



**HAL**  
open science

# Investigation of Nocturnal Atmospheric Reactivity of Furan Compounds with NO<sub>3</sub> Radicals in Simulation Chambers: Kinetics, Products, Mechanisms, and Secondary Organic Aerosol (SOA) Formation.

Fatima Al Ali

► **To cite this version:**

Fatima Al Ali. Investigation of Nocturnal Atmospheric Reactivity of Furan Compounds with NO<sub>3</sub> Radicals in Simulation Chambers: Kinetics, Products, Mechanisms, and Secondary Organic Aerosol (SOA) Formation.. Earth Sciences. Université du Littoral Côte d'Opale, 2023. English. NNT : 2023DUNK0672 . tel-04343100

**HAL Id: tel-04343100**

**<https://theses.hal.science/tel-04343100>**

Submitted on 13 Dec 2023

**HAL** is a multi-disciplinary open access archive for the deposit and dissemination of scientific research documents, whether they are published or not. The documents may come from teaching and research institutions in France or abroad, or from public or private research centers.

L'archive ouverte pluridisciplinaire **HAL**, est destinée au dépôt et à la diffusion de documents scientifiques de niveau recherche, publiés ou non, émanant des établissements d'enseignement et de recherche français ou étrangers, des laboratoires publics ou privés.



## Thèse de Doctorat

*Mention Sciences de la terre et de l'univers  
Spécialité Espace Terre, enveloppes fluides*

présentée à l'Ecole Doctorale en Sciences Technologie et Santé (ED 585)

de l'Université du Littoral Côte d'Opale

par

**Fatima AL ALI**

pour obtenir le grade de Docteur de l'Université du Littoral Côte d'Opale

***Investigation of Nocturnal Atmospheric Reactivity of Furan  
Compounds with NO<sub>3</sub> Radicals in Simulation Chambers:  
Kinetics, Products, Mechanisms, and Secondary Organic  
Aerosol (SOA) Formation***

Soutenue le 11 octobre 2023 après avis des rapporteurs, devant le jury d'examen :

M. Abdelwahid MELOUKI, DR, CNRS Orléans  
M<sup>me</sup> Estelle ROTH, MCF HDR, Université de Reims  
M. Eric VILLENAVE, Pr., Université de Bordeaux  
M<sup>me</sup> Cecile COEUR, MCF HDR, Université du Littoral-Côte d'Opale  
M. Emmanouil ROMANIAS, MCF, IMT Nord Europe  
M. Alexandre TOMAS, Pr., IMT Nord Europe  
M. Matthew COGGON, Dr., NOAA  
M. Nicolas HOUZEL, Université du Littoral-Côte d'Opale

Président  
Rapporteur  
Examineur  
Directeur de thèse  
Co-directeur  
Examineur  
Membre invité  
Membre invité



## Thèse de Doctorat

*Mention Sciences de la terre et de l'univers  
Spécialité Espace Terre, enveloppes fluides*

présentée à l'Ecole Doctorale en Sciences Technologie et Santé (ED 585)

de l'Université du Littoral Côte d'Opale

par

**Fatima AL ALI**

pour obtenir le grade de Docteur de l'Université du Littoral Côte d'Opale

*Étude de la réactivité atmosphérique nocturne des composés furanniques avec les radicaux NO<sub>3</sub> dans des chambres de simulation : cinétique, produits, mécanismes et formation d'aérosols organiques secondaires (SOA)*

Soutenue le 11 octobre 2023 après avis des rapporteurs, devant le jury d'examen :

M. Abdelwahid MELOUKI, DR, CNRS Orléans  
M<sup>me</sup> Estelle ROTH, MCF HDR, Université de Reims  
M. Eric VILLENAVE, Pr., Université de Bordeaux  
M<sup>me</sup> Cecile COEUR, MCF HDR, Université du Littoral-Côte d'Opale  
M. Emmanouil ROMANIAS, MCF, IMT Nord Europe  
M. Alexandre TOMAS, Pr., IMT Nord Europe  
M. Matthew COGGON, Dr., NOAA  
M. Nicolas HOUZEL, Université du Littoral-Côte d'Opale

Président  
Rapporteur  
Examineur  
Directeur de thèse  
Co-directeur  
Examineur  
Membre invité  
Membre invité

Acknowledgement

***1080 days since the beginning... 1080 Thanks..***

It is in meditating on writing these lines that a person realizes he is far from walking the path of life alone. This journey I embarked on, I wasn't alone, this path I walked, I had company, this project I worked on, I had mentors.

I would like to express my gratitude for the jury members **Pr. Wahid Mellouki**, **Pr. Eric Villenave**, and **Dr. Estelle ROTH** for accepting to evaluate this thesis and all the work that was put into it. Thanks for accepting to take time from your busy schedules to participate to our long presentation and debate. Special thanks go to **Dr. Matt Coggon** who accepted to share in this work examination from USA regardless of our time difference.

I would also like to thank my committee members **Dr. Christa Fittschen** and **Pr. Stéphane Sauvage** for their vital comments and valuable suggestions during our annual meetings.

Special acknowledgement goes to our two institutions "Université du Littoral-Côte d'Opale" and "IMT Nord Europe" for granting me a doctoral fellowship. Also, special thanks go to **Labex CAPPA** for financing this project.

First, I would like to express my sincere gratitude to my supervisors, **Dr. Cécile Coeur**, **Dr. Manolis N. Romanias**, **Pr. Alexandre Tomas**. I am extremely lucky to have the three of them as my PhD mentors due your help and guidance throughout these three years, for your continuous support, for our scientific discussions, and for your profound belief in my abilities. My utmost heartfelt gratitude goes to **Dr. Cecile** for being always there for me. This work would have not been possible without your help, dedication, and meticulous work methods. Your insightful feedbacks pushed me to sharpen my critical thinking skills and elevated the quality of my work. Thanks for not only being my PhD mentor, but also my second family in France. I owe sincere thankfulness to **Dr. Manolis**, for all the knowledge you have passed onto me and I will remain forever grateful to all the comments you gave me to lighten my road. I will never forget all of our midnight discussions on the experimental results that ultimately led to be the most productive. I cannot thank you enough for your availability whenever I needed you despite all of your responsibilities. Thank you for all of the technical methods that helped shape this research and your accuracy in the bench work. I extend my gratefulness to **Pr. Alexandre** for all your helpful suggestions, indispensable advices, and encouragement. I am blessed to have had the opportunity to work with you and gain from your rich experience.

I would also like to take this opportunity to express my deepest appreciation to our team research engineer **Nicolas Houzel**. Words cannot express how grateful I am for the support you showed during the three years. Thanks for your time, for your unquestionable support, and for your patience in teaching me each and every experimental detail. Thanks for being a true friend not only a work colleague.

I am also deeply thankful to all of my colleagues and the staff members at Laboratoire de Physico-Chimie de l'Atmosphère for the enjoyable environment, the discussions and the time we shared together during one and a half year. I address many thanks to my old and current PhD colleagues at ULCO including **Ghoufrane**, **Jonas**, **Nhut**, **Jean**, **Yamina**, **Stephanie**, **Souleimane**, **Marc**, **Lamia**, **Malak**. Thanks for our good time and for our late nights in the laboratory spent between hard work and unforgettable moments. I was lucky to also meet new colleagues and office mates during the second part of my PhD at IMT Nord Europe. Special

thanks go to **Anais, Florent, Daria, Jerome, Hichem, Gabriel and Marius**. Thanks to **Vincent Gaudion**, for solving any technical problem in the laboratory whenever needed, sure besides our good moments and discussions.

I also wish to thank the Centre Commun de Mesures at ULCO especially **Paul Genevray** for his help in the LC-MS/MS and GC-EI-MS analysis. I express my sincere acknowledgment to **Pr. Arnaud Cuisset** for his help in the FTIR experiments.

A special thought goes to my friends **Raafa, Ali and Nour**. You stood next to me from the beginning. Thanks for being there through the thin and thick. You all know well what my heart carries for you! I wish you all the good in the world, my friends, and a long and happy life surrounded by your families.

I cannot forget my Lebanese friends in France whom I shared with rememberable time through the past years full of laughs and Lebanese food competitions. Thanks **Hadi, Adel, Ahmad, Douaa, Baby Adam, Hassan, Ghina, Zeinab, Mohammad, Tamara, Salwa, Ibrahim and Alaa**.

*I dedicate this thesis and all the hard work done to the soul of my father **Mashhour** and to my lovely mother **Faten**.*

*Dear **Father**, here our dream come true. Your eldest daughter is getting her highest degree as you always wished. Although you left our world at the beginning of the journey, I always carried your words with me and these words were the base stone to fulfill this adventure. I owe you all the love of this world. Thank you, my hero!*

*All the pages of the world and all the dedication letters are not enough to thank you my **mother**. I cannot thank you enough for having my back since kindergarten, for spending the nights awake during my exam nights, for.... This work would not be possible, and I say this with the highest level of certainty, without your support, love, warmth and prayers. Despite long distances you were sharing each and every moment of the past three years.*

*To the pieces of heart, my sisters **Aya and Yasmina**, my words fail to express my appreciation, gratitude, and love. Thanks for taking care of me since we met. Thanks for always listening to me with complete love and patience. Thanks for believing in me.*

*I am forever indebted to my family for giving me the opportunities that have made me who I am today.*

## Publications & Scientific Activity

The work presented in this manuscript was valued in the form of publications and oral or poster communications. The list is presented below:

## 1. Publications

- **F. Al Ali**, C. CŒUR, N. HOUZEL, H. BOUYA, A. TOMAS, M. N. ROMANIAS. “Rate Coefficients for the Gas-Phase Reactions of Nitrate Radicals with a Series of Furan Compounds”, *J. Phys. Chem. A* 2022, 126, 46, 8674–8681
- **F. Al Ali**, C. CŒUR, N. HOUZEL, P. GENEVRAY, F. CAZIER, A. CUISSET, V. C. PAPADIMITRIOU, A. TOMAS, Manolis N. ROMANIAS, “Atmospheric Degradation of 2-Methylfuran by NO<sub>3</sub> radical. A product study” (submitted).
- M. N. Romanias, M. M. Coggon, **F. Al Ali**, J.B. Burkholder, P. Dagaut, C. Warneke, C. E. Stockwell, Z. Decker, A. Tomas, N. Houzel, C. Cœur, S. S. Brown. “Atmospheric chemistry of furanoids: insights into the sources and atmospheric fate”, *ACS Earth Space Chem.* (under review).
- **F. Al Ali**, C. CŒUR, N. HOUZEL, A. TOMAS, P. Genevray, F. Cazier, M. N. ROMANIAS. “Product and Mechanistic Study of the Atmospheric Degradation of 2,5-Dimethylfuran and 2,3,5-Trimethylfuran with NO<sub>3</sub> radicals” (Under preparation).
- **F. Al Ali**, C. CŒUR, N. HOUZEL, A. TOMAS, M. N. ROMANIAS. “Temperature Dependent Rate Coefficients for Reactions of Methylated-Furan Compounds with NO<sub>3</sub> Radicals” (Under preparation).

## 2. Oral Presentations

- F. AL ALI, C. COEUR, N. HOUZEL, M. ROMANIAS, A. TOMAS, “Reaction of Furan Compounds Emitted from Biomass Burning with the Major Nighttime Oxidant (NO<sub>3</sub> Radical): Rate Coefficient Measurements & Product Characterization”- 26th International Symposium on Gas Kinetics and Related Phenomena – GK2022, Rennes, France (28 August-2 September 2022)
- F. AL ALI, C. COEUR, N. HOUZEL, M. ROMANIAS, A. TOMAS, “Nighttime atmospheric degradation of biomass burning compounds: the fate of methylated furan compounds”- Labex CAPPa scientific day 2022- Lille, France (10 march 2022)
- F. AL ALI, C. COEUR, N. HOUZEL, M. ROMANIAS, A. TOMAS, “Study of the Nighttime Atmospheric Reactivity of Furan Compounds with NO<sub>3</sub> Radical in the Atmospheric Simulation Chamber CHARME” - Comité Scientifique CaPPa –Lille, France (9 november 2021)
- F. AL ALI, C. COEUR, N. HOUZEL, M. ROMANIAS, A. TOMAS, “Kinetic studies of the reactivity of furan compounds with NO<sub>3</sub> in the simulation chamber CHARME”-Labex CAPPa PhD student’s day–Lille, France (9 September 2021).

### 3. Posters

- F. AL ALI, C. COEUR, N. HOUZEL, M. ROMANIAS, A. TOMAS, “NO<sub>3</sub> Initiated Oxidation of Furan Compounds: Rate Coefficients, Gas-Phase Chemical Mechanisms and SOA Formation”-ACM 2022-University of California-Davis-USA (December 2022)
- F. AL ALI, C. COEUR, N. HOUZEL, M. ROMANIAS, A. TOMAS, “Mechanistic Pathways for Reaction of Methylated Furan Compounds with NO<sub>3</sub> Radical”- GDR national conference- Université du Littoral Côte d'Opale -Dunkerque, France (June,2022)
- F. AL ALI, C. COEUR, N. HOUZEL, M. ROMANIAS, A. TOMAS, “Study of the Nighttime Atmospheric Reactivity of Furan Compounds with NO<sub>3</sub> Radical in the Atmospheric Simulation Chamber CHARME”-CLIMIBIO –Lille, France (24 November 2021)

## Table of Contents



<b>ACKNOWLEDGEMENTS</b> .....	ii
<b>PUBLICATIONS &amp; SCIENTIFIC ACTIVITY</b> .....	iv
<b>TABLE OF FIGURES</b> .....	x
<b>TABLE OF TABLES</b> .....	xiv
<b>LIST OF ABBREVIATIONS</b> .....	xvi
<b>GENERAL INTRODUCTION</b> .....	1
<b>I CHAPTER I STATE OF ART</b> .....	<b>7</b>
I.1 INTRODUCTION .....	8
I.2 ATMOSPHERE .....	8
<i>I.2.1 Atmospheric layers</i> .....	8
<i>I.2.2 Atmospheric composition</i> .....	8
<i>I.2.3 Air pollution and climate change</i> .....	10
<i>I.2.4 Oxidative capacity of the troposphere</i> .....	10
I.2.4.1 Hydroxyl radical (OH) sources and levels .....	11
I.2.4.2 Nitrate radical (NO <sub>3</sub> ) sources and levels .....	12
I.2.4.3 Ozone (O <sub>3</sub> ) sources and levels .....	13
I.2.4.4 Chlorine (Cl) sources and levels .....	14
<i>I.2.5 Photolysis</i> .....	14
I.3 VOLATILE ORGANIC COMPOUNDS .....	14
<i>I.3.1 Definition</i> .....	14
<i>I.3.2 Sources</i> .....	15
<i>I.3.3 Chain reactions of tropospheric oxidation of VOCs</i> .....	16
I.4 FURAN COMPOUNDS: IDENTIFICATION, PROPERTIES, EMISSION FACTORS, KINETICS AND PRODUCTS FORMATION .....	17
<i>I.4.1 Chemical structure of furanoids</i> .....	17
<i>I.4.2 Physical properties</i> .....	18
<i>I.4.3 Furan compounds emitted from BB events</i> .....	23
I.4.3.1 Fundamental reactions contributing to furanoid emissions .....	23
I.4.3.2 Open biomass burning connections to fundamental pyrolysis processes .....	25
I.4.3.3 Emission factors of furanoids emitted from fires.....	26
I.5 KINETICS OF THE REACTIONS OF FURAN COMPOUNDS WITH TROPOSPHERIC OXIDANT .....	27
I.5.1.1 Reaction with OH.....	27
I.5.1.2 Reaction with NO <sub>3</sub> .....	31
I.5.1.3 Reaction with O <sub>3</sub> .....	34
I.5.1.4 Reaction with Cl.....	35
I.6 GAS-PHASE PRODUCTS OF THE REACTION OF FURAN COMPOUNDS WITH THE OXIDANTS.....	37
<i>I.6.1 Reaction with OH</i> .....	37
<i>I.6.2 Reaction with NO<sub>3</sub></i> .....	39
<i>I.6.3 Reaction with O<sub>3</sub> and Cl</i> .....	42
I.7 PARTICULATE MATTER .....	42
<i>I.7.1 Definition, sources &amp; classes</i> .....	42
<i>I.7.2 Particles sizes</i> .....	43
<i>I.7.3 Particle aging in the atmosphere</i> .....	43
<i>I.7.4 Chemical composition of atmospheric particles &amp; partitioning of an organic compound</i> .....	43
<i>I.7.5 Secondary Organic Aerosols (SOAs)</i> .....	44
I.7.5.1 Formation mechanism, RH and NO <sub>x</sub> effects.....	44
I.7.5.2 Effect of seed particles on SOA yield .....	44
I.7.5.3 SOA from furan compounds .....	45
I.8 THESIS AIM .....	46
I.9 REFERENCES .....	48
<b>II CHAPTER II - EXPERIMENTAL SETUPS AND METHODS</b> .....	<b>68</b>
II.1 INTRODUCTION .....	69
II.2 THE IMPORTANCE OF LABORATORY STUDIES FOR UNDERSTANDING ATMOSPHERIC CHEMISTRY .....	69

II.3	ATMOSPHERIC SIMULATION CHAMBERS (ACS) USED FOR ATMOSPHERIC PROCESSES ANALYSIS .....	70
II.4	CHARME ATMOSPHERIC SIMULATION CHAMBER .....	70
II.4.1	Chamber presentation .....	70
II.4.2	Pressure and temperature monitoring .....	71
II.4.3	Reaction mixture homogenization .....	71
II.4.4	Cleaning protocol .....	72
II.4.5	Online monitoring of the gas-phase mixture using proton transfer-time of flight-mass spectrometry (PTR-ToF-MS) coupled to CHARME .....	73
II.4.6	Passive sampling of the gas-phase mixture and off-line analysis with gas chromatography-electron impact mass spectrometry (GC-EI-MS) .....	75
II.4.6.1	Adsorption on activated carbon cartridges and analysis with thermo-desorption gas chromatography- mass spectrometry (TD-GC-EI-MS) .....	75
II.4.6.2	Adsorption monotrap™ .....	76
II.4.6.3	Passive sampling of the reaction mixture in a bubbler containing solvent .....	77
II.4.6.4	GC-EI-MS used for analysis of samples collected by the monotrap and the bubbler .....	77
II.4.7	Online monitoring of particles formation using a scanning mobility particle sizer (SMPS) .....	78
II.4.8	Characterization of the SOA composition using passive analytical techniques .....	79
II.4.8.1	Quartz fiber filters .....	79
II.4.8.2	ESI-LC-QToF-MS/MS .....	81
II.4.8.3	Attenuated total reflectance-fourier transform infrared spectroscopy (ATR-FTIR) .....	82
II.5	THALAMOS FACILITY .....	83
II.5.1	Chamber presentation .....	83
II.5.2	Reaction mixture homogenization .....	84
II.5.3	Cleaning protocol and bath gas .....	84
II.5.4	Online monitoring of the gas-phase mixture using selected ion flow tube-mass spectrometer (SIFT-MS) coupled to THALAMOS .....	85
II.5.5	Gas-phase active sampling using tenax cartridges & analysis with TD-GC-MS/FID .....	87
II.6	FOURIER TRANSFORM INFRARED SPECTROSCOPY (FTIR) .....	88
II.6.1	FTIR located at LPCA (Dunkerque, France) .....	88
II.6.2	FTIR located at IMT Nord Europe (Dunkerque, France) .....	89
II.7	COMPLEMENTARITY BETWEEN THE ANALYSIS CONDUCTED IN THE TWO ASC (CHARME & THALAMOS) & SUMMARY OF ANALYTICAL TECHNIQUES .....	90
II.8	EXPERIMENTAL PROTOCOL FOLLOWED .....	92
II.8.1	Background measurement and conditions setting .....	92
II.8.2	Preliminary tests .....	92
II.8.3	Reactant injection .....	92
II.8.4	Reaction analysis .....	95
II.9	MATERIALS .....	97
II.9.1	Materials used .....	97
II.9.2	Synthesis of N <sub>2</sub> O <sub>5</sub> crystals .....	98
II.10	METHODOLOGY .....	101
II.10.1	Determination of rate coefficients .....	101
II.10.1.1	Relative rate method .....	101
II.10.1.2	Error analysis .....	102
II.10.2	Quantification of the products yields .....	103
II.10.3	Determination of SOA yields .....	103
II.11	CONCLUSION OF THE CHAPTER .....	104
II.12	REFERENCES .....	107
<b>III</b>	<b>CHAPTER III: KINETIC STUDIES .....</b>	<b>126</b>
III.1	INTRODUCTION .....	127
III.2	ROOM TEMPERATURE RATE COEFFICIENTS MEASUREMENTS IN CHARME SIMULATION CHAMBER .....	127
III.2.1	Preliminary experiments .....	127
III.2.1.1	Dilution effect .....	127

III.2.1.2 Wall losses .....	128
III.2.1.3 Absence of interference due to reaction with N <sub>2</sub> O <sub>5</sub> and NO <sub>2</sub> .....	129
III.2.2 Rate coefficient of furan reaction with NO <sub>3</sub> .....	129
III.2.3 Rate coefficient of 2-MF reaction with NO <sub>3</sub> .....	131
III.2.4 Rate coefficient of 3-MF reaction with NO <sub>3</sub> .....	132
III.2.5 Rate coefficient of 2,5-DMF reaction with NO <sub>3</sub> .....	133
III.2.6 Rate coefficient of 2,3,5-TMF reaction with NO <sub>3</sub> .....	134
III.3 TEMPERATURE-DEPENDENT RATE COEFFICIENTS FOR THE REACTION OF FURAN COMPOUNDS WITH NO <sub>3</sub> RADICALS ....	138
III.3.1 Temperature dependent rate coefficients of $\alpha$ -P with NO <sub>3</sub> .....	139
III.3.2 Temperature dependent rate coefficients of the reaction of furan with NO <sub>3</sub> .....	144
III.3.3 Temperature-dependent rate coefficient for the reaction of 2-MF with NO <sub>3</sub> .....	147
III.3.4 Temperature dependent rate coefficient for the reaction of 2-carene with NO <sub>3</sub> .....	152
III.3.5 Temperature dependent rate coefficient for the reaction of 2,5-DMF with NO <sub>3</sub> .....	154
III.3.6 Temperature dependence of abstraction and addition pathways .....	157
III.4 DISCUSSION .....	161
III.4.1 Trends in reactivity and first insights about the reaction mechanism .....	161
III.4.2 Average room temperature rate coefficients obtained in CHARME & THALAMOS and comparison with literature data .....	162
III.4.3 Atmospheric implications .....	163
III.5 CONCLUSION.....	164
III.6 REFERENCES.....	165
<b>IV CHAPTER IV PRODUCTS CHARACTERIZATION: COMBINING QUALITATIVE AND QUANTITATIVE APPROACHES WITH MECHANISM PROPOSAL .....</b>	<b>185</b>
IV.1 INTRODUCTION.....	186
IV.2 GAS PHASE PRODUCTS OF THE REACTION OF FURANOIDS WITH NO <sub>3</sub> .....	186
IV.2.1 Furan reaction with NO <sub>3</sub> .....	186
IV.2.1.1 Qualitative identification of the products (TD-GC-EI-MS + SIFT-MS analyses) .....	186
IV.2.1.2 Mechanism in literature and proposition of the major pathways .....	190
IV.2.2 2-Methylfuran reaction with NO <sub>3</sub> .....	190
IV.2.2.1 Offline NO <sub>3</sub> + 2-MF gas-phase reaction products analysis (TD-GC-EI-MS, GC-EI-MS) .....	193
IV.2.2.2 Insights from the online analysis (PTR-ToF-MS, SIFT-MS) of the gas mixture -temporal variation of the reactant and products and yields estimated .....	194
IV.2.2.3 In-situ analysis of NO <sub>3</sub> + 2-MF gas-phase reaction products-results validation- identification and quantification of gas-phase products .....	201
IV.2.3 SOA formation from 2-MF reaction with NO <sub>3</sub> radicals.....	207
IV.2.3.1 SOA yields .....	207
IV.2.3.2 SOA chemical composition .....	209
IV.2.4 Reaction phase mechanism .....	212
IV.2.5 3-Methylfuran reaction with NO <sub>3</sub> .....	215
IV.2.5.1 Qualitative identification of the products (Td-GC-EI-MS chromatograms) .....	215
IV.2.5.2 Mechanism of 3-MF reaction with NO <sub>3</sub> radicals as proposed in literature .....	216
IV.2.6 2,5-DMF reaction with NO <sub>3</sub> .....	217
IV.2.6.1 Insights from the offline analysis of the gas mixture-qualitative identification of the products ( TD-GC-EI-MS, GC-EI-MS) .....	217
IV.2.6.2 Insights from the online analysis (PTR-ToF-MS/SIFT-MS) of the gas mixture- temporal variation of the reactant and products and yields estimated .....	221
IV.2.6.3 Variation of the yield of formation of 5-methylfurfural as function of temperature .....	229
IV.2.7 Mechanism of the reaction of 2,5-DMF with NO <sub>3</sub> .....	230
IV.2.8 SOA formation from the reaction of 2,5-DMF with NO <sub>3</sub> .....	233
IV.2.8.1 SOA yield.....	233
IV.2.8.2 SOA composition .....	235
IV.2.9 2,3,5-TMF reaction with NO <sub>3</sub> .....	237
IV.2.9.1 Insights from the offline analysis of the gas mixture-qualitative identification of the products (TD-GC-EI-MS, GC-EI-MS) .....	237

IV.2.9.2 Insights from the online analysis of the gas mixture- temporal variation of the reactant and products (PTR-ToF-MS) and yields estimated.....	239
IV.2.9.3 Mechanism of the reaction of 2,3,5-TMF with NO <sub>3</sub> .....	241
IV.2.9.4 SOA formation from the reaction of 2,3,5-TMF with NO <sub>3</sub> .....	242
IV.3 CONCLUSION.....	244
IV.4 REFERENCES.....	247
<b>CONCLUSION &amp; PERSPECTIVES.....</b>	<b>263</b>
<b>APPENDICES.....</b>	<b>267</b>
<b>RESUME EN FRANÇAIS.....</b>	<b>275</b>
<b>ABSTRACTS (ENGLISH&amp; FRENCH VERSION).....</b>	<b>306</b>

## TABLE OF FIGURES

Figure I.1: Atmospheric layers and variation of temperature with altitude (Baldwin et al., 2019). .....	8
Figure I.2: Percentage of atmospheric gaseous composition. ....	9
Figure I.3: General description of a chemical mechanism. The main types of reaction considered and classes of organic intermediate and products which are potentially generated. The dominant pathways are highlighted using blue/yellow frame (Zogka & Zogka, 2017). ....	11
Figure I.4: Schematic representation of the free radical catalyzed oxidation of a VOC into its first-generation carbonyl product(s) in the presence of NO, and the associated generation of Ozone (O <sub>3</sub> ) (Jenkin & Hayman, 1999). ....	13
Figure I.5: Mechanism of VOC oxidation or photolysis chain reactions (Ziemann & Atkinson, 2012). ....	16
Figure I.6: Basic structures of (A) aromatic furanoids and (B) partially and fully saturated heterocyclic furanoids. ....	18
Figure I.7: Structure of cellulose, hemicellulose, and lignin. ....	23
Figure I.8: (A) Observed effect of pyrolysis temperature on VOC speciation from measurements of smoke emitted from open burning of temperate forest fuel types. (B) Process diagram showing the connection between pyrolysis, smoldering and flaming combustion, and release of gases and particles from open biomass burning. Graphs adapted from Sekimoto et al. (Sekimoto et al., 2018). Figure taken from review article prepared in the framework of this thesis, and received the contribution of many co-authors. ....	25
Figure I.9: Distribution of furanoid mass for (A) chapparal, (B) peat, and (C) temperate forest fuel types. Species are ordered by the furanoids most commonly reported in literature. ....	26
Figure I.10: Reaction mechanism proposed by Aschmann et al. and Jiang et al. for the degradation of furans by OH radicals in presence of NO <sub>x</sub> at room temperature. Scheme adapted by the work of Jiang et al., (2020). ....	39
Figure I.11: Proposed reaction mechanism for the addition of NO <sub>3</sub> radical to the olefinic double bonds of furan. ....	40
Figure I.12: Size modes and sources of atmospheric particles (Koppmann, 2007). ....	43
Figure II.1: Three-legged stool connecting atmospheric chemistry to sustainable policy (Burkholder et al., 2017). ....	69
Figure II.2: CHARME Atmospheric Simulation Chamber. ....	71
Figure II.3: Homogenization time of one of the furanoids studied (2-MF). ....	72
Figure II.4: Picture of the PTR-ToF-MS connected to CHARME. ....	73
Figure II.5: Scheme of the PTR-ToF-MS and its different parts. ....	74
Figure II.6: (a) Picture of the sampling system composed of an aerosol filter and the bubbler (b) Picture of the bubbler containing the reactive mixture. ....	77
Figure II.7: The two GC-MS techniques used to analyse the samples obtained in CHARME. a: Varian GC-EI-MS, b: AGILENT GC-EI-MS. ....	78
Figure II.8: The SMPS (Model 3081, TSI Inc.) and the CPC (Model 3775, TSI Inc.), coupled to CHARME. ....	78
Figure II.9: Quartz filter with sampled reaction mixture (stained with yellow). ....	80
Figure II.10: ESI-LC-QToF-MS/MS instrument used for the analysis of aerosol filter samples. ....	82
Figure II.11: Diagram and picture of ATR-Spectroscopy (Nicolet iN10 MX) used for aerosols analysis. ....	82
Figure II.12: A picture of the THALAMOS-ASC connected to one of the analytical techniques, SIFT-MS (Voice200). ....	83
Figure II.13: Temperature dynamic in the climatic box determined under heating and cooling experiments (Osseiran et al., 2020). ....	84
Figure II.14: (a) Simplified diagram of the SIFT-MS (b) Picture of the SIFT-MS. ....	86
Figure II.15: Schema representing THALAMOS and the loop connecting it to the SIFT. ....	87
Figure II.16: TD-GC-FID/MS deployed at IMT-NORD-EUROPE. ....	87
Figure II.17: FTIR setup deployed at LPCA-Dunkerque. ....	88

Figure II.18: The impinger used to inject liquid VOCs into CHARME.....	93
Figure II.19: The impinger used to inject solid VOCs into CHARME.....	94
Figure II.20: Setup (consisting of an atomizer and a dryer) utilized to introduce seed particles into CHARME.....	95
Figure II.21: N <sub>2</sub> O <sub>5</sub> synthesis setups. (A) Setup used for CHARME experiments: S-shaped glass tube measuring 2.5 m in length and 2 cm in diameter. (B) Setup used for THALAMOS experiments: glass tube measuring 1 m in length and 4 cm in diameter. (C) Collection of N <sub>2</sub> O <sub>5</sub> crystals.....	100
Figure II.22: FTIR spectrum of the synthesized N <sub>2</sub> O <sub>5</sub> crystals.....	101
Figure II.23: Diagram representing the online and offline analytical techniques coupled to CHARME.....	105
Figure II.24: Diagram representing the online and offline analytical techniques coupled to THALAMOS.....	105
Figure III.1: Typical first-order wall loss reaction plot of 2-MF.....	128
Figure III.2: Time profiles of F and $\alpha$ -P followed by the PTR-ToF-MS.....	130
Figure III.3: Kinetic data plots for the reaction of F with NO <sub>3</sub> using $\alpha$ -P (green circles) and $\beta$ -P (pink triangles) as reference compounds.....	131
Figure III.4: Kinetic data plots for the reaction of 2-MF with NO <sub>3</sub> at 294 $\pm$ 2 K using 2-MB (black squares), $\gamma$ -T (red triangles) and DMB (blue cross) as reference compounds.....	132
Figure III.5: Kinetic data plots for the reaction of 3-MF with NO <sub>3</sub> using three reference compounds 2-MB (black squares), $\gamma$ -T (red triangles) and $\alpha$ -P (green circles).....	133
Figure III.6: Kinetic data plots for the reaction of 2,5-DMF with NO <sub>3</sub> using two reference compounds, $\gamma$ -T (red triangles) and DMB (blue crosses).....	134
Figure III.7: Kinetic data plots for the reaction of 2,3,5-TMF with NO <sub>3</sub> at 294 $\pm$ 2 K using $\alpha$ -T and DMB as reference compounds.....	135
Figure III.8: Workflow of the rate coefficient measurements.....	138
Figure III.9: Arrhenius plot for the reaction of cyclohexene with NO <sub>3</sub> .....	139
Figure III.10: Temporal variation of cyclohexene (black squares) and $\alpha$ -P (red squares) signals by SIFT-MS. Cyclohexene was followed at m/z = 83 and $\alpha$ -P at m/z = 137. Note that m/z includes +1 (protonation). .....	140
Figure III.11: Kinetic data plots for the reaction of $\alpha$ -P with NO <sub>3</sub> relative to that of cyclohexene at increasing temperatures (296-378 K) (slopes obtained using H <sub>3</sub> O <sup>+</sup> specifically are represented).....	141
Figure III.12: Arrhenius plot for the reaction of $\alpha$ -P with NO <sub>3</sub> .....	143
Figure III.13: Relative rate plots for the reaction of F with NO <sub>3</sub> relative to the reaction of cyclohexene at increasing temperatures (296-353 K). Furan was followed at m/z = 68 and cyclohexene at m/z = 82. ....	144
Figure III.14: Arrhenius plot for the reaction of F with NO <sub>3</sub> at temperatures between 263-353 K.....	147
Figure III.15: Relative rate plots for the reaction of 2-MF with NO <sub>3</sub> at increasing temperatures (296-373 K). 2-MF was followed at m/z = 82 and $\alpha$ -P was followed at m/z = 136. ....	148
Figure III.16: Relative rate plots for the reaction of 2-MF with NO <sub>3</sub> at room temperature (296 K) using three references (2-carene, $\alpha$ -P and $\gamma$ -T). 2-MF was followed at m/z = 82 and 2-carene, $\alpha$ -P and $\gamma$ -T were followed at m/z = 93. ....	148
Figure III.17: Arrhenius plot for the reaction of 2-MF with NO <sub>3</sub> .....	151
Figure III.18: Kinetic data plot for the reaction of 2-carene with NO <sub>3</sub> relative to that of 2-MF at increasing temperatures. 2-MF was followed at m/z = 82 and 2-carene at m/z = 136.....	152
Figure III.19: Arrhenius plot for the reaction of 2-carene with NO <sub>3</sub> in the temperature range of 296 to 353 K. .	153
Figure III.20: Kinetic data plots for the reaction of 2,5-DMF with NO <sub>3</sub> relative to that of 2-carene at increasing temperatures. 2,5-DMF was followed at m/z = 96 and 2-carene was followed at m/z = 136. ....	154
Figure III.21: Relative rate plots for the reaction of 2,5-DMF with NO <sub>3</sub> at 296 $\pm$ 2 K using three reference compounds. 2,5-DMF was followed at m/z = 96 and $\alpha$ -T, 2-carene and $\gamma$ -T were followed at m/z = 136. ....	155
Figure III.22: Arrhenius plot for the reaction of 2,5-DMF with NO <sub>3</sub> .....	157
Figure III.23: Calibration of 2,5-DMF and 5-Methylfurfural using three precursor ions of the SIFT. ....	158
Figure III.24: 2,5-DMF consumption and 5-methylfurfural formation versus reaction time (SIFT-MS measurements). ....	158
Figure III.25: 5-Methylfurfural yield of formation from the reaction of 2,5-DMF with NO <sub>3</sub> versus temperature.	159
Figure III.26: Temperature-dependence of the H-abstraction and NO <sub>3</sub> addition rate coefficients of 2,5-DMF....	160

Figure IV.1: Chromatogram (TD-GC-EI-MS) of the gas-phase oxidation products formed during the reaction of furan with NO <sub>3</sub> radicals. The peaks are labelled with their chemical structures. ....	187
Figure IV.2 : Mass scans of the products of Furan/NO <sub>3</sub> obtained with the SIFT-MS using three precursor ions (H <sub>3</sub> O <sup>+</sup> , NO <sup>+</sup> , O <sub>2</sub> <sup>+</sup> ) in THALAMOS. Identified peaks are labelled with their corresponding m/z values. ....	189
Figure IV.3 : Mechanism of the reaction of furan with NO <sub>3</sub> leading to the formation of the major primary products. ....	190
Figure IV.4 : Chromatogram (TD-GC-EI-MS) of the gas-phase oxidation products formed the reaction of 2-MF with NO <sub>3</sub> radicals. The peaks are labelled with their chemical structures and names. ....	193
Figure IV.5: (a) Typical reactants and products temporal profiles detected for the NO <sub>3</sub> radical reaction with 2-MF ([2-MF] <sub>t=0</sub> = 800 ppbv) with PTR-ToF-MS. 2-MF (m/z = 83.0) and the two predominant products detected at m/z = 99.0 and 97.0 are shown with different colors. Note that m/z includes +1 corresponding to ionization by H <sup>+</sup> (b) time profiles of the minor oxidation products. ....	195
Figure IV.6: Typical plots for the determination of the gas-phase product yields formed from the reaction of 2-MF with NO <sub>3</sub> . (a) major oxidation products (b) minor oxidation products. ....	197
Figure IV.7: Mass scans of furfural, 2-MF and products of the reaction of 2-MF with NO <sub>3</sub> obtained using SIFT-MS coupled to THALAMOS employing three precursor ions (H <sub>3</sub> O <sup>+</sup> , NO <sup>+</sup> , O <sub>2</sub> <sup>+</sup> ). ....	200
Figure IV.8: Residual spectrum recorded at 2-MF + NO <sub>3</sub> reaction completion, in presence of O <sub>2</sub> , after subtracting the IR spectra of N <sub>2</sub> O <sub>5</sub> , NO <sub>2</sub> , and HNO <sub>3</sub> . The residual spectrum displays the end-oxidation products. The exact wavenumbers of the peaks are shown in graph. ....	203
Figure IV.9: Residual IR spectrum (black line, left axis), and theoretically obtained cross section spectra of 4-oxo-2-pentenal (blue line, right axis) and dinitrooxy-methylfuran (red line, right axis) calculated at MP2/AUG-ccc-pVDZ level of theory. ....	203
Figure IV.10: Yield Curve (SOA yield Y <sub>SOA</sub> versus the organic aerosols mass formed M <sub>0</sub> ) for the 2-MF/NO <sub>3</sub> (squares). The line represents the Odum fit to the data considering one-product model developed by Odum et al., (1996). ....	208
Figure IV.11 : Chromatogram (ESI-LC-QTOF-MS analysis) of the SOA formed from the gas-phase reaction of 2-MF with NO <sub>3</sub> radical. The compounds corresponding to the labelled peaks are displayed in Table IV.6. ....	210
Figure IV.12 : ATR spectrum (in black) of SOA formed from the NO <sub>3</sub> initiated oxidation of 2-MF. SOA were collected on quartz filter. The atmospheric irradiance spectrum is also given in the graph, to evaluate the formed SOA as potent radiative species. ....	212
Figure IV.13 : Mechanism for the reaction of 2-MF with NO <sub>3</sub> yielding to the different products detected by different analytical techniques. ....	213
Figure IV.14 : Chromatogram (Td-GC-EI-MS) of the gas-phase products formed from the gas-phase reaction of 3-MF with NO <sub>3</sub> radicals. The peaks are labelled with their chemical structures identifications. ....	216
Figure IV.15 : Proposed mechanism for 3-methylfuran oxidation by NO <sub>3</sub> radicals. Selected particle species in Figure IV.2 is colored in green. NO <sub>3</sub> can be added to 2 or 5 position, but addition to 5 position is shown here as the representative case (Joo et al., 2019b). ....	217
Figure IV.16 : Chromatogram (Td-GC-EI-MS) of the gas-phase products formed from the gas-phase reaction of 2,5-DMF with NO <sub>3</sub> radicals. The peaks are labelled with their chemical structures identifications. ....	218
Figure IV. 17 : (a) Typical time profiles of masses detected by PTR-ToF-MS during the oxidation of 2,5-DMF (initial concentration = 800 ppbv), 2,5-DMF (m/z = 97.10), major products : m/z = 111.0 and m/z = 113.0. (b) time profile of the minor oxidation products. Nolte that m/z includes +1 corresponding to ionization by H <sup>+</sup> ....	222
Figure IV.18 : Typical plots for the determination of the gas-phase products yields formed from the reaction of 2,5-DMF with NO <sub>3</sub> (a) major oxidation products (b) minor oxidation products. ....	223
Figure IV. 19 : Mass scan of 5-methylfurfural standard using the SIFT-MS coupled to THALAMOS using the three precursor ions (H <sub>3</sub> O <sup>+</sup> , NO <sup>+</sup> , O <sub>2</sub> <sup>+</sup> ). ....	226
Figure IV.20 : Mass scans of the products of the reaction of 2,5-DMF with NO <sub>3</sub> obtained upon ionization using three precursor ions H <sub>3</sub> O <sup>+</sup> (a), NO <sup>+</sup> (b), O <sub>2</sub> <sup>+</sup> (c) within SIFT-MS coupled to THALAMOS. ....	228
Figure IV.21 : Mechanism of the reaction of 2,5-DMF with NO <sub>3</sub> . First generation products are colored in red while the second-generation products are labelled in blue. ....	232
Figure IV.22 : Plot of Y <sub>SOA</sub> as function of M <sub>0</sub> for the reaction of 2,5-DMF with NO <sub>3</sub> according to the one product model developed by Odum et al. ....	234

Figure IV.23 : Chromatogram (Td-GC-EI-MS) of the gas-phase products formed from the gas-phase reaction of 2,3,5-TMF with NO<sub>3</sub> radicals. The peaks are labelled with their chemical structures' identifications..... 237

Figure IV.24 : (a) Typical time profiles of chemical compounds detected by PTR-ToF-MS during the oxidation of 2,3,5-TMF (initial concentration= 1100 ppbv), 2,3,5-TMF (m/z = 111.0), major products: m/z =125.0, m/z = 127.0). Note that m/z includes +1 corresponding to the ionization by H<sup>+</sup> (b) time profiles of the minor products. .... 239

Figure IV.25 : Typical plots for the determination of the gas-phase product yields formed from the reaction of 2,3,5-TMF with NO<sub>3</sub> (a) major oxidation products (b) minor oxidation products..... 240

Figure IV.26 : Mechanism of the reaction of 2,3,5-TMF with NO<sub>3</sub>. Labeled in red are the first-generation products (1-3) while in blue are the second-generation products (4-7). .... 242

Figure IV.27 : Yield Curve for the reaction of 2,3,5-TMF with NO<sub>3</sub> (squares). The line represents the Odum fit to the data considering one-product model (Odum et al., 1996). .... 244

Figure IV.28: Chemical mechanisms for the gas-phase reaction of furan and methylated-furanoids with NO<sub>3</sub> leading to the formation of the primary products. Products labelled in blue are formed from NO<sub>3</sub> addition while those labelled in red are the products formed from H-abstraction while those. Products yields are also indicated. .... 245



## TABLE OF TABLES

Table I.1: Trace gases and their average atmospheric mixing ratios (ppmv) (Vallero,2004).....	9
Table I.2: Physical properties of furanoids considered in literature studies. Compounds in brackets have not been identified in biomass burning but studied in terms of reactivity with atmospheric oxidants.....	19
Table I.3: Summary of available literature data for the reaction of furanoids with the hydroxyl radical (OH). ....	28
Table I.4: Summary of available literature data for the reaction of furanoids with the nitrate radical (NO <sub>3</sub> ). ....	32
Table I.5: Summary of available literature data for the reaction of furanoids with ozone (O <sub>3</sub> ). ....	34
Table I.6: Summary of available room temperature literature data for the reaction of furanoids with chlorine atom (Cl). ....	35
Table I.7: Experimental determined yields of the major products formed from the photooxidation of furan/methylfurans by OH radicals at room temperature and ambient pressure. ....	38
Table I.8: Summary of the SOA yields from the OH, NO <sub>3</sub> , and O <sub>3</sub> oxidation of furanoids. ....	45
Table II.1: Comparison of the two types of monotraps used for gaseous products sampling. ....	76
Table II.2: Comparison of the features of the two atmospheric simulation chambers used (CHARME & THALAMOS). ....	90
Table II.3: Comparison of the features of the two atmospheric simulation chambers used (CHARME & THALAMOS). ....	91
Table II.4: Ions selected on the PTR-ToF-MS to monitor the concentration profiles of the compounds used in the current study. ....	96
Table II.5: Ion intensities selected on SIFT-MS to monitor the concentration profiles of the compounds used in the current study. ....	96
Table II.6: List of the chemicals used in the experiments, their molar mass, physical state, manufacturer, and the corresponding purity. ....	98
Table III.1: Rate coefficients of the references used for the determination of the rate coefficients of furan compounds. ....	127
Table III.2: Average wall loss rate coefficient (kw) for the VOCs used in CHARME experiments. ....	129
Table III.3: Summary of all rate coefficients for the reactions of furan compounds with NO <sub>3</sub> . ....	136
Table III.4: Summary of the experimental conditions and the rate coefficients measured at increasing temperatures using the three precursor ions of the SIFT-MS (H <sub>3</sub> O <sup>+</sup> , NO <sup>+</sup> , O <sub>2</sub> <sup>+</sup> ). ....	142
Table III.5: Summary of the experimental conditions and the rate coefficients of the reaction of F with NO <sub>3</sub> measured at increasing temperatures (263 – 353 K) using the three precursor ions of the SIFT-MS (H <sub>3</sub> O <sup>+</sup> , NO <sup>+</sup> , O <sub>2</sub> <sup>+</sup> ). ....	145
Table III.6: Experimental conditions, slopes of the relative rate plots and the temperature-dependent rate coefficients for the reaction of 2-MF with NO <sub>3</sub> . ....	149
Table III.7: Experimental conditions including 2-carene and the reference (2-MF) concentrations, the slopes of the relative rate plots and the average rate coefficient measured at each temperature (296-353 K). ....	153
Table III.8: Experimental conditions, relative rate plots slopes obtained with the three precursor ions of the SIFT and the average rate coefficient measured at each temperature. ....	155
Table III.9: 5-Methylfurfural yields versus temperature and the corresponding H-abstraction rate coefficient (k <sub>obs</sub> ). ....	159
Table III.10: Arrhenius expressions for the reaction of F, 2-MF and 2,5-DMF with NO <sub>3</sub> , temperature range of each expression and the corresponding activation energy. ....	161
Table III.11: Comparison of the average rate coefficients measured in CHARME with those in the literature. ..	163
Table IV.1 : Masses of the products of the reaction of furan with NO <sub>3</sub> detected with the SIFT-MS, including the ions obtained upon ionization with H <sub>3</sub> O <sup>+</sup> , NO <sup>+</sup> and O <sub>2</sub> <sup>+</sup> . ....	188

<i>Table IV.2 : Gas-phase products detected using different sampling methods and analytical techniques (products numbers are consistent with the mechanism presented in Figure IV.13). Results obtained for the different solvents have been combined. ....</i>	<i>191</i>
<i>Table IV.3 : NO<sub>3</sub> + 2-MF reaction products molar-yields as determined from the linear least-square analysis of products concentration versus [2-MF] loss. The m/z correspond to compounds fragments masses plus one (H<sup>+</sup> attached). ....</i>	<i>196</i>
<i>Table IV.4 : Experimental conditions and SOA yields of the reaction of 2-MF and NO<sub>3</sub>. ....</i>	<i>207</i>
<i>Table IV.5 : Names and structures of the oxidation products identified in the SOA formed from the 2-MF oxidation by NO<sub>3</sub>. ....</i>	<i>209</i>
<i>Table IV.6 : Compounds detected in the SOA formed from the reaction of 2-MF with NO<sub>3</sub> radical in the particulate phase (ESI-LC-QToF-MS/MS analyses). The main fragments observed by MS/MS analyses and the relative abundance of each detected compound (in %) are also presented.....</i>	<i>211</i>
<i>Table IV.7 : Products of the reaction of 2,5-DMF with NO<sub>3</sub> identified using different sampling and analytical techniques (products numbers are related to their numbering on the mechanism figure.....</i>	<i>219</i>
<i>Table IV.8 : Identification and formation yields of the products formed from the reaction of 2,5-DMF with NO<sub>3</sub> (m/z masses include the addition of H<sup>+</sup>). ....</i>	<i>225</i>
<i>Table IV.9: Yield of formation of 5-methylfurfural from the reaction of 2,5-DMF with NO<sub>3</sub> at temperatures between 298 and 353 K. ....</i>	<i>230</i>
<i>Table IV.10 : Experimental conditions and SOA yields for the reaction of 2,5-DMF with NO<sub>3</sub>. ....</i>	<i>233</i>
<i>Table IV.11 : Names and structures of the oxidation products identified with the GC-EI-MS in the SOAs formed from the 2,5-DMF oxidation by NO<sub>3</sub>. ....</i>	<i>235</i>
<i>Table IV.12 : Compounds detected in the SOA formed from the reaction of 2,5-DMF with NO<sub>3</sub> radical in the particulate phase (ESI-LC-QToF-MS/MS analyses). The main fragments observed by MS/MS analyses and the relative abundance of each detected compound (in %) are also presented.....</i>	<i>236</i>
<i>Table IV.13 : Identification of the products formed from the reaction of 2,3,5-TMF with NO<sub>3</sub> in both the gaseous and particulate phase by the different analytical techniques employed.....</i>	<i>238</i>
<i>Table IV.14 : Identification and formations yields of the products formed from the reaction of 2,3,5-TMF with NO<sub>3</sub> (m/z masses include the addition of H<sup>+</sup>). ....</i>	<i>241</i>
<i>Table IV.15 : Experimental conditions and SOA yield for the reaction of 2,3,5-TMF with NO<sub>3</sub>. ....</i>	<i>243</i>

## **List of Abbreviations**

API-MS/MS	Atmospheric pressure ionization tandem mass spectrometry
AR	Absolute rate method
ASC	Atmospheric simulation chamber
ATR-FTIR	Attenuated total Reflectance-fourier transform infrared spectroscopy
CHARME	Chamber for Atmospheric Reactivity and Metrology of the Environment
CI	Chemical ionisation
Cl	Chlorine atom
CO	Carbon monoxide
CO <sub>2</sub>	Carbon dioxide
CPC	Condensation particle counter
DFT	Discharge flow tube
DMA	Differential mobility analyzer
DMB	2,3-Dimethyl-2-Butene
ESI-LC- QToF-MS/MS	ElectroSpray Ionization - liquid Chromatography- quadrupole time- of flight – tandem mass spectrometry
EU	European union
F	Furan
FID	Flame ionization detector
FP	Flash photolysis
FTIR	Fourier Transform infrared spectroscopy
FT	Flow tube
GC-EI-MS	Gas chromatography-electron impact-mass spectrometry
GC-FID	Gas chromatography –flame ionization detection
GC-FID-MS	Gas chromatography –flame ionization detection-mass spectrometry
GC-MS	Gas chromatography-mass spectrometry
HCOH	Formaldehyde
HNO <sub>3</sub>	Nitric acid

HONO	Nitrous acid
H <sub>2</sub> O <sub>2</sub>	Hydrogen peroxide
H <sub>3</sub> O <sup>+</sup>	Hydronium ions
HR-TOF-CIMS	High-resolution time of flight-chemical ionization mass spectrometer
k	Rate coefficient
LIF	Laser induced fluorescence
MCE	Modified combustion efficiency
MCP	Micro Channel Plate
MSDS	Material safety data sheet
m/z	Mass-to-charge ratio
NH <sub>4</sub> <sup>+</sup>	Ammonium ions
(NH <sub>4</sub> ) <sub>2</sub> SO <sub>4</sub>	Ammonium sulfate
NMVOCS	Non-methane volatile organic compounds
NO <sub>2</sub>	Nitrogen dioxide
NO <sub>3</sub>	Nitrate radical
NO <sub>x</sub>	Nitrogen oxides
N <sub>2</sub> O <sub>5</sub>	Dinitrogen pentoxide
O	Oxygen atom
O <sub>2</sub>	Oxygen molecule
O <sub>3</sub>	Ozone
ODS	Octadecylsilyl groups
OH	Hydroxyl radical
Ox	Oxidant
PA	Proton affinity
PC	Pyrex cell
PCI GC-MS	Positive chemical ionization gas chromatography–mass spectrometry
PLP	Pulse laser fluorescence
PM	Particulate matter
PPR	Pyrex photochemical reactor
PSA	Pressure swing adsorption
PTR-ToF-MS	Proton transfer-time of flight-mass spectrometry

QPR	Quartz photochemical reactor
Ref	Reference compound
RF	Resonance fluorescence
RH	Relative humidity
RO <sub>2</sub>	Peroxy radical
RR	Relative rate method
SAR	Structure activity relationship
SDS	Safety data sheet
SIFT-MS	Selected ion flow tube-mass spectrometer
SOA	Secondary organic aerosols
SO <sub>2</sub>	Sulfur dioxide
SPME-GC-FID detection	Solid-phase microextraction- gas chromatography –flame ionization
ST	Shock tube
SVOC	Semi-volatile organic compounds
S/V	Surface to volume ratio
TD-GC-EI-MS	Thermo-desorption gas chromatography- mass spectrometry
THALAMOS	Thermally regulated atmospheric simulation chamber
UV <sub>abs</sub>	Ultraviolet absorption
VOC	Volatile organic compound
2-MB	2-Methyl-2-Butene
2-MF	2-Methylfuran
3-MF	3-Methylfuran
2,5-DMF	2,5-Dimethylfuran
2,3,5-TMF	2,3,5-Trimethylfuran
α-P	α-Pinene
α-T	α-Terpinene
β-P	β-Pinene
γ-T	γ-Terpinene

## General Introduction

Atmospheric chemistry is an important and complicated discipline for understanding air pollution and its impacts, dealing with atmospheric chemical composition and reactivity of its components. This branch of atmospheric science focuses on physico-chemical processes within the Earth's atmosphere, including oxidation of gaseous compounds, formation and properties of the reaction products and airborne aerosol particles, gas-particle interactions, etc. (Finlayson-Pitts, 2010).

Volatile Organic Compounds (VOCs) are all the organic compounds which have a saturation vapor pressure of 10 Pa or higher at 20°C. VOCs are released in the atmosphere either from natural or anthropogenic sources. Guenther et al. (1995) reported that 90% of the global emissions of organic compounds are from biogenic origins and 10% are from anthropogenic origin (Guenther et al., 1995). Among the various sources of VOCs in the atmosphere, Biomass Burning (BB) has received special attention during the past 10 to 15 years.

BB is the burning of living and dead vegetation, which includes the human-initiated burning for land clearing and land-use change, natural fires, and domestic heating. Due to the increasing population rate and the extra demand for food, the rate of land clearing and land use (directly related to wildfires and BB events) (Durigan et al., 2017; Krause et al., 2014) has increased dramatically during the last few decades (Paquet et al., 2019), and increasing trends are projected over the near future (Stehfest et al., 2019).

BB is a significant source of non-methane volatile organic compounds (NMVOCs) that leads to the formation of pollutants like ozone and secondary organic aerosols (SOA) (Alvarado, 2008; Alvarado et al., 2015). Therefore, biomass burning events are associated with poor air quality and also affects regional and global climate. There have been extensive attempts to quantify the biomass burning emission fluxes of NMVOCs, and investigate their tropospheric chemical reactivity (Hatch et al., 2015; Decker et al., 2019).

One of the important NMVOC families emitted from biomass combustion are furan compounds (Stockwell et al., 2015; Hatch et al., 2017). Furans are highly reactive toward hydroxyl radical (OH) during daytime as well as with nitrate radical (NO<sub>3</sub>) during both daytime and night (Gilman et al., 2015; Hartikainen et al., 2018; Koss et al., 2018; Decker et al., 2019; Al Ali et al., 2022). They have been demonstrated to contribute significantly ( $\cong 20\%$ ) to the overall NO<sub>3</sub> (Decker et al., 2021) and OH reactivities (Coggon et al., 2019). Interestingly, a recent study, based on both experiments and modelisation, showed that during the daytime, furan degradation drives the chemistry inside fresh biomass plumes, forming secondary pollutants like tropospheric ozone (O<sub>3</sub>) and SOA (Coggon et al., 2019).

As a result, it is essential to develop chemical mechanisms involving the atmospheric reactions between furans and oxidants in order to investigate the chemical modifications occurring into fresh plumes and also to determine their impacts on air quality and climate. In literature, studies focusing on the oxidation mechanisms of furans by OH radicals are limited (Bierbach et al., 1995; Gómez Alvarez et al., 2009; Aschmann et al., 2011; Aschmann et al., 2014; Yuan et al., 2017; Joo et al., 2019), while in the case of other atmospheric oxidants (NO<sub>3</sub>, O<sub>3</sub>, Cl), this information is even more scarce (Villanueva et al., 2007; Villanueva et al., 2009; Tapia et al.,

2011; Colmenar et al., 2012). Up to now, the contribution of furan degradation on the nighttime tropospheric chemistry is poorly addressed.

This thesis aims to study the reactivity of selected furan compounds (furan (F) and methylated furans, i.e. 2-methylfuran (2-MF), 3-methylfuran (3-MF), 2,5-dimethylfuran (2,5-DMF) and 2,3,5-trimethylfuran (2,3,5-TMF)) with the nocturnal atmospheric oxidants of NMOC (the  $\text{NO}_3$  radical).

To specify, the selection of methylated-furan compounds and their reaction with  $\text{NO}_3$  in this study is based on several reasons. The existing kinetic studies on the reactions of methylated-furan compounds with  $\text{NO}_3$  indicate that the  $\text{NO}_3$ -initiated oxidation of this class of compounds is extremely fast (lifetime in the range of 1 h - 1 min) and consequently their corresponding role in nighttime chemistry is expected to be dominant and more significant than during daytime (Atkinson et al., 1983b; Kind et al., 1996; Newland et al., 2022). Decker et al., (2019) showed that 60% of the mass fraction of methylated-furans are oxidized by  $\text{NO}_3$  during nighttime, predominantly due to their fast reaction with  $\text{NO}_3$  radical. Second, these compounds are an important part of this family emitted during fires (Liang et al., 2022). Methylated furans, i.e. 2-MF, 3-MF, 2,5-DMF and 2,3,5-TMF, are directly emitted from vegetation fires and they contribute to a major fraction of the total furan emissions (20-25%) (Ciccioli et al., 2001; Gilman et al., 2015). Third, unlike their daytime atmospheric reactivity, which is well studied in literature, their nighttime reactivity with  $\text{NO}_3$  is poorly understood. Finally, since furan compounds are emitted during biomass burning events (first-generation furan compounds), they play a significant role in driving the chemistry of plumes in the early stages of their formation, occurring during both daytime and nighttime. So, there is a need to study the gas-phase mechanism and to characterize the SOA formation as it is connected with nighttime aging in BB plumes.

In view of the poor knowledge on the atmospheric reactivity of furan compounds and their large emissions during BB, there is a need to study their gas-phase reaction with  $\text{NO}_3$  radical and to characterize their SOA formation potential.

This thesis manuscript starts by a “general introduction”, followed by four distinct chapters and then ends by a “general conclusion and perspectives”.

The first chapter provides an overview of the knowledge on the atmospheric constituents and their interactions with a special attention given to the oxidation of VOCs. Further, a literature review covering the atmospheric reactivity of furan compounds with the different atmospheric oxidants (OH,  $\text{NO}_3$ ,  $\text{O}_3$  and Cl) is presented. This review includes kinetics, products of the reactions, mechanisms and SOA formation. Finally, the aims of the thesis are stated.

In the second chapter, the two complementary atmospheric simulation chambers (CHARME and THALAMOS) deployed in this work are described in addition to the various sampling and analytical methods used to monitor the gas- and particulate- phase species which have been used. These methods can be used as a base for future works on the study of the VOC atmospheric reactivity in simulation chambers.

The third chapter concerns the kinetics investigations. The rate coefficients for the gas-phase oxidation of furan and methylated furan (list here the furans studied) with  $\text{NO}_3$  radical at room

temperature as well as the temperature dependence (precise the temperature range) for F, 2-MF, 2,5-DMF are presented. Achieving these kinetic goals allows to determine the furan atmospheric lifetimes at different temperature which enables to apprehend the behavior of these compounds in the atmosphere. In addition, the investigation of the variation of the rate coefficients with the temperature gives insights into the mechanism of the reactions. From a chemical structure side of view, the kinetic studies of furan and different methylated furans allows to understand how the number and position of the methyl groups on the furan ring influence the rate coefficient with  $\text{NO}_3$ . These data are useful to develop Structure Activity Relationships (SAR) which are used to calculate the rate coefficients for the  $\text{NO}_3$  reaction with other furan compounds and also with other VOCs.

In the fourth chapter, qualitative and quantitative characterization of the atmospheric oxidation products formed both in the gas- and particulate- (i.e. SOA formation) phases from the reaction between furan compounds (which ones? Precise here) and  $\text{NO}_3$  was achieved. The SOA formation yields measured are treated using the gas-particle partitioning model (Odum et al., 1996) in order to determine the parameters  $\alpha$  (mass-based stoichiometric coefficient of semi-volatile organic compounds (SVOC)) and  $K$  (gas-particle partitioning equilibrium constant that describes the partitioning of oxidation product). These experiments allow to propose detailed reaction mechanism schemes which can be used in atmospheric chemical models to simulate the evolution of BB plumes composition.

Finally, the main results obtained during this thesis are resumed in a general conclusion, and research perspectives are proposed. The understanding of the atmospheric physico-chemical processes, of the reactivity of trace gases or aerosols, as well as their interactions are required to develop pollution control strategies.

This research was conducted collaboratively between two laboratories: LPCA at ULCO (Dunkerque) and SAGE at IMT Nord Europe (Douai). Two complementary simulation chambers were utilized: the Chamber for Atmospheric Reactivity and Metrology of the Environment (CHARME) at LPCA and the Thermally Regulated Atmospheric Simulation Chamber (THALAMOS) at SAGE. Both chambers are described in Chapter II underlining the complementarity aspects of the two facilities. This complementarity is crucial for cross-validating the results and conducting temperature-dependent studies.



## References

- Al Ali, F., Coeur, C., Houzel, N., Bouya, H., Tomas, A., & Romanias, M. N. (2022). Rate Coefficients for the Gas-Phase Reactions of Nitrate Radicals with a Series of Furan Compounds. *Journal of Physical Chemistry A*, 126(46), 8674–8681. <https://doi.org/10.1021/acs.jpca.2c03828>
- Aschmann, S. M., Nishino, N., Arey, J., & Atkinson, R. (2011). Kinetics of the Reactions of OH Radicals with 2- and 3-Methylfuran, 2,3- and 2,5-Dimethylfuran, and E- and Z-3-Hexene-2,5-dione, and Products of OH p 2,5-Dimethylfuran. *Environmental Science and Technology*, 45(7), 1859–1865. <https://doi.org/10.1002/kin.550140706>
- Aschmann, S. M., Nishino, N., Arey, J., & Atkinson, R. (2014). *Sara M. Aschmann, Noriko Nishino, † Janet Arey, \*, ‡ and Roger Atkinson \*, ‡*.
- Bierbach, A., Barnes, I., & Becker, K. H. (1995). Product and kinetic study of the oh-initiated gas-phase oxidation of Furan, 2-methylfuran and furanaldehydes at  $\approx 300$  K. *Atmospheric Environment*, 29(19), 2651–2660. [https://doi.org/10.1016/1352-2310\(95\)00096-H](https://doi.org/10.1016/1352-2310(95)00096-H)
- Coggon, M. M., Lim, C. Y., Koss, A. R., Sekimoto, K., Yuan, B., Gilman, J. B., Hagan, D. H., Selimovic, V., Zarzana, K. J., Brown, S. S., M Roberts, J., Müller, M., Yokelson, R., Wisthaler, A., Krechmer, J. E., Jimenez, J. L., Cappa, C., Kroll, J. H., De Gouw, J., & Warneke, C. (2019). OH chemistry of non-methane organic gases (NMOGs) emitted from laboratory and ambient biomass burning smoke: Evaluating the influence of furans and oxygenated aromatics on ozone and secondary NMOG formation. *Atmospheric Chemistry and Physics*, 19(23), 14875–14899. <https://doi.org/10.5194/acp-19-14875-2019>
- Colmenar, I., Cabañas, B., Martínez, E., Salgado, M. S., & Martín, P. (2012). Atmospheric fate of a series of furanaldehydes by their NO<sub>3</sub> reactions. *Atmospheric Environment*, 54(3), 177–184. <https://doi.org/10.1016/j.atmosenv.2012.02.087>
- Decker, Z. C. J., Zarzana, K. J., Coggon, M., Min, K. E., Pollack, I., Ryerson, T. B., Peischl, J., Edwards, P., Dubé, W. P., Markovic, M. Z., Roberts, J. M., Veres, P. R., Graus, M., Warneke, C., De Gouw, J., Hatch, L. E., Barsanti, K. C., & Brown, S. S. (2019). Nighttime Chemical Transformation in Biomass Burning Plumes: A Box Model Analysis Initialized with Aircraft Observations. *Environmental Science and Technology*, 53(5), 2529–2538. <https://doi.org/10.1021/acs.est.8b05359>
- Decker, Z., Robinson, M., Barsanti, K., Bourgeois, I., Coggon, M., DiGangi, J., Diskin, G., Flocke, F., Franchin, A., Fredrickson, C., Hall, S., Halliday, H., Holmes, C., Huey, L. G., Lee, Y. R., Lindaas, J., Middlebrook, A., Montzka, D., Moore, R., ... Brown, S. (2021). Nighttime and Daytime Dark Oxidation Chemistry in Wildfire Plumes: An Observation and Model Analysis of FIREX-AQ Aircraft Data. *Atmospheric Chemistry and Physics Discussions*, November, 1–45. <https://doi.org/10.5194/acp-2021-267>
- Durigan, M. R., Cherubin, M. R., de Camargo, P. B., Ferreira, J. N., Berenguer, E., Gardner, T. A., Barlow, J., Dias, C. T. dos S., Signor, D., de Oliveira, R. C., & Cerri, C. E. P. (2017). Soil organic matter responses to anthropogenic forest disturbance and land use change in the eastern Brazilian Amazon. *Sustainability (Switzerland)*, 9(3). <https://doi.org/10.3390/su9030379>
- Finlayson-Pitts, B. J. (2010). Atmospheric chemistry. *Proceedings of the National Academy of*

*Sciences of the United States of America*, 107(15), 6566–6567.  
<https://doi.org/10.1073/pnas.1003038107>

- Gilman, J. B., Lerner, B. M., Kuster, W. C., Goldan, P. D., Warneke, C., Veres, P. R., Roberts, J. M., De Gouw, J. A., Burling, I. R., & Yokelson, R. J. (2015). Biomass burning emissions and potential air quality impacts of volatile organic compounds and other trace gases from fuels common in the US. *Atmospheric Chemistry and Physics*, 15(24), 13915–13938. <https://doi.org/10.5194/acp-15-13915-2015>
- Gómez Alvarez, E., Borrás, E., Viidanoja, J., & Hjorth, J. (2009). Unsaturated dicarbonyl products from the OH-initiated photo-oxidation of furan, 2-methylfuran and 3-methylfuran. *Atmospheric Environment*, 43(9), 1603–1612. <https://doi.org/10.1016/j.atmosenv.2008.12.019>
- Guenther, A., Nicholas, C., Fall, R., Klinger, L., McKay, W. A., & Scholes, B. (1995). A global model of natural volatile organic compound emissions s Raja the balance Triangle changes in the atmospheric accumulation rates of greenhouse Triangle Several inventories of natural and Exposure Assessment global scales have been two classes Fores. *J. Geophys. Res.*, 100(94), 8873–8892.
- Hartikainen, A., Yli-Pirilä, P., Tiitta, P., Leskinen, A., Kortelainen, M., Orasche, J., Schnelle-Kreis, J., Lehtinen, K. E. J., Zimmermann, R., Jokiniemi, J., & Sippula, O. (2018). Volatile Organic Compounds from Logwood Combustion: Emissions and Transformation under Dark and Photochemical Aging Conditions in a Smog Chamber. *Environmental Science and Technology*, 52(8), 4979–4988. <https://doi.org/10.1021/acs.est.7b06269>
- Hatch, L. E., Yokelson, R. J., Stockwell, C. E., Veres, P. R., Simpson, I. J., Blake, D. R., Orlando, J. J., & Barsanti, K. C. (2017). Multi-instrument comparison and compilation of non-methane organic gas emissions from biomass burning and implications for smoke-derived secondary organic aerosol precursors. *Atmospheric Chemistry and Physics*, 17(2), 1471–1489. <https://doi.org/10.5194/acp-17-1471-2017>
- Joo, T., Rivera-Rios, J. C., Takeuchi, M., Alvarado, M. J., & Ng, N. L. (2019). Secondary Organic Aerosol Formation from Reaction of 3-Methylfuran with Nitrate Radicals. *ACS Earth and Space Chemistry*, 3(6), 922–934. <https://doi.org/10.1021/acsearthspacechem.9b00068>
- Koss, A. R., Sekimoto, K., Gilman, J. B., Selimovic, V., Coggon, M. M., Zarzana, K. J., Yuan, B., Lerner, B. M., Brown, S. S., Jimenez, J. L., Krechmer, J., Roberts, J. M., Warneke, C., Yokelson, R. J., & De Gouw, J. (2018). Non-methane organic gas emissions from biomass burning: Identification, quantification, and emission factors from PTR-ToF during the FIREX 2016 laboratory experiment. *Atmospheric Chemistry and Physics*, 18(5), 3299–3319. <https://doi.org/10.5194/acp-18-3299-2018>
- Krause, T., Tubbesing, C., Benzing, K., & Schöler, H. F. (2014). Model reactions and natural occurrence of furans from hypersaline environments. *Biogeosciences*, 11(10), 2871–2882. <https://doi.org/10.5194/bg-11-2871-2014>
- Odum, J. R., Hoffmann, T., Bowman, F., Collins, D., Flagan, R. C., & Seinfeld, J. H. (1996). Gas/particle partitioning and secondary organic aerosol yields. *Environmental Science and Technology*, 30(8), 2580–2585. <https://doi.org/10.1021/es950943+>
- Paquet, M., Arlt, D., Knape, J., Low, M., Forslund, P., & Pärt, T. (2019). Quantifying the links

- between land use and population growth rate in a declining farmland bird. *Ecology and Evolution*, 9(2), 868–879. <https://doi.org/10.1002/ece3.4766>
- Stehfest, E., van Zeist, W. J., Valin, H., Havlik, P., Popp, A., Kyle, P., Tabeau, A., Mason-D’Croz, D., Hasegawa, T., Bodirsky, B. L., Calvin, K., Doelman, J. C., Fujimori, S., Humpenöder, F., Lotze-Campen, H., van Meijl, H., & Wiebe, K. (2019). Key determinants of global land-use projections. *Nature Communications*, 10(1), 1–10. <https://doi.org/10.1038/s41467-019-09945-w>
- Stockwell, C. E., Veres, P. R., Williams, J., & Yokelson, R. J. (2015). Characterization of biomass burning emissions from cooking fires, peat, crop residue, and other fuels with high-resolution proton-transfer-reaction time-of-flight mass spectrometry. *Atmospheric Chemistry and Physics*, 15(2), 845–865. <https://doi.org/10.5194/acp-15-845-2015>
- Tapia, A., Villanueva, F., Salgado, M. S., Cabañas, B., Martínez, E., & Martín, P. (2011). Atmospheric degradation of 3-methylfuran: Kinetic and products study. *Atmospheric Chemistry and Physics*, 11(7), 3227–3241. <https://doi.org/10.5194/acp-11-3227-2011>
- Villanueva, F., Barnes, I., Monedero, E., Salgado, S., Gómez, M. V., & Martin, P. (2007). Primary product distribution from the Cl-atom initiated atmospheric degradation of furan: Environmental implications. *Atmospheric Environment*, 41(38), 8796–8810. <https://doi.org/10.1016/j.atmosenv.2007.07.053>
- Villanueva, F., Cabañas, B., Monedero, E., Salgado, S., Bejan, I., & Martin, P. (2009). Atmospheric degradation of alkylfurans with chlorine atoms: Product and mechanistic study. *Atmospheric Environment*, 43(17), 2804–2813. <https://doi.org/10.1016/j.atmosenv.2009.02.030>
- Yuan, Y., Zhao, X., Wang, S., & Wang, L. (2017). Atmospheric Oxidation of Furan and Methyl-Substituted Furans Initiated by Hydroxyl Radicals. *Journal of Physical Chemistry A*, 121(48), 9306–9319. <https://doi.org/10.1021/acs.jpca.7b09741>

# **Chapter I State of Art**

## I.1 Introduction

## I.2 Atmosphere

### I.2.1 Atmospheric layers

The Earth's atmosphere is classified in four consecutive layers that differ in altitude, temperature gradient, and gaseous density (see Figure I.1). These layers are the troposphere, stratosphere, mesosphere, and thermosphere. The troposphere is of particular interest to environmental scientists since it is where humans live and where almost all weather occurs. It starts from the ground and extends up to 8 to 14.5 km high, depending on the region and season (Holly Zell, 2013). In the troposphere, the temperature decreases as the height increases.

The stratosphere begins just above the troposphere and reaches a height of 50 km (Holly Zell, 2013). A thin ozone layer is located at the bottom of the stratosphere (at 20-25 km height). Stratospheric ozone is responsible for the absorption of harmful ultraviolet radiation at wavelengths less than 290 nm (Atkinson, 2000). This is the major reason why the temperature increases in the stratosphere with height. In the 1970s, scientific interest in this layer increased as the depletion of the ozone layer began due to the release of anthropogenic chlorofluorocarbons. The application of the Montréal protocol (1987) has allowed the partial recovery of the ozone layer (Chipperfield et al., 2017).

Just above the stratosphere, the mesosphere begins and extends up to 85 km high, which progressively becomes colder with altitude, reaching  $-85^{\circ}\text{C}$  at the top of this layer (Alan Buis, 2019). The thermosphere begins just above the mesosphere and reaches a height of 600 km (Holly Zell, 2013). Throughout this layer, due to the extremely low density of molecules found here, the temperature rises with altitude (Alan Buis, 2019).

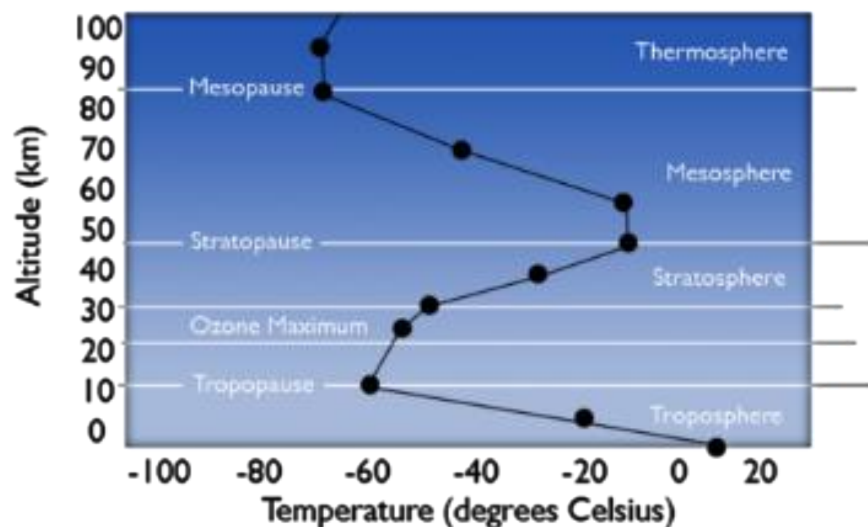


Figure I.1: Atmospheric layers and variation of temperature with altitude (Baldwin et al., 2019).

### I.2.2 Atmospheric composition

The Earth's atmosphere primarily consists of gases such as nitrogen (~78%), oxygen (~21%), and argon (~0.9%) (Figure I.2). The remaining percentage, which is less than 0.1%, comprises a variety of trace compounds (Table I.1) that are crucial for air quality and climate change (U.S.

Department of Commerce, 2023). Water vapor is an important constituent of Earth’s atmosphere, with a wide range of variability, from nearly complete dryness to supersaturation, i.e., between 0% and 4% absolute mixing ratio, depending on the season. CO<sub>2</sub>, CH<sub>4</sub>, N<sub>2</sub>O, and halocarbons are important long-lived trace gases that contribute crucially to the greenhouse effect (Schumann, 2012).

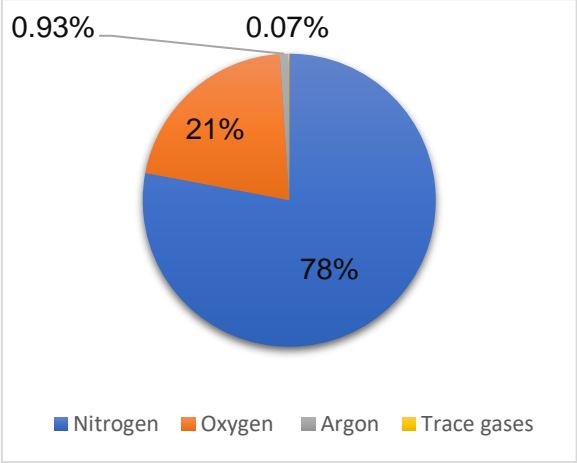


Figure 1.2: Percentage of atmospheric gaseous composition.

Table 1.1: Trace gases and their average atmospheric mixing ratios (ppmv).

Gaseous composition	Mixing ratios (ppmv)
Water	variable
Argon	9×10 <sup>3</sup>
Carbon dioxide	418.5
Neon	18.18
Helium	5.24
Methane	1.70
Krypton	1.14
Nitrous oxide	variable
Hydrogen	0.53
Xenon	0.09
Organic Vapors	0.02

The sources of trace gases in the atmosphere are numerous and have natural or anthropogenic origins. Sources include gas and oil production (CH<sub>4</sub>, volatile organic compounds (VOCs)), traffic (CO<sub>2</sub>, NO<sub>x</sub>, CO), fossil fuel combustion and biomass burning (critical gas emissions: CO<sub>2</sub>, SO<sub>2</sub>, NO<sub>x</sub>, hydrocarbons), livestock and agriculture (CH<sub>4</sub>, N<sub>2</sub>O, NH<sub>3</sub>), vegetation (VOCs), volcanoes (SO<sub>2</sub>, halogens), and oceans/seas (N<sub>2</sub>O, OCS, DMS, halocarbons) (Schumann, 2012).

Although most of the atmosphere is in the gaseous state, particulate matter (PM) is also an important constituent. PM refers to solid or liquid particles suspended in the gaseous phase, also known as "aerosols" (Schumann, 2012). Despite their very small mass fraction in the air,

which rarely exceeds  $10^{-5}$  wt% (George et al., 2015), aerosols can impact both air quality and climate. More details about aerosols can be found in section 1.7.

### 1.2.3 Air pollution and climate change

Air pollution is a significant cause of health diseases (World Health Organization, 2016). An air pollutant is a gas or particle that, when present in high concentrations (above acceptable threshold), poses significant risks to health and the environment. Pollution is combined with various forms of damage i.e. human health, environmental wealth, and properties are all endangered by it. For instance, according to the European Environmental Agency, air pollution is the 3<sup>rd</sup> major cause of premature death worldwide (European Environmental Agency, 2015). A historical example of an air pollution event is the London smog in 1952, where a huge cloud of sulfate aerosols persisted for 2 days and caused the death of around 12,000 individuals (Munger et al., 1983).

The European Union (EU) distinguishes seven primary pollutants (excluding greenhouse gases, GHGs): ammonia ( $\text{NH}_3$ ), nitrogen oxides ( $\text{NO}_x$ ), carbon monoxide (CO), particulate matter (PM), sulfur dioxide ( $\text{SO}_2$ ), ozone, and non-methane volatile organic compounds (NMVOCs) (Koolen and Rothenberg, 2019). Emission limits have been established under transoceanic agreements, of which the so-called Gothenburg Protocol is the most recent. It has set upper limits for  $\text{SO}_2$ ,  $\text{NO}_x$ , NMVOCs, and  $\text{NH}_3$  for 2010, 2020, and beyond (Koolen & Rothenberg, 2019).

Air pollution and climate change are strongly correlated (Molina et al., 2004). Different types of pollutants have various effects on the climate. For instance, greenhouse gases emitted mainly from anthropogenic activities affect the climate by trapping the infrared radiation emitted by earth to space, increasing its temperature. Particulate matter, on the other hand, can either scatter or absorb radiation coming to Earth, resulting in either a cooling or warming effect on the atmosphere. Moreover, precipitation may also be affected due to the increase in nucleation with smaller droplets, thus increasing cloud lifetime (Molina et al., 2004).

### 1.2.4 Oxidative capacity of the troposphere

The oxidative capacity of the troposphere refers to the ability of the Earth's lower atmosphere, known as the troposphere, to undergo chemical reactions that involve the transfer of oxygen atoms. These reactions are crucial for the breakdown and transformation of pollutants and natural substances present in the air. The oxidative capacity of the atmosphere is determined by short-lived species, which play a crucial role in the lifetime of both natural and anthropogenic pollutants. The most important species responsible for this process are the hydroxyl radical (OH), ozone ( $\text{O}_3$ ), nitrate radical ( $\text{NO}_3$ ), and chlorine atom (Cl). In the following section, we will provide a brief overview of the main sources of tropospheric oxidants and their atmospheric level.

Figure 1.3 shows general scheme of the different tropospheric reactions of VOCs (photolysis and reaction with the oxidants). The families of VOCs that reacts with each of the four oxidants (OH, Cl,  $\text{O}_3$  and  $\text{NO}_3$ ) are also indicated with the intermediates and products of these reactions.

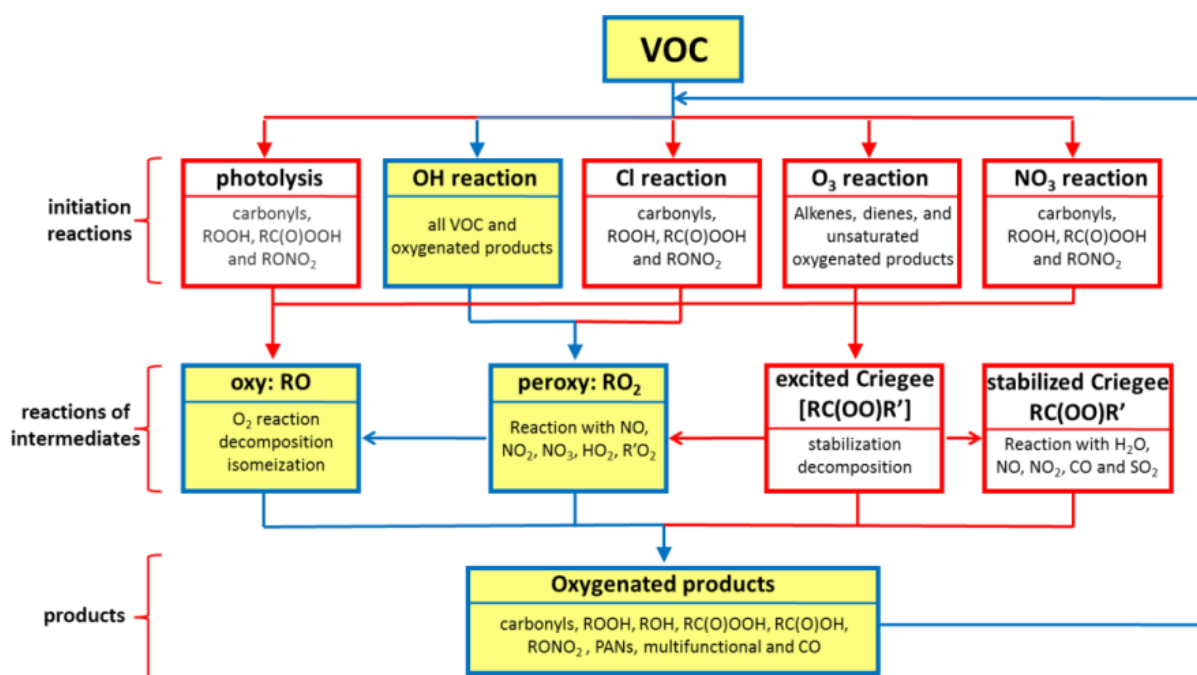
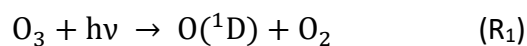


Figure 1.3: General description of a chemical mechanism. The main types of reaction considered and classes of organic intermediate and products which are potentially generated. The dominant pathways are highlighted using blue/yellow frame (Zogka & Zogka, 2017).

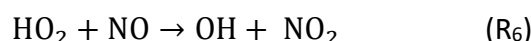
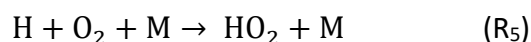
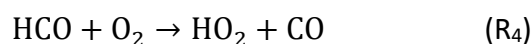
#### 1.2.4.1 Hydroxyl radical (OH) sources and levels

In the troposphere, the hydroxyl radical (OH) is the dominant daytime oxidant. One significant source of OH radicals is the photodissociation of ozone at wavelengths below 310 nm, which occurs in the presence of water vapor (Atkinson and Arey, 2003).

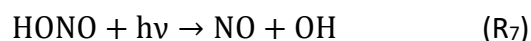


Nonetheless, a majority of the generated O(<sup>1</sup>D) (90%) will be quenched back to the O(<sup>3</sup>P) ground state by N<sub>2</sub> or O<sub>2</sub>.

In highly polluted regions, formaldehyde (HCOH) undergoes photolysis at wavelengths < 356 nm (R<sub>3</sub>) (Carbajo et al., 2008), resulting in the formation of HO<sub>2</sub> radicals (R<sub>4</sub> and R<sub>5</sub>) and ultimately OH radicals (R<sub>6</sub>).



The photodissociation of nitrous acid (HONO) at wavelengths < 400 nm (R<sub>7</sub>) and hydrogen peroxide (H<sub>2</sub>O<sub>2</sub>) at wavelengths < 370 nm (R<sub>8</sub>) (Finlayson-Pitts et al., 1999; Alicke & Platt, 2002) are also significant sources of OH radicals during day (Finlayson-Pitts et al., 1993).





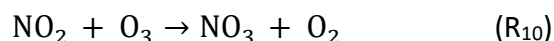
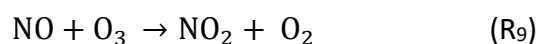


OH radicals can also be generated through non-photolytic sources as ozonolysis of unsaturated compounds (isoprene and alkenes) (Atkinson, 2000) and the reaction of NO<sub>3</sub> with peroxyacetyl nitrates (RC(O)O<sub>2</sub>NO<sub>2</sub>) and alkenes (Ren et al., 2006). Numerous studies have assessed the relative contributions of the various initiation sources to the total initiation rate (PR), and they show that HONO is the main source of OH radicals in the lower atmosphere (Dusanter et al., 2009; Elshorbany et al., 2009; Elshorbany et al., 2010; Ren et al., 2003, 2010). To exemplify, HONO photolysis had the highest contribution (55 %) in OH formation in Santiago de Chile during summer daytime urban conditions. The second major contributor is the ozonolysis of alkenes, POH (24 %), followed by HCHO photolysis (16 %), and ozone photolysis (O<sub>3</sub>) (5 %) (Y. F. Elshorbany et al., 2009; Y. Elshorbany et al., 2010). In addition to urban areas, HONO served as the primary source of OH radicals for remote and rural areas (Zhou et al., 2001).

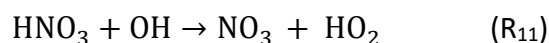
Due to its reactivity with various pollutants, trace gases (VOCs) and tropospheric ozone, the concentration of OH is relatively low compared to other tropospheric oxidants as O<sub>3</sub> and NO<sub>3</sub> (Atkinson et al., 1989). According to several studies (Alvarado et al., 1996; Atkinson, 2000), the levels of OH radicals in the atmosphere typically reach 1 × 10<sup>6</sup> molecules cm<sup>-3</sup> on average over a 24-hour period, but they decrease to about 1 × 10<sup>5</sup> molecules cm<sup>-3</sup> during night.

#### *1.2.4.2 Nitrate radical (NO<sub>3</sub>) sources and levels*

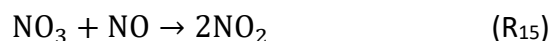
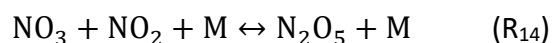
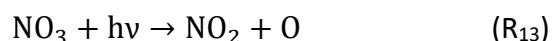
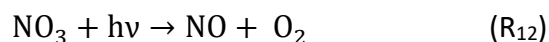
The NO<sub>3</sub> radical is the principal nighttime oxidant of the lower troposphere (Atkinson et al., 1988). Over continental areas, the NO<sub>3</sub> mixing ratio in the lower troposphere was found to be between 2 - 430 pptv. Nitrate radicals are formed in the troposphere according to the following reactions (Atkinson, 1991a):



The reaction of OH and HNO<sub>3</sub> also gives NO<sub>3</sub>:



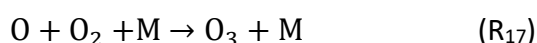
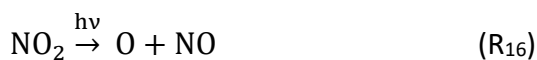
All the following reactions lead to the temporary loss or storage of NO<sub>3</sub>:



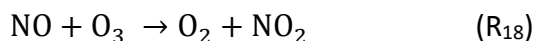
Due to the rapid photolysis of nitrate radicals during daytime hours (R<sub>12</sub>) (R<sub>13</sub>), and the fast reaction between NO<sub>3</sub> and NO (R<sub>15</sub>), NO<sub>3</sub> accumulate during night (Atkinson, 1991a). During nighttime the average NO<sub>3</sub> radical levels are around 2 × 10<sup>8</sup> molecules cm<sup>-3</sup>, while this concentration during daytime falls down to 1 × 10<sup>7</sup> molecules cm<sup>-3</sup> (Brown & Stutz, 2012).

### 1.2.4.3 Ozone (O<sub>3</sub>) sources and levels

Ozone formation in the troposphere occurs through the recombination of an oxygen molecule (O<sub>2</sub>) and an oxygen atom (O), similar to the process observed in the stratosphere (R<sub>17</sub>). However, the photodissociation of molecular oxygen (O<sub>2</sub>) to form oxygen atoms (O) does not occur in the troposphere as this reaction requires short wavelengths of light ( $\lambda < 242$  nm), which are not available in the troposphere. In the troposphere, the only known compound capable of producing oxygen atoms (O) through photodissociation at the radiation available is nitrogen dioxide (NO<sub>2</sub>) (R<sub>16</sub>).



In the presence of NO, O<sub>3</sub> reacts with it, which reaction destroys the ozone and reproduces the NO<sub>2</sub>:



This suggests that because reactions (R<sub>16-18</sub>) simply recycle O<sub>3</sub> and NO<sub>x</sub>, they do not result in a net formation of O<sub>3</sub>. In the presence of other precursors, such as carbon monoxide (CO), methane (CH<sub>4</sub>), non-methane hydrocarbons (NMHC), or specific other organic molecules (volatile organic compounds - VOC), net ozone generation occurs. In the presence of sunlight and nitrogen oxides the latter precursors can be oxidized to generate O<sub>3</sub>. These reactions are summarized in Figure I.4 and thus depending on the VOC/NO<sub>x</sub> ratios, O<sub>3</sub> is formed or consumed. Stratosphere to troposphere transport is another natural source of tropospheric O<sub>3</sub> (Jenkin & Hayman, 1999; Guicherit & Roemer, 2000; Jenkin & Clemitshaw, 2002; Akritidis et al., 2016, 2018). In unpolluted areas, the atmospheric mixing ratio of ozone ranges from 10 to 40 ppbv, while in polluted environments, it can reach up to 100 ppbv (Finlayson-Pitts et al., 1993).

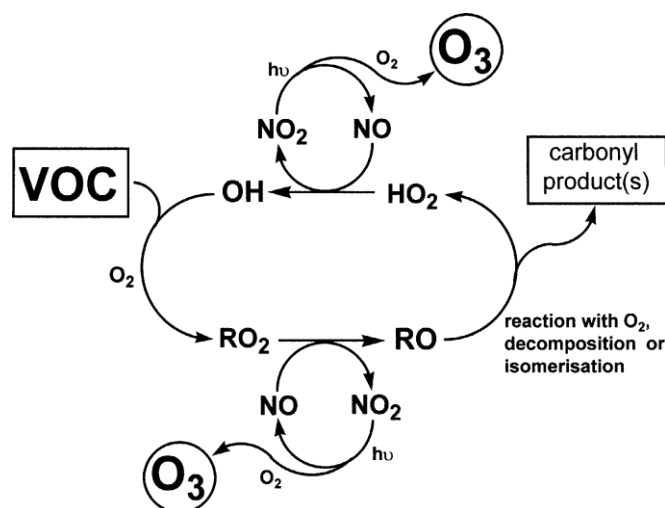
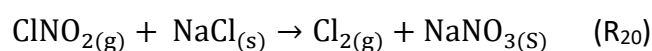
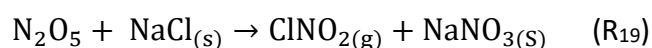


Figure I.4: Schematic representation of the free radical catalyzed oxidation of a VOC into its first-generation carbonyl product(s) in the presence of NO, and the associated generation of Ozone (O<sub>3</sub>) (Jenkin & Hayman, 1999).

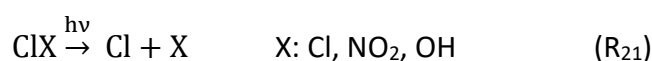
#### 1.2.4.4 Chlorine (Cl) sources and levels

Chlorine atoms (Cl) have a significant impact on both coastal regions and the marine boundary layer, as well as specific continental environments (Atkinson & Arey, 2000; Young et al., 2014). A variety of results from field and laboratory studies proved that Cl atom can be an important oxidant in the marine and arctic regions that rivals the oxidation with OH radical (Finlayson-Pitts et al., 1993). There are several mechanisms by which Cl atoms can enter the troposphere, the most prevalent pathway being through the emission of sea-salt chloride aerosols (Graedel & Keene, 1996).

Sea-salt chloride aerosol is generated by the bursting of air bubbles at the surface of the ocean induced by wind stress (Graedel & Keene, 1996). While larger droplets tend to be rapidly deposited back into the ocean, smaller droplets may persist for several minutes to hours, allowing for their transport within the boundary layer. Sea-salt aerosols react with atmospheric pollutants leading to the formation of Cl reservoir species ( $\text{ClNO}_{2(g)}$  and  $\text{Cl}_{2(g)}$ ).



Then, these active chlorine-containing gases ( $\text{R}_{21}$ ) lead to the production of Cl atoms through photolysis (Finlayson-Pitts et al., 1993).



The concentration of Cl atoms has been reported to be as low as  $1 \times 10^2$  atoms  $\text{cm}^{-3}$  through analysis of VOC ratios (Wingenter et al., 1999), while other studies based on Cl family detection have reported concentrations as high as  $1 \times 10^5$  atoms  $\text{cm}^{-3}$  (Keene et al., 2007).

#### 1.2.5 Photolysis

Sunlight-induced photolysis is recognized as a significant process in the atmosphere for the degradation of certain compounds that absorb ultraviolet-visible (UV-Vis) radiation. This mechanism plays a crucial role in breaking down oxygenated volatile organic compounds (OVOCs) like formaldehyde and acetone (Atkinson & Arey, 2003; Mellouki & Chen, 2015). The resulting byproducts of photolysis contribute to the generation of  $\text{HO}_2$  radicals, which can serve as a precursor for OH radicals (Koppmann, 2007).

### 1.3 Volatile organic compounds

#### 1.3.1 Definition

Volatile organic compounds (VOCs) constitute a large family of chemically and physically different molecules with a common property that is a high vapor pressure at ambient temperature. The **Directive 2004/42/CE of the European Parliament and the Council** defines the VOCs as any organic compound having a boiling point less than or equal to  $250^\circ\text{C}$  measured at a standard atmospheric pressure of 101.3 kPa. In addition, VOCs are defined by the **EPA in Code of Federal Regulation** as "any compound of carbon, excluding carbon monoxide, carbon dioxide, carbonic acid, metallic carbides or carbonates, and ammonium carbonate, which participates in atmospheric photo-chemical reactions". VOCs have grabbed attention due to

their important role in the formation of photo-chemical smog and their contribution to the increase of ozone levels in the troposphere (Zysman & Skelly, 1992).

### 1.3.2 Sources

VOCs are released in the atmosphere either from natural or anthropogenic sources. Guenther (1995) reported that 90% of the global emissions are of biogenic origin and 10% are of anthropogenic origin (Guenther et al., 1995). The dominant natural source of VOCs is vegetation, while biological processes, oceans, volcanic activity, soil and geologic activity contribute also but to a minor extent. Regarding the anthropogenic sources of VOCs, they include vehicles, solvent use, fossil fuel production, processing, combustion, and biomass burning (BB). Anthropogenic volatile organic compounds encompass a wide range of hydrocarbon subclasses, including various functional groups ranging from aromatic to aliphatic compounds. Generally, AVOCs are thought to comprise majorly of alkanes and aromatic hydrocarbons (Rissanen, 2021).

Among the various sources of VOCs in the atmosphere, BB has received special attention in the past 10 to 15 years. BB is the burning of living and dead vegetation, which includes the human-initiated burning for land clearing and land-use change, natural fires, and domestic heating. Due to the increasing population rate and the extra demand of food, the rate of land clearing and land use (directly related to wildfires and BB events) (Collard & Blin, 2014; Wang et al., 2020) has increased dramatically during the last few decades (Akagi et al., 2011), and increasing trends are projected over the near future.

Biomass burning emits a wide spectrum of VOCs and the amount of these emissions depends on fuel composition, and combustion conditions. Unsaturated species including highly reactive alkenes, aromatics and terpenes as well as photolabile OVOCs such as aldehydes and ketones are the major VOCs families emitted from vegetation fires (Collard & Blin, 2014; Wang et al., 2020; Burling et al., 2010; Roberts et al., 2020; Sekimoto et al., 2018; Yokelson et al., 2011). Furanoids, which are the focus of this thesis have recently been identified as major constituents of VOCs emitted during wildfire burning that could contribute to the formation of key atmospheric pollutants, such as O<sub>3</sub> and SOA affecting the climate. Furan compounds comprises about 30% of the total number of VOCs identified in plumes, with significant atmospheric concentration levels ranging between 68 and 118 ppbv relative to 1 ppmv of CO formation (Coggon et al., 2019; Gilman et al., 2015; Hatch et al., 2015; Müller et al., 2016). Furans have been demonstrated to contribute significantly ( $\cong 20\%$ ) to overall NO<sub>3</sub> (Decker et al., 2021) and OH reactivity (Coggon et al., 2019) of emissions from the burning of common wildfire and residential fuels. They also contribute by 6% to the overall O<sub>3</sub> reactivity (Decker et al., 2021).

### 1.3.3 Chain reactions of tropospheric oxidation of VOCs

As previously discussed, among the different removal pathways, the gas-phase chemical degradation by the oxidants of the atmosphere (i.e. OH, NO<sub>3</sub>, O<sub>3</sub> and Cl) and photolysis are considered as the major sinks of VOCs (Koppmann, 2007). The tropospheric oxidation of VOCs occurs via chain reactions leading to the production of numerous organic compounds (Figure 1.5) (Ziemann & Atkinson, 2012).

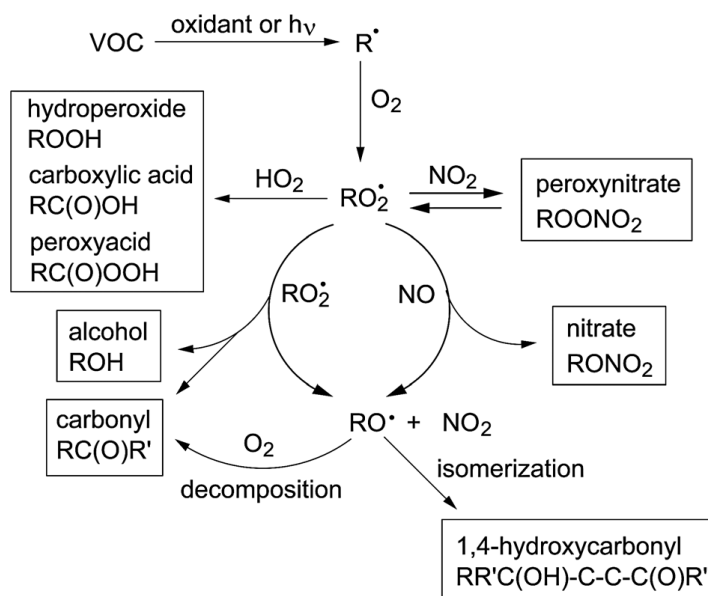
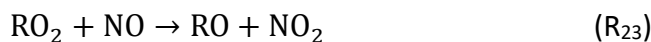


Figure 1.5: Mechanism of VOC oxidation or photolysis chain reactions (Ziemann & Atkinson, 2012).

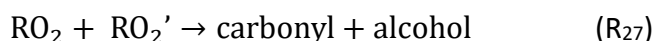
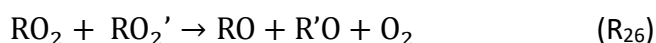
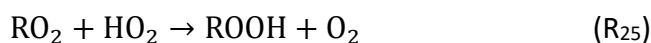
After the initial VOC oxidation step (hydrogen abstraction, oxidant addition to the double/triple bond of unsaturated compounds, ...), a radical R is formed as follows (Atkinson, 2000):



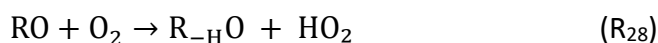
The formed radical reacts immediately with molecular oxygen to form a peroxy radical ( $\text{RO}_2$ ).  $\text{RO}_2$  has different possible reactivity pathways depending on the environment. In a polluted environment,  $\text{RO}_2$  reacts with NO forming either an alkoxy radical RO or an organic nitrate  $\text{RONO}_2$  (if the alkoxy radical has a long carbon chain) (Atkinson, 2000).



However, in a clean environment where  $[\text{NO}_x]$  are low,  $\text{RO}_2$  reacts either with the hydroxyl peroxy radical  $\text{HO}_2$  to generally give a hydroperoxide  $\text{ROOH}$ , or with another peroxy radical  $\text{R}'\text{O}_2$  to give alkoxy radicals, carbonyl compounds or alcohols according to the following reactions (Atkinson, 2000):



Finally, the fate of the alkoxy radical may take three different mechanistic pathways. It can either react with oxygen or decompose or undergo isomerization according to the following reactions (Atkinson, 2000):



For more than 4 decades, scientific research has been dedicated to elucidating the reactivity and fate of several families of VOCs. Some compounds, like the furanoids family, remain much less investigated and require further studies.

## 1.4 Furan compounds: identification, properties, emission factors, kinetics and products formation

This section provides information about furans (or furanoids) compounds, the organic species that were studied in the framework of this thesis. Our focus is to present the compounds that have been identified in BB plumes and are linked to the air quality and climate change, and not to provide an exhausting discussion about all possible furanoid compounds that can be detected in the atmosphere. Therefore, in this section we first introduce to the reader the class of furanoid compounds, and we present their physical properties. Thereafter, the fundamental combustion chemistry linked to the emissions of furanoids in BB, as well as the emission factors for several types of fuels is provided. Afterwards, on the basis of a detailed literature survey and data evaluation, the gas-phase rate coefficients of furanoids by the major atmospheric oxidants and the yields of the gas-phase products formed are discussed. Finally, the formation of secondary organic aerosols (SOA) from furanoids oxidation is discussed.

It is important to note that all these pieces of information are part of a review article prepared in the course of this thesis by several co-authors, experts in the field of atmospheric chemistry and combustion (Romanias et al., submitted to ACS Earth and Space Chemistry, 2023).

### 1.4.1 Chemical structure of furanoids

Furanoids are a class of heterocyclic organic molecules that are present in the atmosphere. Furanoids are broadly defined as a five-membered heterocycle with four carbon atoms and one oxygen. A furanoid can be aromatic (Figure I.6-A), partially saturated, or fully saturated (Figure I.6-B). At each carbon, hydrogen atoms may be replaced by functional groups, including hydroxy (-OH), aldehyde (-H) C=O, ketone (-R) C=O, methyl (-CH<sub>3</sub>), and aromatic (-C<sub>6</sub>H<sub>6</sub>) moieties. The functionality of furanoids makes these molecules reactive towards atmospheric oxidants and potential sources of radicals through the absorption of UV radiation, which has implications for the formation of atmospheric pollutants including ozone (O<sub>3</sub>) and secondary organic aerosol (SOA). Other heterocyclic compounds with backbones similar to furan, including dihydro- and tetrahydro-furans (Figure I.6-B), are also present in the atmosphere and serve as sources of reactive carbon.

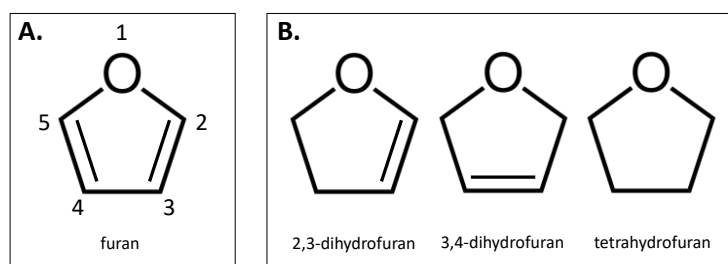

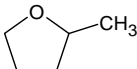
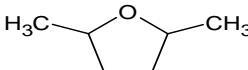
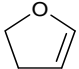
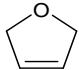
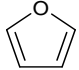
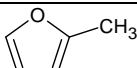
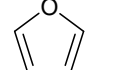
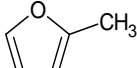


Figure 1.6: Basic structures of (A) aromatic furanoids and (B) partially and fully saturated heterocyclic furanoids.

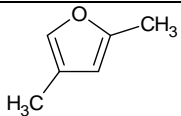
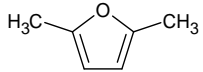
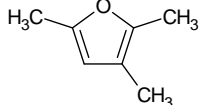
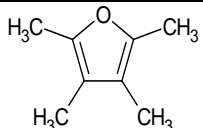
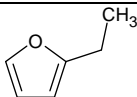
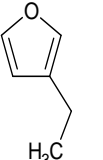
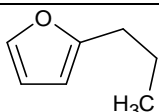
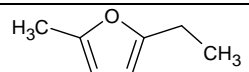
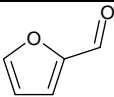
### 1.4.2 Physical properties

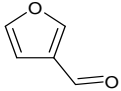
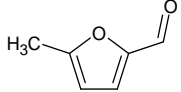
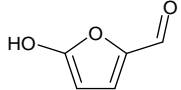
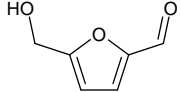
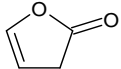
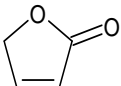
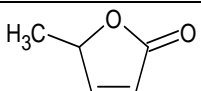
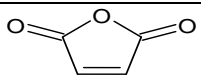
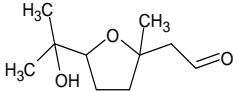
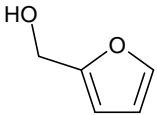
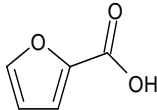
Table 1.2 outlines the physical properties of various furanoids that have been identified as atmospheric pollutants or have been employed in laboratory studies on kinetic or atmospheric degradation mechanisms. Despite their shared heterocyclic ring structure, the presence of different substituents and aromaticity distinguishes these compounds and contributes to their unique physical and chemical properties.

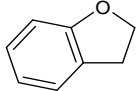
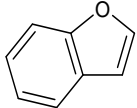
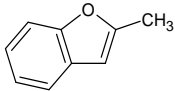
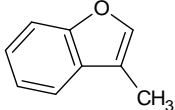
Table 1.2: Physical properties of furanoids considered in literature studies. Compounds in brackets have not been identified in biomass burning but studied in terms of reactivity with atmospheric oxidants.

Compound	Molecular formula	Structure	CAS Number	Phase (298 K)	Molecular weight (g mol <sup>-1</sup> )	Density (g cm <sup>-3</sup> )	Vapor pressure (Torr, 298 ± 5 K)	Flash point (°C)	Melting point (°C)	Boiling point (°C)
Tetrahydrofuran <sup>a</sup>	C <sub>4</sub> H <sub>8</sub> O		109-99-9	Colorless liquid	72.11	0.89	161 <sup>‡</sup>	-17	-108.5	65
(2-methyltetrahydrofuran <sup>a</sup> )	C <sub>5</sub> H <sub>10</sub> O		96-47-9	Colorless liquid	86.13	0.86	No data available	-11	-137	78
(2,5-dimethyltetrahydrofuran <sup>a</sup> )	C <sub>6</sub> H <sub>12</sub> O		1003-38-9	Colorless liquid	100.16	0.83	2.3 <sup>§</sup>	26	-45	90
2,3-Dihydrofuran <sup>b</sup>	C <sub>4</sub> H <sub>6</sub> O		1191-99-7	Light yellow liquid	70.09	1.0	258	-24.4	-83.5	54.5
2,5-Dihydrofuran <sup>b</sup>	C <sub>4</sub> H <sub>6</sub> O		1708-29-8	Clear liquid	70.09	1.0	145.4 <sup>§</sup>	-16	-83.55 <sup>b</sup>	66
Furan <sup>a</sup>	C <sub>4</sub> H <sub>4</sub> O		110-00-9	Colorless liquid	68.08	0.93	596 <sup>‡</sup>	-35	-85.6	31.3
2-methylfuran <sup>a</sup>	C <sub>5</sub> H <sub>6</sub> O		534-22-5	Colorless-Light yellow liquid	82.10	0.91	671 <sup>‡</sup> (333 K)	-22.2	-88.7	63
3-methylfuran <sup>a</sup>	C <sub>5</sub> H <sub>6</sub> O		930-27-8	Colorless liquid	82.10	0.92	161 <sup>§</sup>	>-22 <sup>b</sup>	-67.86 <sup>b</sup>	65
2,3-Dimethylfuran <sup>a</sup>	C <sub>6</sub> H <sub>8</sub> O		14920-89	Colorless-Light yellow liquid	96.12	0.91	41.3 <sup>*</sup>	-1	-48.91 <sup>b</sup>	42



2,4-Dimethylfuran <sup>a</sup>	C <sub>6</sub> H <sub>8</sub> O		3710-43-8	No available data	96.12	0.91	52.4 <sup>§</sup>	0.8±5.6 <sup>b</sup>	-48.91 <sup>b</sup>	95.2
2,5-Dimethylfuran <sup>a</sup>	C <sub>6</sub> H <sub>8</sub> O		625-86-5	Colorless liquid	96.13	0.9	57.1 <sup>§</sup>	-1.7 <sup>b</sup>	-62	92.0
2,3,5-trimethyl furan	C <sub>7</sub> H <sub>10</sub> O		10504-04-8	Colorless to yellow liquid	110.15	0.89	14.4 <sup>§</sup>	20	-30.23 <sup>b</sup>	121
(Tetramethyl-furan <sup>a</sup> )	C <sub>8</sub> H <sub>12</sub> O		15045-43-9	No available data	124.18	0.9	3.08*	42.3	-11.81 <sup>b</sup>	160.6
2-Ethyl-furan <sup>a</sup>	C <sub>6</sub> H <sub>8</sub> O		3208-16-0	Colorless liquid	96.13	0.91	53.9 <sup>§</sup>	-2.2	-55.17 <sup>b</sup>	92
3-Ethylfuran	C <sub>6</sub> H <sub>8</sub> O		67363-95-5	Colorless to yellow liquid	96.13	0.91	65.1	-5.7	-55.17	89.8
2-propyl furan	C <sub>7</sub> H <sub>10</sub> O		4229-91-8	Colorless to Light yellow to Light orange liquid	110.15	0.91	17.7 <sup>§</sup>	14.8	-42.75	121.3
2-ethyl-5-methyl furan	C <sub>7</sub> H <sub>10</sub> O		1703-52-2	Colorless liquid	110.154	0.9	19.3 <sup>§</sup>	15.1	-36.49	119.1
Aldehydes										
Furan-2-aldehyde <sup>a</sup>	C <sub>5</sub> H <sub>4</sub> O <sub>2</sub>		98-01-1	Oily. -reddish brown liquid	96.09	1.16	2.2 <sup>§</sup>	60 <sup>b</sup>	-36	162

Furan-3-aldehyde <sup>a</sup>	C <sub>5</sub> H <sub>4</sub> O <sub>2</sub>		498-60-2	Colorless light yellow liquid	96	1.11	4.88*	48	Not available	144
5-methylfurfural <sup>a</sup>	C <sub>6</sub> H <sub>6</sub> O <sub>2</sub>		620-02-0	Dark yellow	110.11	1.10	0.6 <sup>§</sup>	72.8 <sup>b</sup>	26	187
5-hydroxy-2-furaldehyde	C <sub>5</sub> H <sub>4</sub> O <sub>3</sub>		107997-80-8	Yellow solid	112.08	1.4	0.0 <sup>§</sup>	106.3	32.0	252.2
5-hydroxymethyl-2-furfural <sup>a</sup>	C <sub>6</sub> H <sub>6</sub> O <sub>3</sub>		67-47-0	Light yellow solid	126.11	1.29	0.0 <sup>§</sup>	79	32	114 (1 mmHg)
Ketones										
3H-furan-2-one <sup>b</sup>	C <sub>4</sub> H <sub>4</sub> O <sub>2</sub>		20825-71-2	Colorless liquid	84.07 <sup>b</sup>	1.2 ± 0.1 <sup>b</sup>	0.00912*	105.2 <sup>b</sup>	-40.90 <sup>b</sup>	179.67 <sup>b</sup>
5H-furan-2-one	C <sub>4</sub> H <sub>4</sub> O <sub>2</sub>		497-23-4	Clear colorless to pale yellow	84.07	1.19	0.3	101.1	-40.90	203
(5-Methyl-2(3H)-furanone <sup>b</sup> )	C <sub>5</sub> H <sub>6</sub> O <sub>2</sub>		591-12-8	No available data	98.1	1.1 <sup>b</sup>	0.0 <sup>§</sup>	78.9 ± 16.1 <sup>b</sup>	-33.14 <sup>b</sup>	210.0 <sup>b</sup>
Maleic anhydride <sup>a</sup>	C <sub>4</sub> H <sub>2</sub> O <sub>3</sub>		108-31-6	White crystals	98.06	1.48	0.16*	-51.57	53	202
(5-methyl-5-vinyltetrahydrofuran-2-ol <sup>a</sup> )	C <sub>7</sub> H <sub>12</sub> O <sub>2</sub>		40478-73-7	No available data	128.16	No available data	No available data	No available data	No available data	No available data
Alcohols /acids										
2-Furanmethanol <sup>a</sup>	C <sub>5</sub> H <sub>6</sub> O <sub>2</sub>		98-00-0	Colorless to pale yellow liquid	98.10	1.13	1.0 <sup>§</sup>	75	-31	170
2-furoic acid	C <sub>5</sub> H <sub>4</sub> O <sub>3</sub>		88-14-2	white to light yellow crystal powder	112.08	0.55	0.0 <sup>§</sup>	94.2	38.74	232.1

Furanoids with aromatic ring										
(2,3-dihydrobenzofuran <sup>a</sup> )	C <sub>8</sub> H <sub>8</sub> O		496-16-2	Colorless to Very slight yellow liquid	120.15	1.06	0.836*	66	-21	188
2,3-Benzofuran <sup>a</sup>	C <sub>8</sub> H <sub>6</sub> O		271-89-6	clear to slightly greenish liquid	118.13	1.07	1.65*	50	-18	173
2-Methylbenzofuran <sup>a</sup>	C <sub>9</sub> H <sub>8</sub> O		4265-25-2	Colorless liquid	132.15	1.057	0.6 <sup>§</sup>	67		197
3-Methylbenzofuran <sup>a</sup>	C <sub>9</sub> H <sub>8</sub> O		22367-82-4	Colorless liquid	132.16	1.077	0.608*	73.2	19	198.5

*a: Information taken from Safety Data Sheet (SDS) or Material Safety Data Sheet (MSDS). b: Information taken from Chemspider (<http://www.chemspider.com/Chemical-Structure>). † vapor pressure from Antoine's equation. \* Vapor pressure retrieved from [molbase](#). § Vapor pressure retrieved from [Chemspider](#), estimated using algorithms to predict the physicochemical molecular properties of compounds from Advanced Chemistry Development (ACD) Inc.*

### 1.4.3 Furan compounds emitted from BB events

Since the 1970s, furan compounds have been detected in various environmental areas such as soil and air (Alcock & Jones, 1996). These compounds have both natural and anthropogenic sources, with man-made sources dominating due to processes that occur at high temperatures such as waste incineration, fuel combustion, and temperature-based industrial processes (Mudhoo et al., 2013). Power generation, waste incineration, open burning, and metallurgical industries are the primary sources of furan compounds. All other listed sources are of minor importance in furan emission (Akele & Tarekegn, 2017). Natural sources of furans include volcanic eruptions and wildfires, including those caused by climate change and domestic heating. These events are increasing worldwide due to changing climate and changes in land use, such as deforestation fires, agricultural debris burning, and forest fragmentation in the Amazon and are the major natural sources of furan compounds (Reddington et al., 2016).

Besides, laboratory studies have shown that furanoids are among the most abundant gas-phase products formed from biomass pyrolysis and combustion of several major fuel types (Graham et al., 2002; Lin et al., 2009; Mettler et al., 2012; Simoneit, 2002). It is estimated that furanoids are emitted into the atmosphere at a rate of  $>10 \text{ Tg Yr}^{-1}$  between 1997 – 2020 (Romanias et al., submitted to ACS Earth and Space Chemistry, 2023). For comparison, this global flux is comparable to the emissions of non-heterocyclic aromatic compounds from anthropogenic sources ( $\sim 23 \text{ TgC Yr}^{-1}$ ) (Cabrera-perez et al., 2016). Furthermore, interest in using biomass-derived fuels has developed in recent years (Lange et al., 2010; Mettler et al., 2012; Tuan Hoang & Viet Pham, 2021). Their future use as biofuel or drop-in fuel would contribute to higher emissions of furanoids to the atmosphere through evaporation and incomplete combustion.

#### 1.4.3.1 Fundamental reactions contributing to furanoid emissions

The pyrolysis temperatures alter the mechanism of biomass decomposition, resulting in changes to the VOC profile emitted (Collard & Blin, 2014; Wang et al., 2020; Lange et al., 2010; Lin et al., 2009; Sekimoto et al., 2018). At low- to medium- temperatures ( $300 - 500^\circ\text{C}$ ), cellulose, hemicellulose, and lignin contained in biomasses (Figure 1.7) undergo depolymerization and fragmentation, resulting in emissions enriched with functionalized molecules. At higher temperatures ( $> 500^\circ\text{C}$ ), these processes lead to a greater degree of aromatization, resulting in the formation of char (solid), tar (viscous liquid), and volatile aromatics (e.g. polycyclic aromatic hydrocarbons).

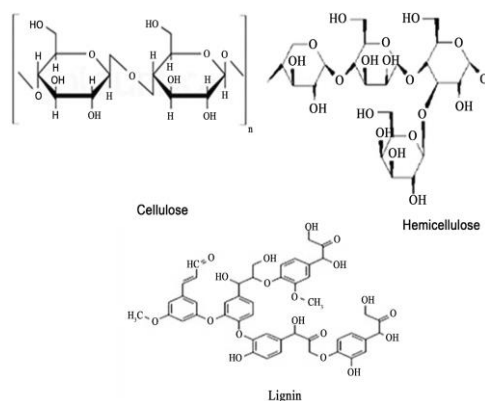


Figure 1.7: Structure of cellulose, hemicellulose, and lignin.

In addition to burning phase, furanoid emissions may also vary by the extent to which biomass is composed of different polymers. Furan derivatives, such as furanaldehydes, are major products of cellulose and hemicellulose. The pyrolysis of hemicellulose has been described in the literature (Yang et al., 2020; Yang et al., 2019; Zhou et al., 2018), and these previous articles show that this polymer has been less studied than other biomass components. 2-Methylfuran is a prominent furanoid that has been detected among the products of hemicellulose pyrolysis (Yang et al., 2019). The pyrolysis of lignin has been investigated experimentally (Ferdous et al., 2002; Jiang et al., 2010; Kawamoto, 2017; Si et al., 2017).

Furanoids functionalized with aromatic rings (e.g., 2,3-dihydro-benzofuran, benzofuran) have been observed to be a large fraction emitted (Si et al., 2017). The pyrolysis of lignocellulosic biomass is a complex chemical process which can result in a wider range of furanoid compounds than the pyrolysis of individual biopolymers, as shown in a relatively recent study presenting extensive speciation of products including furanoids such as 2-furanmethanol, furfural, 2-methylfuran, 2,5-dimethylfuran, 3-methylfuran, and acetyl furan (Lê Thành et al., 2015).

### 1.4.3.2 Open biomass burning connections to fundamental pyrolysis processes

Figure I.8 summarizes the key processes controlling emissions from open biomass burning. Emissions of VOCs begin during distillation, when oils and other higher volatility compounds evaporate. As the temperature rises, the pyrolysis of cellulose, hemicellulose, and lignin results in the breakdown of chemical bonds. In open biomass burning, the VOCs formed by pyrolysis may undergo further transformations through combustion within the flames, leading to the formation of highly oxidized molecules, such as CO<sub>2</sub> (Roberts et al., 2020; Sekimoto et al., 2018). Generally, pyrolysis is considered to occur in the “smoldering” phase of burning and emits VOCs that escape flame processing, while combustion occurs during “flaming.” Smoldering is a slow, non-flaming combustion process that occurs at lower temperatures. It involves the degradation of solid fuels through oxidation without the presence of a visible flame. However, flaming refers to rapid, high-temperature combustion that involves the ignition and burning of fuel in the presence of a visible flame. The modified combustion efficiency (MCE), which relates the ratio between smoldering (CO) and flaming (CO<sub>2</sub>) combustion tracers is a quantity used to estimate the extent to which these different combustion processes contribute to observe trace gas and particle emissions (Yokelson et al., 1997). Furanoid emissions, along with other VOCs, are inversely proportional to MCE and are highest during smoldering combustion (M. O. Andreae, 2001; Burling et al., 2010; Christian et al., 2003; Yokelson et al., 2013). Observations of smoke from ambient wildfires and laboratory simulations of fuel mixtures typically observed in the field show that furanoid emissions are generally well-correlated to CO, regardless of fuel type (Burling et al., 2010).

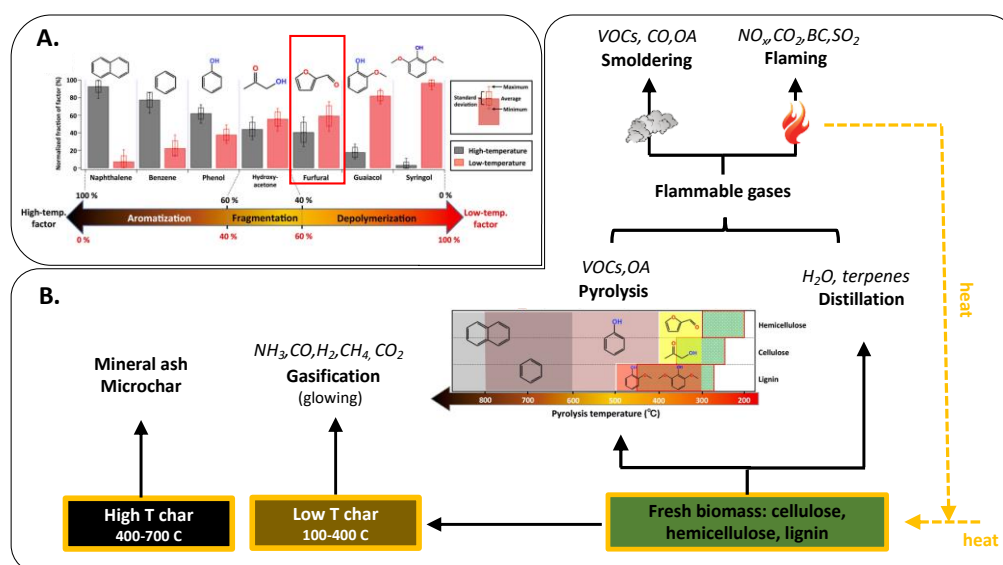


Figure I.8: (A) Observed effect of pyrolysis temperature on VOC speciation from measurements of smoke emitted from open burning of temperature forest fuel types. (B) Process diagram showing the connection between pyrolysis, smoldering and flaming combustion, and release of gases and particles from open biomass burning. Graphs adapted from Sekimoto et al. (Sekimoto et al., 2018). Figure taken from review article prepared in the framework of this thesis, and received the contribution of many co-authors.

### 1.4.3.3 Emission factors of furanoids emitted from fires

The complexity of furanoid emissions observed in the laboratory is challenging to represent in atmospheric models. In ambient biomass burning events, pyrolysis temperatures, combustion conditions, and fuel composition vary significantly, leading to highly variable emissions of VOCs. Models quantify VOC emissions, in part, using ecosystem-specific emission factors, which represent the mass of VOC emitted relative to the mass of fuel consumed by burning ( $\text{g kg}^{-1}$ ) a representative mixture of fuels within a given region. Commonly measured VOCs, such as alkanes, aromatics, and small oxygenates, are widely represented by emission inventories (Akagi et al., 2013; M. O. Andreae, 2001), while furanoid emissions are generally underreported. In our review (Romanias et al., submitted to ACS Earth and Space Chemistry, 2023) a summary of the emission factors of furanoids emitted from biomass burning found in literature studies is provided (Akagi et al., 2013, 2014; Burling et al., 2010; Christian et al., 2003; Ciccioli et al., 2001; Evtugina et al., 2013, 2014; Gilman et al., 2015; Greenberg et al., 1984; Hatch et al., 2017, 2015; Koppmann et al., 1997; Koss et al., 2018; McDonald et al., 2000; Müller et al., 2016; Schellenberg, 2009; Selimovic et al., 2018; Stockwell et al., 2015, 2016; S. Wang et al., 2009; Yokelson et al., 2013, 2022). Here, in Figure I.9 it is shown a summary where the distribution of furans measured for temperate forest, chaparral, and peat fuel types, which have the greatest number of reported furanoid emission factors.

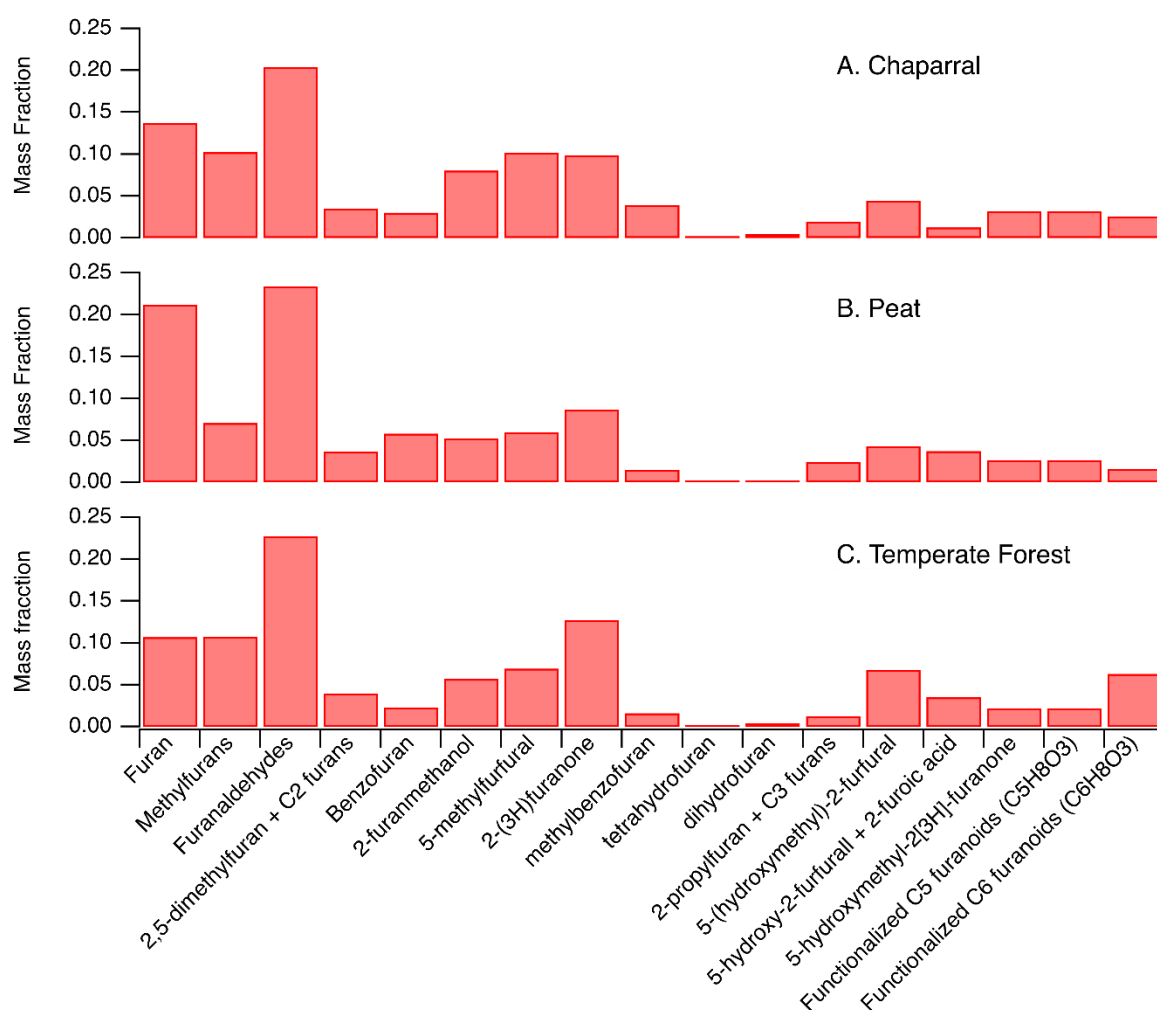


Figure I.9: Distribution of furanoid mass for (A) chaparral, (B) peat, and (C) temperate forest fuel types. Species are ordered by the furanoids most commonly reported in literature.

Furan is the most commonly measured species across fuel types, partly owing to the range of instruments capable of quantifying furan, including Fourier Transfer Infrared Spectroscopy (FTIR), Gas Chromatography-Mass spectrometry (GC-EI-MS), and Proton Transfer -Mass Spectrometry (PTR-MS). Similarly, methyl furans (dominant isomer 2-methylfuran), furanaldehydes (dominant isomer 2-furaldehyde), and dimethyl furans (dominant isomer 2,5-dimethylfuran) are commonly measured by GC-MS and PTR-MS. These species are also among the most abundant furans emitted from most fuel types, and their sum accounts for 48%, 47%, and 55% of the total furan emissions for temperature forest, chaparral, and peat emissions, respectively.

## 1.5 Kinetics of the reactions of furan compounds with tropospheric oxidant

This section includes a brief summary of the literature reported rate coefficients of furanoids with the atmospheric oxidants. Further information can be found elsewhere (Romanias et al., submitted to ACS Earth and Space Chemistry, 2023).

### 1.5.1.1 Reaction with OH

Table I.3 provides the room temperature (i.e.  $295 \pm 5$  K) and temperature dependent rate coefficient values determined for the reaction of differently substituted furan compounds. For compounds with sufficient available studies, a preferred mean of the rate coefficients is provided. In addition, Table I.3 includes the method/technique used in each study, the temperature of the measurements, and/or an Arrhenius expression.

There are multiple studies reporting the reaction rate coefficients of furan and methylated derivatives in literature. The reaction rate coefficients are relatively high, indicating the fast reaction of these compounds. These studied are in relatively good agreement at room temperature, but there are significant variations at high temperatures e.g. for DMF. It is worth mentioning that the reactivity increases with the substitution of an H with a CH<sub>3</sub> group.

There is a limiting number of kinetic data of furan aldehydes, furan ketones and aromatic based furanoids reaction with NO<sub>3</sub> where only one kinetic measurement at ambient temperature is reported (Atkinson et al., 1992; Bierbach et al., 1994; Bierbach et al., 1995).



Table I.3: Summary of available literature data for the reaction of furanoids with the hydroxyl radical (OH).

Compound	Method/technique	Temperature (K)	Pressure (Torr)	A (cm <sup>3</sup> molecule <sup>-1</sup> s <sup>-1</sup> )	E/R (K)	k (295±5) (10 <sup>-11</sup> cm <sup>3</sup> molecule <sup>-1</sup> s <sup>-1</sup> )	Reference	
Tetrahydrofuran	RR-ASC / GC-FID	305 ± 2	760			1.4 ± 0.2	(Winer et al., 1977)	
	AR-QR-FP/ RF	298	20-200			1.63 ± 0.16 (20 Torr) 1.59 ± 0.39 (200 Torr)	(Ravishankara & Davis, 1978)	
	AR-PC / RF	296	25-50			1.78 ± 0.16	(Wallington et al., 1988)	
	RR-ASC / GC-FID	298 ± 2	760			1.80 ± 0.07	(Moriarty et al., 2003)	
	AR-ASC/PLP-LIF	263-372	100	$(9.7 \pm 3.2) \times 10^{-12}$	-(177 ± 67)	1.67 ± 0.07		
	AR-ST / UV <sub>abs</sub>	802-1338			$(1.50 \pm 0.01) \times 10^{-22} (T)^{3.407 \pm 0.001}$	-(2436.7 ± 7.84)	n.d	(Giri et al., 2017)
RR-QR / GC-FID	260-360	825±75		$(5.7 \pm 3.2) \times 10^{-12}$	(349±168)	1.73 ± 0.23	(Illés et al., 2021)	
				$(1.66 \pm 0.80) \times 10^{-12} \times \left(\frac{T}{293}\right)^{1.77 \pm 0.26}$	684±142	<b>1.66 ± 0.26</b>	<b>Mean value</b>	
5-methyl-5-vinyltetrahydrofuran-2-ol	RR-ASC / FTIR	298 ± 5	740			7.40 ± 0.90	(Calogirou et al., 1999)	
2,3-dihydrofuran	RR-PC / GC-FID	298 ± 2	800			11.95 ± 2.79	(Alwe et al., 2014)	
2,5-dihydrofuran	RR-PC / GC-FID	298 ± 2	800			6.45 ± 1.69	(Alwe et al., 2014)	
Furan	AR-DFT / RF	295 ± 1	1.63 – 2.54			10.5 ± 0.8 <sup>†</sup>	(Lee & Tang, 1982)	
	RR-ASC / GC-FID	298 ± 2	735			3.66 ± 0.26	(Atkinson et al., 1983a)	
	AR-PC-FP / RF	245-425	30–150	$(13.3 \pm 2.9) \times 10^{-12}$		4.10 ± 0.62 <sup>§</sup>	(Wine & Thompson, 1984)	
	RR-ASC / GC-FID	300 ± 2	760			4.19 ± 0.21	(Bierbach et al., 1992)	
	AR-ST / UV <sub>abs</sub>	924-1388	889-1482		$783.39 \times T^3$	-1866.7	n.d	(Elwardany et al., 2016)
	AR-PLP / LIF	294-595	3.8–7600		$3.5 \times 10^{-11} \left(\frac{T}{300}\right)^{-1.61} + 9.5 \times 10^{-11} \left(\frac{T}{100}\right)^{-0.44}$	-3079	3.34 ± 0.48 (P<200 mbar) 3.45 ± 0.13 (P>2bar)	(Whelan et al., 2020)
		294–1388	760	$3.75 \times 10^{-11} \times \left(\frac{T}{300}\right)^{-1.6} + 3.5 \times 10^{-11} \times \left(\frac{T}{1000}\right)^{1.8}$	<b>-2456</b>	<b>3.75 ± 0.44</b>	<b>Preferred mean value</b>	
2-methylfuran	RR-ASC / GC-FID	300 ± 2	760			6.19 ± 0.30	(Bierbach et al., 1992)	

	RR-ASC / GC-FID	296 ± 2	735			7.31 ± 0.35	(Aschmann et al., 2011)
	AR-PLP / LIF	295–350	9601-15826	$(1.23 \pm 0.37) \times 10^{-11}$	500	6.69 ± 0.37	(Eble et al., 2015)
	AR-ST / UV <sub>abs</sub>	890-1327	798-1186	$8.85 \times 10^{13}$	-2285	n.d	(Elwardany et al., 2016)
	AR-PLP / LIF	296–668	3.8–7600	$7.3 \times 10^{-11} \left(\frac{T}{300}\right)^{-1.97} + 5.3 \times 10^{-8} \left(\frac{T}{100}\right)^{-4.19}$	-8756	7.34 ± 0.29 (P<200 mbar) 6.80 ± 0.30 (P>2bar)	(Whelan et al., 2020)
						<b>6.89 ± 0.70</b>	<b>Mean value</b>
3-methylfuran	RR-ASC / GC-FID	298 ± 2	740			9.35 ± 1.87	(Atkinson et al., 1989)
	RR-ASC / GC-FID	296 ± 2	735			8.73 ± 0.18	(Aschmann et al., 2011)
	RR-ASC-PC / GC-FID, CG-MS, FTIR	296 ± 2	760			10.7 ± 2.1	(Tapia et al., 2011)
	AR-DFT / LIF	273 - 368	2-6	$(3.2 \pm 0.4) \times 10^{-11}$	310 ± 40	9.1 ± 0.3	(Liljegren & Stevens, 2013)
						<b>9.47 ± 1.23</b>	<b>Mean value</b>
2,3-Dimethylfuran	RR-ASC / GC-FID	296 ± 2	735			12.6 ± 0.4	(Aschmann et al., 2011)
2,5-Dimethylfuran	RR-ASC / GC-FID	300 ± 2	760			14.63 ± 1.02	(Bierbach et al., 1992)
	RR-ASC / GC-FID	296 ± 2	735			12.5 ± 0.4	(Aschmann et al., 2011)
	AR-PLP / LIF	295–350	5025-11701	$(3.38 \pm 1.00) \times 10^{-11}$	-219	7.04 ± 1.00 <sup>†</sup>	(Eble et al., 2015)
	AR-ST / UV <sub>abs</sub>	915-1278	904-1322	$1.03 \times 10^{14}$	2182	n.d	(Elwardany et al., 2016)
	AR-PLP / LIF	295-635	3.8–7600	$9.2 \times 10^{-11} \left(\frac{T}{300}\right)^{-1.78} + 2.0 \times 10^{-8} \left(\frac{T}{100}\right)^{-4.15}$	-7252	11.5 ± 0.7 (P<200 mbar) 9.20 ± 0.40 (P>2bar)	(Whelan et al., 2020)
						<b>11.96 ± 2.76</b>	<b>Preferred mean value</b>
2-ethylfuran	RR-ASC / GC-FID	300 ± 2	760			10.77 ± 2.11	(Bierbach et al., 1992)
Maleic anhydride	RR-ASC / FTIR	296 ± 2	750			0.19 ± 0.01	(Bierbach et al., 1994)
	AR-PLP / LIF-FTIR	283-374	50-200	$(1.55 \pm 0.20) \times 10^{-12}$	-410±44	0.0393 ± 0.0028	(Chattopadhyay et al., 2020)
Furan-2-aldehyde	RR-ASC / GC-FID	298 ± 2	750			3.51 ± 0.11	(Bierbach et al., 1995)
Furan-3-aldehyde	RR-ASC / GC-FID	298 ± 2	750			4.85 ± 0.16	(Bierbach et al., 1995)
5-methylfurfural	RR-ASC / GC-FID	298 ± 2	750			5.10 ± 0.21	(Bierbach et al., 1995)
3H-furan-2-one	RR-ASC / GC-FID	296 ± 2	750			4.45 ± 0.26	(Bierbach et al., 1994)
5-Methyl-2(3H)-furanone	RR-ASC / GC-FID	296 ± 2	750			6.90 ± 0.46	(Bierbach et al., 1994)
2,3-dihydrobenzofuran	RR-ASC / FTIR	298 ± 2	740			3.66 ± 0.56	(Atkinson et al., 1992)

2,3-benzofuran	RR-ASC / GC-FID	298 ± 2	740			3.73 ± 0.74	(Atkinson et al., 1992)
----------------	-----------------	---------	-----	--	--	-------------	-------------------------

Abbreviations used in the table: Relative rate method (RR), Absolute rate method (AR), Atmospheric simulation chamber-Teflon or glass made (ASC), Discharge flow tube (DFT), Shocked tube (ST), Pyrex cell (PC), Quartz reactor (QR), pulse laser fluorescence (PLP), Laser induced fluorescence (LIF), Resonance fluorescence (RF), Flash photolysis (FP), Gas Chromatography –Flame ionization detection (GC-FID), Gas Chromatography mass spectrometry (GC-MS), Ultraviolet absorption ( $UV_{abs}$ ), Fourier-transform infrared spectroscopy (FTIR).

†: Data excluded from the mean value.

§: Value determined averaging results at 298±2 K.

There are multiple studies reporting the reaction rate coefficients of furan and methylated derivatives in literature. The reaction rate coefficients are relatively high (in the order of magnitude of  $10^{-11} \text{ cm}^3 \text{ molecule}^{-1} \text{ s}^{-1}$ ), indicating the fast reaction of these compounds. These studied are in relatively good agreement at room temperature, but there are significant discrepancies at high temperatures e.g. for 2,5-DMF, for which up to a factor of 2 could be observed.

There is a limiting number of kinetic data of furan aldehydes, furan ketones and aromatic based furanoids reaction with  $\text{NO}_3$ . They have been essentially measured by a single group (Atkinson et al., 1992; Bierbach et al., 1994; Bierbach et al., 1995).

In conclusion, there is a need for additional kinetic measurements for furanoids, in particular where there is only one reported study or where results are in poor agreement. Reliable ambient temperature kinetic data for substituted furanoids are necessary to construct structure activity relationships (SAR), which are not currently available. In addition, there is a need for temperature dependent kinetic data at i) tropospheric relevant temperatures, which will enable the more accurate determination of furanoid lifetimes and elucidate reaction mechanisms, ii) combustion relevant temperatures, which are needed since furanoids are proposed biofuels and ideally iii) intermediate temperature ranges (400-800 K) to link the cold and hot temperature regimes and enable comprehensive temperature dependent expressions. Priority should be given to studies of the most abundant furanoids released to the atmosphere from biomass burning, or species considered as promising furanoid-based constituents of biofuels (e.g., methyl and dimethylfurans (Román-Leshkov et al., 2007; Tuan Hoang & Viet Pham, 2021)).

#### *1.5.1.2 Reaction with $\text{NO}_3$*

The  $\text{NO}_3$  radical is a major nighttime tropospheric oxidant. The reaction of nitrate radicals with different classes of organic compounds has been studied for more than four decades. Nevertheless, there are still gaps in the atmospheric  $\text{NO}_3$  oxidation chemistry of organics, including furanoids. Table I.4 summarizes the available furanoid +  $\text{NO}_3$  reaction kinetic data. Below is a discussion of the available  $\text{NO}_3$  kinetic studies. Rate coefficient recommendations are proposed where possible.

Table I.4: Summary of available literature data for the reaction of furanoids with the nitrate radical (NO<sub>3</sub>).

Compound	Method/technique	Temperature (K)	Pressure (Torr)	A factor	E/R (K)	$k$ (295 ± 5) cm <sup>3</sup> molecule <sup>-1</sup> s <sup>-1</sup>	Reference
Tetrahydrofuran	RR-ASC / GC-FID	296 ± 2	740	–		$(4.93 \pm 0.64) \times 10^{-15}$	(Atkinson et al., 1988)
	AR-DFT / LIF	287-340	1.1-1.5	$(2.0 \pm 2) \times 10^{-9}$	-3800 ± 400	$(5.1 \pm 0.2) \times 10^{-15}$	(Cabañas et al., 2004)
						<b><math>(5.02 \pm 0.1) \times 10^{-15}</math></b>	<b>Mean value</b>
Furan	RR-ASC / GC-FID	295 ± 1	735	–		$(1.44 \pm 0.21) \times 10^{-12}$	(Atkinson, Aschmann, Winer, & Carter, 1985a)
	RR-FT / GC-FID	295 ± 2	5.1-150	–		$(9.98 \pm 0.62) \times 10^{-13, \dagger}$	(Kind, Berndt, Bisge, et al., 1996b)
	AR-DFT / LIF	260-345	1.1-1.5	$(1.3 \pm 0.8) \times 10^{-13}$	700 ± 200	$(1.3 \pm 0.2) \times 10^{-12}$	(Cabañas et al., 2004)
	RR-ASC / FTIR	299 ± 2	760			$(1.49 \pm 0.23) \times 10^{-12}$	(Newland et al., 2022)
						<b><math>(1.44 \pm 0.14) \times 10^{-12}</math></b>	<b>Preferred mean value</b>
2-methylfuran	RR-FT / GC-FID	295 ± 2	5.1-150			$(2.57 \pm 0.17) \times 10^{-11}$	(Kind, Berndt, Bisge, et al., 1996b)
	RR-ASC / FTIR	299 ± 2	760			$(2.26 \pm 0.52) \times 10^{-11}$	(Newland et al., 2022)
						<b><math>(2.42 \pm 0.35) \times 10^{-11}</math></b>	<b>Mean value</b>
3-methylfuran	RR-FT / GC-FID	295 ± 2	5.1-150	–		$(2.86 \pm 0.06) \times 10^{-11, \dagger}$	(Kind, Berndt, Bisge, et al., 1996b)
	RR-ASC / GC-FID	296 ± 2	740	–		$(1.31 \pm 0.46) \times 10^{-11}$	(Alvarado et al., 1996)
	RR-ASC / GC-FID, FTIR	296 ± 2	760	–		$(1.26 \pm 0.18) \times 10^{-11}$	(Tapia et al., 2011)128
						<b><math>(1.81 \pm 0.23) \times 10^{-11}</math></b>	<b>Preferred mean value</b>
2,3-Dimethylfuran	RR-FT / GC-FID	295 ± 2	5.1-150			$(5.83 \pm 0.46) \times 10^{-11}$	(Kind, Berndt, Bisge, et al., 1996b)
2,4-Dimethylfuran	RR-FT / GC-FID	295 ± 2	5.1-150			$(2.72 \pm 0.46) \times 10^{-11}$	(Kind, Berndt, Bisge, et al., 1996b)
2,5-Dimethylfuran	RR-FT / GC-FID	295 ± 2	5.1-150			$(5.78 \pm 0.34) \times 10^{-11}$	(Kind, Berndt, Bisge, et al., 1996b)
	RR-ASC / FTIR	299 ± 2	760			$(1.02 \pm 0.31) \times 10^{-10}$	(Newland et al., 2022)

Tetramethylfuran	RR-FT / GC-FID	295 ± 2	5.1-150			$(1.18 \pm 0.16) \times 10^{-10}$	(Kind, Berndt, Bisge, et al., 1996b)
Furan-2-aldehyde	RR-ASC / FTIR	298 ± 2	760			$(1.20 \pm 0.28) \times 10^{-12}$	(Colmenar et al., 2012)
	RR-ASC / FTIR	299 ± 2	760			$(9.07 \pm 2.30) \times 10^{-14}$	(Newland et al., 2022)
Furan-3-aldehyde	RR-ASC / FTIR	298 ± 2	760			$(3.41 \pm 0.79) \times 10^{-12}$	(Colmenar et al., 2012)
5-methylfurfural	RR-ASC / FTIR	298 ± 2	760			$(5.51 \pm 1.27) \times 10^{-12}$	(Colmenar et al., 2012)
$\gamma$ -crotonolactone	RR-ASC / FTIR	299 ± 2	760			$< 1 \times 10^{-16}$	(Newland et al., 2022)
5-Methyl-2(3H)-furanone ( $\alpha$ -angelicalactone)	RR-ASC / FTIR	299 ± 2	760			$(3.01 \pm 0.45) \times 10^{-12}$	(Newland et al., 2022)
5-methyl-5-vinyltetrahydrofuran-2-ol	RR-ASC / FTIR	298 ± 5	740			$(2.0 \pm 0.9) \times 10^{-14}$	(Calogirou et al., 1999)

Abbreviations used in the table: Relative rate method (RR); Absolute rate method (AR); Atmospheric simulation chamber-Teflon or glass made (ASC); Discharge flow tube (DFT); Flow tube (FT); Laser induced fluorescence (LIF); gas chromatography – flame ionization detection (GC-FID); Fourier-transform infrared spectroscopy (FTIR); Proton transfer mass spectrometry (PTR-MS); †: Data not included in the mean value determination.

The kinetics of furan and methyl-substituted furanoids with NO<sub>3</sub> have been studied by multiple research groups using absolute and relative rate methods. Based on the available kinetic data, the rate coefficients for the NO<sub>3</sub> radical reaction with these compounds are high (in the order of magnitude of 10<sup>-12</sup> -10<sup>-10</sup> cm<sup>3</sup> molecule<sup>-1</sup> s<sup>-1</sup>) indicating that this reaction is an important sink for these molecules. Room temperature studies of these reactions are in good agreement except for 2,5-DMF. The reactivity increases with the substitution of H on the furan ring with a methyl group. It also increases with the increase of the number of methyl groups. For all other studied molecules including the aldehyde furans and ketone furans there is one room temperature study per molecule (Colmenar et al., 2012; Newland et al., 2022). Regarding the temperature dependent rate coefficient, there is only one study for the reactions of furan and tetrahydrofuran.

In conclusion, the reaction of NO<sub>3</sub> radicals with methyl-substituted furanoids are considerably faster when compared with the corresponding OH radical reaction rate coefficients. In general, there are limited studies of furanoids reactions with NO<sub>3</sub>, especially for substituted furanoids that have been identified in biomass burning. Furthermore, there is a significant data gap for temperature dependent kinetics. For some furanoids, the reaction with NO<sub>3</sub> can compete with that of OH; therefore, it is important that the current database of NO<sub>3</sub> reaction with this class of compounds be extended with additional laboratory studies to better evaluate the impact of these reactions on tropospheric photochemistry and air quality.

### 1.5.1.3 Reaction with O<sub>3</sub>

The ozonolysis of heterocyclic compounds, such as furans, has not been thoroughly studied. Presently, there are only seven studies reporting kinetic data for furanoid + O<sub>3</sub> reactions. The available kinetic data, method, and measurement technique used in each study are summarized in Table I.5. Aside from furan, each species has only been investigated once.

Table I.5: Summary of available literature data for the reaction of furanoids with ozone (O<sub>3</sub>).

Compound	Method/technique	Temperature (K)	Pressure (Torr)	k (cm <sup>3</sup> molecule <sup>-1</sup> s <sup>-1</sup> )	Reference
Tetrahydrofuran	RR-QPR / FTIR	298 ± 3	700	(7.12 ± 2.11) × 10 <sup>-21</sup>	(Andersen et al., 2016)
	AR-QPR / FTIR	298 ± 3	700	(4.69 ± 1.60) × 10 <sup>-21</sup>	(Andersen et al., 2016)
2-methyltetrahydrofuran	RR-QPR / FTIR	298 ± 3	700	(1.77 ± 0.54) × 10 <sup>-20</sup>	(Andersen et al., 2016)
	AR-QPR / FTIR	298 ± 3	700	(1.97 ± 0.63) × 10 <sup>-20</sup>	(Andersen et al., 2016)
2,5-dimethyltetrahydrofuran	RR-QPR / FTIR	298 ± 3	700	(5.00 ± 1.48) × 10 <sup>-20</sup>	(Andersen et al., 2016)
	AR-QPR / FTIR	298 ± 3	700	(4.15 ± 1.55) × 10 <sup>-20</sup>	(Andersen et al., 2016)
5-methyl-5-vinyltetrahydrofuran-2-ol	RR-ASC / FTIR	298 ± 5	740	(3.8 ± 0.8) × 10 <sup>-18</sup>	(Calogirou et al., 1999)
2,3-dihydrofuran	RR-PC / GC-FID	298 ± 2	800	(4.43 ± 0.79) × 10 <sup>-15</sup>	(Alwe et al., 2014)
2,5-dihydrofuran	RR-PC / GC-FID	298 ± 2	800	(1.65 ± 0.31) × 10 <sup>-17</sup>	(Alwe et al., 2014)
Furan	AR-ASC / GC-FID-O <sub>3</sub> analyzer	298 ± 2	735	(2.42 ± 0.28) × 10 <sup>-18</sup>	(Atkinson et al., 1983a)
	RR-QPR / FTIR	298 ± 3	700	(2.60 ± 0.31) × 10 <sup>-18</sup>	(Andersen et al., 2016)
				<b>(2.51 ± 0.09) × 10<sup>-18</sup></b>	<b>Mean value</b>
3-Methylfuran	RR-ASC / GC-FID	296 ± 2	740	(2.05 ± 0.52) × 10 <sup>-17</sup>	(Alvarado et al., 1996)
2,5-Dimethylfuran	AR-FT / O <sub>3</sub> analyzer	295	n.d	(4.2 ± 0.9) × 10 <sup>-16</sup>	(Matsumoto, 2011)

2,3-dihydrobenzofuran	AR-ASC / O <sub>3</sub> analyzer	298 ± 2	740	<1 × 10 <sup>-19</sup>	(Atkinson et al., 1992)
2,3-benzofuran	AR-ASC / O <sub>3</sub> analyzer	298 ± 2	740	(1.83 ± 0.21) × 10 <sup>-18</sup>	(Atkinson et al., 1992)

Abbreviations used in the table: Relative rate method (RR), Absolute rate method (AR), atmospheric simulation chamber (ASC), quartz photochemical reactor (QPR), flow tube (FT), gas chromatography – flame ionization detection (GC-FID), Fourier-transform infrared spectroscopy (FTIR).

In general, the available studies show that the O<sub>3</sub> kinetics with multi-methylated and oxygenated furanoids appear to be slower than reactions by OH and NO<sub>3</sub> radicals. However, for some species (such as dihydrofurans and tri-substituted furanoids), O<sub>3</sub> kinetics remain important and may require further evaluation in order to fully evaluate the oxidation chemistry of furanoids in fresh and aged biomass burning plumes. Finally, studies on the rate coefficients of the reaction of furanoids with O<sub>3</sub> remain scarce and more studies are needed to propose mean preferred values.

#### 1.5.1.4 Reaction with Cl

The kinetic data for furanoid + Cl atom reactions is relatively scarce. Except for tetrahydrofuran and furan, only single kinetic measurements are reported for the compounds given in Table I.6.

Table I.6: Summary of available room temperature literature data for the reaction of furanoids with chlorine atom (Cl).

Compound	Method/technique	Temperature (K)	Pressure (Torr)	$k \times 10^{-10}$ (cm <sup>3</sup> molecule <sup>-1</sup> s <sup>-1</sup> )	Reference
Tetrahydrofuran	RR-QPR / FTIR	298 ± 3	700	1.96 ± 0.24	(Andersen et al., 2016)
	RR-PC / GC-FID	298 ± 2	800	2.50 ± 0.39	(Alwe et al., 2014)
				<b>2.23 ± 0.27</b>	<b>Mean value</b>
2-methyltetrahydrofuran	RR-QPR / FTIR	298 ± 3	700	2.65 ± 0.43	(Andersen et al., 2016)
2,5-dimethyltetrahydrofuran	RR-QPR / FTIR	298 ± 3	700	2.84 ± 0.34	(Andersen et al., 2016)
2,3-dihydrofuran	RR-PC / GC-FID	298 ± 2	800	4.52 ± 0.99	(Alwe et al., 2014)
2,5-dihydrofuran	RR-PC / GC-FID	298 ± 2	800	4.48 ± 0.39	(Alwe et al., 2014)
Furan	RR-ASC / GC-FID-MS			2.0 ± 0.2	(Cabañas et al., 2005)
	RR-QPR / FTIR	298 ± 3	700	2.39 ± 0.27	(Andersen et al., 2016)
				<b>2.20 ± 0.20</b>	<b>Mean value</b>
2-Methylfuran	RR-ASC / GC-FID-MS	298 ± 2	760	4.1 ± 0.2	(Cabañas et al., 2005)
3-Methylfuran	RR-ASC / GC-FID-MS	298 ± 2	760	4.2 ± 0.3	(Cabañas et al., 2005)
2-Ethylfuran	RR-ASC / GC-FID-MS	298 ± 2	760	4.6 ± 0.3	(Cabañas et al., 2005)
2,5-Dimethylfuran	RR-ASC / GC-FID-MS	298 ± 2	760	5.7 ± 0.3	(Cabañas et al., 2005)
Furan-2-aldehyde	RR-QPR / GC-FID	298 ± 2	708.5	2.61 ± 0.27	(Cabañas et al., 2005)
Furan-3-aldehyde	RR-QPR / GC-FID	298 ± 2	708.5	3.15 ± 0.27	(Cabañas et al., 2005)
5-methylfurfural	RR-QPR / GC-FID	298 ± 2	708.5	4.0 ± 0.5	(Cabañas et al., 2005)
Maleic anhydride	AR-PLP / RF	296	760	0.30	(Chattopadhyay et al., 2020)
	RR-PPR / FTIR	296	620	0.287 ± 0.024 <sup>‡</sup>	

Abbreviations used in the table: Absolute rate method (AR) Relative rate method (RR), Atmospheric simulation chamber (ASC), quartz photochemical reactor (QPR), Pyrex photochemical reactor (PPR), gas chromatography –flame ionization detection-mass spectrometry (GC-FID-MS), solid-phase microextraction- gas chromatography –flame ionization detection (SPME-GC-FID), Fourier-transform infrared spectroscopy (FTIR), pulse laser fluorescence (PLP), Resonance fluorescence (RF).

<sup>‡</sup>: Study carried out as a function of pressure and temperature. Only the room temperature rate coefficient is presented, however the pressure and temperature range where measurements were conducted are discussed in the main manuscript. The room temperature value determined with the relative method is the mean value of the two reference molecules used (ethylene and acetylene). The estimated uncertainty covers the range of the kinetic measurements.



Cl chemistry is expected to be of minor atmospheric loss process for furanoids. However, from the available kinetic data, it is obvious that the rate coefficient of the reaction of furanoids with Cl is faster than their reaction with all other atmospheric oxidants.

Comparing the rate coefficient of furan and methyl substituted furans, the rate coefficient increases with the addition of a methyl group to the ring. However, this increase is less considerable compared to that observed due to the reaction with OH and NO<sub>3</sub>.

Additional room, temperature, and pressure dependent kinetic studies would provide additional insight into the Cl atom initiated atmospheric degradation mechanism and the contribution of the H atom abstraction pathway to the overall rate coefficient.

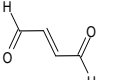
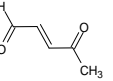
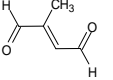
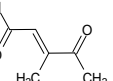
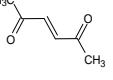
To conclude this section, the OH reaction has been extensively investigated in the literature, but there are still disagreements regarding the rate coefficients at room temperature. Additionally, temperature-dependent rate coefficients have not been studied. As for the NO<sub>3</sub> reaction, there is even less available data; however, the already reported rate coefficient suggests that the reaction is fast, highlighting the urgent need for further studies. The reaction with Cl and O<sub>3</sub> has received significantly less attention, with limited studies conducted thus far. Importantly, additional kinetic studies are necessary for all oxidants to obtain reliable and comprehensive kinetic data. Besides the already investigated compounds, it is necessary to enlarge the list of furanoids to be studied, on the basis of the speciation observed in BB plumes. For instance, furanaldehydes, furan methanol, propyl-furan, and aromatic based furanoids are among the species poorly or not studied at all.

## I.6 Gas-phase products of the reaction of furan compounds with the oxidants

### I.6.1 Reaction with OH

There are several experimental and theoretical literature studies investigating the atmospheric degradation mechanism and gas-phase products of furan and methyl furans oxidation initiated by the OH radical (Tuan Hoang et al., 2021; Aschmann et al., 2014b; Davis & Sarathy, 2013; Gómez Alvarez et al., 2009; Yuan et al., 2017). All experimental studies were conducted under ambient temperature and atmospheric pressure and all the studies were discussed in our review (Romanias et al., submitted to ACS Earth and Space Chemistry, 2023) but here brief summary of the work is presented in Table I.7. These studies used atmospheric simulation chambers coupled to different analytical techniques (PTR-MS, GC-FID, FTIR, etc.) to characterize the products of the furan/methylfurans reaction qualitatively and quantitatively. The oxidation mechanism of the title reaction has also been studied using high-level quantum calculations, which showed agreement with the experimentally determined data. As a result, all studies showed that the major product of the reaction of methylated-furanoids with OH are the unsaturated dicarbonyls. Hydroxyfuranones species that retain the furan ring, were also among the compounds identified. Generally, the radical formed from the addition of OH can either lead to ring opening and subsequent formation of unsaturated dicarbonyl or be stabilized (thermally or with collisions with a third body) such that the ring structure is maintained and subsequent alkoxy decomposition leads to the formation of hydroxy-furanones and epoxides as major products. The yield of the products formed depends on the presence of NO<sub>x</sub>, which enhances the reaction pathway leading to the formation of furanones and epoxides. Comparing the yields of the dicarbonyls formed from the reaction with furan and methylated-furans, the yields of products decrease as the methyl-substitution on the ring increases. This can be due to the stabilization of the ring with the increase of the methyl-groups which favors the formation of hydroxy-furanones over the ring opening (Aschmann et al., 2014b).

Table I.7: Experimental determined yields of the major products formed from the photooxidation of furan/methylfurans by OH radicals at room temperature and ambient pressure.

compound	Method/technique	Temperature (K)	Pressure (Torr)	Unsaturated dicarbonyl		Reference
				Structure	Yield (%) <sup>†</sup>	
Furan	ASC / FTIR	298 ± 2	750		(> 70)	(Bierbach et al., 1995)
	ASC / PTR-MS, GC-FID	n.g <sup>§</sup>	n.g		100 ± 39 <sup>2</sup>	(Gómez Alvarez et al., 2009)
	ASC / PCI GC-MS, API-MS/MS	296 ± 2	735		75 ± 5	(Aschmann et al., 2014a)
					<b>75 ± 5 % in presence of NOx</b>	<b>Preferred value</b>
2-methylfuran	ASC / FTIR	298 ± 2	750		(~70)	(Bierbach et al., 1995)
	ASC / PTR-MS, GC-FID	n.g	n.g		60 ± 24	(Gómez Alvarez et al., 2009)
	ASC / PCI GC-MS, API-MS/MS	296±2	735		31 ± 5	(Aschmann et al., 2014a)
					<b>31 ± 5 % in presence of NOx</b>	<b>Preferred value</b>
3-methylfuran	ASC / PTR-MS, GC-FID	n.g	n.g		83 ± 33	(Gómez Alvarez et al., 2009)
	ASC / GC-FID, CG-MS, FTIR	296 ± 2	760		1.4 ± 0.3	(Tapia et al., 2011)
	ASC / PCI GC-MS, API-MS/MS	296 ± 2	735		38 ± 2	(Aschmann et al., 2014a)
					<b>38 ± 2 % in presence of NOx</b>	<b>Preferred value</b>
2,3-Dimethylfuran	ASC / PCI GC-MS, API-MS/MS	296 ± 2	735	 3-Methyl-4-Oxo-2-pentenal	8 ± 2	(Aschmann et al., 2014a)
2,5-Dimethylfuran	ASC / GC-FID, GC-MS, API-MS/MS	296 ± 2	735		24 ± 3	(Aschmann et al., 2011)
	ASC / PCI GC-MS, API-MS/MS	296 ± 2	735		27	(Aschmann et al., 2014a)
					<b>25 ± 4 % in presence of NOx</b>	<b>Preferred value</b>

Abbreviations used in the table: Atmospheric simulation chamber-Teflon or glass made (ASC); gas chromatography – flame ionization detection (GC-FID); Fourier-transform infrared spectroscopy (FTIR); Proton transfer mass spectrometry (PTR-MS); positive chemical ionization gas chromatography–mass spectrometry (PCI GC-MS); atmospheric pressure ionization tandem mass spectrometry (API-MS/MS);<sup>†</sup>: The yields of dicarbonyl formed in the absence of NOx are shown in brackets. These values are expected to be higher than in presence of NOx (Aschmann et al., 2014b);<sup>§</sup>: not given. However, experiments performed in EUPHORE atmospheric simulation chamber and thus conditions should be close to ambient temperature and atmospheric pressure.

Figure I.10 present the reaction mechanism for the reaction of methylated furan with OH radical as proposed in the study of Jiang et al. (2020). The mechanism only considers the addition of OH in one of the C=C double bonds. The H-atom abstraction (direct or addition-elimination) has not been evaluated, although it is expected to be of minor importance under tropospheric relevant pressures and temperatures (Davis & Sarathy, 2013). However, with the increase of methyl groups in furans, H-atom abstraction mechanism could play a role. It is worth noting that the yields of the dicarbonyls (primary major product formed by OH addition to C-2/C-5 of the ring) was estimated in literature as the standards of these molecules are commercially available which is not the case of furanones which are also major products of these reactions (Table I.7).

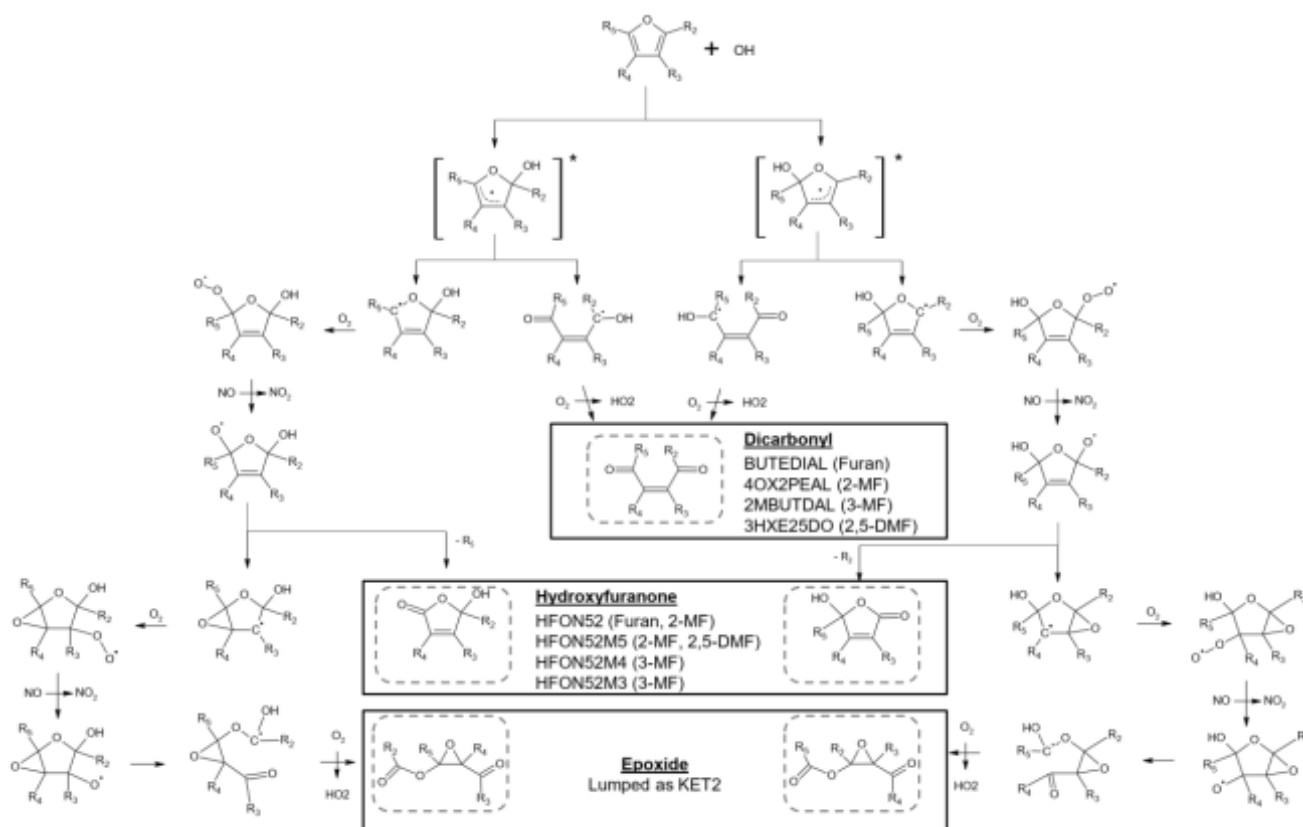


Figure I.10: Reaction mechanism proposed by Aschmann et al. and Jiang et al. for the degradation of furans by OH radicals in presence of NO<sub>x</sub> at room temperature. Scheme adapted by the work of Jiang et al., (2020).

### 1.6.2 Reaction with NO<sub>3</sub>

There is a limited number of literature studies investigating the mechanism of NO<sub>3</sub> reaction with furanoids (Tapia et al., 2011; Berndt et al., 1997; Colmenar et al., 2020; Joo et al., 2019). As the reaction of furanoids with NO<sub>3</sub> is the subject of this thesis, a full illustration of the results on the products of these reactions presented in literature is provided in the following section, as well as to the review article (Romanias et al., submitted to ACS Earth and Space Chemistry, 2023).

**Furan oxidation products.** Atkinson et al. (1985) was the first article proposing a reaction mechanism of furan oxidation by NO<sub>3</sub> radical. Although in their study the authors did not identify or quantify any products, on the basis of the analogy with the alkenes and dialkenes

they proposed that the dominant reaction pathway is the  $\text{NO}_3$  addition to the olefinic double bonds, and in presence of  $\text{O}_2$  and  $\text{NO}_2$ , could lead to the formation of the thermally unstable peroxy nitrates (Atkinson, Aschmann, Winer, & Carter, 1985b).

Berndt et al. (1997) investigated the  $\text{NO}_3$  initiated oxidation of furan inside a low-pressure flow tube reactor (3.75–75 Torr). Pure  $\text{N}_2$  or  $\text{O}_2/\text{N}_2$  mixtures of up to 67%  $\text{O}_2/\text{N}_2$  ratios were used as bath gas. A GC-MS/FID and a FT-IR were coupled to the flow tube for on-line analysis of reactants and products. In the case of furan, the major products identified with FT-IR were 2-butenedial and 3H-furan-2-one with 77% and 19% formation yields, respectively. Products formation were found to be independent of pressure, between 3.75–75 Torr and independent of the bath gas. However, an increase of the 3H-furan-2-one yield was observed with increasing  $\text{O}_2$  concentrations, reaching a maximum value of 38% at 67%  $\text{O}_2/\text{N}_2$  mixtures. The carbon mass balance was above 90% indicating that 2-butenedial and 3H-furan-2-one are the principal compounds formed from  $\text{NO}_3$  initiated oxidation of furan. Regarding the reaction mechanism, Berndt et al. (1997) suggested that  $\text{NO}_3$  adds to C-2 position of furan to form a resonance stabilized radical. The localization of the radical at C-5, and loss of  $\text{NO}_2$  leads to 2-butenedial formation. Localization of radical in position C-2, followed by  $\text{NO}_2$  loss and intramolecular H-transfer from C-2 to C-3 leads to 3H-furan-2-one formation.

A mechanistic scheme can be proposed based on the studies of Atkinson et al. (1985) and Berndt et al. (1997) (Figure I.11).

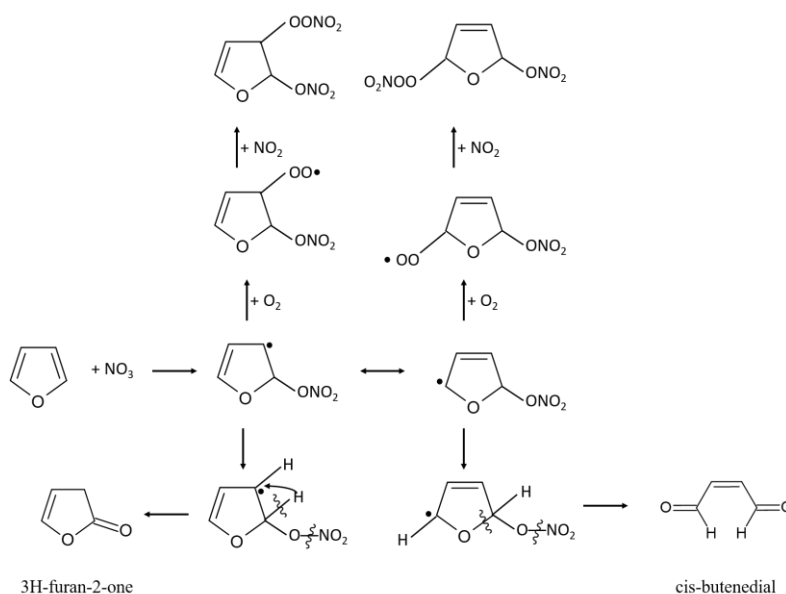


Figure I.11: Proposed reaction mechanism for the addition of  $\text{NO}_3$  radical to the olefinic double bonds of furan.

**3-methylfuran oxidation products.** The gas-phase products reaction mechanism of 3-MF oxidation initiated by reaction with the nitrate radical has been reported in the studies of Tapia et al. (2011) and Joo et al. (2019). In the work of Tapia et al. (2011) the reaction was studied inside atmospheric simulation chambers (Teflon chamber, Pyrex cell). The gas mixture was sampled onto a 30/50  $\mu\text{m}$  SPME fibre and products identification and quantification was achieved deploying GC-EI-MS and GC-FID respectively. Complementary gas phase FT-IR analysis was applied for the detection of organic nitrates. 2-methylbutenedial, 3-

furanaldehyde, 3-methyl-2(3H)-furanone and 3-methyl-2(3H)-furanone were identified. The reported yield for 2-methylbutenedial was unexpected low, below 1%, due to analytical artifacts (Aschmann et al., 2014b). The yield for 3-furanaldehyde was below 1% indicating that possibly the H atom abstraction pathway from the methyl group is of minor importance. The yields for 3-methyl-2(3H)-furanone and 3-methyl-2(3H)-furanone were in the range of 30% and 2% respectively. FTIR analysis evidenced the presence of various oxygenated furans and furan-based organic nitrates, i.e. nitroperoxy- and nitrooxy- compounds. Finally, Tapia et al. (2011), proposed that the NO<sub>3</sub> addition to the double bond of 3-MF is the dominant reaction pathway.

In the study of Joo et al., (2019b) experiments were carried out in a simulation chamber. An iodine high-resolution time of flight-chemical ionization mass spectrometer (HR-TOF-CIMS) was coupled to the chamber for gas-phase products characterization. The particulate matter composition was analyzed with a High Resolution-Time of Flight-Aerosol Mass Spectrometer (HR-TOF-AMS). Different C-2 to C-5 oxygenated and nitro-containing gas-phase species were identified with the HR-ToF-CIMS. Compounds m/z values (extracting the mass of Iodine) were in the range of 45–192. The product peaks with the highest intensity were attributed to a cyclic nitrooxy carbonyl (C<sub>5</sub>H<sub>5</sub>NO<sub>5</sub>) and an organic acid (C<sub>5</sub>H<sub>6</sub>O<sub>3</sub>). These species have the inverse distribution in the particulate phase. Based on the products identified in the gas- and particulate- phases, a mechanism was proposed. According to Joo et al. (2019), the reaction proceeds mainly with the addition of NO<sub>3</sub> to the C-2 or C-5 position of furan ring, which are favored due to the stability of the cyclic nitrooxyalkyl radical produced (Joo et al., 2019b). The radical can either react with O<sub>2</sub> to form a cyclic nitrooxyperoxy radical (RO<sub>2</sub>) or lose NO<sub>2</sub> and give 2-Methylbutenedial. Further details about the reaction mechanism can be found in the corresponding study (Joo et al., 2019b). In conclusion, in both Tapia et al. (2011) and Joo et al. (2019) studies, the first reaction step involves the NO<sub>3</sub> addition to the C-2 or C-5 position of 3-MF. Based on the gas-phase products analysis, the H atom abstraction pathway is considered of minor importance, but still more studies are required to clarify the mechanism of NO<sub>3</sub> reaction with furans and methylated furans.

**Furfural oxidation products.** Colmenar et al., (2012) reported the reaction mechanism of 2-furanaldehyde with NO<sub>3</sub> radical. Experiments were carried out at room temperature (297 ± 2 K) and atmospheric pressure (700 ± 1 Torr) using synthetic air as bath gas inside glass and Teflon made simulation chambers. The glass made chamber was coupled to an FTIR for in situ monitoring of reactants and products. The Teflon chamber was equipped with ports for sampling onto a 30/50 μm SPME, and the gas mixture was injected in a chromatograph column and analyzed with an electron ionization mode time of flight mass spectrometer, GC-ToF-MS.

Maleic anhydride and 2-nitrofuran were identified with GC-EI-MS analyses with molar yields of (58.6 ± 8.6)% and (20 ± 3)%, respectively. A third product was observed, and attributed to 2-furylnitroketone, but its presence was not confirmed. With FTIR, several nitroperoxy and nitrooxy compounds were observed. Authors assigned the IR bands to the presence of 5-hydroxy-2(5H)-furanone, maleic anhydride, or 5-nitrate-2-(5H)-furanone and 2-furylketone but the none of these compounds were confirmed, due to the absence of standards.

Regarding the reaction mechanism Colmenar et al., (2012) proposed a general scheme for NO<sub>3</sub> addition to C5 position, or H atom abstraction of the aldehyde hydrogen, although this reaction pathway is anticipated to be of minor importance. The H-atom abstraction from the furan ring was also considered of minor importance. Maleic anhydride presence was attributed to both addition and abstraction pathways, while that of organic nitrates mainly to the abstraction pathway.

Besides experimental, theoretical calculations were performed to study the degradation mechanism of furfural by NO<sub>3</sub> radical and was found to be in good agreement with experiments observation (Huang et al., 2019). Certainly, more studies are needed to clarify the NO<sub>3</sub> oxidation mechanism of furanoids. The contribution of the H abstraction pathway from the methyl substituted furanoids or furanaldehydes needs also to be evaluated. In addition, considering the challenging step of organic nitrate identification in lab experiments, theoretical studies could provide insights on the reaction mechanism and the formation of these species.

### 1.6.3 Reaction with O<sub>3</sub> and Cl

The reaction of O<sub>3</sub> with furanoids could be an important atmospheric loss process, especially in the case of dihydrofurans and methylated furans. However, until today studies reporting the reaction mechanism, or the gas-phase products formed are very scarce. The Cl atmospheric degradation of furanoids is not expected to be a significant tropospheric loss. There are a few studies reporting the gas-phase products formed, and reaction mechanism (Tapia et al., 2011; Colmenar et al., 2020; Villanueva et al., 2007, 2009). These studies have been carried out by the same group, and thus to draw safe conclusions and eliminate possible systematic uncertainties in the measurements, further studies are needed.

More information on these studies and the provided results in literature are available in our review but are not focused on in this manuscript.

## 1.7 Particulate matter

### 1.7.1 Definition, sources & classes

Atmospheric particulate matter, also known as aerosols, refers to tiny solid or liquid particles suspended in the gaseous phase (Seinfeld et al., 1998). The analysis of these particles has garnered scientific attention due to their significant influence on air quality and climate (Koppmann, 2007). They have the ability to scatter and absorb sunlight radiation, affecting the radiative budget at the Earth's surface, and they also provide sites for heterogeneous reactions in the atmosphere (Koppmann, 2007). In terms of human health, particulate matter has been linked to respiratory diseases as well as vascular and brain disorders (Oh et al., 2020).

Particles are emitted from natural and anthropogenic sources. Natural sources can be suspension of soil and dust, sea spray, forest fires, suspension and release of bacteria, fungi, biological debris of plant and animal decomposition, volcanic eruption particles. Anthropogenic sources include traffic, fossil fuel combustion, industries (as sulfates produced from industrial SO<sub>2</sub>) (Koppmann, 2007).

Two major classes of particles are defined. The first one concerns the **primary particles** which are emitted directly from a given source into the atmosphere, the second class concerns the

**secondary particles** which are due to gas-to-particle conversion processes in the atmosphere (Seinfeld et al., 1998).

### 1.7.2 Particles sizes

The particle size depends first on the formation process and thus PM is classified into two categories (Figure 1.12)(Koppmann, 2007). This classification is necessary since the different categories have different transport and removal process, different chemical composition, optical properties, and different activity in the human's respiratory system (Seinfeld et al., 1998). The first category includes particles with size less than 1  $\mu\text{m}$  or 2.5  $\mu\text{m}$  depending on definition (**fine particles**) and the second category includes particles with size greater than 1  $\mu\text{m}$  or 2.5  $\mu\text{m}$  (**coarse particles**) (Koppmann, 2007). In the first category, the particles are formed or released primarily from combustion processes or from nucleation process and condensational growth (Koppmann, 2007). The particles in the nucleation mode (around 5 to 20 nm) can then continue to grow by uptake of condensable vapors into the Aitken mode (around 20 to 100 nm) and further to particles in the accumulation mode (100-nm range). The coarse particles are mechanically generated such as those released due to ground erosion by wind (Koppmann, 2007).

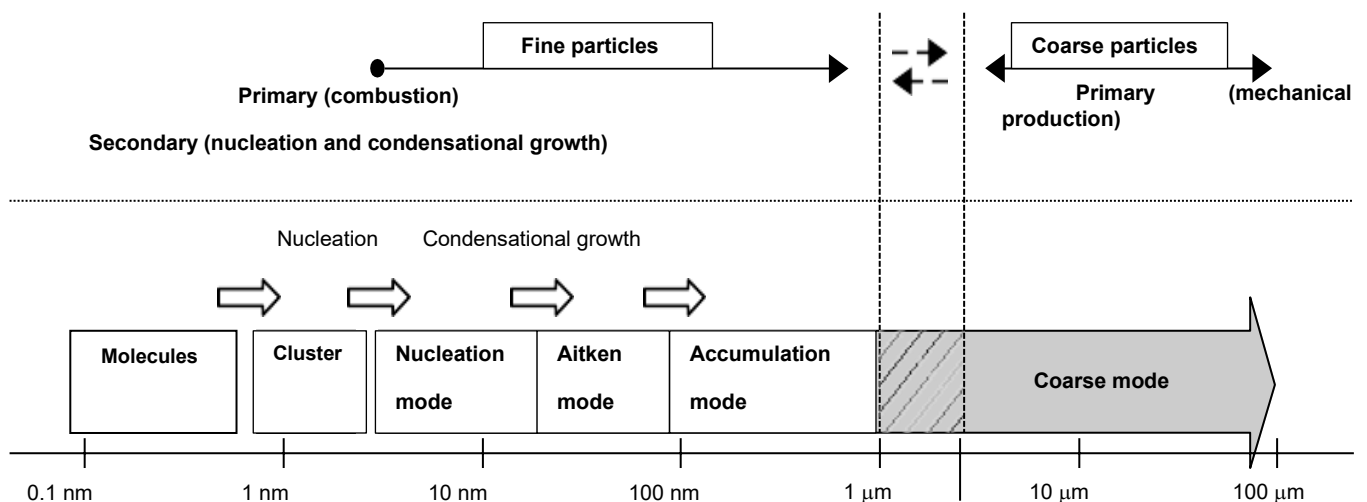


Figure 1.12: Size modes and sources of atmospheric particles (Koppmann, 2007).

### 1.7.3 Particle aging in the atmosphere

Once released into the atmosphere, the size and the composition of the particles can change due to the following processes: uptake of low volatility gaseous compounds, evaporation of compounds from particles, particle coagulation, bulk or surface chemical reactions (Seinfeld et al., 1998). Changes in the chemical composition also alter the physical or physicochemical properties of the particles (light scattering, hygroscopicity, chemical reactivity, etc.), which affect the impact of aerosols on climate (Koppmann, 2007). These parameters will have direct influence on particle transport, lifetime, health impacts, environmental effects and cloud formation ability (Ziemann & Atkinson, 2012).

### 1.7.4 Chemical composition of atmospheric particles & partitioning of an organic compound

PM composition comprises both organic and inorganic fractions. The organic part includes elemental carbon and thousands of organic compounds which range from simple organic



compounds to large oligomeric compounds. The inorganic fraction consists of metals, inorganic ions and crustal fraction (Ziemann & Atkinson, 2012). Water can also occupy part of the particle depending on its hygroscopic property.

The partitioning of an organic compound between the gaseous phase and the condensed phase depends on several parameters: the particle nature, surface area of the particle per unit volume and vapor pressure. Considering the vapor pressure, organic compounds having a  $P_L > 1$  Pa are in a gaseous state, while those having pressure lower than  $10^{-6}$  Pa exists in the condensed phase. However, semi volatile organic compounds have moderate  $P_L$  values that are between  $10^{-6}$  Pa and 1 Pa and exist in both gaseous and particulate phases (Atkinson, 2000).

### 1.7.5 Secondary Organic Aerosols (SOAs)

Secondary organic aerosols (SOA) are aerosols that are not directly emitted, but are produced in the troposphere through chemical reactions between organic compounds and oxidants (Koppmann, 2007).

#### 1.7.5.1 Formation mechanism, RH and $\text{NO}_x$ effects

Precursors of SOA are mainly biogenic VOCs (specially monoterpenes) or anthropogenic VOCs (mainly aromatics) (Koppmann, 2007). These compounds are oxidized in the atmosphere by OH radicals,  $\text{NO}_3$  radical, chlorine atoms, ozone or by photolysis. The oxidation products formed are more functionalized (they can contain hydroxyl, carbonyl, carboxylic groups, etc.) and are less volatile than the VOC precursor. So, they either condense on preexisting particles or form new aerosols (nucleation) (Koppmann, 2007).

The presence of  $\text{NO}_x$  affects the SOA formation due to the reaction of NO with  $\text{RO}_2$  leading to RO which often degrades into smaller molecules with higher volatility, therefore leading to a decrease in the SOA yield (Tajuelo et al., 2021). This means that  $\text{NO}_x$  prevent the formation of new particles and limit the available particle surface inhibiting the condensation of low volatile compounds (Zhao *et al.*, 2018; Tajuelo *et al.*, 2021).

It is expected that mass concentration and yield of SOA increase proportionally with the relative humidity (RH) (Tajuelo et al., 2019a; Tajuelo et al., 2019b; Liu et al., 2019; Tajuelo *et al.*, 2021). Hydrophilic organic compounds can absorb on humid surfaces at high RH, contributing to an increase of the mass concentrations and formation yields of SOA. Hydrophilic organic compounds can absorb on humid surfaces at high RH, contributing to an increase of the mass concentrations and formation yields of SOA (Tajuelo et al., 2021).

#### 1.7.5.2 Effect of seed particles on SOA yield

The presence of seeds enhances the yield of aerosols formation since it acts as a medium of absorption of low volatility products. However, the effect of seeds differs according to its hygroscopic character. To clarify,  $\text{CaCl}_2$  have greater hygroscopic character than  $(\text{NH}_4)_2\text{SO}_4$  and thus Tajuelo *et al.*, (2021) showed that when ammonium sulfate was used as seeds during the OH-photooxidation of 2,5-dimethylfuran, the SOA mass slightly increased after the total consumption of the VOC indicating the slower product condensation. But, in presence of calcium chloride particles, the process of condensation was faster due to the increase of hygroscopic character (3 times higher).

### 1.7.5.3 SOA from furan compounds

Products of furanoids oxidation may partition to the particulate phase to form SOAs. In our review (Romanias et al., submitted to ACS Earth and Space Chemistry, 2023), all the literature studies investigating the SOA formation from furanoids reactions with the key atmospheric oxidants were discussed and just a summary of the different works is presented in Table I.8. In general, the SOA formation yields of furanoids are low (yields < 16 %) and thus, this family of VOCs is unlikely to be significant sources of secondary organic aerosols in the atmosphere beyond concentrated wildfire plumes. However, there remains a number of higher molecular weight furanoids, such as 5-methylfurfural, 2-furanmethanol, and 5-(hydroxymethyl)-2-furfural, for which SOA yields have not been determined yet. A systematic study of the furanoids atmospheric reactivity might elucidate the dependence of SOA formation on furanoids functionality.

Table I.8: Summary of the SOA yields from the OH, NO<sub>3</sub>, and O<sub>3</sub> oxidation of furanoids.

Species	SOA Yield (%)	Initial VOC (ppb)	Initial NOx (ppb)	Seed <sup>1</sup>	RH	Reference
<i>OH Experiments</i>						
furan	0.04 - 5	700 - 780	16-97	NaCl + NaNO <sub>3</sub>	dry - 85%	(Jiang et al., 2020)
furan	1.9 - 7.2	633-830	50	none	dry	(Gómez Alvarez et al., 2009)
2-methylfuran	5.5	750	70	none	dry	(Gómez Alvarez et al., 2009)
3-methylfuran	9	640	120	none	dry	(Gómez Alvarez et al., 2009)
3-methylfuran	9 - 15	10000	10000	DOS or AS	dry - 50%	(Strollo & Ziemann, 2013)
2,5-dimethylfuran	1.4 - 3.7	300 - 800	< 1	none or AS	dry - 25%	(Jiang et al., 2020)
2,5 dimethylfuran	4 - 16	10 - 1000 ppb	< 5 ppb	AS or CaCl <sub>2</sub>	dry - 59%	(Tajuelo et al., 2021)
furfural	0.3	1860 - 1376	Not noted	none	dry	(Colmenar et al., 2012)
<i>NO<sub>3</sub> Experiments</i>						
furan	4 - 10	200	---	none	dry	(Jiang et al., 2020)
3-methylfuran	1.6 - 2.4	96 - 560	---	AS	dry	(Joo et al., 2019b)
<i>O<sub>3</sub> Experiments</i>						
2,5-dimethylfuran	< 1	50 - 500	---	AS or CaCl <sub>2</sub>	dry	(Tajuelo et al., 2021)
furfural	0.5	1860 - 1376	---	none	dry	(Colmenar et al., 2012)

<sup>1</sup> AS = ammonium sulfate, DOS = dioctyl sebacate

## 1.8 Thesis aim

As indicated in the bibliography, biomass burning plays a critical role in air quality, climate, and health. Due to the increasing population rate and the extra demand of food, the rate of land clearing and land use (directly related to wildfires and BB events) (Durigan et al., 2017; Brando et al., 2020) has increased dramatically during the last few decades (Paquet et al., 2019) and increasing trends are projected over the near future (Stehfest et al., 2019). During nighttime, it has been recently shown that the mixing of smoke-derived  $O_3$  with  $NO_x$  in a BB plume leads to the production of  $NO_3$  radicals (the dominant nighttime oxidant) with a rate of approximately  $1 \text{ ppbv h}^{-1}$  (Decker et al., 2019). As a result, significant nighttime chemical transformations potentially occur inside the BB plume that could strongly impact the oxidative capacity of the atmosphere and air quality (Lalchandani et al., 2021). Yet these pathways are poorly studied in literature.

The effect of BB emissions on air quality and climate is correlated to the mixture of gases and particles that are emitted. On the first hand, furans have been identified as major constituents of the VOCs emitted with significant concentrations during BB events from cellulose pyrolysis (see section 1.4.3.3). On the second hand, furans have been demonstrated to significantly contribute ( $\approx 20\%$ ) to overall  $NO_3$  (Decker et al., 2021) and OH reactivity (Coggon et al., 2019) of emissions from residential fuel and wildfire burning.

The objective of this thesis is to enhance our understanding of the nocturnal oxidation of furan compounds (F, 2-MF, 3-MF, 2,5-DMF and 2,3,5-TMF) induced by  $NO_3$ . It is a three-folds objective: the first is related to kinetics determinations of the reactions, the second concerns product characterization and mechanism development and the third is related to SOA formed. To specify, the selection of methylated-furan compounds and their reaction with  $NO_3$  in this study is based on several reasons. First, the very scarce studies on the kinetics of the latter reactions suggests that the  $NO_3$ -initiated oxidation of this class of compounds is extremely fast and consequently their corresponding role in nighttime chemistry is expected to be dominant and more significant than during daytime (Atkinson et al., 1983b; Kind et al., 1996; Newland et al., 2022). Second, these compounds are an important part of this family emitted during fires (Liang et al., 2022). Third, unlike their daytime atmospheric reactivity, which is well studied in literature, their nighttime reactivity with  $NO_3$  is poorly understood. Fourth, these compounds also are expected to be first-generation emitted furan compounds (1.4.3), and thus, they should drive the chemistry in the initial stage of the plume (during daytime and nighttime).

This thesis is composed of four chapters. In the following chapters, a description of the experimental procedures and the results obtained in this work is provided. In the second chapter, the two atmospheric simulation chambers deployed in this work and the associated analytical techniques to monitor the gas- and particulate- phase species are illustrated besides the different methodologies applied to achieve our aims. This chapter describes sampling and analytical methods which have been already previously used in other works (Meng et al., 2020; Fayad et al., 2021) and new methods deployed specially for this research. These methods can be used as a base for future works in atmospheric simulation chambers or more generally in the study of atmospheric reactivity. The third chapter concerns the kinetics data, the rate

coefficients of furan and methylated furan oxidation at room temperature and the temperature dependence for F, 2-MF, 2,5-DMF compounds are presented. Achieving this kinetic goal allows us to determine their lifetimes from one side and to uncover the variation of rate coefficient with temperature, which gives insights into the mechanism of the reaction from the other side. The atmospheric lifetimes enable the behavior of these VOCs in the atmosphere to be more apprehended. A VOC with a short lifetime will have a main impact due to its first- and second-generation products whereas a long lifetime will allow the VOC to be transported for long distances. From a chemical structure side of view, the study of the simplest furan to different methylated furans will show us how the number and the position of methyl functions on the furan ring influence the rate coefficient with  $\text{NO}_3$ . In the fourth chapter, qualitative and quantitative characterization of the atmospheric oxidation products in the gas- and particulate- phase was achieved allowing the proposal of detailed reaction mechanism schemes that can be used in chemical transport models to simulate the chemical evolution of BB plumes. The proposed chemical schemes have many benefits for the scientific community. It helps in the identification of atmospheric tracers common to the methylated furans or unique tracers for each studied furan reaction. It allows the determination of the major products formed, which ones will continue to react and which ones will be ending products. This information is particularly interesting for future reactivity studies to determine the fate of those primary and secondary products in the atmosphere. Moreover, it shows the repartition of the VOCs between gas- and particulate- phase and the mechanism for the formation of SVOCs in SOA. Finally, toxicological studies can be based on the identified products to determine the effect on health. The final objective presented in the last chapter is the estimation of the SOA yields formed from these reactions. It is crucial to know if this family of VOCs are a major SOA contributor. Of course, those data let the door open for further investigations for hygroscopic or optical properties. Finally, the results obtained from achieving all the aims can be included in chemical transport models for air quality and climate. These objectives aim to bridge a significant knowledge gap in the understanding of biomass burning oxidation in the atmosphere.

This research was conducted collaboratively between two laboratories: LPCA at ULCO (Dunkerque) and SAGE at IMT Nord Europe (Douai). Two complementary simulation chambers were utilized: the Chamber for Atmospheric Reactivity and Metrology of the Environment (CHARME) at LPCA and the Thermally Regulated Atmospheric Simulation Chamber (THALAMOS) at SAGE. Both chambers are described in Chapter II underlining the complementarity aspects of the two facilities. This complementarity is crucial for cross-validating the results and conducting temperature-dependent studies.

## I.9 References

- Akagi, S. K., Burling, I. R., Mendoza, A., Johnson, T. J., Cameron, M., Griffith, D. W. T., Paton-Walsh, C., Weise, D. R., Reardon, J., & Yokelson, R. J. (2014). Field measurements of trace gases emitted by prescribed fires in southeastern US pine forests using an open-path FTIR system. *Atmospheric Chemistry and Physics*, *14*(1), 199–215. <https://doi.org/10.5194/acp-14-199-2014>
- Akagi, S. K., Yokelson, R. J., Burling, I. R., Meinardi, S., Simpson, I., Blake, D. R., McMeeking, G. R., Sullivan, A., Lee, T., Kreidenweis, S., Urbanski, S., Reardon, J., Griffith, D. W. T., Johnson, T. J., & Weise, D. R. (2013). Measurements of reactive trace gases and variable O<sub>3</sub> formation rates in some South Carolina biomass burning plumes. In *Atmospheric Chemistry and Physics* (Vol. 13, Issue 3). <https://doi.org/10.5194/acp-13-1141-2013>
- Akagi, S. K., Yokelson, R. J., Wiedinmyer, C., Alvarado, M. J., Reid, J. S., Karl, T., Crouse, J. D., & Wennberg, P. O. (2011). Emission factors for open and domestic biomass burning for use in atmospheric models. *Atmospheric Chemistry and Physics*, *11*(9), 4039–4072. <https://doi.org/10.5194/acp-11-4039-2011>
- Akele, E. S., & Tarekegn, M. M. (2017). Assessment of dioxin and furan emission levels and management practices in Addis Ababa, Ethiopia. *Journal of Health and Pollution*, *7*(15), 85–94. <https://doi.org/10.5696/2156-9614-7.15.85>
- Al Ali, F., Coeur, C., Houzel, N., Bouya, H., Tomas, A., & Romanias, M. N. (2022). Rate Coefficients for the Gas-Phase Reactions of Nitrate Radicals with a Series of Furan Compounds. *Journal of Physical Chemistry A*, *126*(46), 8674–8681. <https://doi.org/10.1021/acs.jpca.2c03828>
- Alan Buis. (2019). *Earth's Atmosphere: A Multi-layered Cake*. <https://climate.nasa.gov/news/2919/earths-atmosphere-a-multi-layered-cake/>
- Alcock, R. E., & Jones, K. C. (1996). Dioxins in the environment: A review of trend data. *Environmental Science and Technology*, *30*(11), 3133–3143. <https://doi.org/10.1021/es960306z>
- Alicke, B., & Platt, U. (2002). *Impact of nitrous acid photolysis on the total hydroxyl radical budget during the Limitation of Oxidant Production / Pianura Padana Produzione di Ozono study in Milan*. 107. <https://doi.org/10.1029/2000JD000075>
- Alvarado, A., Atkinson, R., & Arey, J. (1996). Kinetics of the gas-phase reactions of NO<sub>3</sub> radicals and O<sub>3</sub> with 3-methylfuran and the OH radical yield from the O<sub>3</sub> reaction. *International Journal of Chemical Kinetics*, *28*(12), 905–909. [https://doi.org/10.1002/\(SICI\)1097-4601\(1996\)28:12<905::AID-KIN7>3.0.CO;2-R](https://doi.org/10.1002/(SICI)1097-4601(1996)28:12<905::AID-KIN7>3.0.CO;2-R)
- Alwe, H. D., Walavalkar, M. P., Sharma, A., Dhanya, S., & Naik, P. D. (2014). Tropospheric oxidation of cyclic unsaturated ethers in the day-time: Comparison of the reactions with Cl, OH and O<sub>3</sub> based on the determination of their rate coefficients at 298K. *Atmospheric Environment*, *82*, 113–120. <https://doi.org/10.1016/j.atmosenv.2013.10.009>
- Andersen, C., Nielsen, O. J., Østerstrøm, F. F., Ausmeel, S., Nilsson, E. J. K., & Sulbaek Andersen, M. P. (2016). Atmospheric Chemistry of Tetrahydrofuran, 2-Methyltetrahydrofuran, and 2,5-Dimethyltetrahydrofuran: Kinetics of Reactions with Chlorine Atoms, OH Radicals, and Ozone. *Journal of Physical Chemistry A*, *120*(37), 7320–7326.

<https://doi.org/10.1021/acs.jpca.6b06618>

- Andreae, M. (2019). Emission of trace gases and aerosols from biomass burning. *Global Biogeochemical. Atmospheric Chemistry and Physics*, 15 (4)(April), 955–966. <https://www.atmos-chem-phys-discuss.net/acp-2019-303/acp-2019-303.pdf>
- Andreae, M. O. (2001). [ *Ca Because of the carbon to permits*. 15(4), 955–966.
- Aschmann, S. M., Nishino, N., Arey, J., & Atkinson, R. (2011). Kinetics of the Reactions of OH Radicals with 2- and 3-Methylfuran, 2,3- and 2,5-Dimethylfuran, and E- and Z-3-Hexene-2,5-dione, and Products of OH p 2,5-Dimethylfuran. *Environmental Science and Technology*, 45(7), 1859–1865. <https://doi.org/10.1002/kin.550140706>
- Aschmann, S. M., Nishino, N., Arey, J., & Atkinson, R. (2014a). Products of the OH Radical-Initiated Reactions of Furan, 2- and 3-Methylfuran, and 2,3- and 2,5-Dimethylfuran in the Presence of NO. *The Journal of Physical Chemistry*, 118, 457–466. <https://doi.org/10.1021/jp410345k>
- Aschmann, S. M., Nishino, N., Arey, J., & Atkinson, R. (2014b). *Sara M. Aschmann, Noriko Nishino, † Janet Arey, \*, ‡ and Roger Atkinson \*, ‡*.
- Atkinson, R. (1991a). Kinetics and Mechanisms of the Gas-Phase Reactions of the NO<sub>3</sub> Radical with Organic Compounds. *Journal of Physical and Chemical Reference Data*, 20(3), 459–507. <https://doi.org/10.1063/1.555887>
- Atkinson, R. (1991b). Kinetics and Mechanisms of the Gas-Phase Reactions of the NO<sub>3</sub> Radical with Organic Compounds. *Journal of Physical and Chemical Reference Data*, 20(3), 459–507. <https://doi.org/10.1063/1.555887>
- Atkinson, R. (2000). Atmospheric chemistry of VOCs and NO(x). *Atmospheric Environment*, 34(12–14), 2063–2101. [https://doi.org/10.1016/S1352-2310\(99\)00460-4](https://doi.org/10.1016/S1352-2310(99)00460-4)
- Atkinson, R., & Arey, J. (2003). *ARTICLE IN PRESS Gas-phase tropospheric chemistry of biogenic volatile organic compounds: a review*. 2(2). [https://doi.org/10.1016/S1352-2310\(03\)00391-1](https://doi.org/10.1016/S1352-2310(03)00391-1)
- Atkinson, R., Arey, J., Tuazon, E. C., & Aschmann, S. M. (1992). Gas-phase reactions of 1,4-benzodioxan, 2,3-dihydrobenzofuran, and 2,3-benzofuran with OH radicals and O<sub>3</sub>. *International Journal of Chemical Kinetics*, 24(4), 345–358. <https://doi.org/10.1002/kin.550240404>
- Atkinson, R., Aschmann, S. M., & Carter, P. L. (1983a). *Radicals with Furan and Thiophene at*. 15, 51–61.
- Atkinson, R., Aschmann, S. M., & Carter, W. P. L. (1983b). Kinetics of the reactions of O<sub>3</sub> and OH radicals with furan and thiophene at 298 ± 2 K. *International Journal of Chemical Kinetics*, 15(1), 51–61. <https://doi.org/10.1002/kin.550150106>
- Atkinson, R., Aschmann, S. M., & Carter, W. P. L. (1984). Kinetics of the reactions of O<sub>3</sub> and OH radicals with a series of dialkenes and trialkenes at 294 ± 2 K. *International Journal of Chemical Kinetics*, 16(8), 967–976. <https://doi.org/10.1002/kin.550160804>
- Atkinson, R., Aschmann, S. M., & Pitts, J. N. (1988). Rate constants for the gas-phase reactions of the NO<sub>3</sub> radical with a series of organic compounds at 296 ± 2 K. *Journal of Physical*

*Chemistry*, 92(12), 3454–3457. <https://doi.org/10.1021/j100323a028>

- Atkinson, R., Aschmann, S. M., Tuazon, E. C., Arey, J., & Zielinska, B. (1989). Formation of 3-Methylfuran from the gas-phase reaction of OH radicals with isoprene and the rate constant for its reaction with the OH radical. *International Journal of Chemical Kinetics*, 21(7), 593–604. <https://doi.org/10.1002/kin.550210709>
- Atkinson, R., Aschmann, S. M., Winer, A. M., & Carter, W. P. L. (1985a). *for Reactions with Pyrrole ± 1 Atmospheric. I*, 87–90.
- Atkinson, R., Aschmann, S. M., Winer, A. M., & Carter, W. P. L. (1985b). Rate Constants for the Gas-Phase Reactions of NO<sub>3</sub> Radicals with Furan, Thiophene, and Pyrrole at 295 ± 1 K and Atmospheric Pressure. *Environmental Science and Technology*, 19(1), 87–90. <https://doi.org/10.1021/es00131a010>
- Atkinson, R., Aschmann, S. M., Winer, A. M., & Pitts, J. N. (1985). Kinetics and Atmospheric Implications of the Gas-Phase Reactions of NO<sub>3</sub> Radicals with a Series of Monoterpenes and Related Organics at 294 ± 2 K. *Environmental Science and Technology*, 19(2), 159–163. <https://doi.org/10.1021/es00132a009>
- Atkinson, R., Baulch, D. L., Cox, R. A., Hampson, R. F., Kerr, J. A., Rossi, M. J., & Troe, J. (1997). Evaluated Kinetic, Photochemical and Heterogeneous Data for Atmospheric Chemistry: Supplement V: IUPAC Subcommittee on Gas Kinetic Data Evaluation for Atmospheric Chemistry. *Journal of Physical and Chemical Reference Data*, 26(3), 521–784. <https://doi.org/10.1063/1.556011>
- Bahreini, R., Keywood, M. D., Ng, N. L., Varutbangkul, V., Gao, S., Flagan, R. C., Seinfeld, J. H., Worsnop, D. R., & Jimenez, J. L. (2005). Measurements of secondary organic aerosol from oxidation of cycloalkenes, terpenes, and m-xylene using an aerodyne aerosol mass spectrometer. *Environmental Science and Technology*, 39(15), 5674–5688. <https://doi.org/10.1021/es048061a>
- Berndt, T., Böge, O., & Rolle, W. (1997). Products of the gas-phase reactions of NO<sub>3</sub> radicals with furan and tetramethylfuran. *Environmental Science and Technology*, 31(4), 1157–1162. <https://doi.org/10.1021/es960669z>
- Bierbach, A., Barnes, I., & Becker, K. H. (1992). Rate coefficients for the gas-phase reactions of hydroxyl radicals with furan, 2-methylfuran, 2-ethylfuran and 2,5-dimethylfuran at 300 ± 2 K. *Atmospheric Environment Part A, General Topics*, 26(5), 813–817. [https://doi.org/10.1016/0960-1686\(92\)90241-C](https://doi.org/10.1016/0960-1686(92)90241-C)
- Bierbach, A., Barnes, I., & Becker, K. H. (1995). Product and kinetic study of the oh-initiated gas-phase oxidation of Furan, 2-methylfuran and furanaldehydes at ≈ 300 K. *Atmospheric Environment*, 29(19), 2651–2660. [https://doi.org/10.1016/1352-2310\(95\)00096-H](https://doi.org/10.1016/1352-2310(95)00096-H)
- Bierbach, A., Barnes, I., Becker, K. H., & Wiesen, E. (1994). Atmospheric Chemistry of Unsaturated Carbonyls: Butenedial, 4-Oxo-2-pentenal, 3-Hexene-2,5-dione, Maleic Anhydride, 3H-Furan-2-one, and 5-Methyl-3H-furan-2-one. *Environmental Science and Technology*, 28(4), 715–729. <https://doi.org/10.1021/es00053a028>
- Blake, R., Monks, P., & Ellis, A. (2009). Proton Transfer Reaction Mass Spectrometry (PTR-MS). *Chem.Rev.*, 109(0), 861–896. <https://doi.org/10.1002/9781118180730.ch28>

- Brando, P., Macedo, M., Silvério, D., Rattis, L., Paolucci, L., Alencar, A., Coe, M., & Amorim, C. (2020). Amazon wildfires: Scenes from a foreseeable disaster. *Flora: Morphology, Distribution, Functional Ecology of Plants*, 268. <https://doi.org/10.1016/j.flora.2020.151609>
- Brown, S. S., & Stutz, J. (2012). Nighttime radical observations and chemistry. *Chemical Society Reviews*, 41(19), 6405–6447. <https://doi.org/10.1039/c2cs35181a>
- Burkholder, J. B., Abbatt, J. P. D., Barnes, I., Roberts, J. M., Melamed, M. L., Ammann, M., Bertram, A. K., Cappa, C. D., Carlton, A. G., Carpenter, L. J., Crowley, J. N., Dubowski, Y., George, C., Heard, D. E., Herrmann, H., Keutsch, F. N., Kroll, J. H., McNeill, V. F., Ng, N. L., ... Ziemann, P. J. (2017). The Essential Role for Laboratory Studies in Atmospheric Chemistry. *Environmental Science and Technology*, 51(5), 2519–2528. <https://doi.org/10.1021/acs.est.6b04947>
- Burkholder, J. B., Sander, S. P., Abbatt, J. P. D., Barker, J. R., Huie, R. E., Kolb, C. E., Kurylo, M. J., Orkin, V. L., Wilmouth, D. M., & Wine, P. H. (2020). Chemical Kinetics and Photochemical Data for Use in Atmospheric Studies, Evaluation No. 19. *JPL Publications 19-5*, 19, 1–153. <http://jpldataeval.jpl.nasa.gov/>
- Burling, I. R., Yokelson, R. J., Griffith, D. W. T., Johnson, T. J., Veres, P., Roberts, J. M., Warneke, C., Urbanski, S. P., Reardon, J., Weise, D. R., Hao, W. M., & De Gouw, J. (2010). Laboratory measurements of trace gas emissions from biomass burning of fuel types from the southeastern and southwestern United States. *Atmospheric Chemistry and Physics*, 10(22), 11115–11130. <https://doi.org/10.5194/acp-10-11115-2010>
- Cabañas, B., Baeza, M. T., Salgado, S., Martín, P., Taccone, R., & Martínez, E. (2004). Oxidation of heterocycles in the atmosphere: Kinetic study of their reactions with NO<sub>3</sub> radical. *Journal of Physical Chemistry A*, 108(49), 10818–10823. <https://doi.org/10.1021/jp046524t>
- Cabañas, B., Villanueva, F., Martín, P., Baeza, M. T., Salgado, S., & Jiménez, E. (2005). Study of reaction processes of furan and some furan derivatives initiated by Cl atoms. *Atmospheric Environment*, 39(10), 1935–1944. <https://doi.org/10.1016/j.atmosenv.2004.12.013>
- Cabrera-perez, D., Taraborrelli, D., Sander, R., & Pozzer, A. (2016). *Global atmospheric budget of simple monocyclic aromatic compounds*. 6931–6947. <https://doi.org/10.5194/acp-16-6931-2016>
- Calogirou, A., Jensen, N. R., Nielsen, C. J., Kotzias, D., & Hjorth, J. (1999). Gas-phase reactions of nopinone, 3-isopropenyl-6-oxo-heptanal, and 5-methyl-5-vinyltetrahydrofuran-2-ol with OH, NO<sub>3</sub>, and ozone. *Environmental Science and Technology*, 33(3), 453–460. <https://doi.org/10.1021/es980530j>
- Carbajo, P. G., Smith, S. C., Holloway, A. L., Smith, C. A., Pope, F. D., Shallcross, D. E., & Orr-Ewing, A. J. (2008). Ultraviolet photolysis of HCHO: Absolute HCO quantum yields by direct detection of the HCO radical photoproduct. *Journal of Physical Chemistry A*, 112(48), 12437–12448. <https://doi.org/10.1021/jp8070508>
- Chattopadhyay, A., Papadimitriou, V. C., Marshall, P., & Burkholder, J. B. (2020). Temperature-dependent rate coefficients for the gas-phase OH + furan-2,5-dione (C<sub>4</sub>H<sub>2</sub>O<sub>3</sub>, maleic anhydride) reaction. *International Journal of Chemical Kinetics*, 52(10), 623–631.



<https://doi.org/10.1002/kin.21387>

- Chipperfield, M. P., Bekki, S., Dhomse, S., Harris, N. R. P., Hassler, B., Hossaini, R., Steinbrecht, W., Thiéblemont, R., & Weber, M. (2017). Detecting recovery of the stratospheric ozone layer. *Nature*, *549*(7671), 211–218. <https://doi.org/10.1038/nature23681>
- Christian, T. J., Kleiss, B., Yokelson, R. J., Holzinger, R., Crutzen, P. J., Hao, W. M., Saharjo, B. H., & Ward, D. E. (2003). Comprehensive laboratory measurements of biomass-burning emissions: 1. Emissions from Indonesian, African, and other fuels. *Journal of Geophysical Research: Atmospheres*, *108*(23). <https://doi.org/10.1029/2003jd003704>
- Ciccioli, P., Brancaleoni, E., Frattoni, M., Cecinato, A., & Pinciarelli, L. (2001). Determination of volatile organic compounds (VOC) emitted from biomass burning of Mediterranean vegetation species by GC-MS. *Analytical Letters*, *34*(6), 937–955. <https://doi.org/10.1081/AL-100103604>
- Coeur-tourneur, C., Tomas, A., & Menu, D. (2008). Secondary organic aerosol formation from the gas phase reaction of hydroxyl radicals with *m*-, *o*- and *p*-cresol. *42*, 3035–3045. <https://doi.org/10.1016/j.atmosenv.2007.12.043>
- Coggon, M. M., Lim, C. Y., Koss, A. R., Sekimoto, K., Yuan, B., Gilman, J. B., Hagan, D. H., Selimovic, V., Zarzana, K. J., Brown, S. S., M Roberts, J., Müller, M., Yokelson, R., Wisthaler, A., Krechmer, J. E., Jimenez, J. L., Cappa, C., Kroll, J. H., De Gouw, J., & Warneke, C. (2019). OH chemistry of non-methane organic gases (NMOGs) emitted from laboratory and ambient biomass burning smoke: Evaluating the influence of furans and oxygenated aromatics on ozone and secondary NMOG formation. *Atmospheric Chemistry and Physics*, *19*(23), 14875–14899. <https://doi.org/10.5194/acp-19-14875-2019>
- Collard, F. X., & Blin, J. (2014). A review on pyrolysis of biomass constituents: Mechanisms and composition of the products obtained from the conversion of cellulose, hemicelluloses and lignin. *Renewable and Sustainable Energy Reviews*, *38*, 594–608. <https://doi.org/10.1016/j.rser.2014.06.013>
- Colmenar, I., Cabañas, B., Martínez, E., Salgado, M. S., & Martín, P. (2012). Atmospheric fate of a series of furanaldehydes by their NO<sub>3</sub> reactions. *Atmospheric Environment*, *54*(3), 177–184. <https://doi.org/10.1016/j.atmosenv.2012.02.087>
- Colmenar, I., Martín, P., Cabañas, B., Salgado, S., Villanueva, F., & Ballesteros, B. (2020). Evaluation of the SOA formation in the reaction of furfural with atmospheric oxidants. *Atmosphere*, *11*(9). <https://doi.org/10.3390/atmos11090927>
- Corchnoy, S., & Atkinson, R. (1990). Kinetics of the Gas-Phase Reactions of OH and NO<sub>3</sub> Radicals with 2-Carene, 1,8-Cineole, *p*-Cymene, and Terpinolene. *Environ. Sci. Technol.* *1990*, *24*(10), 1497–1502.
- Crouse, J. D., DeCarlo, P. F., Blake, D. R., Emmons, L. K., Campos, T. L., Apel, E. C., Clarke, A. D., Weinheimer, A. J., McCabe, D. C., Yokelson, R. J., Jimenez, J. L., & Wennberg, P. O. (2009). Biomass burning and urban air pollution over the Central Mexican Plateau. *Atmospheric Chemistry and Physics*, *9*(14), 4929–4944. <https://doi.org/10.5194/acp-9-4929-2009>
- Cuisset, A., Coeur, C., Mouret, G., Ahmad, W., Tomas, A., & Pirali, O. (2016). Infrared

- spectroscopy of methoxyphenols involved as atmospheric secondary organic aerosol precursors: Gas-phase vibrational cross-sections. *Journal of Quantitative Spectroscopy and Radiative Transfer*, 179, 51–58. <https://doi.org/10.1016/j.jqsrt.2016.03.020>
- Davis, A. C., & Sarathy, S. M. (2013). Computational study of the combustion and atmospheric decomposition of 2-methylfuran. *Journal of Physical Chemistry A*, 117(33), 7670–7685. <https://doi.org/10.1021/jp403085u>
- De gouw, J., & Warneke, C. (2007). MEASUREMENTS OF VOLATILE ORGANIC COMPOUNDS IN THE EARTH'S ATMOSPHERE USING PROTON-TRANSFER-REACTION MASS SPECTROMETRY. *Wiley InterScience*, i, 221–235. <https://doi.org/10.1002/mas>
- Decker, Z. C. J., Zarzana, K. J., Coggon, M., Min, K. E., Pollack, I., Ryerson, T. B., Peischl, J., Edwards, P., Dubé, W. P., Markovic, M. Z., Roberts, J. M., Veres, P. R., Graus, M., Warneke, C., De Gouw, J., Hatch, L. E., Barsanti, K. C., & Brown, S. S. (2019). Nighttime Chemical Transformation in Biomass Burning Plumes: A Box Model Analysis Initialized with Aircraft Observations. *Environmental Science and Technology*, 53(5), 2529–2538. <https://doi.org/10.1021/acs.est.8b05359>
- Decker, Z., Robinson, M., Barsanti, K., Bourgeois, I., Coggon, M., DiGangi, J., Diskin, G., Flocke, F., Franchin, A., Fredrickson, C., Hall, S., Halliday, H., Holmes, C., Huey, L. G., Lee, Y. R., Lindaas, J., Middlebrook, A., Montzka, D., Moore, R., ... Brown, S. (2021). Nighttime and Daytime Dark Oxidation Chemistry in Wildfire Plumes: An Observation and Model Analysis of FIREX-AQ Aircraft Data. *Atmospheric Chemistry and Physics Discussions*, November, 1–45. <https://doi.org/10.5194/acp-2021-267>
- Dlugokencky, E. J., & Howard, C. J. (1989a). + (1.28. 17, 1091–1096.
- Dlugokencky, E. J., & Howard, C. J. (1989b). Studies of NO<sub>3</sub> radical reactions with some atmospheric organic compounds at low pressures. *Journal of Physical Chemistry*, 93(3), 1091–1096. <https://doi.org/10.1021/j100340a015>
- Dodge, M. C. (2000). Chemical oxidant mechanisms for air quality modeling: Critical review. *Atmospheric Environment*, 34(12–14), 2103–2130. [https://doi.org/10.1016/S1352-2310\(99\)00461-6](https://doi.org/10.1016/S1352-2310(99)00461-6)
- Durigan, M. R., Cherubin, M. R., de Camargo, P. B., Ferreira, J. N., Berenguer, E., Gardner, T. A., Barlow, J., Dias, C. T. dos S., Signor, D., de Oliveira, R. C., & Cerri, C. E. P. (2017). Soil organic matter responses to anthropogenic forest disturbance and land use change in the eastern Brazilian Amazon. *Sustainability (Switzerland)*, 9(3). <https://doi.org/10.3390/su9030379>
- Dusanter, S., Vimal, D., Stevens, P. S., Volkamer, R., Molina, L. T., Baker, A., Meinardi, S., Blake, D., Sheehy, P., Merten, A., Zhang, R., Zheng, J., Fortner, E. C., Junkermann, W., Dubey, M., Rann, T., Eichinger, B., Lewandowski, P., Prueger, J., & Holder, H. (2009). Measurements of OH and HO<sub>2</sub> concentrations during the MCMA-2006 field campaign - Part 2: Model comparison and radical budget. *Atmospheric Chemistry and Physics*, 9(18), 6655–6675. <https://doi.org/10.5194/acp-9-6655-2009>
- Eble, J., Bänisch, C., & Olzmann, M. (2015). *Kinetic Investigation of the Reactions of 2, 5-Dimethylfuran and 2-Methylfuran with Hydroxyl Radicals*. 2–5.

- Elshorbany, Y., Barnes, I., Becker, K. H., Kleffmann, J., & Wiesen, P. (2010). Sources and cycling of tropospheric hydroxyl radicals - An overview. *Zeitschrift Fur Physikalische Chemie*, 224(7–8), 967–987. <https://doi.org/10.1524/zpch.2010.6136>
- Elshorbany, Y. F., Kurtenbach, R., Wiesen, P., Lissi, E., Rubio, M., Villena, G., Gramsch, E., Rickard, A. R., Pilling, M. J., & Kleffmann, J. (2009). Oxidation capacity of the city air of Santiago, Chile. *Atmospheric Chemistry and Physics*, 9(6), 2257–2273. <https://doi.org/10.5194/acp-9-2257-2009>
- Elwardany, A., Es-Sebbar, E., Khaled, F., & Farooq, A. (2016). A chemical kinetic study of the reaction of hydroxyl with furans. *Fuel*, 166, 245–252. <https://doi.org/10.1016/j.fuel.2015.10.098>
- Evyugina, M., Alves, C., Calvo, A., Nunes, T., Tarelho, L., Duarte, M., Prozil, S. O., Evtugin, D. V., & Pio, C. (2014). VOC emissions from residential combustion of Southern and mid-European woods. *Atmospheric Environment*, 83, 90–98. <https://doi.org/10.1016/j.atmosenv.2013.10.050>
- Evyugina, M., Calvo, A. I., Nunes, T., Alves, C., Fernandes, A. P., Tarelho, L., Vicente, A., & Pio, C. (2013). VOC emissions of smouldering combustion from Mediterranean wildfires in central Portugal. *Atmospheric Environment*, 64, 339–348. <https://doi.org/10.1016/j.atmosenv.2012.10.001>
- Fayad, L. (2019). *Caractérisation de la nouvelle chambre de simulation atmosphérique CHARME et étude de la réaction d'ozonolyse d'un COV biogénique, le  $\gamma$ -terpinène Layal FAYAD Acknowledgments* (Vol. 104).
- Fayad, L., Coeur, C., Fagniez, T., Secordel, X., Houzel, N., & Mouret, G. (2021). Kinetic and mechanistic study of the gas-phase reaction of ozone with  $\gamma$ -terpinene. *Atmospheric Environment*, 246(August 2020). <https://doi.org/10.1016/j.atmosenv.2020.118073>
- Ferdous, D., Dalai, A. K., Bej, S. K., & Thring, R. W. (2002). Pyrolysis of lignins: Experimental and kinetics studies. *Energy and Fuels*, 16(6), 1405–1412. <https://doi.org/10.1021/ef0200323>
- Finlayson-Pitts, B. J. (2010). Atmospheric chemistry. *Proceedings of the National Academy of Sciences of the United States of America*, 107(15), 6566–6567. <https://doi.org/10.1073/pnas.1003038107>
- Finlayson-Pitts, B. J., & Pitts, J. N. (1993). Atmospheric chemistry of tropospheric ozone formation: Scientific and regulatory implications. *Air and Waste*, 43(8), 1091–1100. <https://doi.org/10.1080/1073161X.1993.10467187>
- Finlayson-Pitts, Barbara J., & James N. Pitts Jr. (1999). *Chemistry of the upper and lower atmosphere: theory, experiments, and applications*. El Sevier.
- Fuchs, J. D. H., Seakins, A. K. P., & Editors, J. W. (n.d.). *A Practical Guide to Atmospheric*.
- George, C., Ammann, M., D'Anna, B., Donaldson, D. J., & Nizkorodov, S. A. (2015). Heterogeneous Photochemistry in the Atmosphere. *Chemical Reviews*, 115(10), 4218–4258. <https://doi.org/10.1021/cr500648z>
- Gilman, J. B., Lerner, B. M., Kuster, W. C., Goldan, P. D., Warneke, C., Veres, P. R., Roberts, J. M., De Gouw, J. A., Burling, I. R., & Yokelson, R. J. (2015). Biomass burning emissions and

- potential air quality impacts of volatile organic compounds and other trace gases from fuels common in the US. *Atmospheric Chemistry and Physics*, 15(24), 13915–13938. <https://doi.org/10.5194/acp-15-13915-2015>
- Giri, B. R., Khaled, F., Szori, M., Viskolcz, B., & Farooq, A. (2017). An experimental and theoretical kinetic study of the reaction of OH radicals with tetrahydrofuran. *Proceedings of the Combustion Institute*, 36(1), 143–150. <https://doi.org/10.1016/j.proci.2016.06.016>
- Gómez Alvarez, E., Borrás, E., Viidanoja, J., & Hjorth, J. (2009). Unsaturated dicarbonyl products from the OH-initiated photo-oxidation of furan, 2-methylfuran and 3-methylfuran. *Atmospheric Environment*, 43(9), 1603–1612. <https://doi.org/10.1016/j.atmosenv.2008.12.019>
- Graedel, T. E., & Keene, W. C. (1996). The budget and cycle of Earth's natural chlorine. *Pure and Applied Chemistry*, 68(9), 1689–1697. <https://doi.org/10.1351/pac199668091689>
- Graham, B., Mayol-Bracero, O. L., Guyon, P., Roberts, G. C., Decesari, S., Facchini, M. C., Artaxo, P., Maenhaut, W., Köll, P., & Andreae, M. O. (2002). Water-soluble organic compounds in biomass burning aerosols over Amazonia 1. Characterization by NMR and GC-MS. *Journal of Geophysical Research Atmospheres*, 107(20), LBA 14-1-LBA 14-16. <https://doi.org/10.1029/2001JD000336>
- Greenberg, J. P., Zimmerman, P. R., Heidt, L., & Pollock, W. (1984). Hydrocarbon and carbon monoxide emissions from biomass burning in Brazil. *Journal of Geophysical Research*, 89(D1), 1350–1354. <https://doi.org/10.1029/JD089iD01p01350>
- Gira, A., Amarandei, C., Romanias, M. N., El Dib, G., Canosa, A., Arsene, C., Bejan, I. G., Olariu, R. I., Coddeville, P., & Tomas, A. (2020). Kinetic measurements of Cl atom reactions with C5-C8 unsaturated alcohols. *Atmosphere*, 11(3), 1–15. <https://doi.org/10.3390/ATMOS11030256>
- Guenther, A., Nicholas, C., Fall, R., Klinger, L., McKay, W. A., & Scholes, B. (1995). A global model of natural volatile organic compound emissions s Raja the balance Triangle changes in the atmospheric accumulation rates of greenhouse Triangle Several inventories of natural and Exposure Assessment global scales have been two classes Fores. *J. Geophys. Res.*, 100(94), 8873–8892.
- Hartikainen, A., Yli-Pirilä, P., Tiitta, P., Leskinen, A., Kortelainen, M., Orasche, J., Schnelle-Kreis, J., Lehtinen, K. E. J., Zimmermann, R., Jokiniemi, J., & Sippula, O. (2018). Volatile Organic Compounds from Logwood Combustion: Emissions and Transformation under Dark and Photochemical Aging Conditions in a Smog Chamber. *Environmental Science and Technology*, 52(8), 4979–4988. <https://doi.org/10.1021/acs.est.7b06269>
- Hatch, L. E., Luo, W., Pankow, J. F., Yokelson, R. J., Stockwell, C. E., & Barsanti, K. C. (2015). Identification and quantification of gaseous organic compounds emitted from biomass burning using two-dimensional gas chromatography-time-of-flight mass spectrometry. *Atmospheric Chemistry and Physics*, 15(4), 1865–1899. <https://doi.org/10.5194/acp-15-1865-2015>
- Hatch, L. E., Yokelson, R. J., Stockwell, C. E., Veres, P. R., Simpson, I. J., Blake, D. R., Orlando, J. J., & Barsanti, K. C. (2017). Multi-instrument comparison and compilation of non-methane organic gas emissions from biomass burning and implications for smoke-derived

- secondary organic aerosol precursors. *Atmospheric Chemistry and Physics*, 17(2), 1471–1489. <https://doi.org/10.5194/acp-17-1471-2017>
- Hein, R., Crutzen, P. J., & Heimann, M. (1997). An inverse modeling approach to investigate the global atmospheric methane cycle. *Global Biogeochemical Cycles*, 11(1), 43–76. <https://doi.org/10.1029/96GB03043>
- Holly Zell. (2013). *Earth's Atmospheric Layers*. [https://www.nasa.gov/mission\\_pages/sunearth/science/atmosphere-layers2.html](https://www.nasa.gov/mission_pages/sunearth/science/atmosphere-layers2.html)
- Huang, Z., Zhao, N., Ma, X., Xu, F., Zhang, Q., Zhuang, T., & Wang, W. (2019). Theoretical study on the atmospheric oxidation reaction of 2-furaldehyde initiated by NO<sub>3</sub> radicals. *Chemical Physics Letters*, 722(3), 50–57. <https://doi.org/10.1016/j.cplett.2019.03.009>
- Hynes, R. G., Angove, D. E., Saunders, S. M., Haverd, V., & Azzi, M. (2005). Evaluation of two MCM v3.1 alkene mechanisms using indoor environmental chamber data. *Atmospheric Environment*, 39(38), 7251–7262. <https://doi.org/10.1016/j.atmosenv.2005.09.005>
- Identification, I., Flux, V., & Atkinson, R. (1990). *Radicals with*. 24(10), 1497–1502.
- Illés, Á., Rózsa, Z. B., Thangaraj, R., Décsiné Gombos, E., Dóbbé, S., Giri, B. R., & Szóri, M. (2021). An experimental and theoretical kinetic study of the reactions of hydroxyl radicals with tetrahydrofuran and two deuterated tetrahydrofurans. *Chemical Physics Letters*, 776. <https://doi.org/10.1016/j.cplett.2021.138698>
- IUPAC. (2016). *IUPAC Task Group on Atmospheric Chemical Kinetic Data Evaluation – Data Sheet NO<sub>3</sub>\_VOC*. [iupac.pole-ether.fr](http://iupac.pole-ether.fr)
- Jenkin, M. E., & Hayman, G. D. (1999). Photochemical ozone creation potentials for oxygenated volatile organic compounds: Sensitivity to variations in kinetic and mechanistic parameters. *Atmospheric Environment*, 33(8), 1275–1293. [https://doi.org/10.1016/S1352-2310\(98\)00261-1](https://doi.org/10.1016/S1352-2310(98)00261-1)
- Jiang, G., Nowakowski, D. J., & Bridgwater, A. V. (2010). Effect of the temperature on the composition of lignin pyrolysis products. *Energy and Fuels*, 24(8), 4470–4475. <https://doi.org/10.1021/ef100363c>
- Jiang, J., Carter, W. P. L., Cocker, D. R., & Barsanti, K. C. (2020). Development and Evaluation of a Detailed Mechanism for Gas-Phase Atmospheric Reactions of Furans. *ACS Earth and Space Chemistry*, 4(8), 1254–1268. <https://doi.org/10.1021/acsearthspacechem.0c00058>
- Joo, T., Rivera-Rios, J. C., Takeuchi, M., Alvarado, M. J., & Ng, N. L. (2019a). Secondary Organic Aerosol Formation from Reaction of 3-Methylfuran with Nitrate Radicals. *ACS Earth and Space Chemistry*, 3(6), 922–934. <https://doi.org/10.1021/acsearthspacechem.9b00068>
- Joo, T., Rivera-Rios, J. C., Takeuchi, M., Alvarado, M. J., & Ng, N. L. (2019b). Secondary Organic Aerosol Formation from Reaction of 3-Methylfuran with Nitrate Radicals [Research-article]. *ACS Earth and Space Chemistry*, 3(6), 922–934. <https://doi.org/10.1021/acsearthspacechem.9b00068>
- Kawamoto, H. (2017). Lignin pyrolysis reactions. *Journal of Wood Science*, 63(2), 117–132. <https://doi.org/10.1007/s10086-016-1606-z>
- Keene, W. C., Maring, H., Maben, J. R., Kieber, D. J., Pszenny, A. A. P., Dahl, E. E., Izaguirre, M.

- A., Davis, A. J., Long, M. S., Zhou, X., Smoydzin, L., & Sander, R. (2007). Chemical and physical characteristics of nascent aerosols produced by bursting bubbles at a model air-sea interface. *Journal of Geophysical Research Atmospheres*, *112*(21), 1–16. <https://doi.org/10.1029/2007JD008464>
- Kind, I., Berndt, T., Bisge, O., & Rolle, W. (1996a). *Gas-phase rate constants for the reaction of*. *2614*(3), 2–6.
- Kind, I., Berndt, T., Bisge, O., & Rolle, W. (1996b). *Gas-phase rate constants for the reaction of NO<sub>3</sub> radicals with furan and methyl-substituted furans*. *2614*(3), 2–6.
- Kind, I., Berndt, T., Böge, O., & Rolle, W. (1996). Gas-phase rate constants for the reaction of NO<sub>3</sub> radicals with selected oxiranes. *Chemical Physics Letters*, *249*(1–2), 35–39. [https://doi.org/10.1016/0009-2614\(95\)01327-X](https://doi.org/10.1016/0009-2614(95)01327-X)
- Koolen, C. D., & Rothenberg, G. (2019). Air Pollution in Europe. *ChemSusChem*, *12*(1), 164–172. <https://doi.org/10.1002/cssc.201802292>
- Koppmann, R. (2007). Volatile Organic Compounds in the Atmosphere. In *Volatile Organic Compounds in the Atmosphere*. <https://doi.org/10.1002/9780470988657>
- Koppmann, R., Khedim, A., Rudolph, J., Poppe, D., Andreae, M. O., Helas, G., Welling, M., & Zenker, T. (1997). Emissions of organic trace gases from savanna fires in southern Africa during the 1992 Southern African Fire Atmosphere Research Initiative and their impact on the formation of tropospheric ozone. *Journal of Geophysical Research Atmospheres*, *102*(15), 18879–18888. <https://doi.org/10.1029/97jd00845>
- Koss, A. R., Sekimoto, K., Gilman, J. B., Selimovic, V., Coggon, M. M., Zarzana, K. J., Yuan, B., Lerner, B. M., Brown, S. S., Jimenez, J. L., Krechmer, J., Roberts, J. M., Warneke, C., Yokelson, R. J., & De Gouw, J. (2018). Non-methane organic gas emissions from biomass burning: Identification, quantification, and emission factors from PTR-ToF during the FIREX 2016 laboratory experiment. *Atmospheric Chemistry and Physics*, *18*(5), 3299–3319. <https://doi.org/10.5194/acp-18-3299-2018>
- Krause, T., Tubbesing, C., Benzing, K., & Schöler, H. F. (2014). Model reactions and natural occurrence of furans from hypersaline environments. *Biogeosciences*, *11*(10), 2871–2882. <https://doi.org/10.5194/bg-11-2871-2014>
- Kumar, V., Chandra, B. P., & Sinha, V. (2018). Large unexplained suite of chemically reactive compounds present in ambient air due to biomass fires. *Scientific Reports*, *8*(1), 1–15. <https://doi.org/10.1038/s41598-017-19139-3>
- Lalchandani, V., Srivastava, D., Dave, J., Mishra, S., Tripathi, N., Shukla, A. K., Sahu, R., Thamban, N. M., Gaddamidi, S., Dixit, K., Ganguly, D., Tiwari, S., Srivastava, A. K., Sahu, L., Rastogi, N., Gargava, P., & Tripathi, S. N. (2021). Effect of biomass burning on PM 2.5 composition and secondary aerosol formation during post-monsoon and winter haze episodes in Delhi . *Journal of Geophysical Research: Atmospheres*, 1–21. <https://doi.org/10.1029/2021jd035232>
- Lambe, A. T., Chhabra, P. S., Onasch, T. B., Brune, W. H., Hunter, J. F., Kroll, J. H., Cummings, M. J., Brogan, J. F., Parmar, Y., Worsnop, D. R., Kolb, C. E., & Davidovits, P. (2015). Effect of oxidant concentration, exposure time, and seed particles on secondary organic aerosol

- chemical composition and yield. *Atmospheric Chemistry and Physics*, 15(6), 3063–3075. <https://doi.org/10.5194/acp-15-3063-2015>
- Lancar, I., Daele, V., Le Bras, G., & Poulet, G. (1991). Étude de la réactivité des radicaux NO<sub>3</sub> avec le diméthyl-2,3 butène-2, le butadiène-1,3 et le diméthyl-2,3 butadiène-1,3. *J.Chim. Phys*, 88, 1777–1792. <https://doi.org/10.1051/jcp/1991881777>
- Lançar, I., Daele, V., Le Bras, G., & Poulet, G. (1991). Étude de la réactivité des radicaux NO<sub>3</sub> avec le diméthyl-2,3 butène-2, le butadiène-1,3 et le diméthyl-2,3 butadiène-1,3. *Journal de Chimie Physique*, 88, 1777–1792. <https://doi.org/10.1051/jcp/1991881777>
- Lange, J. P., Price, R., Ayoub, P. M., Louis, J., Petrus, L., Clarke, L., & Gosselink, H. (2010). Valeric biofuels: A platform of cellulosic transportation fuels. *Angewandte Chemie - International Edition*, 49(26), 4479–4483. <https://doi.org/10.1002/anie.201000655>
- Lauraguais, A., Coeur-tourneur, C., Cassez, A., & Seydi, A. (2012). Rate constant and secondary organic aerosol yields for the gas-phase reaction of hydroxyl radicals with syringol (2,6-dimethoxyphenol). *Atmospheric Environment*, 55, 43–48. <https://doi.org/10.1016/j.atmosenv.2012.02.027>
- Lê Thành, K., Commandré, J. M., Valette, J., Volle, G., & Meyer, M. (2015). Detailed identification and quantification of the condensable species released during torrefaction of lignocellulosic biomasses. *Fuel Processing Technology*, 139, 226–235. <https://doi.org/10.1016/j.fuproc.2015.07.001>
- Lee, J. H., & Tang, I. N. (1982). Absolute rate constants for the hydroxyl radical reactions with ethane, furan, and thiophene at room temperature. *The Journal of Chemical Physics*, 77(9), 4459–4463. <https://doi.org/10.1063/1.444367>
- Liang, Y., Weber, R. J., Misztal, P. K., Jen, C. N., & Goldstein, A. H. (2022). Aging of Volatile Organic Compounds in October 2017 Northern California Wildfire Plumes. *Environmental Science and Technology*, 56(3), 1557–1567. <https://doi.org/10.1021/acs.est.1c05684>
- Liley, P. E., Buck, E., & Ch, M. S. E. (1999). 493-Physical and Chemical Data 物性数据. *Perry's Chemical Engineers Handbook*, 2–86.
- Liljegren, J. A., & Stevens, P. S. (2013). Measurements of the kinetics of the reaction of OH radicals with 3-methylfuran at low pressure. *International Journal of Chemical Kinetics*, 45(12), 787–794. <https://doi.org/10.1002/kin.20814>
- Lin, Y., Cho, J., Tompsett, G. A., Westmoreland, P. R., & Huber, G. W. (2009). Kinetics Mechanism Cellulose Pyrolysis. *Phys. Chem. C*, 113, 20097–20107.
- Lindinger, W., Hansel, A., & Jordan, A. (1998). On-line monitoring of volatile organic compounds at pptv levels by means of Proton-Transfer-Reaction Mass Spectrometry (PTR-MS) Medical applications, food control and environmental research. *International Journal of Mass Spectrometry and Ion Processes*, 173(3), 191–241. [https://doi.org/10.1016/s0168-1176\(97\)00281-4](https://doi.org/10.1016/s0168-1176(97)00281-4)
- Ljungström, E., Wängberg, I., & Langer, S. (1993). Absolute rate coefficients for the reaction between nitrate radicals and some cyclic alkenes. *Journal of the Chemical Society, Faraday Transactions*, 89(16), 2977–2982. <https://doi.org/10.1039/FT9938902977>

- Manion, J., Huie, R. E., Burgess, D. R., Orkin, V. L., Tsang, W., McGivern, W. ., Hudgens, J. W., Knyazev, V. D., Atkinson, D. B., Chai, E., Tereza, A. M., Lin, C. Y., Allison, T. C., Mallard, W. G., Westley, F., Herron, J. T., Hampson, R. F., & Frizzell, D. H. (2015). *NIST Chemical Kinetics Database, NIST Standard Reference Database 17, Version 7.0 (Web Version), Release 1.6.8, Data version 2015.09*.
- Martín, P., Cabañas, B., Colmenar, I., Salgado, M. S., Villanueva, F., & Tapia, A. (2013). Reactivity of E-butenedial with the major atmospheric oxidants. *Atmospheric Environment*, *70*, 351–360. <https://doi.org/10.1016/j.atmosenv.2013.01.041>
- Martinez, E., Cabanas, B., Aranda, A., & Martín, P. (1998). Kinetics of the reactions of NO<sub>3</sub> radical with selected monoterpenes: A temperature dependence study. *Environmental Science and Technology*, *32*(23), 3730–3734. <https://doi.org/10.1021/es970899t>
- Martínez, E., Cabañas, B., Aranda, A., Martín, P., Notario, A., & Salgado, S. (1999). Study on the NO<sub>3</sub> Radical Reactivity: Reactions with Cyclic Alkenes. *Journal of Physical Chemistry A*, *103*(27), 5321–5327. <https://doi.org/10.1021/jp9847181>
- Martinez, E., Cabañas, B., Aranda, A., Martin, P., & Salgado, S. (1999). Absolute Rate Coefficients for the Gas-Phase Reactions of NO<sub>3</sub> Radical with a Series of Monoterpenes at T = 298 to 433 K. *Journal of Atmospheric Chemistry*, *33*(3), 265–282. <https://doi.org/10.1023/A:1006178530211>
- Mathematics, A. (2016). 済無No Title No Title No Title. *19*(1), 1–23.
- Matsumoto, J. (2011). Kinetics of the reactions of ozone with 2,5-dimethylfuran and its atmospheric implications. *Chemistry Letters*, *40*(6), 582–583. <https://doi.org/10.1246/cl.2011.582>
- Mcdonald, J. D., Zielinska, B., Fujita, E. M., Sagebiel, J. C., Chow, J. C., & Watson, J. G. (2000). Fine particle and gaseous emission rates from residential wood combustion. *Environmental Science and Technology*, *34*(11), 2080–2091. <https://doi.org/10.1021/es9909632>
- Mellouki, A., & Chen, J. (2015). *Atmospheric Chemistry of Oxygenated Volatile Organic Compounds : Impacts on Air Quality and Climate*. <https://doi.org/10.1021/cr500549n>
- Meng, L., Coeur, C., Fayad, L., Houzel, N., Genevray, P., Bouzidi, H., Tomas, A., & Chen, W. (2020). Secondary organic aerosol formation from the gas-phase reaction of guaiacol (2-methoxyphenol) with NO<sub>3</sub> radicals. *Atmospheric Environment*, *240*(July). <https://doi.org/10.1016/j.atmosenv.2020.117740>
- Mettler, M. S., Mushrif, S. H., Paulsen, A. D., Javadekar, A. D., Vlachos, D. G., & Dauenhauer, P. J. (2012). Revealing pyrolysis chemistry for biofuels production: Conversion of cellulose to furans and small oxygenates. *Energy and Environmental Science*, *5*(1), 5414–5424. <https://doi.org/10.1039/c1ee02743c>
- Molina, M. J., & Molina, L. T. (2004). Megacities and atmospheric pollution. *Journal of the Air and Waste Management Association*, *54*(6), 644–680. <https://doi.org/10.1080/10473289.2004.10470936>
- Moriarty, J., Sidebottom, H., Wenger, J., Mellouki, A., & Le Bras, G. (2003). Kinetic studies on the reactions of hydroxyl radicals with cyclic ethers and aliphatic diethers. *Journal of*



- Physical Chemistry A*, 107(10), 1499–1505. <https://doi.org/10.1021/jp021267i>
- Mudhoo, A., Thayalan, G., Muthoora, N. J., Muthoora, M. N., Oozeer, B. Z., Rago, Y. P., Ramphul, M. P., Valaydon, A. K., & Kumar, S. (2013). *Dioxins and Furans: Sources, Impacts and Remediation*. [https://doi.org/10.1007/978-3-319-02387-8\\_10](https://doi.org/10.1007/978-3-319-02387-8_10)
- Müller, M., Anderson, B. E., Beyersdorf, A. J., Crawford, J. H., Diskin, G. S., Eichler, P., Fried, A., Keutsch, F. N., Mikoviny, T., Thornhill, K. L., Walega, J. G., Weinheimer, A. J., Yang, M., Yokelson, R. J., & Wisthaler, A. (2016). In situ measurements and modeling of reactive trace gases in a small biomass burning plume. *Atmospheric Chemistry and Physics*, 16(6), 3813–3824. <https://doi.org/10.5194/acp-16-3813-2016>
- Müller, M., Graus, M., Wisthaler, A., Hansel, A., Metzger, A., Dommen, J., & Baltensperger, U. (2012). Analysis of high mass resolution PTR-TOF mass spectra from 1,3,5-trimethylbenzene (TMB) environmental chamber experiments. *Atmospheric Chemistry and Physics*, 12(2), 829–843. <https://doi.org/10.5194/acp-12-829-2012>
- Munger, J. W., Jacob, D. J., Waldman, J. M., & Hoffmann, M. R. (1983). Fogwater chemistry in an urban atmosphere. *Journal of Geophysical Research*, 88(C9), 5109–5121. <https://doi.org/10.1029/JC088iC09p05109>
- Newland, M. J., Ren, Y., McGillen, M. R., Michelat, L., Daële, V., & Mellouki, A. (2022). NO<sub>3</sub> chemistry of wildfire emissions: A kinetic study of the gas-phase reactions of furans with the NO<sub>3</sub> radical. *Atmospheric Chemistry and Physics*, 22(3), 1761–1772. <https://doi.org/10.5194/acp-22-1761-2022>
- Nguyen, T. B., Coggon, M. M., Bates, K. H., Zhang, X., Schwantes, R. H., Schilling, K. A., Loza, C. L., Flagan, R. C., Wennberg, P. O., & Seinfeld, J. H. (2014). Organic aerosol formation from the reactive uptake of isoprene epoxydiols (IEPOX) onto non-acidified inorganic seeds. *Atmospheric Chemistry and Physics*, 14(7), 3497–3510. <https://doi.org/10.5194/acp-14-3497-2014>
- Odum, J. R., Hoffmann, T., Bowman, F., Collins, D., Flagan, R. C., & Seinfeld, J. H. (1996). Gas/particle partitioning and secondary organic aerosol yields. *Environmental Science and Technology*, 30(8), 2580–2585. <https://doi.org/10.1021/es950943+>
- Oh, H. J., Ma, Y., & Kim, J. (2020). Human inhalation exposure to aerosol and health effect: Aerosol monitoring and modelling regional deposited doses. *International Journal of Environmental Research and Public Health*, 17(6), 1–2. <https://doi.org/10.3390/ijerph17061923>
- Olariu, R. I., Bejan, I., Barnes, I., Klotz, B., Becker, K. H., & Wirtz, K. (2004). Rate coefficients for the gas-phase reaction of NO<sub>3</sub> radicals with selected dihydroxybenzenes. *International Journal of Chemical Kinetics*, 36(11), 577–583. <https://doi.org/10.1002/kin.20029>
- Olariu, R. I., Cuza, A. I., Chemistry, A., Tomas, A., Douai, M. De, Chimie, D., Barnes, I., Bejan, I., Becker, K. H., Wuppertal, B. U., Wirtz, K., Centro, F., & Ambientales, D. E. (1998). *Atmospheric Ozone Degradation Reaction of 1, 2-dihydroxybenzene : Aerosol Formation Study*. 1–12.
- Osseiran, N., Romanias, M. N., Gaudion, V., Angelaki, M. E., Papadimitriou, V. C., Tomas, A., Coddeville, P., & Thevenet, F. (2020). Development and validation of a thermally

- regulated atmospheric simulation chamber (THALAMOS): A versatile tool to simulate atmospheric processes. *Journal of Environmental Sciences (China)*, 95(xxxx), 141–154. <https://doi.org/10.1016/j.jes.2020.03.036>
- Pankow, J. F. (1994). An absorption model of the gas/aerosol partitioning involved in the formation of secondary organic aerosol. *Atmospheric Environment*, 28(SUPPL.), 189–193. <https://doi.org/10.1016/j.atmosenv.2007.10.060>
- Papadimitriou, V. C., Lazarou, Y. G., Talukdar, R. K., & Burkholder, J. B. (2011). *Atmospheric Chemistry of CF<sub>3</sub>CF<sub>2</sub>*. 2(3), 167–181.
- Paquet, M., Arlt, D., Knape, J., Low, M., Forslund, P., & Pärt, T. (2019). Quantifying the links between land use and population growth rate in a declining farmland bird. *Ecology and Evolution*, 9(2), 868–879. <https://doi.org/10.1002/ece3.4766>
- Qian, Y., Zhu, L., Wang, Y., & Lu, X. (2015). Recent progress in the development of biofuel 2,5-dimethylfuran. *Renewable and Sustainable Energy Reviews*, 41, 633–646. <https://doi.org/10.1016/j.rser.2014.08.085>
- Ravishankara, A. R., & Davis, D. D. (1978). Kinetic rate constants for the reaction of OH with methanol, ethanol, and tetrahydrofuran at 298 K [2]. *Journal of Physical Chemistry*, 82(26), 2852–2853. <https://doi.org/10.1021/j100515a022>
- Reddington, C. L., Spracklen, D. V., Artaxo, P., Ridley, D. A., Rizzo, L. V., & Arana, A. (2016). Analysis of particulate emissions from tropical biomass burning using a global aerosol model and long-term surface observations. *Atmospheric Chemistry and Physics*, 16(17), 11083–11106. <https://doi.org/10.5194/acp-16-11083-2016>
- Ren, X., Brune, W. H., Oliger, A., Metcalf, A. R., Simpas, J. B., Shirley, T., Schwab, J. J., Bai, C., Roychowdhury, U., Li, Y., Cai, C., Demerjian, K. L., He, Y., Zhou, X., Gao, H., & Hou, J. (2006). OH, HO<sub>2</sub>, and OH reactivity during the PMTACS – NY Whiteface Mountain 2002 campaign: Observations and model comparison. 111, 1–12. <https://doi.org/10.1029/2005JD006126>
- Ren, X., Gao, H., Zhou, X., Crouse, J. D., Wennberg, P. O., Browne, E. C., LaFranchi, B. W., Cohen, R. C., McKay, M., Goldstein, A. H., & Mao, J. (2010). Measurement of atmospheric nitrous acid at Bodgett forest during BEARPEX2007. *Atmospheric Chemistry and Physics*, 10(13), 6283–6294. <https://doi.org/10.5194/acp-10-6283-2010>
- Ren, X., Harder, H., Martinez, M., Leshner, R. L., Oliger, A., Simpas, J. B., Brune, W. H., Schwab, J. J., Demerjian, K. L., He, Y., Zhou, X., & Gao, H. (2003). OH and HO<sub>2</sub> chemistry in the urban atmosphere of New York City. *Atmospheric Environment*, 37(26), 3639–3651. [https://doi.org/10.1016/S1352-2310\(03\)00459-X](https://doi.org/10.1016/S1352-2310(03)00459-X)
- Rissanen, M. (2021). Anthropogenic Volatile Organic Compound (AVOC) Autoxidation as a Source of Highly Oxygenated Organic Molecules (HOM). *Journal of Physical Chemistry A*, 125(41), 9027–9039. <https://doi.org/10.1021/acs.jpca.1c06465>
- Roberts, J. M., Stockwell, C. E., Yokelson, R. J., De Gouw, J., Liu, Y., Selimovic, V., Koss, A. R., Sekimoto, K., Coggon, M. M., Yuan, B., Zarzana, K. J., Brown, S. S., Santin, C., Doerr, S. H., & Warneke, C. (2020). The nitrogen budget of laboratory-simulated western US wildfires during the FIREX 2016 Fire Lab study. *Atmospheric Chemistry and Physics*, 20(14), 8807–

8826. <https://doi.org/10.5194/acp-20-8807-2020>

- Román-Leshkov, Y., Barrett, C. J., Liu, Z. Y., & Dumesic, J. A. (2007). Production of dimethylfuran for liquid fuels from biomass-derived carbohydrates. *Nature*, *447*(7147), 982–985. <https://doi.org/10.1038/nature05923>
- Romanias, M. N., Coggon, M., Al Ali, F., Burkholder, J. B., Dagaut, P., Warneke, C., Stockwell, C. E., Decker, Z., Tomas, A., Houzel, N., Coeur, C., & Brown, S. (n.d.-a). Atmospheric chemistry of furanoids: insights into the sources and atmospheric fate. *Atmospheric Environment*.
- Romanias, M. N., Coggon, M. M., Al Ali, F., Burkholder, J. B., Dagaut, P., Warneke, C., Stockwell, C. E., Decker, Z. C. J., Tomas, A., Houzel, N., Coeur, C., & Brown, S. S. (n.d.-b). Atmospheric chemistry of furanoids: insights into the sources and atmospheric fate. *ASC ACS Earth and Space Chemistry*.
- Schellenberg, C. (2009). Conducta irascible y recalcitrante tras una infección de gripe: Efectos de una acupuntura dispersante en el H 3 en lactantes y niños pequeños. *Revista Internacional de Acupuntura*, *3*(2), 78–79. [https://doi.org/10.1016/S1887-8369\(09\)71579-0](https://doi.org/10.1016/S1887-8369(09)71579-0)
- Schumann, U. (2012). Atmospheric Physics. In *Physics Today* (Vol. 15, Issue 5). <https://doi.org/10.1063/1.3058219>
- Seinfeld, J. H., Pandis, S. N., & Noone, K. (1998). Atmospheric Chemistry and Physics: From Air Pollution to Climate Change. In *Physics Today* (Vol. 51, Issue 10). <https://doi.org/10.1063/1.882420>
- Sekimoto, K., Koss, A. R., Gilman, J. B., Selimovic, V., Coggon, M. M., Zarzana, K. J., Yuan, B., Lerner, B. M., Brown, S. S., Warneke, C., Yokelson, R. J., Roberts, J. M., & De Gouw, J. (2018). High-and low-temperature pyrolysis profiles describe volatile organic compound emissions from western US wildfire fuels. *Atmospheric Chemistry and Physics*, *18*(13), 9263–9281. <https://doi.org/10.5194/acp-18-9263-2018>
- Selimovic, V., Yokelson, R. J., Warneke, C., Roberts, J. M., De Gouw, J., Reardon, J., & Griffith, D. W. T. (2018). Aerosol optical properties and trace gas emissions by PAX and OP-FTIR for laboratory-simulated western US wildfires during FIREX. *Atmospheric Chemistry and Physics*, *18*(4), 2929–2948. <https://doi.org/10.5194/acp-18-2929-2018>
- Si, Z., Wang, C. G., Bi, K., Zhang, X. H., Yu, C. L., Dong, R. J., Ma, L. L., & Changle, P. (2017). Py-GC/MS study of lignin pyrolysis and effect of catalysts on product distribution. *International Journal of Agricultural and Biological Engineering*, *10*(5), 214–225. <https://doi.org/10.25165/j.ijabe.20171005.2852>
- Simoneit, B. R. T. (2002). Biomass burning - A review of organic tracers for smoke from incomplete combustion. In *Applied Geochemistry* (Vol. 17, Issue 3). [https://doi.org/10.1016/S0883-2927\(01\)00061-0](https://doi.org/10.1016/S0883-2927(01)00061-0)
- Smith, D., & Španěl, P. (2005). Selected ion flow tube mass spectrometry (SIFT-MS) for on-line trace gas analysis. *Mass Spectrometry Reviews*, *24*(5), 661–700. <https://doi.org/10.1002/mas.20033>
- Song, C., NA, K., & Cocker, D. R. (2005). Impact of the Hydrocarbon to NO. *Environmental*

*Science & Technology*, 39(9), 3143–3149.

- Španěl, P., Dryahina, K., & Smith, D. (2013). A quantitative study of the influence of inhaled compounds on their concentrations in exhaled breath. *Journal of Breath Research*, 7(1). <https://doi.org/10.1088/1752-7155/7/1/017106>
- Stehfest, E., van Zeist, W. J., Valin, H., Havlik, P., Popp, A., Kyle, P., Tabeau, A., Mason-D’Croz, D., Hasegawa, T., Bodirsky, B. L., Calvin, K., Doelman, J. C., Fujimori, S., Humpenöder, F., Lotze-Campen, H., van Meijl, H., & Wiebe, K. (2019). Key determinants of global land-use projections. *Nature Communications*, 10(1), 1–10. <https://doi.org/10.1038/s41467-019-09945-w>
- Stockman, R. A. (2007). Heterocyclic chemistry. In *Annual Reports on the Progress of Chemistry - Section B* (Vol. 103). <https://doi.org/10.1039/b614418g>
- Stockwell, C. E., Christian, T. J., Goetz, J. D., Jayarathne, T., Bhawe, P. V., Praveen, P. S., Adhikari, S., Maharjan, R., DeCarlo, P. F., Stone, E. A., Saikawa, E., Blake, D. R., Simpson, I. J., Yokelson, R. J., & Panday, A. K. (2016). Nepal Ambient Monitoring and Source Testing Experiment (NAMaSTE): Emissions of trace gases and light-absorbing carbon from wood and dung cooking fires, garbage and crop residue burning, brick kilns, and other sources. *Atmospheric Chemistry and Physics*, 16(17), 11043–11081. <https://doi.org/10.5194/acp-16-11043-2016>
- Stockwell, C. E., Veres, P. R., Williams, J., & Yokelson, R. J. (2015). Characterization of biomass burning emissions from cooking fires, peat, crop residue, and other fuels with high-resolution proton-transfer-reaction time-of-flight mass spectrometry. *Atmospheric Chemistry and Physics*, 15(2), 845–865. <https://doi.org/10.5194/acp-15-845-2015>
- Strollo, C. M., & Ziemann, P. J. (2013). Products and mechanism of secondary organic aerosol formation from the reaction of 3-methylfuran with OH radicals in the presence of NOx. *Atmospheric Environment*, 77, 534–543. <https://doi.org/10.1016/j.atmosenv.2013.05.033>
- Tajuelo, M., Rodríguez, A., Baeza-Romero, M. T., Aranda, A., Díaz-de-Mera, Y., & Rodríguez, D. (2019). Secondary organic aerosol formation from  $\alpha$ -methylstyrene atmospheric degradation: Role of NOx level, relative humidity and inorganic seed aerosol. *Atmospheric Research*, 230(July), 104631. <https://doi.org/10.1016/j.atmosres.2019.104631>
- Tajuelo, M., Rodríguez, D., Baeza-Romero, M. T., Díaz-de-Mera, Y., Aranda, A., & Rodríguez, A. (2019). Secondary organic aerosol formation from styrene photolysis and photooxidation with hydroxyl radicals. *Chemosphere*, 231, 276–286. <https://doi.org/10.1016/j.chemosphere.2019.05.136>
- Tajuelo, M., Rodríguez, D., Rodríguez, A., Escalona, A., Viteri, G., Aranda, A., & Diaz-de-Mera, Y. (2021). Secondary organic aerosol formation from the ozonolysis and oh-photooxidation of 2,5-dimethylfuran. *Atmospheric Environment*, 245, 118041. <https://doi.org/10.1016/j.atmosenv.2020.118041>
- Takekawa, H., Minoura, H., & Yamazaki, S. (2003). *Temperature dependence of secondary organic aerosol formation by photo-oxidation of hydrocarbons*. 37, 3413–3424. [https://doi.org/10.1016/S1352-2310\(03\)00359-5](https://doi.org/10.1016/S1352-2310(03)00359-5)

- Tapia, A., Villanueva, F., Salgado, M. S., Cabañas, B., Martínez, E., & Martín, P. (2011). Atmospheric degradation of 3-methylfuran: Kinetic and products study. *Atmospheric Chemistry and Physics*, *11*(7), 3227–3241. <https://doi.org/10.5194/acp-11-3227-2011>
- Thewes, M., Muether, M., Pischinger, S., Budde, M., Brunn, A., Sehr, A., Adomeit, P., & Klankermayer, J. (2011). Analysis of the impact of 2-methylfuran on mixture formation and combustion in a direct-injection spark-ignition engine. *Energy and Fuels*, *25*(12), 5549–5561. <https://doi.org/10.1021/ef201021a>
- Tomas, A., Henry, F., & Visez, N. (2009). *Aerosol formation yields from the reaction of catechol with ozone*. *43*, 2360–2365. <https://doi.org/10.1016/j.atmosenv.2008.12.054>
- Tuan Hoang, A., & Viet Pham, V. (2021). 2-Methylfuran (MF) as a potential biofuel: A thorough review on the production pathway from biomass, combustion progress, and application in engines. *Renewable and Sustainable Energy Reviews*, *148*(June), 111265. <https://doi.org/10.1016/j.rser.2021.111265>
- Tuazon, E. C., Aschmann, S. M., & Atkinson, R. (2000). Atmospheric degradation of volatile methyl-silicon compounds. *Environmental Science and Technology*, *34*(10), 1970–1976. <https://doi.org/10.1021/es9910053>
- Vallero, D. (2008). *Fundamentals of Air Pollution* (Fourth). El Sevier.
- Villanueva, F., Barnes, I., Monedero, E., Salgado, S., Gómez, M. V., & Martin, P. (2007). Primary product distribution from the Cl-atom initiated atmospheric degradation of furan: Environmental implications. *Atmospheric Environment*, *41*(38), 8796–8810. <https://doi.org/10.1016/j.atmosenv.2007.07.053>
- Villanueva, F., Cabañas, B., Monedero, E., Salgado, S., Bejan, I., & Martin, P. (2009). Atmospheric degradation of alkylfurans with chlorine atoms: Product and mechanistic study. *Atmospheric Environment*, *43*(17), 2804–2813. <https://doi.org/10.1016/j.atmosenv.2009.02.030>
- Wallington, T. J., Dagaut, P., Liu, R., & Kurylo, M. J. (1988). The gas phase reactions of hydroxyl radicals with a series of esters over the temperature range 240–440 K. *International Journal of Chemical Kinetics*, *20*(2), 177–186. <https://doi.org/10.1002/kin.550200210>
- Wang, J., Doussin, J. F., Perrier, S., Perraudin, E., Katrib, Y., Pangu, E., & Picquet-Varrault, B. (2011). Design of a new multi-phase experimental simulation chamber for atmospheric photochemistry, aerosol and cloud chemistry research. *Atmospheric Measurement Techniques*, *4*(11), 2465–2494. <https://doi.org/10.5194/amt-4-2465-2011>
- Wang, L., Slowik, J. G., Tripathi, N., Bhattu, D., Rai, P., Kumar, V., Vats, P., Satish, R., Baltensperger, U., Ganguly, D., Rastogi, N., Sahu, L. K., Tripathi, S. N., & Prévôt, A. S. H. (2020). Source characterization of volatile organic compounds measured by proton-transfer-reaction time-of-flight mass spectrometers in Delhi, India. *Atmospheric Chemistry and Physics*, *20*(16), 9753–9770. <https://doi.org/10.5194/acp-20-9753-2020>
- Wang, Q., Song, H., Pan, S., Dong, N., Wang, X., & Sun, S. (2020). Initial pyrolysis mechanism and product formation of cellulose: An Experimental and Density functional theory(DFT) study. *Scientific Reports*, *10*(1), 1–18. <https://doi.org/10.1038/s41598-020-60095-2>
- Wang, S., Wei, W., Du, L., Li, G., & Hao, J. (2009). Characteristics of gaseous pollutants from

- biofuel-stoves in rural China. *Atmospheric Environment*, 43(27), 4148–4154. <https://doi.org/10.1016/j.atmosenv.2009.05.040>
- Whelan, C. A., Eble, J., Mir, Z. S., Blitz, M. A., Seakins, P. W., Olzmann, M., & Stone, D. (2020). Kinetics of the Reactions of Hydroxyl Radicals with Furan and Its Alkylated Derivatives 2-Methyl Furan and 2,5-Dimethyl Furan. *Journal of Physical Chemistry A*, 124(37), 7416–7426. <https://doi.org/10.1021/acs.jpca.0c06321>
- Wine, P. H., & Thompson, R. J. (1984). Kinetics of OH reactions with furan, thiophene, and tetrahydrothiophene. *International Journal of Chemical Kinetics*, 16(7), 867–878. <https://doi.org/10.1002/kin.550160707>
- Winer, M., Darnall, K. R., & Lloyd, A. C. (1977). *REACTION set-BUTYL*. 5(2), 221–226.
- Wingenter, O. W., Blake, D. R., Blake, N. J., Sive, B. C., Rowland, F. S., Atlas, E., & Flocke, F. (1999). Tropospheric hydroxyl and atomic chlorine concentrations, and mixing timescales determined from hydrocarbon and halocarbon measurements made over the Southern Ocean. *Journal of Geophysical Research Atmospheres*, 104(D17), 21819–21828. <https://doi.org/10.1029/1999JD900203>
- Wingenter, O. W., Kubo, M. K., Blake, N. J., Smith, T. W., Blake, D. R., & Rowland, F. S. (1996). Hydrocarbon and halocarbon measurements as photochemical and dynamical indicators of atmospheric hydroxyl, atomic chlorine, and vertical mixing obtained during Lagrangian flights. *Journal of Geophysical Research Atmospheres*, 101(D2), 4331–4340. <https://doi.org/10.1029/95JD02457>
- World Health Organization. (2016). WORLD HEALTH STATISTICS - MONITORING HEALTH FOR THE SDGs. *World Health Organization*, 1.121. <https://doi.org/10.1017/CBO9781107415324.004>
- Xu, L., Guo, H., Weber, R. J., & Ng, N. L. (2017). Chemical Characterization of Water-Soluble Organic Aerosol in Contrasting Rural and Urban Environments in the Southeastern United States. *Environmental Science and Technology*, 51(1), 78–88. <https://doi.org/10.1021/acs.est.6b05002>
- Yang, H., Li, S., Liu, B., Chen, Y., Xiao, J., Dong, Z., Gong, M., & Chen, H. (2020). Hemicellulose pyrolysis mechanism based on functional group evolutions by two-dimensional perturbation correlation infrared spectroscopy. *Fuel*, 267(July 2019), 117302. <https://doi.org/10.1016/j.fuel.2020.117302>
- Yang, X., Zhao, Y., Li, W., Li, R., & Wu, Y. (2019). Unveiling the Pyrolysis Mechanisms of Hemicellulose: Experimental and Theoretical Studies. *Energy and Fuels*, 33(5), 4352–4360. <https://doi.org/10.1021/acs.energyfuels.9b00482>
- Yokelson, R. J., Burling, I. R., Gilman, J. B., Warneke, C., Stockwell, C. E., De Gouw, J., Akagi, S. K., Urbanski, S. P., Veres, P., Roberts, J. M., Kuster, W. C., Reardon, J., Griffith, D. W. T., Johnson, T. J., Hosseini, S., Miller, J. W., Cocker, D. R., Jung, H., & Weise, D. R. (2013). Coupling field and laboratory measurements to estimate the emission factors of identified and unidentified trace gases for prescribed fires. *Atmospheric Chemistry and Physics*, 13(1), 89–116. <https://doi.org/10.5194/acp-13-89-2013>
- Yokelson, R. J., Burling, I. R., Urbanski, S. P., Atlas, E. L., Adachi, K., Buseck, P. R., Wiedinmyer,

- C., Akagi, S. K., Toohey, D. W., & Wold, C. E. (2011). Trace gas and particle emissions from open biomass burning in Mexico. *Atmospheric Chemistry and Physics*, *11*(14), 6787–6808. <https://doi.org/10.5194/acp-11-6787-2011>
- Yokelson, R. J., Saharjo, B. H., Stockwell, C. E., Putra, E. I., Jayarathne, T., Akbar, A., Albar, I., Blake, D. R., Graham, L. L. B., Kurniawan, A., Meinardi, S., Ningrum, D., Nurhayati, A. D., Saad, A., Sakuntaladewi, N., Setianto, E., Simpson, I. J., Stone, E. A., Sutikno, S., ... Cochrane, M. A. (2022). Tropical peat fire emissions: 2019 field measurements in Sumatra and Borneo and synthesis with previous studies. *Atmospheric Chemistry and Physics*, *22*(15), 10173–10194. <https://doi.org/10.5194/acp-22-10173-2022>
- Yokelson, R. J., Susott, R., Ward, D. E., Reardon, J., & Griffith, D. W. T. (1997). Emissions from smoldering combustion of biomass measured by open-path Fourier transform infrared spectroscopy. *Journal of Geophysical Research Atmospheres*, *102*(15), 18865–18877. <https://doi.org/10.1029/97jd00852>
- Young, C. J., Washenfelder, R. A., Edwards, P. M., Parrish, D. D., Gilman, J. B., Kuster, W. C., Mielke, L. H., Osthoff, H. D., Tsai, C., Pikelnaya, O., Stutz, J., Veres, P. R., Roberts, J. M., Griffith, S., Dusanter, S., Stevens, P. S., Flynn, J., Grossberg, N., Lefer, B., ... Brown, S. S. (2014). Chlorine as a primary radical: Evaluation of methods to understand its role in initiation of oxidative cycles. *Atmospheric Chemistry and Physics*, *14*(7), 3427–3440. <https://doi.org/10.5194/acp-14-3427-2014>
- Yuan, Y., Zhao, X., Wang, S., & Wang, L. (2017). Atmospheric Oxidation of Furan and Methyl-Substituted Furans Initiated by Hydroxyl Radicals. *Journal of Physical Chemistry A*, *121*(48), 9306–9319. <https://doi.org/10.1021/acs.jpca.7b09741>
- Zhao, D., Schmitt, S. H., Wang, M., Acir, I. H., Tillmann, R., Tan, Z., Novelli, A., Fuchs, H., Pullinen, I., Wegener, R., Rohrer, F., Wildt, J., Kiendler-Scharr, A., Wahner, A., & Mentel, T. F. (2018). Effects of NO<sub>x</sub> and SO<sub>2</sub> on the secondary organic aerosol formation from photooxidation of  $\alpha$ -pinene and limonene. *Atmospheric Chemistry and Physics*, *18*(3), 1611–1628. <https://doi.org/10.5194/acp-18-1611-2018>
- Zhao, X., & Wang, L. (2017). Atmospheric Oxidation Mechanism of Furfural Initiated by Hydroxyl Radicals. *Journal of Physical Chemistry A*, *121*(17), 3247–3253. <https://doi.org/10.1021/acs.jpca.7b00506>
- Zhou, X., Beine, H. J., Honrath, R. E., Fuentes, J. D., Simpson, W., & Bottenheim, J. W. (2001). Snowpack Photochemical Production of HONO: a Major Source of OH in the Arctic Boundary Layer in Springtime. *Geophysical Research Letters*, *28*, 4087–4090. <https://doi.org/10.1029/2001GL013531>
- Zhou, X., Li, W., Mabon, R., & Broadbelt, L. J. (2018). A mechanistic model of fast pyrolysis of hemicellulose. *Energy and Environmental Science*, *11*(5), 1240–1260. <https://doi.org/10.1039/c7ee03208k>
- Ziemann, P. J., & Atkinson, R. (2012). Kinetics, products, and mechanisms of secondary organic aerosol formation. *Chemical Society Reviews*, *41*(19), 6582–6605. <https://doi.org/10.1039/c2cs35122f>
- Zogka, A. G., Romanias, M. N., & Thevenet, F. (2022). Formaldehyde and glyoxal measurement deploying a selected ion flow tube mass spectrometer (SIFT-MS). *Atmospheric*

*Measurement Techniques*, 15(7), 2001–2019. <https://doi.org/10.5194/amt-15-2001-2022>

Zysman, B., & Skelly, P. D. (1992). *T*: 1992.



# **Chapter II - Experimental Setups and Methods**

## II.1 Introduction

In this thesis, the reaction of furans and methyl-substituted furanoids with nitrate radicals ( $\text{NO}_3$ ) was studied to determine the rate coefficients, to qualitatively and quantitatively characterize the products formed in gas- and particle- phases and establish the chemical mechanism of the reactions.

This chapter presents a comprehensive description of the materials and methods employed, which are divided into four major sections. The first part provides a detailed description of both atmospheric simulation chambers deployed to study the reactions and the associated analytical techniques. The second part outlines the experimental procedures, and the third section details the methods that were deployed to determine the rate coefficients, gas-phase products and SOA formed from the reactions. The final section presents an overview of the chemical compounds (commercially available/synthesized) that were used.

## II.2 The Importance of laboratory studies for understanding atmospheric chemistry

Despite advances in atmospheric chemical composition laboratory studies remain crucial for developing a fundamental understanding of atmospheric chemistry which is necessary for mitigating air quality issues, understanding climate change, and predicting future trends.

Laboratory experiments allow researchers to investigate chemical reactions or reaction systems in detail, guiding interpretation of field observations and identifying critical atmospheric reactions. Laboratory studies importantly contributed to various atmospheric chemistry areas, including oxidation mechanisms, chemical kinetics, multiphase chemistry, and measurement techniques for reactive species and oxidation products. Further research is needed on topics such as the atmospheric oxidation of VOCs, reactions of organic peroxy radicals and oxidants with organic films and particles. Moreover, the interdisciplinary collaboration and integration of laboratory data into models is of crucial importance for having a sustainable global and local environmental policy (Figure II.1) (Burkholder et al., 2017).

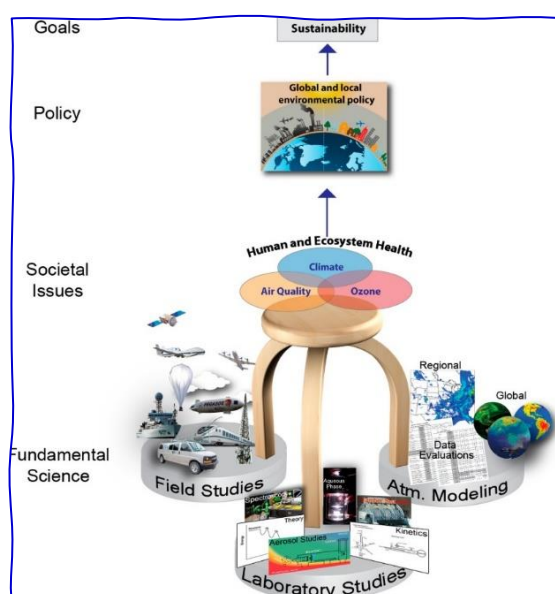


Figure II.1: Three-legged stool connecting atmospheric chemistry to sustainable policy (Burkholder et al., 2017).

## II.3 Atmospheric simulation chambers (ASC) used for atmospheric processes analysis

ASCs are reactors having volumes a few liters to tens cubic meters which provide controlled environments in which atmospheric parameters such as precursor concentrations, pressure, temperature... are regulated.

### Objective of the chambers

To address the challenges posed by the complex nature of atmosphere, ASC have been used for more than 80 years (Fuchs et al., 2021). These chambers were initially developed to generate kinetic data, branching ratios, and product distributions, with the objective of advancing our comprehension of the oxidation mechanisms that occur in the gas- and particulate- phases and improving atmospheric models (Dodge, 2000; Hynes et al., 2005). Furthermore, ASCs are employed to better assess the impacts of atmospheric pollution on air quality and climate change.

### ASC used in this study

In this thesis, two ASC were used, CHARME (Chamber of Atmospheric Reactivity and Metrology of the Environment) and THALAMOS (Thermally Regulated Atmospheric Simulation Chamber) to study the oxidation of furan and methylated furans with  $\text{NO}_3$ . CHARME is located at LPCA-ULCO, Dunkerque, France and THALAMOS at IMT-Nord-Europe, Douai, France. Studies at ambient temperature were conducted in CHARME, while temperature-dependent experiments were carried out in THALAMOS. In the following section, a detailed description of the two facilities is provided together with the corresponding analytical techniques used to meet the objectives of the current study.

## II.4 CHARME atmospheric simulation chamber

### II.4.1 Chamber presentation

CHARME is a  $9.2 \text{ m}^3$  indoor atmospheric simulation chamber of horizontally structured cylindrical shape constructed from chemically inert material, specifically electropolished stainless steel (Figure II.2). The reactor internal surface area ranges from 30 to  $32 \text{ m}^2$  and its surface to volume ratio ( $S/V$ ) is approximately  $3.5 \text{ m}^{-1}$ , which minimizes wall effects such as losses of particles and/or gas-phase species as well as heterogeneous reactions with the reactor walls. CHARME is vacuum compatible and can operate from 0.05 mbar to atmospheric pressure. Experiments within this chamber are operated at  $(298 \pm 2) \text{ K}$ .



Figure II.2: CHARME Atmospheric Simulation Chamber.

The chamber is sealed by two flanges at both ends, which enables the connection of different analytical instruments (the techniques coupled to CHARME are listed in the following sections). Moreover, inlet lines are also coupled to CHARME for the introduction of gas and particles. More details about the chamber can be found in Fayad's thesis (Fayad, 2019).

#### II.4.2 Pressure and temperature monitoring

##### Pressure monitoring

The pressure within CHARME is continuously monitored by a pressure controller comprising two Baratron capacitance manometers. One manometer (MKS Baratron 626B01MDE) measures the pressure below 1 mbar, while the other monitors the pressure up to 1100 mbar (MKS Baratron 626B13MDE). The relative uncertainty on the pressure measurement is 0.25% for both Baratron.

##### Pressure compensation

During the course of the experiments, the sampling of gas and aerosol from the various instruments leads to a pressure decrease within the chamber and this reduction was consistently counter balanced by an electronic pressure compensator (Bronkhorst model P-602C), which allows the introduction of clean air into CHARME.

##### Temperature and RH monitoring

In CHARME, the temperature and relative humidity (RH) are measured with a sensor (Vaisala HMT330 Series HUMICAP). The sensor is inserted into the chamber and a digitalized recorder is present outside the chamber for temperature and humidity follow-up. The sensor accuracy is as followed: error on temperature =  $\pm 0.2^{\circ}\text{C}$  at  $20^{\circ}\text{C}$  and error on RH =  $\pm 1\%$  between 0-90% of RH.

#### II.4.3 Reaction mixture homogenization

To ensure good homogeneity and adequate mixing of gas species and particles within CHARME, four two-blades stainless steel fans having a 50 cm diameter are situated at the bottom of the chamber. A magnetic torque motor located outside the chamber controls the

rotational speed of the fans. The rotational speed of the fans can be adjusted as a function of the input power supply, with a maximum of 330 rpm. In our experiments, the input power was 20 V resulting in a fan speed of 220 rpm. The homogenization of the mixture requires a few min (maximum of 10 min) (Figure II.3).

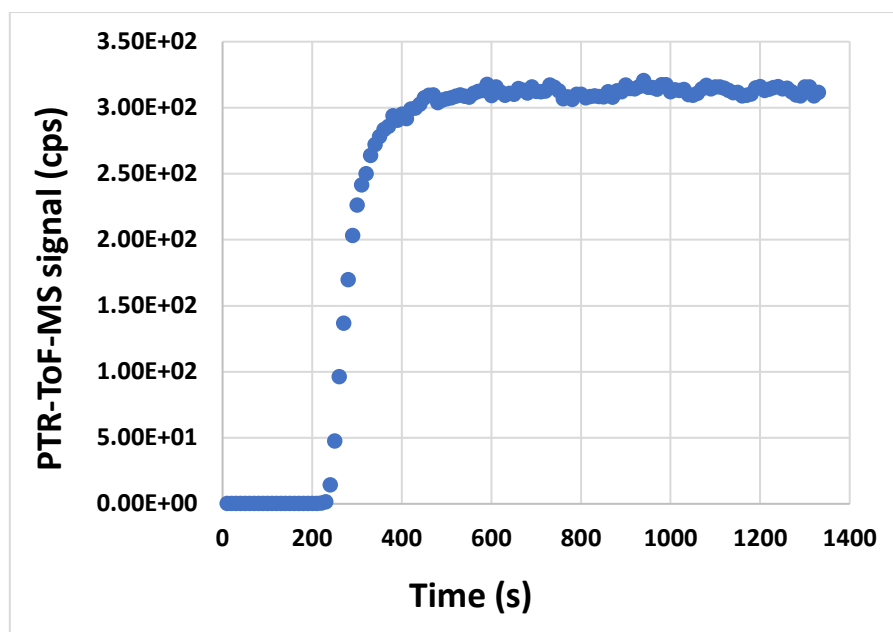


Figure II.3: Homogenization time of one of the furanoids studied (2-MF).

#### II.4.4 Cleaning protocol

Prior to each experiment CHARME was cleaned to ensure the absence of any memory effect contributing to the following experiment. To do so, CHARME was connected to a pumping system (Cobra NC0100-0300B) to pump the gas mixture of the chamber (till 4 mbar). Then, the chamber was filled till atmospheric pressure with dry/clean air at a flow rate of  $1880 \text{ L min}^{-1}$  by the utilization of an air compressor (bub-S 7,5- RENNEN SCROLLine) connected to an air generator (Parker Zander KA-MT 1-8; (total VOCs < 1 ppbv,  $\text{O}_3$  < 1ppbv,  $\text{NO}_2$  < 0.1 ppbv,  $\text{NO}$  < 1ppbv,  $\text{CO}$  < 1ppbv particles <  $0.1 \mu\text{g m}^{-3}$  and dewpoint below  $-30^\circ\text{C}$ ). Prior to each experiment, the background concentrations of gases and aerosols into CHARME were measured with the analytical instruments coupled to the chamber.

This procedure allowed to clean CHARME within 60 min and to perform between 1 to 3 experiments per day, depending on the duration of the reactions which were investigated. T

A manual cleaning of the walls of CHARME was also regularly performed with ethanol when a new series of experiments started.

In this section, the various techniques (online and offline) used for the analysis of gas- and particulate- phase species are described.

## II.4.5 Online monitoring of the gas-phase mixture using proton transfer-time of flight-mass spectrometry (PTR-ToF-MS) coupled to CHARME

### Instrument description

CHARME was coupled to a PTR-ToF-MS (Model 1000, IONICON Analytik, Innsbruck, Austria) mass spectrometer, as shown in Figure II.4.

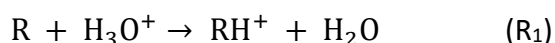


Figure II.4: Picture of the PTR-ToF-MS connected to CHARME.

A PTR-ToF-MS was used to follow the temporal evolution of the VOC concentrations within CHARME, with the goal to determine the kinetics and products of NO<sub>3</sub> reaction with furan (F), 2-methylfuran (2-MF), 3-methylfuran (3-MF), 2,5-dimethylfuran (2,5-DMF) and 2,3,5-trimethylfuran (2,3,5-TMF).

This analytical technique allows the detection and quantification of VOCs via chemical ionization through proton transfer (Lindinger et al., 1998).

The ion source of the PTR-MS is composed of a hollow-cathode discharge source that generates H<sub>2</sub><sup>+</sup>, H<sup>+</sup>, and O<sup>+</sup> ions from water vapor. These ions react with water molecules to produce hydronium ions (H<sub>3</sub>O<sup>+</sup>). The PTR-MS utilizes these hydronium ions to softly ionize VOCs through proton-transfer reaction (R<sub>1</sub>) in the drift tube (De gouw & Warneke, 2007). This ionization reaction is restricted to compounds with proton affinities (PA) that exceed that of water, which is 697 kJ/mol. Thus, air molecules (N<sub>2</sub>, O<sub>2</sub>, Ar, and CO<sub>2</sub>) do not react with H<sub>3</sub>O<sup>+</sup> and are not detected. Detection of VOCs is achieved by measuring the mass of the species plus one, provided that fragmentation does not occur (Blake et al., 2009). The proton-transfer reaction is represented by reaction (R<sub>1</sub>) where R denotes the organic compound undergoing ionization, and RH<sup>+</sup> refers to its protonated form.



Upon exiting the drift tube, the ions are directed into the ToF-MS, where they are sorted based on their mass-to-charge ratio (m/z). The transmission of ions to the ToF-MS is guaranteed through the utilization of transfer optics, which consist of a set of electrostatic lenses. These lenses enable the filtering of neutral molecules and optimization of the transmission process.

Following this, the pulsed ions are directed to the detector by a deflector comprising two pairs of deflecting plates, which adjust the path of the ion flux based on their time of flight in the ToF. The MCPs (Micro Channel Plates) constitute the detector, enabling to achieve high sensitivity. In the ToF-MS, ions with equal charges are uniformly accelerated to the same kinetic energy by an electric field and are subsequently separated based on their mass-to-charge ratio. This separation is based on the fact that ions with higher masses travel slower than ions with lower masses under the same conditions of acceleration as illustrated in Figure II.5.

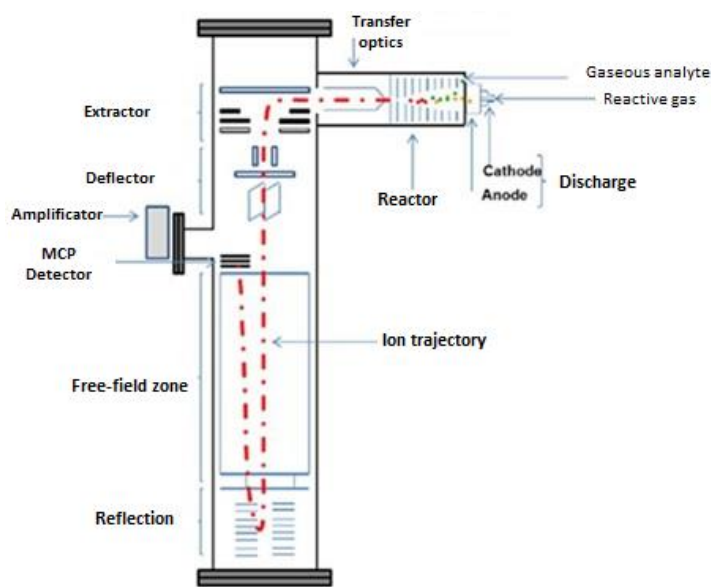


Figure II.5: Scheme of the PTR-ToF-MS and its different parts.

The PTR-ToF-MS technique offers various benefits:

- The analysis of samples without prior preparation or special treatment.
- Soft ionization leading to minimal fragmentation, and the use of air as a buffer gas due to its non-reactivity with  $\text{H}_3\text{O}^+$  ions.
- Measurement of numerous VOCs with high sensitivity (10 – 100 pptv) and rapid response time (0.1 – 10 s).

However, limitations exist (see table xx in appendix) such as:

- The inability to determine the identity of the compounds.
- The duration of the ion flight is directly proportional to their kinetic energy and, consequently, to their mass-to-charge ratio ( $m/z$ ). This implies that it is not feasible to differentiate isomers due to their identical masses.
- The ionization method used presents a significant constraint for our investigation. Organic nitrates, which may be reaction products, undergo significant fragmentations under the standard conditions of instrument operation (Müller et al., 2012).

## PTR-ToF-MS conditions used for CHARME experiments

This instrument used a heated (60°C) inlet capillary line measuring 100 cm to introduce the analyte into the system. Subsequently, this analyte was ionized in the drift tube at a pressure of 2.2 mbar, temperature of 60°C, with a drift tube field of 600 V cm<sup>-1</sup> and electric field E over the number density of air N ratio of (E/N) of 136 Td. The sampling flow was set at 50 mL min<sup>-1</sup>, and continuous VOC quantification was recorded at 10 s intervals.

For quantitative analyses, the PTR-ToF-MS was calibrated by injecting known amounts of the standard VOCs into the chamber. For standards that were not commercially available, their concentrations were theoretically determined using Eq. 1:

$$[R] = \frac{[RH^+]}{[H_3O^+]_0 kt} \quad (\text{Eq. 1})$$

with:

[R]: Concentration of the compound being measured.

[RH<sup>+</sup>]: Signal of the protonated compound.

[H<sub>3</sub>O<sup>+</sup>]: Primary ion signal.

k: The generic H<sub>3</sub>O<sup>+</sup> rate coefficient (k). An estimated value of 2×10<sup>-9</sup> cm<sup>3</sup> molecule<sup>-1</sup> s<sup>-1</sup> was used for those compounds whose experimental or theoretical data do not exist.

t: Reaction time in the drift tube.

Since the rate coefficients for the proton transfer reactions are not available for all the compounds, an estimated generic rate coefficients (k) of 2×10<sup>-9</sup> cm<sup>3</sup> molecule<sup>-1</sup> s<sup>-1</sup> was used for those compounds that lack experimental or theoretical data. The rate coefficients for the proton transfer reactions of most compounds are typically within a range of ±20 % of the estimated k.

### II.4.6 Passive sampling of the gas-phase mixture and off-line analysis with gas chromatography-electron impact mass spectrometry (GC-EI-MS)

Passive sampling methods followed by off-line analysis with GC-EI-MS methods were used to determine the chemical composition of the products formed from the gas-phase reactions of F, 2-MF, 3-MF, 2,5-DMF and 2,3,5-TMF with NO<sub>3</sub>, an information that was not easily obtained with the PTR-ToF-MS. Below are presented the three different adsorption media that were used, and the corresponding analytical techniques deployed for the analyses.

#### II.4.6.1 Adsorption on activated carbon cartridges and analysis with thermo-desorption gas chromatography-mass spectrometry (TD-GC-EI-MS)

A portable TD-GC-EI-MS instrument (HAPSITE® ER from INFICON) was connected to CHARME with a heated transfer line (40 °C) to sample VOCs (at 100 mL.min<sup>-1</sup>) with a sample volume of 100 mL. This system consists of tribed activated carbon trap, a thermal desorption system connected to an Rtx-1 MS (15 m) gas chromatograph column with nitrogen as carrier gas and internal standards for mass calibration validation. Oven temperature was programmed to run from 60°C to 180°C. The desorption temperature was set to range from 350°C to 400°C.

The targeted furan or methylated-furan was introduced into the chamber at a concentration of 2 ppmv. Then, N<sub>2</sub>O<sub>5</sub> was intermittently injected, and the resulting mixtures were analyzed



at different reaction times (before N<sub>2</sub>O<sub>5</sub> injection, at 25%, 50%, 75% and 100% of the initial furan concentration consumption).



The validation of the peaks corresponding to some of the products (maleic anhydride,  $\alpha$ -angelicalactone, and furfural) was carried out by injecting the relevant standards into the simulation chamber and confirming the peaks through their retention times. For oxidation products not commercially available, the identification was performed using the NIST Mass Spectral Database (NIST Mass Spectral Library Version 2.0 d, build Apr 26 2005). Finally, to identify the compounds not included in the NIST database, the mass spectra were also analyzed in order to propose a chemical formula to further to determine the identity of any compounds not included by the database.

#### II.4.6.2 Adsorption monotraps™

MonoTrap™ is a recently developed sorptive media that utilizes advanced silica monolith technology to provide a high surface area. The use of Monotrap is particularly suitable for the analysis of volatile and semi-volatile organic compounds, making it an attractive option for numerous applications such as quality control and environmental monitoring.

Silica monoliths possess a unique three-dimensional network of through-pores and mesopores that result in an unmatched surface area, making them highly efficient in adsorption and desorption processes. Some monotraps can be thermally desorbed and others chemically desorbed. We chose chemical desorption monotraps to avoid the extreme temperature of TD and so avoid the hypothetical degradation of thermo-fragile VOCs. To collect both polar and non-polar products, two different types of Monotrap were utilized with varying adsorption materials, where the first type (RCC18) consists solely of ODS groups (octadecylsilyl groups), and the second type (RSC18) is composed of ODS groups with activated carbon. Both monotraps are effective in adsorbing nonpolar compounds, the activated carbon type performs better in adsorbing polar compounds. The features of the two monotraps are presented in Table II.1. During sampling in the CHARME system, the monotrap was positioned on a long metallic rod (60 cm) at the center of the chamber, away from the walls, and left to adsorb for three hours.

Table II.1: Comparison of the two types of monotraps used for gaseous products sampling.

Description	Appearance	Shape	Size	Material
MonoTrap RCC18		Rod	Diameter : 2.9 mm Length : 5 mm	Active carbon and ODS function
MonoTrap RSC18		Rod	Diameter : 2.9 mm Length : 5 mm	ODS function

To extract the adsorbed compounds from the monotraps, each monotrap was placed in a separate vial, and 150  $\mu$ l of dichloromethane was injected into each insert for the two vials filled with deionized water. After placing the vials in a beaker with deionized water, ultrasonic extraction was performed for 5 min. Please note that the ultrasonic extraction process can

heat the sample, so we wait a few min until the sample cool down to avoid evaporation of VOCs during the transfer. The extracted solution was then transferred to two fresh vials that were ready for analysis. This extraction method is advised by the manufacturer (GL Sciences Inc.) and its efficiency is validated ( $\approx 100\%$ ).

#### *II.4.6.3 Passive sampling of the reaction mixture in a bubbler containing solvent*

A bubbler was also used to sample VOC. The primary objective of this sampling technique was to utilize different solvents to derivatize or dissolve gaseous products formed from the studied chemical reactions. The bubbler apparatus depicted in includes an internal tube with sintered bottom Figure II.6-b. This feature maximizes the surface area between the gas phase products and the solvent, thereby enhancing the quantity of solubilized products. It was connected to the reaction chamber on one end and a flowmeter with a KNF pump (type N811KT.18) on the other end, and the reaction mixture was continuously flushed for three hours with a flow rate of  $5 \text{ L}\cdot\text{min}^{-1}$ .

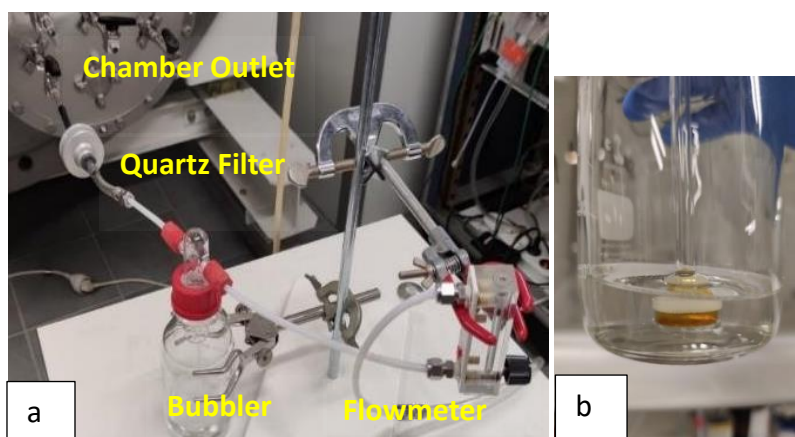


Figure II.6: (a) Picture of the sampling system composed of an aerosol filter and the bubbler (b) Picture of the bubbler containing the reactive mixture.

derivatize specific products (aldehydes), while acetonitrile was used to solubilize the products formed while preserving their structure. Regarding the derivatization reaction, when the sample is exposed to light, aldehydes undergo a photochemical reaction that converts them to their corresponding carboxylic acid forms. These acids then undergo an esterification reaction with methanol used as a solvent, resulting in the formation of ester products.

The bubbler mixture of solvent and VOCs was subsequently dried by purging it with gaseous nitrogen, reducing the volume to  $200 \mu\text{L}$ . This approach provides a comprehensive and efficient way to solubilize and collect reaction oxidation products for further analyses.

#### *II.4.6.4 GC-EI-MS used for analysis of samples collected by the monotrapp and the bubbler*

Two GC-EI-MS instruments with different types of chromatographic column were employed (Figure II.7) in order to be sure to identify as many as possible both polar and non-polar products. Samples collected by the offline techniques presented previously (monotraps & bubbler) were taken from the chamber and analyzed by these two GC-EI-MS.

An AGILENT GC-EI-MS system (6890 Series GC system-MS: 5973 Network Mass Selective Detector) equipped with a Restek RTX-624 chromatographic column was used for separating

polar compounds. The oven temperature program was set to hold at 40°C for 2 min, followed by a heating rate of 10°C/min until 250°C and then a 1-min hold at 250°C.

A Varian GC-EI-MS (Cp-3800-MS: Varian 1200 quadrupole MS/MS), equipped with an Agilent DB5MS UI chromatographic column was employed for separating non-polar compounds. The temperature program used to heat the column consisted of a 2-min hold at 70°C, followed by a heating rate of 30°C min<sup>-1</sup> until 150°C, 5°C min<sup>-1</sup> until 200°C, 4°C min<sup>-1</sup> until 310°C, and finally a 3-min hold at 310°C.

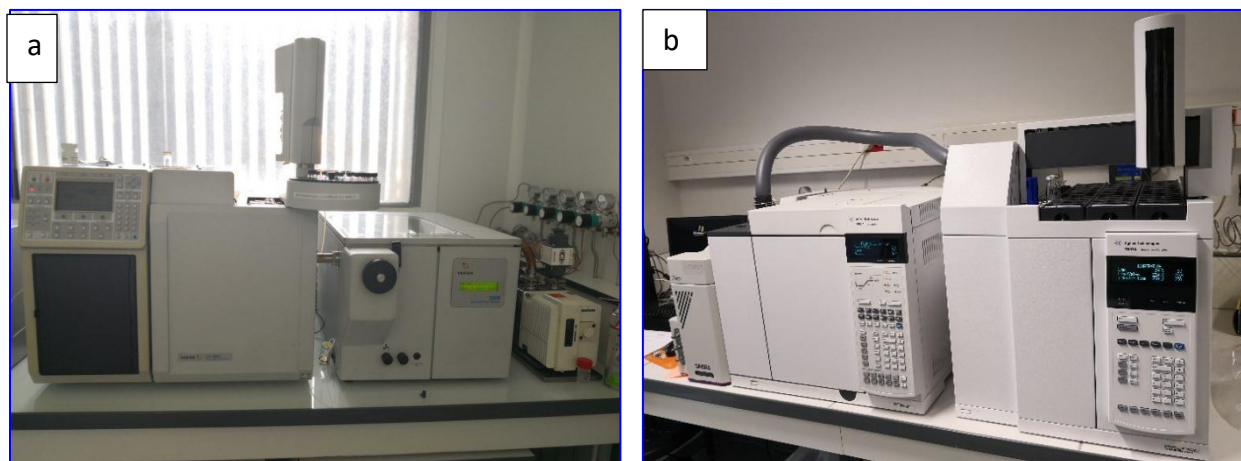


Figure II.7: The two GC-MS techniques used to analyse the samples obtained in CHARME. a: Varian GC-EI-MS, b: AGILENT GC-EI-MS.

#### II.4.7 Online monitoring of particles formation using a scanning mobility particle sizer (SMPS)

To measure the particle size distribution, a Scanning Mobility Particle Sizer (SMPS) instrument was connected to CHARME (Figure II.8) allowing the analysis of the particles resulting from the oxidation of methylated furan compounds (2-MF, 2,5-DMF and 2,3,5-TMF) with NO<sub>3</sub> radicals.

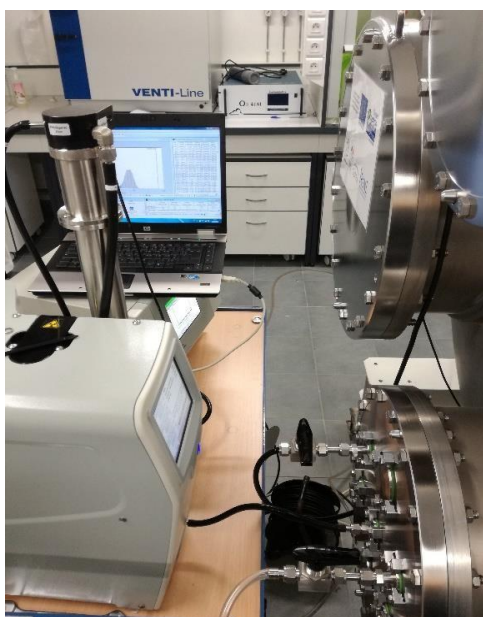


Figure II.8: The SMPS (Model 3081, TSI Inc.) and the CPC (Model 3775, TSI Inc.), coupled to CHARME.

The SMPS employs a differential mobility analyzer (Model 3081 Long DMA, TSI Inc.) to separate particles by their electrical mobility, followed by a condensation particle counter (CPC Model 3775, TSI Inc.) to count the fractionated particles by size class. To reduce electrostatic losses, a 21 cm conductive silicon sampling line from TSI Inc. was utilized to extract the particles generated from the ASC (CHARME). The extracted sample was then passed through an impactor (nozzle size = 0.0457 cm for an aerosol inlet flow of 0.2-0.8 L min<sup>-1</sup>) to remove coarse particles, i.e. captured particles exceeding its cut-off diameter. Subsequently, the sample was neutralized using an X-ray source aerosol neutralizer (model 3088) to minimize the charge level on the particles. In the SMPS, the sample is directed from the top of the system to the bottom of the DMA. The electric field generated inside the DMA is responsible for the separation of particles based on their electrical mobility. The electrical mobility of a charged particle is the velocity at which it moves in an electric field which is directly related to its diameter. The sample particles are then transported into the CPC for enumeration. This counting is presented as a particle concentration value that is displayed as the number of particles detected per cubic centimeter (# cm<sup>-3</sup>) of sampled air.

During the experimental procedures, the DMA was employed with an aerosol flow of 0.3 L min<sup>-1</sup> and a sheath flow of 3.0 L min<sup>-1</sup>. According to TSI's usage recommendations, it is recommended to work with a sheath flow ten times higher than the aerosol flow to reduce uncertainties in electrical mobility. Measurements of aerosol number size distributions were taken at intervals of 120 s over a size range spanning from 20 to 680 nm in diameter.

In order to calculate formation yields of aerosols (see section II.10.3), aerosol mass concentration measurements are necessary. Assuming particles sphericity and non-porosity, the 'Aerosol Instrument Manager<sup>®</sup>' software of the SMPS provides volume concentration (in nm<sup>3</sup> cm<sup>-3</sup>) or mass concentration (in µg m<sup>-3</sup>). The latter is obtained from the number concentration (N<sub>i</sub>) and the geometric diameter (D<sub>i</sub>) for each size class i, provided that the aerosol density (ρ) was assumed or known, according to equation Eq. 2.

$$C_m = \sum_i N_i \times \frac{\pi}{6} \times D_i^3 \times \rho \quad (\text{Eq. 2})$$

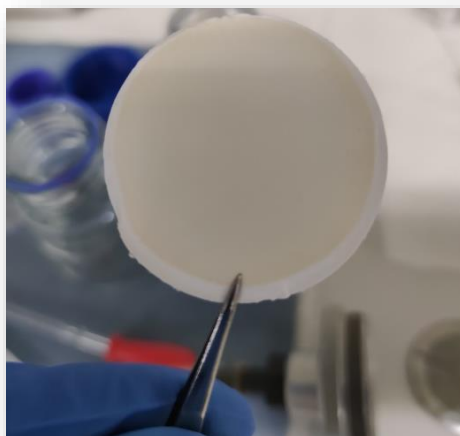
In the present work, we employed a particle density of 1 g cm<sup>-3</sup> to convert aerosol volume concentrations to mass concentrations and determine the SOA yields. Although no definitive value exists for the density of SOA resulting from the NO<sub>3</sub> reaction with furans, most published values indicate a density lower than 1.3 g cm<sup>-3</sup> (Bahreini et al., 2005; J. Wang et al., 2011).

## II.4.8 Characterization of the SOA composition using passive analytical techniques

### II.4.8.1 Quartz fiber filters

Quartz fiber filters were used to sample SOA from CHARME. These filters were then extracted and analysed to determine the SOA chemical composition. For each studied reaction (2-MF, 2,5-DMF and 2,3,5-TMF with NO<sub>3</sub>), two filters (Whatman1851-047 QMA, 47 mm diameter; see Figure II.9) were utilized to collect aerosols in parallel and were placed in filter holders

during the sampling time. To ensure the absence of any contamination, the filters were heated at 500°C for 12 h prior to sampling and stored in aluminum foil at a temperature below 4°C. Moreover, filter holders were subjected to a rigorous cleaning process by washing them three times using 99% pure dichloromethane and flushing them with N<sub>2</sub> for a duration of 15 min. To confirm the level of cleanliness of both the chamber and filters, blank filters were sampled from the chamber prior to each sampling.



*Figure II.9: Quartz filter with sampled reaction mixture (stained with yellow).*

Two different filters were sampled as they were intended to be analyzed by two different analytical techniques, ESI-LC-QToF-MSMS & ATR-IR respectively. The two filters were connected as follows:

- 1) The first filter was connected to the chamber outlet from one side immediately before the bubbler as previously illustrated in Figure II.6 (see section II.4.6.3) so that the aerosols were collected by the filter and the gaseous phase were sampled with the bubbler. Both the filter and the bubbler were connected to a pump and sampled for 3 h with a flow rate of 5 L min<sup>-1</sup>.
- 2) The second filter was connected to the chamber outlet from one side and to another pump from the other side via a filter holder. However, it was sampled with a flow rate of 11.5 L min<sup>-1</sup> since it was intended for analysis with ATR-IR and higher sampling flow was used to improve the aerosols detection on the instrument.

The aerosol extraction was performed by soaking the filter in 5 mL of acetonitrile and conducting ultrasonic extraction for 5 min. The resulting solution was filtered using a PTFE membrane (Whatman) with a pore size of 0.45 µm, and the filtrate was gradually reduced to 200 µL using a gaseous nitrogen flow to obtain a concentrated sample suitable for analysis.

There were several methods that were under consideration to investigate the composition of the particulate phase obtained from the filters. ElectroSpray Ionization - Liquid

Chromatography - Quadrupole - Time of Flight – Tandem Mass Spectrometry (ESI-LC-QToF-MS/MS) was employed as the preferred method to qualitatively assess the composition of the SOA, while the rest of the samples was preserved for future analyses using complementary techniques such as GC-EI-MS (described in section II.4.6.4) and ATR-FTIR, which would provide complementary information on the chemical composition of the particulate phase.

#### *II.4.8.2 ESI-LC-QToF-MS/MS*

The objective of using ESI-LC-QToF-MS/MS technique was to determine the products formed in the particulate phase from the reaction of 2-MF, 2,5-DMF and 2,3,5-TMF with NO<sub>3</sub>. This method allows to analyse high molecular weight organic compounds that were formed in the particulate phase. Additionally, it enables to obtain structure information on targeting of compounds by fragmentation at different energies.

ESI-LC-QToF-MS/MS is a powerful analytical technique for identifying and quantifying complex mixtures of analytes. The sample is separated in the LC system based on the column and solvent properties. The LC effluent is then ionized in the ESI source, creating charged molecules detected by the mass spectrometer. The quadrupole mass filter separates the ions based on their mass-to-charge ratio ( $m/z$ ). Accelerated ions pass through the flight tube, and their time-of-flight provides accurate mass measurements. In MS/MS, selected ions undergo fragmentation in a collision cell with a neutral gas. The second quadrupole and time-of-flight analyzer analyzes the resulting fragments for precise mass measurements.

The ESI-LC-QToF-MS/MS approach is exceptionally sensitive and can detect trace amounts of analytes in complex mixtures with high precision and accuracy. Molecular formulas were determined from exact masses selected in the spectra with mass error below 2 ppm. It has a wide range of applications in fields such as proteomics, metabolomics, pharmaceuticals, environmental analysis, and forensic science.

In this study, the solutions containing SOA obtained through acetonitrile extraction of quartz fiber filter were subjected to analysis by ESI-LC-QToF-MS/MS (Agilent LC 1100-MS 6540) using the positive ionization mode (see Figure II.10). The aim of this technique was to identify the chemical composition of the aerosol while protecting temperature-sensitive molecules and determining low and high mass products such as oligomers. To achieve this, a chromatographic column (ZORBAX Extend-C18; 50 mm long x 2.1 mm i.d., 1.8  $\mu$ m pore size) was used and thermostated at 40°C. The ESI-LC-QToF-MS/MS analyses provide mass-based identification, and the software proposes molecular formulas.

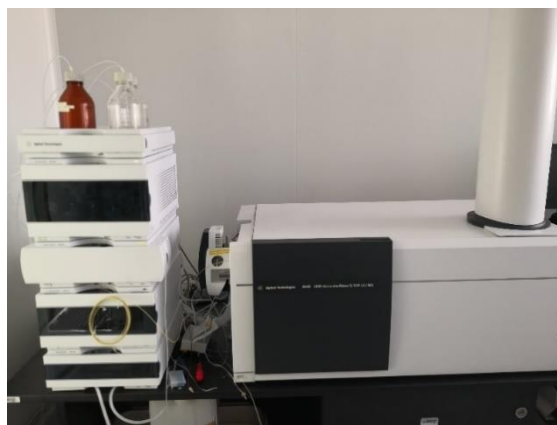


Figure II.10: ESI-LC-QToF-MS/MS instrument used for the analysis of aerosol filter samples.

#### II.4.8.3 Attenuated total reflectance-fourier transform infrared spectroscopy (ATR-FTIR)

The objective of the ATR-FTIR technique was to cross validate the product identification and to try to identify organic nitrates products if they were formed.

In the present study, an aerosol filter (II.4.8.1) was subjected to analysis using ATR-FTIR spectroscopy (Nicolet iN10 MX; Figure II.11). The analysis procedure was two-steps. The first step involves analyzing a blank filter to have the quartz + background air IR signature. In the second step, the SOA sampled filter was analyzed and the background (air and quartz) was excluded from the IR spectrum to retrieve the final IR spectrum of the aerosol. A significant advantage of this technique is that it enables examination of samples in either solid or liquid state without requiring any preparation. The technique operates on the principle of internal reflection of infrared light that passes through the crystal and gets partially absorbed by the sample. This allows for accurate characterization of the sample (Figure II.11).

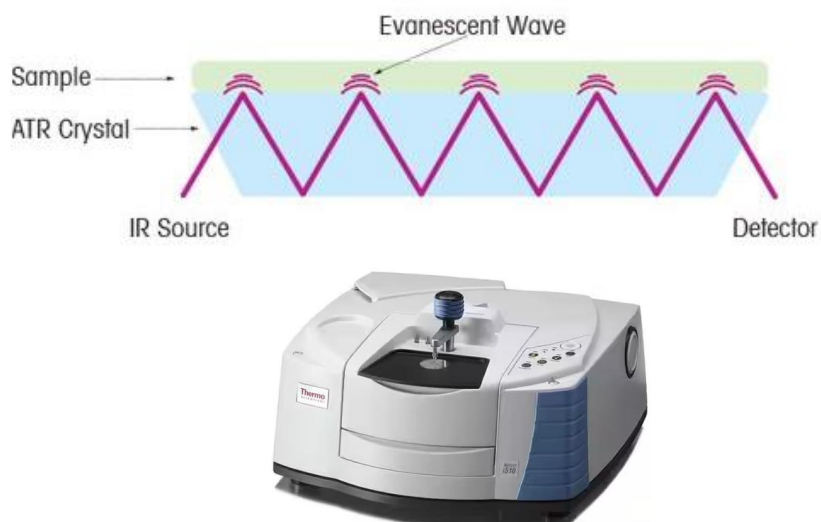


Figure II.11: Diagram and picture of ATR-Spectroscopy (Nicolet iN10 MX) used for aerosols analysis.

## II.5 THALAMOS facility

### II.5.1 Chamber presentation

The THALAMOS-ASC (Figure II.12) is a 600-L cubic Teflon reactor used to study physicochemical processes under controlled conditions. It is a Teflon chamber of cuboid shape fixed inside a 1200 L thermostatic cage (climatic box) capable of maintaining temperatures between 231 and 453 K. THALAMOS was deployed to study the temperature-dependent reaction of  $\text{NO}_3$  with F, 2-MF and 2,5-DMF (kinetics and products analysis).

The climatic box has two fans that were used to homogenize the cold/hot air in the entire box, and thus cooling (or heating) the Teflon chamber. A temperature and pressure sensor were arranged within the center of the Teflon chamber, enabling real-time monitoring of the gas mixture temperature and pressure. One of the major features of THALAMOS is that the



Figure II.12: A picture of the THALAMOS-ASC connected to one of the analytical techniques, SIFT-MS (Voice200).

temperature can be easily tuned within short time (Figure II.13) and both temperature measurements (inside Teflon chamber and the climatic box) were digitized and recorded and stored in a lab computer for further analyses. The box encompassing the Teflon chamber is opaque, thereby enabling nocturnal analysis to be conducted. To enable sampling of the reaction mixture from the chamber, a Restek Sulfinert-treated stainless steel tube was positioned at the center and back-side of the chamber.



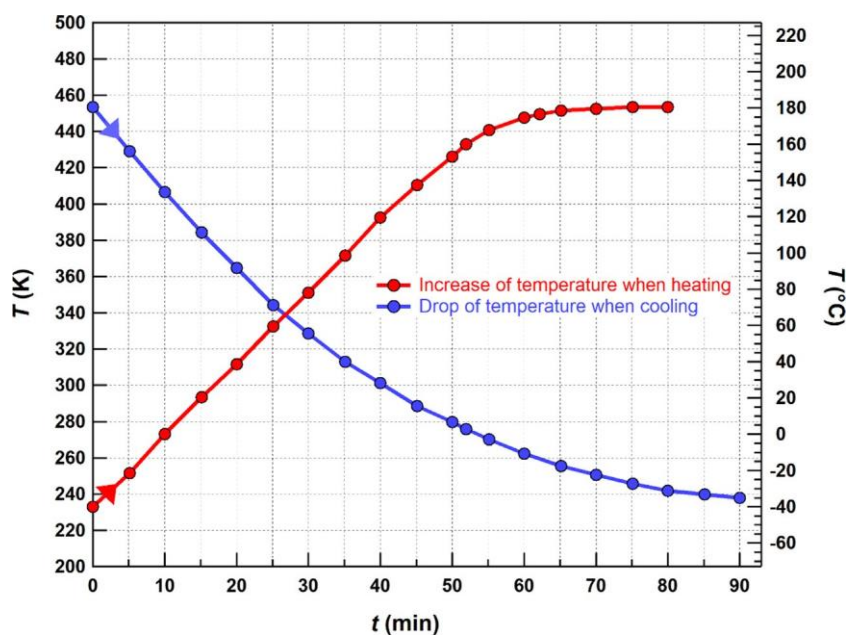


Figure II.13: Temperature dynamic in the climatic box determined under heating and cooling experiments (Osseiran et al., 2020).

### II.5.2 Reaction mixture homogenization

Four fans are installed in the Teflon chamber to ensure the homogenization of the temperature and the concentrations of gas phase species in the chamber (Osseiran et al., 2020). Two of these fans are positioned at the front and bottom-right side of the chamber, placed at a 45-degree angle immediately after the inlet port. This facilitates the efficient transport of the injected compounds into the main part of the chamber. The other two fans are situated at the back and up-left side of the chamber. Typically, less than 1 min is needed to homogenize the mixture in THALAMOS, at a temperature of 296 K. However, it should be noted that the time required for homogenization depends also on factors such as compound volatility, adsorption potential, or condensation on the chamber surface, and the temperature of THALAMOS. To ensure the well mixing in the chamber, the gas-phase concentrations of the stable species are continuously monitored in real-time using the desired analytical instrumentation. This is an experimental validation of the achievement of steady state concentrations of the different species in the chamber.

### II.5.3 Cleaning protocol and bath gas

The chamber was cleaned by continuously flushing and pumping with zero air at a constant flow rate of  $20 \text{ L min}^{-1}$  for at least 2 h. The cleaning process prevents the occurrence of any side reactions or the buildup of reactive species in the chamber, eliminating any memory effects during consecutive experiments. The experimental validation of the chamber cleaning was achieved by recording the background levels of atmospheric species previously injected / formed in the chamber with the analytical instrumentation.

During the majority of the experiments carried out in THALAMOS, the bath gas used was zero air, which was generated by an oil-free air compressor and a water removal system installed in-line. This zero air can be subjected to further purification before being delivered to the chamber. Depending on the method of purification, two different types of zero air flows can

be obtained. In the first method which was used in this work, the air was passed through a zero-air generator (AZ-2020, Claind, Italy), which operates at 673 K and facilitates the catalytic conversion of any organic compounds in the air into CO<sub>2</sub>. The relative humidity of the gas flow, determined using a temperature and relative humidity probe (HQ 210, Kimo, France), was found to be below 2% at room temperature (293 K), with an accuracy of ±1% as per the manufacturer's specifications. Alternatively, the air from the compressor was directed to a high-purification system (zero-air generator equipped with a pressure swing adsorption (PSA) device), which can eliminate VOCs, CO, CO<sub>2</sub> and further reduce the humidity levels to 2 ppm. The remaining impurity levels in the air stream are always lower than the analytical system detection limits: VOCs < 0.1 ppbV, CO<sub>2</sub> < 10 ppbV, CO < 80 ppbV and H<sub>2</sub>O ~ 2 ppmV at 293 K.

The reactants and products were monitored continuously by coupling the chamber in series with multiple detection methods presented in the following sections.

#### II.5.4 Online monitoring of the gas-phase mixture using selected ion flow tube-mass spectrometer (SIFT-MS) coupled to THALAMOS

A SIFT-MS (Voice200<sup>®</sup> manufactured by Syft Technologies in New Zealand) was deployed to follow in real-time the kinetics of the NO<sub>3</sub> reaction with F, 2-MF and 2,5-DMF as a function of temperature. In addition, SIFT-MS was used to analyze the products formed from these reactions and determine the temperature effect on the yields of the major products. SIFT-MS is a soft ionization technique where fragmentation of organic compounds is low and will allow us to validate the results obtained by the PTR-MS and to identify the products that were fragmented by the PTR-MS.

##### **General principle of the technique**

SIFT-MS is a soft chemical ionization technique that involves the chemical ionization (CI) of an analyte (A) using three reagent ions, R<sup>+</sup>: H<sub>3</sub>O<sup>+</sup>, NO<sup>+</sup>, and O<sub>2</sub><sup>+</sup>, simultaneously. The reagent ions are created by the interaction of water vapor and air in a microwave discharge. The ions created are selected by a first quadrupole mass filter (Smith & Španěl, 2005). The selected ion is then introduced into a metal cylinder within a helium carrier gas stream at a pressure of 1 Torr in the flow tube reactor. A gas sample is continuously fed into the tube with a volume (30 mL), via a heated capillary. The molecules of the sample undergo soft ionization reactions depending on their chemical properties, including proton affinity (PA) and ionization energy. The reactions between the reagent ions (R<sup>+</sup>) and the sample components (A) generates ion products (P<sup>+</sup>) and neutral products (N). All these chemical species are then directed into a second quadrupole mass filter to selectively isolate ions according to their m/z ratio. An electron multiplier detector located at the exit of the second quadrupole is utilized to measure the count rates of the ions within the desired m/z range.

Figure II.14 provides a simplified schematic representation of this instrument. It is important to note that in order to prevent any potential contamination of the sampling line and wall reactions along the flow tube, both the sampling port and flow tube of the instrument are heated to 393 K. To maintain accuracy and precision, the mass spectrometer is calibrated internally on a daily basis using a standard mixture of nine compounds provided by the manufacturer. This calibration, combined with the known reaction rate coefficients of the

precursor ions with the analytes, allows for the theoretical concentrations of any organic compound to be estimated (Španěl et al., 2013).

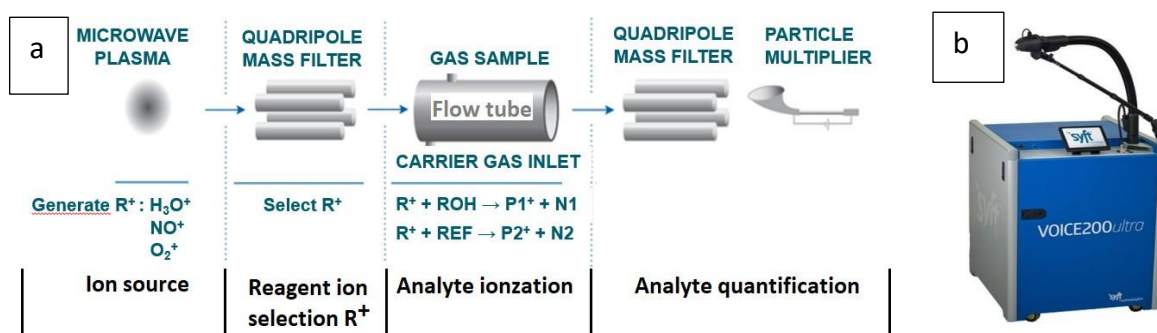


Figure II.14: (a) Simplified diagram of the SIFT-MS (b) Picture of the SIFT-MS.

### SIFT-MS in this study

In this study, the SIFT-MS was connected to THALAMOS chamber. To create a closed loop between the chamber and the analytical instruments (Figure II.15), a Teflon diaphragm pump with a flow rate of  $4 \text{ L min}^{-1}$  was utilized (Osseiran et al., 2020).

The instrument was operated at its standard mode, (i.e., He flow  $380 \text{ mL min}^{-1}$ , flow tube and sampling plate temperatures  $393 \text{ K}$ ). Further information about the instrument can be found elsewhere. In SIFT-MS the fragmentation of compounds is less probable than in PTR-ToF-MS due to the low mean kinetic energy between reactants ( $KE_{cm}$ ) values that were in the range of  $0.04$  to  $0.05 \text{ eV}$  (Zogka et al., 2022). Especially, the use of  $NO^+$  precursor ion could allow the identification of organic nitrate species, which are expected as products of our studied reactions. Therefore, complementary information can be obtained compared to the PTR-ToF-MS analysis, to thoroughly evaluate the reaction mechanism of 2-MF and 2,5-DMF degradation by  $NO_3$  radicals. The SIFT-MS sampling flow was  $10 \text{ mL min}^{-1}$  and had a negligible impact on the pressure and concentrations in the reactor over the duration of an experiment (from a few minutes to maximum one hour). The gas mixture was continuously monitored with the SIFT-MS from reactant injection to the end of the reaction.

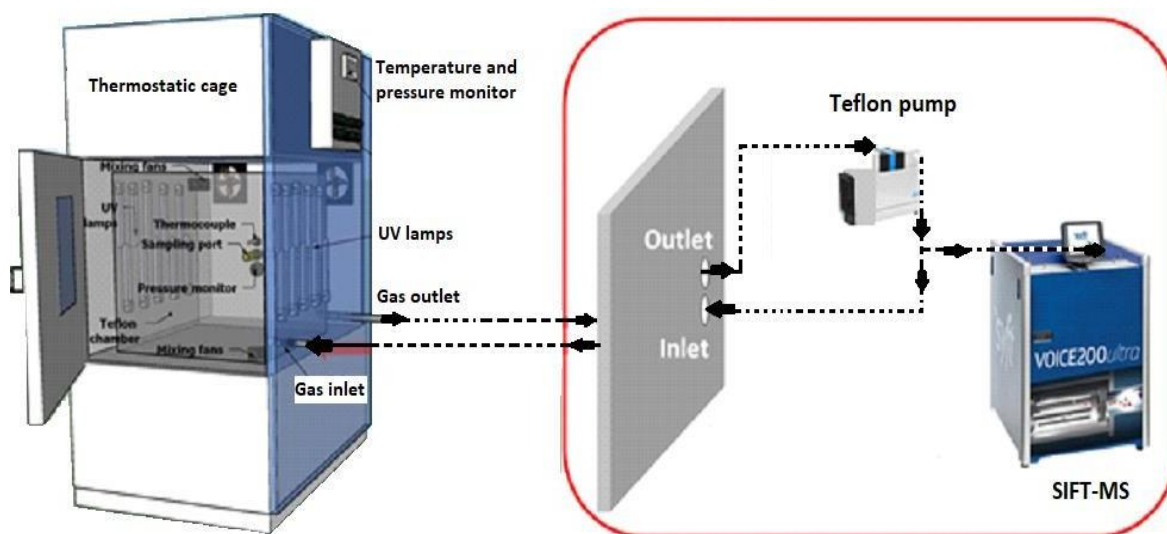


Figure II.15: Schema representing THALAMOS and the loop connecting it to the SIFT.

### II.5.5 Gas-phase active sampling using tenax cartridges & analysis with TD-GC-EI-MS/FID

In the experiments carried out on 2-MF + NO<sub>3</sub>, Tenax cartridges were used to collect samples from the chamber to check the formation of furfural as major primary product and to validate and complement the results obtained by the SIFT-MS. Tenax cartridges containing standards of 2-MF and furfural of 100 µg L<sup>-1</sup> were also prepared and analyzed using GC-FID/MS.

Tenax cartridges are cylindrical stainless-steel tubes (length = 8.8 cm, diameter = 0.6 cm) filled with Tenax adsorbent (Markes International). These cartridges are commonly used in analytical chemistry for the collection and concentration of trace amounts of VOCs from air and gas samples. The cartridges are later thermally desorbed using a TD and analyzed by GC.

To collect organic compounds, Tenax tubes were connected to THALAMOS and sampling was done at a flow rate of 200 mL min<sup>-1</sup> at the end of the reaction for a duration of ≈ 60 min.

The sampled cartridges were then analyzed with the Gas Chromatography depicted in Figure II.16. This technique comprises a thermodesorption system (PERKIN TurboMatrix 350) that is equipped with a transfer line and a GC (Agilent 6890N)-MS/FID.

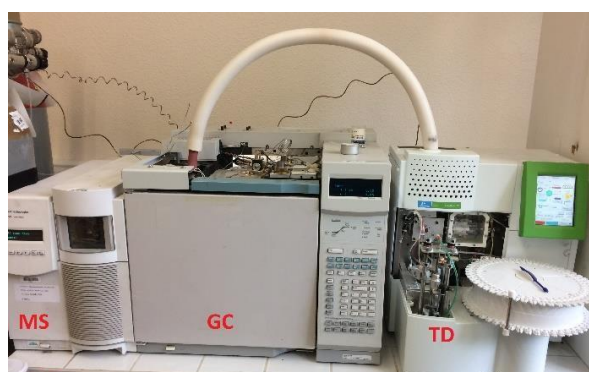


Figure II.16: TD-GC-FID/MS deployed at IMT-NORD-EUROPE.

Tenax<sup>®</sup> cartridges were then desorbed thermally in the TD for 10 min at 250°C utilizing helium gas and cryofocused in a trap that was cooled to 10°C. The trap was quickly heated to 275°C (flash heating) within a few seconds, allowing for rapid injection of the VOC into the Agilent DB-5MS chromatographic column, which measured 30 m × 320 μm × 1 μm. Separation of the compounds was accomplished using the following temperature. The oven temperature program was set to hold at 30°C for 3 min, followed by a heating rate of 10°C min<sup>-1</sup> until 200°C and then hold for 2 min for the first ramp. For ramp 2, a heating rate of 1°C min<sup>-1</sup> was used until 201°C. The total program duration was 45 min. To quantify the detected compounds, the peaks on the chromatogram obtained from the measurement with a FID were integrated after performing calibration of these peaks. Additionally, an inert mass spectrometer (Agilent 5975B MSD) was used to perform structural analysis of the eluted molecules based on their molecular mass/charge ratio. This technique is primarily employed to identify the compounds and quantify products yields.

## II.6 Fourier transform infrared spectroscopy (FTIR)

### II.6.1 FTIR located at LPCA (Dunkerque, France)

FTIR analyses were also performed since some oxidation products, like organic nitrates, are fragmented by ionization when analyzed by PTR-MS while other can be thermally degraded in GC-EI-MS analysis. The resulting spectrum can be used to identify the functional groups present in the sample, which are characteristic of specific chemical compounds, by comparing them to reference spectra of known compounds in a database.

NO<sub>3</sub> reactions of furanoids were studied within a small stainless steel cell (8 L) with in situ analysis by FTIR in order to analyze the end-oxidation products of the reactions and to evaluate the formation of organic nitrates. The setup used is depicted in Figure II.17.

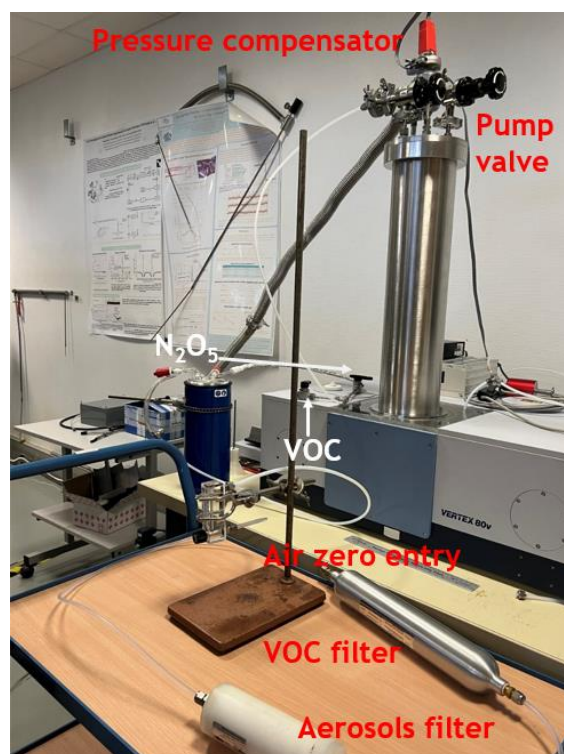


Figure II.17: FTIR setup deployed at LPCA-Dunkerque.

FTIR analyses were performed at  $298 \pm 1$  K using a FTIR spectrometer (Brucker Vertex 80v) coupled to a White-type multi-pass cell aligned on a 32 m optical-path, a KBr beam splitter and MCT detector. A more detailed description of the spectrometer is given in Cuisset et al. (2016).

Prior to each measurement, the multipath IR cell was thoroughly flushed with clean air and pumped-out ( $P < 10^{-3}$  mbar) and this process was repeated at least 3 times. Then, about 3 ppmv of a furanoid compound was introduced inside the IR cell and the system was filled with clean air till atmospheric pressure. After that, the reaction was initiated via a continuous slow flow of dry air through an  $\text{N}_2\text{O}_5$  cold trap ( $0.1 \text{ L min}^{-1}$ ). FTIR spectra were sequentially collected prior and during the reaction until the complete conversion of the furanoids compound. Each IR spectrum was collected with 200 co-added scans at  $0.5 \text{ cm}^{-1}$  resolution, in the range  $600\text{--}4000 \text{ cm}^{-1}$ .

The reaction of VOCs with  $\text{NO}_3$  radicals can be a source of SOA due to the condensation of semi-volatile oxidation products into the particle phase. In order to investigate the SOA formation potential of furan products, different analytical techniques were used.

#### II.6.2 FTIR located at IMT Nord Europe (Dunkerque, France)

Experiments were conducted in-situ in a FTIR cell (Antaris IGS, Thermo Scientific) at 500 torr pressure and room temperature (298 K) to determine the products formed from the  $\text{NO}_3$  oxidation of F, 2-MF and 2,5-DMF and cross validate the results obtained by the FTIR at LPCA. As a reminder, a major reason behind employing this technique is being a non-destructive technique and preserving the structure of the identified products.

#### Instrument illustration & experimental run

The FTIR spectrophotometer was equipped with anti-reflected coated zinc selenide transmission windows and a 10-meter path length White-cell and was linked to a liquid- $\text{N}_2$  cooled MCT detector. The cell was initially evacuated to 100 torr and flushed several times for cleaning. Thereafter filling the cell with zero air, a background spectrum was taken. Furan compound initial concentrations used were between 10 and 100 ppm.  $\text{N}_2\text{O}_5$  was then intermittently injected, and spectra were taken at quarter, half, and complete conversion of the furanoid molecule initial concentration (in experiments under a high concentration of furanoid compound (i.e., 100 ppm) the reaction was stopped after 50% conversion of the furanoid). The total pressure increase in the cell after injecting all reactants reached 500 torr. 100 IR spectra were recorded per run with  $1 \text{ cm}^{-1}$  resolution between  $600$  and  $4000 \text{ cm}^{-1}$  using Result-3 software. The objective of these experiments was to i) ensure that  $\text{NO}_3$  is dominantly reacting with the furanoids compound during the course of the reaction and suppress possible  $\text{NO}_3$  reactivity with first generation products, and ii) to identify products that could be formed even at low yields, i.e., below 5% (detection limit for most VOCs is around 2-3 ppm). To analyze and quantify the data, TQ-Analyst software (Thermo Scientific) was utilized.

## II.7 Complementarity between the analysis conducted in the two ASC (CHARME & THALAMOS) & summary of analytical techniques

A summary of the features of the ASCs utilized in this study can be found in Table II.2. Each chamber has its own set of strengths and weaknesses compared to other ASCs, based on factors such as material, shape, surface-to-volume ratio and operating temperature and pressure ranges.

Table II.2: Comparison of the features of the two atmospheric simulation chambers used (CHARME & THALAMOS).

Name	CHARME	THALAMOS
Acronym	CHamber for the Atmospheric Reactivity and the Metrology of the Environment	Thermally Regulated Atmospheric Simulation Chamber
Localization	LPCA (Dunkerque, France)	IMT Nord Europe (Douai, France)
Material	Stainless steel type 304L electropolished	Teflon
Shape	Cylindrical	Cuboid
Volume (m <sup>3</sup> )	9.2	0.6
Surface/volume (m <sup>-1</sup> )	3.5	7.6
Temperature	(296 ± 2) K	T = (231-453) K
Pressure	0.05 - 1100 mbar	Atmospheric pressure
Reference	Fayad (2019)	Osseiran et al., (2020)

The advantages and complementarity behind this collaboration were multifold. First, the use of both chambers allowed the cross validation of the kinetic and product results, enhancing the accuracy and robustness of our measurements, at least at room temperature conditions. Especially for the oxidation products, deploying two simulation chambers of different material and surface/volume ratios enables to assess whether wall losses and secondary processes contribute or not to the results. Furthermore, in CHARME, the reaction of furanoids with NO<sub>3</sub> was studied at room temperature, while THALAMOS allows to study atmospheric reactions as a function of temperature.

Finally, there was also a complementarity in the analytical techniques used to monitor the gas- and aerosol-phases. Special attention should be given for the PTR-ToF-MS, which was used for CHARME experiments, and SIFT-MS, which was used for THALAMOS experiments. In particular, with the PTR-ToF-MS, some compounds such as the organic nitrates can be fragmented and their identification with this instrument will not be possible or could lead to mislabeling of the masses observed. On the contrary, in the SIFT-MS, due to the low energy minimizing the fragmentation of these chemical species, they can be identified. Moreover, PTR-ToF-MS only use H<sub>3</sub>O<sup>+</sup> as ionisation precursor while SIFT-MS uses simultaneously three different precursors (H<sub>3</sub>O<sup>+</sup>, NO<sup>+</sup> and O<sub>2</sub><sup>+</sup>). This is greatly advantageous in the analytical analysis done especially for kinetic measurements where the rate coefficients of the reaction can be determined using all three ions, allowing us to cross validate the results between the ions, and evaluate the possible discrepancies due to uncontrolled chemical processes that can occur in the flow tube of the instrument.

Table II.3 presents a brief overview of the analytical methods used in this study to detect specific species to achieve our research objectives. The use of complementary detection techniques allowed the identification and quantification of a wide range of chemical species.

Table II.3: Comparison of the features of the two atmospheric simulation chambers used (CHARME & THALAMOS).

Instrument (Model)	Chemical species	CHARME	THALAMOS
Analytical instruments coupled to chambers			
PTR-ToF-MS, IONICON 1000	VOCs	x	
SIFT-MS Voice200 ultra	VOCs		x
TD-GC-EI-MS (Hapsite ER INFICON)	VOCs	x	
AGILENT GC-EI-MS system (6890 Series GC system-MS: 5973 Network MSD)	VOCs	x	
Varian GC-EI-MS (Cp-3800-MS: Varian 1200 quadrupole MS/MS)	VOCs	x	
PERKIN Turbo Matrix 350 Thermodesorber, GC (Agilent 6890N), FID/MS	VOCs		x
FTIR (Brucker Vertex 80v)	VOCs	x	
FTIR (Antaris IGS, Thermo Scientific)	VOCs		x
ESI-LC-QToF-MS/MS	VOCs	x	
SMPS (DMA TSI 3081, CPC TSI 3775)	Aerosols (size distribution, number concentration, mass concentration...)	x	
Aerosol generator (TSI 3076) + dryer (TSI 3062)	Particles production	x	
Ozone generator (Air Tree Ozone Technology C-L010-DTI)	O <sub>3</sub>	x	x
Conditions Monitoring Instruments			
Sensors (VAISALA HMT330) (Sensirion EK-H5 -SensorSHT75)	Humidity, Temperature	x	
Pressure controller with MK Baratron capacitance gauges (Baratron® Basics)	Pressure	x	
Platinum temperature (&pressure) sensor (PT-100, 103 Pico technology)	Temperature, Pressure		x



## II.8 Experimental protocol followed

This section presents the experimental steps / protocols followed to achieve the goals of the current study. Independently of the chamber used, the experimental methods used to investigate the kinetics or the oxidation products of the reactions was common, and are described below.

### II.8.1 Background measurement and conditions setting

After chamber cleaning, the necessary analytical instruments (PTR-ToF-MS, CPC-SMPS for CHARME & SIFT-MS for THALAMOS) were then used to measure the background concentrations of gases and particle and to make sure of the cleanliness of the chamber. After that, the environmental parameters (such as temperature, pressure and RH) were adjusted to achieve the desired objectives of each atmospheric investigation. In THALAMOS, the temperature had to be stable before injecting any species and it took a maximum a half an hour for the extreme temperatures (373-393 K) to be reached. Subsequently, the gases (such as VOCs, oxidants) and/or particles were introduced into the chambers, and their concentrations were continually monitored during the experiments.

### II.8.2 Preliminary tests

Prior to conducting a study, preliminary tests were carried out for each reactant to ensure that the PTR-MS/SIFT-MS signal exhibited linearity with respect to the VOC injected concentrations.

Additionally, the potential contribution of any degradation products to the ion peaks that were used to monitor the furan or reference compounds (in the case of the kinetic studies) was evaluated. In these experiments, each compound of interest was individually introduced into the chamber and allowed to react with  $\text{NO}_3$  until its complete consumption. Although various mass peaks were observed in the PTR-MS/SIFT-MS due to the formation of oxidation products, none of them interfered with the mass peaks that were selected to monitor the furans or reference compounds.

The effect of dilution was also considered by monitoring the signal of acetonitrile, which was introduced into the chamber (CHARME & THALAMOS) as a dilution tracer. The dilution effect was found to be negligible, at least in the timescale of the experiments.

Wall losses were also measured by injecting VOCs and letting them for a minimum of 20 min and a maximum of 1 h to be well mixed before initiating the reaction. The dark decay of the concentrations of organic compounds prior to the introduction of  $\text{N}_2\text{O}_5$  was followed to determine their wall losses in each experiment. Once the reagents achieved stable concentrations (or a steadily decreasing concentration due to wall losses), the experimental inquiry can commence by introducing the oxidant ( $\text{NO}_3$ ).

### II.8.3 Reactant injection

The physical state of the chemical species used in the current work was either solid, liquid or gaseous (see Table II.6). The way in which these species were introduced into the chamber was determined by their physical state and thus necessitating distinct methods.

## Liquid VOCs

In CHARME, liquid VOCs were injected into the chamber at room temperature and atmospheric pressure using different methods depending on the properties of the compounds. One approach involves injecting them through the chamber's inlet and flushing the line with zero air. Alternatively, the liquid may be directly injected into the vacuumed chamber, which promotes its evaporation. Another approach was used both in CHARME and THALAMOS which involves injecting a known quantity of the reactant with a micro-syringe through a septum into a glass impinger (as illustrated in Figure II.18). The impinger was flushed with a stream of purified air (2–10 L min<sup>-1</sup>) to ensure the complete injection of the compound. This method was used with the majority of the reactants except for some of them with a high boiling point (2,5-DMF, 2,3,5-TMF and Methylfurfural) where a mild heating process was required to facilitate its vaporization.

The concentration in the chamber was calculated according to the following equation (Eq. 3):

$$C \left( \frac{\text{mg}}{\text{m}^3} \right) = \frac{\text{Mass}_{\text{injected}} (\text{mg})}{\text{Volume}_{\text{chamber}} (\text{m}^3)} = \frac{\text{Volume}_{\text{injected}} (\text{L}) \times \text{density} \left( \frac{\text{mg}}{\text{L}} \right)}{\text{Volume}_{\text{chamber}} (\text{m}^3)} \quad (\text{Eq. 3})$$



Figure II.18: The impinger used to inject liquid VOCs into CHARME.

## Solid VOCs

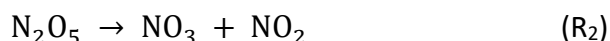
To introduce solid VOCs (maleic anhydride) into CHARME or THALAMOS, a specially designed impinger was used which was gently heated and purged with purified air to collect the vapors of the compound and drive them in the chamber (Figure II.19).



Figure II.19: The impinger used to inject solid VOCs into CHARME.

In the current study,  $N_2O_5$ , the precursor that was used for the in-situ production of  $NO_3$  radicals was in the solid state. Once the organic species have been injected and have achieved a well-mixed and stable concentration, a constant flow of  $\sim 100 \text{ mL min}^{-1}$  of gaseous  $N_2$  was flowed through the cold trap containing the  $N_2O_5$  crystals to vaporize and drive it into the chambers. To control the amount of  $N_2O_5$  injected, the temperature of the cold finger trap was kept between  $-30$  and  $-45^\circ\text{C}$  in a liquid  $N_2$  / ethanol bath, depending on the application and the chamber used.

The thermal decomposition of  $N_2O_5$  leads to the in-situ production of  $NO_3$  according to the following reaction ( $R_2$ ):



$N_2O_5$  injection was carried out either continuously during the course of the reaction, or stepwise injecting certain amounts for a certain time (5-30 s).

Calculation of  $N_2O_5$  concentration in the chamber

The concentration of  $N_2O_5$  injected can be calculated according to the following equation (Eq. 4)

$$[N_2O_5](\text{ppmv}) = \frac{F(N_2) \times (P(N_2O_5) \times t \times 1000000)}{V_{\text{chamber}} \times (760 - P(N_2O_5))} \quad (\text{Eq. 4})$$

where  $F(N_2)$  ( $\text{m}^3 \text{ min}^{-1}$ ) is the nitrogen gas flow flushing the trap,  $P(N_2O_5)$  is the vapor pressure of  $N_2O_5$ ,  $t$  is the time of sample flushing to the chamber and  $V_{\text{chamber}}$  ( $\text{m}^3$ ) is the volume of the chamber. Vapor pressure at different temperatures were retrieved from (Liley et al., 1999).

### Particle injection

In CHARME, the production of seed particles, such as ammonium sulfate ( $(NH_4)_2SO_4$ ), was performed using an atomizer (TSI 3076), as illustrated in Figure II.20. The atomizer was used to nebulize a solution of 0.015 M at a flow rate of  $3 \text{ L min}^{-1}$ , using dry pure nitrogen at a pressure of 2 bar. After nebulization, the particles were dried through a diffusion dryer (TSI 3062) filled with silica gel and then introduced into the chamber.

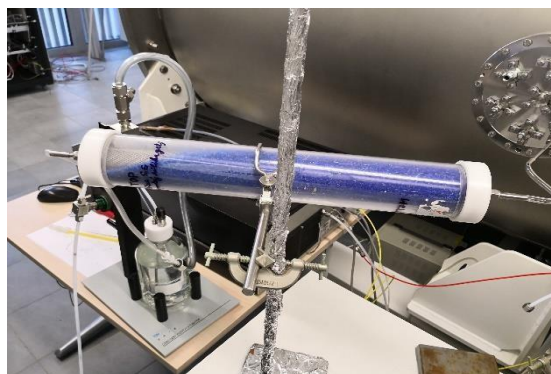


Figure II.20: Setup (consisting of an atomizer and a dryer) utilized to introduce seed particles into CHARME.

#### II.8.4 Reaction analysis

During the course of the experiments, the evolution of the gas mixture was recorded either in real time or using passive methods of analysis, that were attached to the chamber as previously described.

**For the ambient temperature kinetics experiments**, in order to ensure the accuracy and reliability of the measurements, two to three reference compounds were employed for each furan compound, and a minimum of three experiments were performed per reference. Various concentrations of furans and references were utilized, ranging between several hundred ppbv and several thousand ppbv.

$\text{N}_2\text{O}_5$  was introduced into the chamber continuously until a consumption of at least 98% was achieved for both the furan and reference compounds. However, for 2-MF, the relative rate plots were constrained within a consumption range of 50-80% due to the non-linear nature of the plots beyond this range. These measures were taken to ensure accurate and reliable data interpretation, excluding the possible contribution of secondary products to the PTR-MS signal of 2-MF and reference molecules. These experimental conditions were carefully selected to achieve optimal accuracy in the rate coefficient measurements. The references used in this study and their rate coefficients with  $\text{NO}_3$  (in units of  $\text{cm}^3 \text{ molecule}^{-1} \text{ s}^{-1}$ ) were:  $k(\alpha\text{-terpinene}) = (1.82 \pm 1.04) \times 10^{-10}$  (Atkinson, Aschmann, Winer, & Pitts, 1985),  $k(\gamma\text{-terpinene}) = (2.94 \pm 0.81) \times 10^{-11}$  (Atkinson, Aschmann, Winer, & Pitts, 1985),  $k(\alpha\text{-pinene}) = (6.20 \pm 1.42) \times 10^{-12}$  (IUPAC, 2016),  $k(\beta\text{-pinene}) = (2.50 \pm 0.69) \times 10^{-11}$  (IUPAC, 2016),  $k(2\text{-methyl-2-butene}) = (9.38 \pm 0.47) \times 10^{-12}$  (Atkinson et al., 1988), and  $k(2,3\text{-dimethyl-2-butene}) = (4.50 \pm 0.40) \times 10^{-11}$  (Lancar et al., 1991). Except for 2,3-dimethyl-2-butene, for all the other reference molecules the rate coefficients values used were IUPAC recommended. Table II.4 and Table II.5 present a comprehensive list of ion peaks that were chosen to monitor the concentration profiles of both the studied furanoids and the references with PTR-ToF-MS and SIFT-MS.

Table II.4: Ions selected on the PTR-ToF-MS to monitor the concentration profiles of the compounds used in the current study.

Compound	Product ions used	Mass-to-charge ratio (m/z)
Furan	C <sub>4</sub> H <sub>5</sub> O <sup>+</sup>	69
2-methylfuran	C <sub>5</sub> H <sub>6</sub> OH <sup>+</sup>	83
3-methylfuran	C <sub>5</sub> H <sub>6</sub> OH <sup>+</sup>	83
2,5-dimethylfuran	C <sub>6</sub> H <sub>8</sub> OH <sup>+</sup>	97
2,3,5-trimethylfuran	C <sub>7</sub> H <sub>10</sub> OH <sup>+</sup>	111
α-pinene	C <sub>10</sub> H <sub>17</sub> <sup>+</sup>	137
β-pinene	C <sub>10</sub> H <sub>17</sub> <sup>+</sup>	137
α-terpinene	C <sub>10</sub> H <sub>17</sub> <sup>+</sup>	137
γ-terpinene	C <sub>10</sub> H <sub>17</sub> <sup>+</sup>	137
2,3-dimethyl-2-butene	C <sub>6</sub> H <sub>12</sub> H <sup>+</sup>	86
2-methyl-2-butene	C <sub>5</sub> H <sub>10</sub> H <sup>+</sup>	71

**For the temperature dependent kinetic measurements**, due to the scarcity of literature on the temperature-dependent rate coefficients of VOCs reacting with NO<sub>3</sub>, a maximum of two references per furan compound studied were used. For each temperature investigated, a minimum of two experiments were conducted, with the concentration of the targeted furans and reference ranging between 0.8 ppmv and 11 ppmv.

The absence of reliable temperature kinetic measurements as a function of temperature was among the most challenging aspects of the kinetic measurements. To overcome this, cyclohexene was used as a base molecule, due to the satisfactory agreement between the data available in the literature. This compound was used to cross validate the rate coefficients of other reference molecules, α-pinene, and 2-carene, before measuring the T dependence of F, 2-MF, and DMF. Further information is provided in results section.

Table II.5: Ion intensities selected on SIFT-MS to monitor the concentration profiles of the compounds used in the current study.

Compound	Product ions monitored	Mass to Charge Ratio (m/z)	Precursor ion
Furan	C <sub>4</sub> H <sub>5</sub> O <sup>+</sup>	69	H <sub>3</sub> O <sup>+</sup>
	C <sub>4</sub> H <sub>4</sub> O <sup>+</sup>	68	NO <sup>+</sup>
	C <sub>4</sub> H <sub>4</sub> O <sup>+</sup>	68	O <sub>2</sub> <sup>+</sup>
2-methylfuran	C <sub>5</sub> H <sub>6</sub> OH <sup>+</sup>	83	H <sub>3</sub> O <sup>+</sup>
	C <sub>5</sub> H <sub>6</sub> O <sup>+</sup>	82	NO <sup>+</sup>
	C <sub>5</sub> H <sub>6</sub> O <sup>+</sup>	82	O <sub>2</sub> <sup>+</sup>
2,5-dimethylfuran	C <sub>6</sub> H <sub>8</sub> O.H <sup>+</sup>	97	H <sub>3</sub> O <sup>+</sup>
	C <sub>6</sub> H <sub>8</sub> O <sup>+</sup>	96	NO <sup>+</sup>
	C <sub>6</sub> H <sub>6</sub> O <sup>+</sup>	96	O <sub>2</sub> <sup>+</sup>
α-pinene	C <sub>10</sub> H <sub>17</sub> <sup>+</sup>	137	H <sub>3</sub> O <sup>+</sup>
	C <sub>10</sub> H <sub>16</sub> <sup>+</sup>	136	NO <sup>+</sup>
	C <sub>7</sub> H <sub>9</sub> <sup>+</sup>	93	O <sub>2</sub> <sup>+</sup>
cyclohexene	C <sub>6</sub> H <sub>10</sub> H <sup>+</sup>	83	H <sub>3</sub> O <sup>+</sup>
	C <sub>6</sub> H <sub>16</sub> <sup>+</sup>	82	NO <sup>+</sup>
	C <sub>5</sub> H <sub>7</sub> <sup>+</sup>	67	O <sub>2</sub> <sup>+</sup>

$\gamma$ -terpinene	$C_{10}H_{17}^+$	137	$H_3O^+$
	$C_{10}H_{16}^+$	136	$NO^+$
	$C_7H_9^+$	93	$O_2^+$
2-carene	$C_{10}H_{17}^+$	137	$H_3O^+$
	$C_{10}H_{16}^+$	136	$NO^+$
	$C_9H_{13}^+$	121	$O_2^+$

**To qualitatively and quantitatively determine reaction products**, a minimum of five experiments were done per furan compound studied. In particular, the targeted furan compound was injected at a concentration range of 300-2000 ppbv and then  $N_2O_5$  was injected continuously until total consumption of the reactant. The evolution of the gas mixture was recorded in real-time with the PTR-ToF-MS or the SIFT-MS in CHARME and THALAMOS, respectively. This approach allowed us to correlate furanoid consumption with product formation, and finally determine the yields, when possible, of the products formed (see also section II.10.2).

Complementary, in THALAMOS, product characterization was done by injecting  $\approx 2$  ppmv of F/2-MF/2,5-DMF while injecting  $N_2O_5$  stepwise in the chamber. Mass scans of the reaction mixtures were recorded by the SIFT-MS after each  $N_2O_5$  injection in order to identify the products formed, in the mass range from 30 to 200 amu, focusing on the formation of organic nitrates.

In certain experiments, it could be advantageous to collect gaseous and particulate compounds using different sampling methods. In CHARME, at the end of the reaction, i.e., after complete consumption of the furanoids, sampling methods using adsorbents (monotrap and bubbler) were used to sample the gas phase products and further analyze them with GC-EI-MS. Quartz fiber filters were used for particle collection as detailed in previous sections. In THALAMOS, Tenax cartridges were used as sampling supports for the investigation of the oxidation products formed from the reaction between 2-MF and  $NO_3$ .

## II.9 Materials

In this study, most of the materials used were commercially available with stated purity and were used as purchased, except dinitrogen pentoxide ( $N_2O_5$ ) which was used as precursor molecule for  $NO_3$  radicals and which was synthesized. It is worth mentioning that  $NO_3$  in situ synthesis (through  $NO_2 + O_3$  in the chamber) was tried but abandoned as some VOCs were reacting with  $O_3$ , so having  $N_2O_5$  was necessary. This section provides the list of the materials directly used (II.9.1) and detailed description of the  $N_2O_5$  synthesis in the second part (II.9.2).

### II.9.1 Materials used

To carry out the experiments, a range of chemical compounds in solid, liquid, and gas states, without further purification were used. The complete list of chemicals employed in our study can be found in Table II.6. Moreover, during simulation experiments, pure air served as the matrix and carrier gas, with low levels of relative humidity (RH lower than 2%), and a dew-point below  $-30^\circ C$ .

Table II.6: List of the chemicals used in the experiments, their molar mass, physical state, manufacturer, and the corresponding purity.

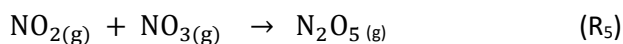
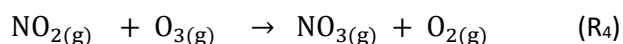
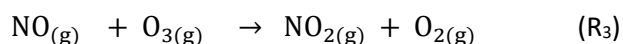
Precursor	Molar Mass (g/mol)	Physical State	Manufacturer	Purity (%)
Acetonitrile <sup>1,2</sup>	41.05	Liquid	Sigma-Aldrich	99.5
Nitrogen monoxide <sup>1</sup>	30.01	Gas	Praxair	99.99
Nitrogen dioxide <sup>2</sup>	46.01	Gas	Not known	>99
Oxygen <sup>1</sup>	31.99	Gas	Praxair	99.5
Furan <sup>1</sup>	68.07	Liquid	Sigma-Aldrich	>99
2-methylfuran <sup>1,2</sup>	82.10	Liquid	Sigma-Aldrich	99
3-methylfuran <sup>1,2</sup>	82.10	Liquid	Sigma-Aldrich	98
Cyclohexene <sup>2</sup>	82.14	Liquid	Sigma-Aldrich	99
2,5-dimethylfuran <sup>1,2</sup>	96.13	Liquid	Sigma-Aldrich	99
2,3,5-trimethylfuran <sup>1,2</sup>	110.15	Liquid	Sigma-Aldrich	99
$\alpha$ -pinene <sup>1,2</sup>	136.23	Liquid	ACROS Organics	98
$\beta$ -pinene <sup>1</sup>	136.23	Liquid	TCI	>94
$\alpha$ -terpinene <sup>1</sup>	136.23	Liquid	Sigma-Aldrich	>95
$\Gamma$ -terpinene <sup>1,2</sup>	136.23	Liquid	Sigma-Aldrich	97
2-methyl-2-butene <sup>1</sup>	70.13	Liquid	Sigma-Aldrich	>99
2,3-dimethyl-2-butene <sup>1</sup>	84.2	Liquid	Sigma-Aldrich	98
$\alpha$ -angelicalactone <sup>1</sup>	98.10	Liquid	Alfa Aesar	98
Maleic anhydride <sup>1</sup>	98.06	Solid	Sigma-Aldrich	>99
Furfural <sup>1,2</sup>	96.08	Liquid	Sigma-Aldrich	99
5-methylfurfural <sup>1,2</sup>	110.11	Liquid	Thermo Scientific	>98
2-carene <sup>2</sup>	136.23	Liquid	Sigma-Aldrich	97
Ammonium sulfate <sup>1</sup>	132.12	Solid	MERCK	

<sup>1</sup> Chemicals used for manipulations done in CHARME.

<sup>2</sup> Chemicals used for manipulations done in THALAMOS.

## II.9.2 Synthesis of N<sub>2</sub>O<sub>5</sub> crystals

Dinitrogen pentoxide (N<sub>2</sub>O<sub>5</sub>) was used as a precursor of nitrate radicals (NO<sub>3</sub>). It was synthesized ex-situ in a glass reactor under flow conditions and atmospheric pressure, either through the consecutive reactions (R<sub>3</sub>-R<sub>5</sub>) or through the reactions (R<sub>4</sub>-R<sub>5</sub>) depending on using nitrogen monoxide (NO) or nitrogen dioxide (NO<sub>2</sub>) as a precursor source of NO<sub>x</sub>.



In reaction (R<sub>3</sub>), NO reacts with an excess of O<sub>3</sub> to form NO<sub>2</sub> and in reaction (R<sub>4</sub>), NO<sub>2</sub> then reacts with O<sub>3</sub> to produce NO<sub>3</sub>. N<sub>2</sub>O<sub>5(g)</sub> was then synthesized from the reaction (R<sub>5</sub>) between NO<sub>2</sub> and NO<sub>3</sub>.

In CHARME N<sub>2</sub>O<sub>5</sub> was formed in a 2.5 m S-shaped glass tube (diameter 2 cm) and in THALAMOS in a 1 m glass tube (diameter 4 cm) as shown in Figure II.21.

The process of producing N<sub>2</sub>O<sub>5</sub> involves the following experimental steps:

1. Drying of the  $\text{N}_2\text{O}_5$  synthesis setup (i.e the glass tube and the cold finger trap) (Figure II.21) for 24 h by heating and purging it with gaseous  $\text{N}_2$  /dry air in order to eliminate the humidity and avoid the heterogeneous hydrolysis reactions on the walls that transform  $\text{NO}_2$  to HONO, or  $\text{N}_2\text{O}_5$  to nitric acid ( $\text{HNO}_3$ ).
2. Introduction of NO (or  $\text{NO}_2$ ) and purging the system for a few min (2-3 min).
3. Production of  $\text{O}_3$  was from pure oxygen ( $\text{O}_2$ ) through a Corona discharge ozone generator (Air Tree Ozone Technology, C-Lasky C-010-DTI) and introduction into the system in excess to the nitrogen oxide.
4. Preparation of the liquid nitrogen / ethanol bath in a Dewar at a temperature ranging from 188 to 193 K, to trap white  $\text{N}_2\text{O}_5$  crystals (Figure II.21-C).  $\text{N}_2\text{O}_5(\text{s})$  was collected and used directly or stored in a freezer (either at 193 K or at 253 K for a few days before being used).



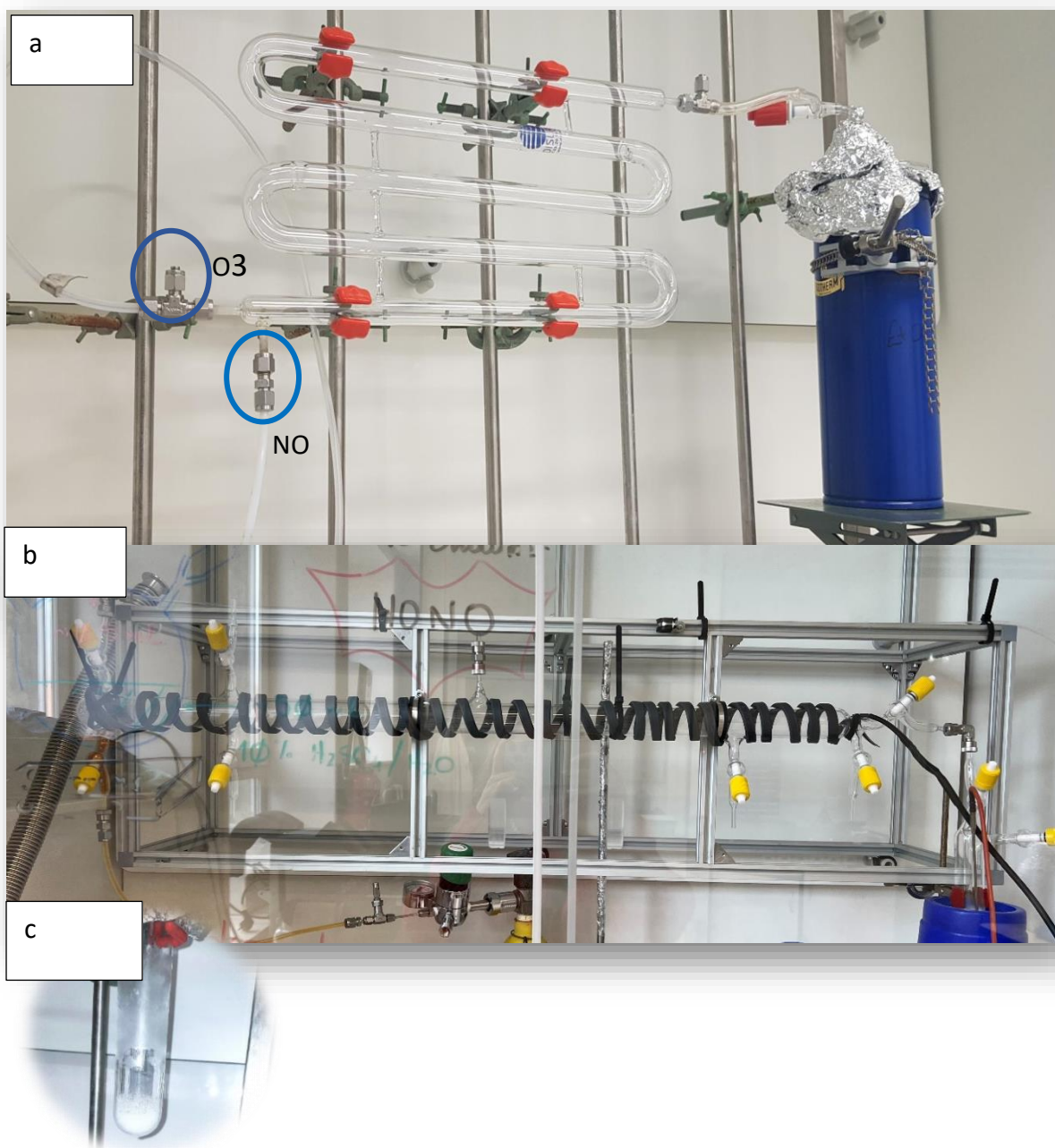


Figure II.21:  $N_2O_5$  synthesis setups. (A) Setup used for CHARME experiments: S-shaped glass tube measuring 2.5 m in length and 2 cm in diameter. (B) Setup used for THALAMOS experiments: glass tube measuring 1 m in length and 4 cm in diameter. (C) Collection of  $N_2O_5$  crystals.

The purity of the  $N_2O_5$  crystals produced was verified by FTIR analysis. Figure II.22 shows the FTIR spectra of  $N_2O_{5(s)}$  validating the purity of this compound.

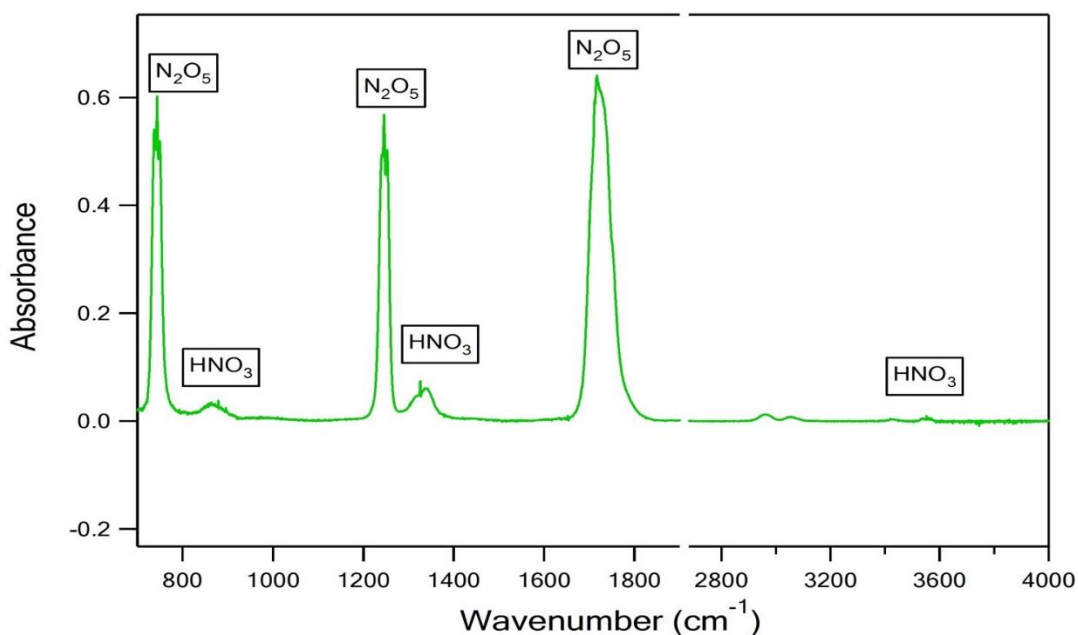


Figure II.22: FTIR spectrum of the synthesized  $N_2O_5$  crystals.

## II.10 Methodology

### II.10.1 Determination of rate coefficients

#### II.10.1.1 Relative rate method

The rate coefficient of a reaction can be determined by deploying either absolute or relative rate methods. The absolute method requires to monitor (at least) one of the reactant concentrations versus the time during the course of the reaction. It is a challenging kinetic measurement method, especially when highly reactive species are present, such as radicals. On the contrary, the relative rate method (RR) is a well-established approach used in chemical kinetics that does not require the determination of the absolute concentration of the reactants. This method permits determining the unknown rate coefficient of a compound ( $k_1$  of (R<sub>6</sub>)) relative to a compound with a known  $NO_3$  rate coefficient ( $k_2$  of (R<sub>7</sub>)). The VOC of interest and reference compound react simultaneously with the oxidant (Ox).



$$-\frac{d[VOC]}{dt} = k_1[VOC][Ox] \quad (Eq. 5)$$

$$-\frac{d[Ref]}{dt} = k_2[Ref][Ox] \quad (Eq. 6)$$

The division of Eq. 5 by Eq. 6 results in the cancellation of the concentration term of Ox, thereby yielding a single expression Eq. 7.

$$\frac{1}{k_1} \frac{d[VOC]}{[VOC]} = \frac{1}{k_2} \frac{d[Ref]}{[Ref]} \quad (Eq. 7)$$

The integration of Eq. 7 gives Eq. 8:

$$\ln \frac{[\text{VOC}]_0}{[\text{VOC}]_t} = \frac{k_1}{k_2} \ln \frac{[\text{Ref}]_0}{[\text{Ref}]_t} \quad (\text{Eq. 8})$$

The variables  $[\text{VOC}]_0$  and  $[\text{Ref}]_0$  represent the initial concentrations of the VOC under investigation and the reference compound, respectively. On the other hand,  $[\text{VOC}]_t$  and  $[\text{Ref}]_t$  refers to the concentrations of the VOC and reference at a given time  $t$ .

In addition to reactions ( $R_6$ ) and ( $R_7$ ), there may be other secondary loss processes ( $R_8$ ) and ( $R_9$ ) occurring simultaneously. For example, VOC and Ref deposition onto the reactor walls may also contribute to the disappearance of the compounds, which cannot be disregarded. To account for these effects, we denote  $k_w$  and  $k_w'$  as the total loss rate coefficient for VOC and Ref, respectively.



The update of equation Eq. 8 will be done as described in Eq.9:

$$\ln \left( \frac{[\text{VOC}]_0}{[\text{VOC}]_t} - k_w t \right) = \frac{k_1}{k_2} \ln \left( \frac{[\text{Ref}]_0}{[\text{Ref}]_t} - k_w' t \right) \quad (\text{Eq. 9})$$

Plotting the first vs last terms of Eq. 8 or Eq. 9 (depending on the need to take secondary losses into account) and extracting the slope through a linear fitting of the experimental results, allows the determination of the relative ratio  $\frac{k_1}{k_2}$ . Then, the rate coefficient of the reaction of interest,  $k_1$ , can be determined by utilizing the known rate coefficient,  $k_2$ , for the reaction between the reference compound (Ref) and (Ox).

For each furan compound, the final value of  $k$  ( $k_{\text{average}}$ ) was obtained by averaging the  $k$  values measured with the different references.

To perform the relative kinetics method, it is important to choose a reference compound that exhibits a reactivity that is similar to that of the compound being studied. This selection ensures that both compounds are consumed at nearly identical rates and improves the precision of the rate coefficient determination. It is also essential that the reference does not act as a precursor or product of the targeted VOC. To improve the accuracy in the determination of the rate coefficient value, it is better if the reference compound has undergone multiple determinations that produce consistent results, or it has been evaluated by the IUPAC or NASA JPL panels.

### *II.10.1.2 Error analysis*

This section provides a detailed explanation of the potential uncertainties that may arise from the kinetic measurements done both in CHARME & THALAMOS.

For experiments done in CHARME, the uncertainty of the measured rate coefficient ( $\Delta k_1$ ) was calculated by considering the slope ( $b$ ) and the known reference rate coefficient ( $k_2$ ) with their corresponding uncertainties ( $\sigma$ ) and  $\Delta k_2$ , respectively, using Eq. 10.

$$\Delta k_1 = \sigma \times k_2 + b \times \Delta k_2 \quad (\text{Eq. 10})$$

The standard deviation ( $\sigma$ ) obtained from the least squares linear regression of the data represents the uncertainty associated with the slope. The uncertainty of the determined rate coefficients considers both the measurement error and the uncertainty associated with the value of the reference rate coefficient.

The final average uncertainty  $\Delta k_{\text{average}}$  (standard error of the mean) was calculated using Eq. 11, where the rate coefficient is denoted by  $k_i$ , while the uncertainty associated with it is represented by  $\Delta k_i$ . These values are determined for each experiment, and  $n$  represents the total number of experiments (Grira et al., 2020 ;Al Ali et al., 2022).

$$\Delta k_{\text{Average}} = \sqrt{\frac{\sum_{i=1}^n (\Delta k_i)^2}{n}} \quad (\text{Eq. 11})$$

In THALAMOS, for the temperature-dependent kinetics experiments, the error on the measured rate coefficient was  $2 \times$  standard deviation of linear regression and the error on the final rate coefficient is standard deviation of the average.

### II.10.2 Quantification of the products yields

The yields of the primary oxidation products ( $Y_P$ ) formed from the gas-phase reaction of furan compounds with  $\text{NO}_3$  radicals were determined by plotting the concentration of the primary products  $[P]$  against the consumed concentration of the furans  $\Delta[\text{Furanoid}]$ , according to Eq. 12.

$$Y_P = \frac{[P]}{\Delta[\text{Furanoid}]} \times 100 \quad (\text{Eq.12})$$

In principal, the plot of this equation is linear (if no secondary processes occur), with the slope corresponding to the formation yield of the primary oxidation product. However, for the primary products that were consumed to form secondary products, the formation yields were determined from the slope of the linear portion of the plot which typically occurs during the first min of the reaction. The products concentrations were not corrected for their losses due to the  $\text{NO}_3$  reaction due to the absence of the rate coefficient.

### II.10.3 Determination of SOA yields

The yield of secondary organic aerosols ( $Y_{\text{SOA}}$ ) is a critical parameter for making comparisons between different organic compounds, as it provides information about their potential to generate particles. The definition of SOA yield ( $Y_{\text{SOA}}$ ) is given by Eq. 13.  $M_{\text{SOA,corr}}$  corresponds to the SOA mass concentration corrected for wall losses. The VOC concentration  $[\text{VOC}]$  was followed using the PTR-ToF-MS and the reacted VOC concentration  $\Delta[\text{VOC}]$  was determined ( $\Delta[\text{VOC}] = [\text{VOC}]_0 - [\text{VOC}]_t$ ).

$$Y_{\text{SOA}}(\%) = \frac{M_{\text{SOA,corr}}}{\Delta[\text{VOC}]} \times 100 \quad (\text{Eq. 13})$$

The slope of ( $M_{\text{SOA,corr}} = f(\Delta[\text{VOC}])$ ) represents the formation yield of SOA ( $Y_{\text{SOA}}$ ). To account for particle losses on the chamber walls, the SOA mass concentrations measured with the SMPS ( $M_{\text{SOA,exp}}$ ) were corrected using Eq. 14.  $k_L$  corresponds to the SOA wall losses measured in

CHARME at the end of each reaction when NO<sub>3</sub> radicals were totally consumed. The SOA wall losses followed a first-order decay.

$$M_{\text{SOA,corr}} = M_{\text{SOA,exp}}(1 + k_L \times t) \quad (\text{Eq. 14})$$

A widely-used semi-empirical model based on absorptive gas-particle partitioning of semi-volatile products ((Odum et al., 1996) and (Pankow, 1994)) simplifies the reaction system by assuming that the reactions lead to the production of a sum of products that are distributed between the particulate and gas phases. It requires knowledge of the SOA formation yield (Y), which is a fundamental feature of SOA production associated with a given precursor. Odum model can be represented by Eq. 15, where M<sub>0</sub> is the SOA mass concentration (μg m<sup>-3</sup>), α<sub>i</sub> is the mass-based stoichiometric coefficient of semi-volatile organic compounds (SVOC), K<sub>p,i</sub> is the gas-particle partitioning equilibrium constant that describes the partitioning of oxidation product (i) between the absorbing organic aerosol phase and the gas phase, respectively, :

$$Y = M_0 \sum \frac{\alpha_i \cdot K_{p,i}}{1 + M_0 \cdot K_{p,i}} \quad (\text{Eq. 15})$$

In some cases, SOA formation can be described by the one-product model represented by Eq. 16:

$$Y = M_0 \times \frac{\alpha_1 \cdot K_{p,1}}{1 + M_0 \cdot K_{p,1}} \quad (\text{Eq. 16})$$

## II.11 Conclusion of the chapter

This chapter offers a detailed description of the atmospheric simulation chambers, analytical techniques, and experimental methods used in this thesis. As a reminder, CHARME was used to measure the rate coefficients for the reactions of F, 2-MF, 3-MF, 2,5-DMF, 2,3,5-TMF with NO<sub>3</sub> radicals at room temperature. Gas- and particulate-phase oxidation products were also characterized besides measuring the SOA formation yield. A detailed diagram categorizing the different analytical techniques used in the CHARME chamber is presented in Figure II.23.

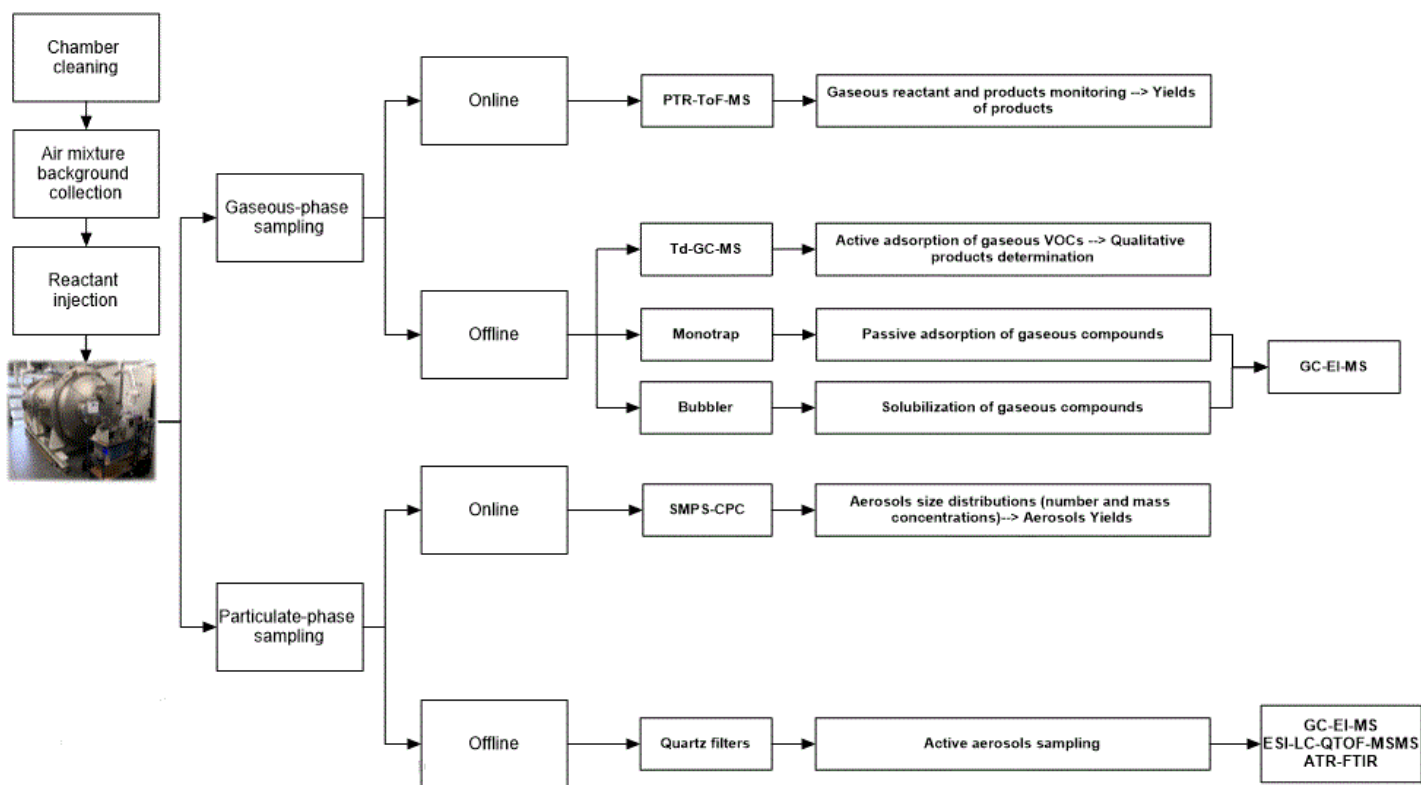


Figure II.23: Diagram representing the online and offline analytical techniques coupled to CHARME.

In addition, THALAMOS was employed for qualitative gas-phase oxidation product determination, as well as for measuring the product yields of 2,5-DMF reaction with  $\text{NO}_3$  at various temperature (296-353 K). T-dependent rate coefficients and Arrhenius equations describing the reactions of the studied VOCs (F, 2-MF, 2,5-DMF,  $\alpha$ -P and 2-carene) with  $\text{NO}_3$  were also performed. The following diagram presents a sum up of the techniques coupled to THALAMOS and the objectives behind using them (Figure II.24).

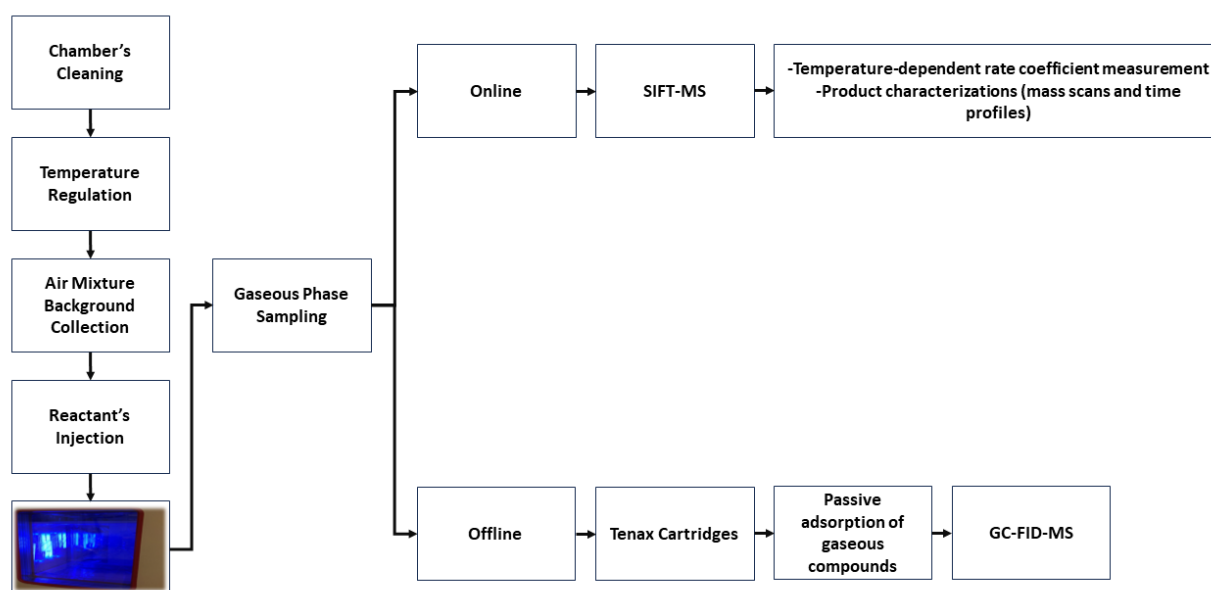


Figure II.24: Diagram representing the online and offline analytical techniques coupled to THALAMOS.

Besides chamber experiments, the reaction of furanoids with  $\text{NO}_3$  radicals was investigated at  $295 \pm 3$  K in White FTIR cells of two different experimental set-ups (one in LPCA and the other at IMT Nord Europe), to try to identify the presence of organic nitrates as final degradation products.

## II.12 References

- Akagi, S. K., Burling, I. R., Mendoza, A., Johnson, T. J., Cameron, M., Griffith, D. W. T., Paton-Walsh, C., Weise, D. R., Reardon, J., & Yokelson, R. J. (2014). Field measurements of trace gases emitted by prescribed fires in southeastern US pine forests using an open-path FTIR system. *Atmospheric Chemistry and Physics*, *14*(1), 199–215. <https://doi.org/10.5194/acp-14-199-2014>
- Akagi, S. K., Yokelson, R. J., Burling, I. R., Meinardi, S., Simpson, I., Blake, D. R., McMeeking, G. R., Sullivan, A., Lee, T., Kreidenweis, S., Urbanski, S., Reardon, J., Griffith, D. W. T., Johnson, T. J., & Weise, D. R. (2013). Measurements of reactive trace gases and variable O<sub>3</sub> formation rates in some South Carolina biomass burning plumes. In *Atmospheric Chemistry and Physics* (Vol. 13, Issue 3). <https://doi.org/10.5194/acp-13-1141-2013>
- Akagi, S. K., Yokelson, R. J., Wiedinmyer, C., Alvarado, M. J., Reid, J. S., Karl, T., Crouse, J. D., & Wennberg, P. O. (2011). Emission factors for open and domestic biomass burning for use in atmospheric models. *Atmospheric Chemistry and Physics*, *11*(9), 4039–4072. <https://doi.org/10.5194/acp-11-4039-2011>
- Akele, E. S., & Tarekegn, M. M. (2017). Assessment of dioxin and furan emission levels and management practices in Addis Ababa, Ethiopia. *Journal of Health and Pollution*, *7*(15), 85–94. <https://doi.org/10.5696/2156-9614-7.15.85>
- Al Ali, F., Coeur, C., Houzel, N., Bouya, H., Tomas, A., & Romanias, M. N. (2022). Rate Coefficients for the Gas-Phase Reactions of Nitrate Radicals with a Series of Furan Compounds. *Journal of Physical Chemistry A*, *126*(46), 8674–8681. <https://doi.org/10.1021/acs.jpca.2c03828>
- Alan Buis. (2019). *Earth's Atmosphere: A Multi-layered Cake*. <https://climate.nasa.gov/news/2919/earths-atmosphere-a-multi-layered-cake/>
- Alcock, R. E., & Jones, K. C. (1996). Dioxins in the environment: A review of trend data. *Environmental Science and Technology*, *30*(11), 3133–3143. <https://doi.org/10.1021/es960306z>
- Alicke, B., & Platt, U. (2002). *Impact of nitrous acid photolysis on the total hydroxyl radical budget during the Limitation of Oxidant Production / Pianura Padana Produzione di Ozono study in Milan*. 107. <https://doi.org/10.1029/2000JD000075>
- Alvarado, A., Atkinson, R., & Arey, J. (1996). Kinetics of the gas-phase reactions of NO<sub>3</sub> radicals and O<sub>3</sub> with 3-methylfuran and the OH radical yield from the O<sub>3</sub> reaction. *International Journal of Chemical Kinetics*, *28*(12), 905–909. [https://doi.org/10.1002/\(SICI\)1097-4601\(1996\)28:12<905::AID-KIN7>3.0.CO;2-R](https://doi.org/10.1002/(SICI)1097-4601(1996)28:12<905::AID-KIN7>3.0.CO;2-R)
- Alwe, H. D., Walavalkar, M. P., Sharma, A., Dhanya, S., & Naik, P. D. (2014). Tropospheric oxidation of cyclic unsaturated ethers in the day-time: Comparison of the reactions with Cl, OH and O<sub>3</sub> based on the determination of their rate coefficients at 298K. *Atmospheric Environment*, *82*, 113–120. <https://doi.org/10.1016/j.atmosenv.2013.10.009>
- Andersen, C., Nielsen, O. J., Østerstrøm, F. F., Ausmeel, S., Nilsson, E. J. K., & Sulbaek Andersen, M. P. (2016). Atmospheric Chemistry of Tetrahydrofuran, 2-Methyltetrahydrofuran, and 2,5-Dimethyltetrahydrofuran: Kinetics of Reactions with Chlorine Atoms, OH Radicals, and Ozone. *Journal of Physical Chemistry A*, *120*(37), 7320–7326.



<https://doi.org/10.1021/acs.jpca.6b06618>

- Andreae, M. (2019). Emission of trace gases and aerosols from biomass burning. *Global Biogeochemical. Atmospheric Chemistry and Physics*, 15 (4)(April), 955–966. <https://www.atmos-chem-phys-discuss.net/acp-2019-303/acp-2019-303.pdf>
- Andreae, M. O. (2001). [ *Ca Because of the carbon to permits*. 15(4), 955–966.
- Aschmann, S. M., Nishino, N., Arey, J., & Atkinson, R. (2011). Kinetics of the Reactions of OH Radicals with 2- and 3-Methylfuran, 2,3- and 2,5-Dimethylfuran, and E- and Z-3-Hexene-2,5-dione, and Products of OH p 2,5-Dimethylfuran. *Environmental Science and Technology*, 45(7), 1859–1865. <https://doi.org/10.1002/kin.550140706>
- Aschmann, S. M., Nishino, N., Arey, J., & Atkinson, R. (2014a). Products of the OH Radical-Initiated Reactions of Furan, 2- and 3-Methylfuran, and 2,3- and 2,5-Dimethylfuran in the Presence of NO. *The Journal of Physical Chemistry*, 118, 457–466. <https://doi.org/10.1021/jp410345k>
- Aschmann, S. M., Nishino, N., Arey, J., & Atkinson, R. (2014b). *Sara M. Aschmann, Noriko Nishino, † Janet Arey, \*, ‡ and Roger Atkinson \*, ‡.*
- Atkinson, R. (1991a). Kinetics and Mechanisms of the Gas-Phase Reactions of the NO<sub>3</sub> Radical with Organic Compounds. *Journal of Physical and Chemical Reference Data*, 20(3), 459–507. <https://doi.org/10.1063/1.555887>
- Atkinson, R. (1991b). Kinetics and Mechanisms of the Gas-Phase Reactions of the NO<sub>3</sub> Radical with Organic Compounds. *Journal of Physical and Chemical Reference Data*, 20(3), 459–507. <https://doi.org/10.1063/1.555887>
- Atkinson, R. (2000). Atmospheric chemistry of VOCs and NO(x). *Atmospheric Environment*, 34(12–14), 2063–2101. [https://doi.org/10.1016/S1352-2310\(99\)00460-4](https://doi.org/10.1016/S1352-2310(99)00460-4)
- Atkinson, R., & Arey, J. (2003). *ARTICLE IN PRESS Gas-phase tropospheric chemistry of biogenic volatile organic compounds: a review*. 2(2). [https://doi.org/10.1016/S1352-2310\(03\)00391-1](https://doi.org/10.1016/S1352-2310(03)00391-1)
- Atkinson, R., Arey, J., Tuazon, E. C., & Aschmann, S. M. (1992). Gas-phase reactions of 1,4-benzodioxan, 2,3-dihydrobenzofuran, and 2,3-benzofuran with OH radicals and O<sub>3</sub>. *International Journal of Chemical Kinetics*, 24(4), 345–358. <https://doi.org/10.1002/kin.550240404>
- Atkinson, R., Aschmann, S. M., & Carter, P. L. (1983a). *Radicals with Furan and Thiophene at*. 15, 51–61.
- Atkinson, R., Aschmann, S. M., & Carter, W. P. L. (1983b). Kinetics of the reactions of O<sub>3</sub> and OH radicals with furan and thiophene at 298 ± 2 K. *International Journal of Chemical Kinetics*, 15(1), 51–61. <https://doi.org/10.1002/kin.550150106>
- Atkinson, R., Aschmann, S. M., & Carter, W. P. L. (1984). Kinetics of the reactions of O<sub>3</sub> and OH radicals with a series of dialkenes and trialkenes at 294 ± 2 K. *International Journal of Chemical Kinetics*, 16(8), 967–976. <https://doi.org/10.1002/kin.550160804>
- Atkinson, R., Aschmann, S. M., & Pitts, J. N. (1988). Rate constants for the gas-phase reactions of the NO<sub>3</sub> radical with a series of organic compounds at 296 ± 2 K. *Journal of Physical*

*Chemistry*, 92(12), 3454–3457. <https://doi.org/10.1021/j100323a028>

- Atkinson, R., Aschmann, S. M., Tuazon, E. C., Arey, J., & Zielinska, B. (1989). Formation of 3-Methylfuran from the gas-phase reaction of OH radicals with isoprene and the rate constant for its reaction with the OH radical. *International Journal of Chemical Kinetics*, 21(7), 593–604. <https://doi.org/10.1002/kin.550210709>
- Atkinson, R., Aschmann, S. M., Winer, A. M., & Carter, W. P. L. (1985a). *for Reactions with Pyrrole ± 1 Atmospheric. I*, 87–90.
- Atkinson, R., Aschmann, S. M., Winer, A. M., & Carter, W. P. L. (1985b). Rate Constants for the Gas-Phase Reactions of NO<sub>3</sub> Radicals with Furan, Thiophene, and Pyrrole at 295 ± 1 K and Atmospheric Pressure. *Environmental Science and Technology*, 19(1), 87–90. <https://doi.org/10.1021/es00131a010>
- Atkinson, R., Aschmann, S. M., Winer, A. M., & Pitts, J. N. (1985). Kinetics and Atmospheric Implications of the Gas-Phase Reactions of NO<sub>3</sub> Radicals with a Series of Monoterpenes and Related Organics at 294 ± 2 K. *Environmental Science and Technology*, 19(2), 159–163. <https://doi.org/10.1021/es00132a009>
- Atkinson, R., Baulch, D. L., Cox, R. A., Hampson, R. F., Kerr, J. A., Rossi, M. J., & Troe, J. (1997). Evaluated Kinetic, Photochemical and Heterogeneous Data for Atmospheric Chemistry: Supplement V: IUPAC Subcommittee on Gas Kinetic Data Evaluation for Atmospheric Chemistry. *Journal of Physical and Chemical Reference Data*, 26(3), 521–784. <https://doi.org/10.1063/1.556011>
- Bahreini, R., Keywood, M. D., Ng, N. L., Varutbangkul, V., Gao, S., Flagan, R. C., Seinfeld, J. H., Worsnop, D. R., & Jimenez, J. L. (2005). Measurements of secondary organic aerosol from oxidation of cycloalkenes, terpenes, and m-xylene using an aerodyne aerosol mass spectrometer. *Environmental Science and Technology*, 39(15), 5674–5688. <https://doi.org/10.1021/es048061a>
- Berndt, T., Böge, O., & Rolle, W. (1997). Products of the gas-phase reactions of NO<sub>3</sub> radicals with furan and tetramethylfuran. *Environmental Science and Technology*, 31(4), 1157–1162. <https://doi.org/10.1021/es960669z>
- Bierbach, A., Barnes, I., & Becker, K. H. (1992). Rate coefficients for the gas-phase reactions of hydroxyl radicals with furan, 2-methylfuran, 2-ethylfuran and 2,5-dimethylfuran at 300 ± 2 K. *Atmospheric Environment Part A, General Topics*, 26(5), 813–817. [https://doi.org/10.1016/0960-1686\(92\)90241-C](https://doi.org/10.1016/0960-1686(92)90241-C)
- Bierbach, A., Barnes, I., & Becker, K. H. (1995). Product and kinetic study of the oh-initiated gas-phase oxidation of Furan, 2-methylfuran and furanaldehydes at ≈ 300 K. *Atmospheric Environment*, 29(19), 2651–2660. [https://doi.org/10.1016/1352-2310\(95\)00096-H](https://doi.org/10.1016/1352-2310(95)00096-H)
- Bierbach, A., Barnes, I., Becker, K. H., & Wiesen, E. (1994). Atmospheric Chemistry of Unsaturated Carbonyls: Butenedial, 4-Oxo-2-pentenal, 3-Hexene-2,5-dione, Maleic Anhydride, 3H-Furan-2-one, and 5-Methyl-3H-furan-2-one. *Environmental Science and Technology*, 28(4), 715–729. <https://doi.org/10.1021/es00053a028>
- Blake, R., Monks, P., & Ellis, A. (2009). Proton Transfer Reaction Mass Spectrometry (PTR-MS). *Chem.Rev.*, 109(0), 861–896. <https://doi.org/10.1002/9781118180730.ch28>

- Brando, P., Macedo, M., Silvério, D., Rattis, L., Paolucci, L., Alencar, A., Coe, M., & Amorim, C. (2020). Amazon wildfires: Scenes from a foreseeable disaster. *Flora: Morphology, Distribution, Functional Ecology of Plants*, 268. <https://doi.org/10.1016/j.flora.2020.151609>
- Brown, S. S., & Stutz, J. (2012). Nighttime radical observations and chemistry. *Chemical Society Reviews*, 41(19), 6405–6447. <https://doi.org/10.1039/c2cs35181a>
- Burkholder, J. B., Abbatt, J. P. D., Barnes, I., Roberts, J. M., Melamed, M. L., Ammann, M., Bertram, A. K., Cappa, C. D., Carlton, A. G., Carpenter, L. J., Crowley, J. N., Dubowski, Y., George, C., Heard, D. E., Herrmann, H., Keutsch, F. N., Kroll, J. H., McNeill, V. F., Ng, N. L., ... Ziemann, P. J. (2017). The Essential Role for Laboratory Studies in Atmospheric Chemistry. *Environmental Science and Technology*, 51(5), 2519–2528. <https://doi.org/10.1021/acs.est.6b04947>
- Burkholder, J. B., Sander, S. P., Abbatt, J. P. D., Barker, J. R., Huie, R. E., Kolb, C. E., Kurylo, M. J., Orkin, V. L., Wilmouth, D. M., & Wine, P. H. (2020). Chemical Kinetics and Photochemical Data for Use in Atmospheric Studies, Evaluation No. 19. *JPL Publications 19-5*, 19, 1–153. <http://jpldataeval.jpl.nasa.gov/>
- Burling, I. R., Yokelson, R. J., Griffith, D. W. T., Johnson, T. J., Veres, P., Roberts, J. M., Warneke, C., Urbanski, S. P., Reardon, J., Weise, D. R., Hao, W. M., & De Gouw, J. (2010). Laboratory measurements of trace gas emissions from biomass burning of fuel types from the southeastern and southwestern United States. *Atmospheric Chemistry and Physics*, 10(22), 11115–11130. <https://doi.org/10.5194/acp-10-11115-2010>
- Cabañas, B., Baeza, M. T., Salgado, S., Martín, P., Taccone, R., & Martínez, E. (2004). Oxidation of heterocycles in the atmosphere: Kinetic study of their reactions with NO<sub>3</sub> radical. *Journal of Physical Chemistry A*, 108(49), 10818–10823. <https://doi.org/10.1021/jp046524t>
- Cabañas, B., Villanueva, F., Martín, P., Baeza, M. T., Salgado, S., & Jiménez, E. (2005). Study of reaction processes of furan and some furan derivatives initiated by Cl atoms. *Atmospheric Environment*, 39(10), 1935–1944. <https://doi.org/10.1016/j.atmosenv.2004.12.013>
- Cabrera-perez, D., Taraborrelli, D., Sander, R., & Pozzer, A. (2016). *Global atmospheric budget of simple monocyclic aromatic compounds*. 6931–6947. <https://doi.org/10.5194/acp-16-6931-2016>
- Calogirou, A., Jensen, N. R., Nielsen, C. J., Kotzias, D., & Hjorth, J. (1999). Gas-phase reactions of nopinone, 3-isopropenyl-6-oxo-heptanal, and 5-methyl-5-vinyltetrahydrofuran-2-ol with OH, NO<sub>3</sub>, and ozone. *Environmental Science and Technology*, 33(3), 453–460. <https://doi.org/10.1021/es980530j>
- Carbajo, P. G., Smith, S. C., Holloway, A. L., Smith, C. A., Pope, F. D., Shallcross, D. E., & Orr-Ewing, A. J. (2008). Ultraviolet photolysis of HCHO: Absolute HCO quantum yields by direct detection of the HCO radical photoproduct. *Journal of Physical Chemistry A*, 112(48), 12437–12448. <https://doi.org/10.1021/jp8070508>
- Chattopadhyay, A., Papadimitriou, V. C., Marshall, P., & Burkholder, J. B. (2020). Temperature-dependent rate coefficients for the gas-phase OH + furan-2,5-dione (C<sub>4</sub>H<sub>2</sub>O<sub>3</sub>, maleic anhydride) reaction. *International Journal of Chemical Kinetics*, 52(10), 623–631.

<https://doi.org/10.1002/kin.21387>

- Chipperfield, M. P., Bekki, S., Dhomse, S., Harris, N. R. P., Hassler, B., Hossaini, R., Steinbrecht, W., Thiéblemont, R., & Weber, M. (2017). Detecting recovery of the stratospheric ozone layer. *Nature*, *549*(7671), 211–218. <https://doi.org/10.1038/nature23681>
- Christian, T. J., Kleiss, B., Yokelson, R. J., Holzinger, R., Crutzen, P. J., Hao, W. M., Saharjo, B. H., & Ward, D. E. (2003). Comprehensive laboratory measurements of biomass-burning emissions: 1. Emissions from Indonesian, African, and other fuels. *Journal of Geophysical Research: Atmospheres*, *108*(23). <https://doi.org/10.1029/2003jd003704>
- Ciccioli, P., Brancaleoni, E., Frattoni, M., Cecinato, A., & Pinciarelli, L. (2001). Determination of volatile organic compounds (VOC) emitted from biomass burning of Mediterranean vegetation species by GC-MS. *Analytical Letters*, *34*(6), 937–955. <https://doi.org/10.1081/AL-100103604>
- Coeur-tourneur, C., Tomas, A., & Menu, D. (2008). *Secondary organic aerosol formation from the gas phase reaction of hydroxyl radicals with m - , o- and p -cresol*. *42*, 3035–3045. <https://doi.org/10.1016/j.atmosenv.2007.12.043>
- Coggon, M. M., Lim, C. Y., Koss, A. R., Sekimoto, K., Yuan, B., Gilman, J. B., Hagan, D. H., Selimovic, V., Zarzana, K. J., Brown, S. S., M Roberts, J., Müller, M., Yokelson, R., Wisthaler, A., Krechmer, J. E., Jimenez, J. L., Cappa, C., Kroll, J. H., De Gouw, J., & Warneke, C. (2019). OH chemistry of non-methane organic gases (NMOGs) emitted from laboratory and ambient biomass burning smoke: Evaluating the influence of furans and oxygenated aromatics on ozone and secondary NMOG formation. *Atmospheric Chemistry and Physics*, *19*(23), 14875–14899. <https://doi.org/10.5194/acp-19-14875-2019>
- Collard, F. X., & Blin, J. (2014). A review on pyrolysis of biomass constituents: Mechanisms and composition of the products obtained from the conversion of cellulose, hemicelluloses and lignin. *Renewable and Sustainable Energy Reviews*, *38*, 594–608. <https://doi.org/10.1016/j.rser.2014.06.013>
- Colmenar, I., Cabañas, B., Martínez, E., Salgado, M. S., & Martín, P. (2012). Atmospheric fate of a series of furanaldehydes by their NO<sub>3</sub> reactions. *Atmospheric Environment*, *54*(3), 177–184. <https://doi.org/10.1016/j.atmosenv.2012.02.087>
- Colmenar, I., Martín, P., Cabañas, B., Salgado, S., Villanueva, F., & Ballesteros, B. (2020). Evaluation of the SOA formation in the reaction of furfural with atmospheric oxidants. *Atmosphere*, *11*(9). <https://doi.org/10.3390/atmos11090927>
- Corchnoy, S., & Atkinson, R. (1990). Kinetics of the Gas-Phase Reactions of OH and NO<sub>3</sub> Radicals with 2-Carene, 1,8-Cineole, p-Cymene, and Terpinolene. *Environ. Sci. Technol.* *1990*, *24*(10), 1497–1502.
- Crouse, J. D., DeCarlo, P. F., Blake, D. R., Emmons, L. K., Campos, T. L., Apel, E. C., Clarke, A. D., Weinheimer, A. J., McCabe, D. C., Yokelson, R. J., Jimenez, J. L., & Wennberg, P. O. (2009). Biomass burning and urban air pollution over the Central Mexican Plateau. *Atmospheric Chemistry and Physics*, *9*(14), 4929–4944. <https://doi.org/10.5194/acp-9-4929-2009>
- Cuisset, A., Coeur, C., Mouret, G., Ahmad, W., Tomas, A., & Pirali, O. (2016). Infrared

- spectroscopy of methoxyphenols involved as atmospheric secondary organic aerosol precursors: Gas-phase vibrational cross-sections. *Journal of Quantitative Spectroscopy and Radiative Transfer*, 179, 51–58. <https://doi.org/10.1016/j.jqsrt.2016.03.020>
- Davis, A. C., & Sarathy, S. M. (2013). Computational study of the combustion and atmospheric decomposition of 2-methylfuran. *Journal of Physical Chemistry A*, 117(33), 7670–7685. <https://doi.org/10.1021/jp403085u>
- De gouw, J., & Warneke, C. (2007). MEASUREMENTS OF VOLATILE ORGANIC COMPOUNDS IN THE EARTH'S ATMOSPHERE USING PROTON-TRANSFER-REACTION MASS SPECTROMETRY. *Wiley InterScience*, i, 221–235. <https://doi.org/10.1002/mas>
- Decker, Z. C. J., Zarzana, K. J., Coggon, M., Min, K. E., Pollack, I., Ryerson, T. B., Peischl, J., Edwards, P., Dubé, W. P., Markovic, M. Z., Roberts, J. M., Veres, P. R., Graus, M., Warneke, C., De Gouw, J., Hatch, L. E., Barsanti, K. C., & Brown, S. S. (2019). Nighttime Chemical Transformation in Biomass Burning Plumes: A Box Model Analysis Initialized with Aircraft Observations. *Environmental Science and Technology*, 53(5), 2529–2538. <https://doi.org/10.1021/acs.est.8b05359>
- Decker, Z., Robinson, M., Barsanti, K., Bourgeois, I., Coggon, M., DiGangi, J., Diskin, G., Flocke, F., Franchin, A., Fredrickson, C., Hall, S., Halliday, H., Holmes, C., Huey, L. G., Lee, Y. R., Lindaas, J., Middlebrook, A., Montzka, D., Moore, R., ... Brown, S. (2021). Nighttime and Daytime Dark Oxidation Chemistry in Wildfire Plumes: An Observation and Model Analysis of FIREX-AQ Aircraft Data. *Atmospheric Chemistry and Physics Discussions*, November, 1–45. <https://doi.org/10.5194/acp-2021-267>
- Dlugokencky, E. J., & Howard, C. J. (1989a). + (1.28. 17, 1091–1096.
- Dlugokencky, E. J., & Howard, C. J. (1989b). Studies of NO<sub>3</sub> radical reactions with some atmospheric organic compounds at low pressures. *Journal of Physical Chemistry*, 93(3), 1091–1096. <https://doi.org/10.1021/j100340a015>
- Dodge, M. C. (2000). Chemical oxidant mechanisms for air quality modeling: Critical review. *Atmospheric Environment*, 34(12–14), 2103–2130. [https://doi.org/10.1016/S1352-2310\(99\)00461-6](https://doi.org/10.1016/S1352-2310(99)00461-6)
- Durigan, M. R., Cherubin, M. R., de Camargo, P. B., Ferreira, J. N., Berenguer, E., Gardner, T. A., Barlow, J., Dias, C. T. dos S., Signor, D., de Oliveira, R. C., & Cerri, C. E. P. (2017). Soil organic matter responses to anthropogenic forest disturbance and land use change in the eastern Brazilian Amazon. *Sustainability (Switzerland)*, 9(3). <https://doi.org/10.3390/su9030379>
- Dusanter, S., Vimal, D., Stevens, P. S., Volkamer, R., Molina, L. T., Baker, A., Meinardi, S., Blake, D., Sheehy, P., Merten, A., Zhang, R., Zheng, J., Fortner, E. C., Junkermann, W., Dubey, M., Rann, T., Eichinger, B., Lewandowski, P., Prueger, J., & Holder, H. (2009). Measurements of OH and HO<sub>2</sub> concentrations during the MCMA-2006 field campaign - Part 2: Model comparison and radical budget. *Atmospheric Chemistry and Physics*, 9(18), 6655–6675. <https://doi.org/10.5194/acp-9-6655-2009>
- Eble, J., Bänsch, C., & Olzmann, M. (2015). *Kinetic Investigation of the Reactions of 2, 5-Dimethylfuran and 2-Methylfuran with Hydroxyl Radicals*. 2–5.

- Elshorbany, Y., Barnes, I., Becker, K. H., Kleffmann, J., & Wiesen, P. (2010). Sources and cycling of tropospheric hydroxyl radicals - An overview. *Zeitschrift Fur Physikalische Chemie*, 224(7–8), 967–987. <https://doi.org/10.1524/zpch.2010.6136>
- Elshorbany, Y. F., Kurtenbach, R., Wiesen, P., Lissi, E., Rubio, M., Villena, G., Gramsch, E., Rickard, A. R., Pilling, M. J., & Kleffmann, J. (2009). Oxidation capacity of the city air of Santiago, Chile. *Atmospheric Chemistry and Physics*, 9(6), 2257–2273. <https://doi.org/10.5194/acp-9-2257-2009>
- Elwardany, A., Es-Sebbar, E., Khaled, F., & Farooq, A. (2016). A chemical kinetic study of the reaction of hydroxyl with furans. *Fuel*, 166, 245–252. <https://doi.org/10.1016/j.fuel.2015.10.098>
- Evyugina, M., Alves, C., Calvo, A., Nunes, T., Tarelho, L., Duarte, M., Prozil, S. O., Evtugin, D. V., & Pio, C. (2014). VOC emissions from residential combustion of Southern and mid-European woods. *Atmospheric Environment*, 83, 90–98. <https://doi.org/10.1016/j.atmosenv.2013.10.050>
- Evyugina, M., Calvo, A. I., Nunes, T., Alves, C., Fernandes, A. P., Tarelho, L., Vicente, A., & Pio, C. (2013). VOC emissions of smouldering combustion from Mediterranean wildfires in central Portugal. *Atmospheric Environment*, 64, 339–348. <https://doi.org/10.1016/j.atmosenv.2012.10.001>
- Fayad, L. (2019). *Caractérisation de la nouvelle chambre de simulation atmosphérique CHARME et étude de la réaction d'ozonolyse d'un COV biogénique, le  $\gamma$ -terpinène Loyal FAYAD Acknowledgments* (Vol. 104).
- Fayad, L., Coeur, C., Fagniez, T., Secordel, X., Houzel, N., & Mouret, G. (2021). Kinetic and mechanistic study of the gas-phase reaction of ozone with  $\gamma$ -terpinene. *Atmospheric Environment*, 246(August 2020). <https://doi.org/10.1016/j.atmosenv.2020.118073>
- Ferdous, D., Dalai, A. K., Bej, S. K., & Thring, R. W. (2002). Pyrolysis of lignins: Experimental and kinetics studies. *Energy and Fuels*, 16(6), 1405–1412. <https://doi.org/10.1021/ef0200323>
- Finlayson-Pitts, B. J. (2010). Atmospheric chemistry. *Proceedings of the National Academy of Sciences of the United States of America*, 107(15), 6566–6567. <https://doi.org/10.1073/pnas.1003038107>
- Finlayson-Pitts, B. J., & Pitts, J. N. (1993). Atmospheric chemistry of tropospheric ozone formation: Scientific and regulatory implications. *Air and Waste*, 43(8), 1091–1100. <https://doi.org/10.1080/1073161X.1993.10467187>
- Finlayson-Pitts, Barbara J., & James N. Pitts Jr. (1999). *Chemistry of the upper and lower atmosphere: theory, experiments, and applications*. El Sevier.
- Fuchs, J. D. H., Seakins, A. K. P., & Editors, J. W. (n.d.). *A Practical Guide to Atmospheric*.
- George, C., Ammann, M., D'Anna, B., Donaldson, D. J., & Nizkorodov, S. A. (2015). Heterogeneous Photochemistry in the Atmosphere. *Chemical Reviews*, 115(10), 4218–4258. <https://doi.org/10.1021/cr500648z>
- Gilman, J. B., Lerner, B. M., Kuster, W. C., Goldan, P. D., Warneke, C., Veres, P. R., Roberts, J. M., De Gouw, J. A., Burling, I. R., & Yokelson, R. J. (2015). Biomass burning emissions and

- potential air quality impacts of volatile organic compounds and other trace gases from fuels common in the US. *Atmospheric Chemistry and Physics*, 15(24), 13915–13938. <https://doi.org/10.5194/acp-15-13915-2015>
- Giri, B. R., Khaled, F., Szori, M., Viskolcz, B., & Farooq, A. (2017). An experimental and theoretical kinetic study of the reaction of OH radicals with tetrahydrofuran. *Proceedings of the Combustion Institute*, 36(1), 143–150. <https://doi.org/10.1016/j.proci.2016.06.016>
- Gómez Alvarez, E., Borrás, E., Viidanoja, J., & Hjorth, J. (2009). Unsaturated dicarbonyl products from the OH-initiated photo-oxidation of furan, 2-methylfuran and 3-methylfuran. *Atmospheric Environment*, 43(9), 1603–1612. <https://doi.org/10.1016/j.atmosenv.2008.12.019>
- Graedel, T. E., & Keene, W. C. (1996). The budget and cycle of Earth's natural chlorine. *Pure and Applied Chemistry*, 68(9), 1689–1697. <https://doi.org/10.1351/pac199668091689>
- Graham, B., Mayol-Bracero, O. L., Guyon, P., Roberts, G. C., Decesari, S., Facchini, M. C., Artaxo, P., Maenhaut, W., Köll, P., & Andreae, M. O. (2002). Water-soluble organic compounds in biomass burning aerosols over Amazonia 1. Characterization by NMR and GC-MS. *Journal of Geophysical Research Atmospheres*, 107(20), LBA 14-1-LBA 14-16. <https://doi.org/10.1029/2001JD000336>
- Greenberg, J. P., Zimmerman, P. R., Heidt, L., & Pollock, W. (1984). Hydrocarbon and carbon monoxide emissions from biomass burning in Brazil. *Journal of Geophysical Research*, 89(D1), 1350–1354. <https://doi.org/10.1029/JD089iD01p01350>
- Gira, A., Amarandei, C., Romanias, M. N., El Dib, G., Canosa, A., Arsene, C., Bejan, I. G., Olariu, R. I., Coddeville, P., & Tomas, A. (2020). Kinetic measurements of Cl atom reactions with C5-C8 unsaturated alcohols. *Atmosphere*, 11(3), 1–15. <https://doi.org/10.3390/ATMOS11030256>
- Guenther, A., Nicholas, C., Fall, R., Klinger, L., McKay, W. A., & Scholes, B. (1995). A global model of natural volatile organic compound emissions s Raja the balance Triangle changes in the atmospheric accumulation rates of greenhouse Triangle Several inventories of natural and Exposure Assessment global scales have been two classes Fores. *J. Geophys. Res.*, 100(94), 8873–8892.
- Hartikainen, A., Yli-Pirilä, P., Tiitta, P., Leskinen, A., Kortelainen, M., Orasche, J., Schnelle-Kreis, J., Lehtinen, K. E. J., Zimmermann, R., Jokiniemi, J., & Sippula, O. (2018). Volatile Organic Compounds from Logwood Combustion: Emissions and Transformation under Dark and Photochemical Aging Conditions in a Smog Chamber. *Environmental Science and Technology*, 52(8), 4979–4988. <https://doi.org/10.1021/acs.est.7b06269>
- Hatch, L. E., Luo, W., Pankow, J. F., Yokelson, R. J., Stockwell, C. E., & Barsanti, K. C. (2015). Identification and quantification of gaseous organic compounds emitted from biomass burning using two-dimensional gas chromatography-time-of-flight mass spectrometry. *Atmospheric Chemistry and Physics*, 15(4), 1865–1899. <https://doi.org/10.5194/acp-15-1865-2015>
- Hatch, L. E., Yokelson, R. J., Stockwell, C. E., Veres, P. R., Simpson, I. J., Blake, D. R., Orlando, J. J., & Barsanti, K. C. (2017). Multi-instrument comparison and compilation of non-methane organic gas emissions from biomass burning and implications for smoke-

- derived secondary organic aerosol precursors. *Atmospheric Chemistry and Physics*, 17(2), 1471–1489. <https://doi.org/10.5194/acp-17-1471-2017>
- Hein, R., Crutzen, P. J., & Heimann, M. (1997). An inverse modeling approach to investigate the global atmospheric methane cycle. *Global Biogeochemical Cycles*, 11(1), 43–76. <https://doi.org/10.1029/96GB03043>
- Holly Zell. (2013). *Earth's Atmospheric Layers*. [https://www.nasa.gov/mission\\_pages/sunearth/science/atmosphere-layers2.html](https://www.nasa.gov/mission_pages/sunearth/science/atmosphere-layers2.html)
- Huang, Z., Zhao, N., Ma, X., Xu, F., Zhang, Q., Zhuang, T., & Wang, W. (2019). Theoretical study on the atmospheric oxidation reaction of 2-furaldehyde initiated by NO<sub>3</sub> radicals. *Chemical Physics Letters*, 722(3), 50–57. <https://doi.org/10.1016/j.cplett.2019.03.009>
- Hynes, R. G., Angove, D. E., Saunders, S. M., Haverd, V., & Azzi, M. (2005). Evaluation of two MCM v3.1 alkene mechanisms using indoor environmental chamber data. *Atmospheric Environment*, 39(38), 7251–7262. <https://doi.org/10.1016/j.atmosenv.2005.09.005>
- Identification, I., Flux, V., & Atkinson, R. (1990). *Radicals with*. 24(10), 1497–1502.
- Illés, Á., Rózsa, Z. B., Thangaraj, R., Décsiné Gombos, E., Dóbbé, S., Giri, B. R., & Szóri, M. (2021). An experimental and theoretical kinetic study of the reactions of hydroxyl radicals with tetrahydrofuran and two deuterated tetrahydrofurans. *Chemical Physics Letters*, 776. <https://doi.org/10.1016/j.cplett.2021.138698>
- IUPAC. (2016). *IUPAC Task Group on Atmospheric Chemical Kinetic Data Evaluation – Data Sheet NO<sub>3</sub>\_VOC*. [iupac.pole-ether.fr](http://iupac.pole-ether.fr)
- Jenkin, M. E., & Hayman, G. D. (1999). Photochemical ozone creation potentials for oxygenated volatile organic compounds: Sensitivity to variations in kinetic and mechanistic parameters. *Atmospheric Environment*, 33(8), 1275–1293. [https://doi.org/10.1016/S1352-2310\(98\)00261-1](https://doi.org/10.1016/S1352-2310(98)00261-1)
- Jiang, G., Nowakowski, D. J., & Bridgwater, A. V. (2010). Effect of the temperature on the composition of lignin pyrolysis products. *Energy and Fuels*, 24(8), 4470–4475. <https://doi.org/10.1021/ef100363c>
- Jiang, J., Carter, W. P. L., Cocker, D. R., & Barsanti, K. C. (2020). Development and Evaluation of a Detailed Mechanism for Gas-Phase Atmospheric Reactions of Furans. *ACS Earth and Space Chemistry*, 4(8), 1254–1268. <https://doi.org/10.1021/acsearthspacechem.0c00058>
- Joo, T., Rivera-Rios, J. C., Takeuchi, M., Alvarado, M. J., & Ng, N. L. (2019a). Secondary Organic Aerosol Formation from Reaction of 3-Methylfuran with Nitrate Radicals. *ACS Earth and Space Chemistry*, 3(6), 922–934. <https://doi.org/10.1021/acsearthspacechem.9b00068>
- Joo, T., Rivera-Rios, J. C., Takeuchi, M., Alvarado, M. J., & Ng, N. L. (2019b). Secondary Organic Aerosol Formation from Reaction of 3-Methylfuran with Nitrate Radicals [Research-article]. *ACS Earth and Space Chemistry*, 3(6), 922–934. <https://doi.org/10.1021/acsearthspacechem.9b00068>
- Kawamoto, H. (2017). Lignin pyrolysis reactions. *Journal of Wood Science*, 63(2), 117–132. <https://doi.org/10.1007/s10086-016-1606-z>



- Keene, W. C., Maring, H., Maben, J. R., Kieber, D. J., Pszenny, A. A. P., Dahl, E. E., Izaguirre, M. A., Davis, A. J., Long, M. S., Zhou, X., Smoydzin, L., & Sander, R. (2007). Chemical and physical characteristics of nascent aerosols produced by bursting bubbles at a model air-sea interface. *Journal of Geophysical Research Atmospheres*, *112*(21), 1–16. <https://doi.org/10.1029/2007JD008464>
- Kind, I., Berndt, T., Bisge, O., & Rolle, W. (1996a). *Gas-phase rate constants for the reaction of* 2614(3), 2–6.
- Kind, I., Berndt, T., Bisge, O., & Rolle, W. (1996b). *Gas-phase rate constants for the reaction of NO<sub>3</sub> radicals with furan and methyl-substituted furans*. 2614(3), 2–6.
- Kind, I., Berndt, T., Böge, O., & Rolle, W. (1996). Gas-phase rate constants for the reaction of NO<sub>3</sub> radicals with selected oxiranes. *Chemical Physics Letters*, *249*(1–2), 35–39. [https://doi.org/10.1016/0009-2614\(95\)01327-X](https://doi.org/10.1016/0009-2614(95)01327-X)
- Koolen, C. D., & Rothenberg, G. (2019). Air Pollution in Europe. *ChemSusChem*, *12*(1), 164–172. <https://doi.org/10.1002/cssc.201802292>
- Koppmann, R. (2007). Volatile Organic Compounds in the Atmosphere. In *Volatile Organic Compounds in the Atmosphere*. <https://doi.org/10.1002/9780470988657>
- Koppmann, R., Khedim, A., Rudolph, J., Poppe, D., Andreae, M. O., Helas, G., Welling, M., & Zenker, T. (1997). Emissions of organic trace gases from savanna fires in southern Africa during the 1992 Southern African Fire Atmosphere Research Initiative and their impact on the formation of tropospheric ozone. *Journal of Geophysical Research Atmospheres*, *102*(15), 18879–18888. <https://doi.org/10.1029/97jd00845>
- Koss, A. R., Sekimoto, K., Gilman, J. B., Selimovic, V., Coggon, M. M., Zarzana, K. J., Yuan, B., Lerner, B. M., Brown, S. S., Jimenez, J. L., Krechmer, J., Roberts, J. M., Warneke, C., Yokelson, R. J., & De Gouw, J. (2018). Non-methane organic gas emissions from biomass burning: Identification, quantification, and emission factors from PTR-ToF during the FIREX 2016 laboratory experiment. *Atmospheric Chemistry and Physics*, *18*(5), 3299–3319. <https://doi.org/10.5194/acp-18-3299-2018>
- Krause, T., Tubbesing, C., Benzing, K., & Schöler, H. F. (2014). Model reactions and natural occurrence of furans from hypersaline environments. *Biogeosciences*, *11*(10), 2871–2882. <https://doi.org/10.5194/bg-11-2871-2014>
- Kumar, V., Chandra, B. P., & Sinha, V. (2018). Large unexplained suite of chemically reactive compounds present in ambient air due to biomass fires. *Scientific Reports*, *8*(1), 1–15. <https://doi.org/10.1038/s41598-017-19139-3>
- Lalchandani, V., Srivastava, D., Dave, J., Mishra, S., Tripathi, N., Shukla, A. K., Sahu, R., Thamban, N. M., Gaddamidi, S., Dixit, K., Ganguly, D., Tiwari, S., Srivastava, A. K., Sahu, L., Rastogi, N., Gargava, P., & Tripathi, S. N. (2021). Effect of biomass burning on PM 2.5 composition and secondary aerosol formation during post-monsoon and winter haze episodes in Delhi . *Journal of Geophysical Research: Atmospheres*, 1–21. <https://doi.org/10.1029/2021jd035232>
- Lambe, A. T., Chhabra, P. S., Onasch, T. B., Brune, W. H., Hunter, J. F., Kroll, J. H., Cummings, M. J., Brogan, J. F., Parmar, Y., Worsnop, D. R., Kolb, C. E., & Davidovits, P. (2015). Effect

- of oxidant concentration, exposure time, and seed particles on secondary organic aerosol chemical composition and yield. *Atmospheric Chemistry and Physics*, 15(6), 3063–3075. <https://doi.org/10.5194/acp-15-3063-2015>
- Lancar, I., Daele, V., Le Bras, G., & Poulet, G. (1991). Étude de la réactivité des radicaux NO<sub>3</sub> avec le diméthyl-2,3 butène-2, le butadiène-1,3 et le diméthyl-2,3 butadiène-1,3. *J.Chim. Phys*, 88, 1777–1792. <https://doi.org/10.1051/jcp/1991881777>
- Lançar, I., Daele, V., Le Bras, G., & Poulet, G. (1991). Étude de la réactivité des radicaux NO<sub>3</sub> avec le diméthyl-2,3 butène-2, le butadiène-1,3 et le diméthyl-2,3 butadiène-1,3. *Journal de Chimie Physique*, 88, 1777–1792. <https://doi.org/10.1051/jcp/1991881777>
- Lange, J. P., Price, R., Ayoub, P. M., Louis, J., Petrus, L., Clarke, L., & Gosselink, H. (2010). Valeric biofuels: A platform of cellulosic transportation fuels. *Angewandte Chemie - International Edition*, 49(26), 4479–4483. <https://doi.org/10.1002/anie.201000655>
- Lauraguais, A., Coeur-tourneur, C., Cassez, A., & Seydi, A. (2012). Rate constant and secondary organic aerosol yields for the gas-phase reaction of hydroxyl radicals with syringol (2,6-dimethoxyphenol). *Atmospheric Environment*, 55, 43–48. <https://doi.org/10.1016/j.atmosenv.2012.02.027>
- Lê Thành, K., Commandré, J. M., Valette, J., Volle, G., & Meyer, M. (2015). Detailed identification and quantification of the condensable species released during torrefaction of lignocellulosic biomasses. *Fuel Processing Technology*, 139, 226–235. <https://doi.org/10.1016/j.fuproc.2015.07.001>
- Lee, J. H., & Tang, I. N. (1982). Absolute rate constants for the hydroxyl radical reactions with ethane, furan, and thiophene at room temperature. *The Journal of Chemical Physics*, 77(9), 4459–4463. <https://doi.org/10.1063/1.444367>
- Liang, Y., Weber, R. J., Misztal, P. K., Jen, C. N., & Goldstein, A. H. (2022). Aging of Volatile Organic Compounds in October 2017 Northern California Wildfire Plumes. *Environmental Science and Technology*, 56(3), 1557–1567. <https://doi.org/10.1021/acs.est.1c05684>
- Liley, P. E., Buck, E., & Ch, M. S. E. (1999). 493-Physical and Chemical Data 物性数据. *Perry's Chemical Engineers Handbook*, 2–86.
- Liljegren, J. A., & Stevens, P. S. (2013). Measurements of the kinetics of the reaction of OH radicals with 3-methylfuran at low pressure. *International Journal of Chemical Kinetics*, 45(12), 787–794. <https://doi.org/10.1002/kin.20814>
- Lin, Y., Cho, J., Tompsett, G. A., Westmoreland, P. R., & Huber, G. W. (2009). Kinetics Mechanism Cellulose Pyrolysis. *Phys. Chem. C*, 113, 20097–20107.
- Lindinger, W., Hansel, A., & Jordan, A. (1998). On-line monitoring of volatile organic compounds at pptv levels by means of Proton-Transfer-Reaction Mass Spectrometry (PTR-MS) Medical applications, food control and environmental research. *International Journal of Mass Spectrometry and Ion Processes*, 173(3), 191–241. [https://doi.org/10.1016/s0168-1176\(97\)00281-4](https://doi.org/10.1016/s0168-1176(97)00281-4)
- Ljungström, E., Wängberg, I., & Langer, S. (1993). Absolute rate coefficients for the reaction between nitrate radicals and some cyclic alkenes. *Journal of the Chemical Society, Faraday Transactions*, 89(16), 2977–2982. <https://doi.org/10.1039/FT9938902977>

- Manion, J., Huie, R. E., Burgess, D. R., Orkin, V. L., Tsang, W., McGivern, W. ., Hudgens, J. W., Knyazev, V. D., Atkinson, D. B., Chai, E., Tereza, A. M., Lin, C. Y., Allison, T. C., Mallard, W. G., Westley, F., Herron, J. T., Hampson, R. F., & Frizzell, D. H. (2015). *NIST Chemical Kinetics Database, NIST Standard Reference Database 17, Version 7.0 (Web Version), Release 1.6.8, Data version 2015.09*.
- Martín, P., Cabañas, B., Colmenar, I., Salgado, M. S., Villanueva, F., & Tapia, A. (2013). Reactivity of E-butenedial with the major atmospheric oxidants. *Atmospheric Environment*, *70*, 351–360. <https://doi.org/10.1016/j.atmosenv.2013.01.041>
- Martinez, E., Cabanas, B., Aranda, A., & Martín, P. (1998). Kinetics of the reactions of NO<sub>3</sub> radical with selected monoterpenes: A temperature dependence study. *Environmental Science and Technology*, *32*(23), 3730–3734. <https://doi.org/10.1021/es970899t>
- Martínez, E., Cabañas, B., Aranda, A., Martín, P., Notario, A., & Salgado, S. (1999). Study on the NO<sub>3</sub> Radical Reactivity: Reactions with Cyclic Alkenes. *Journal of Physical Chemistry A*, *103*(27), 5321–5327. <https://doi.org/10.1021/jp9847181>
- Martinez, E., Cabañas, B., Aranda, A., Martin, P., & Salgado, S. (1999). Absolute Rate Coefficients for the Gas-Phase Reactions of NO<sub>3</sub> Radical with a Series of Monoterpenes at T = 298 to 433 K. *Journal of Atmospheric Chemistry*, *33*(3), 265–282. <https://doi.org/10.1023/A:1006178530211>
- Matsumoto, J. (2011). Kinetics of the reactions of ozone with 2,5-dimethylfuran and its atmospheric implications. *Chemistry Letters*, *40*(6), 582–583. <https://doi.org/10.1246/cl.2011.582>
- Mcdonald, J. D., Zielinska, B., Fujita, E. M., Sagebiel, J. C., Chow, J. C., & Watson, J. G. (2000). Fine particle and gaseous emission rates from residential wood combustion. *Environmental Science and Technology*, *34*(11), 2080–2091. <https://doi.org/10.1021/es9909632>
- Mellouki, A., & Chen, J. (2015). *Atmospheric Chemistry of Oxygenated Volatile Organic Compounds : Impacts on Air Quality and Climate*. <https://doi.org/10.1021/cr500549n>
- Meng, L., Coeur, C., Fayad, L., Houzel, N., Genevray, P., Bouzidi, H., Tomas, A., & Chen, W. (2020). Secondary organic aerosol formation from the gas-phase reaction of guaiacol (2-methoxyphenol) with NO<sub>3</sub> radicals. *Atmospheric Environment*, *240*(July). <https://doi.org/10.1016/j.atmosenv.2020.117740>
- Mettler, M. S., Mushrif, S. H., Paulsen, A. D., Javadekar, A. D., Vlachos, D. G., & Dauenhauer, P. J. (2012). Revealing pyrolysis chemistry for biofuels production: Conversion of cellulose to furans and small oxygenates. *Energy and Environmental Science*, *5*(1), 5414–5424. <https://doi.org/10.1039/c1ee02743c>
- Molina, M. J., & Molina, L. T. (2004). Megacities and atmospheric pollution. *Journal of the Air and Waste Management Association*, *54*(6), 644–680. <https://doi.org/10.1080/10473289.2004.10470936>
- Moriarty, J., Sidebottom, H., Wenger, J., Mellouki, A., & Le Bras, G. (2003). Kinetic studies on the reactions of hydroxyl radicals with cyclic ethers and aliphatic diethers. *Journal of Physical Chemistry A*, *107*(10), 1499–1505. <https://doi.org/10.1021/jp021267i>

- Mudhoo, A., Thayalan, G., Muthoora, N. J., Muthoora, M. N., Oozeer, B. Z., Rago, Y. P., Ramphul, M. P., Valaydon, A. K., & Kumar, S. (2013). *Dioxins and Furans: Sources, Impacts and Remediation*. [https://doi.org/10.1007/978-3-319-02387-8\\_10](https://doi.org/10.1007/978-3-319-02387-8_10)
- Müller, M., Anderson, B. E., Beyersdorf, A. J., Crawford, J. H., Diskin, G. S., Eichler, P., Fried, A., Keutsch, F. N., Mikoviny, T., Thornhill, K. L., Walega, J. G., Weinheimer, A. J., Yang, M., Yokelson, R. J., & Wisthaler, A. (2016). In situ measurements and modeling of reactive trace gases in a small biomass burning plume. *Atmospheric Chemistry and Physics*, *16*(6), 3813–3824. <https://doi.org/10.5194/acp-16-3813-2016>
- Müller, M., Graus, M., Wisthaler, A., Hansel, A., Metzger, A., Dommen, J., & Baltensperger, U. (2012). Analysis of high mass resolution PTR-TOF mass spectra from 1,3,5-trimethylbenzene (TMB) environmental chamber experiments. *Atmospheric Chemistry and Physics*, *12*(2), 829–843. <https://doi.org/10.5194/acp-12-829-2012>
- Munger, J. W., Jacob, D. J., Waldman, J. M., & Hoffmann, M. R. (1983). Fogwater chemistry in an urban atmosphere. *Journal of Geophysical Research*, *88*(C9), 5109–5121. <https://doi.org/10.1029/JC088iC09p05109>
- Newland, M. J., Ren, Y., McGillen, M. R., Michelat, L., Daële, V., & Mellouki, A. (2022). NO<sub>3</sub> chemistry of wildfire emissions: A kinetic study of the gas-phase reactions of furans with the NO<sub>3</sub> radical. *Atmospheric Chemistry and Physics*, *22*(3), 1761–1772. <https://doi.org/10.5194/acp-22-1761-2022>
- Nguyen, T. B., Coggon, M. M., Bates, K. H., Zhang, X., Schwantes, R. H., Schilling, K. A., Loza, C. L., Flagan, R. C., Wennberg, P. O., & Seinfeld, J. H. (2014). Organic aerosol formation from the reactive uptake of isoprene epoxydiols (IEPOX) onto non-acidified inorganic seeds. *Atmospheric Chemistry and Physics*, *14*(7), 3497–3510. <https://doi.org/10.5194/acp-14-3497-2014>
- Odum, J. R., Hoffmann, T., Bowman, F., Collins, D., Flagan, R. C., & Seinfeld, J. H. (1996). Gas/particle partitioning and secondary organic aerosol yields. *Environmental Science and Technology*, *30*(8), 2580–2585. <https://doi.org/10.1021/es950943+>
- Oh, H. J., Ma, Y., & Kim, J. (2020). Human inhalation exposure to aerosol and health effect: Aerosol monitoring and modelling regional deposited doses. *International Journal of Environmental Research and Public Health*, *17*(6), 1–2. <https://doi.org/10.3390/ijerph17061923>
- Olariu, R. I., Bejan, I., Barnes, I., Klotz, B., Becker, K. H., & Wirtz, K. (2004). Rate coefficients for the gas-phase reaction of NO<sub>3</sub> radicals with selected dihydroxybenzenes. *International Journal of Chemical Kinetics*, *36*(11), 577–583. <https://doi.org/10.1002/kin.20029>
- Olariu, R. I., Cuza, A. I., Chemistry, A., Tomas, A., Douai, M. De, Chimie, D., Barnes, I., Bejan, I., Becker, K. H., Wuppertal, B. U., Wirtz, K., Centro, F., & Ambientales, D. E. (1998). *Atmospheric Ozone Degradation Reaction of 1, 2-dihydroxybenzene : Aerosol Formation Study*. 1–12.
- Osseiran, N., Romanias, M. N., Gaudion, V., Angelaki, M. E., Papadimitriou, V. C., Tomas, A., Coddeville, P., & Thevenet, F. (2020). Development and validation of a thermally regulated atmospheric simulation chamber (THALAMOS): A versatile tool to simulate atmospheric processes. *Journal of Environmental Sciences (China)*, *95*(xxxx), 141–154.

<https://doi.org/10.1016/j.jes.2020.03.036>

- Pankow, J. F. (1994). An absorption model of the gas/aerosol partitioning involved in the formation of secondary organic aerosol. *Atmospheric Environment*, 28(SUPPL.), 189–193. <https://doi.org/10.1016/j.atmosenv.2007.10.060>
- Papadimitriou, V. C., Lazarou, Y. G., Talukdar, R. K., & Burkholder, J. B. (2011). *Atmospheric Chemistry of CF 3 CF 2*. 2(3), 167–181.
- Paquet, M., Arlt, D., Knape, J., Low, M., Forslund, P., & Pärt, T. (2019). Quantifying the links between land use and population growth rate in a declining farmland bird. *Ecology and Evolution*, 9(2), 868–879. <https://doi.org/10.1002/ece3.4766>
- Qian, Y., Zhu, L., Wang, Y., & Lu, X. (2015). Recent progress in the development of biofuel 2,5-dimethylfuran. *Renewable and Sustainable Energy Reviews*, 41, 633–646. <https://doi.org/10.1016/j.rser.2014.08.085>
- Ravishankara, A. R., & Davis, D. D. (1978). Kinetic rate constants for the reaction of OH with methanol, ethanol, and tetrahydrofuran at 298 K [2]. *Journal of Physical Chemistry*, 82(26), 2852–2853. <https://doi.org/10.1021/j100515a022>
- Reddington, C. L., Spracklen, D. V., Artaxo, P., Ridley, D. A., Rizzo, L. V., & Arana, A. (2016). Analysis of particulate emissions from tropical biomass burning using a global aerosol model and long-term surface observations. *Atmospheric Chemistry and Physics*, 16(17), 11083–11106. <https://doi.org/10.5194/acp-16-11083-2016>
- Ren, X., Brune, W. H., Oligier, A., Metcalf, A. R., Simpas, J. B., Shirley, T., Schwab, J. J., Bai, C., Roychowdhury, U., Li, Y., Cai, C., Demerjian, K. L., He, Y., Zhou, X., Gao, H., & Hou, J. (2006). OH, HO<sub>2</sub>, and OH reactivity during the PMTACS – NY Whiteface Mountain 2002 campaign: Observations and model comparison. 111, 1–12. <https://doi.org/10.1029/2005JD006126>
- Ren, X., Gao, H., Zhou, X., Crouse, J. D., Wennberg, P. O., Browne, E. C., LaFranchi, B. W., Cohen, R. C., McKay, M., Goldstein, A. H., & Mao, J. (2010). Measurement of atmospheric nitrous acid at Bodgett forest during BEARPEX2007. *Atmospheric Chemistry and Physics*, 10(13), 6283–6294. <https://doi.org/10.5194/acp-10-6283-2010>
- Ren, X., Harder, H., Martinez, M., Leshner, R. L., Oligier, A., Simpas, J. B., Brune, W. H., Schwab, J. J., Demerjian, K. L., He, Y., Zhou, X., & Gao, H. (2003). OH and HO<sub>2</sub> chemistry in the urban atmosphere of New York City. *Atmospheric Environment*, 37(26), 3639–3651. [https://doi.org/10.1016/S1352-2310\(03\)00459-X](https://doi.org/10.1016/S1352-2310(03)00459-X)
- Rissanen, M. (2021). Anthropogenic Volatile Organic Compound (AVOC) Autoxidation as a Source of Highly Oxygenated Organic Molecules (HOM). *Journal of Physical Chemistry A*, 125(41), 9027–9039. <https://doi.org/10.1021/acs.jpca.1c06465>
- Roberts, J. M., Stockwell, C. E., Yokelson, R. J., De Gouw, J., Liu, Y., Selimovic, V., Koss, A. R., Sekimoto, K., Coggon, M. M., Yuan, B., Zarzana, K. J., Brown, S. S., Santin, C., Doerr, S. H., & Warneke, C. (2020). The nitrogen budget of laboratory-simulated western US wildfires during the FIREX 2016 Fire Lab study. *Atmospheric Chemistry and Physics*, 20(14), 8807–8826. <https://doi.org/10.5194/acp-20-8807-2020>
- Román-Leshkov, Y., Barrett, C. J., Liu, Z. Y., & Dumesic, J. A. (2007). Production of

- dimethylfuran for liquid fuels from biomass-derived carbohydrates. *Nature*, 447(7147), 982–985. <https://doi.org/10.1038/nature05923>
- Romanias, M. N., Coggon, M., Al Ali, F., Burkholder, J. B., Dagaut, P., Warneke, C., Stockwell, C. E., Decker, Z., Tomas, A., Houzel, N., Coeur, C., & Brown, S. (n.d.-a). Atmospheric chemistry of furanoids: insights into the sources and atmospheric fate. *Atmospheric Environment*.
- Romanias, M. N., Coggon, M. M., Al Ali, F., Burkholder, J. B., Dagaut, P., Warneke, C., Stockwell, C. E., Decker, Z. C. J., Tomas, A., Houzel, N., Coeur, C., & Brown, S. S. (n.d.-b). Atmospheric chemistry of furanoids: insights into the sources and atmospheric fate. *ASC ACS Earth and Space Chemistry*.
- Schellenberg, C. (2009). Conducta irascible y recalcitrante tras una infección de gripe: Efectos de una acupuntura dispersante en el H 3 en lactantes y niños pequeños. *Revista Internacional de Acupuntura*, 3(2), 78–79. [https://doi.org/10.1016/S1887-8369\(09\)71579-0](https://doi.org/10.1016/S1887-8369(09)71579-0)
- Schumann, U. (2012). Atmospheric Physics. In *Physics Today* (Vol. 15, Issue 5). <https://doi.org/10.1063/1.3058219>
- Seinfeld, J. H., Pandis, S. N., & Noone, K. (1998). Atmospheric Chemistry and Physics: From Air Pollution to Climate Change. In *Physics Today* (Vol. 51, Issue 10). <https://doi.org/10.1063/1.882420>
- Sekimoto, K., Koss, A. R., Gilman, J. B., Selimovic, V., Coggon, M. M., Zarzana, K. J., Yuan, B., Lerner, B. M., Brown, S. S., Warneke, C., Yokelson, R. J., Roberts, J. M., & De Gouw, J. (2018). High-and low-temperature pyrolysis profiles describe volatile organic compound emissions from western US wildfire fuels. *Atmospheric Chemistry and Physics*, 18(13), 9263–9281. <https://doi.org/10.5194/acp-18-9263-2018>
- Selimovic, V., Yokelson, R. J., Warneke, C., Roberts, J. M., De Gouw, J., Reardon, J., & Griffith, D. W. T. (2018). Aerosol optical properties and trace gas emissions by PAX and OP-FTIR for laboratory-simulated western US wildfires during FIREX. *Atmospheric Chemistry and Physics*, 18(4), 2929–2948. <https://doi.org/10.5194/acp-18-2929-2018>
- Si, Z., Wang, C. G., Bi, K., Zhang, X. H., Yu, C. L., Dong, R. J., Ma, L. L., & Changle, P. (2017). Py-GC/MS study of lignin pyrolysis and effect of catalysts on product distribution. *International Journal of Agricultural and Biological Engineering*, 10(5), 214–225. <https://doi.org/10.25165/j.ijabe.20171005.2852>
- Simoneit, B. R. T. (2002). Biomass burning - A review of organic tracers for smoke from incomplete combustion. In *Applied Geochemistry* (Vol. 17, Issue 3). [https://doi.org/10.1016/S0883-2927\(01\)00061-0](https://doi.org/10.1016/S0883-2927(01)00061-0)
- Smith, D., & Španěl, P. (2005). Selected ion flow tube mass spectrometry (SIFT-MS) for on-line trace gas analysis. *Mass Spectrometry Reviews*, 24(5), 661–700. <https://doi.org/10.1002/mas.20033>
- Song, C., NA, K., & Cocker, D. R. (2005). Impact of the Hydrocarbon to NO. *Environmental Science & Technology*, 39(9), 3143–3149.
- Španěl, P., Dryahina, K., & Smith, D. (2013). A quantitative study of the influence of inhaled

- compounds on their concentrations in exhaled breath. *Journal of Breath Research*, 7(1). <https://doi.org/10.1088/1752-7155/7/1/017106>
- Stehfest, E., van Zeist, W. J., Valin, H., Havlik, P., Popp, A., Kyle, P., Tabeau, A., Mason-D’Croz, D., Hasegawa, T., Bodirsky, B. L., Calvin, K., Doelman, J. C., Fujimori, S., Humpenöder, F., Lotze-Campen, H., van Meijl, H., & Wiebe, K. (2019). Key determinants of global land-use projections. *Nature Communications*, 10(1), 1–10. <https://doi.org/10.1038/s41467-019-09945-w>
- Stockman, R. A. (2007). Heterocyclic chemistry. In *Annual Reports on the Progress of Chemistry - Section B* (Vol. 103). <https://doi.org/10.1039/b614418g>
- Stockwell, C. E., Christian, T. J., Goetz, J. D., Jayarathne, T., Bhawe, P. V., Praveen, P. S., Adhikari, S., Maharjan, R., DeCarlo, P. F., Stone, E. A., Saikawa, E., Blake, D. R., Simpson, I. J., Yokelson, R. J., & Panday, A. K. (2016). Nepal Ambient Monitoring and Source Testing Experiment (NAMaSTE): Emissions of trace gases and light-absorbing carbon from wood and dung cooking fires, garbage and crop residue burning, brick kilns, and other sources. *Atmospheric Chemistry and Physics*, 16(17), 11043–11081. <https://doi.org/10.5194/acp-16-11043-2016>
- Stockwell, C. E., Veres, P. R., Williams, J., & Yokelson, R. J. (2015). Characterization of biomass burning emissions from cooking fires, peat, crop residue, and other fuels with high-resolution proton-transfer-reaction time-of-flight mass spectrometry. *Atmospheric Chemistry and Physics*, 15(2), 845–865. <https://doi.org/10.5194/acp-15-845-2015>
- Strollo, C. M., & Ziemann, P. J. (2013). Products and mechanism of secondary organic aerosol formation from the reaction of 3-methylfuran with OH radicals in the presence of NO<sub>x</sub>. *Atmospheric Environment*, 77, 534–543. <https://doi.org/10.1016/j.atmosenv.2013.05.033>
- Tajuelo, M., Rodríguez, A., Baeza-Romero, M. T., Aranda, A., Díaz-de-Mera, Y., & Rodríguez, D. (2019). Secondary organic aerosol formation from  $\alpha$ -methylstyrene atmospheric degradation: Role of NO<sub>x</sub> level, relative humidity and inorganic seed aerosol. *Atmospheric Research*, 230(July), 104631. <https://doi.org/10.1016/j.atmosres.2019.104631>
- Tajuelo, M., Rodríguez, D., Baeza-Romero, M. T., Díaz-de-Mera, Y., Aranda, A., & Rodríguez, A. (2019). Secondary organic aerosol formation from styrene photolysis and photooxidation with hydroxyl radicals. *Chemosphere*, 231, 276–286. <https://doi.org/10.1016/j.chemosphere.2019.05.136>
- Tajuelo, M., Rodríguez, D., Rodríguez, A., Escalona, A., Viteri, G., Aranda, A., & Diaz-de-Mera, Y. (2021). Secondary organic aerosol formation from the ozonolysis and oh-photooxidation of 2,5-dimethylfuran. *Atmospheric Environment*, 245, 118041. <https://doi.org/10.1016/j.atmosenv.2020.118041>
- Takekawa, H., Minoura, H., & Yamazaki, S. (2003). *Temperature dependence of secondary organic aerosol formation by photo-oxidation of hydrocarbons*. 37, 3413–3424. [https://doi.org/10.1016/S1352-2310\(03\)00359-5](https://doi.org/10.1016/S1352-2310(03)00359-5)
- Tapia, A., Villanueva, F., Salgado, M. S., Cabañas, B., Martínez, E., & Martín, P. (2011). Atmospheric degradation of 3-methylfuran: Kinetic and products study. *Atmospheric*

- Chemistry and Physics*, 11(7), 3227–3241. <https://doi.org/10.5194/acp-11-3227-2011>
- Thewes, M., Muether, M., Pischinger, S., Budde, M., Brunn, A., Sehr, A., Adomeit, P., & Klankermayer, J. (2011). Analysis of the impact of 2-methylfuran on mixture formation and combustion in a direct-injection spark-ignition engine. *Energy and Fuels*, 25(12), 5549–5561. <https://doi.org/10.1021/ef201021a>
- Tomas, A., Henry, F., & Visez, N. (2009). *Aerosol formation yields from the reaction of catechol with ozone*. 43, 2360–2365. <https://doi.org/10.1016/j.atmosenv.2008.12.054>
- Tuan Hoang, A., & Viet Pham, V. (2021). 2-Methylfuran (MF) as a potential biofuel: A thorough review on the production pathway from biomass, combustion progress, and application in engines. *Renewable and Sustainable Energy Reviews*, 148(June), 111265. <https://doi.org/10.1016/j.rser.2021.111265>
- Tuazon, E. C., Aschmann, S. M., & Atkinson, R. (2000). Atmospheric degradation of volatile methyl-silicon compounds. *Environmental Science and Technology*, 34(10), 1970–1976. <https://doi.org/10.1021/es9910053>
- Vallero, D. (2008). *Fundamentals of Air Pollution* (Fourth). El Sevier.
- Villanueva, F., Barnes, I., Monedero, E., Salgado, S., Gómez, M. V., & Martin, P. (2007). Primary product distribution from the Cl-atom initiated atmospheric degradation of furan: Environmental implications. *Atmospheric Environment*, 41(38), 8796–8810. <https://doi.org/10.1016/j.atmosenv.2007.07.053>
- Villanueva, F., Cabañas, B., Monedero, E., Salgado, S., Bejan, I., & Martin, P. (2009). Atmospheric degradation of alkylfurans with chlorine atoms: Product and mechanistic study. *Atmospheric Environment*, 43(17), 2804–2813. <https://doi.org/10.1016/j.atmosenv.2009.02.030>
- Wallington, T. J., Dagaut, P., Liu, R., & Kurylo, M. J. (1988). The gas phase reactions of hydroxyl radicals with a series of esters over the temperature range 240–440 K. *International Journal of Chemical Kinetics*, 20(2), 177–186. <https://doi.org/10.1002/kin.550200210>
- Wang, J., Doussin, J. F., Perrier, S., Perraudin, E., Katrib, Y., Pangui, E., & Picquet-Varrault, B. (2011). Design of a new multi-phase experimental simulation chamber for atmospheric photo-smog, aerosol and cloud chemistry research. *Atmospheric Measurement Techniques*, 4(11), 2465–2494. <https://doi.org/10.5194/amt-4-2465-2011>
- Wang, L., Slowik, J. G., Tripathi, N., Bhattu, D., Rai, P., Kumar, V., Vats, P., Satish, R., Baltensperger, U., Ganguly, D., Rastogi, N., Sahu, L. K., Tripathi, S. N., & Prévôt, A. S. H. (2020). Source characterization of volatile organic compounds measured by proton-transfer-reaction time-of-flight mass spectrometers in Delhi, India. *Atmospheric Chemistry and Physics*, 20(16), 9753–9770. <https://doi.org/10.5194/acp-20-9753-2020>
- Wang, Q., Song, H., Pan, S., Dong, N., Wang, X., & Sun, S. (2020). Initial pyrolysis mechanism and product formation of cellulose: An Experimental and Density functional theory(DFT) study. *Scientific Reports*, 10(1), 1–18. <https://doi.org/10.1038/s41598-020-60095-2>
- Wang, S., Wei, W., Du, L., Li, G., & Hao, J. (2009). Characteristics of gaseous pollutants from biofuel-stoves in rural China. *Atmospheric Environment*, 43(27), 4148–4154. <https://doi.org/10.1016/j.atmosenv.2009.05.040>



- Whelan, C. A., Eble, J., Mir, Z. S., Blitz, M. A., Seakins, P. W., Olzmann, M., & Stone, D. (2020). Kinetics of the Reactions of Hydroxyl Radicals with Furan and Its Alkylated Derivatives 2-Methyl Furan and 2,5-Dimethyl Furan. *Journal of Physical Chemistry A*, *124*(37), 7416–7426. <https://doi.org/10.1021/acs.jpca.0c06321>
- Wine, P. H., & Thompson, R. J. (1984). Kinetics of OH reactions with furan, thiophene, and tetrahydrothiophene. *International Journal of Chemical Kinetics*, *16*(7), 867–878. <https://doi.org/10.1002/kin.550160707>
- Winer, M., Darnall, K. R., & Lloyd, A. C. (1977). *REACTION set-BUTYL*. *5*(2), 221–226.
- Wingenter, O. W., Blake, D. R., Blake, N. J., Sive, B. C., Rowland, F. S., Atlas, E., & Flocke, F. (1999). Tropospheric hydroxyl and atomic chlorine concentrations, and mixing timescales determined from hydrocarbon and halocarbon measurements made over the Southern Ocean. *Journal of Geophysical Research Atmospheres*, *104*(D17), 21819–21828. <https://doi.org/10.1029/1999JD900203>
- Wingenter, O. W., Kubo, M. K., Blake, N. J., Smith, T. W., Blake, D. R., & Rowland, F. S. (1996). Hydrocarbon and halocarbon measurements as photochemical and dynamical indicators of atmospheric hydroxyl, atomic chlorine, and vertical mixing obtained during Lagrangian flights. *Journal of Geophysical Research Atmospheres*, *101*(D2), 4331–4340. <https://doi.org/10.1029/95JD02457>
- World Health Organization. (2016). WORLD HEALTH STATISTICS - MONITORING HEALTH FOR THE SDGs. *World Health Organization*, 1.121. <https://doi.org/10.1017/CBO9781107415324.004>
- Xu, L., Guo, H., Weber, R. J., & Ng, N. L. (2017). Chemical Characterization of Water-Soluble Organic Aerosol in Contrasting Rural and Urban Environments in the Southeastern United States. *Environmental Science and Technology*, *51*(1), 78–88. <https://doi.org/10.1021/acs.est.6b05002>
- Yang, H., Li, S., Liu, B., Chen, Y., Xiao, J., Dong, Z., Gong, M., & Chen, H. (2020). Hemicellulose pyrolysis mechanism based on functional group evolutions by two-dimensional perturbation correlation infrared spectroscopy. *Fuel*, *267*(July 2019), 117302. <https://doi.org/10.1016/j.fuel.2020.117302>
- Yang, X., Zhao, Y., Li, W., Li, R., & Wu, Y. (2019). Unveiling the Pyrolysis Mechanisms of Hemicellulose: Experimental and Theoretical Studies. *Energy and Fuels*, *33*(5), 4352–4360. <https://doi.org/10.1021/acs.energyfuels.9b00482>
- Yokelson, R. J., Burling, I. R., Gilman, J. B., Warneke, C., Stockwell, C. E., De Gouw, J., Akagi, S. K., Urbanski, S. P., Veres, P., Roberts, J. M., Kuster, W. C., Reardon, J., Griffith, D. W. T., Johnson, T. J., Hosseini, S., Miller, J. W., Cocker, D. R., Jung, H., & Weise, D. R. (2013). Coupling field and laboratory measurements to estimate the emission factors of identified and unidentified trace gases for prescribed fires. *Atmospheric Chemistry and Physics*, *13*(1), 89–116. <https://doi.org/10.5194/acp-13-89-2013>
- Yokelson, R. J., Burling, I. R., Urbanski, S. P., Atlas, E. L., Adachi, K., Buseck, P. R., Wiedinmyer, C., Akagi, S. K., Toohey, D. W., & Wold, C. E. (2011). Trace gas and particle emissions from open biomass burning in Mexico. *Atmospheric Chemistry and Physics*, *11*(14), 6787–6808. <https://doi.org/10.5194/acp-11-6787-2011>

- Yokelson, R. J., Saharjo, B. H., Stockwell, C. E., Putra, E. I., Jayarathne, T., Akbar, A., Albar, I., Blake, D. R., Graham, L. L. B., Kurniawan, A., Meinardi, S., Ningrum, D., Nurhayati, A. D., Saad, A., Sakuntaladewi, N., Setianto, E., Simpson, I. J., Stone, E. A., Sutikno, S., ... Cochrane, M. A. (2022). Tropical peat fire emissions: 2019 field measurements in Sumatra and Borneo and synthesis with previous studies. *Atmospheric Chemistry and Physics*, *22*(15), 10173–10194. <https://doi.org/10.5194/acp-22-10173-2022>
- Yokelson, R. J., Susott, R., Ward, D. E., Reardon, J., & Griffith, D. W. T. (1997). Emissions from smoldering combustion of biomass measured by open-path Fourier transform infrared spectroscopy. *Journal of Geophysical Research Atmospheres*, *102*(15), 18865–18877. <https://doi.org/10.1029/97jd00852>
- Young, C. J., Washenfelder, R. A., Edwards, P. M., Parrish, D. D., Gilman, J. B., Kuster, W. C., Mielke, L. H., Osthoff, H. D., Tsai, C., Pikelnaya, O., Stutz, J., Veres, P. R., Roberts, J. M., Griffith, S., Dusanter, S., Stevens, P. S., Flynn, J., Grossberg, N., Lefer, B., ... Brown, S. S. (2014). Chlorine as a primary radical: Evaluation of methods to understand its role in initiation of oxidative cycles. *Atmospheric Chemistry and Physics*, *14*(7), 3427–3440. <https://doi.org/10.5194/acp-14-3427-2014>
- Yuan, Y., Zhao, X., Wang, S., & Wang, L. (2017). Atmospheric Oxidation of Furan and Methyl-Substituted Furans Initiated by Hydroxyl Radicals. *Journal of Physical Chemistry A*, *121*(48), 9306–9319. <https://doi.org/10.1021/acs.jpca.7b09741>
- Zhao, D., Schmitt, S. H., Wang, M., Acir, I. H., Tillmann, R., Tan, Z., Novelli, A., Fuchs, H., Pullinen, I., Wegener, R., Rohrer, F., Wildt, J., Kiendler-Scharr, A., Wahner, A., & Mentel, T. F. (2018). Effects of NO<sub>x</sub> and SO<sub>2</sub> on the secondary organic aerosol formation from photooxidation of  $\alpha$ -pinene and limonene. *Atmospheric Chemistry and Physics*, *18*(3), 1611–1628. <https://doi.org/10.5194/acp-18-1611-2018>
- Zhao, X., & Wang, L. (2017). Atmospheric Oxidation Mechanism of Furfural Initiated by Hydroxyl Radicals. *Journal of Physical Chemistry A*, *121*(17), 3247–3253. <https://doi.org/10.1021/acs.jpca.7b00506>
- Zhou, X., Beine, H. J., Honrath, R. E., Fuentes, J. D., Simpson, W., & Bottenheim, J. W. (2001). Snowpack Photochemical Production of HONO: a Major Source of OH in the Arctic Boundary Layer in Springtime. *Geophysical Research Letters*, *28*, 4087–4090. <https://doi.org/10.1029/2001GL013531>
- Zhou, X., Li, W., Mabon, R., & Broadbelt, L. J. (2018). A mechanistic model of fast pyrolysis of hemicellulose. *Energy and Environmental Science*, *11*(5), 1240–1260. <https://doi.org/10.1039/c7ee03208k>
- Ziemann, P. J., & Atkinson, R. (2012). Kinetics, products, and mechanisms of secondary organic aerosol formation. *Chemical Society Reviews*, *41*(19), 6582–6605. <https://doi.org/10.1039/c2cs35122f>
- Zogka, A. G., Romanias, M. N., & Thevenet, F. (2022). Formaldehyde and glyoxal measurement deploying a selected ion flow tube mass spectrometer (SIFT-MS). *Atmospheric Measurement Techniques*, *15*(7), 2001–2019. <https://doi.org/10.5194/amt-15-2001-2022>
- Zysman, B., & Skelly, P. D. (1992). *T : 1992*.

## **Chapter III: Kinetic Studies**

### III.1 Introduction

This chapter includes the results obtained from the kinetic investigation of Furan (F), (2-methylfuran (2-MF), 3-methylfuran (3-MF), 2,5-dimethylfuran (2,5-DMF), and 2,3,5-trimethylfuran (2,3,5-TMF) reaction with NO<sub>3</sub> radicals. At first, in section III.2 are discussed the room temperature kinetics of the targeted compounds with the nitrate radical (NO<sub>3</sub>). Subsequently, in section III.3 the temperature dependent kinetics of F, 2-MF and 2,5-DMF with NO<sub>3</sub> are presented. This section also includes the temperature dependent study of  $\alpha$ -pinene and 2-carene, two monoterpenes that were used as reference molecules and for which it was necessary to validate their kinetics versus temperature in order to provide accurate results. The temperature dependent kinetics not only provide important information about the reaction mechanism, e.g. addition or abstraction pathways, but they are also necessary to evaluate the VOC reactivity under tropospheric relevant temperatures (essentially in atmospheric modeling), or elevated temperatures like those occurring in BB plumes. Finally, in section III.4 results discussion is provided in which the atmospheric lifetimes of the furanoids with NO<sub>3</sub> radicals and other tropospheric oxidants, i.e. OH, Cl, O<sub>3</sub>, are presented and the corresponding atmospheric implications are discussed.

### III.2 Room temperature rate coefficients measurements in CHARME simulation chamber

As a reminder, CHARME studies were conducted under dry conditions, at atmospheric pressure and room temperature ( $294 \pm 2$  K), which are typical laboratory conditions. In this investigations, the initial mixing ratios of the reactants were carefully controlled within a range of 500 to 1200 ppbv for both furan compounds and reference compounds. NO<sub>3</sub> radicals were produced by the thermal decomposition of dinitrogen pentoxide (N<sub>2</sub>O<sub>5</sub>). The concentration of VOCs was continuously monitored using a PTR-ToF-MS with a high temporal resolution of 10 s. Table III.1 represents the rate coefficients used for the reference compounds ( $k_{\text{Ref}}$ ).

Table III.1: Rate coefficients of the references used for the determination of the rate coefficients of furan compounds.

Reference Compound	$k_{\text{Ref}}$ (cm <sup>3</sup> molecule <sup>-1</sup> s <sup>-1</sup> )	Reference literature
$\alpha$ -Pinene ( $\alpha$ -P)	$(6.20 \pm 1.42) \times 10^{-12}$	(IUPAC, 2016)
$\beta$ -Pinene ( $\beta$ -P)	$(2.50 \pm 0.69) \times 10^{-12}$	
$\gamma$ -Terpinene ( $\gamma$ -T)	$(2.94 \pm 0.81) \times 10^{-11}$	
2-Methyl-2-Butene (2-MB)	$(9.38 \pm 0.47) \times 10^{-12}$	
$\alpha$ -Terpinene ( $\alpha$ -T)	$(1.82 \pm 1.04) \times 10^{-10}$	
2,3-Dimethyl-2-Butene (DMB)	$(4.50 \pm 0.40) \times 10^{-11}$	(Lançar et al., 1991)

#### III.2.1 Preliminary experiments

##### III.2.1.1 Dilution effect

A pressure compensator linked to the purified air generator enabled the chamber CHARME to be maintained at its original pressure. For this reason, in certain experiments an inert tracer, acetonitrile, was added to reactional mixture in order to measure the total dilution rate. The concentration of acetonitrile was monitored at  $m/z = 42.0$  using a PTR-ToF-MS. The average loss rate of acetonitrile calculated during each experiment was used as the dilution rate for all

stable species during the simulations. The dilution rate of acetonitrile was found to be  $k = 4.0 \times 10^{-6} \text{ s}^{-1}$ , which is consistent with Fayad (2019) who previously performed similar experiments in the same chamber. Given that the duration of the experiment was maximum 3 h, the dilution rate was considered to be negligible and the concentrations of the various species in the chamber were not adjusted for dilution.

### III.2.1.2 Wall losses

It is crucial to calculate the wall loss rates of all the species of interest in order to evaluate their possible contribution during the reaction kinetics with  $\text{NO}_3$ . The rate of gas- and particle- losses on the chamber walls are influenced by various factors, such as the chamber history, the cleaning process, the coating material, and the technology utilized in the coating process (Wang et al., 2011). The wall loss rate of a specific compound introduced into a reactor corresponds to its concentration decay over time in the absence of other reagents. This concentration decrease may result from its deposition and/or conversion on the chamber walls. To assess the wall losses of each VOC, a specific concentration range (300 ppbv - 800 ppbv) was injected into CHARME and was then constantly monitored before  $\text{N}_2\text{O}_5$  introduction. The decay of the compounds follows a first-order reaction according to Eq.1 where  $[\text{2-MF}]_0$  represents 2-MF initial concentration,  $[\text{2-MF}]_t$  represents instantaneous 2-MF concentration,  $k_w$  is the wall loss rate coefficient and  $t$  is the time of the analysis. Figure III.1 presents the typical wall loss kinetics of 2-MF.

$$\ln\left(\frac{[\text{2-MF}]_0}{[\text{2-MF}]_t}\right) = k_w \times t \quad \text{Eq.1}$$

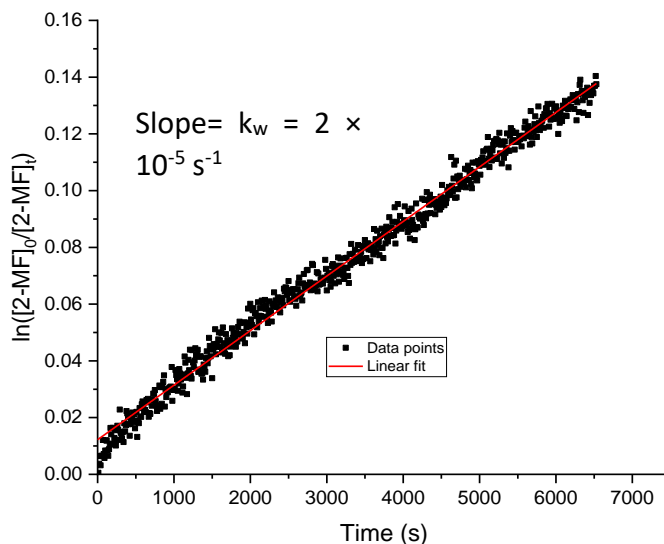


Figure III.1: Typical first-order wall loss reaction plot of 2-MF.

The wall loss rate coefficient, denoted as  $k_w$ , (see Table III.2) was considered in the case of furan with a value of  $6 \times 10^{-5} \text{ s}^{-1}$ , but was disregarded for all other organic compounds, where  $k_w$  was less than  $5 \times 10^{-5} \text{ s}^{-1}$  (see Table III.2).

Table III.2: Average wall loss rate coefficient ( $k_w$ ) for the VOCs used in CHARME experiments.

Compound	$k_w$ ( $s^{-1}$ )
2-MB	$8.1 \times 10^{-6}$
2,3-DMB	$1.0 \times 10^{-5}$
$\alpha$ -T	$2.0 \times 10^{-6}$
$\gamma$ -T	$9.6 \times 10^{-6}$
$\alpha$ -P	$8.7 \times 10^{-6}$
$\beta$ -P	$3.9 \times 10^{-5}$
Furan	$6.0 \times 10^{-5}$
2-MF	$1.9 \times 10^{-5}$
3-MF	$1.8 \times 10^{-5}$
2,5-DMF	$2.9 \times 10^{-5}$
2,3,5-TMF	$2.0 \times 10^{-5}$

### III.2.1.3 Absence of interference due to reaction with $N_2O_5$ and $NO_2$

The verification of the non-interference with  $N_2O_5$  and  $NO_2$  reactivity has already been achieved by Atkinson et al., (1985b) for double bonds in aromatic furan rings. Recently, another study done by Newland et al., (2022) has already showed that even for the organic compounds used in their study with the fastest reactivity with  $NO_2$ , there is still no effect on the kinetic with  $NO_3$  due to the compound's very slow reaction with  $NO_2$ . In literature (Atkinson et al., 1984), we can see that rate coefficient for some compounds reactivity with  $NO_2$  is slower by a factor of 1 to 100 million with the present kinetic values in this work. So even with a very high  $NO_2$  concentrations, the reaction of the studied VOCs will be sensibly slower than the  $NO_3$  reactivity. Table III.3 of this present work shows a very good agreement between the different references and between high and low  $N_2O_5$  concentrations, leading to the fact that furans and references only react to one oxidant,  $NO_3$ .

### III.2.2 Rate coefficient of furan reaction with $NO_3$

For the measurement of furan reaction rate coefficient with  $NO_3$ , seven experiments were conducted using two reference compounds,  $\alpha$ -P and  $\beta$ -P. The range of concentrations used for furan and the reference compounds was within 500 and 1300 ppbv. A continuous injection of  $N_2O_5$  was performed into the chamber until both the furan and reference compounds were consumed by at least 98%. As an example, the intensity (in counts) of F and  $\alpha$ -P measured versus the time with the PTR-MS during one representative experiment are presented in Figure III.2.

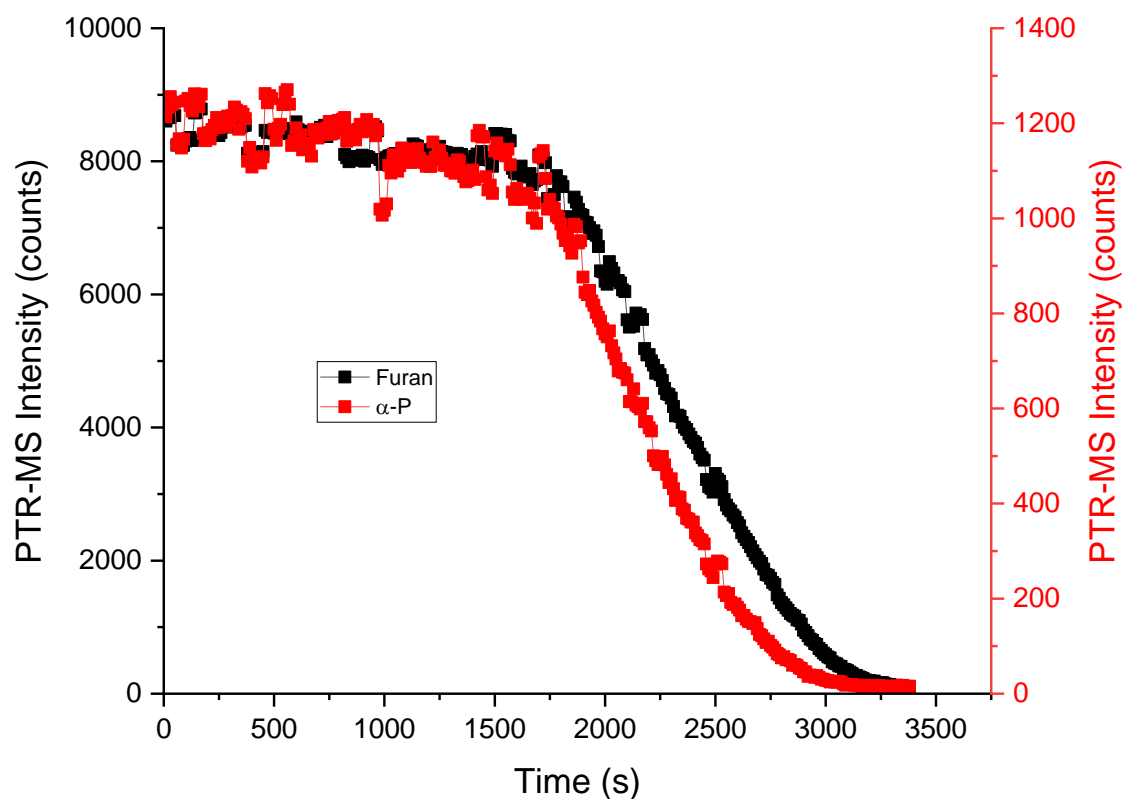


Figure III.2: Time profiles of F and  $\alpha$ -P followed by the PTR-ToF-MS.

A typical relative rate plot is presented in Figure III.3. A linear relationship with a correlation coefficient greater than 0.98 and nearly zero intercept was observed. These observations suggest that no secondary reactions, beyond those that result in accounted losses (wall losses), are taking place into the chamber.

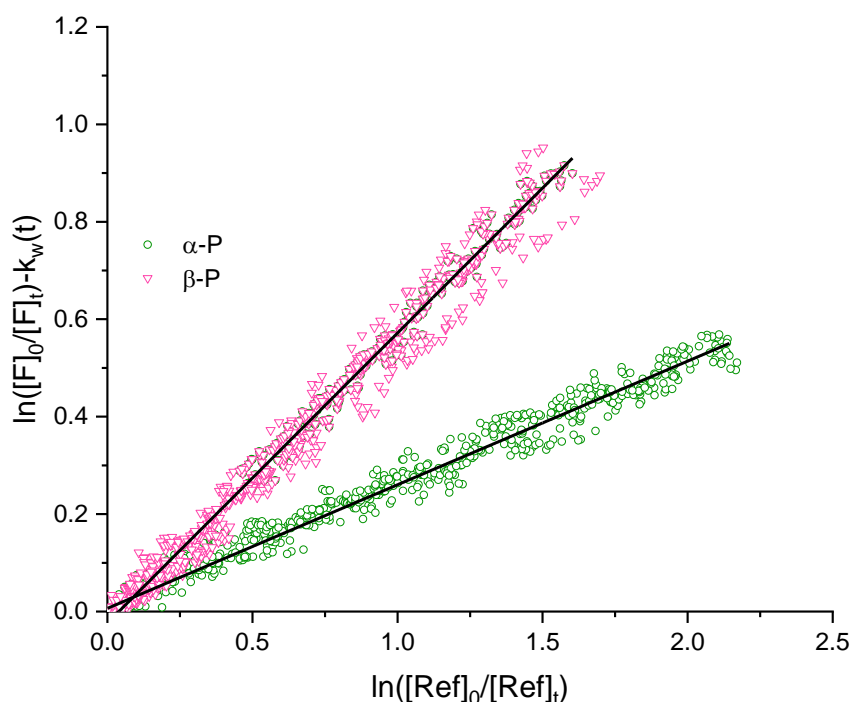


Figure III.3: Kinetic data plots for the reaction of F with  $\text{NO}_3$  using  $\alpha$ -P (green circles) and  $\beta$ -P (pink triangles) as reference compounds.

Table III.3 presents the experimental conditions, the relative rate ratios ( $k_{\text{FC}}/k_{\text{Ref}}$ ) obtained from the relative rate plots, and the measured rate coefficients for each experiment ( $k_{\text{FC}}$ ). Table III.3 also presents the average rate coefficient ( $k_{\text{FC average}}$ ), which was obtained from the values of the two references. The reported errors on the slope represent twice the standard deviation resulting from the linear regression. The error on the rate coefficient is calculated according to Eq. 10 taking into account the error on our measurements and on the reference rate coefficient. The average rate coefficient obtained for the reaction of F with  $\text{NO}_3$  is  $(1.51 \pm 0.38) \times 10^{-12} \text{ cm}^3 \text{ molecule}^{-1} \text{ s}^{-1}$  (this value was obtained by calculating the arithmetic mean of the values determined with both references with average error calculated according to Eq. 11).

### III.2.3 Rate coefficient of 2-MF reaction with $\text{NO}_3$

The relative rate constant for the gas-phase reaction between 2-MF and  $\text{NO}_3$  was measured using three reference compounds  $\gamma$ -T, 2-MB, and DMB (Table III.1). Nine experiments were conducted, three per reference with concentration ranging for 2-MF and the references between 400 and 1350 ppbv. Figure S1 depicts a typical temporal profile of the 2-MF concentrations (in counts) versus one of the references employed (2-MB). Figure III.4 illustrates the comparison of 2-MF's relative loss with that of the three reference compounds in the presence of  $\text{NO}_3$  radicals. The high correlation coefficient exceeding 0.98 and a near-zero intercept for all the reference compounds demonstrate that there are no secondary reactions.



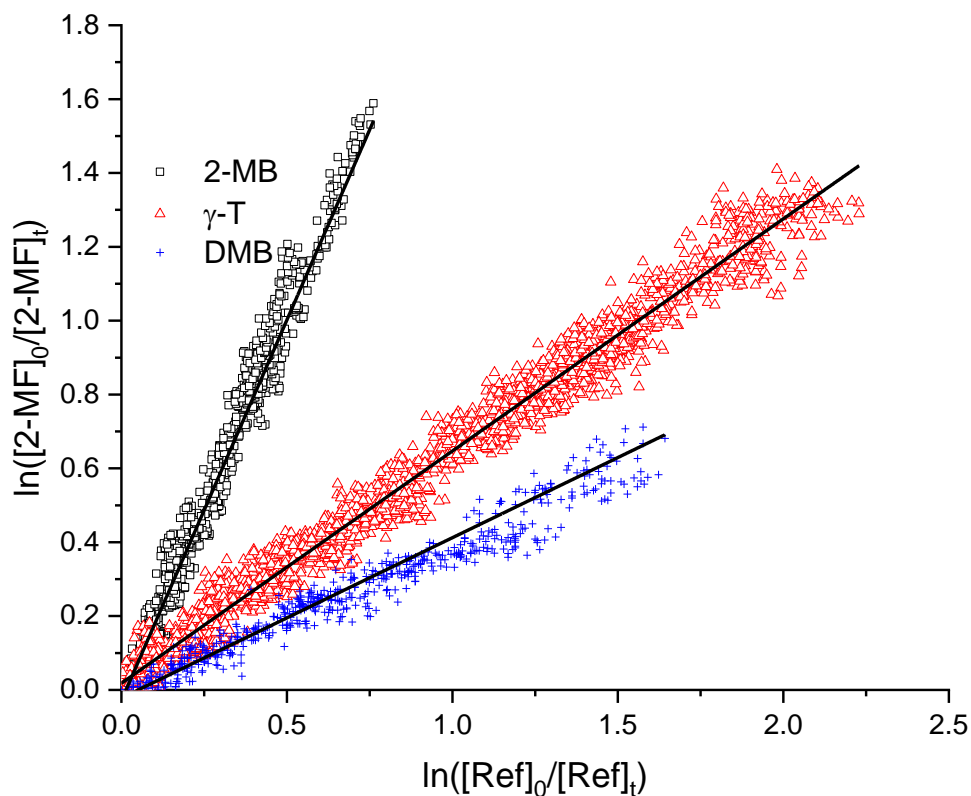


Figure III.4: Kinetic data plots for the reaction of 2-MF with  $\text{NO}_3$  at  $294 \pm 2$  K using 2-MB (black squares),  $\gamma$ -T (red triangles) and DMB (blue cross) as reference compounds.

The slopes ( $k_{2\text{-MF}}/k_{\text{Ref}}$ ) and the relative rate constants (2-MF) were determined for each reference compound, and the average of all the obtained values was measured to be  $(1.91 \pm 0.32) \times 10^{-11} \text{ cm}^3 \text{ molecule}^{-1} \text{ s}^{-1}$  (see Table III.3).

#### III.2.4 Rate coefficient of 3-MF reaction with $\text{NO}_3$

To determine the reaction rate coefficient of 3-MF, nine experiments were carried out using three reference compounds,  $\alpha$ -P,  $\gamma$ -T and 2-MB (Table III.1) with concentration ranges of 250 to 1100 ppbv. Figure S2 shows a typical temporal variation observed for one of the utilized references ( $\alpha$ -P) and 3-MF.

Figure III.5 compares the relative loss of 3-MF with that of the three reference compounds in the presence of  $\text{NO}_3$  radicals. The correlation coefficient was greater than 0.98 and the almost-zero intercept observed for all the reference compounds indicate the absence of any secondary reactions and the insignificance of wall losses for 3-MF and all references.

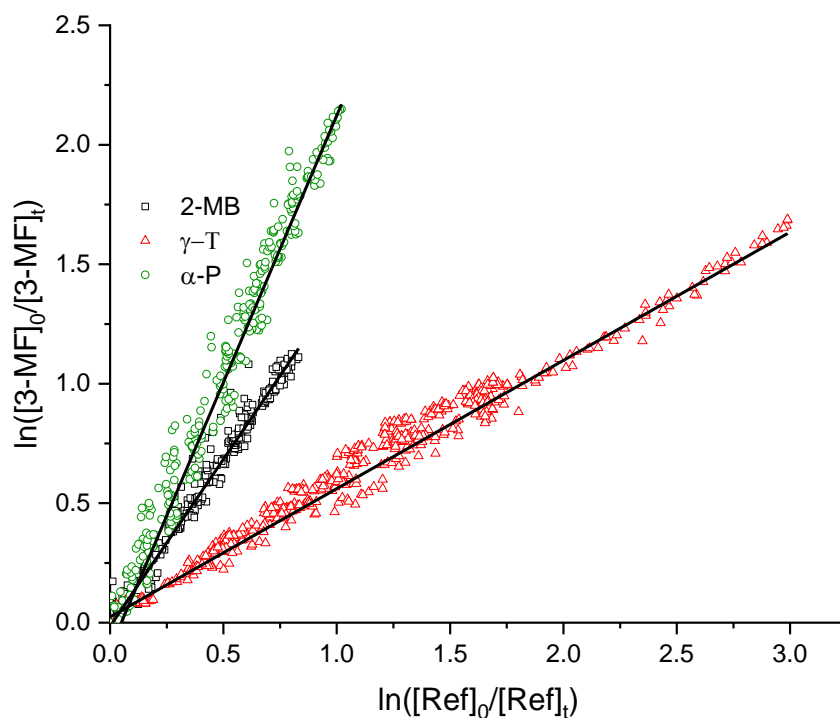


Figure III.5: Kinetic data plots for the reaction of 3-MF with  $\text{NO}_3$  using three reference compounds 2-MB (black squares),  $\gamma$ -T (red triangles) and  $\alpha$ -P (green circles).

The slopes ( $k_{3\text{-MF}}/k_{\text{Ref}}$ ) and relative rate constants ( $k_{3\text{-MF}}$ ) were measured for each reference compound, and the mean value of these measurements was computed. A summary of these results is also presented in Table III.3. The average 3-MF rate coefficient obtained from the three references is  $k_{3\text{-MF}} = (1.49 \pm 0.33) \times 10^{-11} \text{ cm}^3 \text{ molecule}^{-1} \text{ s}^{-1}$ .

### III.2.5 Rate coefficient of 2,5-DMF reaction with $\text{NO}_3$

The kinetics of 2,5-DMF with  $\text{NO}_3$  radicals were determined in respect of two different reference compounds:  $\gamma$ -T and DMB (Table III.1). Six experiments were done using variable concentrations of 2,5-DMF between 600 ppbv and 1400 ppbv. A summary of the experimental conditions and the obtained results is given in Table III.3. A typical temporal variation of one of the used references ( $\gamma$ -T) and 2,5-DMF is illustrated in Figure S3.

Figure III.6 shows the plot of  $\ln([2,5\text{-DMF}]_0/[2,5\text{-DMF}]_t)$  against  $\ln([Ref]_0/[Ref]_t)$ . The experimental data points exhibit good linearity, and the regression line passes through the origin, indicating that both 2,5-DMF and references are consumed only through their reaction with  $\text{NO}_3$ .

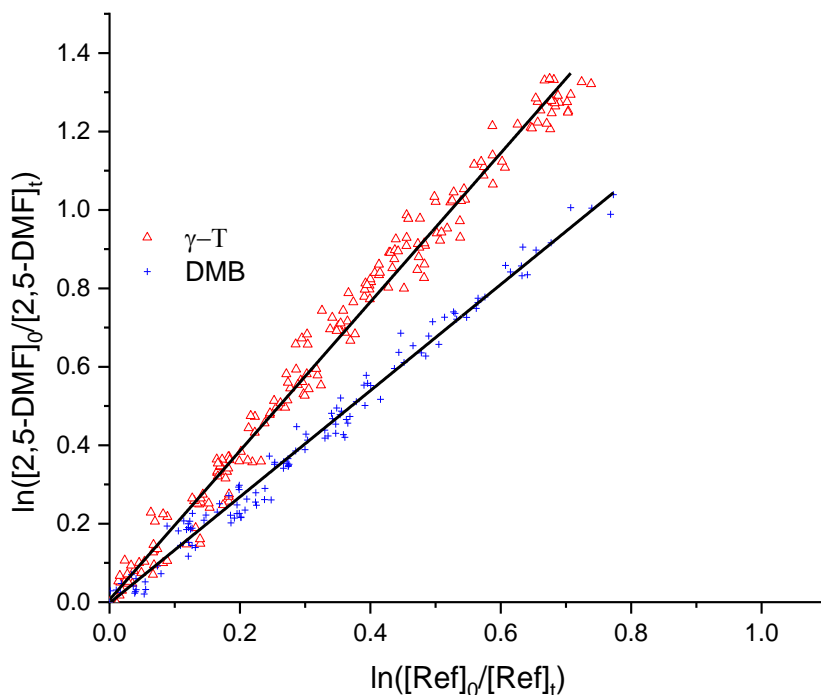


Figure III.6: Kinetic data plots for the reaction of 2,5-DMF with  $\text{NO}_3$  using two reference compounds,  $\gamma$ -T (red triangles) and DMB (blue crosses).

The values of the constant for the reaction between 2,5-DMF and nitrate radicals obtained with both references are consistent. The average value is  $k_{2,5\text{-DMF}} = (5.82 \pm 1.21) \times 10^{-11} \text{ cm}^3 \text{ molecule}^{-1} \text{ s}^{-1}$ . The error indicated for  $k_{2,5\text{-DMF}}$  takes into account the error on the constant of the reference compounds.

### III.2.6 Rate coefficient of 2,3,5-TMF reaction with $\text{NO}_3$

To establish the reaction rate coefficient of 2,3,5-TMF, relative rate kinetics were performed using  $\alpha$ -T and DMB (Table III.1). A total of six experiments were conducted and the concentration of 2,3,5-TMF and the two reference compounds ranged from 400 to 1200 ppbv. A characteristic temporal profile for the decay of 2,3,5-TMF relative to one of the reference compounds ( $\alpha$ -T) is shown in Figure S4.

A typical relative rate plot for the decay of 2,3,5-TMF and the two used references is presented in Figure III.7. The total average rate coefficient for the reaction of 2,3,5-TMF with  $\text{NO}_3$  is  $(1.66 \pm 0.69) \times 10^{-10} \text{ cm}^3 \text{ molecule}^{-1} \text{ s}^{-1}$ . A summary of the experimental conditions and results obtained is given in Table III.3.

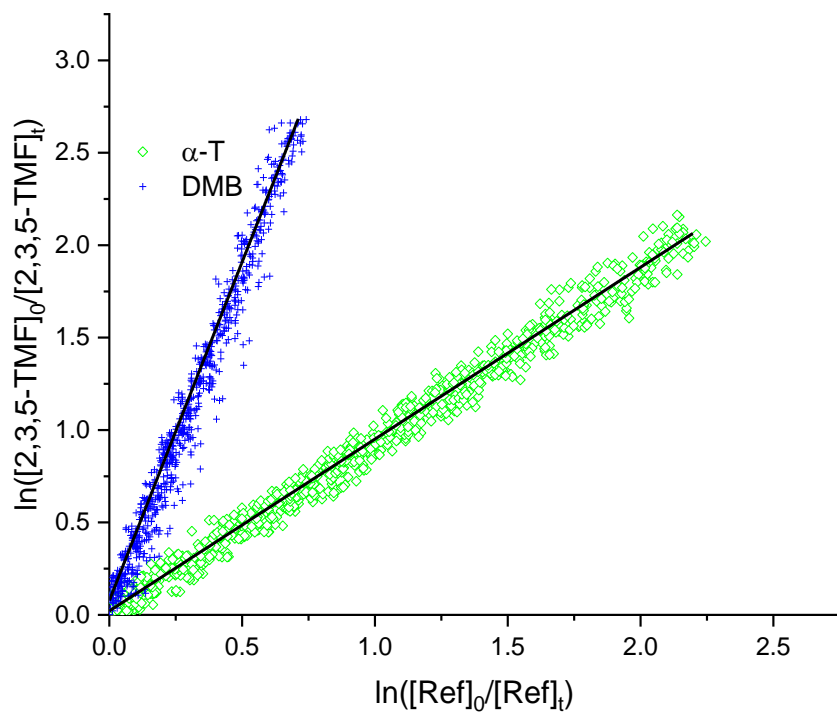
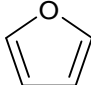
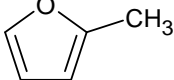
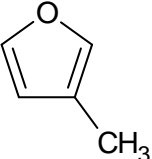
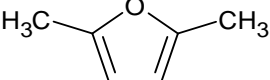
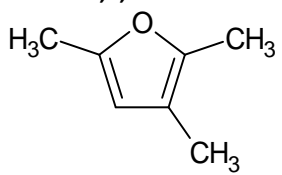


Figure III.7: Kinetic data plots for the reaction of 2,3,5-TMF with  $\text{NO}_3$  at  $294 \pm 2$  K using  $\alpha\text{-T}$  and DMB as reference compounds.

Table III.3: Summary of all rate coefficients for the reactions of furan compounds with NO<sub>3</sub>.

Compound	Reference	[FC] <sub>0</sub> (ppbv)	[Ref] <sub>0</sub> (ppbv)	[N <sub>2</sub> O <sub>5</sub> ] <sub>0</sub> (ppbv)	$k_{FC}/k_{ref}^a$	$k_{FC}^{b,c}$	$k_{FC}^{b,d,e}$ (average)
<b>F</b> 	α-P	590	600	1850	$(24.5 \pm 0.2) \times 10^{-2}$	$(1.52 \pm 0.36) \times 10^{-12}$	$(1.51 \pm 0.38) \times 10^{-12}$
		790	800	1760	$(24.6 \pm 0.1) \times 10^{-2}$	$(1.52 \pm 0.35) \times 10^{-12}$	
		1000	1000	3660	$(25.2 \pm 0.1) \times 10^{-2}$	$(1.56 \pm 0.36) \times 10^{-12}$	
		1300	1300	8770	$(25.3 \pm 0.3) \times 10^{-2}$	$(1.57 \pm 0.37) \times 10^{-12}$	
	β-P	500	500	1740	$(56.5 \pm 0.2) \times 10^{-2}$	$(1.41 \pm 0.39) \times 10^{-12}$	
		990	1000	2000	$(62.1 \pm 0.3) \times 10^{-2}$	$(1.55 \pm 0.43) \times 10^{-12}$	
1300		1300	4170	$(59.5 \pm 0.2) \times 10^{-2}$	$(1.48 \pm 0.41) \times 10^{-12}$		
<b>2-MF</b> 	2-MB	630	640	9400	$2.06 \pm 0.01$	$(1.93 \pm 0.10) \times 10^{-11}$	$(1.91 \pm 0.32) \times 10^{-11}$
		830	860	6520	$2.17 \pm 0.01$	$(2.03 \pm 0.11) \times 10^{-11}$	
		1100	870	5120	$2.21 \pm 0.02$	$(2.07 \pm 0.12) \times 10^{-11}$	
	γ-T	410	500	2500	$(61.0 \pm 0.4) \times 10^{-2}$	$(1.79 \pm 0.50) \times 10^{-11}$	
		550	500	2700	$(62.8 \pm 0.3) \times 10^{-2}$	$(1.84 \pm 0.51) \times 10^{-11}$	
		1100	830	2870	$(63.6 \pm 0.3) \times 10^{-2}$	$(1.87 \pm 0.52) \times 10^{-11}$	
	DMB	550	1340	8400	$(41.8 \pm 0.7) \times 10^{-2}$	$(1.88 \pm 0.19) \times 10^{-11}$	
		280	540	3400	$(43.4 \pm 0.7) \times 10^{-2}$	$(1.95 \pm 0.20) \times 10^{-11}$	
800		800	2140	$(41.2 \pm 0.4) \times 10^{-2}$	$(1.85 \pm 0.18) \times 10^{-11}$		
<b>3-MF</b> 	α-P	830	830	3400	$2.38 \pm 0.01$	$(1.48 \pm 0.34) \times 10^{-11}$	$(1.49 \pm 0.33) \times 10^{-11}$
		630	630	1400	$2.37 \pm 0.04$	$(1.47 \pm 0.36) \times 10^{-11}$	
		1100	1100	3100	$2.23 \pm 0.01$	$(1.38 \pm 0.32) \times 10^{-11}$	
	γ-T	280	250	1140	$(53.7 \pm 0.5) \times 10^{-2}$	$(1.57 \pm 0.45) \times 10^{-11}$	
		600	830	2700	$(53.6 \pm 0.3) \times 10^{-2}$	$(1.57 \pm 0.44) \times 10^{-11}$	
		700	600	3580	$(56.8 \pm 0.4) \times 10^{-2}$	$(1.67 \pm 0.47) \times 10^{-11}$	
	2-MB	550	740	1370	$(14.9 \pm 0.2) \times 10^{-1}$	$(1.41 \pm 0.09) \times 10^{-11}$	
		830	1060	5219	$(13.99 \pm 0.08) \times 10^{-1}$	$(1.31 \pm 0.07) \times 10^{-11}$	
280		420	1420	$(17.0 \pm 0.2) \times 10^{-1}$	$(1.59 \pm 0.10) \times 10^{-11}$		
<b>2,5-DMF</b> 	γ-T	800	800	1430	$1.91 \pm 0.02$	$(5.61 \pm 1.60) \times 10^{-11}$	$(5.82 \pm 1.21) \times 10^{-11}$
		1400	1300	2800	$1.98 \pm 0.01$	$(5.82 \pm 1.63) \times 10^{-11}$	
		600	600	1790	$1.89 \pm 0.02$	$(5.55 \pm 1.58) \times 10^{-11}$	
	DMB	600	620	1890	$(13.5 \pm 0.2) \times 10^{-1}$	$(6.07 \pm 0.62) \times 10^{-11}$	

<p style="text-align: center;"><b>2,3,5-TMF</b></p> 		800	800	1500	$(13.2 \pm 0.2) \times 10^{-1}$	$(5.98 \pm 0.60) \times 10^{-11}$	$(1.66 \pm 0.69) \times 10^{-10}$
		1011.3	1020.82	7580	$(13.21 \pm 0.27) \times 10^{-1}$	$(5.94 \pm 0.64) \times 10^{-11}$	
	DMB	615	940	1650	$3.62 \pm 0.02$	$(1.62 \pm 0.15) \times 10^{-10}$	
		410	671	1560	$3.74 \pm 0.06$	$(1.68 \pm 0.17) \times 10^{-10}$	
		821	1208	2190	$3.66 \pm 0.01$	$(1.64 \pm 0.15) \times 10^{-10}$	
	$\alpha$ -T	600	600	5700	$(92.96 \pm 0.48) \times 10^{-2}$	$(1.69 \pm 0.97) \times 10^{-10}$	
		840	850	1990	$(91.23 \pm 0.38) \times 10^{-2}$	$(1.66 \pm 0.95) \times 10^{-10}$	
		410	450	1080	$(93.09 \pm 0.46) \times 10^{-2}$	$(1.69 \pm 0.97) \times 10^{-10}$	

<sup>a</sup> Indicated error is twice the standard deviation arising from the linear regression analysis. <sup>b</sup> Expressed in  $\text{cm}^3 \text{ molecule}^{-1} \text{ s}^{-1}$ . <sup>c</sup> Indicated error calculated using Eq. 12. <sup>d</sup> Average rate coefficients obtained from all reference measurements. <sup>e</sup> Average error according to Eq.13.

### III.3 Temperature-dependent rate coefficients for the reaction of furan compounds with NO<sub>3</sub> radicals

According to the available literature, only room temperature kinetic studies have been conducted on the reaction of NO<sub>3</sub> radicals with furanoids compounds, except for furan (Cabañas et al., 2004). In this latter case, an Arrhenius equation has been proposed in the range of 263-335 K.

In this work, the temperature dependent rate coefficient was studied for the reaction of F, 2-MF, and 2,5-DMF between 263 and 373 K, at atmospheric pressure (around 1 atm) and using the relative rate method, deploying the THALAMOS facility.

The application of the relative rate approach to determine the temperature dependent rate coefficients of NO<sub>3</sub> radicals with organic compounds requires reliable references, i.e. reference compounds where their rate coefficient as a function of temperature is well established. In addition, as mentioned in the Materials and method section (see Chapter II), the rate coefficient of the reference molecule should be close, ideally, up to a factor of 5 differences are acceptable, to obtain results with good precision. However, in the case of NO<sub>3</sub>, there is a limited number of temperature dependent studies and the reported kinetic measurements mainly disagree with each other (Manion et al., 2015; IUPAC, 2016; Burkholder et al., 2020). Actually, the vast majority of the temperature dependent studies performed the last 30 years with NO<sub>3</sub> radical have been carried out by two research groups, and different temperature dependent trends were reported (Dlugokencky & Howard, 1989; Martinez et al., 1998). Both groups applied the absolute method to perform their kinetic measurements in low pressure flow tube reactors. Especially in the case of the Spanish group (Martinez et al., 1998), kinetic measurements were considered as questionable and were excluded from review articles. Therefore, for the above mentioned reasons, several reference molecules that were used for the room temperature studies, cannot be applied for the temperature dependence.

To overcome this, we performed several kinetic measurements to first validate rate coefficients of reference compounds, which were further used to determine the temperature dependent rate coefficients of furanoids. The workflow of our approach is displayed in Figure III.8.

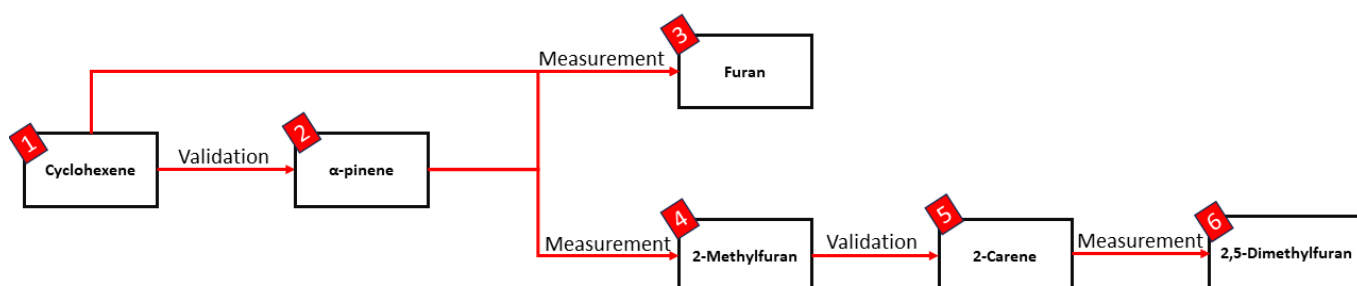


Figure III.8: Workflow of the rate coefficient measurements.

In particular, after a thorough literature search, cyclohexene was found to be the only suitable reference where the temperature dependent rate coefficients reported are in well agreement

(Ljungström et al., 1993; Martínez et al., 1999). These results are presented in Figure III.9. We fitted these results using the following modified Arrhenius expression:

$$k_{\text{cyclohexene}} = 10^{-14} \times \left(\frac{T}{298}\right)^{5.49 \pm 0.18} e^{\frac{1264.5 \pm 15.2}{T}} \text{ cm}^3 \text{ molecule}^{-1} \text{ s}^{-1}.$$

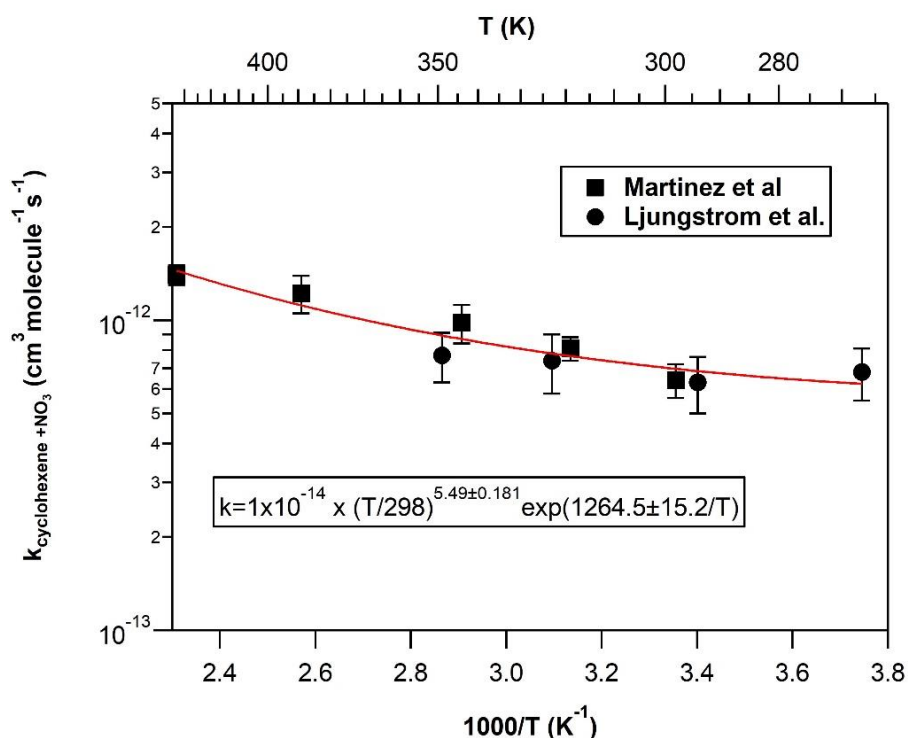


Figure III.9: Arrhenius plot for the reaction of cyclohexene with NO<sub>3</sub>.

On this basis, a series of measurements were performed using cyclohexene to validate the temperature dependence of α-P + NO<sub>3</sub>. These two compounds were the primary reference molecules used in the current study. Both cyclohexene and α-P were both used as references for furan rate coefficient measurement and α-P was used for 2-MF reaction rate coefficient measurement. Then, using 2-MF as a reference, the rate coefficient of 2-carene reaction with NO<sub>3</sub> was measured and the latter was used as a reference to measure the rate coefficient of 2,5-DMF reaction.

In the following the presentation of the temperature dependent kinetic results will be based on the strategy and the different steps followed in the work flow chart (Figure III.8).

### III.3.1 Temperature dependent rate coefficients of α-P with NO<sub>3</sub>

There are two literature studies reporting the temperature dependent rate coefficient of α-P with NO<sub>3</sub> radical (Dlugokencky & Howard, 1989; Martínez et al., 1998). In both studies, experiments were performed deploying the absolute method under low pressure flow tube reactors (pressure of ~1.3-1.4 mbar) using Laser Induced Fluorescence (LIF). In the first study, experiments were done at a temperature range of 261-384 K (Dlugokencky & Howard, 1989b) while in the second one, experiments were operated between 298 K and 423 K (Martínez et al., 1998). Although there is an excellent agreement at room temperature, there is a significant



disagreement at higher temperatures (see also Figure III.12). In the latest IUPAC evaluation, the panel recommended the results obtained by Dlugokencky & Howard,  $k_{\alpha\text{-pinene}} = 1.2 \times 10^{-12} \times e^{\frac{490 \pm 300}{T}}$  (260 – 390 K), **while the uncertainty that was given to the proposed Arrhenius expression were up to 61%.**

Therefore, a series of relative rate experiments were performed as a function of temperature, using cyclohexene as a reference compound. The objective was twofold. First, we aimed to address the disagreement between the previous literature studies. In case of our measurements agree with one of the studies, and given the different methods and conditions deployed to measure the rate coefficients, this could be also an extra validation that cyclohexene is a reliable reference to be used. Secondly, the goal was to improve the precision of the Arrhenius expression proposed by the IUPAC panel.

A series of kinetic experiments were carried out in the temperature range 296 - 393 K. Variable concentrations of  $\alpha$ -P and cyclohexene were used, between 1 and 12 ppmv, to eliminate any possible concentration effects that could be related with experimental artifacts. Considering that cyclohexene rate coefficient is slower than  $\alpha$ -P, it was injected in higher concentrations to ensure that both compounds removed with comparable kinetics losses by  $\text{NO}_3$  during the experiments. Two  $\text{N}_2\text{O}_5$  injection protocols were deployed, continuous and discontinuous. In the first case,  $\text{N}_2\text{O}_5$  was injected continuously under a constant flow of zero air, while in the second case,  $\text{N}_2\text{O}_5$  was injected in doses, i.e. step-by-step injections. The three precursor ions of the SIFT-MS (i.e.  $\text{H}_3\text{O}^+$ ,  $\text{NO}^+$ , and  $\text{O}_2^+$ ) were used to monitor the  $\alpha$ -P and cyclohexene with a time constant of 10 s. Figure III.10 depicts the temporal variation of the targeted molecules and reference ions upon reaction with  $\text{NO}_3$  at 339 K using  $\text{H}_3\text{O}^+$  as precursor ion.

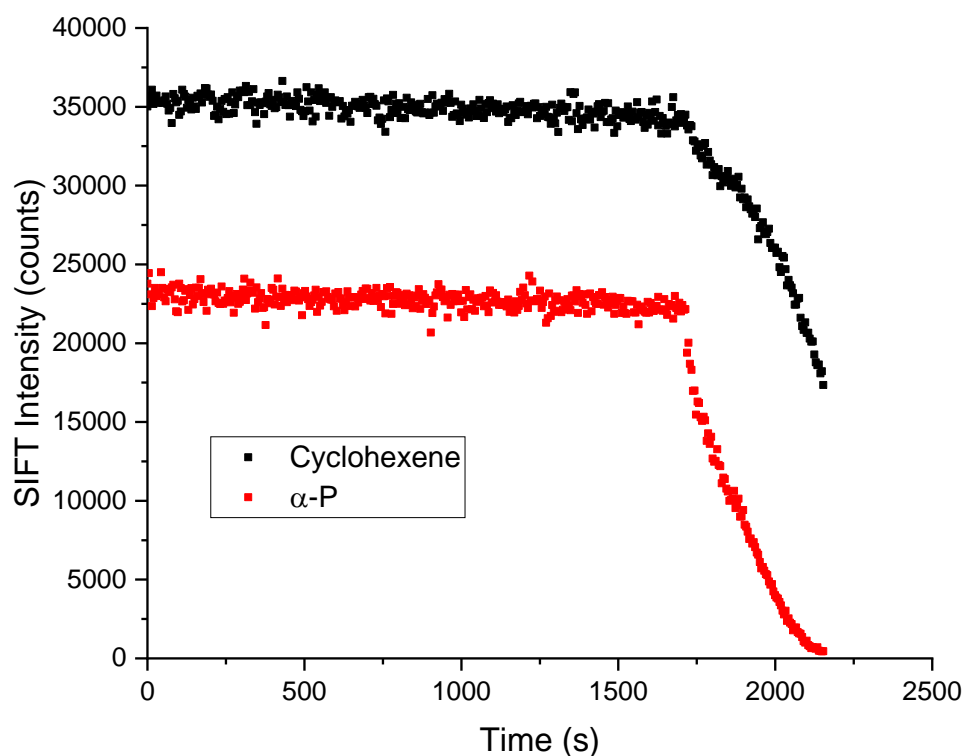


Figure III.10: Temporal variation of cyclohexene (black squares) and  $\alpha$ -P (red squares) signals by SIFT-MS. Cyclohexene was followed at  $m/z = 83$  and  $\alpha$ -P at  $m/z = 137$ . Note that  $m/z$  includes +1 (protonation).

Following these intensities obtained with the three precursor ions of the SIFT and upon applying the relative rate equation, three slopes of the equation were obtained per each experiment. The three slopes ( $\frac{k_{\alpha-P}^{H3O^+}}{k_{cyclohexene}^{H3O^+}}$ ,  $\frac{k_{\alpha-P}^{NO^+}}{k_{cyclohexene}^{NO^+}}$ ,  $\frac{k_{\alpha-P}^{O2^+}}{k_{cyclohexene}^{O2^+}}$ ) obtained in each experiment were averaged and the mean value was used to determine the overall relative ratio  $k_{\alpha-P}/k_{cyclohexene}$  of all ions, which was further used to determine the rate coefficient of  $\alpha$ -P using the reference's rate coefficient at each studied temperature. Figure III.11 shows typical relative rate plots showing the variation of the slope versus temperature. It should be mentioned that at 296 K and 326 K the rate coefficient of  $\alpha$ -P is almost by a factor of 8 greater than cyclohexane, which is actually a significant difference. Practically, this means that 50% consumption of the initial cyclohexene concentration is associated with a 99% consumption of  $\alpha$ -P concentration. Nevertheless, the signal recorded with the SIFT-MS were of such a good quality that allowed us to determine the relative rate ratios for each ion with a precision lower than 5 % (see Table III.4). Furthermore, the room temperature rate coefficient measured is in excellent agreement with the IUPAC recommended values, and the measurements performed in the CHARME chamber. Overall, the results of the kinetic measurements, are displayed in Table III.4.

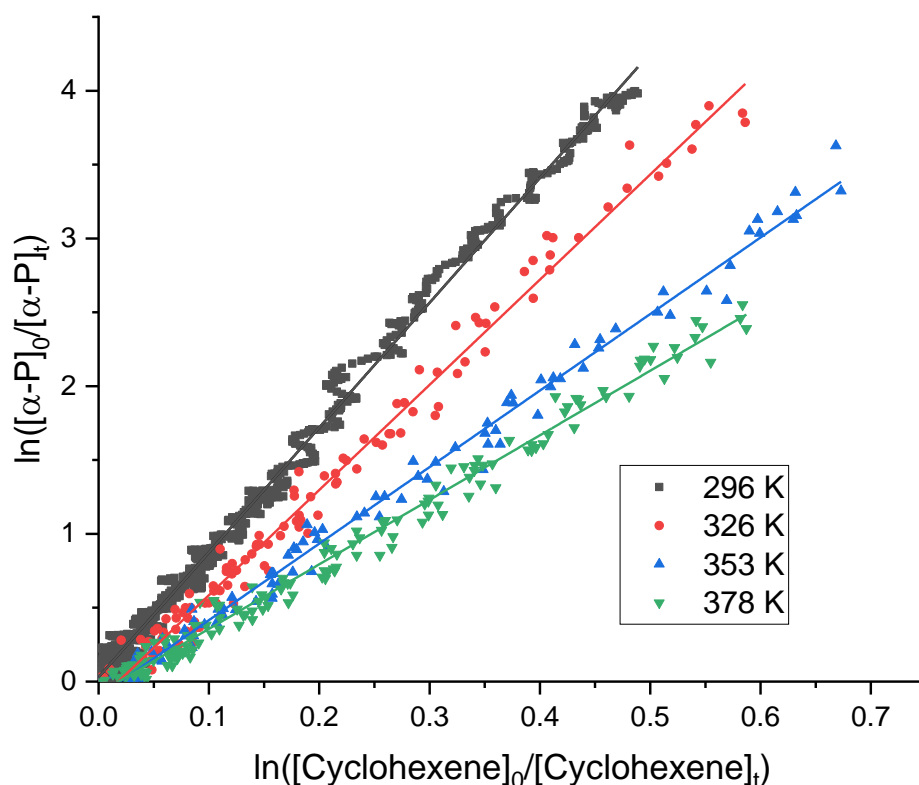


Figure III.11: Kinetic data plots for the reaction of  $\alpha$ -P with  $NO_3$  relative to that of cyclohexene at increasing temperatures (296-378 K) (slopes obtained using  $H3O^+$  specifically are represented).

Table III.4: Summary of the experimental conditions and the rate coefficients measured at increasing temperatures using the three precursor ions of the SIFT-MS ( $H_3O^+$ ,  $NO^+$ ,  $O_2^+$ ).

Temperature (K)	[Cyclohexene] <sub>0</sub> (ppbv)	[ $\alpha$ -P] <sub>0</sub> (ppbv)	$\frac{k_{\alpha-P}^{H3O^+}}{k_{cyclohexene}^{H3O^+}}$	$\frac{k_{\alpha-P}^{NO^+}}{k_{cyclohexene}^{NO^+}}$	$\frac{k_{\alpha-P}^{O2^+}}{k_{cyclohexene}^{O2^+}}$	$k_{\alpha-P} / k_{cyclohexene}$ All ions	$k_{average}$ ( $10^{-12} \text{ cm}^3 \text{ molecule}^{-1} \text{ s}^{-1}$ )
<b>296</b>	11860	6300	8.45 ± 0.02	10.4 ± 0.03	8.29 ± 0.02	9.06 ± 0.02	<b>6.33 ± 0.54</b>
	8360	7150	9.40 ± 0.06	9.39 ± 0.23	8.97 ± 0.14	9.25 ± 0.16	
<b>313</b>	6270	1330	7.13 ± 0.08	8.46 ± 0.07	7.32 ± 0.07	7.64 ± 0.07	<b>5.93 ± 0.46</b>
	2670	1250	7.95 ± 0.14	8.85 ± 0.19	7.21 ± 0.12	8.00 ± 0.15	
	1250	800	8.09 ± 0.15	8.54 ± 0.17	8.22 ± 0.19	8.28 ± 0.17	
<b>326</b>	1300	830	7.12 ± 0.07	7.47 ± 0.11	7.19 ± 0.09	7.26 ± 0.09	<b>5.74 ± 0.15</b>
<b>333</b>	1330	850	6.84 ± 0.09	6.83 ± 0.09	6.59 ± 0.11	6.75 ± 0.10	<b>5.54 ± 0.13</b>
<b>339</b>	1360	870	6.19 ± 0.07	6.27 ± 0.10	6.19 ± 0.10	6.22 ± 0.09	<b>5.24 ± 0.03</b>
	1360	870	6.15 ± 0.07	6.17 ± 0.07	6.18 ± 0.10	6.17 ± 0.08	
<b>353</b>	1410	900	5.28 ± 0.06	5.43 ± 0.07	5.08 ± 0.07	5.26 ± 0.07	<b>4.75 ± 0.13</b>
	1410	900	5.18 ± 0.05	5.25 ± 0.05	5.07 ± 0.07	5.17 ± 0.06	
<b>368</b>	1470	940	4.60 ± 0.04	5.04 ± 0.05	4.55 ± 0.04	4.73 ± 0.04	<b>4.72 ± 0.23</b>
	1470	940	4.94 ± 0.06	4.89 ± 0.06	4.59 ± 0.06	4.81 ± 0.06	
<b>378</b>	1510	960	4.37 ± 0.04	4.60 ± 0.03	4.21 ± 0.03	4.39 ± 0.03	<b>4.44 ± 0.38</b>
	1510	960	3.98 ± 0.04	4.66 ± 0.02	3.71 ± 0.03	4.12 ± 0.03	
<b>393</b>	1000	1000	3.29 ± 0.03	3.62 ± 0.04	3.24 ± 0.07	3.38 ± 0.05	<b>3.79 ± 0.55</b>
	1500	1000	3.08 ± 0.02	3.62 ± 0.03	3.07 ± 0.02	3.26 ± 0.02	

*In italics are the experiments done by discontinuous (step by step)  $NO_3$  injections.*

In Figure III.12, are presented the rate coefficients measured in the frame of this study, together with those reported in literature. Our values are in excellent agreement with those reported by Dlugokencky & Howard (1989), which has been also indicated by the IUPAC panel as the most reliable. The rate coefficient of  $\alpha$ -P with  $\text{NO}_3$  radicals decreases as temperature increase, indicating that the corresponding reaction mechanism proceeds mainly through addition of  $\text{NO}_3$  to the double bond of  $\alpha$ -P.

To obtain the Arrhenius dependance of the rate coefficient, the results of our study and those of Dlugokencky & Howard were fitted and the following expression was obtained:

$$k_{\alpha\text{-P}+\text{NO}_3} = (1.32 \pm 0.01) \times e^{\frac{462 \pm 60}{T}} \text{ cm}^3 \text{ molecule}^{-1} \text{ s}^{-1}$$

in the temperature range of 263-378 K. The uncertainties given in the pre-exponential and exponential factors correspond to the  $2\sigma$  of the fit precision. The associated uncertainties are significantly lower than those indicated by the IUPAC panel. It should be noted that the measurements we performed at 393 K, were not included in this fit, since they were found to be systematically lower. Although we do not have a clear explanation of this, it could be related to a change in the reaction mechanism of  $\text{NO}_3$  with  $\alpha$ -P. This expression was further used to measure the temperature dependent rate coefficients of several furanoids with  $\text{NO}_3$ .

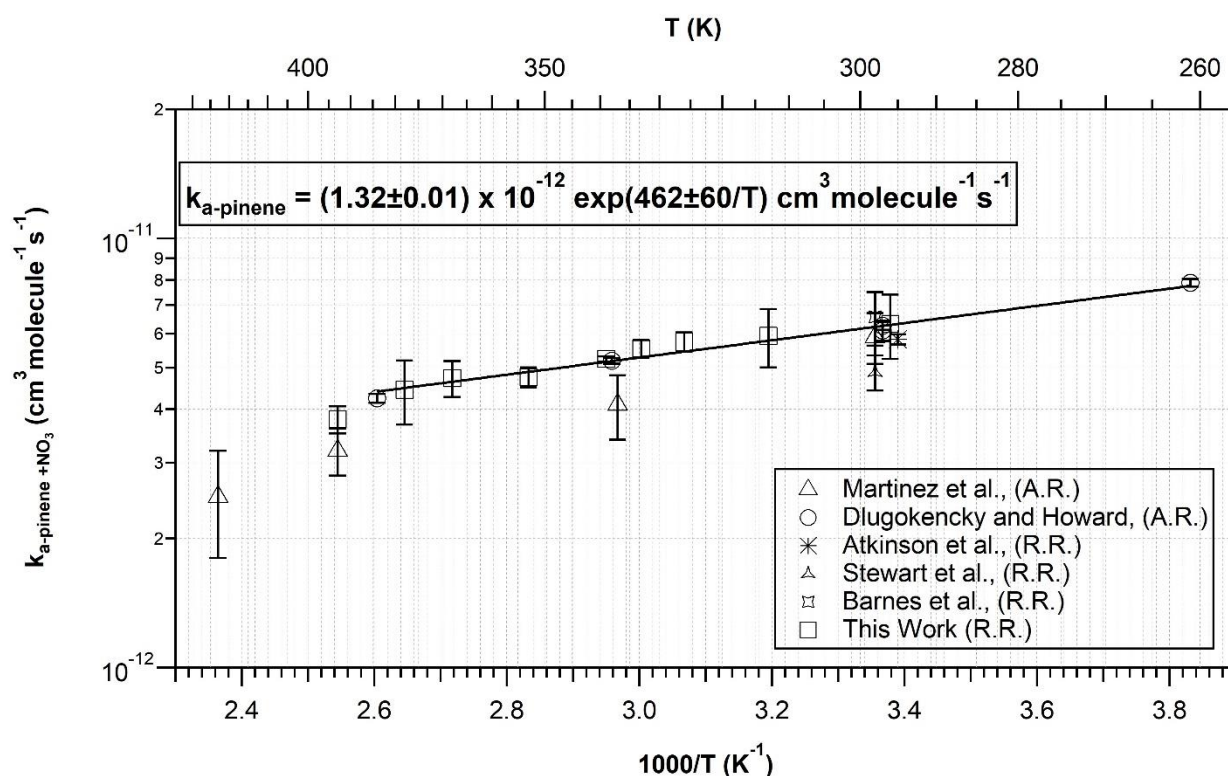


Figure III.12: Arrhenius plot for the reaction of  $\alpha$ -P with  $\text{NO}_3$ .

### III.3.2 Temperature dependent rate coefficients of the reaction of furan with NO<sub>3</sub>

There is only one literature study providing the temperature dependent rate coefficient of furan with NO<sub>3</sub> (Cabañas et al., 2004). In this study, absolute kinetics experiments were conducted within a discharge flow tube reactor equipped with NO<sub>3</sub> LIF detection at 1.47-2.0 mbar and 263-335 K temperature ranges. The proposed Arrhenius equation by this study was

$$k_{F+NO_3} = (1.3 \pm 0.8) \times 10^{-13} \times e^{\frac{(700 \pm 200)}{T}} \text{ cm}^3 \text{ molecule}^{-1} \text{ s}^{-1}.$$

In the current study, a series of relative rate experiments were performed versus temperature using both cyclohexene and  $\alpha$ -P as reference compounds in the temperature range of 263-353 K. The concentrations of F and the reference molecules used were between 1.4 and 1.9 ppmv and 1.1 and 1.7 ppmv, respectively and N<sub>2</sub>O<sub>5</sub> was then continuously injected.

Comparable concentrations of the F and reference compounds were used since their NO<sub>3</sub> reaction rate coefficients are comparable and they fulfill the criteria we follow to choose the references ( $k_F/k_{\text{Ref}} < 5$ ) (see section III.3).

Similar concept was followed, and the slopes of the relative rate plots were obtained using the three precursor ions of the SIFT. Figure III.13 shows the relative rate plots recorded with NO<sup>+</sup> precursor ion at different temperatures using cyclohexene as reference. All the kinetics results are presented in Table III.5.

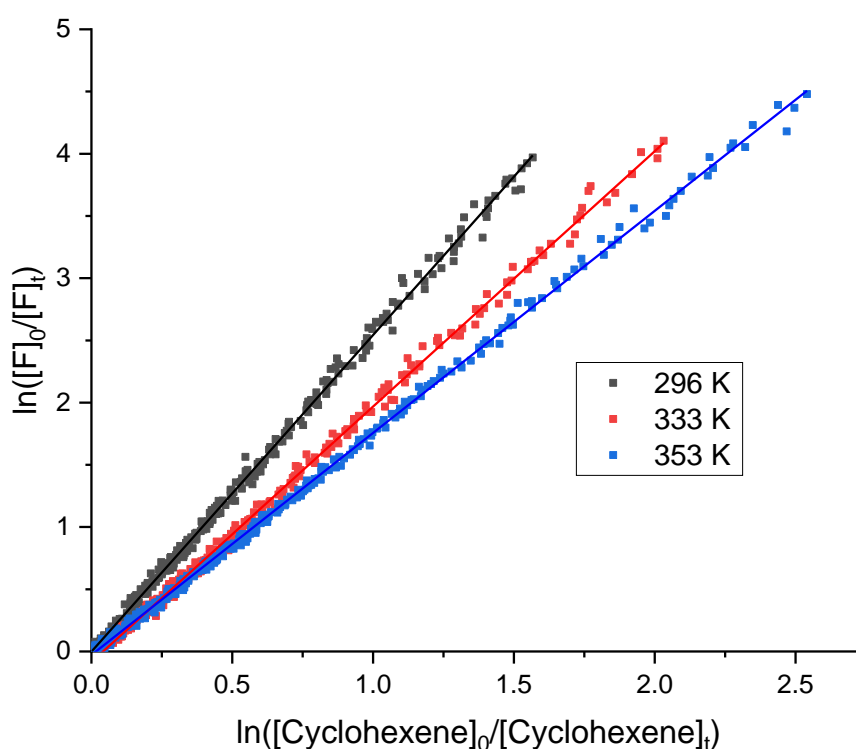


Figure III.13: Relative rate plots for the reaction of F with NO<sub>3</sub> relative to the reaction of cyclohexene at increasing temperatures (296-353 K). Furan was followed at  $m/z = 68$  and cyclohexene at  $m/z = 82$ .

Table III.5: Summary of the experimental conditions and the rate coefficients of the reaction of F with NO<sub>3</sub> measured at increasing temperatures (263 – 353 K) using the three precursor ions of the SIFT-MS (H<sub>3</sub>O<sup>+</sup>, NO<sup>+</sup>, O<sub>2</sub><sup>+</sup>).

Temperature (K)	[F] <sub>0</sub> (ppbv)	[Ref] <sub>0</sub> (ppbv)	$\frac{k_F^{H3O^+}}{k_{Ref}^{H3O^+}}$	$\frac{k_F^{NO^+}}{k_{Ref}^{NO^+}}$	$\frac{k_F^{O2^+}}{k_{Ref}^{O2^+}}$	k <sub>average</sub> (10 <sup>-12</sup> cm <sup>3</sup> molecule <sup>-1</sup> s <sup>-1</sup> )
263	1470	1120 <sup>α</sup>	0.28 ± 0.01	0.29 ± 0.01	0.29 ± 0.01	2.13 ± 0.13
	1470	1120 <sup>α</sup>	0.27 ± 0.01	0.27 ± 0.01	0.27 ± 0.01	
	1470	1120 <sup>α</sup>	0.28 ± 0.01	0.28 ± 0.01	0.28 ± 0.01	
273	1520	1270*	-	2.66 ± 0.01	3.05 ± 0.01	1.81 ± 0.19
	1520	1270*	-	2.33 ± 0.01	3.02 ± 0.01	
	1520	1160 <sup>α</sup>	0.26 ± 0.01	0.25 ± 0.01	0.27 ± 0.01	
	1520	1160 <sup>α</sup>	0.27 ± 0.01	0.25 ± 0.01	0.27 ± 0.01	
296	1650	1380*	-	2.56 ± 0.01	2.40 ± 0.01	1.70 ± 0.12
	1650	1380*	-	2.55 ± 0.01	2.55 ± 0.01	
	1650	1260 <sup>α</sup>	0.27 ± 0.01	0.26 ± 0.01	0.27 ± 0.01	
	1650	1260 <sup>α</sup>	0.26 ± 0.01	0.26 ± 0.01	0.26 ± 0.01	
313	1750	1460*	-	2.31 ± 0.01	2.16 ± 0.01	1.66 ± 0.17
333	1850	1550*	-	2.05 ± 0.01	2.11 ± 0.01	1.71 ± 0.07
353	1960	1650*	-	1.68 ± 0.01	1.79 ± 0.01	1.55 ± 0.01
	1960	1650*	-	1.72 ± 0.01	1.64 ± 0.01	
	1960	1650*	-	1.67 ± 0.01	1.68 ± 0.01	
	1960	1650*	-	1.78 ± 0.01	1.82 ± 0.01	
	1970	1500 <sup>α</sup>	0.33 ± 0.01	0.32 ± 0.01	0.34 ± 0.01	
	1970	1500 <sup>α</sup>	0.30 ± 0.01	0.30 ± 0.01	0.31 ± 0.01	
	1970	1500 <sup>α</sup>	0.32 ± 0.01	0.31 ± 0.01	0.33 ± 0.01	

\* Reference used was cyclohexene <sup>α</sup> reference used was α-P.

The rate coefficients obtained for the reaction between F and NO<sub>3</sub> using the two references are in excellent agreement within 5% error (see Table III.5). The measurements performed in THALAMOS at 298 K also agree with those done in CHARME to 11 % (Al Ali et al., 2022) (presented in Table III.3). Both the rate coefficients measured in this work and those measured in literature are presented in Figure III.14. The rate coefficient obtained in THALAMOS at 298 K is in very good agreement with the previous studies with less than 15% difference considering the experimental uncertainties (Atkinson et al., 1985a; Cabañas et al., 2004; Newland et al., 2022) except for Kind et al. study (1996 a), where the rate coefficient was systematically lower (by 40%) than other literature studies. The reasons for the lower value obtained by Kind et al. (1996 a) are unclear.

Regarding the temperature dependent rate coefficients, both studies, this work and that of Cabañas et al. (2004), observed a decrease in the rate coefficients as the temperature increases indicating that the major reaction pathway is the NO<sub>3</sub> addition to one of the double bonds of the furan ring. When addition is the major pathway, the rate coefficient decreases as the temperature increase due to unstability of the adduct formed resulting from the excess vibrational energy. As shown in Figure III.14, the rate coefficients determined in our study were fitted with an Arrhenius type equation yielding the following expression:  $k_{F+NO_3} = (7.55 \pm 0.12) \times 10^{-13} \times e^{\frac{254 \pm 138}{T}} \text{ cm}^3 \text{ molecule}^{-1} \text{ s}^{-1}$  in the temperature range of 263-353 K. Similar calculation methods of the uncertainty were used as those mentioned in the previous section. Interestingly, the temperature dependent trend observed in our study is less sharp than Cabañas et al., (2004). In particular the activation energies determined in our work and Cabañas et al., (2004) were  $2.1 \pm 1.1 \text{ kJ mol}^{-1}$  and  $5.8 \pm 1.7 \text{ kJ mol}^{-1}$ , respectively. This difference does not necessarily means that the two studies disagree. In particular, in case that F reaction with NO<sub>3</sub> proceeds through an association mechanism, i.e. formation of an adduct, then the stability of the adduct is strongly dependent on the temperature and the total pressure. The lowest the temperature, the better the adduct can be stabilized thermally, distributing its excess of vibrational energy efficiently, increasing its lifetime, and thus the probability of leading to final products. The pressure effect is mainly correlated with the transfer of the excess energy to the bath gas through collisions. At high pressures the transfer of energy from the adduct to the bath gas is more efficient due to the highest number of collisions. Therefore, it is possible that close to ambient temperatures, the adduct formed is stable even at low pressures. However, at higher temperatures, where the stability of the adduct is not that efficient, the total pressure could play a more important role (fall-off of a typical termolecular reaction) (Papadimitriou et al., 2011).

As a consequence in the study of Cabañas et al. (2004) where experiments were performed under a few torr total pressure, the stability of the adduct may be not achieved at high temperatures, leading to lower rate coefficient. In other words, under our experiments the reaction of F + NO<sub>3</sub> is out of the falloff regime of a typical termolecular reaction, which is not the case of Cabañas et al. (2004).

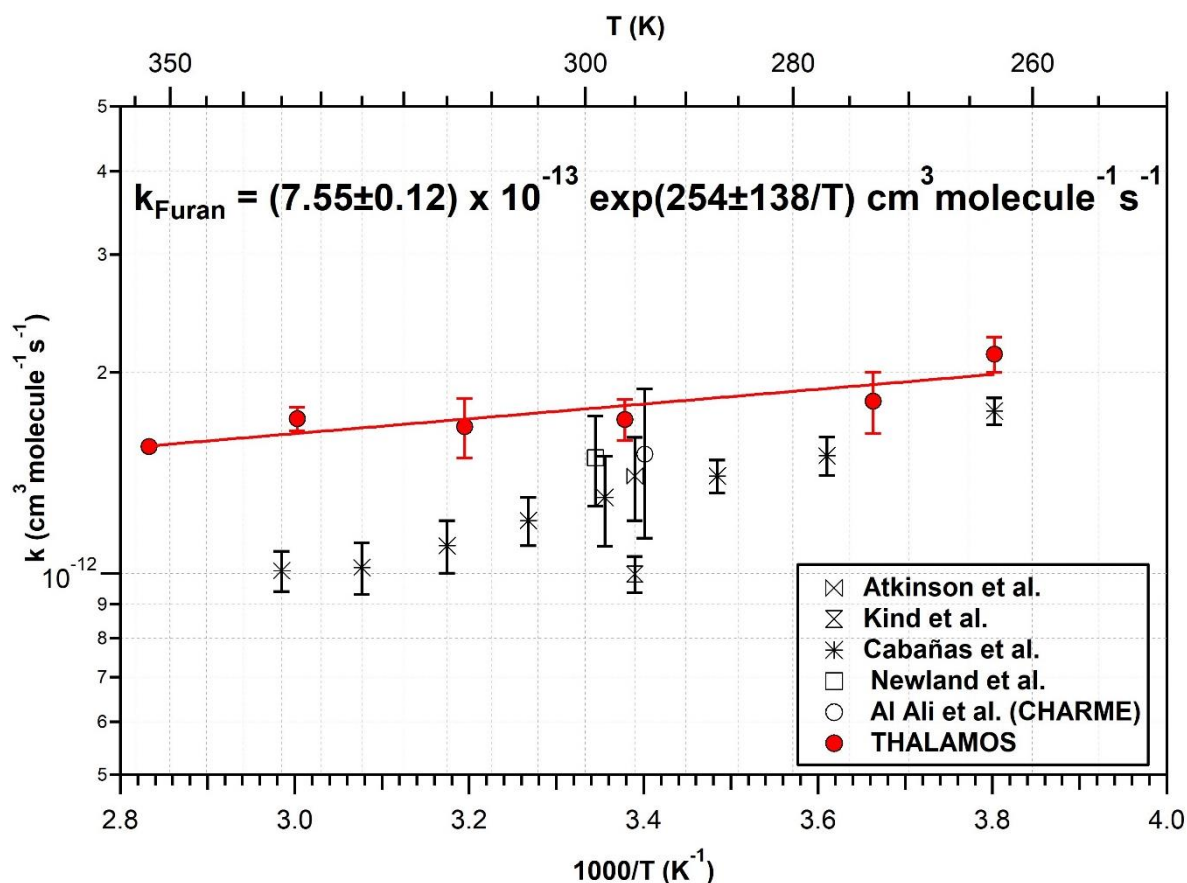


Figure III.14: Arrhenius plot for the reaction of F with  $\text{NO}_3$  at temperatures between 263–353 K.

### III.3.3 Temperature-dependent rate coefficient for the reaction of 2-MF with $\text{NO}_3$

There are several literature studies reporting the rate coefficient of 2-MF reaction with  $\text{NO}_3$  at room temperature (Kind et al., 1996a; Al Ali et al., 2022; Newland et al., 2022). However, to the best of our knowledge, there are no temperature-dependent data of the title reaction. The objective of this temperature dependent measurements is to have an Arrhenius expression of the reaction. Relative rate experiments were carried out in the range of 263 and 373 K using  $\alpha$ -P as a reference molecule. At room temperature, besides  $\alpha$ -P, 2-carene and  $\gamma$ -T were used to measure the room temperature rate coefficient.

2-MF and  $\alpha$ -P concentrations were injected in almost equal concentrations ranging between 800 and 2300 ppbv as this reference fulfill the criteria of having comparable rate coefficient to that of 2-MF ( $k_{2\text{-MF}}/k_{\alpha\text{-P}} \approx 3$ ). At room temperature, two  $\text{N}_2\text{O}_5$  injection protocols were deployed, continuous and discontinuous.

Similar concept to the one described previously i.e., following the signal using the three precursor ions of the SIFT to obtain the slopes of the relative rate plots was followed. Figure III.15 shows the relative rate plots obtained using  $\text{NO}^+$  as precursor ion at the selected temperatures studied showing the observable decrease of the slope as the temperature increases. Figure III.16 shows the room temperature relative rate plots using the three references ( $\alpha$ -P, 2-carene and  $\gamma$ -T) obtained with discontinuous experiments using  $\text{O}_2^+$  as the precursor ion.



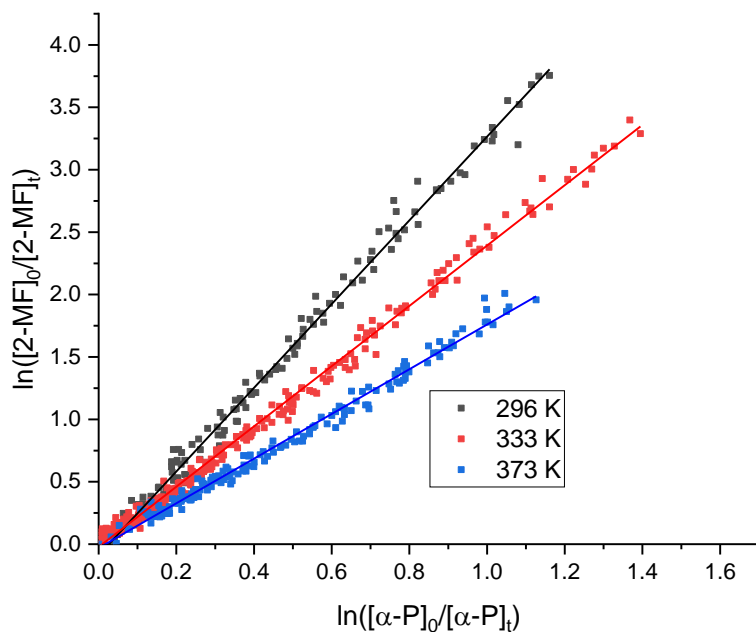


Figure III.15: Relative rate plots for the reaction of 2-MF with  $\text{NO}_3$  at increasing temperatures (296-373 K). 2-MF was followed at  $m/z = 82$  and  $\alpha$ -P was followed at  $m/z = 136$ .

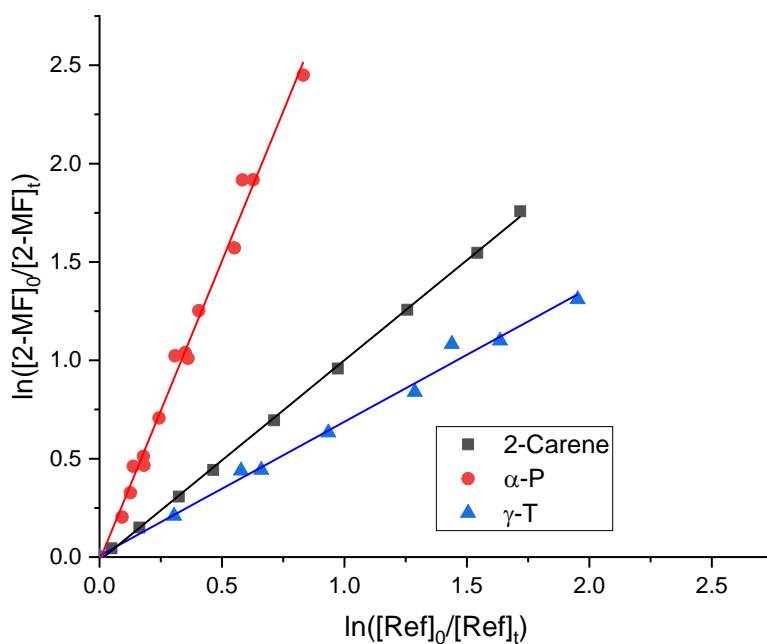


Figure III.16: Relative rate plots for the reaction of 2-MF with  $\text{NO}_3$  at room temperature (296 K) using three references (2-carene,  $\alpha$ -P and  $\gamma$ -T). 2-MF was followed at  $m/z = 82$  and 2-carene,  $\alpha$ -P and  $\gamma$ -T were followed at  $m/z = 93$ .

The room temperature rate coefficients obtained using the three references were in excellent agreement within  $\approx 6\%$  error (see Table III.6). The average room temperature rate coefficient measured for the title reaction is in high agreement with all three literature studies to within 22%. These measurements done in THALAMOS also agree with the measurement done in CHARME to 5%. All temperature-dependent measurements are presented in Table III.6.

Table III.6: Experimental conditions, slopes of the relative rate plots and the temperature-dependent rate coefficients for the reaction of 2-MF with NO<sub>3</sub>.

Temperature (K)	[2-MF] <sub>0</sub> (ppbv)	[α-P] <sub>0</sub> (ppbv)	$\frac{k_{2-MF}^{H3O+}}{k_{\alpha-P}^{H3O+}}$	$\frac{k_{2-MF}^{NO+}}{k_{\alpha-P}^{NO+}}$	$\frac{k_{2-MF}^{O2+}}{k_{\alpha-P}^{O2+}}$	$\frac{k_{average}^{All\ ions}}{k_{average}^{All\ ions}}$	$k_{average}$ (10 <sup>-11</sup> cm <sup>3</sup> molecule <sup>-1</sup> s <sup>-1</sup> )
263	800	780	3.47 ± 0.03	3.20 ± 0.02	3.54 ± 0.04	3.40 ± 0.03	2.58 ± 0.23
	800	780	3.46 ± 0.01	3.36 ± 0.02	3.23 ± 0.02	3.34 ± 0.02	
273	830	810	2.68 ± 0.03	2.69 ± 0.02	2.79 ± 0.04	2.72 ± 0.03	2.05 ± 0.18
	830	810	2.98 ± 0.02	2.99 ± 0.02	2.93 ± 0.04	2.96 ± 0.03	
280	850	830	2.81 ± 0.04	2.85 ± 0.03	2.93 ± 0.04	2.86 ± 0.04	1.95 ± 0.12
283	860	840	2.73 ± 0.04	2.95 ± 0.01	2.92 ± 0.03	2.86 ± 0.03	
296	<b>α-P</b>						2.01 ± 0.16
	900	880	3.45 ± 0.04	3.24 ± 0.02	3.41 ± 0.05	3.36 ± 0.04	
	900	880	3.25 ± 0.04	3.35 ± 0.03	3.22 ± 0.04	3.27 ± 0.03	
	2260	2270	2.94 ± 0.12	3.09 ± 0.04	3.04 ± 0.07	3.02 ± 0.04	
	<b>2-carene</b>						
	2260	2270	1.03 ± 0.02	0.96 ± 0.01	1.01 ± 0.01	1.00 ± 0.01	
	<b>γ-T</b>						
2260	2270	0.73 ± 0.02	0.70 ± 0.02	0.68 ± 0.02	0.70 ± 0.02		
313	950	930	2.80 ± 0.05	3.09 ± 0.02	2.88 ± 0.03	2.92 ± 0.04	1.61 ± 0.21
	950	930	2.69 ± 0.06	2.90 ± 0.06	2.77 ± 0.05	2.78 ± 0.05	
	2260	2270	2.45 ± 0.08	2.84 ± 0.10	2.60 ± 0.08	2.63 ± 0.09	
333	1020	990	2.20 ± 0.02	2.42 ± 0.01	2.19 ± 0.02	2.27 ± 0.02	1.29 ± 0.21
	1020	990	2.65 ± 0.04	2.63 ± 0.02	2.51 ± 0.03	2.59 ± 0.03	
353	1080	1050	2.31 ± 0.03	2.11 ± 0.02	2.09 ± 0.02	2.17 ± 0.02	1.05 ± 0.10

	1080	1050	2.15 ± 0.02	2.09 ± 0.01	2.19 ± 0.02	2.14 ± 0.02	
	1080	1050	2.33 ± 0.03	2.08 ± 0.02	2.06 ± 0.02	2.15 ± 0.02	
373	1140	1110	1.92 ± 0.05	1.77 ± 0.01	1.85 ± 0.01	1.84 ± 0.03	0.85 ± 0.07
	1140	1110	1.84 ± 0.02	1.79 ± 0.01	1.73 ± 0.01	1.78 ± 0.01	
	1140	1110	2.00 ± 0.04	1.88 ± 0.03	1.91 ± 0.03	1.93 ± 0.03	

*Written in italic are the experiments done with discontinuous injections.*

Figure III.17 shows the rate coefficients measured in this work versus temperature together with those measured in literature at room temperature (Kind et al., 1996a; Al Ali et al., 2022; Newland et al., 2022). The rate coefficient of 2-MF reaction with NO<sub>3</sub> radicals decreases as the temperature increases, implying that the reaction mainly occurs by NO<sub>3</sub> addition. It can be NO<sub>3</sub> addition to one of the double bonds or addition elimination mechanism, but this can only be proved by characterizing the products formed (Chapter 4). The rate coefficient decrease by a factor of ~2 as the temperature increases from 263 K to 373 K.

The Arrhenius plot of experimental results provides the following expression:  $k_{2-MF+NO_3} = (7.76 \pm 0.14) \times 10^{-13} \times e^{\frac{922 \pm 151}{T}} \text{ cm}^3 \text{ molecule}^{-1} \text{ s}^{-1}$  in the temperature range of 263-373 K. More studies are needed to be able to have a recommended Arrhenius expression.

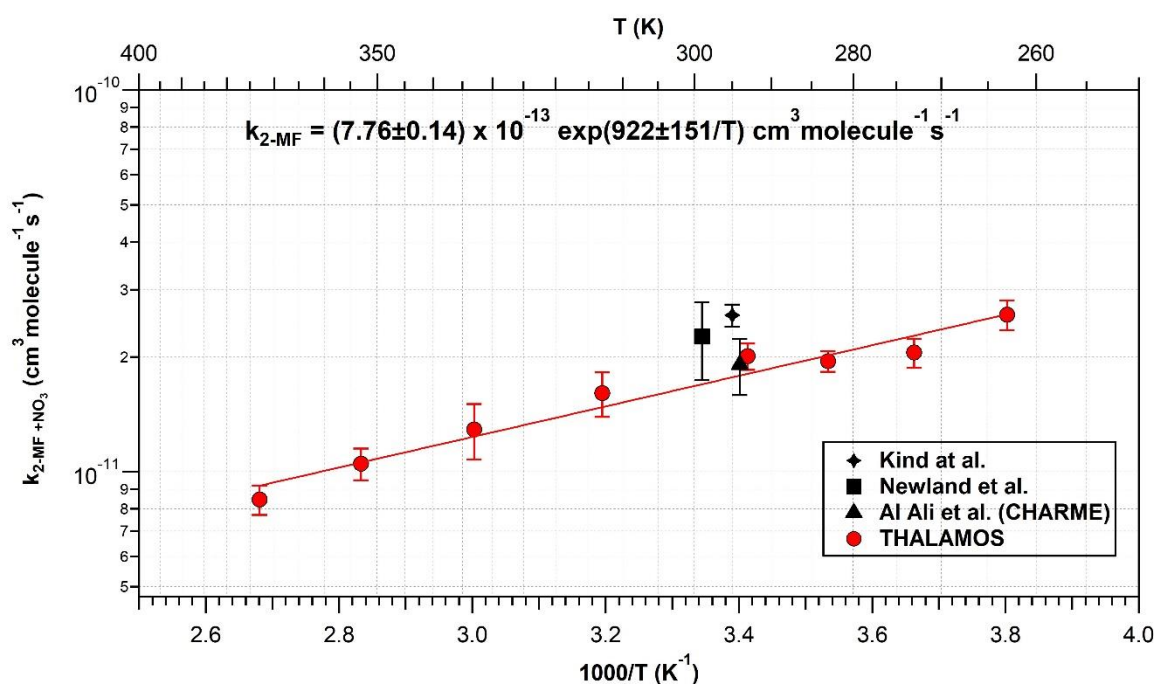


Figure III.17: Arrhenius plot for the reaction of 2-MF with NO<sub>3</sub>.

Interestingly, it was observed that the rate coefficient of 2-MF is 10 times faster than the rate coefficient of F (further discussion about this increasing trend is provided in section III.4.1). Considering this increasing trend of the rate coefficient with CH<sub>3</sub> substitution of furan, in the case of 2,5-DMF, a faster rate coefficient than 2-MF reaction is anticipated. Therefore, α-P is no more a suitable reference molecule because it has a significantly slower rate coefficient. For that reason, preliminary experiments were performed to evaluate whether 2-MF is an appropriate reference, however, it was found that the product of 2-MF reaction contributes to the mass of 2,5-DMF. Therefore, to overcome this, we decided to first validate the temperature dependence of another reference, 2-carene (a compound that has a rate coefficient comparable to that of 2,5-DMF), using 2-MF as reference molecule. **Therefore, in the following section the temperature-dependent rate coefficient of 2-carene with NO<sub>3</sub> was remeasured to use it as a reference for the reaction of 2,5-DMF with NO<sub>3</sub> (See flowchart Figure III.8).**

### III.3.4 Temperature dependent rate coefficient for the reaction of 2-carene with NO<sub>3</sub>

There is one literature study reporting the temperature dependent rate coefficient for the reaction of 2-carene with NO<sub>3</sub> (Martinez et al., 1999). In this study, experiments were carried out applying the absolute method over the temperature range of 298–393 K, using a discharge flow system coupled to LIF at a total pressure of 1 torr. The following Arrhenius expression was provided:  $k_{2\text{-carene}+\text{NO}_3} = (1.40 \pm 0.70) \times 10^{-12} \times e^{\frac{741 \pm 190}{T}} \text{ cm}^3 \text{ molecule}^{-1} \text{ s}^{-1}$ . No recommendation was proposed by the IUPAC panel for the temperature dependent rate coefficients. At room temperature, literature studies exhibit very good agreement (Corchnoy & Atkinson, 1990; Martinez et al., 1999) and the IUPAC recommended value was  $(2.00 \pm 1.32) \times 10^{-12} \text{ cm}^3 \text{ molecule}^{-1} \text{ s}^{-1}$ . Therefore, relative rate experiments as a function of temperature were done, using 2-MF as a reference compound. The objective was twofold. First, we aimed to validate the expression already presented in literature to have more precision on the rate coefficients that will be used in our study. Second, in case our measurements agree with those in literature (Martinez et al., 1999), given the different methods and conditions used, this can be an additional validation of the measurements done for 2-MF reaction and as a result for the protocol followed since the beginning (Figure III.8).

Experiments were carried out in the temperature range of 296–353 K. 2-Carene and 2-MF were injected into THALAMOS with equal concentrations as the reference achieved the criteria of being with comparable rate coefficient with the studied molecule. The concentration ranged between 1.1 and 1.6 ppmv, N<sub>2</sub>O<sub>5</sub> was injected continuously in excess and the signals followed by SIFT-MS using the three precursor ions (H<sub>3</sub>O<sup>+</sup>, NO<sup>+</sup> and O<sub>2</sub><sup>+</sup>). Figure III.18 shows typical relative rate plots at increasing temperatures obtained using NO<sup>+</sup> as precursor ion. The slope was always close to 1 at the different temperatures, which corresponds to almost similar rate coefficients for both molecules towards NO<sub>3</sub> at increasing temperatures.

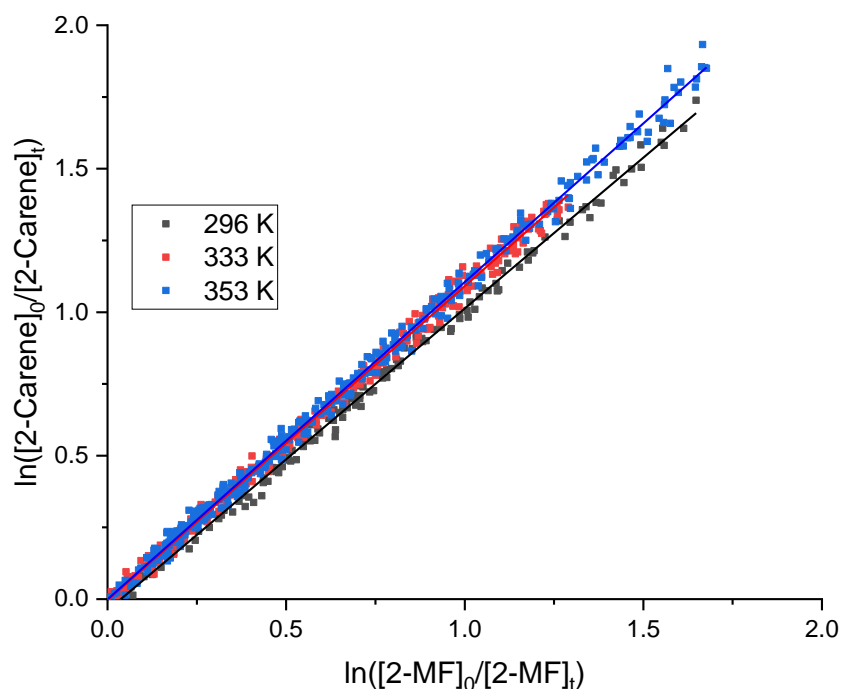


Figure III.18: Kinetic data plot for the reaction of 2-carene with NO<sub>3</sub> relative to that of 2-MF at increasing temperatures. 2-MF was followed at  $m/z = 82$  and 2-carene at  $m/z = 136$ .

The room temperature rate coefficient measured is in excellent agreement with that recommended by the IUPAC panel with ~6% difference. The results of the kinetics measurements are presented in Table III.7.

Table III.7: Experimental conditions including 2-carene and the reference (2-MF) concentrations, the slopes of the relative rate plots and the average rate coefficient measured at each temperature (296-353 K).

Temperature (K)	[2-carene] <sub>0</sub> (ppbv)	[2-MF] <sub>0</sub> (ppbv)	$\frac{k_{2\text{-carene}}^{\text{H3O}^+}}{k_{\text{Ref}}^{\text{H3O}^+}}$	$\frac{k_{2\text{-carene}}^{\text{NO}^+}}{k_{\text{Ref}}^{\text{NO}^+}}$	$\frac{k_{2\text{-carene}}^{\text{O2}^+}}{k_{\text{Ref}}^{\text{O2}^+}}$	$k_{\text{average}} (10^{-11} \text{ cm}^3 \text{ molecule}^{-1} \text{ s}^{-1})$
296	1140	1350	1.03 ± 0.01	1.04 ± 0.01	1.07 ± 0.01	1.88 ± 0.12
	1140	1350	1.13 ± 0.01	1.05 ± 0.01	1.13 ± 0.01	
	1140	1350	1.11 ± 0.01	1.03 ± 0.01	1.05 ± 0.01	
313	1210	1430	1.05 ± 0.01	1.04 ± 0.01	1.04 ± 0.01	1.52 ± 0.05
	1210	1430	0.98 ± 0.01	1.03 ± 0.01	1.01 ± 0.01	
333	1280	1520	1.03 ± 0.01	1.06 ± 0.01	1.11 ± 0.01	1.34 ± 0.05
	1280	1520	1.02 ± 0.01	1.10 ± 0.01	1.09 ± 0.01	
353	1360	1610	1.05 ± 0.01	1.09 ± 0.01	1.11 ± 0.01	1.15 ± 0.04
	1360	1610	1.07 ± 0.01	1.10 ± 0.01	1.09 ± 0.01	

In Figure III.19 are presented the rate coefficients measured in this study, together with those reported in the literature studies (Martinez et al., 1998; Corchnoy et al., 1990; Atkinson & Arey, 2003). Our values are in excellent agreement with the temperature dependent rate coefficients proposed by Martinez et al. The rate coefficient decreases as the temperature increases indicating that 2-carene reaction also proceeds by NO<sub>3</sub> addition to the double bonds. To obtain the Arrhenius dependence of the rate coefficient, the results of our study and those of literature were plotted in Figure III.19. The following Arrhenius expression is proposed  $k_{2\text{-carene}+\text{NO}_3} = (8.77 \pm 0.12) \times 10^{-13} \times e^{\frac{904 \pm 119}{T}} \text{ cm}^3 \text{ molecule}^{-1} \text{ s}^{-1}$  over the temperature range of 296 – 433 K. The uncertainties on the pre-exponential and the exponential factor reflects the 2σ precision of the fit.

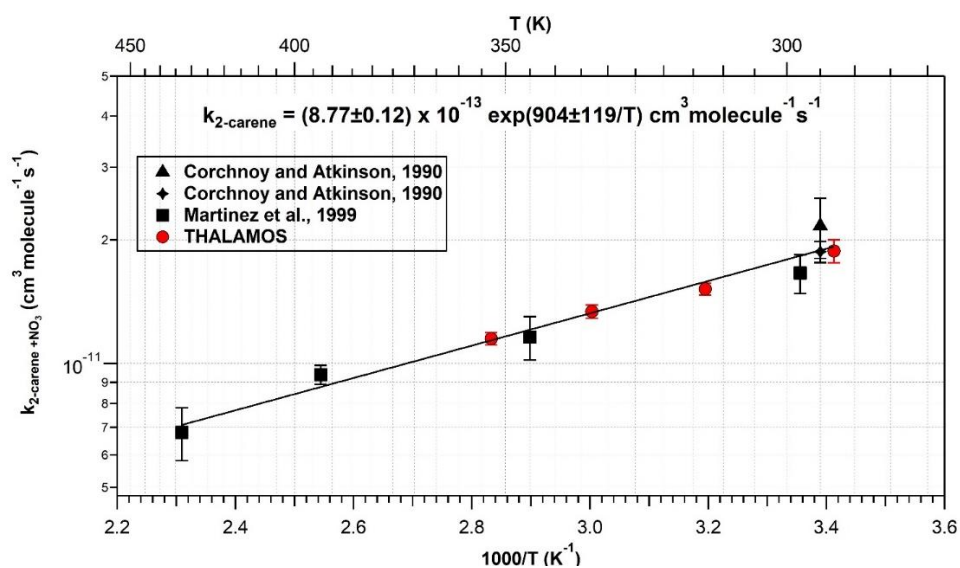


Figure III.19: Arrhenius plot for the reaction of 2-carene with NO<sub>3</sub> in the temperature range of 296 to 353 K.

Using the temperature dependent expression defined for 2-carene, the rate coefficient of 2,5-DMF was studied, as presented in the following section.

### III.3.5 Temperature dependent rate coefficient for the reaction of 2,5-DMF with $\text{NO}_3$

There is no literature studies reporting the temperature dependent rate coefficient of 2,5-DMF with  $\text{NO}_3$  but only for room temperature kinetics (Kind et al., 1996a; Al Ali et al., 2022; Newland et al., 2022). Kind et al. reported a measurement in excellent agreement with our measurement done in CHARME (less than 1% difference); however, Newland et al. gave a 100% higher rate coefficient. The reason for this discrepancy is unknown, but for the common reference (2,3-dimethyl-2-butene) between the two studies, the rate coefficient used by Newland et al. is  $\sim 1.3$  times higher than the value used by us.

Thus, a series of temperature dependent relative rate kinetics methods were performed using 2-carene as a reference compound. At room temperature, two other references were used which are  $\alpha$ -T and  $\gamma$ -T in order to have more precise determinations and cross validate the room temperature rate coefficient provided in literature.

Kinetic experiments were done in the temperature range of 296-353 K. To make a better comparison between the kinetics losses of 2,5-DMF and 2-carene when reacting with  $\text{NO}_3$ , the concentration of 2-carene was injected twice the concentration of 2,5-DMF. The concentrations of 2-carene and 2,5-DMF range was 1.1 -7.4 ppmv and 1.1 – 3.7 ppmv, respectively. These variable concentrations also ensure the absence of any concentration effect that could be related to experimental artifacts. Figure III.20 shows the relative rate plots obtained using  $\text{NO}^+$  as a precursor ion at the studied temperatures, showing a slope decrease as the temperature increases.

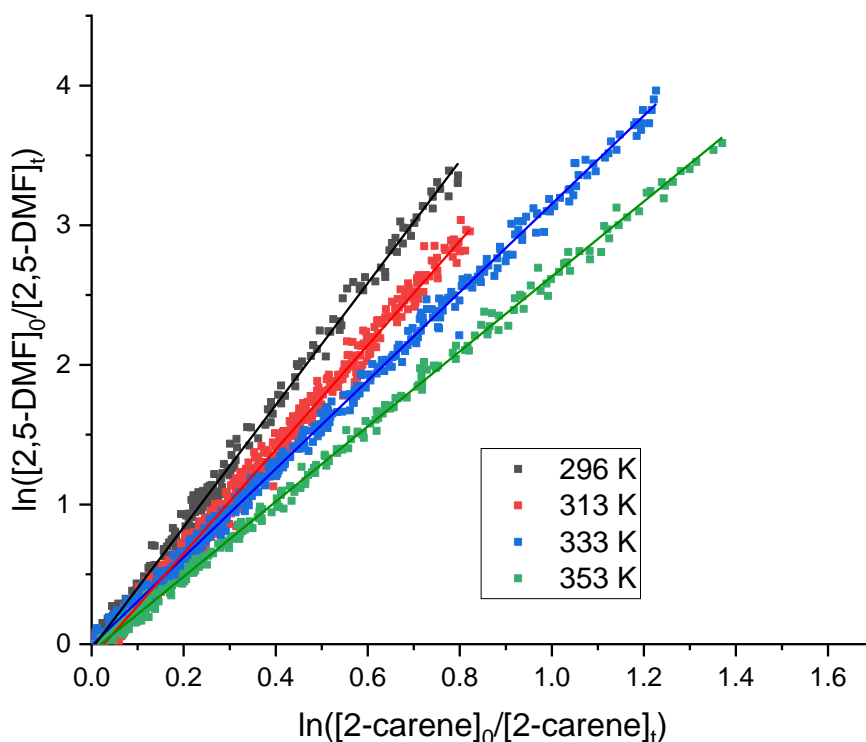


Figure III.20: Kinetic data plots for the reaction of 2,5-DMF with  $\text{NO}_3$  relative to that of 2-carene at increasing temperatures. 2,5-DMF was followed at  $m/z = 96$  and 2-carene was followed at  $m/z = 136$ .

Figure III.21 shows the room temperature relative rate plots obtained using the three different references and using  $\text{NO}^+$  as a precursor ion. The average coefficient obtained from the three references is  $(7.16 \pm 0.59) \times 10^{-11} \text{ cm}^3 \text{ molecule}^{-1} \text{ s}^{-1}$ . The rate coefficients acquired from the three references are in accordance with a difference of  $\sim 5\%$ . Compared to literature, the rate coefficient values measured in THALAMOS are in agreement with that of Kind et al. within 20% while the difference with the determination done by Newland et al. reaches 35%. The room temperature rate coefficient measured in THALAMOS is between Newland et al. and Kind et al. studies (Kind et al., 1996b; Newland et al., 2022). Comparing the rate coefficient measured in THALAMOS to that measured in our work in CHARME, they are in very good agreement with less than 20% difference. Overall, the results are presented in Table III.8.

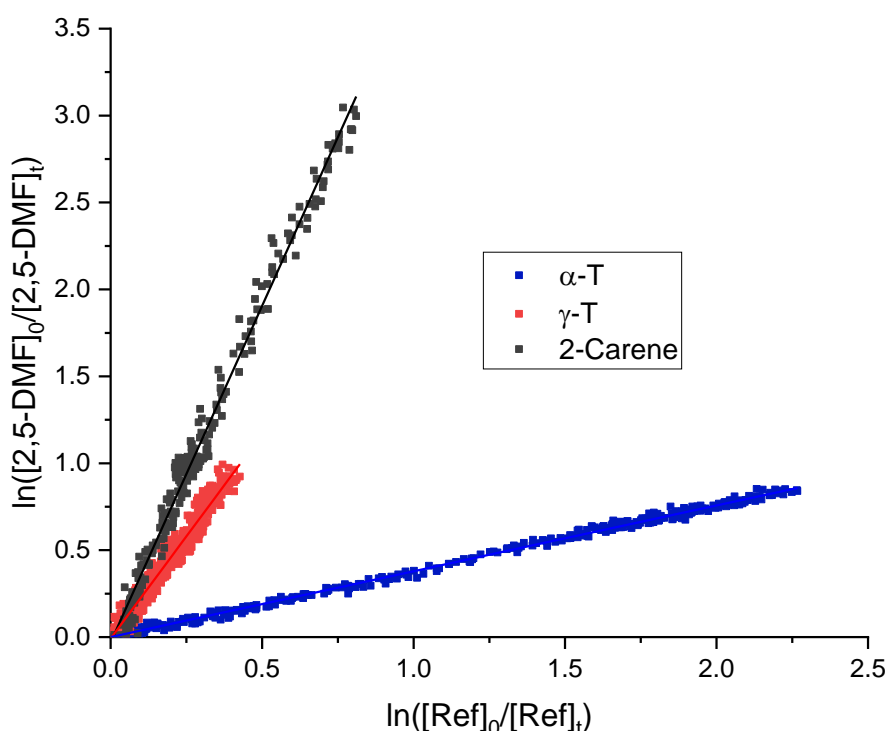


Figure III.21: Relative rate plots for the reaction of 2,5-DMF with  $\text{NO}_3$  at  $296 \pm 2 \text{ K}$  using three reference compounds. 2,5-DMF was followed at  $m/z = 96$  and  $\alpha\text{-T}$ , 2-carene and  $\gamma\text{-T}$  were followed at  $m/z = 136$ .

Table III.8: Experimental conditions, relative rate plots slopes obtained with the three precursor ions of the SIFT and the average rate coefficient measured at each temperature.

Temperature (k)	[2-carene] (ppbv)	[2,5-DMF] (ppbv)	$\frac{k_{2,5\text{-DMF}}^{\text{H3O}^+}}{k_{\text{Ref}}^{\text{H3O}^+}}$	$\frac{k_{2,5\text{-DMF}}^{\text{NO}^+}}{k_{\text{Ref}}^{\text{NO}^+}}$	$\frac{k_{2,5\text{-DMF}}^{\text{O2}^+}}{k_{\text{Ref}}^{\text{O2}^+}}$	$k_{\text{average}} \times 10^{-11}$ ( $\text{cm}^3 \cdot \text{molecule}^{-1} \cdot \text{s}^{-1}$ )
296	2-carene					
	2020	1110	$3.89 \pm 0.03$	$4.36 \pm 0.02$	$3.87 \pm 0.03$	$7.16 \pm 0.59$
	2020	1110	$4.14 \pm 0.06$	$4.27 \pm 0.03$	$4.01 \pm 0.05$	
	2020	1110	$4.18 \pm 0.06$	$4.12 \pm 0.02$	$3.66 \pm 0.04$	
	$\alpha\text{-T}$					
7370	3700	$0.40 \pm 0.03$	$0.40 \pm 0.01$	$0.38 \pm 0.01$		



	γ- T					
	1120	1670	2.43 ± 0.01	2.40 ± 0.03	2.35 ± 0.02	
313	2140	1170	3.75 ± 0.02	3.73 ± 0.01	3.40 ± 0.02	5.87 ± 0.63
	2140	1170	3.90 ± 0.02	3.90 ± 0.01	3.59 ± 0.03	
333	2280	1250	3.39 ± 0.03	3.35 ± 0.01	3.21 ± 0.02	4.26 ± 0.35
	2280	1250	3.23 ± 0.01	3.16 ± 0.03	3.02 ± 0.01	
353	2410	1320	2.77 ± 0.01	2.77 ± 0.01	2.55 ± 0.01	3.07 ± 0.22
	2410	1320	2.67 ± 0.01	2.80 ± 0.01	2.68 ± 0.01	
	2410	1320	2.65 ± 0.02	2.67 ± 0.01	2.61 ± 0.01	

Figure III.22 represents the rate coefficient as function of temperature measured in this study with those measured in literature at room temperature. The rate coefficient clearly decreases as the temperature increase indicating that the reaction of 2,5-DMF with NO<sub>3</sub> proceeds by NO<sub>3</sub> addition to the double bonds. It is worth mentioning that this mechanism can include addition of NO<sub>3</sub> forming NO<sub>3</sub> adduct products or addition elimination leading to the formation of H-abstracted products. The mechanism can only be well understood from products analysis (To be discussed in the next chapter).

The Arrhenius temperature dependence of the rate coefficient is obtained from the plot and the following expression is proposed:  $k_{2,5-DMF + NO_3} = (5.04 \pm 0.19) \times 10^{-13} \times e^{\frac{1467 \pm 338}{T}}$  cm<sup>3</sup> molecule<sup>-1</sup> s<sup>-1</sup> for the temperature range of 298 – 353 K. The rate coefficient decreases by a factor of ~2 as the temperature increases from 298 to 353 K.

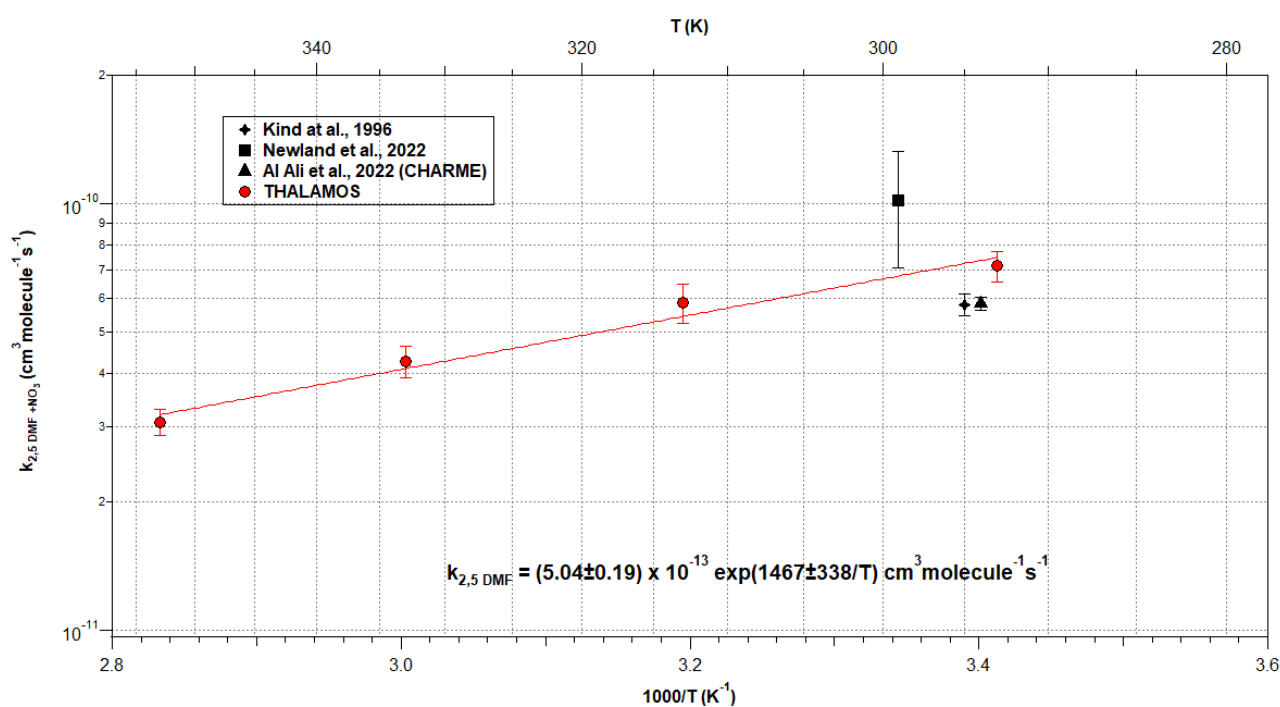
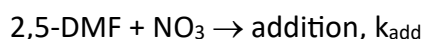


Figure III.22: Arrhenius plot for the reaction of 2,5-DMF with NO<sub>3</sub>.

### III.3.6 Temperature dependence of abstraction and addition pathways

In the case of 2,5-DMF reaction with NO<sub>3</sub>, a series of experiments were performed to evaluate the kinetics of the abstraction and addition pathways as a function of temperature. In particular, the reaction of 2,5-DMF with NO<sub>3</sub> radical can proceed through the following pathways:



In the case of the H abstraction pathway, we consider the case where NO<sub>3</sub> radicals abstract an H atom from one of the two methyl groups of 2,5-DMF. This pathway does not necessarily occur through a classical direct abstraction, but it could be linked with an addition elimination mechanism. In any case, the H atom abstraction would lead to the formation of 5-methylfurfural and HNO<sub>3</sub>. 5-Methylfurfural is not expected to be formed from the addition pathway, at least as primary product. Therefore, the rate coefficient of abstraction pathway can be extracted by multiplying the yield of 5-methylfurfural formation with the total rate coefficient of the reaction, i.e.  $k_{\text{abs}} = \text{Yield} \times k_{\text{total}}$ . Note that further information about the products of 2,5-DMF reaction and mechanism are provided in Chapter 4. Here, we only discuss the kinetics of addition and abstraction paths, and their contribution to the total rate.

5-Methylfurfural and 2,5-DMF were calibrated in separate experiments (see also Figure III.23), by injecting known amounts in the chamber. To monitor their concentrations, the three different ions of the SIFT-MS were used. In Figure III.24 is presented a typical experiment of 2,5-DMF consumption and 5-methylfurfural formation at 298 K.

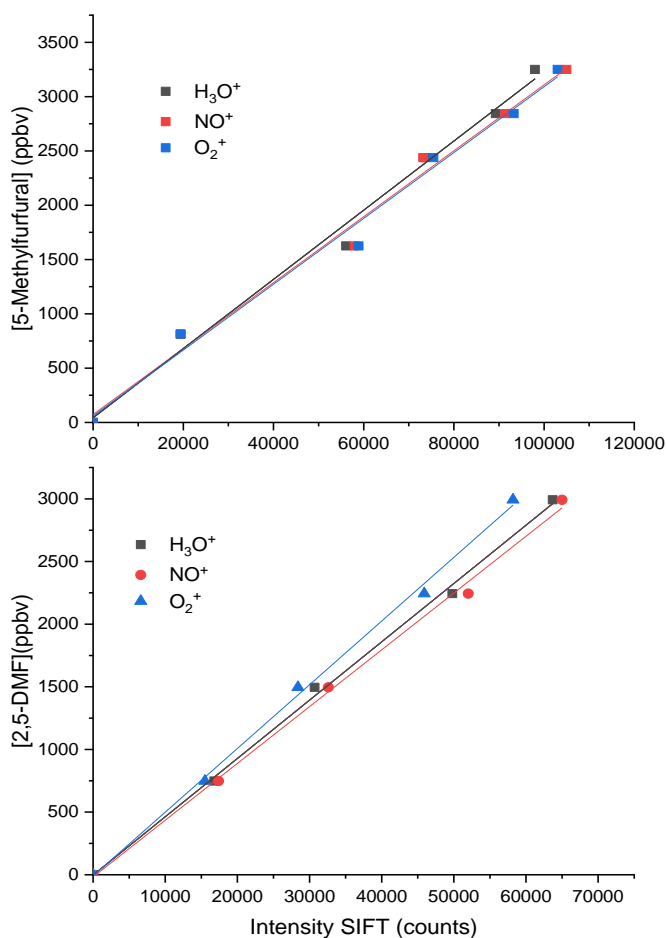


Figure III.23: Calibration of 2,5-DMF and 5-Methylfurfural using three precursor ions of the SIFT.

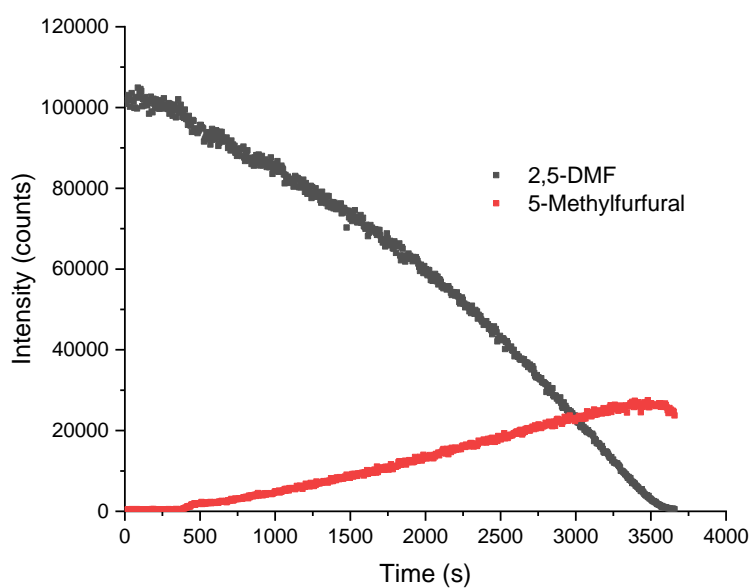


Figure III.24: 2,5-DMF consumption and 5-methylfurfural formation versus reaction time (SIFT-MS measurements).

Plotting the 5-methylfurfural concentration formed versus 2,5-DMF consumption, allows the determination of the product yield. Figure III.25 summarizes the product yield plots versus temperature, recorded with the  $\text{NO}^+$  ion. Beyond  $\Delta[2,5\text{-DMF}] = 2200$  ppbv, a slight curvature is observed which is due to the reaction of 5-methylfurfural with  $\text{NO}_3$  and it is worth mentioning that no corrections were made on 5-methylfurfural concentration due to the absence of rate coefficient of its reaction with  $\text{NO}_3$ . However, only the first part of the graph (until  $\Delta[2,5\text{-DMF}] = 1500$  ppbv) is used in 5-methylfurfural yield measurement. Table III.9 presents the yields determined for each ion, their average values, as well as the rate coefficient of the abstraction pathway.

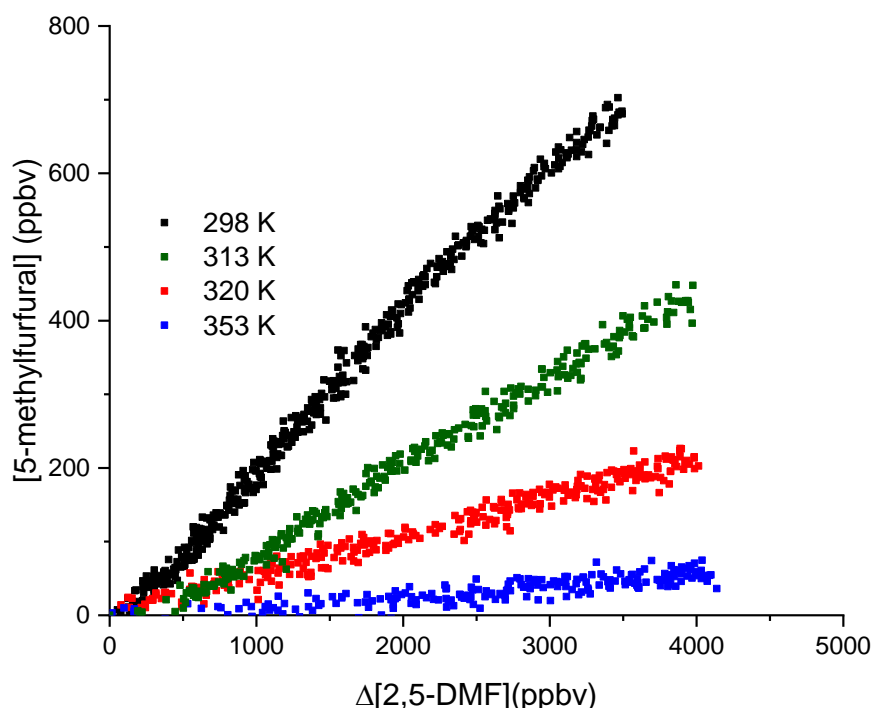


Figure III.25: 5-Methylfurfural yield of formation from the reaction of 2,5-DMF with  $\text{NO}_3$  versus temperature.

Table III.9: 5-Methylfurfural yields versus temperature and the corresponding H-abstraction rate coefficient ( $k_{\text{abs}}$ ).

Temperature	5-Methylfurfural yield			Average yield	$k_{\text{abs}} \times 10^{-11}$ ( $\text{cm}^3 \text{ molecule}^{-1} \text{ s}^{-1}$ )
	$\text{H}_3\text{O}^+$	$\text{NO}^+$	$\text{O}_2^+$		
298	0.276	0.223	0.234	0.244	5.23
303	0.236	0.195	0.189	0.207	5.06
313	0.149	0.111	0.119	0.126	4.78
313	0.153	0.119	0.129	0.134	4.74
318	0.081	0.065	0.069	0.072	4.71
320	0.060	0.052	0.052	0.055	4.67
328	0.015	0.016	0.016	0.016	4.34
333	0.018	0.014	0.018	0.017	4.06
353	0.016	0.015	0.016	0.015	3.17

The temperature dependence of abstraction and addition pathways are displayed in Figure III.26. Interestingly, a very sharp negative temperature dependence was noticed for the abstraction pathway. This is not a classical temperature dependence of a direct abstraction pathway, where the rate coefficient increases with temperature, due to the higher probability of the effective collisions leading to products. In the case of 2,5-DMF, the abstraction pathway is probably related with an adduct formation, pointing to an addition elimination mechanism. Furthermore, interestingly, above 320 K there is a sharp decrease of the abstraction rate coefficient, that is certainly related with the stability of the adduct. It should be noted, that  $k_{abs}$  seems to be somewhat lower than the general trends for the temperatures 328 K and 333 K, but this was observed systematically in our measurements. The Arrhenius plot of the rate coefficient of the abstraction channel leads to the following expression:

$$k_{abs} = (5.70 \pm 0.74) \times 10^{-23} \times e^{\frac{65478 \pm 8896}{T}} \text{ cm}^3 \text{ molecule}^{-1} \text{ s}^{-1} \text{ for the temperature range of 298 – 353 K.}$$

In the case of the addition pathway (defined as the difference between the total and abstraction rate coefficients respectively), a slight negative temperature dependence was observed, pointing that the adduct formed is relative stable or at least more stable than in the case of the abstraction channel. Interestingly, as displayed in Figure III.26 at high temperatures, the addition pathway is actually the dominant one. The plot of the experimental results leads to the following Arrhenius expression:

$$k_{add} = (2.56 \pm 0.07) \times 10^{-12} \times e^{\frac{7594 \pm 939}{T}} \text{ cm}^3 \text{ molecule}^{-1} \text{ s}^{-1} \text{ for the temperature range of 298 – 353 K.}$$

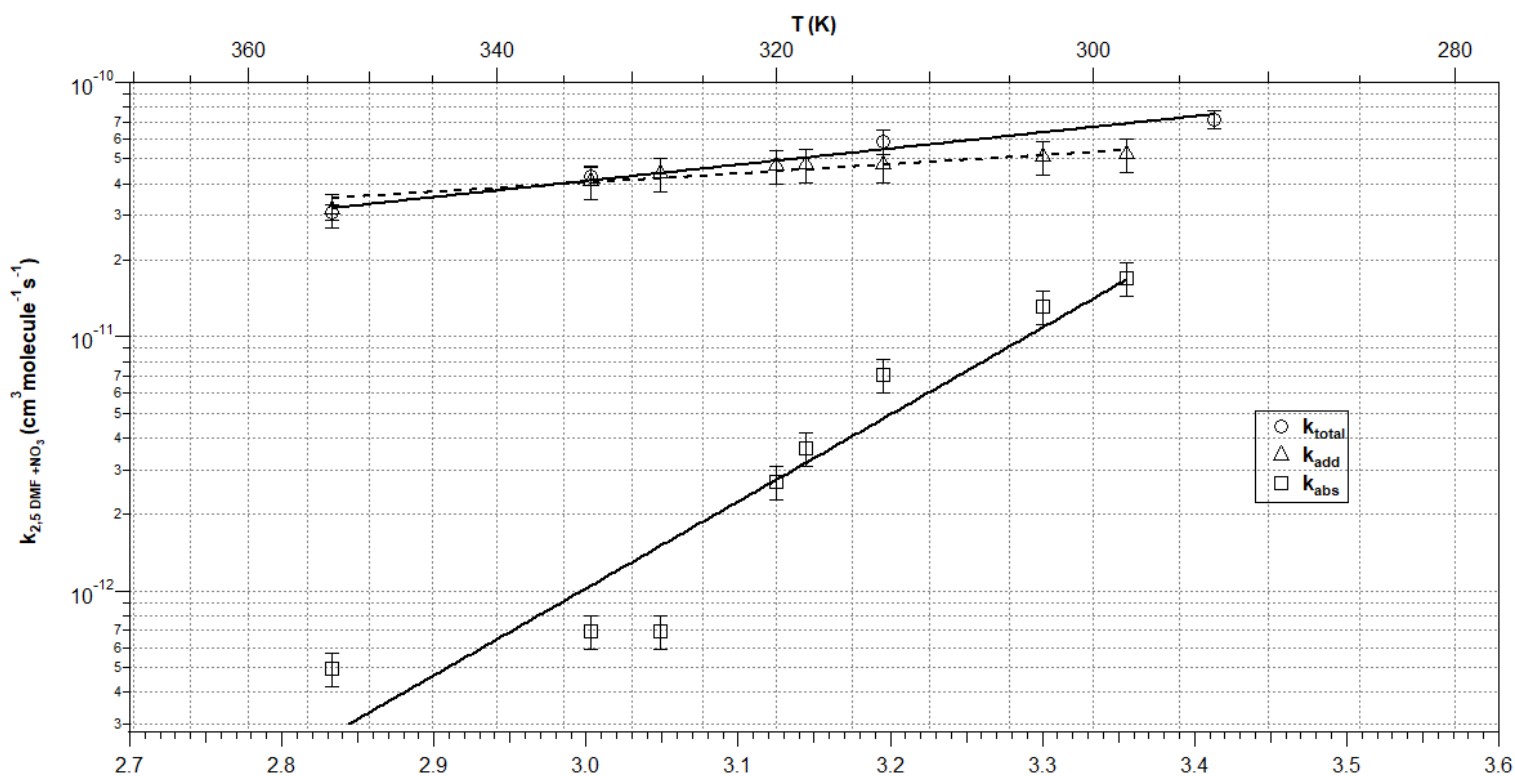


Figure III.26: Temperature-dependence of the H-abstraction and  $\text{NO}_3$  addition rate coefficients of 2,5-DMF.

### III.4 Discussion

#### III.4.1 Trends in reactivity and first insights about the reaction mechanism

Regarding the room temperature rate coefficients, it is crucial to compare the rate coefficients between the different furans to understand the effect of the structure on the NO<sub>3</sub> kinetics. Comparing the rate coefficient of F with those of 2-MF and 3-MF, it was observed that adding a methyl group to the furan ring increases the rate coefficient by approximately one order of magnitude. This increase could be due to the positive inductive effect of the methyl group, which leads to an increase in the electron density of the ring and favors the addition of NO<sub>3</sub> which is proposed to be the major pathway of the reaction. However, the position of the methyl group on C-2 or C-3 does not significantly affect the rate coefficient, suggesting a negligible effect of the position of the methyl group on the kinetics. Comparison of the rate coefficients of single alkylated furans (2-MF and 3-MF) with that of 2,5-DMF indicated an increase by approximately three times, which is also attributed to the increase of the positive inductive effect on the ring. A similar trend was observed when comparing the NO<sub>3</sub> rate coefficients of 2,5-DMF and 2,3,5-TMF, which is supported by a previous literature study (Kind et al., 1996).

Regarding the temperature dependent rate coefficients, the Arrhenius expressions of the reaction of F, 2-MF and 2,5-DMF with NO<sub>3</sub> were obtained and presented in Table III.10. Comparing the Arrhenius equations, all the three reactions exhibit negative-temperature dependence. However, for the reaction of F, a slight temperature dependence was observed which increases with the presence of the methyl groups attached to the furan ring. The reactions proceed without any potential energy barrier. This is typical for association reactions with rather weak T-dependence. Furans + NO<sub>3</sub> form an excited adduct that can either decompose back to the reactant or be stabilized by collision. The rate-determining step is generally the formation of the adduct (consistent with the structure – reactivity effect that we observed). As temperature increases, there are more internal energy in the adduct and the way back to the reactants increases.

Table III.10 : Arrhenius expressions for the reaction of F, 2-MF and 2,5-DMF with NO<sub>3</sub>, temperature range of each expression and the corresponding activation energy.

Compound	Arrhenius Equation	Temperature Range (K)	Activation Energy (kJ/mol)
F	$(7.55 \pm 0.12) \times 10^{-13} \times e^{\frac{254 \pm 138}{T}}$	263 - 353	-(2.1 ± 1.1)
2-MF	$(7.76 \pm 0.14) \times 10^{-13} \times e^{\frac{922 \pm 151}{T}}$	263 - 373	-(7.7 ± 1.3)
2,5-DMF	$(5.04 \pm 0.19) \times 10^{-13} \times e^{\frac{1467 \pm 338}{T}}$	298 - 353	-(12.2 ± 2.8)

After analyzing the experimental results, an effort was made to draw conclusions regarding the mechanisms involved in the investigated reactions. To gain a broader perspective, the reactivity of other organic compounds with NO<sub>3</sub> radicals was taken into consideration, as described in previous studies (Atkinson, 1991; Atkinson et al., 1997). It was observed that rate coefficients in the range of 10<sup>-17</sup> to 10<sup>-14</sup> cm<sup>3</sup> molecule<sup>-1</sup> s<sup>-1</sup> typically correspond to H-abstraction mechanisms and display positive activation energies. In contrast, reactions showing rate coefficients between 10<sup>-14</sup> and 10<sup>-11</sup> cm<sup>3</sup> molecule<sup>-1</sup> s<sup>-1</sup> are usually attributed to a

double bond addition mechanism and display negative activation energies. To specify, regarding our studied reactions the rates are in the range of  $10^{-12}$ - $10^{-11}$   $\text{cm}^3 \text{ molecule}^{-1} \text{ s}^{-1}$  with negative activation energy showing that the primary reaction step occurs by  $\text{NO}_3$  addition to the double bond of the furan ring or by addition elimination pathway which ends by H-abstraction from the methyl group attached to the ring. At higher temperatures, the formation of adduct intermediate species may become less favorable because the reverse reaction (adduct back to reactants) increases due to the higher internal energy in the adduct (more difficult to stabilize through collision), which could slow down the overall reaction rate.

Furthermore, due to the significant similarities in the kinetic and mechanistic properties of reactions involving OH and  $\text{NO}_3$  radicals with organic compounds, further insights can be gained by comparing our experimental results with studies on OH reactions (Eble et al., 2015; Romanias et al., submitted). Notably, the reactions between OH and F, 2-MF and 2,5-DMF were found to exhibit negative activation energies too, indicating an addition mechanism to the double bonds for these reactions in the temperature range studied in our experiments.

#### III.4.2 Average room temperature rate coefficients obtained in CHARME & THALAMOS and comparison with literature data

Table III.11 presents a compilation of the rate coefficients ( $k_{\text{FC}}$ ) measured in CHARME and THALAMOS. Average rate coefficients for the title reactions is also calculated by averaging the rate coefficients obtained from experiments done in both chambers with the different reference molecules (Table III.1). These results are also compared to the rate coefficients measured in the different literature studies.

The literature values of the rate coefficients for F are in good agreement. In terms of the 2-MF +  $\text{NO}_3$  reaction, the present study shows satisfactory agreement with the only two existing literature studies, with discrepancies between the studies being less than 25%. For the 3-MF reaction, the present work is consistent with the findings of Alvarado et al., (1996) and Tapia et al., (2011) within a 15% margin. As for the F reaction, there is a lack of understanding regarding the reasons for the disagreement between the current study and that of Kind et al. Additional research may be necessary to further investigate this matter. Concerning 2,5-DMF, there are only two previous studies that have determined its rate coefficient. The result from Kind et al. is in excellent agreement to within 10% with the present work, whereas Newland et al. reported a 40% higher rate coefficient. It is unclear why there is such a discrepancy, but one possible reason is that for the common reference compound (DMB), Newland et al. used a rate coefficient value that is approximately 1.3 times higher than the one used in this study (Newland et al., 2022). As far as we know, the present study is the first to determine the rate coefficient for the reaction of  $\text{NO}_3$  with 2,3,5-TMF.

Table III.11: Comparison of the average rate coefficients measured in CHARME with those in the literature.

Compound	$k_{FC, \text{average}}$ (CHARME) $\text{cm}^3 \text{ molecule}^{-1} \text{ s}^{-1}$	$k_{FC, \text{average}}$ (THALAMOS) $\text{cm}^3 \text{ molecule}^{-1} \text{ s}^{-1}$	$k_{FC, \text{average}}$ (CHARME & THALAMOS) $\text{cm}^3 \text{ molecule}^{-1} \text{ s}^{-1}$	$k_{FC, \text{average}}$ (literature) $\text{cm}^3 \text{ molecule}^{-1} \text{ s}^{-1}$	Setup / Technique
F	$(1.51 \pm 0.38) \times 10^{-12}$	$(1.70 \pm 0.12) \times 10^{-12}$	$(1.61 \pm 0.28) \times 10^{-12}$	$(1.40 \pm 0.20) \times 10^{-12}$	RR-ASC / GC-FID (Atkinson et al., 1985a)
				$(9.98 \pm 0.62) \times 10^{-13}$	RR-FT / GC-FID (Kind et al., 1996)
				$(1.3 \pm 0.2) \times 10^{-12}$	AR-DFT / LIF (Cabañas et al., 2004)
				$(1.50 \pm 0.23) \times 10^{-12}$	RR-ASC / FTIR (Newland et al., 2022)
2-MF	$(1.91 \pm 0.32) \times 10^{-11}$	$(2.01 \pm 0.16) \times 10^{-11}$	$(1.96 \pm 0.25) \times 10^{-11}$	$(2.57 \pm 0.17) \times 10^{-11}$	RR-FT / GC-FID (Kind et al., 1996)
				$(2.37 \pm 0.55) \times 10^{-11}$	RR-ASC / FTIR (Newland et al., 2022)
3-MF*	$(1.49 \pm 0.33) \times 10^{-11}$	-	$(1.49 \pm 0.33) \times 10^{-11}$	$(2.86 \pm 0.06) \times 10^{-11}$	RR-FT / GC-FID (Kind et al., 1996)
				$(1.31 \pm 0.46) \times 10^{-11}$	RR-ASC / GC-FID (Alvarado et al., 1996)
				$(1.26 \pm 0.18) \times 10^{-11}$	RR-ASC / GC-FID, FTIR (Tapia et al., 2011)
2,5-DMF	$(5.82 \pm 1.21) \times 10^{-11}$	$(7.16 \pm 0.59) \times 10^{-11}$	$(6.49 \pm 0.95) \times 10^{-11}$	$(5.78 \pm 0.34) \times 10^{-11}$	RR-FT / GC-FID (Kind et al., 1996)
				$(1.10 \pm 0.33) \times 10^{-10}$	RR-ASC/FTIR (Newland et al., 2022)
2,3,5-TMF*	$(1.66 \pm 0.69) \times 10^{-10}$	-	$(1.66 \pm 0.69) \times 10^{-10}$	*	

Abbreviations used in the table: Relative rate (RR) method, absolute rate (AR) method, atmospheric simulation chamber-Teflon or glass made (ASC), discharge flow tube (DFT), flow tube (FT), laser-induced fluorescence (LIF), gas chromatography-flame ionization detection (GC-FID), Fourier transform infrared (FTIR) spectroscopy. -No data.\*Only measured in CHARME.

### III.4.3 Atmospheric implications

The atmospheric lifetimes of F and its methylated derivatives with respect to  $\text{NO}_3$  radical reaction have been determined using the room temperature (298 K) rate coefficients obtained in this study. Results are presented in Table 1 together with the lifetimes of furanoids with the other tropospheric oxidants. It should be noted that the lifetimes were calculated based on the average radical/atom concentrations reported in the atmosphere:  $\text{NO}_3$  nighttime and day time concentrations of  $2 \times 10^8 \text{ molecules cm}^{-3}$  and  $1 \times 10^7 \text{ molecules cm}^{-3}$ , respectively (Brown & Stutz, 2012), OH day-time concentration of  $2 \times 10^6 \text{ molecules cm}^{-3}$  (Hein et al., 1997), Cl atoms average mixing ratio of  $1 \times 10^4 \text{ molecules cm}^{-3}$  (Wingenter et al., 1996), and ozone concentration of  $7.5 \times 10^{11} \text{ molecules cm}^{-3}$  (Matsumoto, 2011). As displayed in the table, in the case of furan, the dominant removal source is the reaction with OH radicals, with an estimated lifetime of  $\sim 3.3 \text{ h}$ . However, in the case of methylated derivatives, i.e. 2-MF, 3-MF, 2,5-DMF, and 2,3,5-TMF, the major removal pathway is the reaction with  $\text{NO}_3$  radicals, with lifetimes in the order of minutes. Very interestingly, even during day-time,  $\text{NO}_3$  chemistry of furanoids dominates compared to OH radicals.

Moreover, it is worth mentioning that the reaction of F and 3-MF with ozone is considered insignificant, however, it may compete with OH radical for 2,5-DMF. Therefore, the  $\text{O}_3$  chemistry of dimethyl or trimethyl derivatives of furanoids could be significant in the atmosphere (Matsumoto, 2011). The reaction with chlorine atoms was found to be less



significant compared to other reactions, but it could have a greater impact in coastal areas with higher concentrations of Cl (Matsumoto, 2011).

It is worth noting that in fire plumes, the concentration of nitrate radicals can increase significantly during day and nighttime. As a result, the reactivity of these compounds inside plumes can be very important, with lifetimes in the range from minutes to hours during night and daytime. These findings have implications for understanding the chemistry of biomass burning plumes. Fresh biomass burning plumes are expected to contain primarily methylated furans, while their tropospheric oxidation will generate gas and potentially particulate phase products that are anticipated to be present in aged biomass burning plumes.

Table 1: Atmospheric lifetimes of furan compounds with respect to their reaction with NO<sub>3</sub>, OH, O<sub>3</sub> and Cl.

Compound	$\tau(\text{NO}_3)$ (min) <sup>a, b</sup> (Nighttime)	$\tau(\text{NO}_3)$ (min) <sup>c</sup> (Daytime)	$\tau(\text{OH})$ (min) <sup>d</sup>	$\tau(\text{O}_3)$ (min) <sup>e</sup>	$\tau(\text{Cl})$ (min) <sup>f</sup> (Matsumoto, 2011)
F	52	1035	199 (Olariu et al., 2004)	8550 (~6 days) (Cabañas et al., 2005)	8160 (~5 days)
2-MF	4	85	114 (Aschmann et al., 2011)	–	4380 (~3 days)
3-MF	6	112	95 (Aschmann et al., 2011)	1080(~1 day) (Cabañas et al., 2004)	4200(~3 days)
2,5-DMF	1	26	66 (Aschmann et al., 2011)	54 (Hein et al., 1997)	3480 (~2 days)
2,3,5-TMF	0.5	10	-	-	-

<sup>a</sup> This work.

<sup>b</sup>  $[\text{NO}_3] = 2 \times 10^8$  molecules  $\text{cm}^{-3}$  (Average nighttime concentration) (Brown & Stutz, 2012).

<sup>c</sup>  $[\text{NO}_3] = 1 \times 10^7$  molecules  $\text{cm}^{-3}$  (Average daytime concentration) (Brown & Stutz, 2012).

<sup>d</sup>  $[\text{OH}] = 2 \times 10^6$  12-h daytime average (Hein et al., 1997).

<sup>e</sup>  $[\text{O}_3] = 7.5 \times 10^{11}$  molecules  $\text{cm}^{-3}$  (Matsumoto, 2011).

<sup>f</sup>  $[\text{Cl}] = 1 \times 10^4$  molecules  $\text{cm}^{-3}$  (Wingenter et al., 1996).

### III.5 Conclusion

In this chapter, the room temperature rate coefficients of F, 2-MF, 3-MF, 2,5-DMF and 2,3,5-TMF with NO<sub>3</sub> have been determined, together with the temperature dependence data of F, 2-MF, 2,5-DMF and two monoterpenes ( $\alpha$ -pinene, 2-carene), using the relative rate method. The measurement of the rate coefficients allowed to calculate the atmospheric lifetimes of these furan compounds. These lifetimes, indicate that the reaction of the targeted compounds with NO<sub>3</sub> is their dominant sink during nighttime, but also during daytime, in the case of methyl-, dimethyl- and trimethyl- furanoids. Moreover, these rate coefficients are impacted by the number of the methyl groups attached to the furan ring, probably due to their donor inductive effect. The more methyl groups attached to the ring, the higher is the rate coefficient of the reaction. The negative temperature dependence evidenced in the reaction rates of furanoids with NO<sub>3</sub> shows that the major reaction pathway is governed by NO<sub>3</sub> addition or addition-elimination to the ring.

In the next chapter, the qualitative and quantitative characterization of the gaseous and particulate reaction products will be presented. From these results, chemical mechanisms of the furanoid + NO<sub>3</sub> reactions will tentatively be suggested.

### III.6 References

- Akagi, S. K., Burling, I. R., Mendoza, A., Johnson, T. J., Cameron, M., Griffith, D. W. T., Paton-Walsh, C., Weise, D. R., Reardon, J., & Yokelson, R. J. (2014). Field measurements of trace gases emitted by prescribed fires in southeastern US pine forests using an open-path FTIR system. *Atmospheric Chemistry and Physics*, *14*(1), 199–215. <https://doi.org/10.5194/acp-14-199-2014>
- Akagi, S. K., Yokelson, R. J., Burling, I. R., Meinardi, S., Simpson, I., Blake, D. R., McMeeking, G. R., Sullivan, A., Lee, T., Kreidenweis, S., Urbanski, S., Reardon, J., Griffith, D. W. T., Johnson, T. J., & Weise, D. R. (2013). Measurements of reactive trace gases and variable O<sub>3</sub> formation rates in some South Carolina biomass burning plumes. In *Atmospheric Chemistry and Physics* (Vol. 13, Issue 3). <https://doi.org/10.5194/acp-13-1141-2013>
- Akagi, S. K., Yokelson, R. J., Wiedinmyer, C., Alvarado, M. J., Reid, J. S., Karl, T., Crouse, J. D., & Wennberg, P. O. (2011). Emission factors for open and domestic biomass burning for use in atmospheric models. *Atmospheric Chemistry and Physics*, *11*(9), 4039–4072. <https://doi.org/10.5194/acp-11-4039-2011>
- Akele, E. S., & Tarekegn, M. M. (2017). Assessment of dioxin and furan emission levels and management practices in Addis Ababa, Ethiopia. *Journal of Health and Pollution*, *7*(15), 85–94. <https://doi.org/10.5696/2156-9614-7.15.85>
- Al Ali, F., Coeur, C., Houzel, N., Bouya, H., Tomas, A., & Romanias, M. N. (2022). Rate Coefficients for the Gas-Phase Reactions of Nitrate Radicals with a Series of Furan Compounds. *Journal of Physical Chemistry A*, *126*(46), 8674–8681. <https://doi.org/10.1021/acs.jpca.2c03828>
- Alan Buis. (2019). *Earth's Atmosphere: A Multi-layered Cake*. <https://climate.nasa.gov/news/2919/earths-atmosphere-a-multi-layered-cake/>
- Alcock, R. E., & Jones, K. C. (1996). Dioxins in the environment: A review of trend data. *Environmental Science and Technology*, *30*(11), 3133–3143. <https://doi.org/10.1021/es960306z>
- Alicke, B., & Platt, U. (2002). *Impact of nitrous acid photolysis on the total hydroxyl radical budget during the Limitation of Oxidant Production / Pianura Padana Produzione di Ozono study in Milan*. 107. <https://doi.org/10.1029/2000JD000075>
- Alvarado, A., Atkinson, R., & Arey, J. (1996). Kinetics of the gas-phase reactions of NO<sub>3</sub> radicals and O<sub>3</sub> with 3-methylfuran and the OH radical yield from the O<sub>3</sub> reaction. *International Journal of Chemical Kinetics*, *28*(12), 905–909. [https://doi.org/10.1002/\(SICI\)1097-4601\(1996\)28:12<905::AID-KIN7>3.0.CO;2-R](https://doi.org/10.1002/(SICI)1097-4601(1996)28:12<905::AID-KIN7>3.0.CO;2-R)
- Alwe, H. D., Walavalkar, M. P., Sharma, A., Dhanya, S., & Naik, P. D. (2014). Tropospheric oxidation of cyclic unsaturated ethers in the day-time: Comparison of the reactions with Cl, OH and O<sub>3</sub> based on the determination of their rate coefficients at 298K. *Atmospheric Environment*, *82*, 113–120. <https://doi.org/10.1016/j.atmosenv.2013.10.009>
- Andersen, C., Nielsen, O. J., Østerstrøm, F. F., Ausmeel, S., Nilsson, E. J. K., & Sulbaek Andersen, M. P. (2016). Atmospheric Chemistry of Tetrahydrofuran, 2-Methyltetrahydrofuran, and 2,5-Dimethyltetrahydrofuran: Kinetics of Reactions with Chlorine Atoms, OD Radicals, and Ozone. *Journal of Physical Chemistry A*, *120*(37), 7320–7326.

<https://doi.org/10.1021/acs.jpca.6b06618>

- Andreae, M. (2019). Emission of trace gases and aerosols from biomass burning. *Global Biogeochemical. Atmospheric Chemistry and Physics*, 15 (4)(April), 955–966. <https://www.atmos-chem-phys-discuss.net/acp-2019-303/acp-2019-303.pdf>
- Andreae, M. O. (2001). [ *Ca Because of the carbon to permits*. 15(4), 955–966.
- Aschmann, S. M., Nishino, N., Arey, J., & Atkinson, R. (2011). Kinetics of the Reactions of OH Radicals with 2- and 3-Methylfuran, 2,3- and 2,5-Dimethylfuran, and E- and Z-3-Hexene-2,5-dione, and Products of OH p 2,5-Dimethylfuran. *Environmental Science and Technology*, 45(7), 1859–1865. <https://doi.org/10.1002/kin.550140706>
- Aschmann, S. M., Nishino, N., Arey, J., & Atkinson, R. (2014a). Products of the OH Radical-Initiated Reactions of Furan, 2- and 3-Methylfuran, and 2,3- and 2,5-Dimethylfuran in the Presence of NO. *The Journal of Physical Chemistry*, 118, 457–466. <https://doi.org/10.1021/jp410345k>
- Aschmann, S. M., Nishino, N., Arey, J., & Atkinson, R. (2014b). *Sara M. Aschmann, Noriko Nishino, † Janet Arey, \*, ‡ and Roger Atkinson \*, ‡*.
- Atkinson, R. (1991a). Kinetics and Mechanisms of the Gas-Phase Reactions of the NO<sub>3</sub> Radical with Organic Compounds. *Journal of Physical and Chemical Reference Data*, 20(3), 459–507. <https://doi.org/10.1063/1.555887>
- Atkinson, R. (1991b). Kinetics and Mechanisms of the Gas-Phase Reactions of the NO<sub>3</sub> Radical with Organic Compounds. *Journal of Physical and Chemical Reference Data*, 20(3), 459–507. <https://doi.org/10.1063/1.555887>
- Atkinson, R. (2000). Atmospheric chemistry of VOCs and NO(x). *Atmospheric Environment*, 34(12–14), 2063–2101. [https://doi.org/10.1016/S1352-2310\(99\)00460-4](https://doi.org/10.1016/S1352-2310(99)00460-4)
- Atkinson, R., & Arey, J. (2003). *ARTICLE IN PRESS Gas-phase tropospheric chemistry of biogenic volatile organic compounds: a review*. 2(2). [https://doi.org/10.1016/S1352-2310\(03\)00391-1](https://doi.org/10.1016/S1352-2310(03)00391-1)
- Atkinson, R., Arey, J., Tuazon, E. C., & Aschmann, S. M. (1992). Gas-phase reactions of 1,4-benzodioxan, 2,3-dihydrobenzofuran, and 2,3-benzofuran with OH radicals and O<sub>3</sub>. *International Journal of Chemical Kinetics*, 24(4), 345–358. <https://doi.org/10.1002/kin.550240404>
- Atkinson, R., Aschmann, S. M., & Carter, P. L. (1983a). *Radicals with Furan and Thiophene at*. 15, 51–61.
- Atkinson, R., Aschmann, S. M., & Carter, W. P. L. (1983b). Kinetics of the reactions of O<sub>3</sub> and OH radicals with furan and thiophene at 298 ± 2 K. *International Journal of Chemical Kinetics*, 15(1), 51–61. <https://doi.org/10.1002/kin.550150106>
- Atkinson, R., Aschmann, S. M., & Carter, W. P. L. (1984). Kinetics of the reactions of O<sub>3</sub> and OH radicals with a series of dialkenes and trialkenes at 294 ± 2 K. *International Journal of Chemical Kinetics*, 16(8), 967–976. <https://doi.org/10.1002/kin.550160804>
- Atkinson, R., Aschmann, S. M., & Pitts, J. N. (1988). Rate constants for the gas-phase reactions of the NO<sub>3</sub> radical with a series of organic compounds at 296 ± 2 K. *Journal of Physical*

*Chemistry*, 92(12), 3454–3457. <https://doi.org/10.1021/j100323a028>

- Atkinson, R., Aschmann, S. M., Tuazon, E. C., Arey, J., & Zielinska, B. (1989). Formation of 3-Methylfuran from the gas-phase reaction of OH radicals with isoprene and the rate constant for its reaction with the OH radical. *International Journal of Chemical Kinetics*, 21(7), 593–604. <https://doi.org/10.1002/kin.550210709>
- Atkinson, R., Aschmann, S. M., Winer, A. M., & Carter, W. P. L. (1985a). *for Reactions with Pyrrole ± 1 Atmospheric. I*, 87–90.
- Atkinson, R., Aschmann, S. M., Winer, A. M., & Carter, W. P. L. (1985b). Rate Constants for the Gas-Phase Reactions of NO<sub>3</sub> Radicals with Furan, Thiophene, and Pyrrole at 295 ± 1 K and Atmospheric Pressure. *Environmental Science and Technology*, 19(1), 87–90. <https://doi.org/10.1021/es00131a010>
- Atkinson, R., Aschmann, S. M., Winer, A. M., & Pitts, J. N. (1985). Kinetics and Atmospheric Implications of the Gas-Phase Reactions of NO<sub>3</sub> Radicals with a Series of Monoterpenes and Related Organics at 294 ± 2 K. *Environmental Science and Technology*, 19(2), 159–163. <https://doi.org/10.1021/es00132a009>
- Atkinson, R., Baulch, D. L., Cox, R. A., Hampson, R. F., Kerr, J. A., Rossi, M. J., & Troe, J. (1997). Evaluated Kinetic, Photochemical and Heterogeneous Data for Atmospheric Chemistry: Supplement V: IUPAC Subcommittee on Gas Kinetic Data Evaluation for Atmospheric Chemistry. *Journal of Physical and Chemical Reference Data*, 26(3), 521–784. <https://doi.org/10.1063/1.556011>
- Bahreini, R., Keywood, M. D., Ng, N. L., Varutbangkul, V., Gao, S., Flagan, R. C., Seinfeld, J. H., Worsnop, D. R., & Jimenez, J. L. (2005). Measurements of secondary organic aerosol from oxidation of cycloalkenes, terpenes, and m-xylene using an aerodyne aerosol mass spectrometer. *Environmental Science and Technology*, 39(15), 5674–5688. <https://doi.org/10.1021/es048061a>
- Berndt, T., Böge, O., & Rolle, W. (1997). Products of the gas-phase reactions of NO<sub>3</sub> radicals with furan and tetramethylfuran. *Environmental Science and Technology*, 31(4), 1157–1162. <https://doi.org/10.1021/es960669z>
- Bierbach, A., Barnes, I., & Becker, K. H. (1992). Rate coefficients for the gas-phase reactions of hydroxyl radicals with furan, 2-methylfuran, 2-ethylfuran and 2,5-dimethylfuran at 300 ± 2 K. *Atmospheric Environment Part A, General Topics*, 26(5), 813–817. [https://doi.org/10.1016/0960-1686\(92\)90241-C](https://doi.org/10.1016/0960-1686(92)90241-C)
- Bierbach, A., Barnes, I., & Becker, K. H. (1995). Product and kinetic study of the oh-initiated gas-phase oxidation of Furan, 2-methylfuran and furanaldehydes at ≈ 300 K. *Atmospheric Environment*, 29(19), 2651–2660. [https://doi.org/10.1016/1352-2310\(95\)00096-H](https://doi.org/10.1016/1352-2310(95)00096-H)
- Bierbach, A., Barnes, I., Becker, K. H., & Wiesen, E. (1994). Atmospheric Chemistry of Unsaturated Carbonyls: Butenedial, 4-Oxo-2-pentenal, 3-Hexene-2,5-dione, Maleic Anhydride, 3H-Furan-2-one, and 5-Methyl-3H-furan-2-one. *Environmental Science and Technology*, 28(4), 715–729. <https://doi.org/10.1021/es00053a028>
- Blake, R., Monks, P., & Ellis, A. (2009). Proton Transfer Reaction Mass Spectrometry (PTR-MS). *Chem.Rev.*, 109(0), 861–896. <https://doi.org/10.1002/9781118180730.ch28>

- Brando, P., Macedo, M., Silvério, D., Rattis, L., Paolucci, L., Alencar, A., Coe, M., & Amorim, C. (2020). Amazon wildfires: Scenes from a foreseeable disaster. *Flora: Morphology, Distribution, Functional Ecology of Plants*, 268. <https://doi.org/10.1016/j.flora.2020.151609>
- Brown, S. S., & Stutz, J. (2012). Nighttime radical observations and chemistry. *Chemical Society Reviews*, 41(19), 6405–6447. <https://doi.org/10.1039/c2cs35181a>
- Burkholder, J. B., Abbatt, J. P. D., Barnes, I., Roberts, J. M., Melamed, M. L., Ammann, M., Bertram, A. K., Cappa, C. D., Carlton, A. G., Carpenter, L. J., Crowley, J. N., Dubowski, Y., George, C., Heard, D. E., Herrmann, H., Keutsch, F. N., Kroll, J. H., McNeill, V. F., Ng, N. L., ... Ziemann, P. J. (2017). The Essential Role for Laboratory Studies in Atmospheric Chemistry. *Environmental Science and Technology*, 51(5), 2519–2528. <https://doi.org/10.1021/acs.est.6b04947>
- Burkholder, J. B., Sander, S. P., Abbatt, J. P. D., Barker, J. R., Huie, R. E., Kolb, C. E., Kurylo, M. J., Orkin, V. L., Wilmouth, D. M., & Wine, P. H. (2020). Chemical Kinetics and Photochemical Data for Use in Atmospheric Studies, Evaluation No. 19. *JPL Publications 19-5*, 19, 1–153. <http://jpldataeval.jpl.nasa.gov/>
- Burling, I. R., Yokelson, R. J., Griffith, D. W. T., Johnson, T. J., Veres, P., Roberts, J. M., Warneke, C., Urbanski, S. P., Reardon, J., Weise, D. R., Hao, W. M., & De Gouw, J. (2010). Laboratory measurements of trace gas emissions from biomass burning of fuel types from the southeastern and southwestern United States. *Atmospheric Chemistry and Physics*, 10(22), 11115–11130. <https://doi.org/10.5194/acp-10-11115-2010>
- Cabañas, B., Baeza, M. T., Salgado, S., Martín, P., Taccone, R., & Martínez, E. (2004). Oxidation of heterocycles in the atmosphere: Kinetic study of their reactions with NO<sub>3</sub> radical. *Journal of Physical Chemistry A*, 108(49), 10818–10823. <https://doi.org/10.1021/jp046524t>
- Cabañas, B., Villanueva, F., Martín, P., Baeza, M. T., Salgado, S., & Jiménez, E. (2005). Study of reaction processes of furan and some furan derivatives initiated by Cl atoms. *Atmospheric Environment*, 39(10), 1935–1944. <https://doi.org/10.1016/j.atmosenv.2004.12.013>
- Cabrera-perez, D., Taraborrelli, D., Sander, R., & Pozzer, A. (2016). *Global atmospheric budget of simple monocyclic aromatic compounds*. 6931–6947. <https://doi.org/10.5194/acp-16-6931-2016>
- Calogirou, A., Jensen, N. R., Nielsen, C. J., Kotzias, D., & Hjorth, J. (1999). Gas-phase reactions of nopinone, 3-isopropenyl-6-oxo-heptanal, and 5-methyl-5-vinyltetrahydrofuran-2-ol with OH, NO<sub>3</sub>, and ozone. *Environmental Science and Technology*, 33(3), 453–460. <https://doi.org/10.1021/es980530j>
- Carbajo, P. G., Smith, S. C., Holloway, A. L., Smith, C. A., Pope, F. D., Shallcross, D. E., & Orr-Ewing, A. J. (2008). Ultraviolet photolysis of HCHO: Absolute HCO quantum yields by direct detection of the HCO radical photoproduct. *Journal of Physical Chemistry A*, 112(48), 12437–12448. <https://doi.org/10.1021/jp8070508>
- Chattopadhyay, A., Papadimitriou, V. C., Marshall, P., & Burkholder, J. B. (2020). Temperature-dependent rate coefficients for the gas-phase OH + furan-2,5-dione (C<sub>4</sub>H<sub>2</sub>O<sub>3</sub>, maleic anhydride) reaction. *International Journal of Chemical Kinetics*, 52(10), 623–631.

<https://doi.org/10.1002/kin.21387>

- Chipperfield, M. P., Bekki, S., Dhomse, S., Harris, N. R. P., Hassler, B., Hossaini, R., Steinbrecht, W., Thiéblemont, R., & Weber, M. (2017). Detecting recovery of the stratospheric ozone layer. *Nature*, *549*(7671), 211–218. <https://doi.org/10.1038/nature23681>
- Christian, T. J., Kleiss, B., Yokelson, R. J., Holzinger, R., Crutzen, P. J., Hao, W. M., Saharjo, B. H., & Ward, D. E. (2003). Comprehensive laboratory measurements of biomass-burning emissions: 1. Emissions from Indonesian, African, and other fuels. *Journal of Geophysical Research: Atmospheres*, *108*(23). <https://doi.org/10.1029/2003jd003704>
- Ciccioli, P., Brancaleoni, E., Frattoni, M., Cecinato, A., & Pinciarelli, L. (2001). Determination of volatile organic compounds (VOC) emitted from biomass burning of Mediterranean vegetation species by GC-MS. *Analytical Letters*, *34*(6), 937–955. <https://doi.org/10.1081/AL-100103604>
- Coeur-tourneur, C., Tomas, A., & Menu, D. (2008). *Secondary organic aerosol formation from the gas phase reaction of hydroxyl radicals with m - , o- and p -cresol*. *42*, 3035–3045. <https://doi.org/10.1016/j.atmosenv.2007.12.043>
- Coggon, M. M., Lim, C. Y., Koss, A. R., Sekimoto, K., Yuan, B., Gilman, J. B., Hagan, D. H., Selimovic, V., Zarzana, K. J., Brown, S. S., M Roberts, J., Müller, M., Yokelson, R., Wisthaler, A., Krechmer, J. E., Jimenez, J. L., Cappa, C., Kroll, J. H., De Gouw, J., & Warneke, C. (2019). OH chemistry of non-methane organic gases (NMOGs) emitted from laboratory and ambient biomass burning smoke: Evaluating the influence of furans and oxygenated aromatics on ozone and secondary NMOG formation. *Atmospheric Chemistry and Physics*, *19*(23), 14875–14899. <https://doi.org/10.5194/acp-19-14875-2019>
- Collard, F. X., & Blin, J. (2014). A review on pyrolysis of biomass constituents: Mechanisms and composition of the products obtained from the conversion of cellulose, hemicelluloses and lignin. *Renewable and Sustainable Energy Reviews*, *38*, 594–608. <https://doi.org/10.1016/j.rser.2014.06.013>
- Colmenar, I., Cabañas, B., Martínez, E., Salgado, M. S., & Martín, P. (2012). Atmospheric fate of a series of furanaldehydes by their NO<sub>3</sub> reactions. *Atmospheric Environment*, *54*(3), 177–184. <https://doi.org/10.1016/j.atmosenv.2012.02.087>
- Colmenar, I., Martín, P., Cabañas, B., Salgado, S., Villanueva, F., & Ballesteros, B. (2020). Evaluation of the SOA formation in the reaction of furfural with atmospheric oxidants. *Atmosphere*, *11*(9). <https://doi.org/10.3390/atmos11090927>
- Corchnoy, S., & Atkinson, R. (1990). Kinetics of the Gas-Phase Reactions of OH and NO<sub>3</sub> Radicals with 2-Carene, 1,8-Cineole, p-Cymene, and Terpinolene. *Environ. Sci. Technol.* *1990*, *24*(10), 1497–1502.
- Crouse, J. D., DeCarlo, P. F., Blake, D. R., Emmons, L. K., Campos, T. L., Apel, E. C., Clarke, A. D., Weinheimer, A. J., McCabe, D. C., Yokelson, R. J., Jimenez, J. L., & Wennberg, P. O. (2009). Biomass burning and urban air pollution over the Central Mexican Plateau. *Atmospheric Chemistry and Physics*, *9*(14), 4929–4944. <https://doi.org/10.5194/acp-9-4929-2009>
- Cuisset, A., Coeur, C., Mouret, G., Ahmad, W., Tomas, A., & Pirali, O. (2016). Infrared

- spectroscopy of methoxyphenols involved as atmospheric secondary organic aerosol precursors: Gas-phase vibrational cross-sections. *Journal of Quantitative Spectroscopy and Radiative Transfer*, 179, 51–58. <https://doi.org/10.1016/j.jqsrt.2016.03.020>
- Davis, A. C., & Sarathy, S. M. (2013). Computational study of the combustion and atmospheric decomposition of 2-methylfuran. *Journal of Physical Chemistry A*, 117(33), 7670–7685. <https://doi.org/10.1021/jp403085u>
- De gouw, J., & Warneke, C. (2007). MEASUREMENTS OF VOLATILE ORGANIC COMPOUNDS IN THE EARTH'S ATMOSPHERE USING PROTON-TRANSFER-REACTION MASS SPECTROMETRY. *Wiley InterScience*, i, 221–235. <https://doi.org/10.1002/mas>
- Decker, Z. C. J., Zarzana, K. J., Coggon, M., Min, K. E., Pollack, I., Ryerson, T. B., Peischl, J., Edwards, P., Dubé, W. P., Markovic, M. Z., Roberts, J. M., Veres, P. R., Graus, M., Warneke, C., De Gouw, J., Hatch, L. E., Barsanti, K. C., & Brown, S. S. (2019). Nighttime Chemical Transformation in Biomass Burning Plumes: A Box Model Analysis Initialized with Aircraft Observations. *Environmental Science and Technology*, 53(5), 2529–2538. <https://doi.org/10.1021/acs.est.8b05359>
- Decker, Z., Robinson, M., Barsanti, K., Bourgeois, I., Coggon, M., DiGangi, J., Diskin, G., Flocke, F., Franchin, A., Fredrickson, C., Hall, S., Halliday, H., Holmes, C., Huey, L. G., Lee, Y. R., Lindaas, J., Middlebrook, A., Montzka, D., Moore, R., ... Brown, S. (2021). Nighttime and Daytime Dark Oxidation Chemistry in Wildfire Plumes: An Observation and Model Analysis of FIREX-AQ Aircraft Data. *Atmospheric Chemistry and Physics Discussions*, November, 1–45. <https://doi.org/10.5194/acp-2021-267>
- Dlugokencky, E. J., & Howard, C. J. (1989a). + (1.28. 17, 1091–1096.
- Dlugokencky, E. J., & Howard, C. J. (1989b). Studies of NO<sub>3</sub> radical reactions with some atmospheric organic compounds at low pressures. *Journal of Physical Chemistry*, 93(3), 1091–1096. <https://doi.org/10.1021/j100340a015>
- Dodge, M. C. (2000). Chemical oxidant mechanisms for air quality modeling: Critical review. *Atmospheric Environment*, 34(12–14), 2103–2130. [https://doi.org/10.1016/S1352-2310\(99\)00461-6](https://doi.org/10.1016/S1352-2310(99)00461-6)
- Durigan, M. R., Cherubin, M. R., de Camargo, P. B., Ferreira, J. N., Berenguer, E., Gardner, T. A., Barlow, J., Dias, C. T. dos S., Signor, D., de Oliveira, R. C., & Cerri, C. E. P. (2017). Soil organic matter responses to anthropogenic forest disturbance and land use change in the eastern Brazilian Amazon. *Sustainability (Switzerland)*, 9(3). <https://doi.org/10.3390/su9030379>
- Dusanter, S., Vimal, D., Stevens, P. S., Volkamer, R., Molina, L. T., Baker, A., Meinardi, S., Blake, D., Sheehy, P., Merten, A., Zhang, R., Zheng, J., Fortner, E. C., Junkermann, W., Dubey, M., Rann, T., Eichinger, B., Lewandowski, P., Prueger, J., & Holder, H. (2009). Measurements of OH and HO<sub>2</sub> concentrations during the MCMA-2006 field campaign - Part 2: Model comparison and radical budget. *Atmospheric Chemistry and Physics*, 9(18), 6655–6675. <https://doi.org/10.5194/acp-9-6655-2009>
- Eble, J., Bänsch, C., & Olzmann, M. (2015). *Kinetic Investigation of the Reactions of 2, 5-Dimethylfuran and 2-Methylfuran with Hydroxyl Radicals*. 2–5.

- Elshorbany, Y., Barnes, I., Becker, K. H., Kleffmann, J., & Wiesen, P. (2010). Sources and cycling of tropospheric hydroxyl radicals - An overview. *Zeitschrift Fur Physikalische Chemie*, 224(7–8), 967–987. <https://doi.org/10.1524/zpch.2010.6136>
- Elshorbany, Y. F., Kurtenbach, R., Wiesen, P., Lissi, E., Rubio, M., Villena, G., Gramsch, E., Rickard, A. R., Pilling, M. J., & Kleffmann, J. (2009). Oxidation capacity of the city air of Santiago, Chile. *Atmospheric Chemistry and Physics*, 9(6), 2257–2273. <https://doi.org/10.5194/acp-9-2257-2009>
- Elwardany, A., Es-Sebbar, E., Khaled, F., & Farooq, A. (2016). A chemical kinetic study of the reaction of hydroxyl with furans. *Fuel*, 166, 245–252. <https://doi.org/10.1016/j.fuel.2015.10.098>
- Evyugina, M., Alves, C., Calvo, A., Nunes, T., Tarelho, L., Duarte, M., Prozil, S. O., Evtuguin, D. V., & Pio, C. (2014). VOC emissions from residential combustion of Southern and mid-European woods. *Atmospheric Environment*, 83, 90–98. <https://doi.org/10.1016/j.atmosenv.2013.10.050>
- Evyugina, M., Calvo, A. I., Nunes, T., Alves, C., Fernandes, A. P., Tarelho, L., Vicente, A., & Pio, C. (2013). VOC emissions of smouldering combustion from Mediterranean wildfires in central Portugal. *Atmospheric Environment*, 64, 339–348. <https://doi.org/10.1016/j.atmosenv.2012.10.001>
- Fayad, L. (2019). *Caractérisation de la nouvelle chambre de simulation atmosphérique CHARME et étude de la réaction d'ozonolyse d'un COV biogénique, le  $\gamma$ -terpinène Loyal FAYAD Acknowledgments* (Vol. 104).
- Fayad, L., Coeur, C., Fagniez, T., Secordel, X., Houzel, N., & Mouret, G. (2021). Kinetic and mechanistic study of the gas-phase reaction of ozone with  $\gamma$ -terpinene. *Atmospheric Environment*, 246(August 2020). <https://doi.org/10.1016/j.atmosenv.2020.118073>
- Ferdous, D., Dalai, A. K., Bej, S. K., & Thring, R. W. (2002). Pyrolysis of lignins: Experimental and kinetics studies. *Energy and Fuels*, 16(6), 1405–1412. <https://doi.org/10.1021/ef0200323>
- Finlayson-Pitts, B. J. (2010). Atmospheric chemistry. *Proceedings of the National Academy of Sciences of the United States of America*, 107(15), 6566–6567. <https://doi.org/10.1073/pnas.1003038107>
- Finlayson-Pitts, B. J., & Pitts, J. N. (1993). Atmospheric chemistry of tropospheric ozone formation: Scientific and regulatory implications. *Air and Waste*, 43(8), 1091–1100. <https://doi.org/10.1080/1073161X.1993.10467187>
- Finlayson-Pitts, Barbara J., & James N. Pitts Jr. (1999). *Chemistry of the upper and lower atmosphere: theory, experiments, and applications*. El Sevier.
- Fuchs, J. D. H., Seakins, A. K. P., & Editors, J. W. (n.d.). *A Practical Guide to Atmospheric*.
- George, C., Ammann, M., D'Anna, B., Donaldson, D. J., & Nizkorodov, S. A. (2015). Heterogeneous Photochemistry in the Atmosphere. *Chemical Reviews*, 115(10), 4218–4258. <https://doi.org/10.1021/cr500648z>
- Gilman, J. B., Lerner, B. M., Kuster, W. C., Goldan, P. D., Warneke, C., Veres, P. R., Roberts, J. M., De Gouw, J. A., Burling, I. R., & Yokelson, R. J. (2015). Biomass burning emissions and



- potential air quality impacts of volatile organic compounds and other trace gases from fuels common in the US. *Atmospheric Chemistry and Physics*, 15(24), 13915–13938. <https://doi.org/10.5194/acp-15-13915-2015>
- Giri, B. R., Khaled, F., Szori, M., Viskolcz, B., & Farooq, A. (2017). An experimental and theoretical kinetic study of the reaction of OH radicals with tetrahydrofuran. *Proceedings of the Combustion Institute*, 36(1), 143–150. <https://doi.org/10.1016/j.proci.2016.06.016>
- Gómez Alvarez, E., Borrás, E., Viidanoja, J., & Hjorth, J. (2009). Unsaturated dicarbonyl products from the OH-initiated photo-oxidation of furan, 2-methylfuran and 3-methylfuran. *Atmospheric Environment*, 43(9), 1603–1612. <https://doi.org/10.1016/j.atmosenv.2008.12.019>
- Graedel, T. E., & Keene, W. C. (1996). The budget and cycle of Earth's natural chlorine. *Pure and Applied Chemistry*, 68(9), 1689–1697. <https://doi.org/10.1351/pac199668091689>
- Graham, B., Mayol-Bracero, O. L., Guyon, P., Roberts, G. C., Decesari, S., Facchini, M. C., Artaxo, P., Maenhaut, W., Köll, P., & Andreae, M. O. (2002). Water-soluble organic compounds in biomass burning aerosols over Amazonia 1. Characterization by NMR and GC-MS. *Journal of Geophysical Research Atmospheres*, 107(20), LBA 14-1-LBA 14-16. <https://doi.org/10.1029/2001JD000336>
- Greenberg, J. P., Zimmerman, P. R., Heidt, L., & Pollock, W. (1984). Hydrocarbon and carbon monoxide emissions from biomass burning in Brazil. *Journal of Geophysical Research*, 89(D1), 1350–1354. <https://doi.org/10.1029/JD089iD01p01350>
- Gira, A., Amarandei, C., Romanias, M. N., El Dib, G., Canosa, A., Arsene, C., Bejan, I. G., Olariu, R. I., Coddeville, P., & Tomas, A. (2020). Kinetic measurements of Cl atom reactions with C5-C8 unsaturated alcohols. *Atmosphere*, 11(3), 1–15. <https://doi.org/10.3390/ATMOS11030256>
- Guenther, A., Nicholas, C., Fall, R., Klinger, L., McKay, W. A., & Scholes, B. (1995). A global model of natural volatile organic compound emissions s Raja the balance Triangle changes in the atmospheric accumulation rates of greenhouse Triangle Several inventories of natural and Exposure Assessment global scales have been two classes Fores. *J. Geophys. Res.*, 100(94), 8873–8892.
- Hartikainen, A., Yli-Pirilä, P., Tiitta, P., Leskinen, A., Kortelainen, M., Orasche, J., Schnelle-Kreis, J., Lehtinen, K. E. J., Zimmermann, R., Jokiniemi, J., & Sippula, O. (2018). Volatile Organic Compounds from Logwood Combustion: Emissions and Transformation under Dark and Photochemical Aging Conditions in a Smog Chamber. *Environmental Science and Technology*, 52(8), 4979–4988. <https://doi.org/10.1021/acs.est.7b06269>
- Hatch, L. E., Luo, W., Pankow, J. F., Yokelson, R. J., Stockwell, C. E., & Barsanti, K. C. (2015). Identification and quantification of gaseous organic compounds emitted from biomass burning using two-dimensional gas chromatography-time-of-flight mass spectrometry. *Atmospheric Chemistry and Physics*, 15(4), 1865–1899. <https://doi.org/10.5194/acp-15-1865-2015>
- Hatch, L. E., Yokelson, R. J., Stockwell, C. E., Veres, P. R., Simpson, I. J., Blake, D. R., Orlando, J. J., & Barsanti, K. C. (2017). Multi-instrument comparison and compilation of non-methane organic gas emissions from biomass burning and implications for smoke-

- derived secondary organic aerosol precursors. *Atmospheric Chemistry and Physics*, 17(2), 1471–1489. <https://doi.org/10.5194/acp-17-1471-2017>
- Hein, R., Crutzen, P. J., & Heimann, M. (1997). An inverse modeling approach to investigate the global atmospheric methane cycle. *Global Biogeochemical Cycles*, 11(1), 43–76. <https://doi.org/10.1029/96GB03043>
- Holly Zell. (2013). *Earth's Atmospheric Layers*. [https://www.nasa.gov/mission\\_pages/sunearth/science/atmosphere-layers2.html](https://www.nasa.gov/mission_pages/sunearth/science/atmosphere-layers2.html)
- Huang, Z., Zhao, N., Ma, X., Xu, F., Zhang, Q., Zhuang, T., & Wang, W. (2019). Theoretical study on the atmospheric oxidation reaction of 2-furaldehyde initiated by NO<sub>3</sub> radicals. *Chemical Physics Letters*, 722(3), 50–57. <https://doi.org/10.1016/j.cplett.2019.03.009>
- Hynes, R. G., Angove, D. E., Saunders, S. M., Haverd, V., & Azzi, M. (2005). Evaluation of two MCM v3.1 alkene mechanisms using indoor environmental chamber data. *Atmospheric Environment*, 39(38), 7251–7262. <https://doi.org/10.1016/j.atmosenv.2005.09.005>
- Identification, I., Flux, V., & Atkinson, R. (1990). *Radicals with*. 24(10), 1497–1502.
- Illés, Á., Rózsa, Z. B., Thangaraj, R., Décsiné Gombos, E., Dóbbé, S., Giri, B. R., & Szóri, M. (2021). An experimental and theoretical kinetic study of the reactions of hydroxyl radicals with tetrahydrofuran and two deuterated tetrahydrofurans. *Chemical Physics Letters*, 776. <https://doi.org/10.1016/j.cplett.2021.138698>
- IUPAC. (2016). *IUPAC Task Group on Atmospheric Chemical Kinetic Data Evaluation – Data Sheet NO<sub>3</sub>\_VOC*. [iupac.pole-ether.fr](http://iupac.pole-ether.fr)
- Jenkin, M. E., & Hayman, G. D. (1999). Photochemical ozone creation potentials for oxygenated volatile organic compounds: Sensitivity to variations in kinetic and mechanistic parameters. *Atmospheric Environment*, 33(8), 1275–1293. [https://doi.org/10.1016/S1352-2310\(98\)00261-1](https://doi.org/10.1016/S1352-2310(98)00261-1)
- Jiang, G., Nowakowski, D. J., & Bridgwater, A. V. (2010). Effect of the temperature on the composition of lignin pyrolysis products. *Energy and Fuels*, 24(8), 4470–4475. <https://doi.org/10.1021/ef100363c>
- Jiang, J., Carter, W. P. L., Cocker, D. R., & Barsanti, K. C. (2020). Development and Evaluation of a Detailed Mechanism for Gas-Phase Atmospheric Reactions of Furans. *ACS Earth and Space Chemistry*, 4(8), 1254–1268. <https://doi.org/10.1021/acsearthspacechem.0c00058>
- Joo, T., Rivera-Rios, J. C., Takeuchi, M., Alvarado, M. J., & Ng, N. L. (2019a). Secondary Organic Aerosol Formation from Reaction of 3-Methylfuran with Nitrate Radicals. *ACS Earth and Space Chemistry*, 3(6), 922–934. <https://doi.org/10.1021/acsearthspacechem.9b00068>
- Joo, T., Rivera-Rios, J. C., Takeuchi, M., Alvarado, M. J., & Ng, N. L. (2019b). Secondary Organic Aerosol Formation from Reaction of 3-Methylfuran with Nitrate Radicals [Research-article]. *ACS Earth and Space Chemistry*, 3(6), 922–934. <https://doi.org/10.1021/acsearthspacechem.9b00068>
- Kawamoto, H. (2017). Lignin pyrolysis reactions. *Journal of Wood Science*, 63(2), 117–132. <https://doi.org/10.1007/s10086-016-1606-z>

- Keene, W. C., Maring, H., Maben, J. R., Kieber, D. J., Pszenny, A. A. P., Dahl, E. E., Izaguirre, M. A., Davis, A. J., Long, M. S., Zhou, X., Smoydzin, L., & Sander, R. (2007). Chemical and physical characteristics of nascent aerosols produced by bursting bubbles at a model air-sea interface. *Journal of Geophysical Research Atmospheres*, *112*(21), 1–16. <https://doi.org/10.1029/2007JD008464>
- Kind, I., Berndt, T., Bisge, O., & Rolle, W. (1996a). *Gas-phase rate constants for the reaction of* 2614(3), 2–6.
- Kind, I., Berndt, T., Bisge, O., & Rolle, W. (1996b). *Gas-phase rate constants for the reaction of NO<sub>3</sub> radicals with furan and methyl-substituted furans*. 2614(3), 2–6.
- Kind, I., Berndt, T., Böge, O., & Rolle, W. (1996). Gas-phase rate constants for the reaction of NO<sub>3</sub> radicals with selected oxiranes. *Chemical Physics Letters*, *249*(1–2), 35–39. [https://doi.org/10.1016/0009-2614\(95\)01327-X](https://doi.org/10.1016/0009-2614(95)01327-X)
- Koolen, C. D., & Rothenberg, G. (2019). Air Pollution in Europe. *ChemSusChem*, *12*(1), 164–172. <https://doi.org/10.1002/cssc.201802292>
- Koppmann, R. (2007). Volatile Organic Compounds in the Atmosphere. In *Volatile Organic Compounds in the Atmosphere*. <https://doi.org/10.1002/9780470988657>
- Koppmann, R., Khedim, A., Rudolph, J., Poppe, D., Andreae, M. O., Helas, G., Welling, M., & Zenker, T. (1997). Emissions of organic trace gases from savanna fires in southern Africa during the 1992 Southern African Fire Atmosphere Research Initiative and their impact on the formation of tropospheric ozone. *Journal of Geophysical Research Atmospheres*, *102*(15), 18879–18888. <https://doi.org/10.1029/97jd00845>
- Koss, A. R., Sekimoto, K., Gilman, J. B., Selimovic, V., Coggon, M. M., Zarzana, K. J., Yuan, B., Lerner, B. M., Brown, S. S., Jimenez, J. L., Krechmer, J., Roberts, J. M., Warneke, C., Yokelson, R. J., & De Gouw, J. (2018). Non-methane organic gas emissions from biomass burning: Identification, quantification, and emission factors from PTR-ToF during the FIREX 2016 laboratory experiment. *Atmospheric Chemistry and Physics*, *18*(5), 3299–3319. <https://doi.org/10.5194/acp-18-3299-2018>
- Krause, T., Tubbesing, C., Benzing, K., & Schöler, H. F. (2014). Model reactions and natural occurrence of furans from hypersaline environments. *Biogeosciences*, *11*(10), 2871–2882. <https://doi.org/10.5194/bg-11-2871-2014>
- Kumar, V., Chandra, B. P., & Sinha, V. (2018). Large unexplained suite of chemically reactive compounds present in ambient air due to biomass fires. *Scientific Reports*, *8*(1), 1–15. <https://doi.org/10.1038/s41598-017-19139-3>
- Lalchandani, V., Srivastava, D., Dave, J., Mishra, S., Tripathi, N., Shukla, A. K., Sahu, R., Thamban, N. M., Gaddamidi, S., Dixit, K., Ganguly, D., Tiwari, S., Srivastava, A. K., Sahu, L., Rastogi, N., Gargava, P., & Tripathi, S. N. (2021). Effect of biomass burning on PM 2.5 composition and secondary aerosol formation during post-monsoon and winter haze episodes in Delhi. *Journal of Geophysical Research: Atmospheres*, 1–21. <https://doi.org/10.1029/2021jd035232>
- Lambe, A. T., Chhabra, P. S., Onasch, T. B., Brune, W. H., Hunter, J. F., Kroll, J. H., Cummings, M. J., Brogan, J. F., Parmar, Y., Worsnop, D. R., Kolb, C. E., & Davidovits, P. (2015). Effect

- of oxidant concentration, exposure time, and seed particles on secondary organic aerosol chemical composition and yield. *Atmospheric Chemistry and Physics*, 15(6), 3063–3075. <https://doi.org/10.5194/acp-15-3063-2015>
- Lancar, I., Daele, V., Le Bras, G., & Poulet, G. (1991). Étude de la réactivité des radicaux NO<sub>3</sub> avec le diméthyl-2,3 butène-2, le butadiène-1,3 et le diméthyl-2,3 butadiène-1,3. *J.Chim. Phys*, 88, 1777–1792. <https://doi.org/10.1051/jcp/1991881777>
- Lançar, I., Daele, V., Le Bras, G., & Poulet, G. (1991). Étude de la réactivité des radicaux NO<sub>3</sub> avec le diméthyl-2,3 butène-2, le butadiène-1,3 et le diméthyl-2,3 butadiène-1,3. *Journal de Chimie Physique*, 88, 1777–1792. <https://doi.org/10.1051/jcp/1991881777>
- Lange, J. P., Price, R., Ayoub, P. M., Louis, J., Petrus, L., Clarke, L., & Gosselink, H. (2010). Valeric biofuels: A platform of cellulosic transportation fuels. *Angewandte Chemie - International Edition*, 49(26), 4479–4483. <https://doi.org/10.1002/anie.201000655>
- Lauraguais, A., Coeur-tourneur, C., Cassez, A., & Seydi, A. (2012). Rate constant and secondary organic aerosol yields for the gas-phase reaction of hydroxyl radicals with syringol (2,6-dimethoxyphenol). *Atmospheric Environment*, 55, 43–48. <https://doi.org/10.1016/j.atmosenv.2012.02.027>
- Lê Thành, K., Commandré, J. M., Valette, J., Volle, G., & Meyer, M. (2015). Detailed identification and quantification of the condensable species released during torrefaction of lignocellulosic biomasses. *Fuel Processing Technology*, 139, 226–235. <https://doi.org/10.1016/j.fuproc.2015.07.001>
- Lee, J. H., & Tang, I. N. (1982). Absolute rate constants for the hydroxyl radical reactions with ethane, furan, and thiophene at room temperature. *The Journal of Chemical Physics*, 77(9), 4459–4463. <https://doi.org/10.1063/1.444367>
- Liang, Y., Weber, R. J., Misztal, P. K., Jen, C. N., & Goldstein, A. H. (2022). Aging of Volatile Organic Compounds in October 2017 Northern California Wildfire Plumes. *Environmental Science and Technology*, 56(3), 1557–1567. <https://doi.org/10.1021/acs.est.1c05684>
- Liley, P. E., Buck, E., & Ch, M. S. E. (1999). 493-Physical and Chemical Data 物性数据. *Perry's Chemical Engineers Handbook*, 2–86.
- Liljegren, J. A., & Stevens, P. S. (2013). Measurements of the kinetics of the reaction of OH radicals with 3-methylfuran at low pressure. *International Journal of Chemical Kinetics*, 45(12), 787–794. <https://doi.org/10.1002/kin.20814>
- Lin, Y., Cho, J., Tompsett, G. A., Westmoreland, P. R., & Huber, G. W. (2009). Kinetics Mechanism Cellulose Pyrolysis. *Phys. Chem. C*, 113, 20097–20107.
- Lindinger, W., Hansel, A., & Jordan, A. (1998). On-line monitoring of volatile organic compounds at pptv levels by means of Proton-Transfer-Reaction Mass Spectrometry (PTR-MS) Medical applications, food control and environmental research. *International Journal of Mass Spectrometry and Ion Processes*, 173(3), 191–241. [https://doi.org/10.1016/s0168-1176\(97\)00281-4](https://doi.org/10.1016/s0168-1176(97)00281-4)
- Ljungström, E., Wängberg, I., & Langer, S. (1993). Absolute rate coefficients for the reaction between nitrate radicals and some cyclic alkenes. *Journal of the Chemical Society, Faraday Transactions*, 89(16), 2977–2982. <https://doi.org/10.1039/FT9938902977>

- Manion, J., Huie, R. E., Burgess, D. R., Orkin, V. L., Tsang, W., McGivern, W. ., Hudgens, J. W., Knyazev, V. D., Atkinson, D. B., Chai, E., Tereza, A. M., Lin, C. Y., Allison, T. C., Mallard, W. G., Westley, F., Herron, J. T., Hampson, R. F., & Frizzell, D. H. (2015). *NIST Chemical Kinetics Database, NIST Standard Reference Database 17, Version 7.0 (Web Version), Release 1.6.8, Data version 2015.09*.
- Martín, P., Cabañas, B., Colmenar, I., Salgado, M. S., Villanueva, F., & Tapia, A. (2013). Reactivity of E-butenedial with the major atmospheric oxidants. *Atmospheric Environment*, *70*, 351–360. <https://doi.org/10.1016/j.atmosenv.2013.01.041>
- Martinez, E., Cabanas, B., Aranda, A., & Martín, P. (1998). Kinetics of the reactions of NO<sub>3</sub> radical with selected monoterpenes: A temperature dependence study. *Environmental Science and Technology*, *32*(23), 3730–3734. <https://doi.org/10.1021/es970899t>
- Martínez, E., Cabañas, B., Aranda, A., Martín, P., Notario, A., & Salgado, S. (1999). Study on the NO<sub>3</sub> Radical Reactivity: Reactions with Cyclic Alkenes. *Journal of Physical Chemistry A*, *103*(27), 5321–5327. <https://doi.org/10.1021/jp9847181>
- Martinez, E., Cabañas, B., Aranda, A., Martin, P., & Salgado, S. (1999). Absolute Rate Coefficients for the Gas-Phase Reactions of NO<sub>3</sub> Radical with a Series of Monoterpenes at T = 298 to 433 K. *Journal of Atmospheric Chemistry*, *33*(3), 265–282. <https://doi.org/10.1023/A:1006178530211>
- Mathematics, A. (2016). 済無No Title No Title No Title. *19*(1), 1–23.
- Matsumoto, J. (2011). Kinetics of the reactions of ozone with 2,5-dimethylfuran and its atmospheric implications. *Chemistry Letters*, *40*(6), 582–583. <https://doi.org/10.1246/cl.2011.582>
- Mcdonald, J. D., Zielinska, B., Fujita, E. M., Sagebiel, J. C., Chow, J. C., & Watson, J. G. (2000). Fine particle and gaseous emission rates from residential wood combustion. *Environmental Science and Technology*, *34*(11), 2080–2091. <https://doi.org/10.1021/es9909632>
- Mellouki, A., & Chen, J. (2015). *Atmospheric Chemistry of Oxygenated Volatile Organic Compounds : Impacts on Air Quality and Climate*. <https://doi.org/10.1021/cr500549n>
- Meng, L., Coeur, C., Fayad, L., Houzel, N., Genevray, P., Bouzidi, H., Tomas, A., & Chen, W. (2020). Secondary organic aerosol formation from the gas-phase reaction of guaiacol (2-methoxyphenol) with NO<sub>3</sub> radicals. *Atmospheric Environment*, *240*(July). <https://doi.org/10.1016/j.atmosenv.2020.117740>
- Mettler, M. S., Mushrif, S. H., Paulsen, A. D., Javadekar, A. D., Vlachos, D. G., & Dauenhauer, P. J. (2012). Revealing pyrolysis chemistry for biofuels production: Conversion of cellulose to furans and small oxygenates. *Energy and Environmental Science*, *5*(1), 5414–5424. <https://doi.org/10.1039/c1ee02743c>
- Molina, M. J., & Molina, L. T. (2004). Megacities and atmospheric pollution. *Journal of the Air and Waste Management Association*, *54*(6), 644–680. <https://doi.org/10.1080/10473289.2004.10470936>
- Moriarty, J., Sidebottom, H., Wenger, J., Mellouki, A., & Le Bras, G. (2003). Kinetic studies on the reactions of hydroxyl radicals with cyclic ethers and aliphatic diethers. *Journal of*

- Physical Chemistry A*, 107(10), 1499–1505. <https://doi.org/10.1021/jp021267i>
- Mudhoo, A., Thayalan, G., Muthoora, N. J., Muthoora, M. N., Oozeer, B. Z., Rago, Y. P., Ramphul, M. P., Valaydon, A. K., & Kumar, S. (2013). *Dioxins and Furans: Sources, Impacts and Remediation*. [https://doi.org/10.1007/978-3-319-02387-8\\_10](https://doi.org/10.1007/978-3-319-02387-8_10)
- Müller, M., Anderson, B. E., Beyersdorf, A. J., Crawford, J. H., Diskin, G. S., Eichler, P., Fried, A., Keutsch, F. N., Mikoviny, T., Thornhill, K. L., Walega, J. G., Weinheimer, A. J., Yang, M., Yokelson, R. J., & Wisthaler, A. (2016). In situ measurements and modeling of reactive trace gases in a small biomass burning plume. *Atmospheric Chemistry and Physics*, 16(6), 3813–3824. <https://doi.org/10.5194/acp-16-3813-2016>
- Müller, M., Graus, M., Wisthaler, A., Hansel, A., Metzger, A., Dommen, J., & Baltensperger, U. (2012). Analysis of high mass resolution PTR-TOF mass spectra from 1,3,5-trimethylbenzene (TMB) environmental chamber experiments. *Atmospheric Chemistry and Physics*, 12(2), 829–843. <https://doi.org/10.5194/acp-12-829-2012>
- Munger, J. W., Jacob, D. J., Waldman, J. M., & Hoffmann, M. R. (1983). Fogwater chemistry in an urban atmosphere. *Journal of Geophysical Research*, 88(C9), 5109–5121. <https://doi.org/10.1029/JC088iC09p05109>
- Newland, M. J., Ren, Y., McGillen, M. R., Michelat, L., Daële, V., & Mellouki, A. (2022). NO<sub>3</sub> chemistry of wildfire emissions: A kinetic study of the gas-phase reactions of furans with the NO<sub>3</sub> radical. *Atmospheric Chemistry and Physics*, 22(3), 1761–1772. <https://doi.org/10.5194/acp-22-1761-2022>
- Nguyen, T. B., Coggon, M. M., Bates, K. H., Zhang, X., Schwantes, R. H., Schilling, K. A., Loza, C. L., Flagan, R. C., Wennberg, P. O., & Seinfeld, J. H. (2014). Organic aerosol formation from the reactive uptake of isoprene epoxydiols (IEPOX) onto non-acidified inorganic seeds. *Atmospheric Chemistry and Physics*, 14(7), 3497–3510. <https://doi.org/10.5194/acp-14-3497-2014>
- Odum, J. R., Hoffmann, T., Bowman, F., Collins, D., Flagan, R. C., & Seinfeld, J. H. (1996). Gas/particle partitioning and secondary organic aerosol yields. *Environmental Science and Technology*, 30(8), 2580–2585. <https://doi.org/10.1021/es950943+>
- Oh, H. J., Ma, Y., & Kim, J. (2020). Human inhalation exposure to aerosol and health effect: Aerosol monitoring and modelling regional deposited doses. *International Journal of Environmental Research and Public Health*, 17(6), 1–2. <https://doi.org/10.3390/ijerph17061923>
- Olariu, R. I., Bejan, I., Barnes, I., Klotz, B., Becker, K. H., & Wirtz, K. (2004). Rate coefficients for the gas-phase reaction of NO<sub>3</sub> radicals with selected dihydroxybenzenes. *International Journal of Chemical Kinetics*, 36(11), 577–583. <https://doi.org/10.1002/kin.20029>
- Olariu, R. I., Cuza, A. I., Chemistry, A., Tomas, A., Douai, M. De, Chimie, D., Barnes, I., Bejan, I., Becker, K. H., Wuppertal, B. U., Wirtz, K., Centro, F., & Ambientales, D. E. (1998). *Atmospheric Ozone Degradation Reaction of 1, 2-dihydroxybenzene : Aerosol Formation Study*. 1–12.
- Osseiran, N., Romanias, M. N., Gaudion, V., Angelaki, M. E., Papadimitriou, V. C., Tomas, A., Coddeville, P., & Thevenet, F. (2020). Development and validation of a thermally

- regulated atmospheric simulation chamber (THALAMOS): A versatile tool to simulate atmospheric processes. *Journal of Environmental Sciences (China)*, 95(xxxx), 141–154. <https://doi.org/10.1016/j.jes.2020.03.036>
- Pankow, J. F. (1994). An absorption model of the gas/aerosol partitioning involved in the formation of secondary organic aerosol. *Atmospheric Environment*, 28(SUPPL.), 189–193. <https://doi.org/10.1016/j.atmosenv.2007.10.060>
- Papadimitriou, V. C., Lazarou, Y. G., Talukdar, R. K., & Burkholder, J. B. (2011). *Atmospheric Chemistry of CF 3 CF 2*. 2(3), 167–181.
- Paquet, M., Arlt, D., Knape, J., Low, M., Forslund, P., & Pärt, T. (2019). Quantifying the links between land use and population growth rate in a declining farmland bird. *Ecology and Evolution*, 9(2), 868–879. <https://doi.org/10.1002/ece3.4766>
- Qian, Y., Zhu, L., Wang, Y., & Lu, X. (2015). Recent progress in the development of biofuel 2,5-dimethylfuran. *Renewable and Sustainable Energy Reviews*, 41, 633–646. <https://doi.org/10.1016/j.rser.2014.08.085>
- Ravishankara, A. R., & Davis, D. D. (1978). Kinetic rate constants for the reaction of OH with methanol, ethanol, and tetrahydrofuran at 298 K [2]. *Journal of Physical Chemistry*, 82(26), 2852–2853. <https://doi.org/10.1021/j100515a022>
- Reddington, C. L., Spracklen, D. V., Artaxo, P., Ridley, D. A., Rizzo, L. V., & Arana, A. (2016). Analysis of particulate emissions from tropical biomass burning using a global aerosol model and long-term surface observations. *Atmospheric Chemistry and Physics*, 16(17), 11083–11106. <https://doi.org/10.5194/acp-16-11083-2016>
- Ren, X., Brune, W. H., Oligier, A., Metcalf, A. R., Simpas, J. B., Shirley, T., Schwab, J. J., Bai, C., Roychowdhury, U., Li, Y., Cai, C., Demerjian, K. L., He, Y., Zhou, X., Gao, H., & Hou, J. (2006). *OH, HO 2, and OH reactivity during the PMTACS – NY Whiteface Mountain 2002 campaign: Observations and model comparison*. 111, 1–12. <https://doi.org/10.1029/2005JD006126>
- Ren, X., Gao, H., Zhou, X., Crouse, J. D., Wennberg, P. O., Browne, E. C., LaFranchi, B. W., Cohen, R. C., McKay, M., Goldstein, A. H., & Mao, J. (2010). Measurement of atmospheric nitrous acid at Bodgett forest during BEARPEX2007. *Atmospheric Chemistry and Physics*, 10(13), 6283–6294. <https://doi.org/10.5194/acp-10-6283-2010>
- Ren, X., Harder, H., Martinez, M., Leshner, R. L., Oligier, A., Simpas, J. B., Brune, W. H., Schwab, J. J., Demerjian, K. L., He, Y., Zhou, X., & Gao, H. (2003). OH and HO<sub>2</sub> chemistry in the urban atmosphere of New York City. *Atmospheric Environment*, 37(26), 3639–3651. [https://doi.org/10.1016/S1352-2310\(03\)00459-X](https://doi.org/10.1016/S1352-2310(03)00459-X)
- Rissanen, M. (2021). Anthropogenic Volatile Organic Compound (AVOC) Autoxidation as a Source of Highly Oxygenated Organic Molecules (HOM). *Journal of Physical Chemistry A*, 125(41), 9027–9039. <https://doi.org/10.1021/acs.jpca.1c06465>
- Roberts, J. M., Stockwell, C. E., Yokelson, R. J., De Gouw, J., Liu, Y., Selimovic, V., Koss, A. R., Sekimoto, K., Coggon, M. M., Yuan, B., Zarzana, K. J., Brown, S. S., Santin, C., Doerr, S. H., & Warneke, C. (2020). The nitrogen budget of laboratory-simulated western US wildfires during the FIREX 2016 Fire Lab study. *Atmospheric Chemistry and Physics*, 20(14), 8807–

8826. <https://doi.org/10.5194/acp-20-8807-2020>

- Román-Leshkov, Y., Barrett, C. J., Liu, Z. Y., & Dumesic, J. A. (2007). Production of dimethylfuran for liquid fuels from biomass-derived carbohydrates. *Nature*, *447*(7147), 982–985. <https://doi.org/10.1038/nature05923>
- Romanias, M. N., Coggon, M., Al Ali, F., Burkholder, J. B., Dagaut, P., Warneke, C., Stockwell, C. E., Decker, Z., Tomas, A., Houzel, N., Coeur, C., & Brown, S. (n.d.-a). Atmospheric chemistry of furanoids: insights into the sources and atmospheric fate. *Atmospheric Environment*.
- Romanias, M. N., Coggon, M. M., Al Ali, F., Burkholder, J. B., Dagaut, P., Warneke, C., Stockwell, C. E., Decker, Z. C. J., Tomas, A., Houzel, N., Coeur, C., & Brown, S. S. (n.d.-b). Atmospheric chemistry of furanoids: insights into the sources and atmospheric fate. *ASC ACS Earth and Space Chemistry*.
- Schellenberg, C. (2009). Conducta irascible y recalcitrante tras una infección de gripe: Efectos de una acupuntura dispersante en el H 3 en lactantes y niños pequeños. *Revista Internacional de Acupuntura*, *3*(2), 78–79. [https://doi.org/10.1016/S1887-8369\(09\)71579-0](https://doi.org/10.1016/S1887-8369(09)71579-0)
- Schumann, U. (2012). Atmospheric Physics. In *Physics Today* (Vol. 15, Issue 5). <https://doi.org/10.1063/1.3058219>
- Seinfeld, J. H., Pandis, S. N., & Noone, K. (1998). Atmospheric Chemistry and Physics: From Air Pollution to Climate Change . In *Physics Today* (Vol. 51, Issue 10). <https://doi.org/10.1063/1.882420>
- Sekimoto, K., Koss, A. R., Gilman, J. B., Selimovic, V., Coggon, M. M., Zarzana, K. J., Yuan, B., Lerner, B. M., Brown, S. S., Warneke, C., Yokelson, R. J., Roberts, J. M., & De Gouw, J. (2018). High-and low-temperature pyrolysis profiles describe volatile organic compound emissions from western US wildfire fuels. *Atmospheric Chemistry and Physics*, *18*(13), 9263–9281. <https://doi.org/10.5194/acp-18-9263-2018>
- Selimovic, V., Yokelson, R. J., Warneke, C., Roberts, J. M., De Gouw, J., Reardon, J., & Griffith, D. W. T. (2018). Aerosol optical properties and trace gas emissions by PAX and OP-FTIR for laboratory-simulated western US wildfires during FIREX. *Atmospheric Chemistry and Physics*, *18*(4), 2929–2948. <https://doi.org/10.5194/acp-18-2929-2018>
- Si, Z., Wang, C. G., Bi, K., Zhang, X. H., Yu, C. L., Dong, R. J., Ma, L. L., & Changle, P. (2017). Py-GC/MS study of lignin pyrolysis and effect of catalysts on product distribution. *International Journal of Agricultural and Biological Engineering*, *10*(5), 214–225. <https://doi.org/10.25165/j.ijabe.20171005.2852>
- Simoneit, B. R. T. (2002). Biomass burning - A review of organic tracers for smoke from incomplete combustion. In *Applied Geochemistry* (Vol. 17, Issue 3). [https://doi.org/10.1016/S0883-2927\(01\)00061-0](https://doi.org/10.1016/S0883-2927(01)00061-0)
- Smith, D., & Španěl, P. (2005). Selected ion flow tube mass spectrometry (SIFT-MS) for on-line trace gas analysis. *Mass Spectrometry Reviews*, *24*(5), 661–700. <https://doi.org/10.1002/mas.20033>
- Song, C., NA, K., & Cocker, D. R. (2005). Impact of the Hydrocarbon to NO. *Environmental*



*Science & Technology*, 39(9), 3143–3149.

- Španěl, P., Dryahina, K., & Smith, D. (2013). A quantitative study of the influence of inhaled compounds on their concentrations in exhaled breath. *Journal of Breath Research*, 7(1). <https://doi.org/10.1088/1752-7155/7/1/017106>
- Stehfest, E., van Zeist, W. J., Valin, H., Havlik, P., Popp, A., Kyle, P., Tabeau, A., Mason-D’Croz, D., Hasegawa, T., Bodirsky, B. L., Calvin, K., Doelman, J. C., Fujimori, S., Humpenöder, F., Lotze-Campen, H., van Meijl, H., & Wiebe, K. (2019). Key determinants of global land-use projections. *Nature Communications*, 10(1), 1–10. <https://doi.org/10.1038/s41467-019-09945-w>
- Stockman, R. A. (2007). Heterocyclic chemistry. In *Annual Reports on the Progress of Chemistry - Section B* (Vol. 103). <https://doi.org/10.1039/b614418g>
- Stockwell, C. E., Christian, T. J., Goetz, J. D., Jayarathne, T., Bhawe, P. V., Praveen, P. S., Adhikari, S., Maharjan, R., DeCarlo, P. F., Stone, E. A., Saikawa, E., Blake, D. R., Simpson, I. J., Yokelson, R. J., & Panday, A. K. (2016). Nepal Ambient Monitoring and Source Testing Experiment (NAMaSTE): Emissions of trace gases and light-absorbing carbon from wood and dung cooking fires, garbage and crop residue burning, brick kilns, and other sources. *Atmospheric Chemistry and Physics*, 16(17), 11043–11081. <https://doi.org/10.5194/acp-16-11043-2016>
- Stockwell, C. E., Veres, P. R., Williams, J., & Yokelson, R. J. (2015). Characterization of biomass burning emissions from cooking fires, peat, crop residue, and other fuels with high-resolution proton-transfer-reaction time-of-flight mass spectrometry. *Atmospheric Chemistry and Physics*, 15(2), 845–865. <https://doi.org/10.5194/acp-15-845-2015>
- Strollo, C. M., & Ziemann, P. J. (2013). Products and mechanism of secondary organic aerosol formation from the reaction of 3-methylfuran with OH radicals in the presence of NOx. *Atmospheric Environment*, 77, 534–543. <https://doi.org/10.1016/j.atmosenv.2013.05.033>
- Tajuelo, M., Rodríguez, A., Baeza-Romero, M. T., Aranda, A., Díaz-de-Mera, Y., & Rodríguez, D. (2019). Secondary organic aerosol formation from  $\alpha$ -methylstyrene atmospheric degradation: Role of NOx level, relative humidity and inorganic seed aerosol. *Atmospheric Research*, 230(July), 104631. <https://doi.org/10.1016/j.atmosres.2019.104631>
- Tajuelo, M., Rodríguez, D., Baeza-Romero, M. T., Díaz-de-Mera, Y., Aranda, A., & Rodríguez, A. (2019). Secondary organic aerosol formation from styrene photolysis and photooxidation with hydroxyl radicals. *Chemosphere*, 231, 276–286. <https://doi.org/10.1016/j.chemosphere.2019.05.136>
- Tajuelo, M., Rodríguez, D., Rodríguez, A., Escalona, A., Viteri, G., Aranda, A., & Diaz-de-Mera, Y. (2021). Secondary organic aerosol formation from the ozonolysis and oh-photooxidation of 2,5-dimethylfuran. *Atmospheric Environment*, 245, 118041. <https://doi.org/10.1016/j.atmosenv.2020.118041>
- Takekawa, H., Minoura, H., & Yamazaki, S. (2003). Temperature dependence of secondary organic aerosol formation by photo-oxidation of hydrocarbons. 37, 3413–3424. [https://doi.org/10.1016/S1352-2310\(03\)00359-5](https://doi.org/10.1016/S1352-2310(03)00359-5)

- Tapia, A., Villanueva, F., Salgado, M. S., Cabañas, B., Martínez, E., & Martín, P. (2011). Atmospheric degradation of 3-methylfuran: Kinetic and products study. *Atmospheric Chemistry and Physics*, *11*(7), 3227–3241. <https://doi.org/10.5194/acp-11-3227-2011>
- Thewes, M., Muether, M., Pischinger, S., Budde, M., Brunn, A., Sehr, A., Adomeit, P., & Klankermayer, J. (2011). Analysis of the impact of 2-methylfuran on mixture formation and combustion in a direct-injection spark-ignition engine. *Energy and Fuels*, *25*(12), 5549–5561. <https://doi.org/10.1021/ef201021a>
- Tomas, A., Henry, F., & Visez, N. (2009). Aerosol formation yields from the reaction of catechol with ozone. *43*, 2360–2365. <https://doi.org/10.1016/j.atmosenv.2008.12.054>
- Tuan Hoang, A., & Viet Pham, V. (2021). 2-Methylfuran (MF) as a potential biofuel: A thorough review on the production pathway from biomass, combustion progress, and application in engines. *Renewable and Sustainable Energy Reviews*, *148*(June), 111265. <https://doi.org/10.1016/j.rser.2021.111265>
- Tuazon, E. C., Aschmann, S. M., & Atkinson, R. (2000). Atmospheric degradation of volatile methyl-silicon compounds. *Environmental Science and Technology*, *34*(10), 1970–1976. <https://doi.org/10.1021/es9910053>
- Vallero, D. (2008). *Fundamentals of Air Pollution* (Fourth). El Sevier.
- Villanueva, F., Barnes, I., Monedero, E., Salgado, S., Gómez, M. V., & Martin, P. (2007). Primary product distribution from the Cl-atom initiated atmospheric degradation of furan: Environmental implications. *Atmospheric Environment*, *41*(38), 8796–8810. <https://doi.org/10.1016/j.atmosenv.2007.07.053>
- Villanueva, F., Cabañas, B., Monedero, E., Salgado, S., Bejan, I., & Martin, P. (2009). Atmospheric degradation of alkylfurans with chlorine atoms: Product and mechanistic study. *Atmospheric Environment*, *43*(17), 2804–2813. <https://doi.org/10.1016/j.atmosenv.2009.02.030>
- Wallington, T. J., Dagaut, P., Liu, R., & Kurylo, M. J. (1988). The gas phase reactions of hydroxyl radicals with a series of esters over the temperature range 240–440 K. *International Journal of Chemical Kinetics*, *20*(2), 177–186. <https://doi.org/10.1002/kin.550200210>
- Wang, J., Doussin, J. F., Perrier, S., Perraudin, E., Katrib, Y., Pangu, E., & Picquet-Varrault, B. (2011). Design of a new multi-phase experimental simulation chamber for atmospheric photochemistry, aerosol and cloud chemistry research. *Atmospheric Measurement Techniques*, *4*(11), 2465–2494. <https://doi.org/10.5194/amt-4-2465-2011>
- Wang, L., Slowik, J. G., Tripathi, N., Bhattu, D., Rai, P., Kumar, V., Vats, P., Satish, R., Baltensperger, U., Ganguly, D., Rastogi, N., Sahu, L. K., Tripathi, S. N., & Prévôt, A. S. H. (2020). Source characterization of volatile organic compounds measured by proton-transfer-reaction time-of-flight mass spectrometers in Delhi, India. *Atmospheric Chemistry and Physics*, *20*(16), 9753–9770. <https://doi.org/10.5194/acp-20-9753-2020>
- Wang, Q., Song, H., Pan, S., Dong, N., Wang, X., & Sun, S. (2020). Initial pyrolysis mechanism and product formation of cellulose: An Experimental and Density functional theory(DFT) study. *Scientific Reports*, *10*(1), 1–18. <https://doi.org/10.1038/s41598-020-60095-2>
- Wang, S., Wei, W., Du, L., Li, G., & Hao, J. (2009). Characteristics of gaseous pollutants from

- biofuel-stoves in rural China. *Atmospheric Environment*, 43(27), 4148–4154. <https://doi.org/10.1016/j.atmosenv.2009.05.040>
- Whelan, C. A., Eble, J., Mir, Z. S., Blitz, M. A., Seakins, P. W., Olzmann, M., & Stone, D. (2020). Kinetics of the Reactions of Hydroxyl Radicals with Furan and Its Alkylated Derivatives 2-Methyl Furan and 2,5-Dimethyl Furan. *Journal of Physical Chemistry A*, 124(37), 7416–7426. <https://doi.org/10.1021/acs.jpca.0c06321>
- Wine, P. H., & Thompson, R. J. (1984). Kinetics of OH reactions with furan, thiophene, and tetrahydrothiophene. *International Journal of Chemical Kinetics*, 16(7), 867–878. <https://doi.org/10.1002/kin.550160707>
- Winer, M., Darnall, K. R., & Lloyd, A. C. (1977). *REACTION set-BUTYL*. 5(2), 221–226.
- Wingenter, O. W., Blake, D. R., Blake, N. J., Sive, B. C., Rowland, F. S., Atlas, E., & Flocke, F. (1999). Tropospheric hydroxyl and atomic chlorine concentrations, and mixing timescales determined from hydrocarbon and halocarbon measurements made over the Southern Ocean. *Journal of Geophysical Research Atmospheres*, 104(D17), 21819–21828. <https://doi.org/10.1029/1999JD900203>
- Wingenter, O. W., Kubo, M. K., Blake, N. J., Smith, T. W., Blake, D. R., & Rowland, F. S. (1996). Hydrocarbon and halocarbon measurements as photochemical and dynamical indicators of atmospheric hydroxyl, atomic chlorine, and vertical mixing obtained during Lagrangian flights. *Journal of Geophysical Research Atmospheres*, 101(D2), 4331–4340. <https://doi.org/10.1029/95JD02457>
- World Health Organization. (2016). WORLD HEALTH STATISTICS - MONITORING HEALTH FOR THE SDGs. *World Health Organization*, 1.121. <https://doi.org/10.1017/CBO9781107415324.004>
- Xu, L., Guo, H., Weber, R. J., & Ng, N. L. (2017). Chemical Characterization of Water-Soluble Organic Aerosol in Contrasting Rural and Urban Environments in the Southeastern United States. *Environmental Science and Technology*, 51(1), 78–88. <https://doi.org/10.1021/acs.est.6b05002>
- Yang, H., Li, S., Liu, B., Chen, Y., Xiao, J., Dong, Z., Gong, M., & Chen, H. (2020). Hemicellulose pyrolysis mechanism based on functional group evolutions by two-dimensional perturbation correlation infrared spectroscopy. *Fuel*, 267(July 2019), 117302. <https://doi.org/10.1016/j.fuel.2020.117302>
- Yang, X., Zhao, Y., Li, W., Li, R., & Wu, Y. (2019). Unveiling the Pyrolysis Mechanisms of Hemicellulose: Experimental and Theoretical Studies. *Energy and Fuels*, 33(5), 4352–4360. <https://doi.org/10.1021/acs.energyfuels.9b00482>
- Yokelson, R. J., Burling, I. R., Gilman, J. B., Warneke, C., Stockwell, C. E., De Gouw, J., Akagi, S. K., Urbanski, S. P., Veres, P., Roberts, J. M., Kuster, W. C., Reardon, J., Griffith, D. W. T., Johnson, T. J., Hosseini, S., Miller, J. W., Cocker, D. R., Jung, H., & Weise, D. R. (2013). Coupling field and laboratory measurements to estimate the emission factors of identified and unidentified trace gases for prescribed fires. *Atmospheric Chemistry and Physics*, 13(1), 89–116. <https://doi.org/10.5194/acp-13-89-2013>
- Yokelson, R. J., Burling, I. R., Urbanski, S. P., Atlas, E. L., Adachi, K., Buseck, P. R., Wiedinmyer,

- C., Akagi, S. K., Toohey, D. W., & Wold, C. E. (2011). Trace gas and particle emissions from open biomass burning in Mexico. *Atmospheric Chemistry and Physics*, *11*(14), 6787–6808. <https://doi.org/10.5194/acp-11-6787-2011>
- Yokelson, R. J., Saharjo, B. H., Stockwell, C. E., Putra, E. I., Jayarathne, T., Akbar, A., Albar, I., Blake, D. R., Graham, L. L. B., Kurniawan, A., Meinardi, S., Ningrum, D., Nurhayati, A. D., Saad, A., Sakuntaladewi, N., Setianto, E., Simpson, I. J., Stone, E. A., Sutikno, S., ... Cochrane, M. A. (2022). Tropical peat fire emissions: 2019 field measurements in Sumatra and Borneo and synthesis with previous studies. *Atmospheric Chemistry and Physics*, *22*(15), 10173–10194. <https://doi.org/10.5194/acp-22-10173-2022>
- Yokelson, R. J., Susott, R., Ward, D. E., Reardon, J., & Griffith, D. W. T. (1997). Emissions from smoldering combustion of biomass measured by open-path Fourier transform infrared spectroscopy. *Journal of Geophysical Research Atmospheres*, *102*(15), 18865–18877. <https://doi.org/10.1029/97jd00852>
- Young, C. J., Washenfelder, R. A., Edwards, P. M., Parrish, D. D., Gilman, J. B., Kuster, W. C., Mielke, L. H., Osthoff, H. D., Tsai, C., Pikelnaya, O., Stutz, J., Veres, P. R., Roberts, J. M., Griffith, S., Dusanter, S., Stevens, P. S., Flynn, J., Grossberg, N., Lefer, B., ... Brown, S. S. (2014). Chlorine as a primary radical: Evaluation of methods to understand its role in initiation of oxidative cycles. *Atmospheric Chemistry and Physics*, *14*(7), 3427–3440. <https://doi.org/10.5194/acp-14-3427-2014>
- Yuan, Y., Zhao, X., Wang, S., & Wang, L. (2017). Atmospheric Oxidation of Furan and Methyl-Substituted Furans Initiated by Hydroxyl Radicals. *Journal of Physical Chemistry A*, *121*(48), 9306–9319. <https://doi.org/10.1021/acs.jpca.7b09741>
- Zhao, D., Schmitt, S. H., Wang, M., Acir, I. H., Tillmann, R., Tan, Z., Novelli, A., Fuchs, H., Pullinen, I., Wegener, R., Rohrer, F., Wildt, J., Kiendler-Scharr, A., Wahner, A., & Mentel, T. F. (2018). Effects of NO<sub>x</sub> and SO<sub>2</sub> on the secondary organic aerosol formation from photooxidation of  $\alpha$ -pinene and limonene. *Atmospheric Chemistry and Physics*, *18*(3), 1611–1628. <https://doi.org/10.5194/acp-18-1611-2018>
- Zhao, X., & Wang, L. (2017). Atmospheric Oxidation Mechanism of Furfural Initiated by Hydroxyl Radicals. *Journal of Physical Chemistry A*, *121*(17), 3247–3253. <https://doi.org/10.1021/acs.jpca.7b00506>
- Zhou, X., Beine, H. J., Honrath, R. E., Fuentes, J. D., Simpson, W., & Bottenheim, J. W. (2001). Snowpack Photochemical Production of HONO: a Major Source of OH in the Arctic Boundary Layer in Springtime. *Geophysical Research Letters*, *28*, 4087–4090. <https://doi.org/10.1029/2001GL013531>
- Zhou, X., Li, W., Mabon, R., & Broadbelt, L. J. (2018). A mechanistic model of fast pyrolysis of hemicellulose. *Energy and Environmental Science*, *11*(5), 1240–1260. <https://doi.org/10.1039/c7ee03208k>
- Ziemann, P. J., & Atkinson, R. (2012). Kinetics, products, and mechanisms of secondary organic aerosol formation. *Chemical Society Reviews*, *41*(19), 6582–6605. <https://doi.org/10.1039/c2cs35122f>
- Zogka, A. G., Romanias, M. N., & Thevenet, F. (2022). Formaldehyde and glyoxal measurement deploying a selected ion flow tube mass spectrometer (SIFT-MS). *Atmospheric*

*Measurement Techniques*, 15(7), 2001–2019. <https://doi.org/10.5194/amt-15-2001-2022>

Zysman, B., & Skelly, P. D. (1992). *T*: 1992.

**Chapter IV Product  
Characterization: Combining  
Qualitative and Quantitative  
Approaches with Mechanism  
Proposal**

## IV.1 Introduction

This chapter encompasses three main objectives:

- Firstly, it aims to thoroughly examine the NO<sub>3</sub> oxidation products of furan and methylated-furan compounds (2-MF, 3-MF, 2,5-DMF and 2,3,5-TMF) at room temperature, both qualitatively and quantitatively.

- Secondly, based on the products identified in each reaction, this chapter aims to propose reaction pathways for their formation, along with secondary mechanisms for the resultant secondary products. There is a limited number of literature studies investigating the mechanism of NO<sub>3</sub> reaction with furanoids (Tapia et al., 2011; Berndt et al., 1997; Colmenar et al., 2020; Joo et al., 2019). In addition to room temperature product analysis, the variation of the major product yields of the reactions of 2-MF and 2,5-DMF with NO<sub>3</sub> at temperature between 298 and 353 K was investigated. Studying the temperature dependence of product yields helps in understanding the complex chemistry involved and provides insights into the reaction mechanisms. As mentioned in the previous chapters, furanoids are mainly emitted from BB where temperature can highly exceed ambient temperature and as a result understanding the temperature impact on product yields, will help better understand their nighttime chemistry in fire plumes.

- Thirdly, this chapter seeks to determine the yields of secondary organic aerosol (SOA) for three specific furan molecules (2-MF, 2,5-DMF and 2,3,5-TMF), through their respective reactions. Understanding the SOA yields resulting from these reactions contributes to our knowledge of secondary aerosol formation and its impact on air quality and climate.

Finally, by having these results, researchers can refine existing atmospheric models and improve predictions of atmospheric composition and reactivity.

## IV.2 Gas phase products of the reaction of furanoids with NO<sub>3</sub>

The identification and quantification of the products formed from the reaction of the studied furanoids with NO<sub>3</sub> was investigated in the chambers CHARME and THALAMOS using several online and offline analytical techniques as already described in chapter 2. In this section, the results illustrating the gas-phase and particulate phase products of the reaction of furanoids with NO<sub>3</sub> are presented in detail.

### IV.2.1 Furan reaction with NO<sub>3</sub>

The reaction of furan has been previously studied in the literature, and the investigation of its oxidation products in this study was primarily focused on qualitative analyses. The aim was to cross-validate the reaction mechanism proposed in the existing literature demonstrating the formation of the primary major products.

#### *IV.2.1.1 Qualitative identification of the products (TD-GC-EI-MS + SIFT-MS analyses)*

During and after the reaction of furan with NO<sub>3</sub> in CHARME, TD-GC-EI-MS analyses were performed to identify the furan gas-phase oxidation products. A typical chromatogram obtained during the reaction is presented in Figure IV.1, where the peaks are labelled with the corresponding structures and names of the identified compounds. Referring to the NIST library

of the mass spectra and analyzing the mass spectra corresponding to each peak, the reactant (furan) and three degradation products, but-2-ene-1,4-dione, 2(3H)-furanone and maleic anhydride (MAH), are clearly identified.

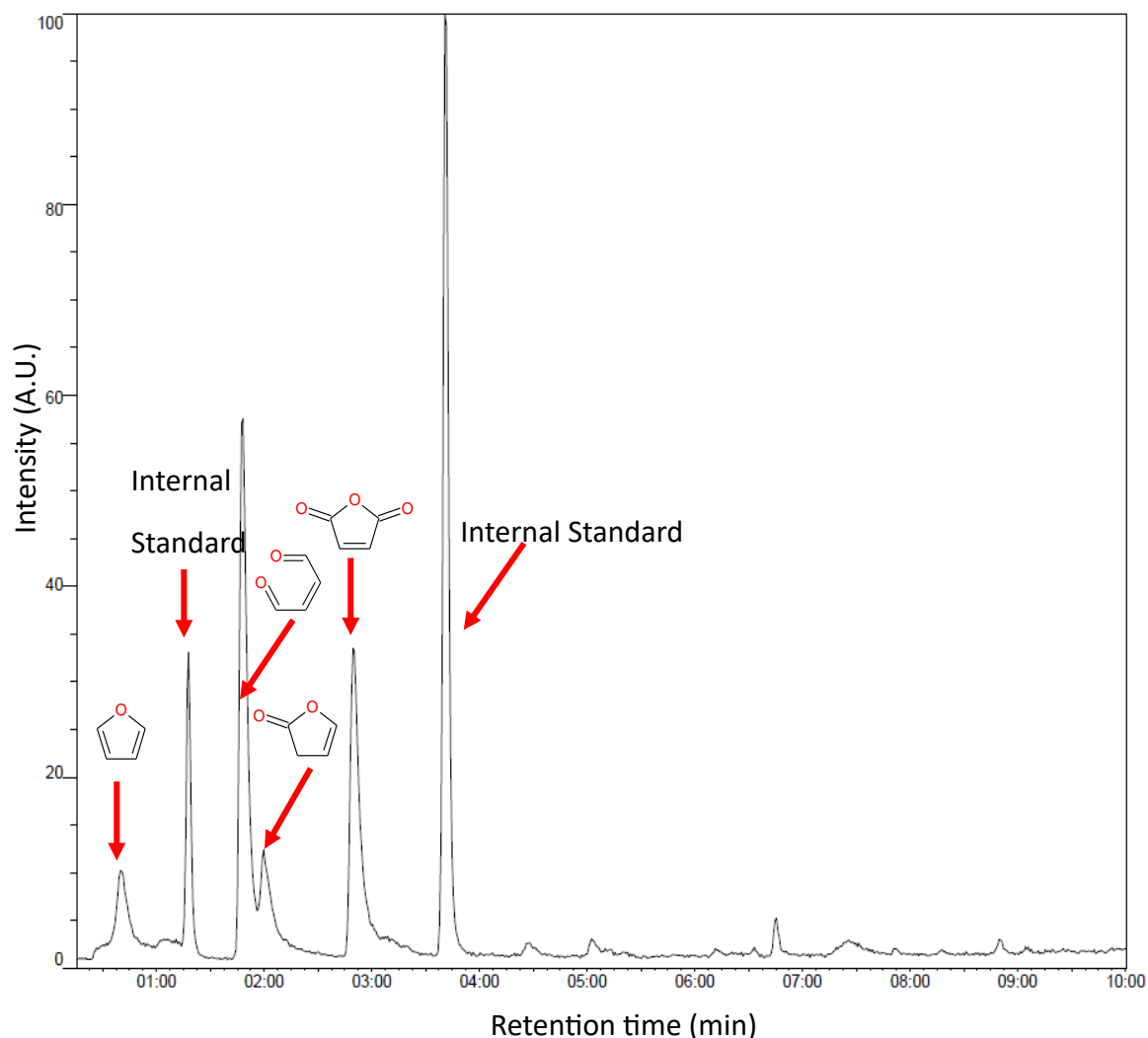


Figure IV.1: Chromatogram (TD-GC-EI-MS) of the gas-phase oxidation products formed during the reaction of furan with  $\text{NO}_3$  radicals. The peaks are labelled with their chemical structures.

In THALAMOS, the products of furan reaction with  $\text{NO}_3$  radicals were studied with SIFT-MS. The products and their corresponding masses obtained upon ionization with the three precursor ions ( $\text{H}_3\text{O}^+$ ,  $\text{NO}^+$  and  $\text{O}_2^+$ ) are presented in Table IV.1. In this series of experiments, SIFT-MS was operated in mass scan mode. The three mass scans obtained are presented in Figure IV.2. In the case of  $\text{H}_3\text{O}^+$  the two major products, 3H-furan-2-one and 2-butenedial, have the same mass and thus in the SIFT-MS, they were detected at the mass peak  $m/z = 85$  (parent peak +  $\text{H}^+$ ). On the contrary, using  $\text{NO}^+$  and  $\text{O}_2^+$  as precursor ions, 3H-furan-2-one was detected at  $m/z = 84$  (parent peak) and 2-butenedial at  $m/z = 83$  (loss of  $\text{H}^+$ ). Note that this interpretation was based on the SIFT-MS library and the fragmentation of aldehydes of similar structure. However, this does not preclude that mass 83 with  $\text{NO}^+$  and  $\text{O}_2^+$  is only attributed to 2-



butenedial. In particular, 4-oxo-2-butenoic acid  $m/z = 100$  (parent mass) can be a secondary product of the reaction. This compound can be detected at the mass peak  $m/z = 101$  with  $H_3O^+$  (parent +  $H^+$ ) and  $m/z = 83$  (OH elimination from the main structure). The same compound is observed at  $m/z = 130$  (parent +  $NO^+$ ),  $m/z = 99$  (elimination of H atom), and  $m/z = 83$  (OH elimination from the main structure). With  $O_2^+$  4-oxo-2-butenoic acid is observed at mass peak 99 (elimination of H atom) and  $m/z = 83$  (OH elimination from the main structure). Our interpretation was based on the analysis of the fragmentation of aldehydes and carboxylic acids in SIFT-MS. To wrap up, mass peak 83 with  $NO^+$  and  $O_2^+$  is attributed to two compounds 2-butenedial and 4-oxo-2-butenoic acid. Maleic anhydride (MAH) was also a product of the reaction. The standard of this compound was injected in the chamber and it was observed at the mass peaks  $m/z = 99$ ,  $m/z = 128$ ,  $m/z = 99$  with  $H_3O^+$ ,  $NO^+$ , and  $O_2^+$ , respectively, with relative ratios:  $\frac{I_{99}^{H_3O^+}}{I_{128}^{NO^+}}=0.15$ ,  $\frac{I_{99}^{H_3O^+}}{I_{99}^{O_2^+}}=10$ . Therefore, the mass peak 99 observed in the  $H_3O^+$  spectrum of the products (Figure IV.2) is attributed mainly to MAH. Around 10% of the counts measured at the mass peak 99 of  $O_2^+$  of the product spectrum could be also attributed to MAH. However, note that due to its sticky nature, the calibration of the SIFT-MS was challenging and for that reason maleic anhydride yield was not determined. 2(5H)-furanone-5-nitrooxy ( $m/z = 145$ ) can be attributed to masses 146 and 175 obtained with  $H_3O^+$  and  $NO^+$  respectively ( $m/z$  obtained with  $NO^+$  includes the mass of the product +  $NO^+$  mass). Nitric acid ( $HNO_3$ ,  $m/z = 63$ ) was also detected with  $H_3O^+$  at mass peak 64. Nitric acid can be a product of the title reaction, but also, predominantly, due to heterogeneous reactions of  $NO_y$  and  $NO_x$  species with chamber walls. The results obtained within the two chambers are in agreement between each other and with that in literature (Berndt et al., 1997). However, the results obtained with the SIFT-MS in THALAMOS provide further information on the formation of additionally identified products especially organic nitrates.

Table IV.1: Masses of the products of the reaction of furan with  $NO_3$  detected with the SIFT-MS, including the ions obtained upon ionization with  $H_3O^+$ ,  $NO^+$  and  $O_2^+$ .

Product	m/z detected by SIFT-MS		
	$H_3O^+$	$NO^+$	$O_2^+$
2-Butenedial	85	83	83
3H-furan-2-one	85	84	84
4-oxo-2-butenoic acid	83, 101	83, 99, 130	83, 99
Maleic anhydride	99	128	99
2(5H)-furanone-5-nitrooxy	146	175	
Nitric acid	64		

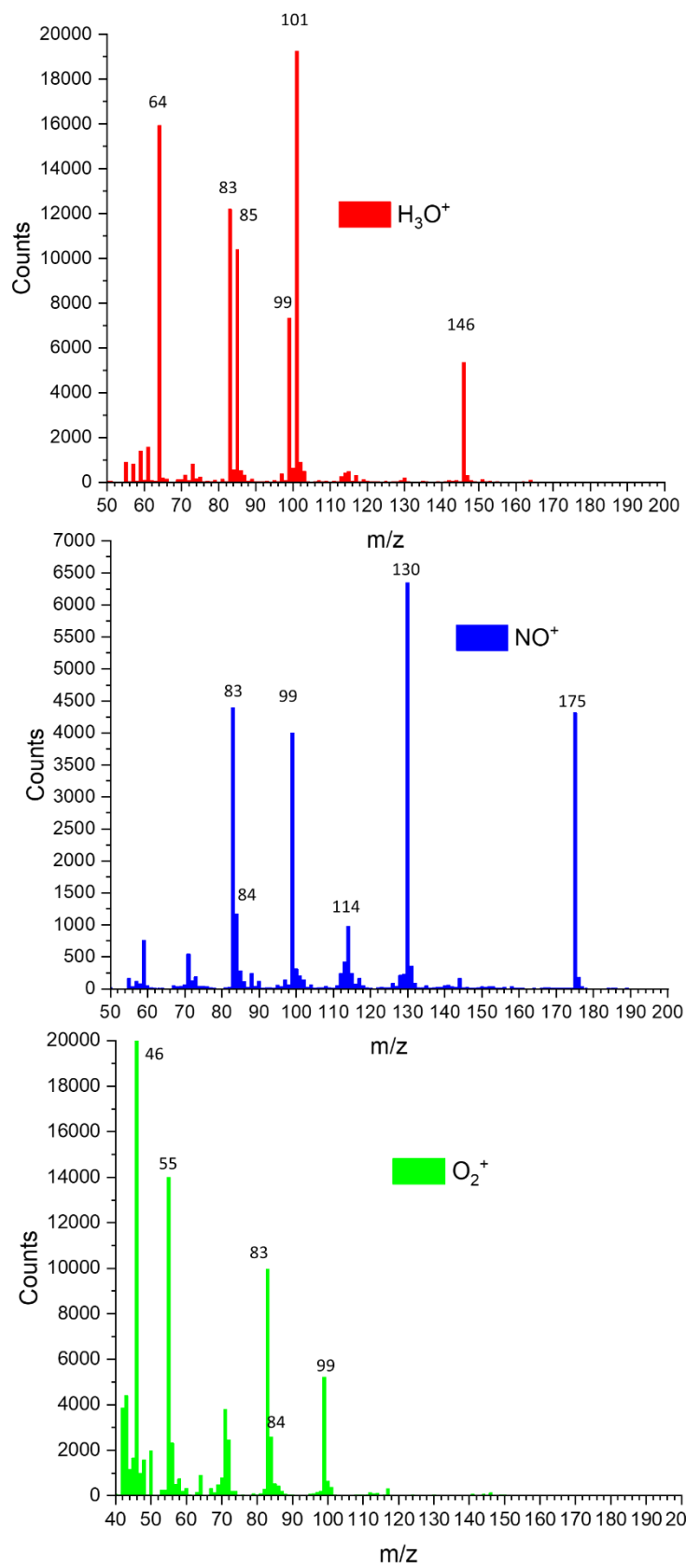


Figure IV.2: Mass scans of the products of Furan/ $NO_3$  obtained with the SIFT-MS using three precursor ions ( $H_3O^+$ ,  $NO^+$ ,  $O_2^+$ ) in THALAMOS. Identified peaks are labelled with their corresponding m/z values.

#### IV.2.1.2 Mechanism in literature and proposition of the major pathways

A similar reaction mechanism to that proposed by Berndt et al., (1997) is presented in Figure IV.3. The main reaction of  $\text{NO}_3$  radicals occurs by addition to carbon C-2/C-5 of the ring, as anticipated based on information from previous studies (Stockman, 2007). The structure of the observed products confirms this finding. The resulting adduct forms a resonance-stabilized radical. Either  $\text{NO}_2$  elimination and intramolecular 1,2 H-transfer occurs leading to the formation of 3H-furan-2-one (**1**), or  $\text{NO}_2$  elimination and rearrangement occur forming 2-butenedial (**2**) (Berndt et al., 1997). Another product that can be formed and was not proposed in the previous literature study is 2(5H)-furanone-5-nitrooxy (**3**). This product can be formed by the reaction of a cyclic nitrooxyalkyl radical with  $\text{O}_2$  to form a cyclic nitrooxyperoxy radical. The latter will react with  $\text{NO}_3$  /  $\text{RO}_2$  to form the corresponding nitroalkoxy radical, which will react with  $\text{O}_2$  to form 2(5H)-furanone-5-nitrooxy (**3**). Regarding maleic anhydride (**4**), it is probably formed from the oxidation of 2-butenedial, a mechanism proved to occur upon oxidation of unsaturated dicarbonyls with OH radical (Bierbach et al., 1994). Another product that can be formed from the oxidation of 2-butenedial is 4-oxo-2-butenic acid (**5**). The latter can be formed by H-abstraction from the aldehyde group.

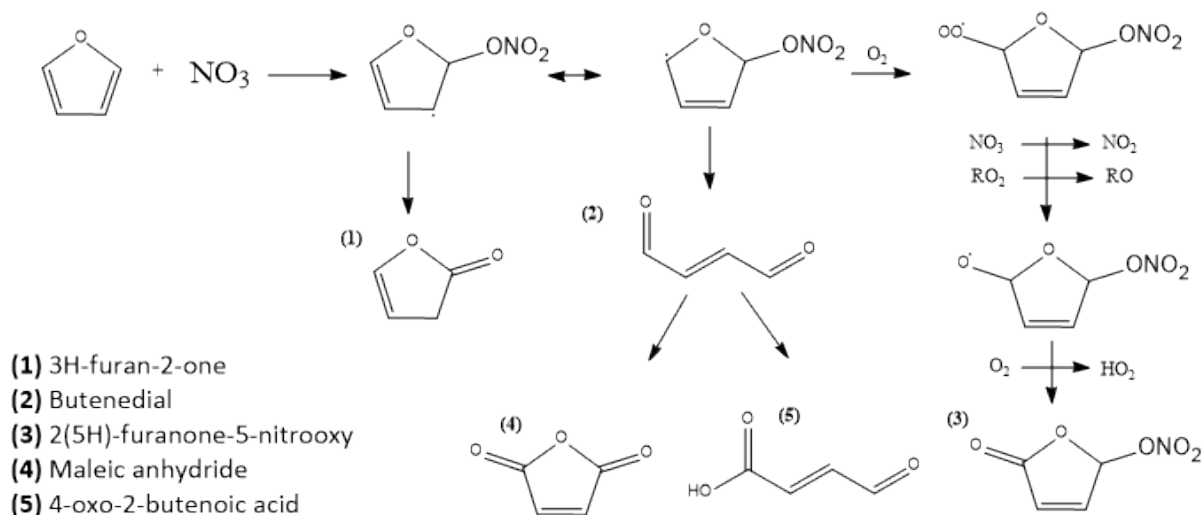
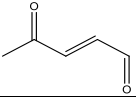
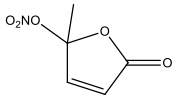
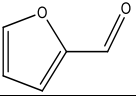
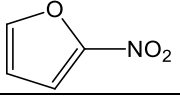
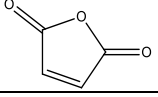
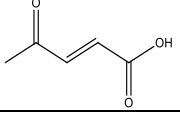
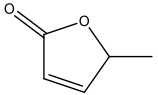
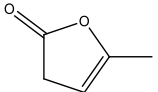


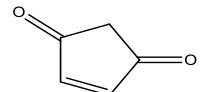
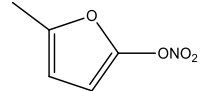
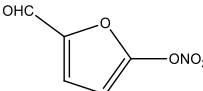
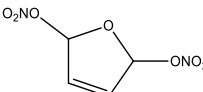
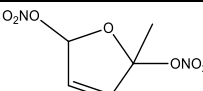
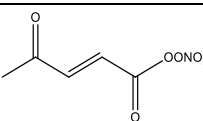
Figure IV.3: Mechanism of the reaction of furan with  $\text{NO}_3$  leading to the formation of the major primary products.

#### IV.2.2 2-Methylfuran reaction with $\text{NO}_3$

In this section, the results of the gas-phase product analysis for  $\text{NO}_3$  radical reaction with 2-MF are presented and discussed. Several analytical techniques and sampling methods were used to qualitatively and quantitatively analyze the end-oxidation products and to provide comprehensive information. The identified compounds in the present study are summarized in Table IV.2. Off-line, real-time and in-situ product analyses are presented in three separate sections and the results are critically compared and discussed. Quantum mechanical molecular calculations results are included in the in-situ FTIR monitoring section.

Table IV.2: Gas-phase products detected using different sampling methods and analytical techniques (products numbers are consistent with the mechanism presented in Figure IV.13). Results obtained for the different solvents have been combined.

Product	Structure	m/z <sup>1</sup>	PTR-ToF-MS <sup>2</sup>	SIFT-MS <sup>3</sup>	GC-EI-MS (Offline)				FTIR
					TD-GC-EI-MS <sup>2</sup>	Monotrap <sup>2</sup>	Bubbler (Methanol/Acetonitrile) <sup>2</sup>	Tenax cartridges <sup>3</sup>	
4-oxo-2-pentenal (1)		99	✓	✓	✓	✓	✓	✓	✓
5-methyl-5-nitrooxy- 2(5H)-furanone (2)		160 (fragments: 97, 114)	✓	✓	✓				
2-furfural (3)		97			✓	✓	✓	✓	
2-Nitrofuran (4)					✓				
Maleic anhydride (5)		99	✓	✓	✓	✓	✓	✓	
4-oxopent-2-enoic acid (6)		115	✓	✓			✓	✓	
5-methyl-2(3H)- furanone (7)		99	✓	✓	✓	✓	✓		
5-methyl -2(5H)-furanone(8)		99	✓	✓	✓	✓	✓	✓	

2-Cyclopentene-1,4-dione		98	√	√	√	√	√	√	
2-methylfuran-5-nitrooxy					√				
5-nitro-2-furfural							√		
2,5-dinitrooxy-furan									√
2-methyl, 2,5-dinitrooxy-furan									√
4-oxopent-2-enoyl nitrate		176	√						

<sup>1</sup> *m/z* corresponds to the compound mass +1 (charge,  $z=1$ ) detected with PTR-ToF-MS/ SIFT-MS with the plus one being due to the ionization method ( $H_3O^+$ ).

<sup>2</sup> Results obtained in CHARME.

<sup>3</sup> Results obtained in THALAMOS.

#### IV.2.2.1 Offline $\text{NO}_3$ + 2-MF gas-phase reaction products analysis (TD-GC-EI-MS, GC-EI-MS)

GC-EI-MS analyses were performed to identify the gas-phase oxidation products of the title reaction. A typical chromatogram obtained with active sampling analysis on tri-bed activated carbon cartridges with TD-GC-EI-MS is presented in Figure IV.4, labelling the corresponding structures and names of the identified compounds. In Table IV.2 are summarized the results of the major products identified using the existing NIST library and in the case of 2-furfural, maleic anhydride and 5-methyl-2(3H)-furanone with the use of standards. Several oxygenated species were identified, such as aldehydes, ketones and organic nitrates. Besides 4-oxo-2-pentenal and 4-oxopent-2-enoic acid all the other compounds identified retain the main structure of the furan ring. Furthermore, as displayed in Table IV.2, the compounds identified from the analysis of the gas mixture of THALAMOS chamber trapped in Tenax<sup>®</sup> cartridges, agree with those measured in CHARME.

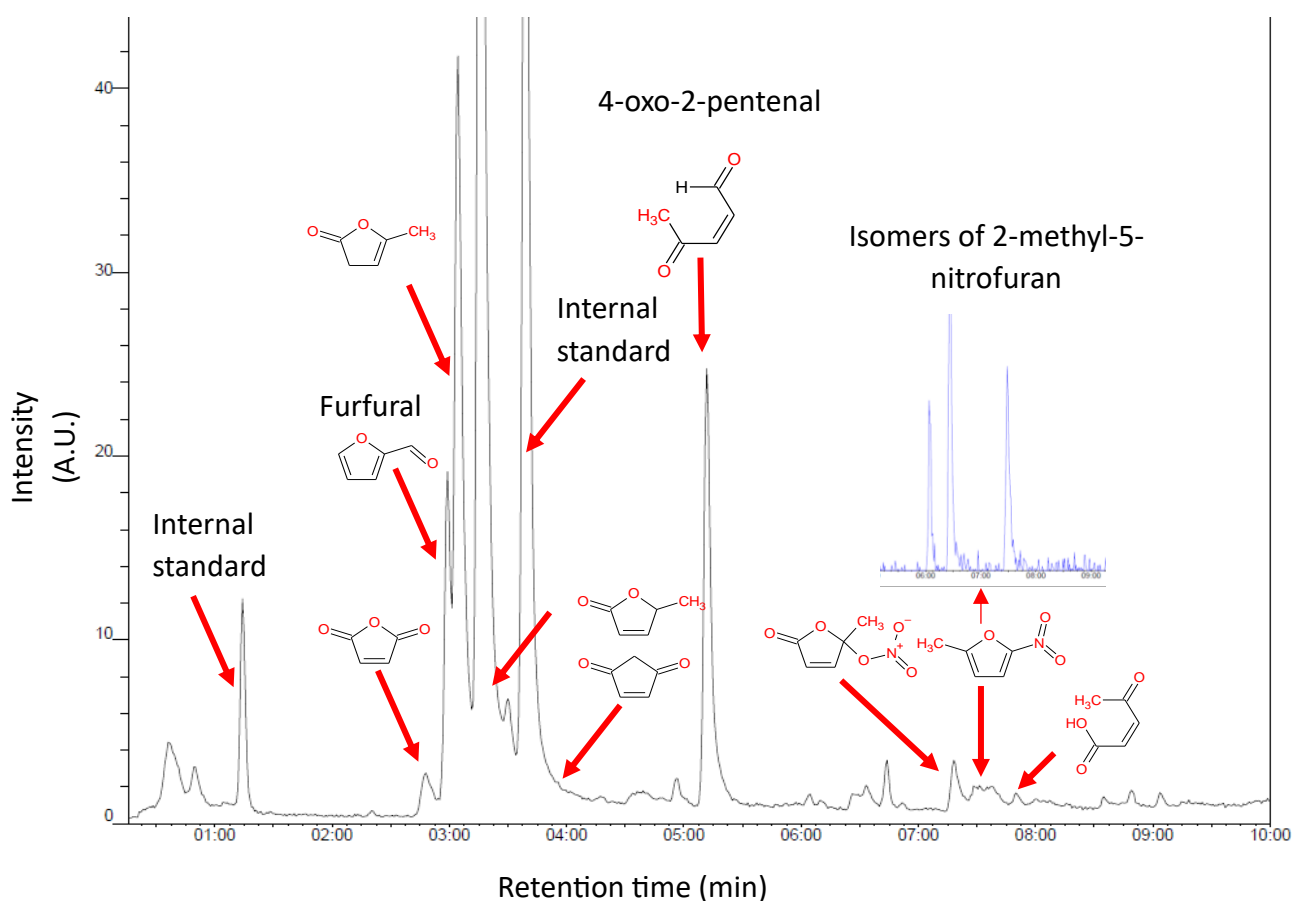


Figure IV.4: Chromatogram (TD-GC-EI-MS) of the gas-phase oxidation products formed in the reaction of 2-MF with  $\text{NO}_3$  radicals. The peaks are labelled with their chemical structures and names.

#### *IV.2.2.2 Insights from the online analysis (PTR-ToF-MS, SIFT-MS) of the gas mixture: temporal variation of the reactant and products and yields estimated*

In CHARME, a series of 6 experiments were performed to qualitatively and quantitatively determine the gas-phase oxidation products from 2-MF + NO<sub>3</sub>. NO<sub>3</sub> + 2-MF reaction progress was continually followed with PTR-ToF-MS detection. 2-MF temporal profile was monitored using 83 mass peak (2-MF•H<sup>+</sup>), while the mass peaks that correspond to the products were (m/z masses + H<sup>+</sup>): 96.0, 97.0, 98.0, 99.0, 100.0, 101.0, 113.0, 114.0, 115.0, 160.0. Note that possible fragmentation of ionized molecules might occur with PTR-ToF-MS detection; thus, the mass peaks detected might not correspond to the parent peaks of the compounds. The products that the observed mass spectral intensities have been attributed to are presented in Table IV.2. Typical temporal profiles of the most prominent mass spectral intensities, i.e., 97.0 and 99.0, are shown in Figure IV.5, together with those of minor masses.

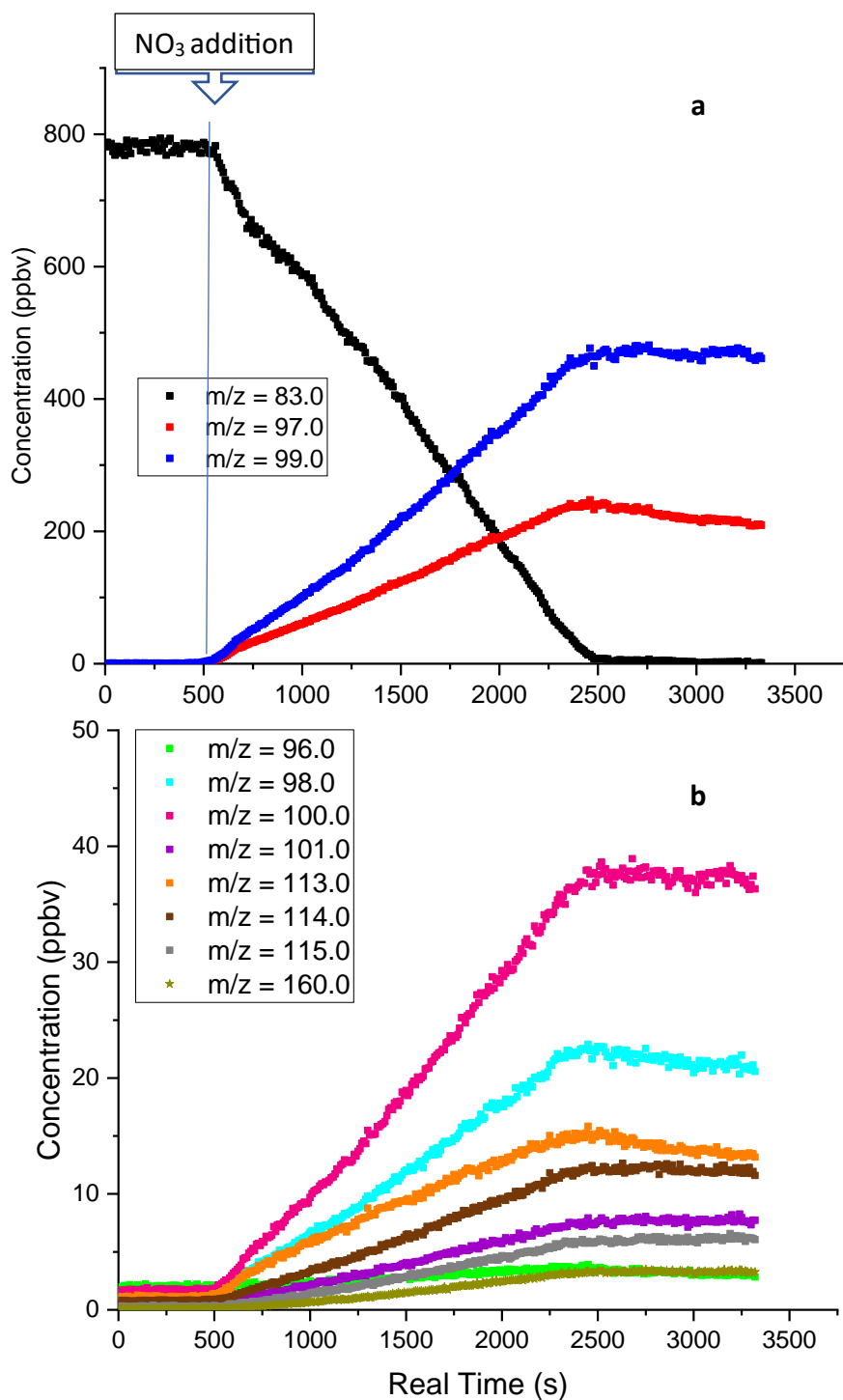


Figure IV.5: Typical reactant and product temporal profiles for the NO<sub>3</sub> radical reaction with 2-MF ( $[2\text{-MF}]_{t=0} = 800$  ppbv) with PTR-ToF-MS. Note that  $m/z$  includes +1 corresponding to ionization by H<sup>+</sup>. (a) 2-MF ( $m/z = 83$ ) and the two predominant products detected at  $m/z = 99.0$  and  $97.0$ . (b) Minor oxidation products and fragments of major products.



For PTR-ToF-MS calibration in quantitative analysis, known volumes of 2-MF were used. For the reaction products, the concentrations were theoretically calculated using a rate coefficient of  $2 \times 10^{-9} \text{ cm}^3 \text{ molecule}^{-1} \text{ s}^{-1}$  for the  $\text{H}_3\text{O}^+$  protonation reaction. The product concentrations were corrected for their background signals measured before the introduction of the corresponding compounds. The masses at  $m/z$  97.0 and 99.0 were initially attributed to 2-furfural and 4-oxo-2-pentenal, respectively. Although the calibration of 2-furfural standards with the PTR-ToF-MS showed that it is detected at the exact  $m/z = 97.0$ , it is highly apparent that there is a contribution from isobaric fragments due to the high probability of organic nitrate fragmentation in the PTR-ToF-MS. Product yields were determined via fitting the product concentration as a function of [2-MF] loss (see Figure IV.6) and the results are presented in Table IV.3. Note that in PTR-ToF-MS the 2-furfural yield was determined to be  $\sim 26\%$ , while in GC-EI-MS measurements it was found to be 1%.

Table IV.3:  $\text{NO}_3 + 2\text{-MF}$  reaction products molar-yields as determined from the linear least-square analysis of products concentration versus [2-MF] loss. The  $m/z$  correspond to compounds fragments masses plus one ( $\text{H}^+$  attached).

[2-MF] <sub>0</sub> (ppbv) ( $m/z=83.0$ )	% Product yields				
	$m/z = 97.0^a$	$m/z = 98.0^b$	$m/z = 99.0^c$	$m/z = 114.0^d$	$m/z = 115.0^e$
320	25.8	1.0	53.0	1.0	1.0
665	28.1	3.1	66.0	1.1	1.1
865	26.4	2.8	62.7	1.5	0.7
1260	28.1	3.1	65.2	2.0	1.0
1540	25.2	3.0	70.3	1.8	1.0
1770	24.1	2.9	52.1	1.3	1.1
Average yield	$26.2 \pm 3.1$	$2.9 \pm 2.3$	$61.5 \pm 14.7$	$1.4 \pm 0.7$	$0.9 \pm 0.2$

<sup>a</sup> Yields determined using 2-furfural standard. SIFT-MS experiments (see below) identified 5-methyl-5-nitrooxy-2(5H)-furanone as additional product that will be also detected at  $m/z = 97$  in PTR. Organic nitrate yields can be indirectly estimated assuming that this is the sole contribution at 97 mass peak.

<sup>b</sup> Attributed to 2-cyclopentene-1,4-dione

<sup>c</sup> Attributed to 4-oxo-2-pentenal

<sup>d</sup> Attributed to 5-methyl-5-nitrooxy-2(5H)-furanone

<sup>e</sup> Attributed to oxopent-2-enoic acid

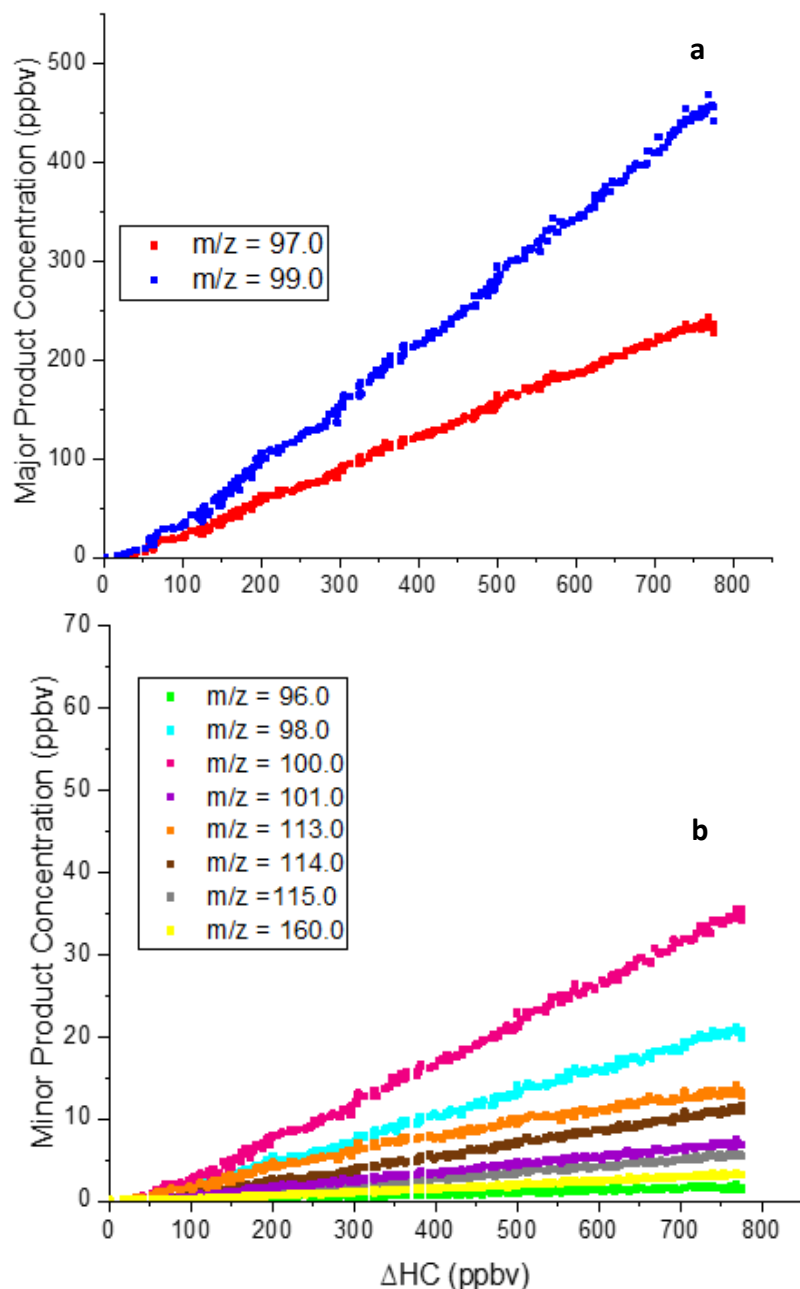


Figure IV.6: Typical plots for the determination of the gas-phase product yields formed from the reaction of 2-MF with  $\text{NO}_3$ . (a) major oxidation products (b) minor oxidation products.

The masses with  $m/z$  97.0 and 99.0 correspond to the dominant products formed from the gas-phase reaction of 2-MF with  $\text{NO}_3$ . They were attributed to 2-furfural ( $m/z$  97.0) and 4-oxo-2-pentenal ( $m/z$  99.0). In separate experiments, the standard of furfural was injected in the chamber to elucidate the exact position of the peak. It was found to be exactly the same with that of the product (i.e.  $m/z = 97.0$ ). Nevertheless, due to the high probability of organic nitrates fragmentation in the PTR-ToF-MS, the peak at  $m/z = 97$  might not be solely attributed to furfural.

In order to further investigate the origin of  $m/z = 97.0$ , a series of experiments were conducted in THALAMOS using SIFT-MS detection. First, the parent ion peak of a 2-furfural standard was measured with SIFT-MS using  $\text{H}_3\text{O}^+$  ( $m/z: 97.0$ ),  $\text{NO}^+$  ( $m/z: 95.0$  and  $126.0$ ) and  $\text{O}_2^+$  ( $m/z = 96.0$ ).

Then the unique relative ratios of 2-furfural peaks were determined to be,  $\frac{I_{97}^{\text{H}_3\text{O}^+}}{I_{95}^{\text{NO}^+}}=5.08$ ,

$\frac{I_{97}^{\text{H}_3\text{O}^+}}{I_{96}^{\text{O}_2^+}}=3.44$ ,  $\frac{I_{97}^{\text{H}_3\text{O}^+}}{I_{126}^{\text{NO}^+}}=3.51$ ,  $\frac{I_{126}^{\text{NO}^+}}{I_{95}^{\text{NO}^+}}=1.46$ ,  $\frac{I_{97}^{\text{H}_3\text{O}^+}}{I_{96}^{\text{O}_2^+}}=1.13$ . A typical mass-scan spectrum of 2-furfural is

shown in Figure IV.7. Next, 2 ppmv of 2-MF were injected in the chamber and left to react with  $\text{NO}_3$  until its complete consumption. Reactant and product temporal profiles recorded with SIFT-MS were in excellent agreement with the ones measured in CHARME (Figure IV.5). The major mass peaks detected with SIFT-MS were 97.0, 99.0, 115.0 for  $\text{H}_3\text{O}^+$ , 97.0 and 98.0 for  $\text{NO}^+$  and mainly fragments of  $\text{O}_2^+$ . The products growth with  $m/z 97.0$  and  $99.0$  for  $\text{H}_3\text{O}^+$ , and  $97.0$  and  $98.0$  for  $\text{NO}^+$  were found to correlate linearly with  $\Delta[2\text{-MF}]$ , similarly with the observations in CHARME (Figure IV.6). Mass peaks 99.0 for  $\text{H}_3\text{O}^+$ , and  $97.0$  and  $98.0$  for  $\text{NO}^+$  were attributed to 4-oxo-2-pentenal.

Interestingly, the relative ratios  $\frac{I_{97}^{\text{H}_3\text{O}^+}}{I_{95}^{\text{NO}^+}} > 10$ ,  $\frac{I_{97}^{\text{H}_3\text{O}^+}}{I_{126}^{\text{NO}^+}} > 6$ ,  $\frac{I_{126}^{\text{NO}^+}}{I_{95}^{\text{NO}^+}}=4.71$ ,  $\frac{I_{97}^{\text{H}_3\text{O}^+}}{I_{96}^{\text{O}_2^+}} > 10$ ,  $\frac{I_{97}^{\text{H}_3\text{O}^+}}{I_{96}^{\text{O}_2^+}}=3.36$ ,

were significantly higher than those determined using 2-furfural standard. Therefore, it is highly likely that the mass 97 in PTR-ToF-MS and SIFT-MS determinations does not stem only from 2-furfural (see also panels a and c,d,e of Figure IV.7). Although SIFT-MS data show that 2-furfural can only be a minor reaction product, it is hard to estimate an upper limit for the yield. The latter is consistent with the 2-furfural  $\sim 1\%$  yield determined using GC-EI-MS. It is worth to note that 2-furfural is formed via the oxidation of the dehydrogenated 2-MF radical, following the H atom abstraction from the methyl group.

Looking into the higher masses of  $\text{NO}_3 + 2\text{-MF}$  reaction product mass spectrum recorded using  $\text{H}_3\text{O}^+$ , we also observed mass peaks at  $m/z 160.0$  and  $113.0$ . The peak with  $m/z 160.0$  was attributed to the protonated form of an organic nitrate ketone, i.e., 5-methyl-5-nitrooxy-2(5H)-furanone (molecular mass of  $159.0$  amu), that can be formed from  $\text{NO}_3$  addition to the C5 preserving the furan ring (see Figure IV.13). We suggest that this organic nitrate fragmentates in the flow tube / DRIFT tube of SIFT-MS / PTR-ToF-MS, leading to fragments with  $m/z 113.0$  and  $46.0$ , and  $97.0$  and  $64.0$  (Figure IV.7). Interestingly, the organic nitrate product yield can be indirectly estimated using the PTR-ToF-MS data, based on the instrument response at  $m/z = 97.0$ . Assuming a unity fragmentation yield, i.e., all the organic nitrate ketone molecules are fragmented to give  $m/z 97.0$  and  $64.0$ , which is a reasonable approximation due to the low relative abundance mass peaks  $113.0$  and  $160.0$  (the sum of their intensities is  $\sim 7\%$  of the one at  $m/z 97.0$ ), the theoretically calculated yield was estimated to be  $28\%$  (upper limit). The corresponding product yield determined based on mass peak  $97.0$ , using 2-furfural standard, was found to be  $\sim 26\%$ , which is in consistency (Table IV.3). The yields for all the other products detected were between 1 and 3% and thus, they can be considered as minor products.

To wrap up, the online monitoring of  $\text{NO}_3$  radical reaction with 2-MF revealed 4-oxo-2-pentenal and 5-methyl-5-nitrooxy-2(5H)-furanone as the two major reaction products, with

estimated yields of 61% and 26%, respectively. Taking that into account and the low 2-furfural product yield at room temperature, we suggest that  $\text{NO}_3$  radical is preferably added to the C-2/C-5 double bond of 2-MF. The subsequent oxidation of the  $\text{NO}_3$  adduct can either exhibit a ring opening and lead to unsaturated aldehyde or preserve the furan ring and form the organic nitrate.

Masses of lower intensities were also detected with SIFT-MS (Figure IV.7) and the corresponding attributed reaction products are included in the proposed reaction mechanism (Figure IV.13). In SIFT-MS analysis with  $\text{NO}^+$  precursor ion, a mass peak at  $m/z = 175.0$  was observed that was attributed to PeroxyAcyl Nitrate (PAN). PAN could be a secondary product formed via the  $\text{NO}_3$  reaction with 4-oxo-2-pentenal. PAN fragmentation in SIFT-MS could give the mass peak 146.0 that was also detected with  $\text{H}_3\text{O}^+$  ion. This is the first time that SIFT-MS capability to detect easily fragmentated species, such as PANs, is demonstrated.

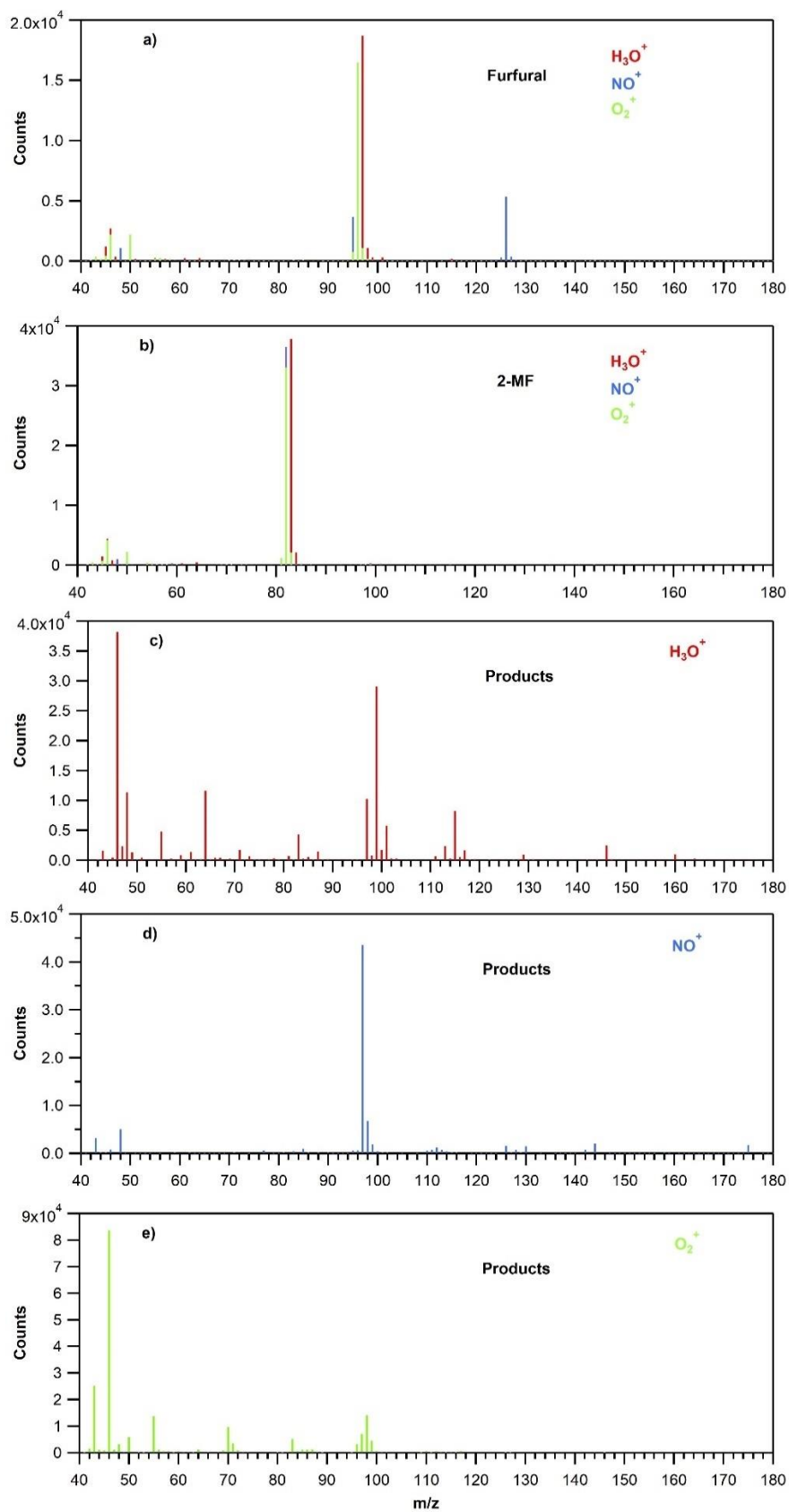


Figure IV.7: Mass scans of furfural, 2-MF and products of the reaction of 2-MF with  $NO_3$  obtained using SIFT-MS coupled to THALAMOS employing three precursor ions ( $H_3O^+$ ,  $NO^+$ ,  $O_2^+$ ).

#### IV.2.2.3 In-situ analysis of $\text{NO}_3 + 2\text{-MF}$ gas-phase reaction products using FTIR spectroscopy

FTIR spectroscopy was employed to monitor end-oxidation products of  $\text{NO}_3 + 2\text{-MF}$  and to evaluate possible formation of organic nitrates.

Figure IV.8 shows the residual spectrum recorded in the first experimental setup located in Dunkerque (injected concentrations  $\cong 3$  ppmv), after the complete oxidation of 2-MF and subtracting the IR spectra of  $\text{N}_2\text{O}_5$ ,  $\text{NO}_2$  and  $\text{HNO}_3$ . The attribution of the different absorption bands is also presented. In Figure IV.9 is also displayed the IR spectrum recorded in the second experimental setup after 50% consumption of 2-MF (injected concentrations  $\cong 100$  ppmv) to evaluate the formation of products formed at low yields. Identical features were observed comparing the residual experimental spectra. Due to the lack of experimental reference spectra, the different absorption bands observed in the residual spectra were attributed to specific vibration modes of the proposed end-products using the calculated IR spectra (performed in collaboration with our colleagues at Crete University). The capability of MP2/AUG-cc-pVDZ level of theory to predict both peak positions and heights for furanoid compounds is first evaluated comparing the calculated cross-section spectra of three furans, i.e., 2-MF, maleic anhydride (MAH) and furfural with the experimentally determined ones (Figure S5, Figure S6, Figure S7). In the case of furfural, two different conformers were found (Figure S7 upper panel), with relative abundance of 41% (oxygens in the same side) and 59% (oxygens at opposite sides) as calculated based on the energetics and the equilibrium Boltzmann distribution. The resulted calculated spectrum is presented in Figure S7 along with the experimentally measured one, for comparison purposes.

As shown in Figure S5, Figure S6, Figure S7, the calculated spectra of the above mentioned compounds were in reasonable agreement with the experimental reference spectra, both in terms of bands positioning and intensities with the only exception of the region where C-H stretch appears, i.e.,  $3000\text{ cm}^{-1}$ , where the calculations led to a substantial blue-shift. The agreement in integrated band strengths is better than 30% in all cases. Particularly in the region of  $1000\text{-}2000\text{ cm}^{-1}$ , where the strong absorbing features for the majority of the species of interest appear, the agreement is always better than 20%. Therefore, since most of the end-products were expected to be oxygenated compounds and thus, the spectra deviations were expected to follow similar trends with those observed for the three furans (2-MF, MAH and furfural), we decided to run our IR spectra calculations using the same level of theory. The inter-comparison of the experimentally determined residual spectrum with the calculated IR spectra allows to identify  $\text{NO}_3 + 2\text{-MF}$  end-products as well as to estimate their yields.

Thus, based on our proposed oxidation scheme and the theoretically calculated spectra, we suggest 2,5-dinitrooxy-furan and 4-oxo-2 pentenal as the major end-products for the  $\text{NO}_3 + 2\text{-MF}$  reaction; the calculated IR cross section spectra for these two end-products are given in Figure S5 and S6. In the case of 4-oxo-2 pentenal, two different conformers were found with an equilibrium abundance of 90 and 10% ( $\sim 5\text{ kJ mol}^{-1}$  energy difference). This ratio (Figure S7) is used to convolve the composite IR spectrum. The full list of the compounds tested as potent end-products is given in Table S1. Among these compounds, a particular attention should be

drawn to 2,5-dinitrooxy-methyl furan, for which the IR spectrum is very similar with the one calculated for 2,5-dinitrooxy-furan (Figure S7). However, in the case of 2,5-dinitrooxy-furan, the two bands observed in the region  $964 - 1044 \text{ cm}^{-1}$ , better describe the experimental residual spectrum (

Figure IV.8 & Figure IV.9), while a single absorption band is observed in the case of 2,5-dinitrooxy-methyl furan. Thus, 2,5-dinitrooxy-furan is suggested to be the most likely organic nitrate end-product formed.

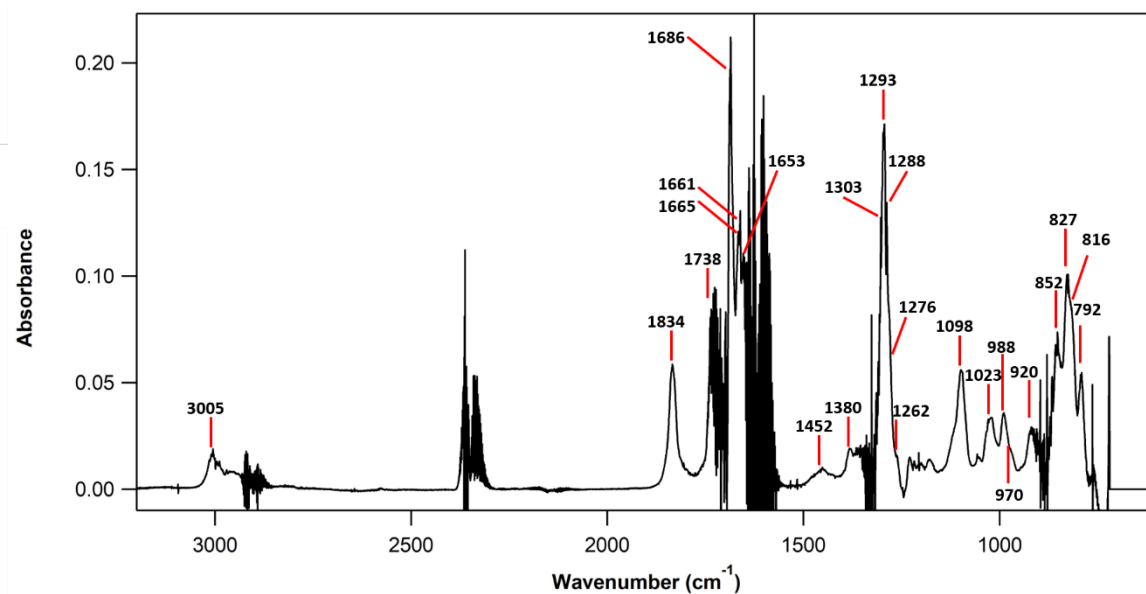


Figure IV.8: Residual spectrum recorded at 2-MF + NO<sub>3</sub> reaction completion, in presence of O<sub>2</sub>, after subtracting the IR spectra of N<sub>2</sub>O<sub>5</sub>, NO<sub>2</sub>, and HNO<sub>3</sub>. The residual spectrum displays the end-oxidation products. The exact wavenumbers of the peaks are shown in graph.

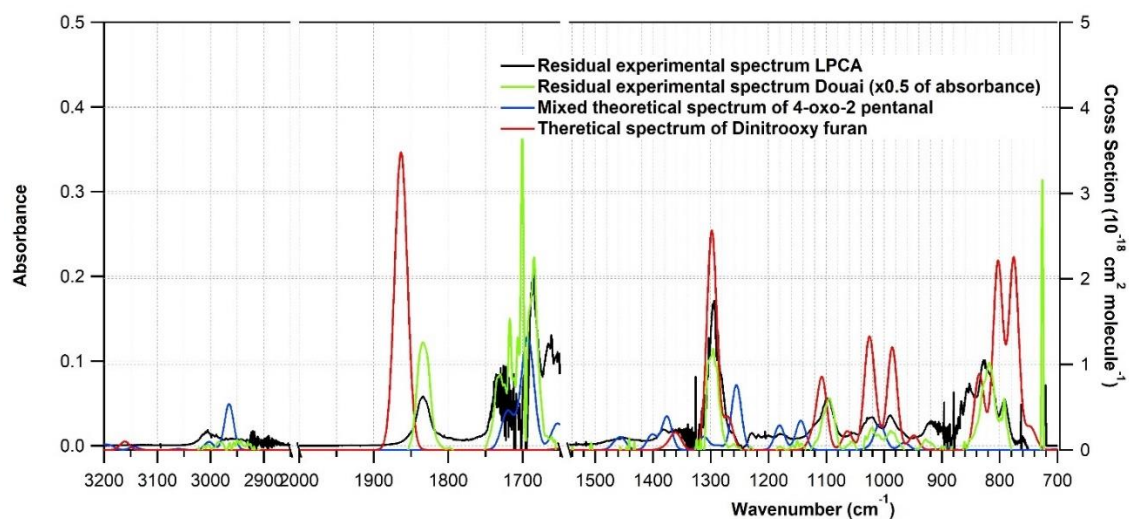


Figure IV.9: Residual IR spectrum (black line, left axis), and theoretically obtained cross section spectra of 4-oxo-2-pentanal (blue line, right axis) and dinitrooxy-methylfuran (red line, right axis) calculated at MP2/AUG-ccc-pVDZ level of theory.



Interestingly, no characteristic band features were observed in the residual IR spectrum that correspond to furfural or MA. Furfural and MA are formed via direct or indirect H-atom abstraction as primary and secondary oxidation product, respectively. The absence of furfural in both experimentally determined products also confirms that the H-atom abstraction pathway is of minor importance. To suppress possible reaction of furfural formed with  $\text{NO}_3$  radicals, the experiments in the second experimental setup were performed under high excess of 2-MF (ca. 100 ppmv), and the reaction products were evaluated after ca. 44% of 2-MF conversion. It should be also noted that the reaction rate coefficient of furfural with  $\text{NO}_3$  radicals is slower by a factor of 10 compared to 2-MF and thus possible reaction of furfural with  $\text{NO}_3$  is unlikely to occur in our system. To give an upper limit to furfural formation (and thus of the abstraction channel), the standard was injected in the FTIR gas cell (in second experimental setup experiments), to estimate a limit of detection. On this basis, an upper yield of 5% can be given. In addition, a series of experiments were performed reacting furfural (15 ppmv) with  $\text{NO}_3$  radicals to compare the final reaction products with those of 2-MF. It was evidenced that the final reaction products of furfural +  $\text{NO}_3$  and 2-MF +  $\text{NO}_3$  were different.

In the case of  $\text{NO}_3$  addition to the 2-MF ring, the primary oxidation product is 4-oxo-2-pentenal (ring opening), which is also present in the residual IR spectrum. This observation indicates that the reactivity of  $\text{NO}_3$  towards 4-oxo-2-pentenal is relatively slow (but occurs) compared to the one towards 2-MF, which is not surprising considering that the  $\text{NO}_3$  rate coefficients with furans are greater than the ones for straight chain unsaturated compounds (Martín et al., 2013; Newland et al., 2022). The PAN arising from 4-oxo-2-pentenal which was previously detected with SIFT-MS, is not observed with FTIR, probably due to low formation yields. Nevertheless, it should be noted that this compound is expected to give similar absorption features with other organic nitrates formed, and thus its identification is challenging.

The formation of 2,5-dinitrooxy-furan or 2,5-dinitrooxy-furans is also attributed to the  $\text{NO}_3$  addition pathway, where the furan ring is retained forming the organic nitrate with mass peak 159 previously observed with the SIFT-MS.

A comparison of the experimentally determined residual spectrum with the proposed products is given in Figure IV.9. The theoretical spectrum of 2,5-dinitrooxy-furan overlaps with the experimental in the region of  $1261\text{-}1323\text{ cm}^{-1}$  which is the main vibration feature of nitrooxy compounds ( $-\text{ONO}_2$ ). The slight red- and blue-shifts observed in the region  $755\text{-}823\text{ cm}^{-1}$  and  $1777\text{-}1876\text{ cm}^{-1}$ , respectively, were attributed to limitations of the level of theory used and the harmonic oscillator and rigid rotor corrections that have not been applied. Nevertheless, the satisfactory representation of all the features of the absorption bands in both terms of positioning and band intensities appearing in the residual spectrum provides with evidence that 2,5-dinitrooxy-furan is formed as end-product. However, the presence of other non-identified end-products, either due to weak absorbance features, that overlap with the observed ones in the residual spectrum or due to low yields or even due to phase-change, e.g., polymerization, condensation, or gas-phase and wall loss cannot be excluded.

The absorption band at 774-874  $\text{cm}^{-1}$  is attributed to the  $-\text{ONO}_2-$  group bending mode of the organic nitrates formed. In particular, the absorption peaks at 792 and 827  $\text{cm}^{-1}$  are assigned to the asymmetric and symmetric vibrational bending modes of two  $\text{O}-\text{NO}_2$  groups attached to the  $\text{C}_2$  and  $\text{C}_5$  carbons of the 2,5-dinitrooxy-furan, respectively. The peak at 852  $\text{cm}^{-1}$  is attributed to the stretching vibration mode of the furan-ring of 2,5-dinitrooxy-furan. It is noted that the weak absorption broad band centered at  $\sim 920 \text{ cm}^{-1}$  indicates the parallel formation of 2,5-dinitrooxy-methyl furan since, based on the theoretical spectra, this feature could result from the twisting mode of the C-H connected to the double bond ( $\text{H}-\text{C}=\text{C}-\text{H}$ ) and the C-H vibration of the methyl substituted 2,5-dinitrooxy-methyl furan.

The two absorption bands at 955-1002  $\text{cm}^{-1}$  and 1002-1044  $\text{cm}^{-1}$  were consistent with vibration modes of 2,5-dinitrooxy-furan. In particular, the broad absorption peaks centred at 988  $\text{cm}^{-1}$  and 1023  $\text{cm}^{-1}$  were attributed to the antisymmetric and symmetric stretching of the two  $\text{C}-\text{ONO}_2$  of 2,5-dinitrooxy furan. The right shoulder at around 970  $\text{cm}^{-1}$  is assigned to the  $(\text{O})\text{C}-\text{CH}_3$  vibration mode of the  $\text{C}_4-\text{C}_5$  carbons of 4-oxo-2-pentenal. Furthermore, the C-H vibrations of the aldehyde group and the  $\text{C}_2-\text{H}$  and  $\text{C}_3-\text{H}$  vibrations of the double bond in 4-oxo-2-pentenal, appear at around 1005  $\text{cm}^{-1}$ . The broad band at 1070-1149  $\text{cm}^{-1}$  with a peak at 1098  $\text{cm}^{-1}$ , and a left shoulder at around 1107  $\text{cm}^{-1}$  is chiefly attributed to the nitrooxy substituted carbons  $\text{C}_2-\text{O}-\text{C}_5$  of the furanoid ring. Interestingly, in the calculated spectrum of 2,5-dinitrooxy furan this vibration mode appears at around 1107  $\text{cm}^{-1}$ , and thus overlaps with the left shoulder of the peak, while in the case of 2,5-dinitrooxy methyl-furan this vibration mode appears at 1095  $\text{cm}^{-1}$ .

The absorption band feature around 1293  $\text{cm}^{-1}$  (blue-shifted to 1298  $\text{cm}^{-1}$  in the theoretical spectrum) corresponds to the symmetric and antisymmetric stretching vibration modes of the  $\text{O}-\text{NO}_2$  of the 2,5-dinitrooxy furan. The absorption feature appearing as a shoulder at  $\sim 1262 \text{ cm}^{-1}$  is consistent with the formation of 4-oxo-2-pentenal and corresponds to the  $-\text{C}(\text{O})-\text{H}$  bending mode of the aldehyde group of the most stable conformer of the compound (1256  $\text{cm}^{-1}$  in the theoretical spectrum), the C-H vibrations of the double bond, and C-C vibrations of the  $\text{C}_4$  carbon.

The weak broad absorption band with a peak around 1380  $\text{cm}^{-1}$  is assigned to the C-H wagging modes of the  $\text{CH}_3$  group of 4-oxo-2-pentenal and the C-H vibrations of the four carbon ring in the furanoid nitrooxy compound. In a similar way, the very weak but broad absorption band between 1418 – 1500  $\text{cm}^{-1}$  corresponds to scissoring C-H vibrations of the  $\text{CH}_3$  group in dinitrooxy-methyl furan and 4-oxo-2-pentenal.

The absorption band at 1653  $\text{cm}^{-1}$  represents the  $\text{C}=\text{C}$  vibration mode of 4-oxo-2-pentenal, which appears in the composite theoretical spectrum at 1651  $\text{cm}^{-1}$ . The sharp peak at 1686  $\text{cm}^{-1}$  (1693  $\text{cm}^{-1}$  in the calculated spectrum) is assigned to the  $\text{C}=\text{O}$  stretching mode of the carbonyl group of the same compound. There is also a vibration mode at around 1720 - 1730  $\text{cm}^{-1}$  that is assigned to C=O vibrations of the carbonyl group of 4-oxo-2-pentenal.

The broad absorption feature at  $1834\text{ cm}^{-1}$  represents the O=N=O vibration frequencies of the dinitrooxy-furan. Note that it has been proposed in the literature that nitroperoxy compounds ( $-\text{OONO}_2$ ) can be also formed as products during  $\text{NO}_3$  oxidation of methyl furans (Tapia et al., 2011). Based on our theoretical calculations, nitroperoxy compounds IR spectra have a characteristic absorption band around  $1950\text{ cm}^{-1}$  that corresponds to the O- $\text{ONO}_2$  stretching. However, no evidence for nitroperoxy compounds were found in the experimental residual spectrum. Finally, the very broad absorption feature appeared between  $2966 - 3040\text{ cm}^{-1}$  and centered at  $3005\text{ cm}^{-1}$ , is consistent with the C-H stretching modes of 4-oxo-2-pentenal aldehyde group.

Additionally, to the qualitative analysis and the peak assignments, our calculated cross-section spectra were also used to quantitatively estimate the end-products yields. In particular, in the case of dinitrooxy furan, the integrated absorption band cross sections at  $1247.2\text{-}1317.4\text{ cm}^{-1}$  and  $761.44\text{-}951.22\text{ cm}^{-1}$  ( $714.4\text{-}904.6\text{ cm}^{-1}$  in the theoretical spectrum), that correspond to organic nitrate vibration modes, were used to estimate its concentration, employing Beer's law. The estimated yield of organic nitrates formed were  $33\pm 17\%$ , where the uncertainty denotes the discrepancies between the integration of the peaks and mainly due to the variation between the experiments carried out in the first and second experimental setups. In the case of 4-oxo-2-pentenal, the peak cross section at  $1686\text{ cm}^{-1}$  is used to estimate the concentration due to problems with the baseline that is shifted by 0.062 in the first experimental setup spectrum, but this is not the case for the second setup. In the calculated IR spectrum, the referred peak appears at  $1694\text{ cm}^{-1}$  and the peak cross-section is  $1.33 \times 10^{-18}\text{ cm}^2\text{ molecule}^{-1}$ . The estimated yield of 4-oxo-2-pentenal is around  $31\pm 5\%$ . This value is relatively lower than the yield observed by the PTR-ToF-MS. However, it should be noted that our approach to employ theoretically obtained IR spectra for quantitative analysis of end-product-yields is mainly used as an indicative tool to test the results consistency.

## IV.2.3 SOA formation from 2-MF reaction with NO<sub>3</sub> radicals

### IV.2.3.1 SOA yields

A total of 7 experiments were carried out in the CHARME chamber to investigate the SOA formation potential from the gas-phase reaction of 2-MF with NO<sub>3</sub> radical in presence of ammonium sulfate seeds of 25 µg.m<sup>-3</sup>. Similar approaches were also followed in literature in the case of 3-MF oxidation by NO<sub>3</sub> (Joo et al., 2019a). The initial 2-MF concentrations used were in the range of 80 ppbv - 531 ppbv. Results are summarized in

Table IV.4. The aerosol yields were calculated as the ratio of ΔM<sub>0</sub> (in µg.m<sup>-3</sup>) to the reacted concentration of 2-MF (in µg.m<sup>-3</sup>) according to the following equation (Eq.1).

$$Y = \frac{\Delta M_0}{\Delta[2-MF]} \quad (\text{Eq.1})$$

Table IV.4: Experimental conditions and SOA yields of the reaction of 2-MF and NO<sub>3</sub>.

Experiment number	[2-MF] <sub>0</sub> (ppbv) <sup>a</sup>	Δ[2-MF] (µg.m <sup>-3</sup> ) <sup>b</sup>	ΔM <sub>0</sub> (µg.m <sup>-3</sup> ) <sup>c</sup>	Yield (%) <sup>d</sup>
1	80	273.0	2.8	1.0
2	110	358.4	5.6	1.6
3	150	494.9	9.5	1.9
4	300	1027.4	21.9	2.1
5	420	1430.2	31.2	2.2
6	470	1604.3	35.9	2.2
7	530	1809.1	40.8	2.3

<sup>a</sup> Initial 2-MF volume ratios.

<sup>b</sup> 2-MF reacted concentration (2-MF was totally consumed in all experiments, so the reacted 2-MF concentration corresponds to the initial 2-MF concentration).

<sup>c</sup> ΔM<sub>0</sub> = M<sub>0</sub> - [seeds]<sub>0</sub>, where M<sub>0</sub> corresponds to the SOA mass concentration corrected for the wall losses formed into the chamber and determined using a particle density of 1.0 g cm<sup>-3</sup>.

<sup>d</sup> Aerosols yield determined from the ratio of the SOA mass concentration formed corrected for the wall losses to the 2-MF reacted concentration.

As shown in

Table IV.4 and Figure IV.10, the increase of 2-MF concentration leads to an augmentation of the SOA yields. The SOA mass concentrations formed (ΔM<sub>0</sub>) were in the range from 2.83 to 40.79 µg.m<sup>-3</sup> corresponding to yields between 1.0 to 2.2 %. The obtained results were fitted using Odum expression (Odum et al., (1996)), which is a semi-empirical model based on semi-volatile products adsorptive gas-particle partitioning according to the following equation (Eq.2):

$$Y = \sum_i \Delta M_0 \frac{\alpha_i K_{om,i}}{1 + K_{om,i} M_0} \quad (\text{Eq.2})$$

where α<sub>i</sub> and K<sub>om,i</sub> are the mass-based stoichiometric coefficient of semi-volatile organic compound (SVOC) and gas-particle partitioning equilibrium constant respectively.

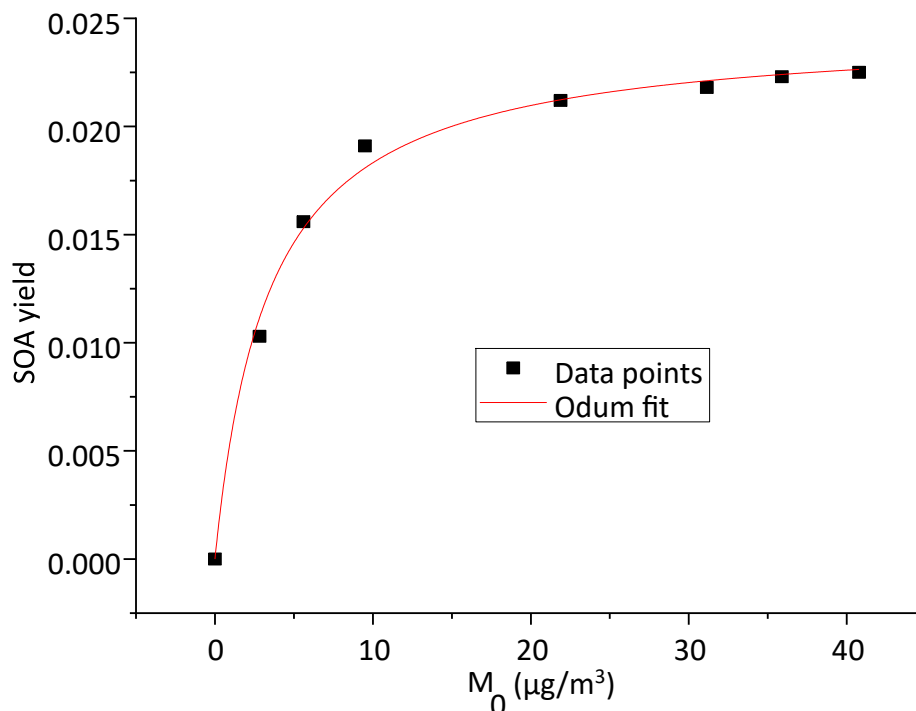


Figure IV.10: Yield curve for the 2-MF + NO<sub>3</sub> reaction (squares). The line represents the Odum fit to the data considering one-product model developed by Odum et al., (1996).

The one product model is able to get satisfactory reproduction of the experimental data ( $R^2 = 0.99$ ) as shown in Figure IV.10 and lead to  $\alpha_i = (2.45 \pm 0.05) \times 10^{-2}$  and  $K_{om,i} = 0.29 \pm 0.03$  ( $\text{m}^3 \cdot \mu\text{g}^{-1}$ ). The two-products model is also able to describe the experimental data, however, the uncertainties on  $\alpha_i$  and  $K_{om,i}$  were higher than their respective values. The one-product model indicates that either only one semi-volatile organic compound is the major constituent of the SOA or that the organic compounds present in the condensed phase have similar  $\alpha_i$  and  $K_{om,i}$ .

It is interesting to compare  $\alpha$  (0.024) to the highest SOA yields determined for the reaction of 2-MF with NO<sub>3</sub> ( $Y = 0.02$ ; see

Table IV.4) and seems to represent the high-limit aerosol yield for this reaction.  $\alpha$  represents the total amount of semi-volatile products present both in the gas- and aerosol-phases, whereas  $Y$  corresponds to the semi-volatile products that have partitioned into the particle phase only. Since  $\alpha$  and  $Y$  were almost equal, this means that the low-volatility organic products formed from the reaction of 2-MF and NO<sub>3</sub> were completely transferred into the particulate matter.

To the best of our knowledge, this work is the first study reporting SOA formation from the gas-phase reaction of 2-MF with NO<sub>3</sub> and there are no literature studies on SOA formation from the reaction of 2-MF with other oxidants (OH, O<sub>3</sub> and Cl). Yet, these results are consistent with the SOA yields formed from the reaction of 3-MF with NO<sub>3</sub> obtained by Joo et al., (2019). In their study, the initial 3-MF concentration varied between 95.9 and 562.8 ppbv, the aerosol mass concentrations  $M_0$  ranged from 5.1 to 45  $\mu\text{g} \cdot \text{m}^{-3}$  corresponding to aerosol yields from 1.62 % to 2.4 %.

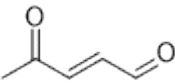
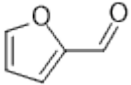
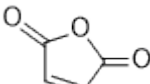
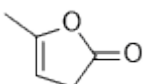
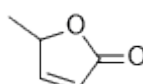
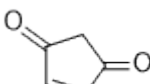
#### IV.2.3.2 SOA chemical composition

The characterization of the chemical composition of aerosols formed from the gas-phase reaction of 2-MF with NO<sub>3</sub> and collected on aerosol filters was performed using GC-EI-MS, ESI-LC-QToF-MS/MS, and ATR-FTIR analyses. Below are described the obtained results separately.

##### IV.2.3.2.1 Qualitative identification with GC-EI-MS

As displayed in Table IV.5, GC-EI-MS revealed 6 oxidation products: 4-oxo-2-pentenal, 2-furfural, maleic anhydride, 5-methyl-2(3H)-furanone, 5-methyl-2(5H)-furanone and 2-cyclopentene-1,4-dione. All these chemical species were also present in the gas phase indicating that they are semi-volatile organic compounds and that they partition between the gas- and aerosol- phases. The formation of organic nitrates in the particulate phase is not observed with this technique probably due to their thermal decomposition in the column of the GC.

Table IV.5: Names and structures of the oxidation products identified in the SOA formed from the 2-MF oxidation by NO<sub>3</sub>.

Product	Structure
4-oxo-2-pentenal	
Furfural	
Maleic anhydride	
5-methyl-2(3H)-furanone	
5-methyl-2(5H)-furanone	
2-Cyclopentene-1,4-dione	

##### IV.2.3.2.2 ESI-LC-QToF-MS/MS analyses of SOA

SOA analyses were performed by ESI-LC-QToF-MS. Identified compounds are ionised either with H<sup>+</sup> within the mobile phase or using ammonium ions (NH<sub>4</sub><sup>+</sup>) added to the mobile phase depending on the organic compound's proton affinity. A typical total ion chromatogram obtained from ESI-LC-QToF-MS/MS analyses of SOA is shown in Figure IV.11. The indicated masses correspond to the [M+NH<sub>4</sub>]<sup>+</sup> product ions of each detected compound. Each peak was then fragmented (MS/MS analyses) using three different energy values 10, 20 and 40 A.U. The different levels of energy applied leads to light and heavy fragmentations of the molecules and

the identification of the functional groups allow then to determine the molecular structures of the 2-MF oxidation products.

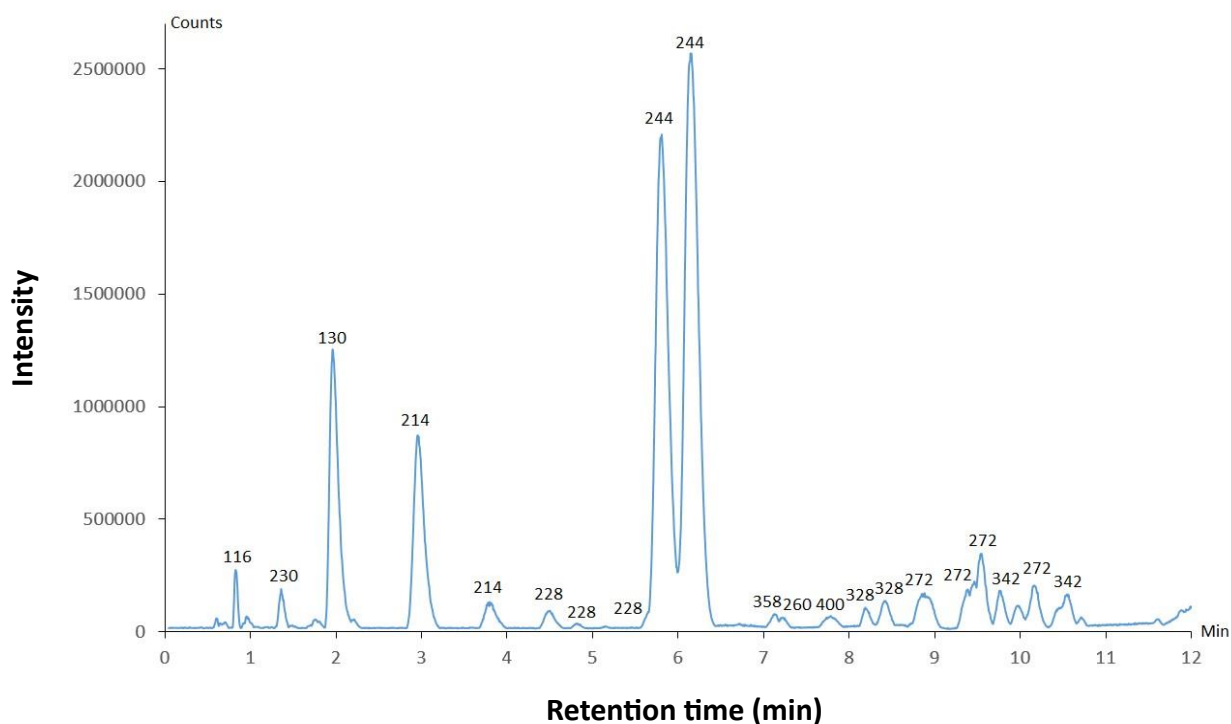
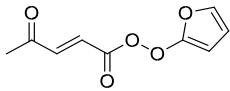
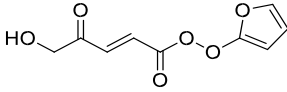
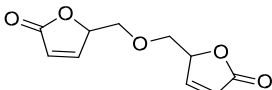
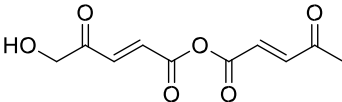
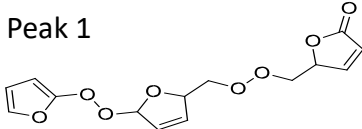
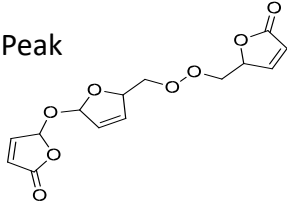
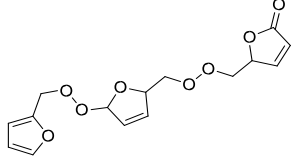


Figure IV.11: Chromatogram (ESI-LC-QTOF-MS analysis) of the SOA formed from the gas-phase reaction of 2-MF with  $\text{NO}_3$  radical. The compounds corresponding to the labelled peaks are displayed in Table IV.6.

The major compounds (relative abundance higher than 1 %) detected in the SOA are listed in Table IV.6 with their masses corresponding to the  $[\text{M}+\text{NH}_4]^+$  product ions. The relative abundances were determined from the ratio of the sum of the chromatographic areas of the peaks of the different isomers to the sum of the chromatographic areas of all the peaks. This strategy assumes that every chemical compound detected by the mass spectrometer produces the same response.

Table IV.6: Compounds detected in the SOA formed from the reaction of 2-MF with NO<sub>3</sub> radical in the particulate phase (ESI-LC-QToF-MS/MS analyses). The main fragments observed by MS/MS analyses and the relative abundance of each detected compound (in %) are also presented.

Molecular ion	Main Fragments	Brut Formula with its adduct	Probability of molecular formula (%)	Structure	R (%)
214.0720	[C <sub>5</sub> H <sub>5</sub> O <sub>2</sub> ] <sup>+</sup> [C <sub>4</sub> H <sub>3</sub> O <sub>2</sub> ] <sup>+</sup> [C <sub>4</sub> H <sub>5</sub> O] <sup>+</sup>	([C <sub>9</sub> H <sub>8</sub> O <sub>5</sub> ]+NH <sub>4</sub> ) <sup>+</sup>	95.28		8.13
230.0665	[C <sub>9</sub> H <sub>7</sub> O <sub>5</sub> ] <sup>+</sup> [C <sub>5</sub> H <sub>5</sub> O <sub>3</sub> ] <sup>+</sup> [C <sub>4</sub> H <sub>3</sub> O <sub>2</sub> ] <sup>+</sup> [C <sub>3</sub> H <sub>3</sub> O] <sup>+</sup>	([C <sub>9</sub> H <sub>8</sub> O <sub>6</sub> ]+NH <sub>4</sub> ) <sup>+</sup>	98.41		1.11
228.0872	[C <sub>5</sub> H <sub>7</sub> O <sub>3</sub> ] <sup>+</sup> [C <sub>5</sub> H <sub>5</sub> O <sub>2</sub> ] <sup>+</sup> [C <sub>4</sub> H <sub>5</sub> O] <sup>+</sup>	([C <sub>10</sub> H <sub>10</sub> O <sub>5</sub> ]+NH <sub>4</sub> ) <sup>+</sup>	98.59		0.96
244.0820	[C <sub>5</sub> H <sub>5</sub> O <sub>2</sub> ] <sup>+</sup> [C <sub>5</sub> H <sub>5</sub> O <sub>3</sub> ] <sup>+</sup> [C <sub>4</sub> H <sub>5</sub> O <sub>2</sub> ] <sup>+</sup> [C <sub>4</sub> H <sub>5</sub> O] <sup>+</sup> [C <sub>2</sub> H <sub>3</sub> O <sub>2</sub> ] <sup>+</sup>	([C <sub>10</sub> H <sub>10</sub> O <sub>6</sub> ]+NH <sub>4</sub> ) <sup>+</sup>	99.69		30.92
328.1033	[C <sub>10</sub> H <sub>11</sub> O <sub>5</sub> ] <sup>+</sup> [C <sub>9</sub> H <sub>9</sub> O <sub>4</sub> ] <sup>+</sup> [C <sub>5</sub> H <sub>5</sub> O <sub>3</sub> ] <sup>+</sup> [C <sub>5</sub> H <sub>7</sub> O <sub>2</sub> ] <sup>+</sup> [C <sub>4</sub> H <sub>3</sub> O <sub>2</sub> ] <sup>+</sup>	([C <sub>10</sub> H <sub>10</sub> O <sub>6</sub> ]+NH <sub>4</sub> ) <sup>+</sup>	98.76	Peak 1 	1.18
				Peak 	2.82
342.1197	[C <sub>10</sub> H <sub>11</sub> O <sub>5</sub> ] <sup>+</sup> [C <sub>5</sub> H <sub>5</sub> O <sub>3</sub> ] <sup>+</sup> [C <sub>5</sub> H <sub>5</sub> O] <sup>+</sup> [C <sub>4</sub> H <sub>5</sub> O <sub>2</sub> ] <sup>+</sup>	([C <sub>15</sub> H <sub>16</sub> O <sub>8</sub> ]+NH <sub>4</sub> ) <sup>+</sup>	94.34		2.13

The fragments used to identify the product chemical structure are also listed in the table. Figure S8 displays the peaks (M + NH<sub>4</sub>)<sup>+</sup> of one identified product and the corresponding fragments obtained upon increasing fragmentation energy. Since the SOA was sampled after the complete consumption of 2-MF by NO<sub>3</sub>, this means that it is more probable that they were formed into the chamber from reactions in the gas- and/or in the particulate- phase(s) than formed on the sampling filter. A set of gas phase ROOR' formation is proposed from peroxy radicals (RO<sub>2</sub> + R'O<sub>2</sub>) reactions to explain the determined structures. In our reactions, the formation of these products is probable due to the large RO<sub>2</sub> radicals that can have higher



vibrational modes. These modes help in distributing collisional energy through ROOR' molecule preventing its breakage. Figure S9 shows the RO<sub>2</sub> radicals or the second-generation products (labelled in gray) that can lead to the formation of these products.

#### IV.2.3.2.3 IR absorption of SOA with ATR

Figure IV.12 shows the ATR spectrum of the SOA formed from the NO<sub>3</sub> initiated oxidation of 2-MF. Note that quartz substrates used for recording the spectra do not transmit IR light between 870 – 1260 cm<sup>-1</sup> and thus, this region is not shown in the graph for clarity purposes. Three major absorption bands can be observed. The first absorption band is observed between 780-820 cm<sup>-1</sup>, assigned to the –ONO<sub>2</sub>– vibration modes providing with evidence for the formation of organic nitrates. There is also an absorption band in the region 1270 – 1310 cm<sup>-1</sup> that can be similarly attributed to the presence of organic nitrates and is assigned to the vibrations of O–NO<sub>2</sub> functional groups. Finally, there is a broad absorption band between 1590 – 1880 cm<sup>-1</sup> assigned to the presence of carbonyl functional groups. All the main absorption features of the ATR spectrum are in excellent agreement with the gas phase IR residual spectrum, indicating the presence of similar functional groups in both gas and particulate phases. In addition, in Figure IV.12 is shown the overlap of the solar irradiance spectrum measured at the Earth's surface. Interestingly, we can observe that the SOA are absorbing radiation in the actinic window reaching Earth's surface. Although quantitative contribution of SOA formation cannot be extracted, due to the IR spectrum quality, it is clear that the absorption features around 870 cm<sup>-1</sup> will strongly interfere with the solar irradiance. The rest of the features observed shows that SOA do not absorb within the atmospheric window and thus these bands contribution is expected to have a minor impact in atmospheric irradiance.

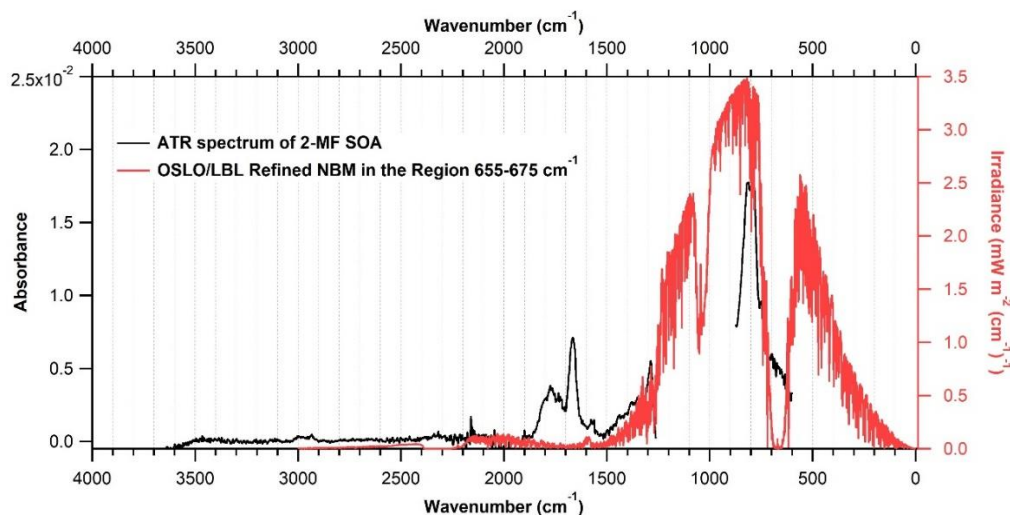


Figure IV.12: ATR spectrum (in black) of SOA formed from the NO<sub>3</sub> initiated oxidation of 2-MF. SOA were collected on quartz filter. The atmospheric irradiance spectrum is also given in the graph, to evaluate the formed SOA as potent radiative species.

#### IV.2.4 Reaction phase mechanism

Very scarce studies have been performed to study the gas-phase reaction of methylated furan compounds with NO<sub>3</sub> radical (Berndt et al., 1997; Tapia et al., 2011; Joo et al., 2019). To our knowledge, there is only two studies describing the nocturnal reactivity of 3-methyl furan with

this oxidant (Tapia et al., 2011; Joo et al., 2019a) and no literature data is available on 2-MF oxidation.

The products formed in the gas phase from the 2-MF reaction with  $\text{NO}_3$  as well as the article on the 3-MF reactivity (Joo et al., 2019b) were used to propose a chemical reaction mechanism (Figure IV.13).

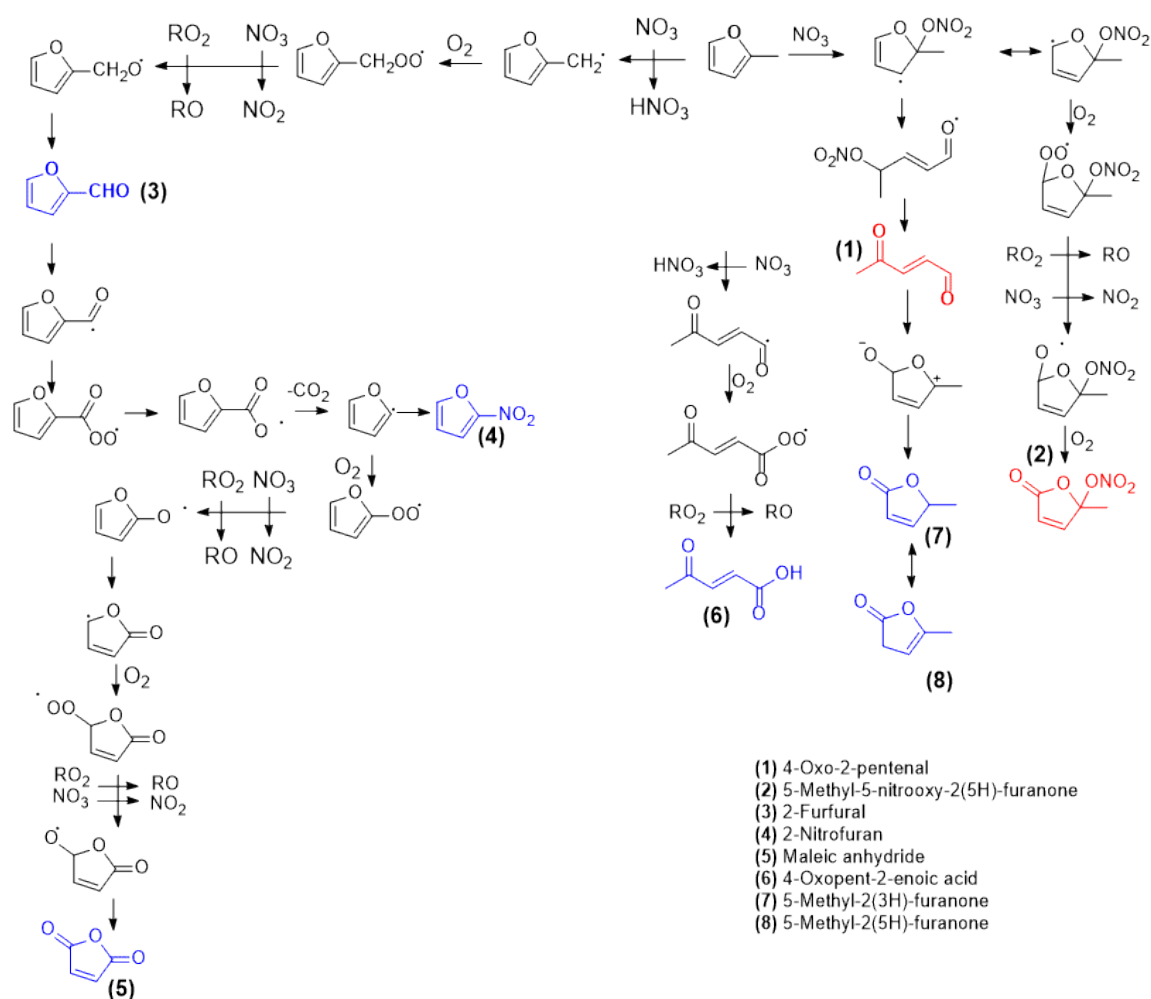


Figure IV.13: Mechanism for the reaction of 2-MF with  $\text{NO}_3$  yielding to the different products detected by different analytical techniques. Major products are colored in red and minor are colored in blue.

The reaction of 2-MF with  $\text{NO}_3$  can start by two primary pathways: (i) either  $\text{NO}_3$  addition to the carbon atoms C-2 or C-5 of the ring or (ii) by hydrogen atom abstraction from the methyl group attached to the ring. At room temperature, the addition is the dominant pathway due to the higher stability of the adduct formed than the intermediate formed from H-abstraction. According to our measurements, the yield of abstraction pathway which is linked to the formation of 2-furfural (Figure IV.13), is < 1% and < 5% based on the GC-EI-MS and FTIR analyses, respectively.

The carbon atoms C-2 and C-5 are favoured for the  $\text{NO}_3$  addition on the ring due to the formation of the resonance-stabilized intermediate radical (Tapia et al., 2011; Joo et al., 2019).

The cyclic nitrooxyalkyl radical can undergo ring opening, followed by rearrangement and  $\text{NO}_2$  loss to form the unsaturated dicarbonyl which is 4-oxo-2-pentenal (**1**) that is observed with a yield of  $61.5 \pm 14.7$  %. According to literature, dicarbonyls are among the major oxidation products of furanoids by OH and  $\text{NO}_3$  (Bierbach et al., 1995; Berndt et al., 1997; Gómez Alvarez et al., 2009; Aschmann et al., 2011; Tapia et al., 2011; Aschmann et al., 2014b; Joo et al., 2019a).

The formation of the other first generation major product 5-methyl-5-nitrooxy-2(5H)-furanone (**2**) is also linked with the addition pathway, and its yield is estimated to be  $26 \pm 3$  %. It can be formed by the reaction of cyclic nitrooxyalkyl radical with  $\text{O}_2$  to form cyclic nitrooxyperoxy radical. The latter will react with  $\text{NO}_3$  /  $\text{RO}_2$  to form the corresponding nitroalkoxy radical, which will react with  $\text{O}_2$  to form 5-methyl-5-nitrooxy-2(5H)-furanone (**2**). Further reaction of the primarily formed organic nitrates with  $\text{NO}_3$  radicals could also lead to the formation of organic dinitrates, species that were detected based on FTIR analysis and quantum chemical calculations (not shown in the reaction mechanism). This pathway leading to the formation of cyclic nitrooxy carbonyl product which is 5-methyl-5-nitrooxy-2(5H)-furanone (**2**) as one of the major products was also validated by Tapia et al., (2011) and Joo et al., (2019) in the analysis of the products of 3-MF reaction with  $\text{NO}_3$ .

The formation of 2-furfural (**3**) can be explained by H-atom abstraction from methyl group of 2-MF to form 2-MF radical. This radical then react with  $\text{O}_2$  to form the corresponding peroxy radical. This latter radical can react with other peroxy radicals, or  $\text{NO}_2$  to form alkoxy radicals which will in turn react with  $\text{O}_2$  to form 2-furfural. H-atom abstraction from the methyl group was shown to be a minor process in previous studies performed on the atmospheric gas-phase reaction of 3-MF with  $\text{NO}_3$  (Tapia et al., 2011). H-abstraction directly from the furan ring had been validated to be negligible (Clifford et al., 2005; Colmenar et al., 2012).

In the reaction of 2-furfural with  $\text{NO}_3$  radical, the presence of the CHO group (mesomere acceptor) on the furan ring deactivates the carbon atoms C-3 and C-5 and decrease the probability of being attacked by  $\text{NO}_3$ . In addition, C-5 is hindered by the carbonyl group attached to it which even makes the attack less probable. For that reason, although  $\text{NO}_3$  attack to both C-2 and C-5 will lead to the formation of resonance stable intermediate, but  $\text{NO}_3$  addition will be favoured on C-2. A similar mechanism was proposed by Colmenar et al., (2012) who studied the reaction of 2-furfural with  $\text{NO}_3$  and was theoretically confirmed by Zhao & Wang, (2017) who studied 2-furfural reaction with OH.

The second pathway can occur by H-atom abstraction from the carbonyl group. As a result, 2-Nitrofuran (**4**) can also be formed from the decarboxylation of furfural. Maleic anhydride (**5**) is identified by all analytical techniques used (PTR-ToF-MS, SIFT-MS, GC-EI-MS). This compound can be formed from H-abstraction from the aldehyde group of furfural followed by the reaction of the resulting radical with  $\text{O}_2$  to form a peroxy radical. Then, this radical either reacts with another  $\text{RO}_2$  or with NO to form the corresponding alkoxy radical. When the alkoxy radical undergoes decarboxylation ( $-\text{CO}_2$ ), maleic anhydride can be formed according to the detailed steps shown in Figure IV.13.

Another possible pathway for the formation of maleic anhydride is from the  $\text{NO}_3$  addition on the C-5 carbon atom and the formation of the corresponding alkoxy radical which will undergo rearrangement and  $\text{NO}_2$  loss to form maleic anhydride. 4-Oxo-2-pentenal can undergo H-abstraction from the aldehyde group leading to the formation of an acylperoxy radical. This pathway is favoured over the addition of  $\text{NO}_3$  to the double bond, since the presence of the aldehydic group decreases the C=C double bond reactivity (Joo et al., 2019a). The acylperoxy radical can react with  $\text{RO}_2$  to form 4-oxopent-2-enoic acid (**6**).

5-methyl-2(3H)-furanone (**7**) is also identified by the various analytical techniques used. This molecule may be formed by intramolecular isomerization of 4-oxo-2-pentenal as described in the mechanism. This pathway is favoured due to the presence of  $\text{HNO}_3$  which stabilizes the zwitterionic intermediate. This pathway was also proposed by Tapia et al., (2011). 5-methyl-2(5H)-furanone (**8**) is also identified in the oxidation products and its formation can be explained by the tautomerization of 5-methyl-2(3H)-furanone. The proposed reaction pathways leading to their formation are in accordance with the literature (Joo et al., 2019a) Tapia et al., (2011) and are presented in Figure IV.13.

#### IV.2.5 3-Methylfuran reaction with $\text{NO}_3$

##### *IV.2.5.1 Qualitative identification of the products (Td-GC-EI-MS chromatograms)*

The reaction of 3-MF with  $\text{NO}_3$  was been thoroughly studied in literature (Tapia et al., 2011; Joo et al., 2019b) where they provided quantitative and qualitative characterization for the products of the reaction. In this study, only qualitative products analysis for 3-MF reaction is provided which was done using the TD-GC-EI-MS during the reaction in CHARME. The objective was to evaluate whether the gas phase products identified in CHARME are in accordance with those observed in literature. Figure IV.14 shows typical chromatogram of the products of the title reaction.

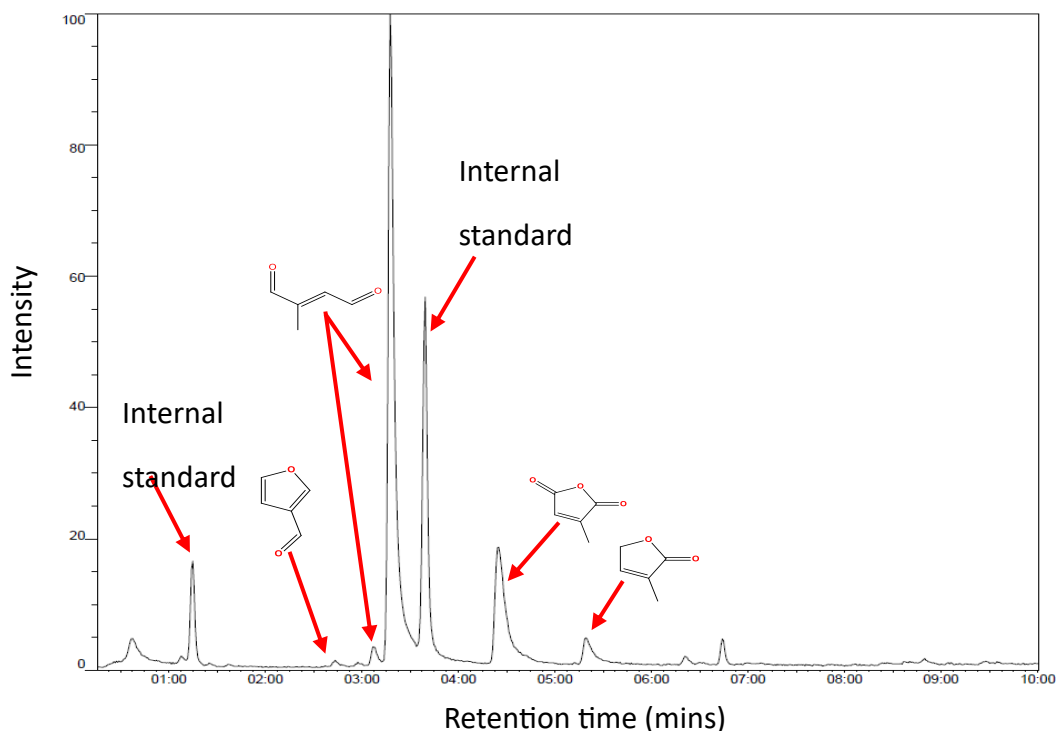


Figure IV.14: Chromatogram (Td-GC-EI-MS) of the gas-phase products formed from the gas-phase reaction of 3-MF with  $\text{NO}_3$  radicals. The peaks are labelled with their chemical structures identifications.

#### IV.2.5.2 Mechanism of 3-MF reaction with $\text{NO}_3$ radicals as proposed in literature

In both Tapia et al., (2011) and Joo et al., (2019a) studies, the first reaction step involves the  $\text{NO}_3$  addition to the C-2 or C-5 position of 3-MF which will lead to the formation of the unsaturated dicarbonyl which is 2-methylbutenedial in this case. This product formation is validated in our experiment. According to literature, 3-Furfural is a minor product formed by H-abstraction from the methyl group attached to the furan ring. In our experiments, the presence of this product in the reaction mixture is validated. Joo et al proposed the formation of a major product which is 2-methyl-5-nitrooxy-2(5H)-Furanone, however in our GC analyses we were not able to detect this compound which may be due to its decomposition / fragmentation in the GC-EI-MS analyses. The reaction of 2-methylbutenedial with  $\text{NO}_3$  leads to the formation of secondary products which were also identified by Joo et al., (2019b). These products are 2,5-furandione,3-methyl and 3-methyl-2(5H)-furanone. To clarify, 2,5-furandione,3-methyl can be produced from H-abstraction of the carbonyl group of 2-methylbutenedial, but the rearrangement of the latter product can form 3-methyl-2(5H)-furanone. Figure IV.15 shows the mechanism of the reaction proposed by Joo et al., (2019a).

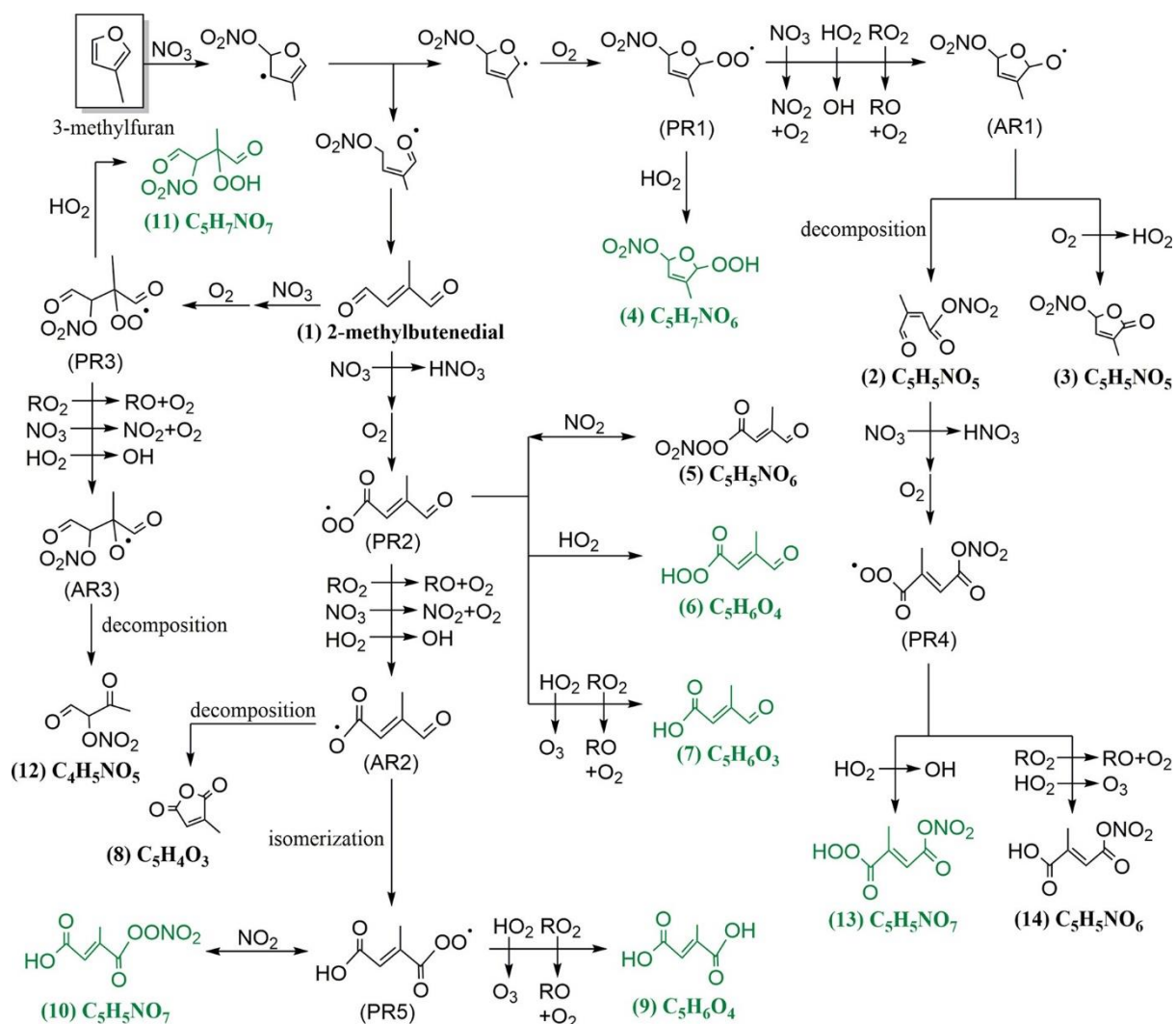


Figure IV.15: Proposed mechanism for 3-methylfuran oxidation by  $\text{NO}_3$  radicals.  $\text{NO}_3$  can be added to 2 or 5 position, but addition to 5 position is shown here as the representative case (Joo et al., 2019b).

## IV.2.6 2,5-DMF reaction with $\text{NO}_3$

### IV.2.6.1 Insights from the offline analysis of the gas mixture-qualitative identification of the products (TD-GC-EI-MS, GC-EI-MS)

Similarly, to the previous reactions, TD-GC-EI-MS analysis were also performed to identify the gas-phase oxidation products of the reaction between 2,5-DMF with  $\text{NO}_3$ . Figure IV.16 displays the typical chromatogram of the gas-phase products formed after the complete reaction of 2,5-DMF with  $\text{NO}_3$ , where the peaks are labelled with the corresponding species identified. The formation of 5-methylfurfural, maleic anhydride and 5-methyl-2(3H)-furanone is validated by comparing their retention times to that of the commercial standards. Analysis of the gas-phase products adsorbed on the monotraps and solubilized in the bubbler was also performed to complete the results provided by the TD-GC-EI-MS and remove any possible misinterpretation due to the decomposition of organic nitrates. The products observed using both the online and the offline analyses are presented in Table IV.7.

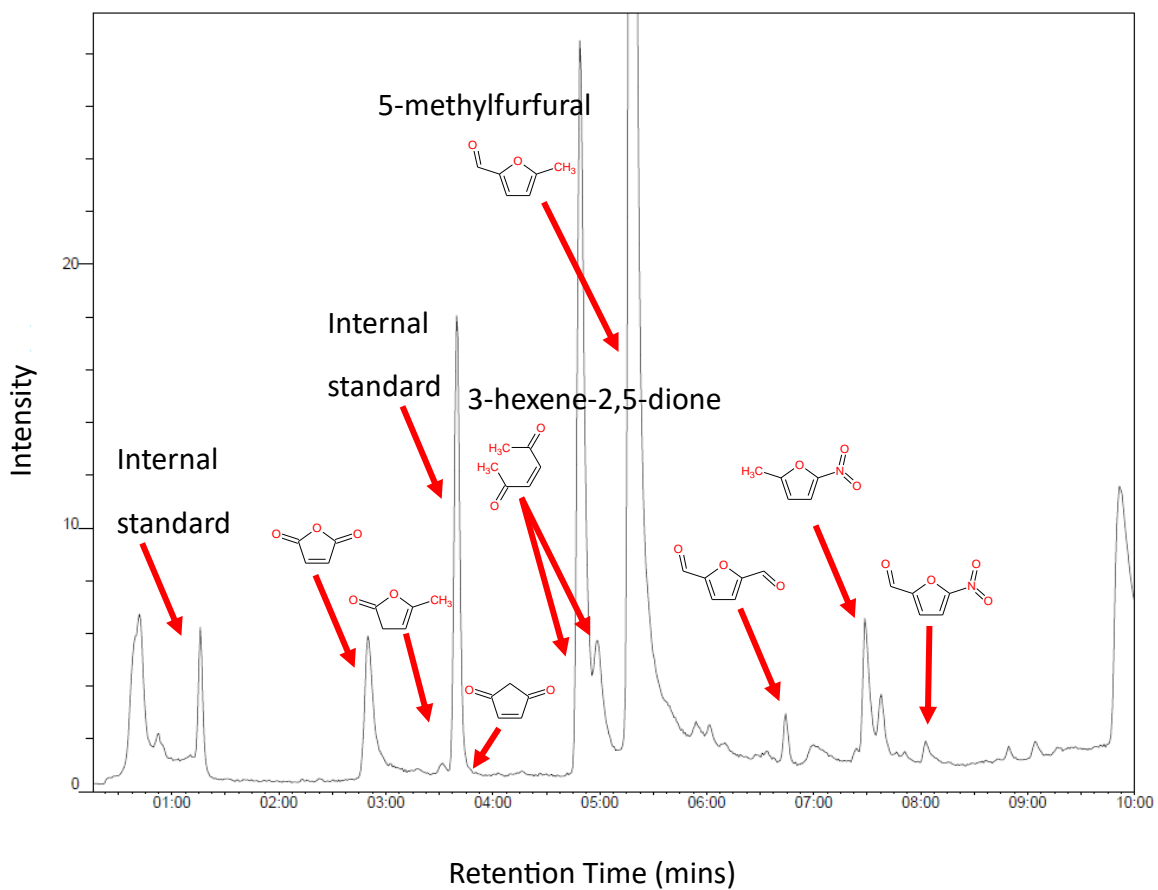
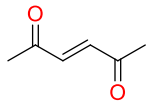
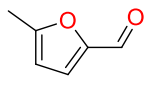
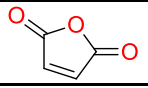
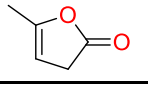
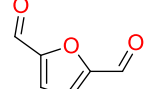
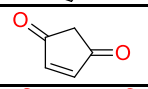
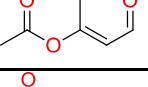
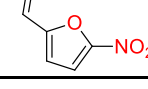
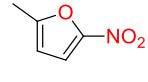
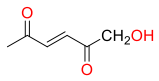
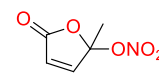
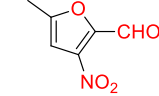
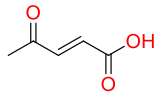


Figure IV.16: Chromatogram (Td-GC-EI-MS) of the gas-phase products formed from the gas-phase reaction of 2,5-DMF with  $\text{NO}_3$  radicals. The peaks are labelled with their chemical structures identifications.

Table IV.7: Products of the reaction of 2,5-DMF with NO<sub>3</sub> identified using different sampling and analytical techniques (products numbers are related to their numbering on the mechanism figure).

Product	Structure	m/z <sup>1</sup>	PTR-ToF-MS <sup>2</sup>	SIFT-MS <sup>3</sup>	TD-GC-EI-MS <sup>2</sup>	GC-EI-MS		
						Monotrap <sup>2</sup>	Bubbler <sup>2</sup>	
							Acetonitrile	Methanol
3-hexene-2,5-dione		111.0	√	√	√	√	√	√
5-methylfurfural		113.0	√	√	√	√	√	√
Maleic anhydride		99.0	√	√	√	√	√	√
5-methyl-2(3H)-furanone		99.0	√	√	√		√	√
2,5-furandicarboxaldehyde		125.0			√	√	√	√
2-Cyclopentene-1,4-dione		97.0	√	√	√	√	√	√
4-Oxobut-2-en-2-yl acetate		129.0	√	√		√	√	√
5-Nitro-2-furfural		142.0		√	√	√	√	√
2-Methylfuran-5-nitro		128.0			√			



1-Hydroxy-3-hexene-2,5-dione		129.0			√	√		
5-Methyl-5-nitrooxy-2(5H)-Furanone		160.0	√		√		√	
3-Nitro-5-methylfurfural		156.0					√	
β-Acetylacrylic acid		115.0	√	√			√	

<sup>1</sup>  $m/z$  is the mass of the compound measured by PTR-ToF-MS/ SIFT-MS, it includes +1 of ionization by  $H_3O^+$ .

<sup>2</sup> Results obtained in CHARME.

<sup>3</sup> Results obtained in THALAMOS.

#### *IV.2.6.2 Insights from the online analysis (PTR-ToF-MS/SIFT-MS) of the gas mixture- temporal variation of the reactant and products and yields estimated*

To study quantitatively the products resulting from the gas phase oxidation of 2,5-DMF with  $\text{NO}_3$ , a series of five experiments were conducted in CHARME chamber at room temperature ( $294 \pm 2$  K), atmospheric pressure and under dark conditions. Reactants and products were continuously monitored with PTR-ToF-MS, and 2,5-DMF was rapidly oxidized by  $\text{NO}_3$  forming several oxidation products. The time profile of the reactants and products is presented in Figure IV.17, with the list of the masses monitored presented in Table IV.8.

The mass peak detected with the PTR-ToF-MS at  $m/z = 111.0$  is attributed to 5-methylfurfural and was validated in separate experiments by introducing the standard of the compound in the chamber. Nevertheless, possible contribution from the fragmentation of organic nitrates cannot be excluded (similar to what observed in the case of 2-MF). The mass peak detected at  $m/z = 113.0$  corresponds to the unsaturated dicarbonyl 3-hexene-2,5-dione.

These product concentrations exhibited a continuous increase throughout the experiment until reaching a plateau. It is interesting to note that after around 50% of 2,5 DMF consumption, 5-methylfurfural concentrations deviate from linearity, that indicate secondary losses of this compound in the chamber. It could be either reaction with  $\text{NO}_3$  radicals, competitive with that of 2,5-DMF +  $\text{NO}_3$  radicals, which is in contradiction with the literature study of Colmenar et al., (2012) where the rate coefficient of 5-methylfurfural was reported to be 10 times lower slower than 2,5 DMF. A second explanation is the partitioning of this compound on the aerosols formed, in the chamber, where their absolute mass increase with DMF consumption.

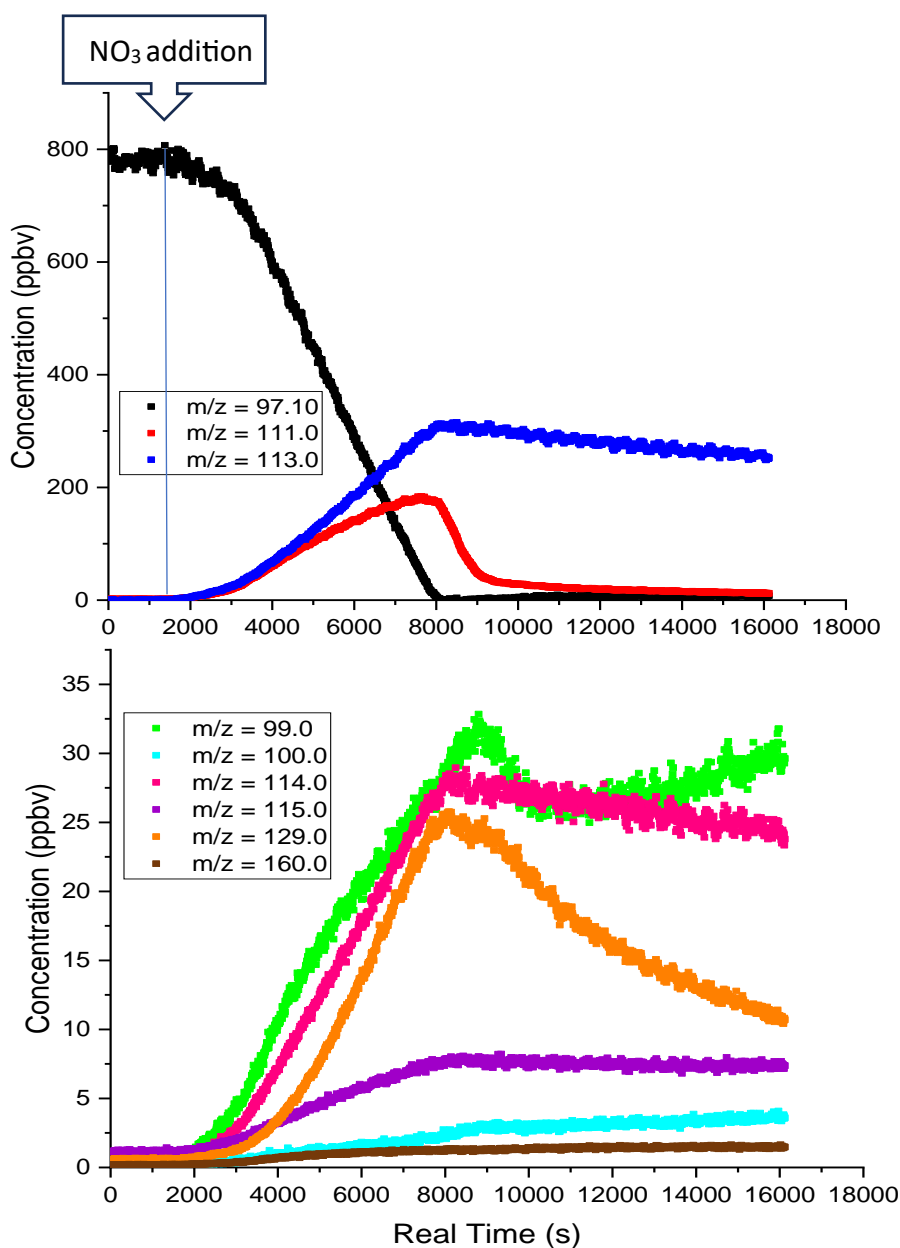


Figure IV.17: (a) Typical time profiles of masses detected by PTR-ToF-MS during the oxidation of 2,5-DMF (initial concentration = 800 ppbv), 2,5-DMF ( $m/z = 97.10$ ), major products:  $m/z = 111.0$  and  $m/z = 113.0$ . (b) time profile of the minor oxidation products. Note that  $m/z$  includes +1 corresponding to ionization by  $H^+$ .

The PTR-ToF-MS was calibrated by introducing known concentrations of 2,5-DMF and 5-methylfurfural into CHARME. In the case of other products formed, concentrations were calculated using a generic  $H_3O^+$  rate coefficient for their protonation reaction which is equal to  $2 \times 10^{-9} \text{ cm}^3 \text{ molecule}^{-1} \text{ s}^{-1}$ . Typical yield plots of the major and minor products formed are shown in Figure IV.18. As displayed, not all data points were considered to calculate the product yields (only slopes at the origin) and the resulting yields are displayed in Table IV.8.

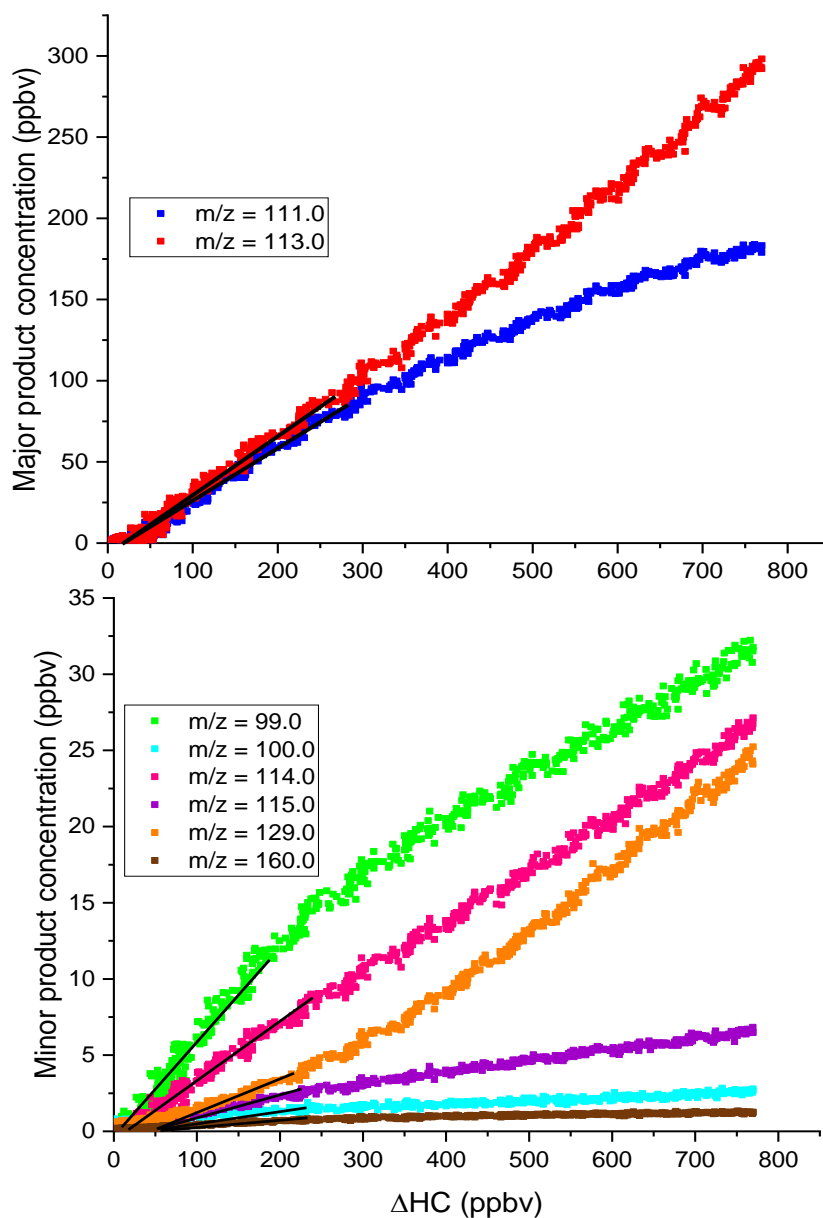


Figure IV.18: Typical plots for the determination of the gas-phase products yields formed from the reaction of 2,5-DMF with  $\text{NO}_3$  (a) major oxidation products (b) minor oxidation products.

Interestingly, the yields of the major products identified ( $m/z$ : 111.0, 113.0, 99.0), were slightly but systematically increased with 2,5-DMF concentration in the chamber. Although it is quite surprising, considering that only the linear part of the slopes was taken into account for the calculations of the yields, it could be related to secondary reactions occurring in the chamber. A possible explanation could be the fast reaction of these products with  $\text{NO}_3$  radicals, that could lead to underestimation of their yield under low 2,5-DMF concentrations. Nevertheless, the kinetic profiles of the products formed and shown in Figure IV.18 indicate that the reactivity towards  $\text{NO}_3$  is different for each species, and thus cannot explain the up to 20% systematic increase in the yields for all major species with increasing 2,5-DMF concentration. Still this increase is unclear.

Considering the experimental uncertainties, as shown in Table IV.8 equivalent yields of 5-methylfurfural and 3-Hexene-2,5-dione were monitored. Interestingly, the yield of 3-hexene-2,5-dione ( $41.9 \pm 4.9 \%$ ) formation from the reaction of 2,5-DMF with  $\text{NO}_3$ , is 40% higher than the corresponding yield obtained upon 2,5-DMF reaction with OH radicals,  $25.0 \pm 4.0 \%$  (Aschmann et al., 2011, 2014b). The  $m/z = 99.0$  is attributed to two products of the reaction, maleic anhydride and 5-Methyl-2(3H)-furanone where the yield of formation is estimated to be  $8.1 \pm 2.1 \%$ . All other products were identified with yield lower than 1%. The pathways leading to the formation of all the products is presented in the mechanism in Figure IV.21.

Table IV.8: Identification and formation yields of the products formed from the reaction of 2,5-DMF with NO<sub>3</sub> (m/z masses include the addition of H<sup>+</sup>).

Experiment number	[2,5-dimethylfuran] (ppbv)	m/z = 111.0 5-methylfurfural	m/z = 113.0 3-Hexene-2,5-dione	m/z = 99.0 Maleic anhydride / 5-Methyl-2(3H)-furanone	m/z = 114.0 5-methyl-5-nitrate-2(5H)-Furanone	m/z = 115.0 β-Acetylacrylic acid	m/z = 129.0 4-oxobut-2-en-2-yl acetate	m/z = 160.0 5-methyl-5-nitrooxy-2(5H)-Furanone
1	428	32.8	35.2	7.4	4.6	1.4	1.6	<1.0
2	860	29.7	33.8	5.5	3.4	1.0	0.5	<1.0
3	1300	34.7	35.4	5.8	3.8	0.9	0.4	<1.0
4	1100	38.1	39.8	7.9	5.3	1.4	1.8	<1.0
5	1900	39.9	44.3	10.1	5.2	1.3	2.2	<1.0
Average Yield (%)		35.0 ± 4.1	37.7 ± 4.3	7.3 ± 1.9	4.4 ± 0.8	1.2 ± 0.2	1.3 ± 0.8	<1.0

Product analysis was also performed in THAMALOS chamber, deploying the SIFT-MS as detection technique. The objective was to get more insights about the species formed and confirm the formation of 5-methylfurfural formation excluding any possible fragmentation organic nitrates in PTR- ToF-MS as in the case of the reaction  $2MF + NO_3$ . The first group of experiments involved the injection of 5-methylfurfural standard in THALAMOS to identify the characteristic mass peaks for each precursor ion. SIFT-MS was operated in mass scan mode and Figure IV. 19 shows the mass spectra collected. Three major masses were obtained for this molecule which are  $m/z = 110.0$  with  $NO^+$  and  $O_2^+$  and  $m/z = 111.0$  with  $H_3O^+$ . The relative ratio of these peaks is as follows  $\frac{I_{111}^{H_3O^+}}{I_{110}^{NO^+}} = 0.92$ ,  $\frac{I_{111}^{H_3O^+}}{I_{110}^{O_2^+}} = 0.96$  and  $\frac{I_{110}^{NO^+}}{I_{110}^{O_2^+}} = 1.04$  and are unique for this compound.

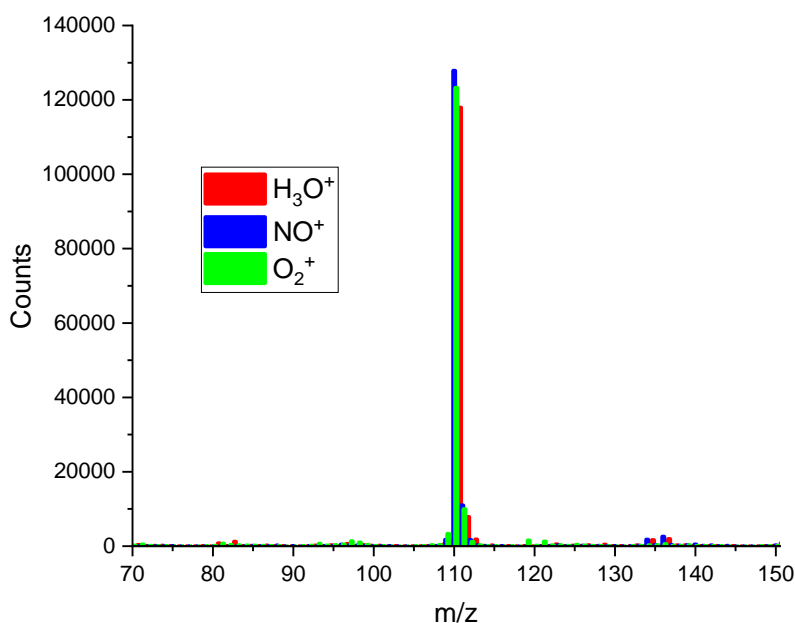


Figure IV. 19: Mass scan of 5-methylfurfural standard using the SIFT-MS coupled to THALAMOS using the three precursor ions:  $H_3O^+$  (red),  $NO^+$  (blue),  $O_2^+$  (green).

Thereafter experiments were carried out, where  $\approx 2$  ppmv of 2,5-DMF were injected in the chamber and allowed to react with  $NO_3$  until its complete consumption. With the SIFT-MS, the temporal variation of the reaction mixture composition was followed, and similar profiles were obtained with those obtained for this reaction using CHARME chamber. The major mass peaks identified at  $m/z 111.0$  with  $H_3O^+$  and at  $m/z 110.0$  for  $NO^+$  and  $O_2^+$  corresponds to 5-methylfurfural. Interestingly, the ratios of 5-methylfurfural standard are in agreement with

the ratios of these masses in the mass scan of the products which are as follows  $\frac{I_{111}^{H_3O^+}}{I_{110}^{NO^+}} = 1.0$ ,

$\frac{I_{111}^{H_3O^+}}{I_{110}^{O_2^+}} = 1.1$  and  $\frac{I_{110}^{NO^+}}{I_{110}^{O_2^+}} = 1.1$  validating the formation of 5-methylfurfural from this reaction with

a significant yield. 3-Hexene-2,5-dione is detected at  $m/z 113.0$  upon ionization with  $H_3O^+$  and at  $m/z 112.0$  upon ionization with  $NO^+$  and  $O_2^+$ . Several other masses were also detected with SIFT-MS as shown in Figure IV.20, these masses were commonly identified by the PTR-ToF-MS and the products identified are presented in Table IV.7. Maleic anhydride is observed with  $H_3O^+$

and NO<sup>+</sup> ions at m/z = 99.0 and 128.0 respectively. With O<sub>2</sub><sup>+</sup>, it is detected at the mass peaks 42.0, 54.0 as well as at mass 99.0. However, the relative ratio of the mass peaks of the major peaks identified in MAH standard ( $\frac{I_{99}^{H_3O^+}}{I_{128}^{NO^+}}=0.15$ ,  $\frac{I_{99}^{H_3O^+}}{I_{99}^{O_2^+}}=10$ ) is different in the spectrum of the products. Therefore, other species could contribute to the specific masses. Nitric acid (HNO<sub>3</sub>) is observed with H<sub>3</sub>O<sup>+</sup> at mass peak 64.0. 4-oxobut-2-en-2-yl acetate is detected at mass peaks 129.0 and 158.0 upon ionization with H<sub>3</sub>O<sup>+</sup> and NO<sup>+</sup> respectively. 5-nitro-2-furfural can be attributed to the mass peak observed with NO<sup>+</sup> at m/z =142.0 and to fragments at m/z 97.0 with both H<sub>3</sub>O<sup>+</sup> and O<sub>2</sub><sup>+</sup>. All products masses identified with the SIFT-MS are presented in Table IV.7.



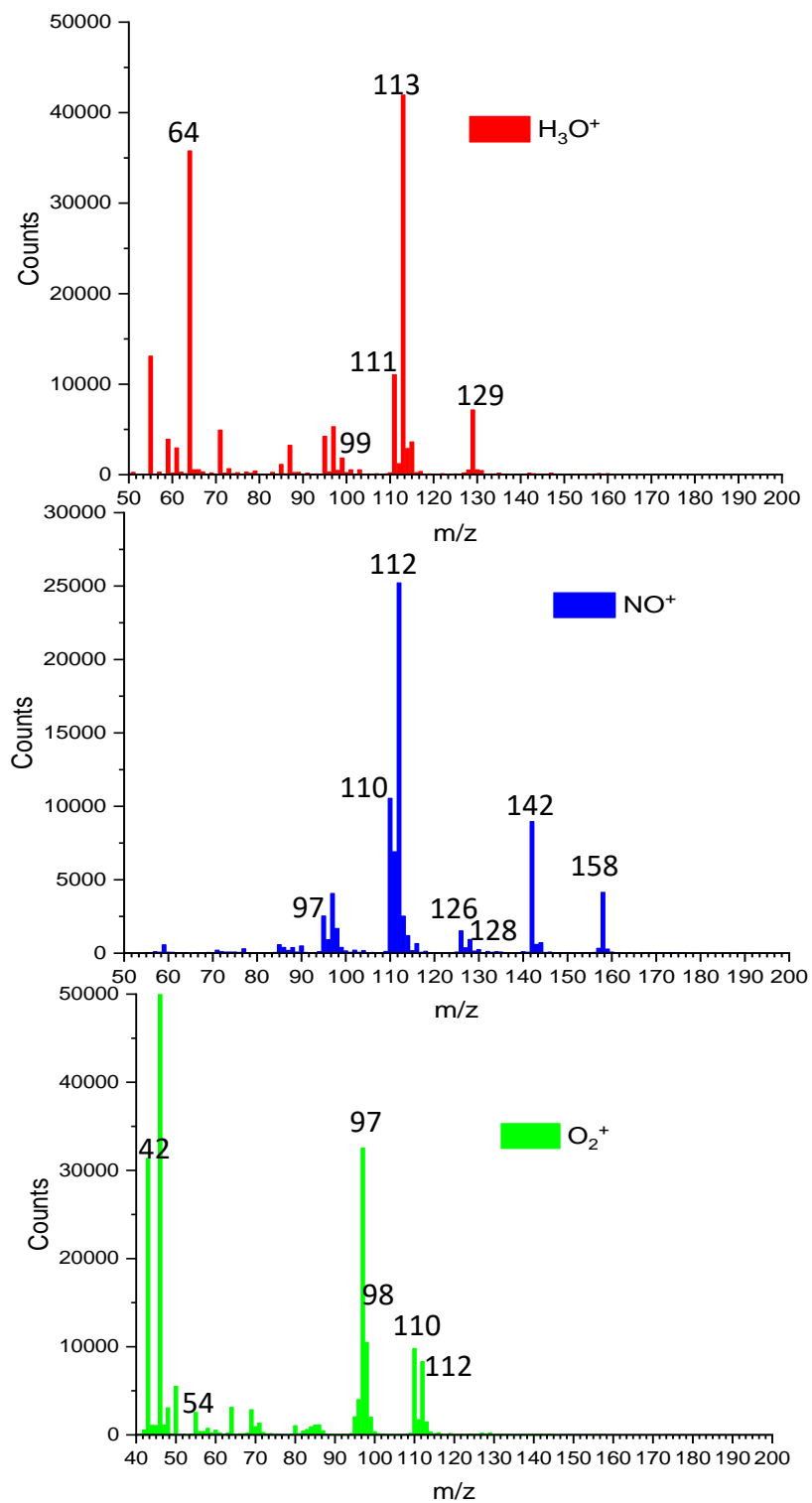


Figure IV.20: Mass scans of the products of the reaction of 2,5-DMF with  $\text{NO}_3$  obtained upon ionization using three precursor ions  $\text{H}_3\text{O}^+$ (a),  $\text{NO}^+$ (b),  $\text{O}_2^+$ (c) within SIFT-MS coupled to THALAMOS.

#### *IV.2.6.3 Variation of the yield of formation of 5-methylfurfural as function of temperature*

As mentioned in the chapter III, 9 experiments were done to measure the temperature-dependent yield of 5-methylfurfural formation from the reaction of 2,5-DMF with  $\text{NO}_3$  at temperatures between 298-353 K. 5-methylfurfural is proposed to be formed from H-abstraction from the methyl group attached to the furan ring. The objective of these experiments was twofold, to evaluate the rate coefficient of the two major pathways of the reaction ( $\text{NO}_3$  addition and H-abstraction) from one side and to validate the reaction mechanism. Table IV.9 shows the yield of 5-methylfurfural formation measured with the SIFT-MS using the three precursor ions ( $\text{H}_3\text{O}^+$ ,  $\text{NO}^+$  and  $\text{O}_2^+$ ) and the average yield. The average yield decreases from 24% to 1% as the temperature increases from 298 to 353 K. It is important to note that the room temperature yield of 5-methylfurfural measured in THALAMOS chamber is ca. 30% lower than CHARME. It is hard to explain this discrepancy. Several tests were performed to identify possible sources of uncertainties during THALAMOS experiments (e.g. wall losses in THALAMOS, calibration experiments, volume of the chamber, etc.) but still, the difference between results is 30%. In particular, to elucidate the contribution of wall losses, the standard of 5-methylfurfural was injected in the chamber, and its concentration was monitored in real-time. Wall losses were found to be in the same range as for other furanoid species. In addition, the temperature of the chamber was increased, to evaluate possible desorption of the molecule from the walls. The SIF-MS signals recorded were found to be invariant during the temperature increase. Similar conclusions were drawn during the calibration experiments. It is also important to note, that the room temperature rate coefficient measured in two chambers were in good agreement, but around 18% faster in THALAMOS. Although the differences between the rate coefficients measured in the two chambers are in the range of experimental uncertainties, it is unclear whether they are related with the discrepancy in the yields of 5-methylfurfural. Regarding the temperature dependence of the yield, it can be linked to an association mechanism. In particular, 2,5-DMF reaction with  $\text{NO}_3$  proceeds either through addition or H atom abstraction. However, the abstraction pathway, is probably linked with a formation of an intermediate (addition elimination mechanism), and not a classical direct abstraction mechanism. Therefore, the increase of temperature, the intermediate becomes less stable, (due to the higher internal energy adduct can decompose leading back to reactants), leading to a reduction of the product yield. Interestingly, at temperatures above 320 K the yield decreases significantly pointing diminishing yield of 5-methylfurfural (more difficult to stabilize through collision), which could slow down the overall reaction rate. On the contrary the adduct leading to  $\text{NO}_3$  addition to the double bonds of 2,5-DMF is slightly impacted by temperature (see chapter three). To conclude, the formation of 5-methylfurfural occurs from the addition of  $\text{NO}_3$  to C-2/C-5 of the ring followed by H-abstraction from the methyl group attached to the ring and not by direct H-abstraction. Further details on the mechanism of the reaction is provided in the following section. Information on the kinetics of the addition and the abstraction pathways for the reaction of 2,5-DMF with  $\text{NO}_3$  was presented in Chapter III.

Table IV.9: Yield of formation of 5-methylfurfural from the reaction of 2,5-DMF with NO<sub>3</sub> at temperatures between 298 and 353 K.

Temperature (K)	5-Methylfurfural Yield (%)			Average Yield (%)
	H <sub>3</sub> O <sup>+</sup>	NO <sup>+</sup>	O <sub>2</sub> <sup>+</sup>	
298	27.6	22.3	23.4	24.4 ± 1.6
303	23.6	19.5	18.9	20.7 ± 1.5
313	14.9	11.1	11.9	12.6 ± 1.2
313	15.3	11.9	12.9	13.4 ± 1.0
318	8.1	6.5	6.9	7.2 ± 0.5
320	6.0	5.2	5.2	5.5 ± 0.3
328	1.5	1.6	1.6	1.6 ± 0.1
333	1.8	1.4	1.8	1.7 ± 0.1
353	1.6	1.5	1.6	1.5 ± 0.1

#### IV.2.7 Mechanism of the reaction of 2,5-DMF with NO<sub>3</sub>

To the best of our knowledge, there are no literature data reporting the products and mechanism of 2,5-DMF reaction with NO<sub>3</sub>. The reaction mechanism proposed for the gaseous phase reaction of 2,5-DMF with NO<sub>3</sub> radical is shown in Figure IV.21 with products numbered **(1-12)**. Based on the quantification of the products and the determination of the two major ones, it can be inferred that the reaction proceeds through two primary pathways. Either NO<sub>3</sub> addition to C-2/C-5 of the ring or NO<sub>3</sub> addition followed by hydrogen abstraction from the methyl group attached to the ring. In the first case, after NO<sub>3</sub> addition, the cyclic nitrooxyalkyl radical can undergo ring opening, rearrangement and NO<sub>2</sub> loss to form the unsaturated dicarbonyl which is 3-hexene-2,5-dione **(1)**. This is also validated to be the dominant pathway in the reaction of 2,5-DMF with OH (Yuan et al., 2017). The formation of 5-methylfurfural **(2)**, is attributed to H-abstraction from a methyl group of 2,5-Dimethylfuran through addition elimination mechanism to form 2,5-Dimethylfuran radical. The latter radical then reacts with O<sub>2</sub> to form the corresponding peroxy radical. This radical can react with NO to form alkoxy radical which in turn reacts with O<sub>2</sub> to form 5-methylfurfural. H-atom abstraction from the methyl group is shown as minor process in previous literature studies in the reaction of 3-MF with NO<sub>3</sub> (Tapia et al., 2011; Cabañas et al., 2005), as well as for 2-MF reaction with NO<sub>3</sub> however in the case of 2,5-DMF its contribution, at least at room temperature is significant.

NO<sub>3</sub> addition can also lead to another primary product which is cyclic nitrooxy carbonyl which is minor in the case of the title reaction. It is formed by the reaction of cyclic nitrooxyalkyl radical with O<sub>2</sub> to form cyclic nitrooxyperoxy radical. The latter reacts with NO to form the corresponding nitroalkoxy radical which reacts with O<sub>2</sub> to form 5-methyl-5-nitrooxy-2(5H)-furanone (product with retention of configuration) **(3)**. The second corresponding resonance stable cyclic nitrooxyalkyl radical formed from the latter pathway also reacts with O<sub>2</sub> and undergo the same consecutive steps as the first radical but the decomposition undergoes ring opening leading to the formation of 4-oxo-buten-2-en-2-yl acetate **(4)** which is also a minor primary pathway.

A series of second-generation compounds can be formed from the reaction of the primary products with NO<sub>3</sub>. Some identified secondary products are produced from the reaction of 3-

hexene-2,5-dione with  $\text{NO}_3$  such as 5-methyl-2(3H)-furanone (**5**) which is formed from rearrangement of 3-hexene-2,5-dione. 5-methyl-2(3H)-furanone (**6**) can be formed from tautomerization of 5-methyl-2(3H)-furanone (**5**). 1-Hydroxy-3-hexene-2,5-dione (**7**) can be formed from the H-abstraction from one of the methyl group of 3-hexene-2,5-dione.

5-methylfurfural (**2**) undergoes fast reaction with  $\text{NO}_3$  which is visible from the reaction time profile recorded with the PTR-MS (see Figure IV.17). The latter reaction leads to the formation of several secondary products. The reaction can proceed by H-abstraction from the methyl group leading to the formation of 5-methylfurfural radical. The latter reacts with  $\text{O}_2$  to form 2,5-furandicarboxaldehyde (**8**). If 2,5-furandicarboxaldehyde undergoes further H-abstraction from one of the carbonyl groups attached to the ring, the formed radical can react with  $\text{NO}_2$  leading to the formation of 5-nitro-2-furfural (**9**). 2-methylfuran radical formed can also react with oxygen and after several steps illustrated in Figure IV.21 it may lead to the formation of maleic anhydride (**10**). If the reaction of 5-methylfurfural (**2**) with  $\text{NO}_3$  occurs by H-abstraction from the carbonyl group, decarboxylation can occur which form 2-methylfuran radical which upon reaction with  $\text{NO}_2$  forms 5-nitro-2-methylfuran (**11**). In case 5-Methylfurfural (**2**) reaction goes by  $\text{NO}_3$  addition to C-2 of the ring it can give 5-methyl-5-nitrooxy-2(5H)-Furanone (**12**) as a product. The presence of CHO group on the furan ring deactivates C-3/C-5 by induction. Eventhough, the attack of  $\text{NO}_3$  to C-5 is favored due to the stability of the intermediate by resonance. C-5 is not included in the reaction due to the hindering effect of CHO group, these facts were also validated in literature (Colmenar et al., 2012) and was theoretically confirmed (Zhao & Wang, 2017).  $\beta$ -Acetylacrylic acid (**12**) can be formed from rearrangement of 25-methyl-5-nitrooxy-2(5H)-Furanone and  $\text{NO}_2$  loss.

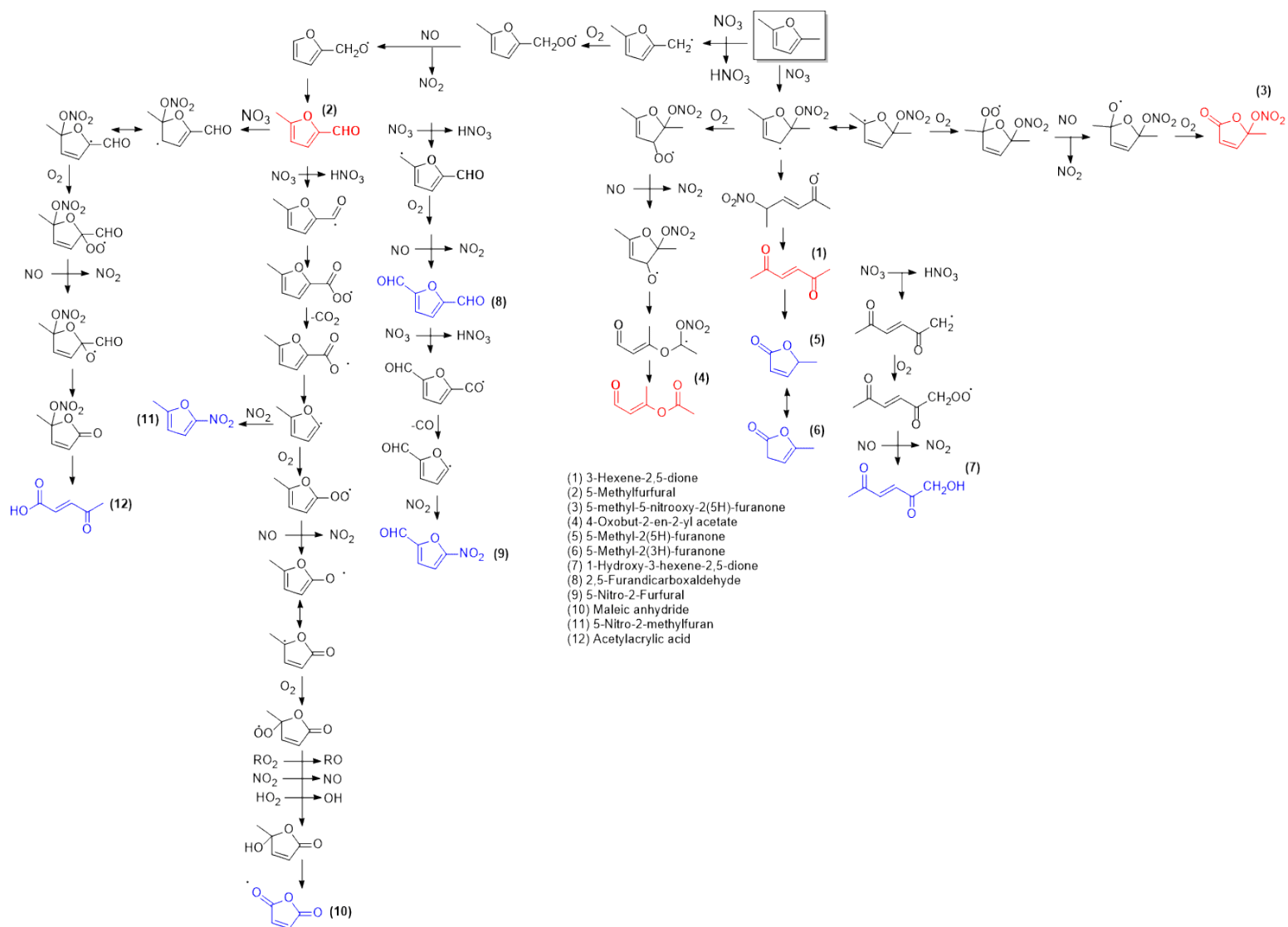


Figure IV.21: Mechanism of the reaction of 2,5-DMF with  $\text{NO}_3$ . First generation products are colored in red while the second-generation products are labelled in blue.

## IV.2.8 SOA formation from the reaction of 2,5-DMF with NO<sub>3</sub>

### IV.2.8.1 SOA yield

To investigate the SOA formation in the reaction of 2,5-DMF with NO<sub>3</sub> radicals, experiments were performed in the absence of light, relative humidity RH < 2%, at atmospheric pressure, and temperature 294 ± 2 K. The initial concentrations of 2,5-DMF ([2,5-DMF]<sub>0</sub>), as well as the reacted concentration (Δ[2,5-DMF]), the corrected mass concentrations of organic aerosols (M<sub>0</sub>) considering wall losses, and the overall yields of SOA are summarized in Table IV.10. In all experiments, 2,5-DMF was completely consumed within a time frame of 15 to 60 min, so the reacted concentrations (Δ[2,5-DMF]) represents the initial concentration ([2,5-DMF]<sub>0</sub>). All the experiments involving the investigation of SOA yields for this reaction did not include any inorganic seeds, and they were conducted until the suspended aerosol mass (M<sub>0</sub>) reached a stable state, accounting for wall losses.

Table IV.10: Experimental conditions and SOA yields for the reaction of 2,5-DMF with NO<sub>3</sub>.

Experiment number	[2,5-DMF] <sub>0</sub> (ppbv)	Δ([2,5-DMF]) (μg.m <sup>-3</sup> )	M <sub>0</sub> (μg.m <sup>-3</sup> )	Yield
1	84	332	0.1	≅ 0.0
2	338	1347	10	0.7
3	358	1431	45	3.0
4	529	2114	186	9.0
5	580	2314	216	10.0
6	703	2810	355	13.0
7	1210	4836	617	13.0

The aerosols mass concentration (M<sub>0</sub>) formed from the reaction were in the range of 0.1-617 μg.m<sup>-3</sup> corresponding to an aerosol yield of 0-13%. The aerosols yield increase with the increase of 2,5-DMF concentration until reaching a plateau which is reached at [2,5-DMF]<sub>0</sub> ≥ 2800 μg.m<sup>-3</sup>.

The simulation of Y versus M<sub>0</sub> using Odum et al., (1996) fit is presented Figure IV.22. One-product model is able to satisfactorily reproduce the experimental data (R<sup>2</sup> = 0.95) while the two-products model is not retained as it leads to high uncertainties on the values of α<sub>i</sub> and K<sub>om,i</sub> (sometimes more than 100% error). The fitting parameters α<sub>i</sub> and K<sub>om,i</sub> corresponding to the one-product semi-empirical model are (18.0 ± 1.0) × 10<sup>-2</sup> and (5.60 ± 1.3) × 10<sup>-3</sup> m<sup>3</sup>.μg<sup>-1</sup>, respectively. Many studies on SOA formation from aromatic compounds have reported that the aerosol yields data should be fitted assuming two hypothetical products (Odum et al., 1996; Song et al., 2005). However, a number of recent works have shown that the organic aerosol yields formed in aromatic photo-oxidation systems could be well described by assuming only one hypothetical product (Olariu et al., 1998; Takekawa et al., 2003; Coeur-tourneur et al., 2008; Tomas et al., 2009; Lauraguais et al., 2012). Although the organic aerosol-phase is often composed of many oxidation products, the present simulation with the one-product model indicates either that one semi-volatile organic compound is the major component of the condensed phase or that the few organics present in SOA have similar α<sub>i</sub>

and  $K_{om,i}$  values. In this latter case, the obtained constants  $\alpha_i$  and  $K_{om,i}$  would not have any intrinsic physical meaning but would rather represent mean values.

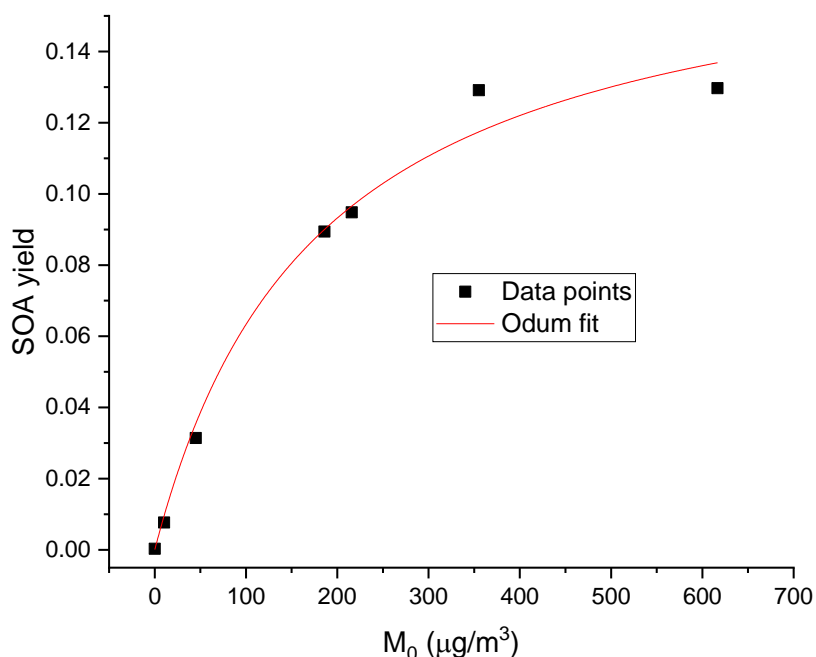


Figure IV.22: Plot of  $Y_{SOA}$  as function of  $M_0$  for the reaction of 2,5-DMF with  $\text{NO}_3$  according to the one product model developed by Odum et al.

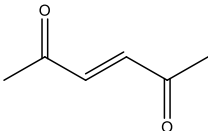
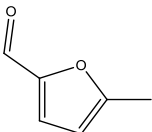
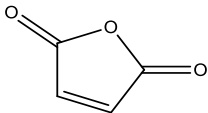
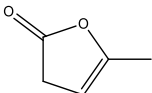
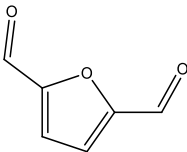
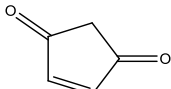
It is interesting to examine the relationship between  $\alpha$  (0.18) and the maximum SOA yield observed in Table IV.10 (0.13). The value of  $\alpha$  represents the combined quantity of semi-volatile products generated in both the gas and aerosol phases. On the other hand,  $Y$  represents the quantification of the semi-volatile products specifically formed in the particle phase. This implies that approximately 72% of the low volatile compounds produced during the 2,5-DMF reaction with  $\text{NO}_3$  radicals are transferred to the particle phase. Comparing the SOA yield obtained from the reaction of 2-MF and 2,5-DMF with  $\text{NO}_3$ , the maximum yield obtained from the reaction of 2-MF is  $\approx 2\%$  which is 6 times lower than that obtained from the reaction of 2,5-DMF which is  $\approx 12\%$ . However, it is worth mentioning that the presence of seeds (case of 2-MF) is expected to increase SOA yields (Lambe et al., 2015). Therefore, the 6-times difference that we observed between 2-MF and 2,5-DMF is a minimum (we would have got higher SOA yields for 2,5-DMF if seeds had been presented). This shows that as the number of methyl groups on the furan ring increases, the SOA yield increases too. This can be attributed to the formation of products with lower volatility. Comparing the SOA yield of formation obtained for these reactions with those formed from other VOCs such as terpenes (Fayad, 2019), furan compounds reactions are considered as low SOA source.

## IV.2.8.2 SOA composition

### IV.2.8.2.1 Identification of SOA with GC-EI-MS

SOA formed by the reaction of 2,5-DMF with  $\text{NO}_3$  was analysed using GC-EI-MS. 6 oxidation products were observed in the particulate phase (see Table IV.11): 3-hexene-2,5-dione, 5-methylfurfural, maleic anhydride, 5-methyl-2(3H)-furanone, 2,5-furandicarboxaldehyde and 2-cyclopentene-1,4-dione. All these chemical species were also present in the gas phase indicating that they are semi-volatile organic compounds and that they partition between the gas- and aerosol- phases.

Table IV.11: Names and structures of the oxidation products identified with the GC-EI-MS in the SOAs formed from the 2,5-DMF oxidation by  $\text{NO}_3$ .

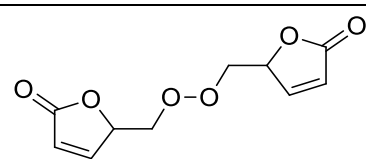
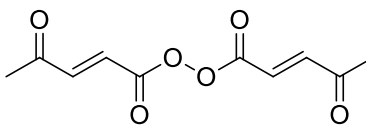
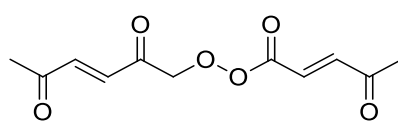
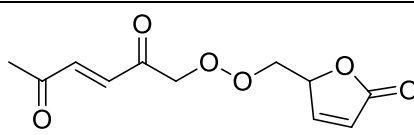
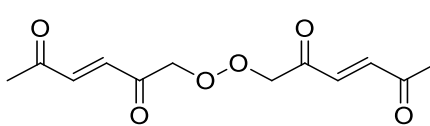
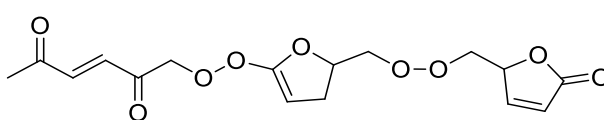
Product	Structure
3-Hexene-2,5-dione	
5-methylfurfural	
Maleic anhydride	
5-methyl-2(3H)-furanone	
2,5-Furandicarboxaldehyde	
2-Cyclopentene-1,4-dione	

### IV.2.8.2.2 Identifications of SOA with ESI-LC-QToF-MS/MS

The SOA sampled on quartz filters were also analyzed by ESI-LC-QToF-MS. Identified compounds were ionized with ammonium adducts ( $\text{NH}_4^+$ ). The major compounds (relative abundance higher than 1 %) detected in the SOA are listed in Table IV.12 with their masses corresponding to the  $[\text{M}+\text{NH}_4]^+$  product ions.



Table IV.12: Compounds detected in the SOA formed from the reaction of 2,5-DMF with NO<sub>3</sub> radical in the particulate phase (ESI-LC-QToF-MS/MS analyses). The main fragments observed by MS/MS analyses and the relative abundance of each detected compound (in %) are also presented.

Molecular Ion	Main Fragments	Brut Formula	Structure	R (%)
244.08	[C <sub>5</sub> H <sub>7</sub> O <sub>4</sub> ] <sup>+</sup> [C <sub>5</sub> H <sub>5</sub> O <sub>3</sub> ] <sup>+</sup> [C <sub>5</sub> H <sub>5</sub> O <sub>2</sub> ] <sup>+</sup>	([C <sub>10</sub> H <sub>10</sub> O <sub>6</sub> ]+NH <sub>4</sub> <sup>+</sup> )		99.92
244.08	[C <sub>5</sub> H <sub>5</sub> O <sub>3</sub> ] <sup>+</sup> [C <sub>5</sub> H <sub>5</sub> O <sub>2</sub> ] <sup>+</sup> [C <sub>4</sub> H <sub>5</sub> O] <sup>+</sup>	([C <sub>10</sub> H <sub>10</sub> O <sub>6</sub> ]+NH <sub>4</sub> <sup>+</sup> )		98.73
258.10	[C <sub>5</sub> H <sub>5</sub> O <sub>2</sub> ] <sup>+</sup> [C <sub>6</sub> H <sub>7</sub> O <sub>3</sub> ] <sup>+</sup> [C <sub>6</sub> H <sub>7</sub> O <sub>2</sub> ] <sup>+</sup>	([C <sub>11</sub> H <sub>12</sub> O <sub>6</sub> ]+NH <sub>4</sub> <sup>+</sup> )		99.65
258.10	[C <sub>4</sub> H <sub>5</sub> O <sub>2</sub> ] <sup>+</sup> [C <sub>5</sub> H <sub>5</sub> O <sub>2</sub> ] <sup>+</sup> [C <sub>5</sub> H <sub>5</sub> O <sub>2</sub> ] <sup>+</sup> [C <sub>6</sub> H <sub>7</sub> O <sub>2</sub> ] <sup>+</sup> [C <sub>6</sub> H <sub>7</sub> O <sub>3</sub> ] <sup>+</sup>	([C <sub>11</sub> H <sub>12</sub> O <sub>6</sub> ]+NH <sub>4</sub> <sup>+</sup> )		99.65
272.11	[C <sub>4</sub> H <sub>5</sub> O] <sup>+</sup> [C <sub>6</sub> H <sub>7</sub> O <sub>2</sub> ] <sup>+</sup> [C <sub>6</sub> H <sub>7</sub> O <sub>3</sub> ] <sup>+</sup>	([C <sub>12</sub> H <sub>14</sub> O <sub>6</sub> ]+NH <sub>4</sub> <sup>+</sup> )		99.92
372.13	[C <sub>4</sub> H <sub>5</sub> O] <sup>+</sup> [C <sub>4</sub> H <sub>5</sub> O <sub>2</sub> ] <sup>+</sup> [C <sub>5</sub> H <sub>5</sub> O <sub>2</sub> ] <sup>+</sup> [C <sub>6</sub> H <sub>7</sub> O <sub>2</sub> ] <sup>+</sup> [C <sub>6</sub> H <sub>9</sub> O <sub>2</sub> ] <sup>+</sup> [C <sub>11</sub> H <sub>13</sub> O <sub>5</sub> ] <sup>+</sup>	([C <sub>16</sub> H <sub>18</sub> O <sub>9</sub> ]+NH <sub>4</sub> <sup>+</sup> )		100

The fragments used to identify the product chemical structures are also listed in Table IV.12. Since the SOA was sampled just after the complete consumption of 2,5-DMF by NO<sub>3</sub>, it is more probable that these compounds were formed in the chamber from reactions in the gas- and/or in the particulate- phase(s) than formed on the filter during the sampling step. A set of gas phase accretion reactions leading to ROOR' formation is proposed. These products are formed from the peroxy radicals (RO<sub>2</sub> + R'O<sub>2</sub>) that are formed during the course of the reaction. From mechanistic point of view, this pathway is proposed to be minor, but in these reactions their probability of formation is higher due to the larger RO<sub>2</sub> radicals. The larger radicals will lead to the formation of stable ROOR' due to higher vibrational modes that helps distributes collisional energy through the molecule.

## IV.2.9 2,3,5-TMF reaction with NO<sub>3</sub>

### IV.2.9.1 Insights from the offline analysis of the gas mixture-qualitative identification of the products (TD-GC-EI-MS, GC-EI-MS)

TD-GC-EI-MS analyses were performed to study the gas-phase oxidation products formed from the reaction of 2,3,5-TMF with NO<sub>3</sub>. The typical chromatogram obtained after the complete reaction of 2,3,5-TMF is presented in Figure IV.23 where the peaks are labelled with the corresponding structures. The identification was also carried out by analyzing the extract of the bubbler and the monotrap by the GC-EI-MS. The products observed using all the analytical techniques are presented in Table IV.13. To the best of our knowledge, except for maleic anhydride there is no available commercial standards for the 2,3,5 TMF oxidation products identified.

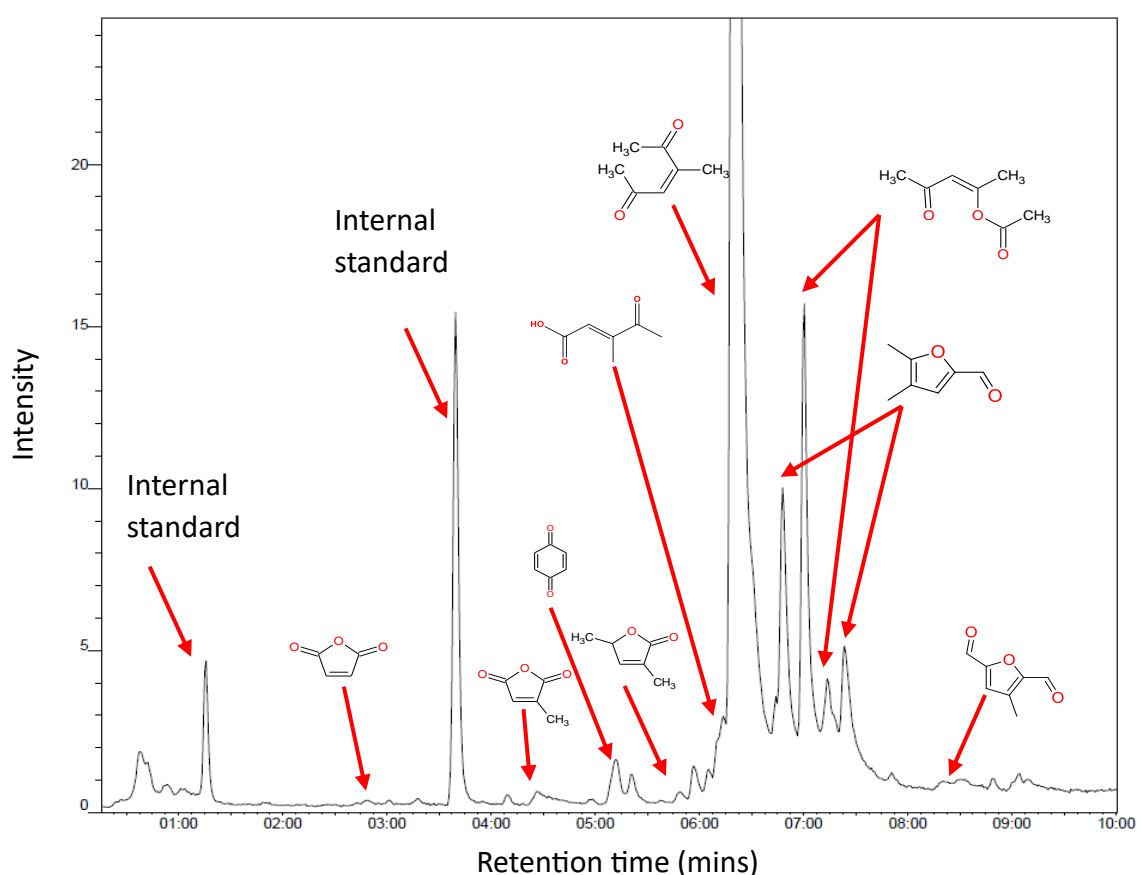


Figure IV.23: Chromatogram (Td-GC-EI-MS) of the gas-phase products formed from the gas-phase reaction of 2,3,5-TMF with NO<sub>3</sub> radicals. The peaks are labelled with their chemical structures' identifications.

Table IV.13: Identification of the products formed from the reaction of 2,3,5-TMF with NO<sub>3</sub> in both the gaseous and particulate phase by the different analytical techniques employed.

Product	Structure	PTR-ToF-MS	TD-GC-EI-MS	GC-EI-MS		
				Mono-trap	Bubbler	
					Acetonitrile	Methanol
5-methyl-3-hexene-2,5-dione		√	√	√	√	√
3,5-dimethyl-2-furaldehyde		√	√	√	√	√
3-methyl-2,5-furandicarboxaldehyde		√	√	√	√	
4,5-dimethyl-2(3H)-furanone		√	√		√	√
2,5-dihydro-3,5-dimethyl-2-Furanone		√	√	√	√	√
Maleic Anhydride		√	√		√	
3-methyl-2,5-dione		√	√	√	√	√
3-Methyl-4-oxo-2-pentenoic acid		√	√			
2-cyclohexene-1,4-dione		√		√	√	
4-oxopent-2-en-2-yl acetate		√	√			

#### IV.2.9.2 Insights from the online analysis of the gas mixture- temporal variation of the reactant and products (PTR-ToF-MS) and yields estimated

The gas-phase products characterization for the reaction of 2,3,5-TMF with  $\text{NO}_3$  or with any other atmospheric oxidant have never been studied in literature. In CHARME, a set of four experiments was conducted under room temperature ( $294 \pm 2$ ) K and atmospheric pressure to study qualitatively and quantitatively the gas-phase oxidation products of the title reaction. The concentrations of 2,3,5-TMF and its corresponding products were followed versus time using the PTR-ToF-MS (see Figure IV.24). In a typical experiment, 2,3,5-TMF exhibited rapid oxidation (within an average time of 30 min) by the  $\text{NO}_3$  radicals, leading to the formation of multiple oxidation products detected with different masses using the PTR-ToF-MS.

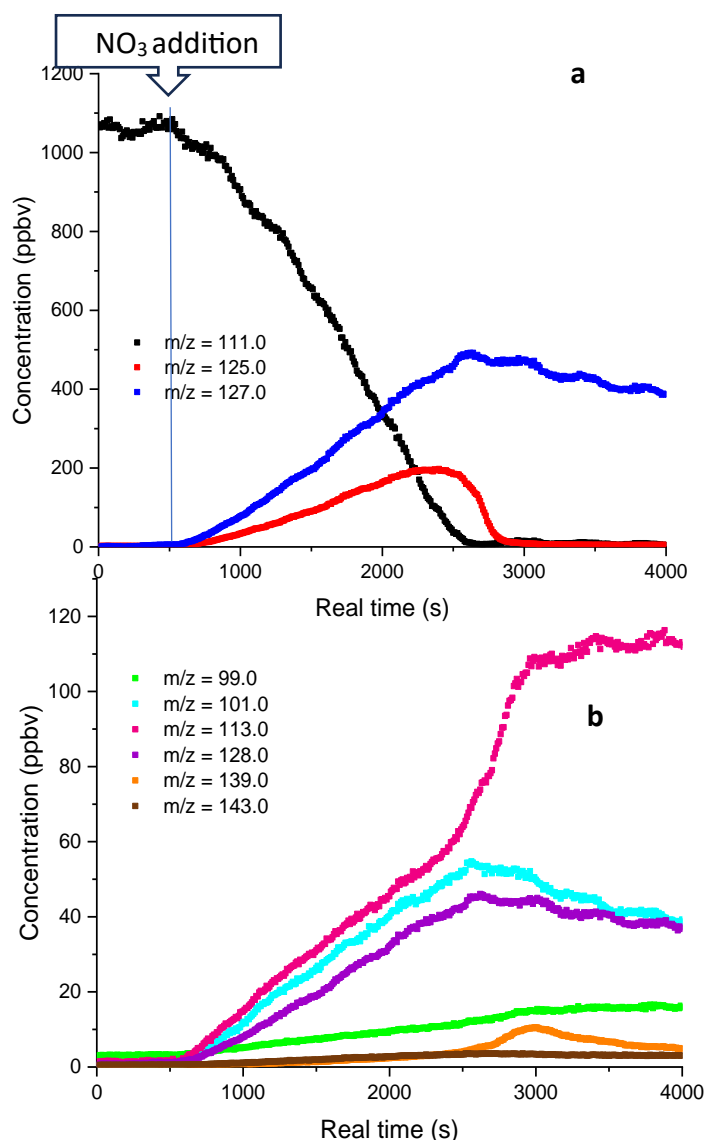


Figure IV.24: (a) Typical time profiles of chemical compounds detected by PTR-ToF-MS during the oxidation of 2,3,5-TMF (initial concentration= 1100 ppbv), 2,3,5-TMF ( $m/z = 111.0$ ), major products:  $m/z = 125.0$ ,  $m/z = 127.0$ ). Note that  $m/z$  includes +1 corresponding to the ionization by  $\text{H}^+$  (b) time profiles of the minor products.

The yields of the products were estimated from the plot of their concentration versus that of the reacted concentration of 2,3,5-TMF (Figure IV.25). The yields are equal to slopes of the linear least-squares fit to the data and are displayed in Table IV.14. However, due to the absence of the commercial standard, only yields obtained from the slope at the origin is provided.

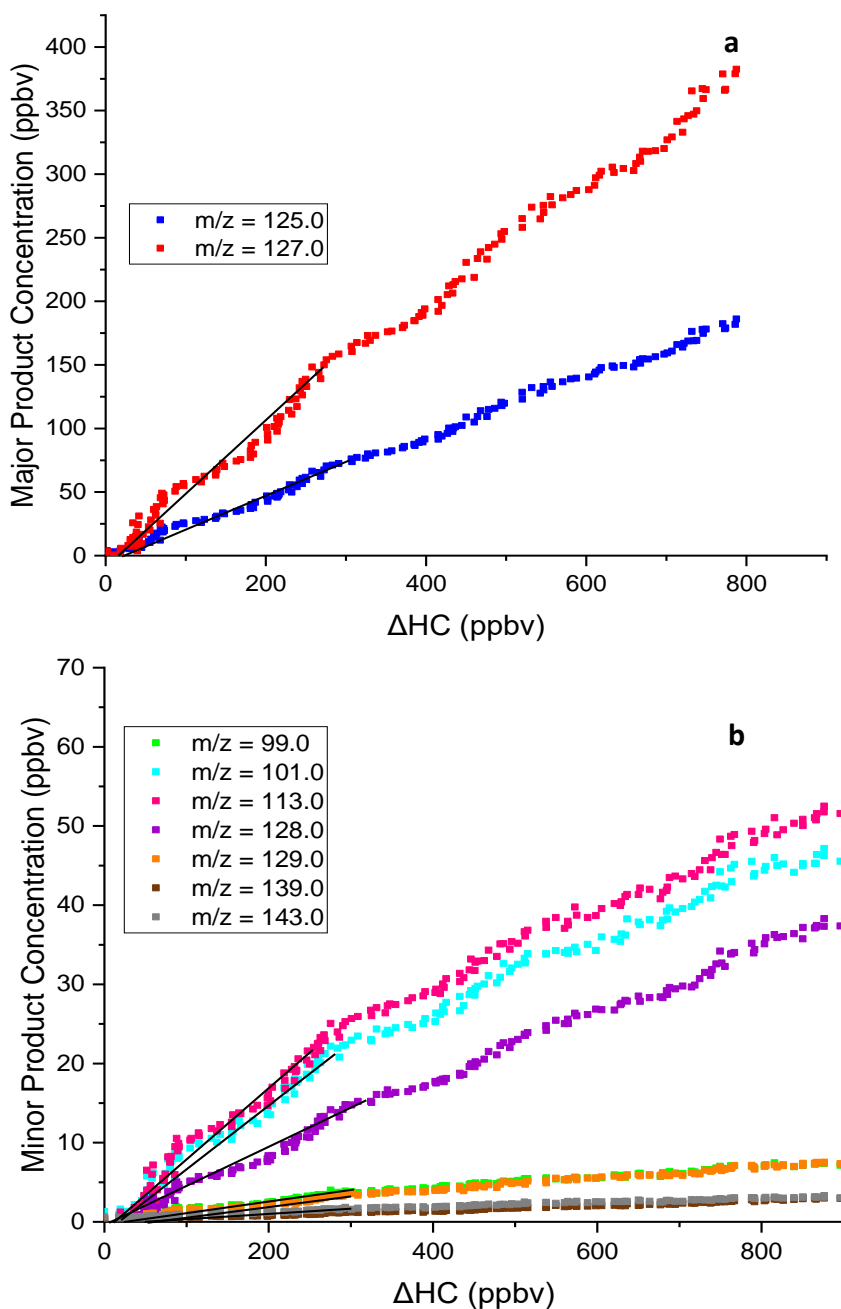


Figure IV.25: Typical plots for the determination of the gas-phase product yields formed from the reaction of 2,3,5-TMF with  $\text{NO}_3$  (a) major oxidation products (b) minor oxidation products.

Table IV.14: Identification and formations yields of the products formed from the reaction of 2,3,5-TMF with NO<sub>3</sub> (m/z masses include the addition of H<sup>+</sup>).

[2,3,5-trimethylfuran] (ppbv)	m/z = 125.0	m/z = 127.0	m/z = 113.0	m/z = 128.0
900	24.3	55.3	9.3	5.2
1000	25.9	54.9	5.8	5.1
1050	18.6	54.2	5.3	5.1
1130	27.9	58.3	7.9	5.6
Average yield (%)	24.2 ± 4.0	55.7 ± 1.8	7.1 ± 1.9	5.2 ± 0.2

9 peaks were observed in mass spectrum recorded with the PTR-ToF-MS and the identified products are also presented in Table IV.13. The 2 major products formed from the gas-phase reaction of 2,3,5-TMF with NO<sub>3</sub> correspond to m/z 125.0 and 127.0.

The peak corresponding to m/z = 127.0 in the PTR-ToF-MS analysis is attributed to 3-methylhex-3-ene-2,5-dione with a theoretical yield of 55.7 ± 1.8 % , while the peak observed at m/z 125 is linked to 3,5-Dimethyl-2-furfural with a yield estimated to be 24.2 ± 4.0 %. 3-methylhex-3-ene-2,5-dione is formed from NO<sub>3</sub> addition to the C-2/C-5 of the 2,3,5-TMF (m/z = 111.0). However, 3,5-Dimethyl-2-furfural is formed from the NO<sub>3</sub> addition followed by H abstraction from the methyl-group of the furan ring. The product with m/z 113.0 can be attributed to 3-methyl-furan-2,5-dione/4,5-dimethyl-2(3H)-furanone and its average yield of formation 7.1 ± 1.9 %. Regarding the minor products, m/z 99.0, m/z 129.0, m/z 139.0, m/z 146.0 can be attributed to maleic anhydride, 3-Methyl-4-oxo-2-pentenoic acid, 3-methyl-2,5-furandicarboxaldehyde, 4-oxopent-2-en-2-yl acetate respectively. All other minor products were formed with yields below 1%. The pathways leading to the formation of all products is presented in Figure IV.26.

#### IV.2.9.3 Mechanism of the reaction of 2,3,5-TMF with NO<sub>3</sub>

This work presents the first literature study characterizing the products formed from the reaction of 2,3,5-TMF with NO<sub>3</sub>. A similar reaction mechanism than the one of 2,5-DMF is proposed for the reaction of 2,3,5-TMF with NO<sub>3</sub> and a brief description is provided here. Figure IV.27 shows the mechanism proposed leading to the formation of the primary and secondary products numbered **(1-7)**. The two major primary pathways of the reaction occur by NO<sub>3</sub> addition to C-2/C-5 of the ring leading to the formation of the unsaturated dicarbonyl 5-methyl-3-hexene-2,5-dione **(1)**. The second major primary product 3,5-dimethyl-2-furfural or 4,5-dimethyl-2-furfural **(2)** is formed by NO<sub>3</sub> addition to C-2/C-5 of the ring followed by H-abstraction from the methyl group attached to the corresponding carbon. Both reaction pathways are major with the NO<sub>3</sub> addition being the dominant pathway. 4-oxopent-2-en-2-yl acetate **(3)** is a minor first-generation product formed from NO<sub>3</sub> addition to C-2/C-5 of the ring as illustrated in Figure IV.26.

Several second-generation products were formed from the reaction of the major primary products with NO<sub>3</sub>. The reaction of 3,5-dimethyl-2-furfural with NO<sub>3</sub> can occur by H-abstraction from the aldehyde group attached to the ring, H-abstraction from the methyl group attached to C-5 of the ring or NO<sub>3</sub> addition to C-5 of the ring. These three reaction

pathways lead to the formation of 3-methyl-2,5-furandicarboxaldehyde (**4**), 3-methyl-2,5-dione (**5**) and 3-Methyl-4-oxo-2-pentenoic acid (**6**) respectively. 4,5-dimethyl-2(3H)-furanone (**7**) can be formed from the rearrangement of 5-methyl-3-hexene-2,5-dione.

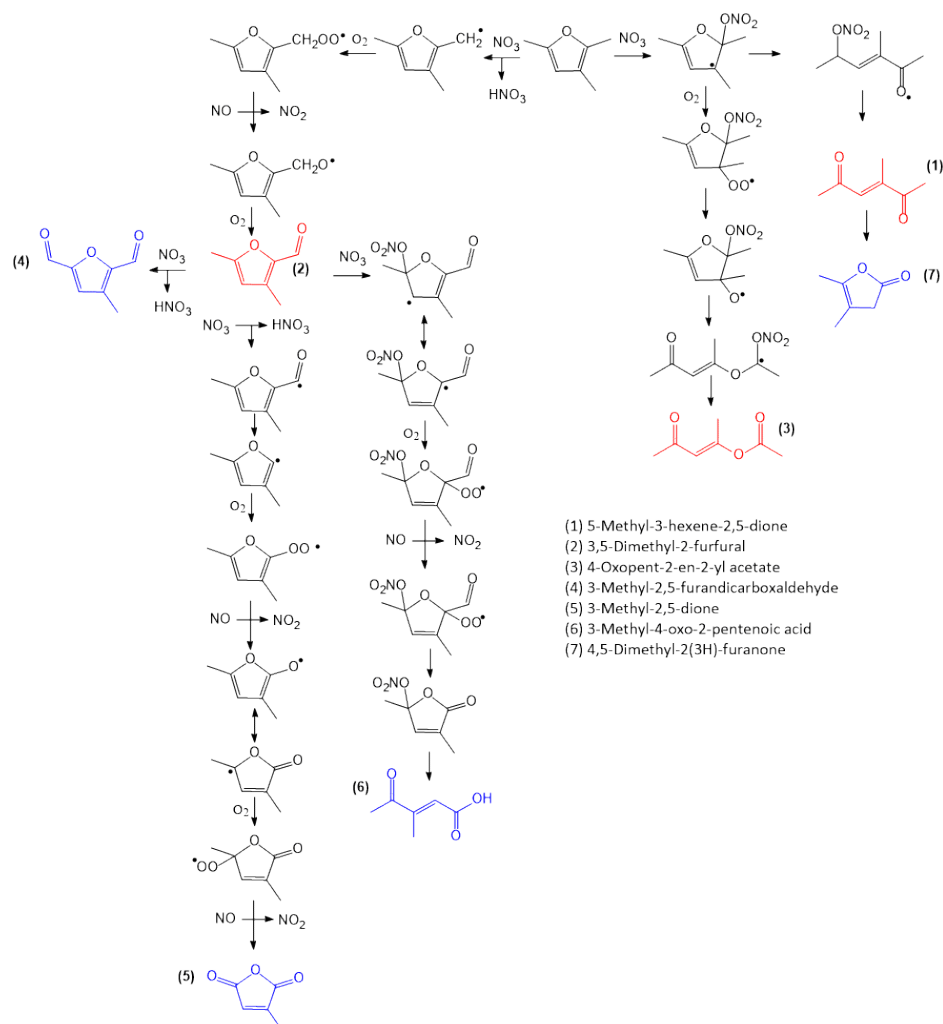


Figure IV.27: Mechanism of the reaction of 2,3,5-TMF with  $\text{NO}_3$ . Labeled in red are the first-generation products (1-3) while in blue are the second-generation products (4-7).

#### IV.2.9.4 SOA formation from the reaction of 2,3,5-TMF with $\text{NO}_3$

To the best of our knowledge, this is the first literature study reporting the SOA yield of formation from the reaction of 2,3,5-TMF with  $\text{NO}_3$ . In CHARME chamber, a total of 8 experiments were run to examine the SOA formation potential. The range of initial 2,3,5-TMF concentrations employed was 80 ppbv to 1100 ppbv. The initial 2,3,5-TMF volume ratios ( $[\text{2,3,5-TMF}]_0$ , in ppbv), the 2,3,5-TMF reacting concentrations ( $[\text{2,3,5-TMF}]$ , in  $\mu\text{g}\cdot\text{m}^{-3}$ ), the organic aerosol mass concentrations ( $M_0$ , in  $\mu\text{g}\cdot\text{m}^{-3}$ ) corrected for wall losses, and the overall SOA yields are all summarized in Table IV.15. In all experiments, 2,3,5-TMF was completely reacted (within 30 min), therefore the reactive concentrations  $\Delta[\text{2,3,5-TMF}]$  are equal to the initial ones ( $[\text{2,3,5-TMF}]_0$ ).

Table IV.15: Experimental conditions and SOA yield for the reaction of 2,3,5-TMF with NO<sub>3</sub>.

<b>[2,3,5-TMF]<sub>0</sub></b> <b>(ppbv)</b>	<b>Δ[2,3,5-TMF]</b> <b>(μg.m<sup>-3</sup>)</b>	<b>M<sub>0</sub></b> <b>(μg.m<sup>-3</sup>)</b>	<b>Yield</b> <b>(%)</b>
85	389.1	1.5	0.3
250	1190.8	36.2	3.0
415	1899.7	59.7	3.1
560	2563.5	108.0	4.2
808	3694.1	222.6	6.0
998	4614.3	282.3	6.1
1040	4943.8	415.8	8.4
1090	5035.9	486.1	9.6

Interpreting the results in Table IV.15, it is clear that the aerosols yield varies with concentration of 2,3,5-TMF. As the initial concentration of 2,3,5-TMF increases, the SOA yield also increases. The aerosols mass concentration (M<sub>0</sub>) formed from the reaction were in the range of 1.51-486 μg.m<sup>-3</sup> corresponding to an aerosol yield of 0.3-9.6%.

The yields of the SOA formation and the aerosols mass concentrations were fitted using the model proposed by Odum et al., (1996) (see Figure IV.28). The one product model is able to satisfactory reproduce the experimental data ( $R^2 = 0.94$ ) as shown in Figure IV.28 and lead to  $\alpha_i = (12.44 \pm 1.97) \times 10^{-2}$  and  $K_{om,i} = (4.90 \pm 1.80) \times 10^{-3} (\text{m}^3 \cdot \mu\text{g}^{-1})$ . The two products model is not retained since the uncertainties on  $\alpha_i$  and  $K_{om,i}$  were higher than their values.



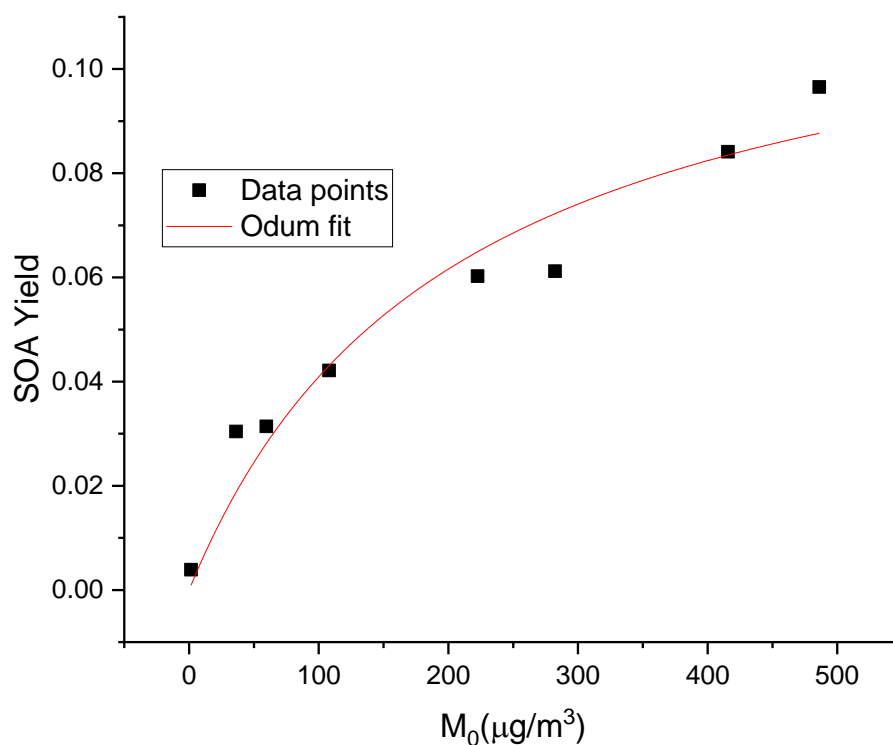


Figure IV.28: Yield Curve for the reaction of 2,3,5-TMF with  $\text{NO}_3$  (squares). The line represents the Odum fit to the data considering one-product model (Odum et al., 1996).

It is interesting to compare the value of  $\alpha$  (0.12) and the maximum SOA yield observed in Table IV.15 (0.10).  $\alpha$  represents the semi-volatile products generated in both the gas- and aerosol-phases whereas  $Y$  represents the semi-volatile products formed in the particle phase only. These 2 values indicate that approximately 80% of the low volatile compounds formed during the 2,3,5-TMF reaction with  $\text{NO}_3$  radicals are transferred into the particle phase.

### IV.3 Conclusion

#### *General mechanism for the reaction of furan and methylated-furanoids with $\text{NO}_3$ radical*

A general chemical mechanism is proposed for the gas-phase reaction of F, 2-MF, 3-MF, 2,5-DMF and 2,3,5-TMF with  $\text{NO}_3$ . Figure IV.29 shows the general chemical mechanism leading to the formation of both major and minor primary oxidation products with their yields (data from this work; Tapia et al., (2011); Berndt et al., 1997). For the five studied furan compounds, the major pathway occurs by  $\text{NO}_3$  addition to Carbon-2/Carbon-5 of the ring leading to the formation of unsaturated dicarbonyls. For single methylated furan compounds (2-MF and 3-MF), cyclic nitrooxy carbonyls are also formed as major primary product from the  $\text{NO}_3$  addition to C-2. For multi-methylated furanoids (2,5-DMF and 2,3,5-TMF), another major pathway occurs by  $\text{NO}_3$  addition followed by H atom-abstraction from one of the methyl groups attached to the furan ring leading to the formation of methylated-furfurals as second major products.

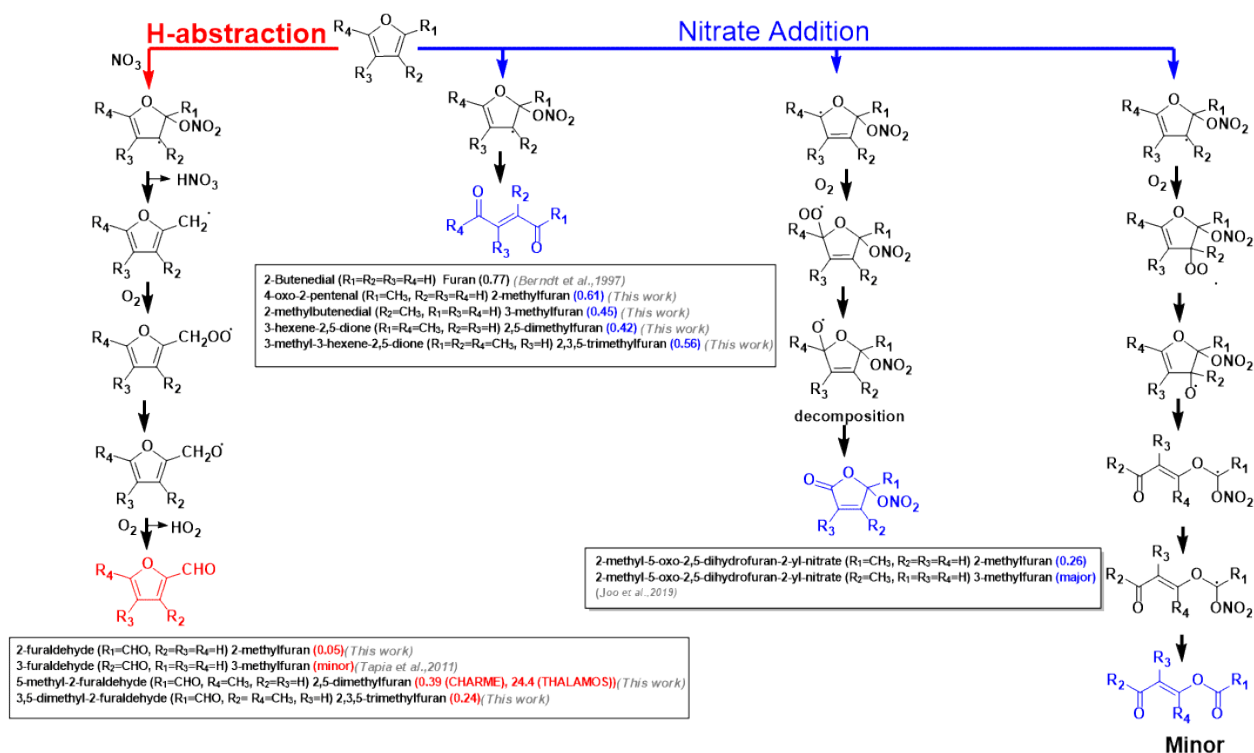


Figure IV.29: Chemical mechanisms for the gas-phase reaction of furan and methylated-furanoids with  $NO_3$  leading to the formation of the primary products. Products labelled in blue are formed from  $NO_3$  addition while those labelled in red are the products formed from H-abstraction while those. Products yields are also indicated.

Regarding the second-generation products, there is a common product formed from the reaction of furan and methylated furans with  $NO_3$  which is maleic anhydride. This compound can be considered as a signature of the presence and oxidation of these compounds within the fires plumes. In the study of Wang et al., (2020), maleic anhydride is considered as sign of the aging of the fire plumes. In addition, methylated-furfurals showed fast reaction with  $NO_3$  which probably occurs by H-abstraction from the aldehydic group attached to the ring.

#### SOA formed from the reaction of furan and methylated-furanoids reaction with $NO_3$ radical

Comparing the SOA yield obtained from the reaction of 2-MF, 2,5-DMF AND 2,3,5-TMF with  $NO_3$ , the maximum aerosol yield obtained from the reaction of 2-MF is  $\approx 2\%$  which is 5-6 times lower than those obtained from the reaction of 2,5-DMF ( $\approx 12\%$ ) and 2,3,5-TMF ( $\approx 10\%$ ). This shows that increasing the methylation on the furan ring increases the SOA yield obtained from the reaction. This is due to the presence of methyl groups on the ring reducing the volatility or the vapor pressure of a compound.

One product model obtained from fitting the data using odum model indicates that either only one semi-volatile organic compounds is the major constituent of the SOA or that the organic compounds present in the condensed phase have similar  $\alpha_i$  and  $K_{om,i}$ .

Regarding the composition of the SOA formed from title reaction, it can be concluded that some products identified in the gas-phase were also identified in the particulate phase including the major ones, this shows that these products partition between the gas- and particulate- phase. Higher-generation oxidation products and possibly multiphase accretion reactions contribute significantly to SOA formation from the methylated furanoids +  $NO_3$

reaction. The slow  $\text{N}_2\text{O}_5$  injection used in this study as well as the fact that these radicals have some of the fastest  $\text{RO}_2 + \text{RO}_2$  reaction rates can lead to considerable dimer formation ( $\text{ROOR}'$ ) and multifunctional species. The carbonyl groups can also participate in accretion reactions or be oxidized in the condensed phase. The molecular formulas of the observed products imply that the compounds in the particle phase are multifunctional and likely to engage in accretion reactions. If other VOCs in biomass burning plumes have similar products, it is expected that these compounds will form SOA efficiently through multigeneration and multiphase chemistry.

The maximum concentration of furanoids observed in the fire plumes are below 10 ppb per 1 ppm of CO where the maximum CO detected in fire plumes is 5-6 ppm. As a result, the maximum concentrations of furanoids in plumes you is estimated to be  $\approx 50$  ppb. Under these conditions, the SOA contribution of the methylated furanoids is expected to be non-important. If typical nighttime RH conditions are considered, which are higher than in this study, the SOA yield may increase owing to oligomerization or reactive uptake of water-soluble compounds (Nguyen et al., 2014; Xu et al., 2017).

## IV.4 References

- Akagi, S. K., Burling, I. R., Mendoza, A., Johnson, T. J., Cameron, M., Griffith, D. W. T., Paton-Walsh, C., Weise, D. R., Reardon, J., & Yokelson, R. J. (2014). Field measurements of trace gases emitted by prescribed fires in southeastern US pine forests using an open-path FTIR system. *Atmospheric Chemistry and Physics*, *14*(1), 199–215. <https://doi.org/10.5194/acp-14-199-2014>
- Akagi, S. K., Yokelson, R. J., Burling, I. R., Meinardi, S., Simpson, I., Blake, D. R., McMeeking, G. R., Sullivan, A., Lee, T., Kreidenweis, S., Urbanski, S., Reardon, J., Griffith, D. W. T., Johnson, T. J., & Weise, D. R. (2013). Measurements of reactive trace gases and variable O<sub>3</sub> formation rates in some South Carolina biomass burning plumes. In *Atmospheric Chemistry and Physics* (Vol. 13, Issue 3). <https://doi.org/10.5194/acp-13-1141-2013>
- Akagi, S. K., Yokelson, R. J., Wiedinmyer, C., Alvarado, M. J., Reid, J. S., Karl, T., Crouse, J. D., & Wennberg, P. O. (2011). Emission factors for open and domestic biomass burning for use in atmospheric models. *Atmospheric Chemistry and Physics*, *11*(9), 4039–4072. <https://doi.org/10.5194/acp-11-4039-2011>
- Akele, E. S., & Tarekegn, M. M. (2017). Assessment of dioxin and furan emission levels and management practices in Addis Ababa, Ethiopia. *Journal of Health and Pollution*, *7*(15), 85–94. <https://doi.org/10.5696/2156-9614-7.15.85>
- Al Ali, F., Coeur, C., Houzel, N., Bouya, H., Tomas, A., & Romanias, M. N. (2022). Rate Coefficients for the Gas-Phase Reactions of Nitrate Radicals with a Series of Furan Compounds. *Journal of Physical Chemistry A*, *126*(46), 8674–8681. <https://doi.org/10.1021/acs.jpca.2c03828>
- Alan Buis. (2019). *Earth's Atmosphere: A Multi-layered Cake*. <https://climate.nasa.gov/news/2919/earths-atmosphere-a-multi-layered-cake/>
- Alcock, R. E., & Jones, K. C. (1996). Dioxins in the environment: A review of trend data. *Environmental Science and Technology*, *30*(11), 3133–3143. <https://doi.org/10.1021/es960306z>
- Alicke, B., & Platt, U. (2002). *Impact of nitrous acid photolysis on the total hydroxyl radical budget during the Limitation of Oxidant Production / Pianura Padana Produzione di Ozono study in Milan*. 107. <https://doi.org/10.1029/2000JD000075>
- Alvarado, A., Atkinson, R., & Arey, J. (1996). Kinetics of the gas-phase reactions of NO<sub>3</sub> radicals and O<sub>3</sub> with 3-methylfuran and the OH radical yield from the O<sub>3</sub> reaction. *International Journal of Chemical Kinetics*, *28*(12), 905–909. [https://doi.org/10.1002/\(SICI\)1097-4601\(1996\)28:12<905::AID-KIN7>3.0.CO;2-R](https://doi.org/10.1002/(SICI)1097-4601(1996)28:12<905::AID-KIN7>3.0.CO;2-R)
- Alwe, H. D., Walavalkar, M. P., Sharma, A., Dhanya, S., & Naik, P. D. (2014). Tropospheric oxidation of cyclic unsaturated ethers in the day-time: Comparison of the reactions with Cl, OH and O<sub>3</sub> based on the determination of their rate coefficients at 298K. *Atmospheric Environment*, *82*, 113–120. <https://doi.org/10.1016/j.atmosenv.2013.10.009>
- Andersen, C., Nielsen, O. J., Østerstrøm, F. F., Ausmeel, S., Nilsson, E. J. K., & Sulbaek Andersen, M. P. (2016). Atmospheric Chemistry of Tetrahydrofuran, 2-Methyltetrahydrofuran, and 2,5-Dimethyltetrahydrofuran: Kinetics of Reactions with Chlorine Atoms, OD Radicals, and Ozone. *Journal of Physical Chemistry A*, *120*(37), 7320–7326. <https://doi.org/10.1021/acs.jpca.6b06618>
- Andreae, M. (2019). Emission of trace gases and aerosols from biomass burning. Global Biogeochemical. *Atmospheric Chemistry and Physics*, *15* (4)(April), 955–966. <https://www.atmos-chem-phys-discuss.net/acp-2019-303/acp-2019-303.pdf>
- Andreae, M. O. (2001). [ *Ca Because of the carbon to permits*. *15*(4), 955–966.
- Aschmann, S. M., Nishino, N., Arey, J., & Atkinson, R. (2011). Kinetics of the Reactions of OH Radicals

- with 2- and 3-Methylfuran, 2,3- and 2,5-Dimethylfuran, and E- and Z-3-Hexene-2,5-dione, and Products of OH  $\beta$  2,5-Dimethylfuran. *Environmental Science and Technology*, 45(7), 1859–1865. <https://doi.org/10.1002/kin.550140706>
- Aschmann, S. M., Nishino, N., Arey, J., & Atkinson, R. (2014a). Products of the OH Radical-Initiated Reactions of Furan, 2- and 3-Methylfuran, and 2,3- and 2,5-Dimethylfuran in the Presence of NO. *The Journal of Physical Chemistry*, 118, 457–466. <https://doi.org/10.1021/jp410345k>
- Aschmann, S. M., Nishino, N., Arey, J., & Atkinson, R. (2014b). Sara M. Aschmann, Noriko Nishino, † Janet Arey, \*, ‡ and Roger Atkinson \*, ‡.
- Atkinson, R. (1991a). Kinetics and Mechanisms of the Gas-Phase Reactions of the NO<sub>3</sub> Radical with Organic Compounds. *Journal of Physical and Chemical Reference Data*, 20(3), 459–507. <https://doi.org/10.1063/1.555887>
- Atkinson, R. (1991b). Kinetics and Mechanisms of the Gas-Phase Reactions of the NO<sub>3</sub> Radical with Organic Compounds. *Journal of Physical and Chemical Reference Data*, 20(3), 459–507. <https://doi.org/10.1063/1.555887>
- Atkinson, R. (2000). Atmospheric chemistry of VOCs and NO(x). *Atmospheric Environment*, 34(12–14), 2063–2101. [https://doi.org/10.1016/S1352-2310\(99\)00460-4](https://doi.org/10.1016/S1352-2310(99)00460-4)
- Atkinson, R., & Arey, J. (2003). *ARTICLE IN PRESS Gas-phase tropospheric chemistry of biogenic volatile organic compounds : a review*. 2(2). [https://doi.org/10.1016/S1352-2310\(03\)00391-1](https://doi.org/10.1016/S1352-2310(03)00391-1)
- Atkinson, R., Arey, J., Tuazon, E. C., & Aschmann, S. M. (1992). Gas-phase reactions of 1,4-benzodioxan, 2,3-dihydrobenzofuran, and 2,3-benzofuran with OH radicals and O<sub>3</sub>. *International Journal of Chemical Kinetics*, 24(4), 345–358. <https://doi.org/10.1002/kin.550240404>
- Atkinson, R., Aschmann, S. M., & Carter, P. L. (1983a). *Radicals with Furan and Thiophene at. 15*, 51–61.
- Atkinson, R., Aschmann, S. M., & Carter, W. P. L. (1983b). Kinetics of the reactions of O<sub>3</sub> and OH radicals with furan and thiophene at 298 ± 2 K. *International Journal of Chemical Kinetics*, 15(1), 51–61. <https://doi.org/10.1002/kin.550150106>
- Atkinson, R., Aschmann, S. M., & Carter, W. P. L. (1984). Kinetics of the reactions of O<sub>3</sub> and OH radicals with a series of dialkenes and trialkenes at 294 ± 2 K. *International Journal of Chemical Kinetics*, 16(8), 967–976. <https://doi.org/10.1002/kin.550160804>
- Atkinson, R., Aschmann, S. M., & Pitts, J. N. (1988). Rate constants for the gas-phase reactions of the NO<sub>3</sub> radical with a series of organic compounds at 296 ± 2 K. *Journal of Physical Chemistry*, 92(12), 3454–3457. <https://doi.org/10.1021/j100323a028>
- Atkinson, R., Aschmann, S. M., Tuazon, E. C., Arey, J., & Zielinska, B. (1989). Formation of 3-Methylfuran from the gas-phase reaction of OH radicals with isoprene and the rate constant for its reaction with the OH radical. *International Journal of Chemical Kinetics*, 21(7), 593–604. <https://doi.org/10.1002/kin.550210709>
- Atkinson, R., Aschmann, S. M., Winer, A. M., & Carter, W. P. L. (1985a). *for Reactions with Pyrrole ± 1 Atmospheric. I*, 87–90.
- Atkinson, R., Aschmann, S. M., Winer, A. M., & Carter, W. P. L. (1985b). Rate Constants for the Gas-Phase Reactions of NO<sub>3</sub> Radicals with Furan, Thiophene, and Pyrrole at 295 ± 1 K and Atmospheric Pressure. *Environmental Science and Technology*, 19(1), 87–90. <https://doi.org/10.1021/es00131a010>
- Atkinson, R., Aschmann, S. M., Winer, A. M., & Pitts, J. N. (1985). Kinetics and Atmospheric Implications

- of the Gas-Phase Reactions of NO<sub>3</sub> Radicals with a Series of Monoterpenes and Related Organics at 294 ± 2 K. *Environmental Science and Technology*, 19(2), 159–163. <https://doi.org/10.1021/es00132a009>
- Atkinson, R., Baulch, D. L., Cox, R. A., Hampson, R. F., Kerr, J. A., Rossi, M. J., & Troe, J. (1997). Evaluated Kinetic, Photochemical and Heterogeneous Data for Atmospheric Chemistry: Supplement V: IUPAC Subcommittee on Gas Kinetic Data Evaluation for Atmospheric Chemistry. *Journal of Physical and Chemical Reference Data*, 26(3), 521–784. <https://doi.org/10.1063/1.556011>
- Bahreini, R., Keywood, M. D., Ng, N. L., Varutbangkul, V., Gao, S., Flagan, R. C., Seinfeld, J. H., Worsnop, D. R., & Jimenez, J. L. (2005). Measurements of secondary organic aerosol from oxidation of cycloalkenes, terpenes, and m-xylene using an aerodyne aerosol mass spectrometer. *Environmental Science and Technology*, 39(15), 5674–5688. <https://doi.org/10.1021/es048061a>
- Berndt, T., Böge, O., & Rolle, W. (1997). Products of the gas-phase reactions of NO<sub>3</sub> radicals with furan and tetramethylfuran. *Environmental Science and Technology*, 31(4), 1157–1162. <https://doi.org/10.1021/es960669z>
- Bierbach, A., Barnes, I., & Becker, K. H. (1992). Rate coefficients for the gas-phase reactions of hydroxyl radicals with furan, 2-methylfuran, 2-ethylfuran and 2,5-dimethylfuran at 300 ± 2 K. *Atmospheric Environment Part A, General Topics*, 26(5), 813–817. [https://doi.org/10.1016/0960-1686\(92\)90241-C](https://doi.org/10.1016/0960-1686(92)90241-C)
- Bierbach, A., Barnes, I., & Becker, K. H. (1995). Product and kinetic study of the OH-initiated gas-phase oxidation of Furan, 2-methylfuran and furanaldehydes at ≈ 300 K. *Atmospheric Environment*, 29(19), 2651–2660. [https://doi.org/10.1016/1352-2310\(95\)00096-H](https://doi.org/10.1016/1352-2310(95)00096-H)
- Bierbach, A., Barnes, I., Becker, K. H., & Wiesen, E. (1994). Atmospheric Chemistry of Unsaturated Carbonyls: Butenedial, 4-Oxo-2-pentenal, 3-Hexene-2,5-dione, Maleic Anhydride, 3H-Furan-2-one, and 5-Methyl-3H-furan-2-one. *Environmental Science and Technology*, 28(4), 715–729. <https://doi.org/10.1021/es00053a028>
- Blake, R., Monks, P., & Ellis, A. (2009). Proton Transfer Reaction Mass Spectrometry (PTR-MS). *Chem.Rev.*, 109(0), 861–896. <https://doi.org/10.1002/9781118180730.ch28>
- Brando, P., Macedo, M., Silvério, D., Rattis, L., Paolucci, L., Alencar, A., Coe, M., & Amorim, C. (2020). Amazon wildfires: Scenes from a foreseeable disaster. *Flora: Morphology, Distribution, Functional Ecology of Plants*, 268. <https://doi.org/10.1016/j.flora.2020.151609>
- Brown, S. S., & Stutz, J. (2012). Nighttime radical observations and chemistry. *Chemical Society Reviews*, 41(19), 6405–6447. <https://doi.org/10.1039/c2cs35181a>
- Burkholder, J. B., Abbatt, J. P. D., Barnes, I., Roberts, J. M., Melamed, M. L., Ammann, M., Bertram, A. K., Cappa, C. D., Carlton, A. G., Carpenter, L. J., Crowley, J. N., Dubowski, Y., George, C., Heard, D. E., Herrmann, H., Keutsch, F. N., Kroll, J. H., McNeill, V. F., Ng, N. L., ... Ziemann, P. J. (2017). The Essential Role for Laboratory Studies in Atmospheric Chemistry. *Environmental Science and Technology*, 51(5), 2519–2528. <https://doi.org/10.1021/acs.est.6b04947>
- Burkholder, J. B., Sander, S. P., Abbatt, J. P. D., Barker, J. R., Huie, R. E., Kolb, C. E., Kurylo, M. J., Orkin, V. L., Wilmouth, D. M., & Wine, P. H. (2020). Chemical Kinetics and Photochemical Data for Use in Atmospheric Studies, Evaluation No. 19. *JPL Publications 19-5*, 19, 1–153. <http://jpldataeval.jpl.nasa.gov/>
- Burling, I. R., Yokelson, R. J., Griffith, D. W. T., Johnson, T. J., Veres, P., Roberts, J. M., Warneke, C., Urbanski, S. P., Reardon, J., Weise, D. R., Hao, W. M., & De Gouw, J. (2010). Laboratory measurements of trace gas emissions from biomass burning of fuel types from the southeastern

- and southwestern United States. *Atmospheric Chemistry and Physics*, 10(22), 11115–11130. <https://doi.org/10.5194/acp-10-11115-2010>
- Cabañas, B., Baeza, M. T., Salgado, S., Martín, P., Taccone, R., & Martínez, E. (2004). Oxidation of heterocycles in the atmosphere: Kinetic study of their reactions with NO<sub>3</sub> radical. *Journal of Physical Chemistry A*, 108(49), 10818–10823. <https://doi.org/10.1021/jp046524t>
- Cabañas, B., Villanueva, F., Martín, P., Baeza, M. T., Salgado, S., & Jiménez, E. (2005). Study of reaction processes of furan and some furan derivatives initiated by Cl atoms. *Atmospheric Environment*, 39(10), 1935–1944. <https://doi.org/10.1016/j.atmosenv.2004.12.013>
- Cabrera-perez, D., Taraborrelli, D., Sander, R., & Pozzer, A. (2016). *Global atmospheric budget of simple monocyclic aromatic compounds*. 6931–6947. <https://doi.org/10.5194/acp-16-6931-2016>
- Calogirou, A., Jensen, N. R., Nielsen, C. J., Kotzias, D., & Hjorth, J. (1999). Gas-phase reactions of nopinone, 3-isopropenyl-6-oxo-heptanal, and 5-methyl-5-vinyltetrahydrofuran-2-ol with OH, NO<sub>3</sub>, and ozone. *Environmental Science and Technology*, 33(3), 453–460. <https://doi.org/10.1021/es980530j>
- Carbajo, P. G., Smith, S. C., Holloway, A. L., Smith, C. A., Pope, F. D., Shallcross, D. E., & Orr-Ewing, A. J. (2008). Ultraviolet photolysis of HCHO: Absolute HCO quantum yields by direct detection of the HCO radical photoproduct. *Journal of Physical Chemistry A*, 112(48), 12437–12448. <https://doi.org/10.1021/jp8070508>
- Chattopadhyay, A., Papadimitriou, V. C., Marshall, P., & Burkholder, J. B. (2020). Temperature-dependent rate coefficients for the gas-phase OH + furan-2,5-dione (C<sub>4</sub>H<sub>2</sub>O<sub>3</sub>, maleic anhydride) reaction. *International Journal of Chemical Kinetics*, 52(10), 623–631. <https://doi.org/10.1002/kin.21387>
- Chipperfield, M. P., Bekki, S., Dhomse, S., Harris, N. R. P., Hassler, B., Hossaini, R., Steinbrecht, W., Thiéblemont, R., & Weber, M. (2017). Detecting recovery of the stratospheric ozone layer. *Nature*, 549(7671), 211–218. <https://doi.org/10.1038/nature23681>
- Christian, T. J., Kleiss, B., Yokelson, R. J., Holzinger, R., Crutzen, P. J., Hao, W. M., Saharjo, B. H., & Ward, D. E. (2003). Comprehensive laboratory measurements of biomass-burning emissions: 1. Emissions from Indonesian, African, and other fuels. *Journal of Geophysical Research: Atmospheres*, 108(23). <https://doi.org/10.1029/2003jd003704>
- Ciccioli, P., Brancaleoni, E., Frattoni, M., Cecinato, A., & Pinciarelli, L. (2001). Determination of volatile organic compounds (VOC) emitted from biomass burning of Mediterranean vegetation species by GC-MS. *Analytical Letters*, 34(6), 937–955. <https://doi.org/10.1081/AL-100103604>
- Coeur-tourneur, C., Tomas, A., & Menu, D. (2008). *Secondary organic aerosol formation from the gas phase reaction of hydroxyl radicals with m-, o- and p-cresol*. 42, 3035–3045. <https://doi.org/10.1016/j.atmosenv.2007.12.043>
- Coggon, M. M., Lim, C. Y., Koss, A. R., Sekimoto, K., Yuan, B., Gilman, J. B., Hagan, D. H., Selimovic, V., Zarzana, K. J., Brown, S. S., M Roberts, J., Müller, M., Yokelson, R., Wisthaler, A., Krechmer, J. E., Jimenez, J. L., Cappa, C., Kroll, J. H., De Gouw, J., & Warneke, C. (2019). OH chemistry of non-methane organic gases (NMOGs) emitted from laboratory and ambient biomass burning smoke: Evaluating the influence of furans and oxygenated aromatics on ozone and secondary NMOG formation. *Atmospheric Chemistry and Physics*, 19(23), 14875–14899. <https://doi.org/10.5194/acp-19-14875-2019>
- Collard, F. X., & Blin, J. (2014). A review on pyrolysis of biomass constituents: Mechanisms and composition of the products obtained from the conversion of cellulose, hemicelluloses and lignin.

- Colmenar, I., Cabañas, B., Martínez, E., Salgado, M. S., & Martín, P. (2012). Atmospheric fate of a series of furanaldehydes by their NO<sub>3</sub> reactions. *Atmospheric Environment*, 54(3), 177–184. <https://doi.org/10.1016/j.atmosenv.2012.02.087>
- Colmenar, I., Martín, P., Cabañas, B., Salgado, S., Villanueva, F., & Ballesteros, B. (2020). Evaluation of the SOA formation in the reaction of furfural with atmospheric oxidants. *Atmosphere*, 11(9). <https://doi.org/10.3390/atmos11090927>
- Corchnoy, S., & Atkinson, R. (1990). Kinetics of the Gas-Phase Reactions of OH and NO<sub>3</sub> Radicals with 2-Carene, 1,8-Cineole, p-Cymene, and Terpinolene. *Environ. Sci. Technol.* 1990, 24(10), 1497–1502.
- Crouse, J. D., DeCarlo, P. F., Blake, D. R., Emmons, L. K., Campos, T. L., Apel, E. C., Clarke, A. D., Weinheimer, A. J., McCabe, D. C., Yokelson, R. J., Jimenez, J. L., & Wennberg, P. O. (2009). Biomass burning and urban air pollution over the Central Mexican Plateau. *Atmospheric Chemistry and Physics*, 9(14), 4929–4944. <https://doi.org/10.5194/acp-9-4929-2009>
- Cuisset, A., Coeur, C., Mouret, G., Ahmad, W., Tomas, A., & Pirali, O. (2016). Infrared spectroscopy of methoxyphenols involved as atmospheric secondary organic aerosol precursors: Gas-phase vibrational cross-sections. *Journal of Quantitative Spectroscopy and Radiative Transfer*, 179, 51–58. <https://doi.org/10.1016/j.jqsrt.2016.03.020>
- Davis, A. C., & Sarathy, S. M. (2013). Computational study of the combustion and atmospheric decomposition of 2-methylfuran. *Journal of Physical Chemistry A*, 117(33), 7670–7685. <https://doi.org/10.1021/jp403085u>
- De gouw, J., & Warneke, C. (2007). MEASUREMENTS OF VOLATILE ORGANIC COMPOUNDS IN THE EARTH'S ATMOSPHERE USING PROTON-TRANSFER-REACTION MASS SPECTROMETRY. *Wiley InterScience*, i, 221–235. <https://doi.org/10.1002/mas>
- Decker, Z. C. J., Zarzana, K. J., Coggon, M., Min, K. E., Pollack, I., Ryerson, T. B., Peischl, J., Edwards, P., Dubé, W. P., Markovic, M. Z., Roberts, J. M., Veres, P. R., Graus, M., Warneke, C., De Gouw, J., Hatch, L. E., Barsanti, K. C., & Brown, S. S. (2019). Nighttime Chemical Transformation in Biomass Burning Plumes: A Box Model Analysis Initialized with Aircraft Observations. *Environmental Science and Technology*, 53(5), 2529–2538. <https://doi.org/10.1021/acs.est.8b05359>
- Decker, Z., Robinson, M., Barsanti, K., Bourgeois, I., Coggon, M., DiGangi, J., Diskin, G., Flocke, F., Franchin, A., Fredrickson, C., Hall, S., Halliday, H., Holmes, C., Huey, L. G., Lee, Y. R., Lindaas, J., Middlebrook, A., Montzka, D., Moore, R., ... Brown, S. (2021). Nighttime and Daytime Dark Oxidation Chemistry in Wildfire Plumes: An Observation and Model Analysis of FIREX-AQ Aircraft Data. *Atmospheric Chemistry and Physics Discussions*, November, 1–45. <https://doi.org/10.5194/acp-2021-267>
- Dlugokencky, E. J., & Howard, C. J. (1989a). + (1.28. 17, 1091–1096.
- Dlugokencky, E. J., & Howard, C. J. (1989b). Studies of NO<sub>3</sub> radical reactions with some atmospheric organic compounds at low pressures. *Journal of Physical Chemistry*, 93(3), 1091–1096. <https://doi.org/10.1021/j100340a015>
- Dodge, M. C. (2000). Chemical oxidant mechanisms for air quality modeling: Critical review. *Atmospheric Environment*, 34(12–14), 2103–2130. [https://doi.org/10.1016/S1352-2310\(99\)00461-6](https://doi.org/10.1016/S1352-2310(99)00461-6)
- Durigan, M. R., Cherubin, M. R., de Camargo, P. B., Ferreira, J. N., Berenguer, E., Gardner, T. A., Barlow,



- J., Dias, C. T. dos S., Signor, D., de Oliveira, R. C., & Cerri, C. E. P. (2017). Soil organic matter responses to anthropogenic forest disturbance and land use change in the eastern Brazilian Amazon. *Sustainability (Switzerland)*, 9(3). <https://doi.org/10.3390/su9030379>
- Dusanter, S., Vimal, D., Stevens, P. S., Volkamer, R., Molina, L. T., Baker, A., Meinardi, S., Blake, D., Sheehy, P., Merten, A., Zhang, R., Zheng, J., Fortner, E. C., Junkermann, W., Dubey, M., Rann, T., Eichinger, B., Lewandowski, P., Prueger, J., & Holder, H. (2009). Measurements of OH and HO<sub>2</sub> concentrations during the MCMA-2006 field campaign - Part 2: Model comparison and radical budget. *Atmospheric Chemistry and Physics*, 9(18), 6655–6675. <https://doi.org/10.5194/acp-9-6655-2009>
- Eble, J., Bänisch, C., & Olzmann, M. (2015). *Kinetic Investigation of the Reactions of 2, 5-Dimethylfuran and 2-Methylfuran with Hydroxyl Radicals*. 2–5.
- Elshorbany, Y., Barnes, I., Becker, K. H., Kleffmann, J., & Wiesen, P. (2010). Sources and cycling of tropospheric hydroxyl radicals - An overview. *Zeitschrift Fur Physikalische Chemie*, 224(7–8), 967–987. <https://doi.org/10.1524/zpch.2010.6136>
- Elshorbany, Y. F., Kurtenbach, R., Wiesen, P., Lissi, E., Rubio, M., Villena, G., Gramsch, E., Rickard, A. R., Pilling, M. J., & Kleffmann, J. (2009). Oxidation capacity of the city air of Santiago, Chile. *Atmospheric Chemistry and Physics*, 9(6), 2257–2273. <https://doi.org/10.5194/acp-9-2257-2009>
- Elwardany, A., Es-Sebbar, E., Khaled, F., & Farooq, A. (2016). A chemical kinetic study of the reaction of hydroxyl with furans. *Fuel*, 166, 245–252. <https://doi.org/10.1016/j.fuel.2015.10.098>
- Evtugina, M., Alves, C., Calvo, A., Nunes, T., Tarelho, L., Duarte, M., Prozil, S. O., Evtuguin, D. V., & Pio, C. (2014). VOC emissions from residential combustion of Southern and mid-European woods. *Atmospheric Environment*, 83, 90–98. <https://doi.org/10.1016/j.atmosenv.2013.10.050>
- Evtugina, M., Calvo, A. I., Nunes, T., Alves, C., Fernandes, A. P., Tarelho, L., Vicente, A., & Pio, C. (2013). VOC emissions of smouldering combustion from Mediterranean wildfires in central Portugal. *Atmospheric Environment*, 64, 339–348. <https://doi.org/10.1016/j.atmosenv.2012.10.001>
- Fayad, L. (2019). *Caractérisation de la nouvelle chambre de simulation atmosphérique CHARME et étude de la réaction d'ozonolyse d'un COV biogénique, le  $\gamma$ -terpinène* Loyal FAYAD *Acknowledgments* (Vol. 104).
- Fayad, L., Coeur, C., Fagniez, T., Secordel, X., Houzel, N., & Mouret, G. (2021). Kinetic and mechanistic study of the gas-phase reaction of ozone with  $\gamma$ -terpinene. *Atmospheric Environment*, 246(August 2020). <https://doi.org/10.1016/j.atmosenv.2020.118073>
- Ferdous, D., Dalai, A. K., Bej, S. K., & Thring, R. W. (2002). Pyrolysis of lignins: Experimental and kinetics studies. *Energy and Fuels*, 16(6), 1405–1412. <https://doi.org/10.1021/ef0200323>
- Finlayson-Pitts, B. J. (2010). Atmospheric chemistry. *Proceedings of the National Academy of Sciences of the United States of America*, 107(15), 6566–6567. <https://doi.org/10.1073/pnas.1003038107>
- Finlayson-Pitts, B. J., & Pitts, J. N. (1993). Atmospheric chemistry of tropospheric ozone formation: Scientific and regulatory implications. *Air and Waste*, 43(8), 1091–1100. <https://doi.org/10.1080/1073161X.1993.10467187>
- Finlayson-Pitts, Barbara J., & James N. Pitts Jr. (1999). *Chemistry of the upper and lower atmosphere: theory, experiments, and applications*. El Sevier.
- Fuchs, J. D. H., Seakins, A. K. P., & Editors, J. W. (n.d.). *A Practical Guide to Atmospheric*.
- George, C., Ammann, M., D'Anna, B., Donaldson, D. J., & Nizkorodov, S. A. (2015). Heterogeneous Photochemistry in the Atmosphere. *Chemical Reviews*, 115(10), 4218–4258.

<https://doi.org/10.1021/cr500648z>

- Gilman, J. B., Lerner, B. M., Kuster, W. C., Goldan, P. D., Warneke, C., Veres, P. R., Roberts, J. M., De Gouw, J. A., Burling, I. R., & Yokelson, R. J. (2015). Biomass burning emissions and potential air quality impacts of volatile organic compounds and other trace gases from fuels common in the US. *Atmospheric Chemistry and Physics*, *15*(24), 13915–13938. <https://doi.org/10.5194/acp-15-13915-2015>
- Giri, B. R., Khaled, F., Szori, M., Viskolcz, B., & Farooq, A. (2017). An experimental and theoretical kinetic study of the reaction of OH radicals with tetrahydrofuran. *Proceedings of the Combustion Institute*, *36*(1), 143–150. <https://doi.org/10.1016/j.proci.2016.06.016>
- Gómez Alvarez, E., Borrás, E., Viidanoja, J., & Hjorth, J. (2009). Unsaturated dicarbonyl products from the OH-initiated photo-oxidation of furan, 2-methylfuran and 3-methylfuran. *Atmospheric Environment*, *43*(9), 1603–1612. <https://doi.org/10.1016/j.atmosenv.2008.12.019>
- Graedel, T. E., & Keene, W. C. (1996). The budget and cycle of Earth's natural chlorine. *Pure and Applied Chemistry*, *68*(9), 1689–1697. <https://doi.org/10.1351/pac199668091689>
- Graham, B., Mayol-Bracero, O. L., Guyon, P., Roberts, G. C., Decesari, S., Facchini, M. C., Artaxo, P., Maenhaut, W., Köll, P., & Andreae, M. O. (2002). Water-soluble organic compounds in biomass burning aerosols over Amazonia 1. Characterization by NMR and GC-MS. *Journal of Geophysical Research Atmospheres*, *107*(20), LBA 14-1-LBA 14-16. <https://doi.org/10.1029/2001JD000336>
- Greenberg, J. P., Zimmerman, P. R., Heidt, L., & Pollock, W. (1984). Hydrocarbon and carbon monoxide emissions from biomass burning in Brazil. *Journal of Geophysical Research*, *89*(D1), 1350–1354. <https://doi.org/10.1029/JD089iD01p01350>
- Girra, A., Amarandei, C., Romanias, M. N., El Dib, G., Canosa, A., Arsene, C., Bejan, I. G., Olariu, R. I., Coddeville, P., & Tomas, A. (2020). Kinetic measurements of Cl atom reactions with C5-C8 unsaturated alcohols. *Atmosphere*, *11*(3), 1–15. <https://doi.org/10.3390/ATMOS11030256>
- Guenther, A., Nicholas, C., Fall, R., Klinger, L., McKay, W. A., & Scholes, B. (1995). A global model of natural volatile organic compound emissions s Raja the balance Triangle changes in the atmospheric accumulation rates of greenhouse Triangle Several inventories of natural and Exposure Assessment global scales have been two classes Fores. *J. Geophys. Res.*, *100*(94), 8873–8892.
- Hartikainen, A., Yli-Pirilä, P., Tiitta, P., Leskinen, A., Kortelainen, M., Orasche, J., Schnelle-Kreis, J., Lehtinen, K. E. J., Zimmermann, R., Jokiniemi, J., & Sippula, O. (2018). Volatile Organic Compounds from Logwood Combustion: Emissions and Transformation under Dark and Photochemical Aging Conditions in a Smog Chamber. *Environmental Science and Technology*, *52*(8), 4979–4988. <https://doi.org/10.1021/acs.est.7b06269>
- Hatch, L. E., Luo, W., Pankow, J. F., Yokelson, R. J., Stockwell, C. E., & Barsanti, K. C. (2015). Identification and quantification of gaseous organic compounds emitted from biomass burning using two-dimensional gas chromatography-time-of-flight mass spectrometry. *Atmospheric Chemistry and Physics*, *15*(4), 1865–1899. <https://doi.org/10.5194/acp-15-1865-2015>
- Hatch, L. E., Yokelson, R. J., Stockwell, C. E., Veres, P. R., Simpson, I. J., Blake, D. R., Orlando, J. J., & Barsanti, K. C. (2017). Multi-instrument comparison and compilation of non-methane organic gas emissions from biomass burning and implications for smoke-derived secondary organic aerosol precursors. *Atmospheric Chemistry and Physics*, *17*(2), 1471–1489. <https://doi.org/10.5194/acp-17-1471-2017>
- Hein, R., Crutzen, P. J., & Heimann, M. (1997). An inverse modeling approach to investigate the global

- atmospheric methane cycle. *Global Biogeochemical Cycles*, 11(1), 43–76. <https://doi.org/10.1029/96GB03043>
- Holly Zell. (2013). *Earth's Atmospheric Layers*. [https://www.nasa.gov/mission\\_pages/sunearth/science/atmosphere-layers2.html](https://www.nasa.gov/mission_pages/sunearth/science/atmosphere-layers2.html)
- Huang, Z., Zhao, N., Ma, X., Xu, F., Zhang, Q., Zhuang, T., & Wang, W. (2019). Theoretical study on the atmospheric oxidation reaction of 2-furaldehyde initiated by NO<sub>3</sub> radicals. *Chemical Physics Letters*, 722(3), 50–57. <https://doi.org/10.1016/j.cplett.2019.03.009>
- Hynes, R. G., Angove, D. E., Saunders, S. M., Haverd, V., & Azzi, M. (2005). Evaluation of two MCM v3.1 alkene mechanisms using indoor environmental chamber data. *Atmospheric Environment*, 39(38), 7251–7262. <https://doi.org/10.1016/j.atmosenv.2005.09.005>
- Identification, I., Flux, V., & Atkinson, R. (1990). *Radicals with*. 24(10), 1497–1502.
- Illés, Á., Rózsa, Z. B., Thangaraj, R., Décsiné Gombos, E., Dóbbé, S., Giri, B. R., & Szóri, M. (2021). An experimental and theoretical kinetic study of the reactions of hydroxyl radicals with tetrahydrofuran and two deuterated tetrahydrofurans. *Chemical Physics Letters*, 776. <https://doi.org/10.1016/j.cplett.2021.138698>
- IUPAC. (2016). *IUPAC Task Group on Atmospheric Chemical Kinetic Data Evaluation – Data Sheet NO<sub>3</sub> VOC*. [iupac.pole-ether.fr](http://iupac.pole-ether.fr)
- Jenkin, M. E., & Hayman, G. D. (1999). Photochemical ozone creation potentials for oxygenated volatile organic compounds: Sensitivity to variations in kinetic and mechanistic parameters. *Atmospheric Environment*, 33(8), 1275–1293. [https://doi.org/10.1016/S1352-2310\(98\)00261-1](https://doi.org/10.1016/S1352-2310(98)00261-1)
- Jiang, G., Nowakowski, D. J., & Bridgwater, A. V. (2010). Effect of the temperature on the composition of lignin pyrolysis products. *Energy and Fuels*, 24(8), 4470–4475. <https://doi.org/10.1021/ef100363c>
- Jiang, J., Carter, W. P. L., Cocker, D. R., & Barsanti, K. C. (2020). Development and Evaluation of a Detailed Mechanism for Gas-Phase Atmospheric Reactions of Furans. *ACS Earth and Space Chemistry*, 4(8), 1254–1268. <https://doi.org/10.1021/acsearthspacechem.0c00058>
- Joo, T., Rivera-Rios, J. C., Takeuchi, M., Alvarado, M. J., & Ng, N. L. (2019a). Secondary Organic Aerosol Formation from Reaction of 3-Methylfuran with Nitrate Radicals. *ACS Earth and Space Chemistry*, 3(6), 922–934. <https://doi.org/10.1021/acsearthspacechem.9b00068>
- Joo, T., Rivera-Rios, J. C., Takeuchi, M., Alvarado, M. J., & Ng, N. L. (2019b). Secondary Organic Aerosol Formation from Reaction of 3-Methylfuran with Nitrate Radicals [Research-article]. *ACS Earth and Space Chemistry*, 3(6), 922–934. <https://doi.org/10.1021/acsearthspacechem.9b00068>
- Kawamoto, H. (2017). Lignin pyrolysis reactions. *Journal of Wood Science*, 63(2), 117–132. <https://doi.org/10.1007/s10086-016-1606-z>
- Keene, W. C., Maring, H., Maben, J. R., Kieber, D. J., Pszenny, A. A. P., Dahl, E. E., Izaguirre, M. A., Davis, A. J., Long, M. S., Zhou, X., Smoydzin, L., & Sander, R. (2007). Chemical and physical characteristics of nascent aerosols produced by bursting bubbles at a model air-sea interface. *Journal of Geophysical Research Atmospheres*, 112(21), 1–16. <https://doi.org/10.1029/2007JD008464>
- Kind, I., Berndt, T., Bisge, O., & Rolle, W. (1996a). *Gas-phase rate constants for the reaction of*. 2614(3), 2–6.
- Kind, I., Berndt, T., Bisge, O., & Rolle, W. (1996b). *Gas-phase rate constants for the reaction of NO<sub>3</sub> radicals with furan and methyl-substituted furans*. 2614(3), 2–6.

- Kind, I., Berndt, T., Böge, O., & Rolle, W. (1996). Gas-phase rate constants for the reaction of NO<sub>3</sub> radicals with selected oxiranes. *Chemical Physics Letters*, 249(1–2), 35–39. [https://doi.org/10.1016/0009-2614\(95\)01327-X](https://doi.org/10.1016/0009-2614(95)01327-X)
- Koolen, C. D., & Rothenberg, G. (2019). Air Pollution in Europe. *ChemSusChem*, 12(1), 164–172. <https://doi.org/10.1002/cssc.201802292>
- Koppmann, R. (2007). Volatile Organic Compounds in the Atmosphere. In *Volatile Organic Compounds in the Atmosphere*. <https://doi.org/10.1002/9780470988657>
- Koppmann, R., Khedim, A., Rudolph, J., Poppe, D., Andreae, M. O., Helas, G., Welling, M., & Zenker, T. (1997). Emissions of organic trace gases from savanna fires in southern Africa during the 1992 Southern African Fire Atmosphere Research Initiative and their impact on the formation of tropospheric ozone. *Journal of Geophysical Research Atmospheres*, 102(15), 18879–18888. <https://doi.org/10.1029/97jd00845>
- Koss, A. R., Sekimoto, K., Gilman, J. B., Selimovic, V., Coggon, M. M., Zarzana, K. J., Yuan, B., Lerner, B. M., Brown, S. S., Jimenez, J. L., Krechmer, J., Roberts, J. M., Warneke, C., Yokelson, R. J., & De Gouw, J. (2018). Non-methane organic gas emissions from biomass burning: Identification, quantification, and emission factors from PTR-ToF during the FIREX 2016 laboratory experiment. *Atmospheric Chemistry and Physics*, 18(5), 3299–3319. <https://doi.org/10.5194/acp-18-3299-2018>
- Krause, T., Tubbesing, C., Benzing, K., & Schöler, H. F. (2014). Model reactions and natural occurrence of furans from hypersaline environments. *Biogeosciences*, 11(10), 2871–2882. <https://doi.org/10.5194/bg-11-2871-2014>
- Kumar, V., Chandra, B. P., & Sinha, V. (2018). Large unexplained suite of chemically reactive compounds present in ambient air due to biomass fires. *Scientific Reports*, 8(1), 1–15. <https://doi.org/10.1038/s41598-017-19139-3>
- Lalchandani, V., Srivastava, D., Dave, J., Mishra, S., Tripathi, N., Shukla, A. K., Sahu, R., Thamban, N. M., Gaddamidi, S., Dixit, K., Ganguly, D., Tiwari, S., Srivastava, A. K., Sahu, L., Rastogi, N., Gargava, P., & Tripathi, S. N. (2021). Effect of biomass burning on PM 2.5 composition and secondary aerosol formation during post-monsoon and winter haze episodes in Delhi. *Journal of Geophysical Research: Atmospheres*, 1–21. <https://doi.org/10.1029/2021jd035232>
- Lambe, A. T., Chhabra, P. S., Onasch, T. B., Brune, W. H., Hunter, J. F., Kroll, J. H., Cummings, M. J., Brogan, J. F., Parmar, Y., Worsnop, D. R., Kolb, C. E., & Davidovits, P. (2015). Effect of oxidant concentration, exposure time, and seed particles on secondary organic aerosol chemical composition and yield. *Atmospheric Chemistry and Physics*, 15(6), 3063–3075. <https://doi.org/10.5194/acp-15-3063-2015>
- Lancar, I., Daele, V., Le Bras, G., & Poulet, G. (1991). Étude de la réactivité des radicaux NO<sub>3</sub> avec le diméthyl-2,3 butène-2, le butadiène-1,3 et le diméthyl-2,3 butadiène-1,3. *J. Chim. Phys*, 88, 1777–1792. <https://doi.org/10.1051/jcp/1991881777>
- Lançar, I., Daele, V., Le Bras, G., & Poulet, G. (1991). Étude de la réactivité des radicaux NO<sub>3</sub> avec le diméthyl-2,3 butène-2, le butadiène-1,3 et le diméthyl-2,3 butadiène-1,3. *Journal de Chimie Physique*, 88, 1777–1792. <https://doi.org/10.1051/jcp/1991881777>
- Lange, J. P., Price, R., Ayoub, P. M., Louis, J., Petrus, L., Clarke, L., & Gosselink, H. (2010). Valeric biofuels: A platform of cellulosic transportation fuels. *Angewandte Chemie - International Edition*, 49(26), 4479–4483. <https://doi.org/10.1002/anie.201000655>
- Lauraguais, A., Coeur-tourneur, C., Cassez, A., & Seydi, A. (2012). Rate constant and secondary organic

- aerosol yields for the gas-phase reaction of hydroxyl radicals with syringol ( 2,6-dimethoxyphenol ). *Atmospheric Environment*, 55, 43–48. <https://doi.org/10.1016/j.atmosenv.2012.02.027>
- Lê Thành, K., Commandré, J. M., Valette, J., Volle, G., & Meyer, M. (2015). Detailed identification and quantification of the condensable species released during torrefaction of lignocellulosic biomasses. *Fuel Processing Technology*, 139, 226–235. <https://doi.org/10.1016/j.fuproc.2015.07.001>
- Lee, J. H., & Tang, I. N. (1982). Absolute rate constants for the hydroxyl radical reactions with ethane, furan, and thiophene at room temperature. *The Journal of Chemical Physics*, 77(9), 4459–4463. <https://doi.org/10.1063/1.444367>
- Liang, Y., Weber, R. J., Misztal, P. K., Jen, C. N., & Goldstein, A. H. (2022). Aging of Volatile Organic Compounds in October 2017 Northern California Wildfire Plumes. *Environmental Science and Technology*, 56(3), 1557–1567. <https://doi.org/10.1021/acs.est.1c05684>
- Liley, P. E., Buck, E., & Ch, M. S. E. (1999). 493-Physical and Chemical Data 物性数据. *Perry's Chemical Engineers Handbook*, 2–86.
- Liljegren, J. A., & Stevens, P. S. (2013). Measurements of the kinetics of the reaction of OH radicals with 3-methylfuran at low pressure. *International Journal of Chemical Kinetics*, 45(12), 787–794. <https://doi.org/10.1002/kin.20814>
- Lin, Y., Cho, J., Tompsett, G. A., Westmoreland, P. R., & Huber, G. W. (2009). Kinetics Mechanism Cellulose Pyrolysis. *Phys. Chem. C*, 113, 20097–20107.
- Lindinger, W., Hansel, A., & Jordan, A. (1998). On-line monitoring of volatile organic compounds at pptv levels by means of Proton-Transfer-Reaction Mass Spectrometry (PTR-MS) Medical applications, food control and environmental research. *International Journal of Mass Spectrometry and Ion Processes*, 173(3), 191–241. [https://doi.org/10.1016/s0168-1176\(97\)00281-4](https://doi.org/10.1016/s0168-1176(97)00281-4)
- Ljungström, E., Wängberg, I., & Langer, S. (1993). Absolute rate coefficients for the reaction between nitrate radicals and some cyclic alkenes. *Journal of the Chemical Society, Faraday Transactions*, 89(16), 2977–2982. <https://doi.org/10.1039/FT9938902977>
- Manion, J., Huie, R. E., Burgess, D. R., Orkin, V. L., Tsang, W., McGivern, W. ., Hudgens, J. W., Knyazev, V. D., Atkinson, D. B., Chai, E., Tereza, A. M., Lin, C. Y., Allison, T. C., Mallard, W. G., Westley, F., Herron, J. T., Hampson, R. F., & Frizzell, D. H. (2015). *NIST Chemical Kinetics Database, NIST Standard Reference Database 17, Version 7.0 (Web Version), Release 1.6.8, Data version 2015.09*.
- Martín, P., Cabañas, B., Colmenar, I., Salgado, M. S., Villanueva, F., & Tapia, A. (2013). Reactivity of E-butenedial with the major atmospheric oxidants. *Atmospheric Environment*, 70, 351–360. <https://doi.org/10.1016/j.atmosenv.2013.01.041>
- Martinez, E., Cabanas, B., Aranda, A., & Martín, P. (1998). Kinetics of the reactions of NO<sub>3</sub> radical with selected monoterpenes: A temperature dependence study. *Environmental Science and Technology*, 32(23), 3730–3734. <https://doi.org/10.1021/es970899t>
- Martínez, E., Cabañas, B., Aranda, A., Martín, P., Notario, A., & Salgado, S. (1999). Study on the NO<sub>3</sub> Radical Reactivity: Reactions with Cyclic Alkenes. *Journal of Physical Chemistry A*, 103(27), 5321–5327. <https://doi.org/10.1021/jp9847181>
- Martinez, E., Cabañas, B., Aranda, A., Martin, P., & Salgado, S. (1999). Absolute Rate Coefficients for the Gas-Phase Reactions of NO<sub>3</sub> Radical with a Series of Monoterpenes at T = 298 to 433 K. *Journal of Atmospheric Chemistry*, 33(3), 265–282. <https://doi.org/10.1023/A:1006178530211>

- Mathematics, A. (2016). 濟無No Title No Title No Title. *19*(1), 1–23.
- Matsumoto, J. (2011). Kinetics of the reactions of ozone with 2,5-dimethylfuran and its atmospheric implications. *Chemistry Letters*, *40*(6), 582–583. <https://doi.org/10.1246/cl.2011.582>
- Mcdonald, J. D., Zielinska, B., Fujita, E. M., Sagebiel, J. C., Chow, J. C., & Watson, J. G. (2000). Fine particle and gaseous emission rates from residential wood combustion. *Environmental Science and Technology*, *34*(11), 2080–2091. <https://doi.org/10.1021/es9909632>
- Mellouki, A., & Chen, J. (2015). *Atmospheric Chemistry of Oxygenated Volatile Organic Compounds : Impacts on Air Quality and Climate*. <https://doi.org/10.1021/cr500549n>
- Meng, L., Coeur, C., Fayad, L., Houzel, N., Genevray, P., Bouzidi, H., Tomas, A., & Chen, W. (2020). Secondary organic aerosol formation from the gas-phase reaction of guaiacol (2-methoxyphenol) with NO<sub>3</sub> radicals. *Atmospheric Environment*, *240*(July). <https://doi.org/10.1016/j.atmosenv.2020.117740>
- Mettler, M. S., Mushrif, S. H., Paulsen, A. D., Javadekar, A. D., Vlachos, D. G., & Dauenhauer, P. J. (2012). Revealing pyrolysis chemistry for biofuels production: Conversion of cellulose to furans and small oxygenates. *Energy and Environmental Science*, *5*(1), 5414–5424. <https://doi.org/10.1039/c1ee02743c>
- Molina, M. J., & Molina, L. T. (2004). Megacities and atmospheric pollution. *Journal of the Air and Waste Management Association*, *54*(6), 644–680. <https://doi.org/10.1080/10473289.2004.10470936>
- Moriarty, J., Sidebottom, H., Wenger, J., Mellouki, A., & Le Bras, G. (2003). Kinetic studies on the reactions of hydroxyl radicals with cyclic ethers and aliphatic diethers. *Journal of Physical Chemistry A*, *107*(10), 1499–1505. <https://doi.org/10.1021/jp021267i>
- Mudhoo, A., Thayalan, G., Muthoora, N. J., Muthoora, M. N., Oozer, B. Z., Rago, Y. P., Ramphul, M. P., Valaydon, A. K., & Kumar, S. (2013). *Dioxins and Furans: Sources, Impacts and Remediation*. [https://doi.org/10.1007/978-3-319-02387-8\\_10](https://doi.org/10.1007/978-3-319-02387-8_10)
- Müller, M., Anderson, B. E., Beyersdorf, A. J., Crawford, J. H., Diskin, G. S., Eichler, P., Fried, A., Keutsch, F. N., Mikoviny, T., Thornhill, K. L., Walega, J. G., Weinheimer, A. J., Yang, M., Yokelson, R. J., & Wisthaler, A. (2016). In situ measurements and modeling of reactive trace gases in a small biomass burning plume. *Atmospheric Chemistry and Physics*, *16*(6), 3813–3824. <https://doi.org/10.5194/acp-16-3813-2016>
- Müller, M., Graus, M., Wisthaler, A., Hansel, A., Metzger, A., Dommen, J., & Baltensperger, U. (2012). Analysis of high mass resolution PTR-TOF mass spectra from 1,3,5-trimethylbenzene (TMB) environmental chamber experiments. *Atmospheric Chemistry and Physics*, *12*(2), 829–843. <https://doi.org/10.5194/acp-12-829-2012>
- Munger, J. W., Jacob, D. J., Waldman, J. M., & Hoffmann, M. R. (1983). Fogwater chemistry in an urban atmosphere. *Journal of Geophysical Research*, *88*(C9), 5109–5121. <https://doi.org/10.1029/JC088iC09p05109>
- Newland, M. J., Ren, Y., Mcgillen, M. R., Michelat, L., Daële, V., & Mellouki, A. (2022). NO<sub>3</sub> chemistry of wildfire emissions: A kinetic study of the gas-phase reactions of furans with the NO<sub>3</sub> radical. *Atmospheric Chemistry and Physics*, *22*(3), 1761–1772. <https://doi.org/10.5194/acp-22-1761-2022>
- Nguyen, T. B., Coggon, M. M., Bates, K. H., Zhang, X., Schwantes, R. H., Schilling, K. A., Loza, C. L., Flagan, R. C., Wennberg, P. O., & Seinfeld, J. H. (2014). Organic aerosol formation from the reactive uptake of isoprene epoxydiols (IEPOX) onto non-acidified inorganic seeds. *Atmospheric Chemistry*

- and Physics*, 14(7), 3497–3510. <https://doi.org/10.5194/acp-14-3497-2014>
- Odum, J. R., Hoffmann, T., Bowman, F., Collins, D., Flagan, R. C., & Seinfeld, J. H. (1996). Gas/particle partitioning and secondary organic aerosol yields. *Environmental Science and Technology*, 30(8), 2580–2585. <https://doi.org/10.1021/es950943+>
- Oh, H. J., Ma, Y., & Kim, J. (2020). Human inhalation exposure to aerosol and health effect: Aerosol monitoring and modelling regional deposited doses. *International Journal of Environmental Research and Public Health*, 17(6), 1–2. <https://doi.org/10.3390/ijerph17061923>
- Olariu, R. I., Bejan, I., Barnes, I., Klotz, B., Becker, K. H., & Wirtz, K. (2004). Rate coefficients for the gas-phase reaction of NO<sub>3</sub> radicals with selected dihydroxybenzenes. *International Journal of Chemical Kinetics*, 36(11), 577–583. <https://doi.org/10.1002/kin.20029>
- Olariu, R. I., Cuza, A. I., Chemistry, A., Tomas, A., Douai, M. De, Chimie, D., Barnes, I., Bejan, I., Becker, K. H., Wuppertal, B. U., Wirtz, K., Centro, F., & Ambientales, D. E. (1998). *Atmospheric Ozone Degradation Reaction of 1, 2-dihydroxybenzene : Aerosol Formation Study*. 1–12.
- Osseiran, N., Romanias, M. N., Gaudion, V., Angelaki, M. E., Papadimitriou, V. C., Tomas, A., Coddeville, P., & Thevenet, F. (2020). Development and validation of a thermally regulated atmospheric simulation chamber (THALAMOS): A versatile tool to simulate atmospheric processes. *Journal of Environmental Sciences (China)*, 95(xxxx), 141–154. <https://doi.org/10.1016/j.jes.2020.03.036>
- Pankow, J. F. (1994). An absorption model of the gas/aerosol partitioning involved in the formation of secondary organic aerosol. *Atmospheric Environment*, 28(SUPPL.), 189–193. <https://doi.org/10.1016/j.atmosenv.2007.10.060>
- Papadimitriou, V. C., Lazarou, Y. G., Talukdar, R. K., & Burkholder, J. B. (2011). *Atmospheric Chemistry of CF<sub>3</sub>CF<sub>2</sub>*. 2(3), 167–181.
- Paquet, M., Arlt, D., Knape, J., Low, M., Forslund, P., & Pärt, T. (2019). Quantifying the links between land use and population growth rate in a declining farmland bird. *Ecology and Evolution*, 9(2), 868–879. <https://doi.org/10.1002/ece3.4766>
- Qian, Y., Zhu, L., Wang, Y., & Lu, X. (2015). Recent progress in the development of biofuel 2,5-dimethylfuran. *Renewable and Sustainable Energy Reviews*, 41, 633–646. <https://doi.org/10.1016/j.rser.2014.08.085>
- Ravishankara, A. R., & Davis, D. D. (1978). Kinetic rate constants for the reaction of OH with methanol, ethanol, and tetrahydrofuran at 298 K [2]. *Journal of Physical Chemistry*, 82(26), 2852–2853. <https://doi.org/10.1021/j100515a022>
- Reddington, C. L., Spracklen, D. V., Artaxo, P., Ridley, D. A., Rizzo, L. V., & Arana, A. (2016). Analysis of particulate emissions from tropical biomass burning using a global aerosol model and long-term surface observations. *Atmospheric Chemistry and Physics*, 16(17), 11083–11106. <https://doi.org/10.5194/acp-16-11083-2016>
- Ren, X., Brune, W. H., Oliger, A., Metcalf, A. R., Simpas, J. B., Shirley, T., Schwab, J. J., Bai, C., Roychowdhury, U., Li, Y., Cai, C., Demerjian, K. L., He, Y., Zhou, X., Gao, H., & Hou, J. (2006). *OH, HO<sub>2</sub>, and OH reactivity during the PMTACS – NY Whiteface Mountain 2002 campaign : Observations and model comparison*. 111, 1–12. <https://doi.org/10.1029/2005JD006126>
- Ren, X., Gao, H., Zhou, X., Crouse, J. D., Wennberg, P. O., Browne, E. C., LaFranchi, B. W., Cohen, R. C., McKay, M., Goldstein, A. H., & Mao, J. (2010). Measurement of atmospheric nitrous acid at Bodgett forest during BEARPEX2007. *Atmospheric Chemistry and Physics*, 10(13), 6283–6294. <https://doi.org/10.5194/acp-10-6283-2010>

- Ren, X., Harder, H., Martinez, M., Leshner, R. L., Oligier, A., Simpas, J. B., Brune, W. H., Schwab, J. J., Demerjian, K. L., He, Y., Zhou, X., & Gao, H. (2003). OH and HO<sub>2</sub> chemistry in the urban atmosphere of New York City. *Atmospheric Environment*, 37(26), 3639–3651. [https://doi.org/10.1016/S1352-2310\(03\)00459-X](https://doi.org/10.1016/S1352-2310(03)00459-X)
- Rissanen, M. (2021). Anthropogenic Volatile Organic Compound (AVOC) Autoxidation as a Source of Highly Oxygenated Organic Molecules (HOM). *Journal of Physical Chemistry A*, 125(41), 9027–9039. <https://doi.org/10.1021/acs.jpca.1c06465>
- Roberts, J. M., Stockwell, C. E., Yokelson, R. J., De Gouw, J., Liu, Y., Selimovic, V., Koss, A. R., Sekimoto, K., Coggon, M. M., Yuan, B., Zarzana, K. J., Brown, S. S., Santin, C., Doerr, S. H., & Warneke, C. (2020). The nitrogen budget of laboratory-simulated western US wildfires during the FIREX 2016 Fire Lab study. *Atmospheric Chemistry and Physics*, 20(14), 8807–8826. <https://doi.org/10.5194/acp-20-8807-2020>
- Román-Leshkov, Y., Barrett, C. J., Liu, Z. Y., & Dumesic, J. A. (2007). Production of dimethylfuran for liquid fuels from biomass-derived carbohydrates. *Nature*, 447(7147), 982–985. <https://doi.org/10.1038/nature05923>
- Romanias, M. N., Coggon, M., Al Ali, F., Burkholder, J. B., Dagaut, P., Warneke, C., Stockwell, C. E., Decker, Z., Tomas, A., Houzel, N., Coeur, C., & Brown, S. (n.d.-a). Atmospheric chemistry of furanoids: insights into the sources and atmospheric fate. *Atmospheric Environment*.
- Romanias, M. N., Coggon, M. M., Al Ali, F., Burkholder, J. B., Dagaut, P., Warneke, C., Stockwell, C. E., Decker, Z. C. J., Tomas, A., Houzel, N., Coeur, C., & Brown, S. S. (n.d.-b). Atmospheric chemistry of furanoids: insights into the sources and atmospheric fate. *ASC ACS Earth and Space Chemistry*.
- Schellenberg, C. (2009). Conducta irascible y recalcitrante tras una infección de gripe: Efectos de una acupuntura dispersante en el H 3 en lactantes y niños pequeños. *Revista Internacional de Acupuntura*, 3(2), 78–79. [https://doi.org/10.1016/S1887-8369\(09\)71579-0](https://doi.org/10.1016/S1887-8369(09)71579-0)
- Schumann, U. (2012). Atmospheric Physics. In *Physics Today* (Vol. 15, Issue 5). <https://doi.org/10.1063/1.3058219>
- Seinfeld, J. H., Pandis, S. N., & Noone, K. (1998). Atmospheric Chemistry and Physics: From Air Pollution to Climate Change. In *Physics Today* (Vol. 51, Issue 10). <https://doi.org/10.1063/1.882420>
- Sekimoto, K., Koss, A. R., Gilman, J. B., Selimovic, V., Coggon, M. M., Zarzana, K. J., Yuan, B., Lerner, B. M., Brown, S. S., Warneke, C., Yokelson, R. J., Roberts, J. M., & De Gouw, J. (2018). High-and low-temperature pyrolysis profiles describe volatile organic compound emissions from western US wildfire fuels. *Atmospheric Chemistry and Physics*, 18(13), 9263–9281. <https://doi.org/10.5194/acp-18-9263-2018>
- Selimovic, V., Yokelson, R. J., Warneke, C., Roberts, J. M., De Gouw, J., Reardon, J., & Griffith, D. W. T. (2018). Aerosol optical properties and trace gas emissions by PAX and OP-FTIR for laboratory-simulated western US wildfires during FIREX. *Atmospheric Chemistry and Physics*, 18(4), 2929–2948. <https://doi.org/10.5194/acp-18-2929-2018>
- Si, Z., Wang, C. G., Bi, K., Zhang, X. H., Yu, C. L., Dong, R. J., Ma, L. L., & Changle, P. (2017). Py-GC/MS study of lignin pyrolysis and effect of catalysts on product distribution. *International Journal of Agricultural and Biological Engineering*, 10(5), 214–225. <https://doi.org/10.25165/j.ijabe.20171005.2852>
- Simoneit, B. R. T. (2002). Biomass burning - A review of organic tracers for smoke from incomplete combustion. In *Applied Geochemistry* (Vol. 17, Issue 3). <https://doi.org/10.1016/S0883->



- Smith, D., & Španěl, P. (2005). Selected ion flow tube mass spectrometry (SIFT-MS) for on-line trace gas analysis. *Mass Spectrometry Reviews*, *24*(5), 661–700. <https://doi.org/10.1002/mas.20033>
- Song, C., NA, K., & Cocker, D. R. (2005). Impact of the Hydrocarbon to NO. *Environmental Science & Technology*, *39*(9), 3143–3149.
- Španěl, P., Dryahina, K., & Smith, D. (2013). A quantitative study of the influence of inhaled compounds on their concentrations in exhaled breath. *Journal of Breath Research*, *7*(1). <https://doi.org/10.1088/1752-7155/7/1/017106>
- Stehfest, E., van Zeist, W. J., Valin, H., Havlik, P., Popp, A., Kyle, P., Tabeau, A., Mason-D’Croz, D., Hasegawa, T., Bodirsky, B. L., Calvin, K., Doelman, J. C., Fujimori, S., Humpenöder, F., Lotze-Campen, H., van Meijl, H., & Wiebe, K. (2019). Key determinants of global land-use projections. *Nature Communications*, *10*(1), 1–10. <https://doi.org/10.1038/s41467-019-09945-w>
- Stockman, R. A. (2007). Heterocyclic chemistry. In *Annual Reports on the Progress of Chemistry - Section B* (Vol. 103). <https://doi.org/10.1039/b614418g>
- Stockwell, C. E., Christian, T. J., Goetz, J. D., Jayarathne, T., Bhave, P. V., Praveen, P. S., Adhikari, S., Maharjan, R., DeCarlo, P. F., Stone, E. A., Saikawa, E., Blake, D. R., Simpson, I. J., Yokelson, R. J., & Panday, A. K. (2016). Nepal Ambient Monitoring and Source Testing Experiment (NAMaSTE): Emissions of trace gases and light-absorbing carbon from wood and dung cooking fires, garbage and crop residue burning, brick kilns, and other sources. *Atmospheric Chemistry and Physics*, *16*(17), 11043–11081. <https://doi.org/10.5194/acp-16-11043-2016>
- Stockwell, C. E., Veres, P. R., Williams, J., & Yokelson, R. J. (2015). Characterization of biomass burning emissions from cooking fires, peat, crop residue, and other fuels with high-resolution proton-transfer-reaction time-of-flight mass spectrometry. *Atmospheric Chemistry and Physics*, *15*(2), 845–865. <https://doi.org/10.5194/acp-15-845-2015>
- Strollo, C. M., & Ziemann, P. J. (2013). Products and mechanism of secondary organic aerosol formation from the reaction of 3-methylfuran with OH radicals in the presence of NO<sub>x</sub>. *Atmospheric Environment*, *77*, 534–543. <https://doi.org/10.1016/j.atmosenv.2013.05.033>
- Tajuelo, M., Rodríguez, A., Baeza-Romero, M. T., Aranda, A., Díaz-de-Mera, Y., & Rodríguez, D. (2019). Secondary organic aerosol formation from  $\alpha$ -methylstyrene atmospheric degradation: Role of NO<sub>x</sub> level, relative humidity and inorganic seed aerosol. *Atmospheric Research*, *230*(July), 104631. <https://doi.org/10.1016/j.atmosres.2019.104631>
- Tajuelo, M., Rodríguez, D., Baeza-Romero, M. T., Díaz-de-Mera, Y., Aranda, A., & Rodríguez, A. (2019). Secondary organic aerosol formation from styrene photolysis and photooxidation with hydroxyl radicals. *Chemosphere*, *231*, 276–286. <https://doi.org/10.1016/j.chemosphere.2019.05.136>
- Tajuelo, M., Rodríguez, D., Rodríguez, A., Escalona, A., Viteri, G., Aranda, A., & Diaz-de-Mera, Y. (2021). Secondary organic aerosol formation from the ozonolysis and oh-photooxidation of 2,5-dimethylfuran. *Atmospheric Environment*, *245*, 118041. <https://doi.org/10.1016/j.atmosenv.2020.118041>
- Takekawa, H., Minoura, H., & Yamazaki, S. (2003). *Temperature dependence of secondary organic aerosol formation by photo-oxidation of hydrocarbons*. *37*, 3413–3424. [https://doi.org/10.1016/S1352-2310\(03\)00359-5](https://doi.org/10.1016/S1352-2310(03)00359-5)
- Tapia, A., Villanueva, F., Salgado, M. S., Cabañas, B., Martínez, E., & Martín, P. (2011). Atmospheric degradation of 3-methylfuran: Kinetic and products study. *Atmospheric Chemistry and Physics*, *11*(7), 3227–3241. <https://doi.org/10.5194/acp-11-3227-2011>

- Thewes, M., Muether, M., Pischinger, S., Budde, M., Brunn, A., Sehr, A., Adomeit, P., & Klankermayer, J. (2011). Analysis of the impact of 2-methylfuran on mixture formation and combustion in a direct-injection spark-ignition engine. *Energy and Fuels*, 25(12), 5549–5561. <https://doi.org/10.1021/ef201021a>
- Tomas, A., Henry, F., & Visez, N. (2009). Aerosol formation yields from the reaction of catechol with ozone. 43, 2360–2365. <https://doi.org/10.1016/j.atmosenv.2008.12.054>
- Tuan Hoang, A., & Viet Pham, V. (2021). 2-Methylfuran (MF) as a potential biofuel: A thorough review on the production pathway from biomass, combustion progress, and application in engines. *Renewable and Sustainable Energy Reviews*, 148(June), 111265. <https://doi.org/10.1016/j.rser.2021.111265>
- Tuazon, E. C., Aschmann, S. M., & Atkinson, R. (2000). Atmospheric degradation of volatile methylsilicon compounds. *Environmental Science and Technology*, 34(10), 1970–1976. <https://doi.org/10.1021/es9910053>
- Vallero, D. (2008). *Fundamentals of Air Pollution* (Fourth). El Sevier.
- Villanueva, F., Barnes, I., Monedero, E., Salgado, S., Gómez, M. V., & Martin, P. (2007). Primary product distribution from the Cl-atom initiated atmospheric degradation of furan: Environmental implications. *Atmospheric Environment*, 41(38), 8796–8810. <https://doi.org/10.1016/j.atmosenv.2007.07.053>
- Villanueva, F., Cabañas, B., Monedero, E., Salgado, S., Bejan, I., & Martin, P. (2009). Atmospheric degradation of alkylfurans with chlorine atoms: Product and mechanistic study. *Atmospheric Environment*, 43(17), 2804–2813. <https://doi.org/10.1016/j.atmosenv.2009.02.030>
- Wallington, T. J., Dagaut, P., Liu, R., & Kurylo, M. J. (1988). The gas phase reactions of hydroxyl radicals with a series of esters over the temperature range 240–440 K. *International Journal of Chemical Kinetics*, 20(2), 177–186. <https://doi.org/10.1002/kin.550200210>
- Wang, J., Doussin, J. F., Perrier, S., Perraudin, E., Katrib, Y., Pangui, E., & Picquet-Varrault, B. (2011). Design of a new multi-phase experimental simulation chamber for atmospheric photochemistry, aerosol and cloud chemistry research. *Atmospheric Measurement Techniques*, 4(11), 2465–2494. <https://doi.org/10.5194/amt-4-2465-2011>
- Wang, L., Slowik, J. G., Tripathi, N., Bhattu, D., Rai, P., Kumar, V., Vats, P., Satish, R., Baltensperger, U., Ganguly, D., Rastogi, N., Sahu, L. K., Tripathi, S. N., & Prévôt, A. S. H. (2020). Source characterization of volatile organic compounds measured by proton-transfer-reaction time-of-flight mass spectrometers in Delhi, India. *Atmospheric Chemistry and Physics*, 20(16), 9753–9770. <https://doi.org/10.5194/acp-20-9753-2020>
- Wang, Q., Song, H., Pan, S., Dong, N., Wang, X., & Sun, S. (2020). Initial pyrolysis mechanism and product formation of cellulose: An Experimental and Density functional theory(DFT) study. *Scientific Reports*, 10(1), 1–18. <https://doi.org/10.1038/s41598-020-60095-2>
- Wang, S., Wei, W., Du, L., Li, G., & Hao, J. (2009). Characteristics of gaseous pollutants from biofuel-stoves in rural China. *Atmospheric Environment*, 43(27), 4148–4154. <https://doi.org/10.1016/j.atmosenv.2009.05.040>
- Whelan, C. A., Eble, J., Mir, Z. S., Blitz, M. A., Seakins, P. W., Olzmann, M., & Stone, D. (2020). Kinetics of the Reactions of Hydroxyl Radicals with Furan and Its Alkylated Derivatives 2-Methyl Furan and 2,5-Dimethyl Furan. *Journal of Physical Chemistry A*, 124(37), 7416–7426. <https://doi.org/10.1021/acs.jpca.0c06321>
- Wine, P. H., & Thompson, R. J. (1984). Kinetics of OH reactions with furan, thiophene, and

- tetrahydrothiophene. *International Journal of Chemical Kinetics*, 16(7), 867–878. <https://doi.org/10.1002/kin.550160707>
- Winer, M., Darnall, K. R., & Lloyd, A. C. (1977). *REACTION set-BUTYL*. 5(2), 221–226.
- Wingenter, O. W., Blake, D. R., Blake, N. J., Sive, B. C., Rowland, F. S., Atlas, E., & Flocke, F. (1999). Tropospheric hydroxyl and atomic chlorine concentrations, and mixing timescales determined from hydrocarbon and halocarbon measurements made over the Southern Ocean. *Journal of Geophysical Research Atmospheres*, 104(D17), 21819–21828. <https://doi.org/10.1029/1999JD900203>
- Wingenter, O. W., Kubo, M. K., Blake, N. J., Smith, T. W., Blake, D. R., & Rowland, F. S. (1996). Hydrocarbon and halocarbon measurements as photochemical and dynamical indicators of atmospheric hydroxyl, atomic chlorine, and vertical mixing obtained during Lagrangian flights. *Journal of Geophysical Research Atmospheres*, 101(D2), 4331–4340. <https://doi.org/10.1029/95JD02457>
- World Health Organization. (2016). WORLD HEALTH STATISTICS - MONITORING HEALTH FOR THE SDGs. *World Health Organization*, 1.121. <https://doi.org/10.1017/CBO9781107415324.004>
- Xu, L., Guo, H., Weber, R. J., & Ng, N. L. (2017). Chemical Characterization of Water-Soluble Organic Aerosol in Contrasting Rural and Urban Environments in the Southeastern United States. *Environmental Science and Technology*, 51(1), 78–88. <https://doi.org/10.1021/acs.est.6b05002>
- Yang, H., Li, S., Liu, B., Chen, Y., Xiao, J., Dong, Z., Gong, M., & Chen, H. (2020). Hemicellulose pyrolysis mechanism based on functional group evolutions by two-dimensional perturbation correlation infrared spectroscopy. *Fuel*, 267(July 2019), 117302. <https://doi.org/10.1016/j.fuel.2020.117302>
- Yang, X., Zhao, Y., Li, W., Li, R., & Wu, Y. (2019). Unveiling the Pyrolysis Mechanisms of Hemicellulose: Experimental and Theoretical Studies. *Energy and Fuels*, 33(5), 4352–4360. <https://doi.org/10.1021/acs.energyfuels.9b00482>
- Yokelson, R. J., Burling, I. R., Gilman, J. B., Warneke, C., Stockwell, C. E., De Gouw, J., Akagi, S. K., Urbanski, S. P., Veres, P., Roberts, J. M., Kuster, W. C., Reardon, J., Griffith, D. W. T., Johnson, T. J., Hosseini, S., Miller, J. W., Cocker, D. R., Jung, H., & Weise, D. R. (2013). Coupling field and laboratory measurements to estimate the emission factors of identified and unidentified trace gases for prescribed fires. *Atmospheric Chemistry and Physics*, 13(1), 89–116. <https://doi.org/10.5194/acp-13-89-2013>
- Yokelson, R. J., Burling, I. R., Urbanski, S. P., Atlas, E. L., Adachi, K., Buseck, P. R., Wiedinmyer, C., Akagi, S. K., Toohey, D. W., & Wold, C. E. (2011). Trace gas and particle emissions from open biomass burning in Mexico. *Atmospheric Chemistry and Physics*, 11(14), 6787–6808. <https://doi.org/10.5194/acp-11-6787-2011>
- Yokelson, R. J., Saharjo, B. H., Stockwell, C. E., Putra, E. I., Jayarathne, T., Akbar, A., Albar, I., Blake, D. R., Graham, L. L. B., Kurniawan, A., Meinardi, S., Ningrum, D., Nurhayati, A. D., Saad, A., Sakuntaladewi, N., Setianto, E., Simpson, I. J., Stone, E. A., Sutikno, S., ... Cochrane, M. A. (2022). Tropical peat fire emissions: 2019 field measurements in Sumatra and Borneo and synthesis with previous studies. *Atmospheric Chemistry and Physics*, 22(15), 10173–10194. <https://doi.org/10.5194/acp-22-10173-2022>
- Yokelson, R. J., Susott, R., Ward, D. E., Reardon, J., & Griffith, D. W. T. (1997). Emissions from smoldering combustion of biomass measured by open-path Fourier transform infrared spectroscopy. *Journal of Geophysical Research Atmospheres*, 102(15), 18865–18877. <https://doi.org/10.1029/97jd00852>

- Young, C. J., Washenfelder, R. A., Edwards, P. M., Parrish, D. D., Gilman, J. B., Kuster, W. C., Mielke, L. H., Osthoff, H. D., Tsai, C., Pikelnaya, O., Stutz, J., Veres, P. R., Roberts, J. M., Griffith, S., Dusanter, S., Stevens, P. S., Flynn, J., Grossberg, N., Lefer, B., ... Brown, S. S. (2014). Chlorine as a primary radical: Evaluation of methods to understand its role in initiation of oxidative cycles. *Atmospheric Chemistry and Physics*, 14(7), 3427–3440. <https://doi.org/10.5194/acp-14-3427-2014>
- Yuan, Y., Zhao, X., Wang, S., & Wang, L. (2017). Atmospheric Oxidation of Furan and Methyl-Substituted Furans Initiated by Hydroxyl Radicals. *Journal of Physical Chemistry A*, 121(48), 9306–9319. <https://doi.org/10.1021/acs.jpca.7b09741>
- Zhao, D., Schmitt, S. H., Wang, M., Acir, I. H., Tillmann, R., Tan, Z., Novelli, A., Fuchs, H., Pullinen, I., Wegener, R., Rohrer, F., Wildt, J., Kiendler-Scharr, A., Wahner, A., & Mentel, T. F. (2018). Effects of NO<sub>x</sub> and SO<sub>2</sub> on the secondary organic aerosol formation from photooxidation of  $\alpha$ -pinene and limonene. *Atmospheric Chemistry and Physics*, 18(3), 1611–1628. <https://doi.org/10.5194/acp-18-1611-2018>
- Zhao, X., & Wang, L. (2017). Atmospheric Oxidation Mechanism of Furfural Initiated by Hydroxyl Radicals. *Journal of Physical Chemistry A*, 121(17), 3247–3253. <https://doi.org/10.1021/acs.jpca.7b00506>
- Zhou, X., Beine, H. J., Honrath, R. E., Fuentes, J. D., Simpson, W., & Bottenheim, J. W. (2001). Snowpack Photochemical Production of HONO: a Major Source of OH in the Arctic Boundary Layer in Springtime. *Geophysical Research Letters*, 28, 4087–4090. <https://doi.org/10.1029/2001GL013531>
- Zhou, X., Li, W., Mabon, R., & Broadbelt, L. J. (2018). A mechanistic model of fast pyrolysis of hemicellulose. *Energy and Environmental Science*, 11(5), 1240–1260. <https://doi.org/10.1039/c7ee03208k>
- Ziemann, P. J., & Atkinson, R. (2012). Kinetics, products, and mechanisms of secondary organic aerosol formation. *Chemical Society Reviews*, 41(19), 6582–6605. <https://doi.org/10.1039/c2cs35122f>
- Zogka, A. G., Romanias, M. N., & Thevenet, F. (2022). Formaldehyde and glyoxal measurement deploying a selected ion flow tube mass spectrometer (SIFT-MS). *Atmospheric Measurement Techniques*, 15(7), 2001–2019. <https://doi.org/10.5194/amt-15-2001-2022>
- Zysman, B., & Skelly, P. D. (1992). *T*: 1992.

## Conclusion & Perspectives

The aim of this work was to understand the nighttime reactivity of methylated furan compounds (F, 2-MF, 3-MF, 2,5-DMF and 2,3,5-TMF) governed by the  $\text{NO}_3$  radicals through kinetics and products investigations. This was achieved by i) measuring the room temperature rate coefficient of the five studied reactions making it possible to determine the lifetimes of these compounds, ii) determining the temperature dependent rate coefficient described by the Arrhenius equation for the reaction of F, 2-MF and 2,5-DMF with  $\text{NO}_3$ , iii) qualitative and quantitative products characterization both in the gaseous and particulate phases (SOA) iv) proposition of the mechanism of the reaction of each compound making it possible to propose an overall mechanism for the formation of first-generation products for methylated furans .

For this purpose, two atmospheric simulation chambers (CHARME & THALAMOS) were deployed to experimentally study these reactions. Analyses were carried out using a variety of techniques: PTR-ToF-MS, GC-EI-MS and ESI-LC-QToF-MS/MS for measurements carried out in CHARME and SIFT-MS, GC-EI-MS for those carried out in THALAMOS. In addition, two FTIR instruments were used to validate the identification of products observed or to provide additional elements for the study of SOA.

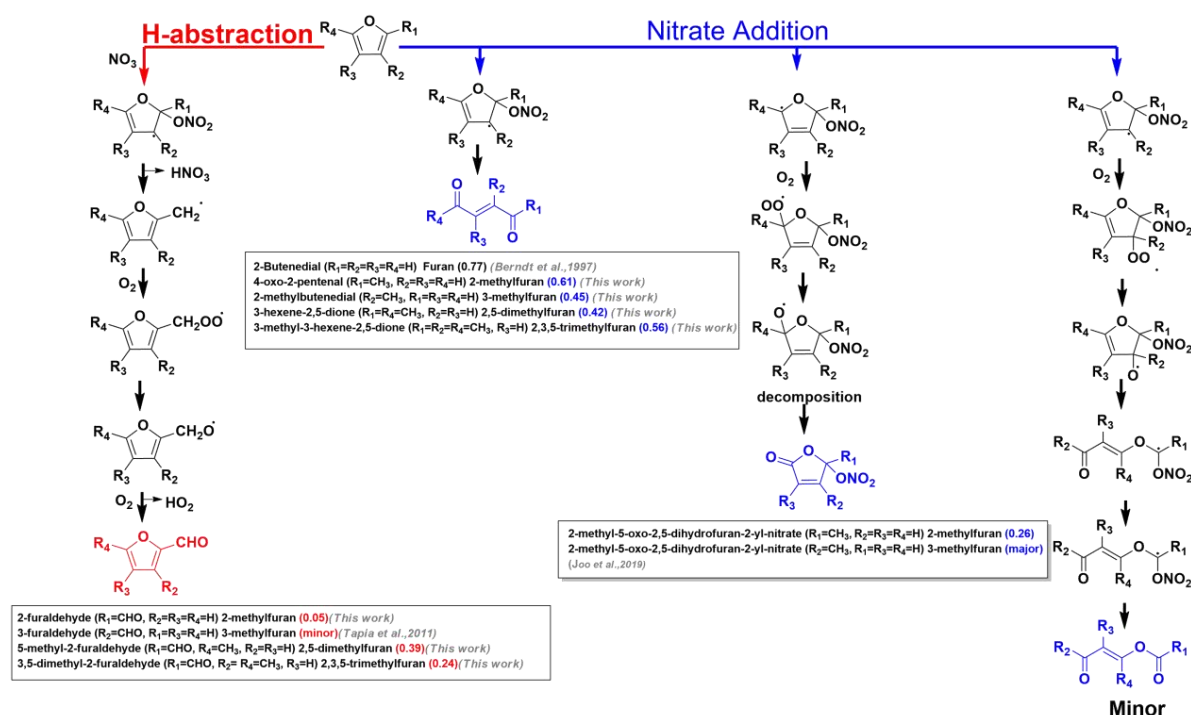
For the room temperature kinetics, experiments were performed in the dark, under dry conditions ( $\text{RH} < 2\%$ ), atmospheric pressure and temperature  $294 \pm 2$  K using the relative rate method in both simulation chambers (CHARME & THALAMOS). The lifetimes measured of the five studied molecules were in the range of 0.5-52 min indicating that the reaction of the targeted compounds with  $\text{NO}_3$  is their dominant sink during nighttime, but also during daytime, in the case of methyl-, dimethyl- and trimethyl- furanoids. Moreover, comparing the rate coefficients of methylated furanoids with different numbers of methyl groups it can be inferred that the rate coefficient is impacted by the number of the methyl groups attached to the furan ring, probably due to their donor inductive effect. The more methyl groups attached to the ring, the higher is the rate coefficient of the reaction.

The temperature-dependent kinetic studies were studied in THALAMOS in the dark, under dry conditions ( $\text{RH} < 2\%$ ), atmospheric pressure using relative rate method too. Negative temperature dependence was observed for the reaction rate coefficient of furanoids with  $\text{NO}_3$  which shows that the major reaction pathway occurs by  $\text{NO}_3$  addition to the double bond of the ring or  $\text{NO}_3$  addition-H abstraction from the methyl group attached to the ring. The room temperature average rate coefficient measured in both chambers besides the temperature dependent Arrhenius equation are summarized in the following table.

Compound	Rate Coefficient (294 ± 2 K) (CHARME & THALAMOS)	Arrhenius equation (temperature range)
F	$(1.61 \pm 0.28) \times 10^{-12}$	$(7.55 \pm 0.12) \times 10^{-13} \times e^{\frac{254 \pm 138}{T}}$ (263 – 353 K)
2-MF	$(1.96 \pm 0.25) \times 10^{-11}$	$(7.76 \pm 0.14) \times 10^{-13} \times e^{\frac{922 \pm 151}{T}}$ (263 – 373 K)
3-MF	$(1.49 \pm 0.33) \times 10^{-11}$	-
2,5-DMF	$(6.49 \pm 0.95) \times 10^{-11}$	$(5.04 \pm 0.19) \times 10^{-13} \times e^{\frac{1467 \pm 338}{T}}$ (298 – 353 K)
2,3,5-TMF	$(1.66 \pm 0.69) \times 10^{-10}$	-

The second part of this research focused on the qualitative and quantitative products determination formed in the gas- and particulate- phase formed from these reactions and the mechanism leading to these oxidation products.

The major product formed with the highest yield from the reaction of furan and the four studied methylated furans with NO<sub>3</sub> was the unsaturated dicarbonyl. This product is formed from the NO<sub>3</sub> addition to C-2/C-5 of the ring followed by ring opening and NO<sub>2</sub> loss. For the second major primary product, in the case of single methylated furan compounds (2-MF and 3-MF), cyclic nitrooxy carbonyls are also formed as major primary product from the NO<sub>3</sub> addition to C-2. For multi-methylated furanoids (2,5-DMF and 2,3,5-TMF), methylated-furfurals are the second major primary products formed by NO<sub>3</sub> addition followed by H atom-abstraction from one of the methyl groups attached to the furan ring. To wrap up, the figure below shows the general chemical mechanism leading to the formation of both major and minor primary oxidation products with their yields (data from this work; Tapia et al., (2011); Berndt et al., 1997).



Chemical mechanisms for the gas-phase reaction of furan and methylated-furanoids with NO<sub>3</sub> leading to the formation of the primary products. Products labelled in blue are formed from NO<sub>3</sub> addition while those labelled in red are the products formed from H-abstraction while those. Products yields are also indicated.

Regarding the second-generation products, there is common product formed from the reaction of furan and methylated furans with  $\text{NO}_3$  which is maleic anhydride. The latter is formed from the reaction of the primary products formed from the studied reactions with  $\text{NO}_3$ . This compound can be considered as an indication of the presence of these compounds within the fires plumes. In the study of Wang et al., (2020), maleic anhydride was considered as sign of the aging of the fire plumes.

In addition, methylated-furfurals which are the second major products formed from the reaction multi-methylated furans with  $\text{NO}_3$ , shows a fast reaction with  $\text{NO}_3$  which probably occurs by H-abstraction from the aldehydic group attached to the ring.

Considering the relatively large emission rates of furans during biomass burning, a 2-12% SOA yield from this study suggests that furans can potentially be an important nighttime SOA precursor. If typical nighttime RH conditions are considered, which are higher than in this study, the SOA yield may increase owing to oligomerization or reactive uptake of water-soluble compounds (Nguyen et al., 2014; Xu et al., 2017). Future studies are warranted to investigate SOA formation from furan oxidation under various reaction conditions.

Comparing the SOA yield obtained from the reaction of 2-MF, 2,5-DMF AND 2,3,5-TMF with  $\text{NO}_3$ , the maximum aerosol yield obtained from the reaction of 2-MF was  $\approx 2\%$  which is 5-6 times lower than those obtained from the reaction of 2,5-DMF ( $\approx 12\%$ ) and 2,3,5-TMF ( $\approx 10\%$ ). This shows that increasing the methylation on the furan ring increases the SOA yield of formation from the reaction. This is due to the presence of methyl groups on the ring reducing the volatility or the vapor pressure of a compound.

One product model obtained from fitting the data using odum model indicates that either only one semi-volatile organic compounds is the major constituent of the SOA or that the organic compounds present in the condensed phase have similar  $\alpha_i$  and  $K_{om,i}$ .

Regarding the composition of the SOA formed from title reaction, it can be concluded that some products identified in the gas-phase were also identified in the particulate phase including the major ones, this shows that these products partition between the gas- and particulate- phase. Higher-generation oxidation products and possibly multiphase accretion reactions contribute significantly to SOA formation from the methylated furanoids +  $\text{NO}_3$  reaction. The slow  $\text{N}_2\text{O}_5$  injection used in this study as well as the fact that these radicals have some of the fastest  $\text{RO}_2 + \text{RO}_2$  reaction rates can lead to considerable dimer formation ( $\text{ROOR}'$ ) and multifunctional species. The carbonyl groups can also participate in accretion reactions or be oxidized in the condensed phase. The molecular formulas of the observed products imply that the compounds in the particle phase are multifunctional and likely to engage in accretion reactions. If other VOCs in biomass burning plumes have similar products, it is expected that these compounds will form SOA efficiently through multigeneration and multiphase chemistry.

As already mentioned, the reactivity of furans with  $\text{NO}_3$  is still poorly understood, especially under biomass combustion conditions where they are mainly found. This thesis has therefore attempted to pave the way for this new field of research. Many objectives have been achieved during these years of research, but others have yet to be undertaken, because even if we have

answered a certain number of questions, others remain unanswered or new questions have been raised by our work. So, the prospects are numerous and multidisciplinary.

The FTIR analysis of the reaction of F, 3-MF, 2,5-DMF and 2,3,5-TMF was also investigated in this work, and the data will be treated in the future and compared to theoretical calculations and the results obtained with other experimental techniques which were discussed in chapter iv. FTIR experiments will extend the products characterization and validate the results already presented. Moreover, FTIR analysis was done for the SOA formed from the reaction of 2,5-DMF and 2,3,5-TMF and the results will be treated in the future and will be compared with the results obtained with GC-EI-MS and ESI-LC-QToF-MS/MS to draw final conclusion on the pathways leading to the formation of the SOAs in the multi-methylated furan compounds. SOA products characterization experiments were done for the reaction of 2,3,5-TMF with  $\text{NO}_3$  using ESI-LC-QToF-MS/MS and data will be treated in the future. The results will then be compared to those obtained for the reaction of 2-MF and 2,5-DMF and the general idea on the formation of the products in the particulate phase can be illustrated.

In addition, structure-activity relationships on the kinetics of the studied reactions could be developed and explicit atmospheric chemistry models be improved.

From the point of view of atmospheric chemistry, this work has identified primary and secondary products which also have significant reactivity with  $\text{NO}_3$ . There is therefore a real interest in studying their reactivity in order to determine their atmospheric implications. Product and SOA formation studies will also be carried out on methylated-furfurals which are major products from the reaction of 2,5-DMF and 2,3,5-TMF with  $\text{NO}_3$ , for which literature data are unavailable and in our work these compounds showed fast reaction with  $\text{NO}_3$ .

The difference in chemistry between simply methylated and multi-methylated furans is also still to be answered. Why do some promote the formation of nitrate compounds and others promote the formation of furfural.

Regarding the particulate phase, even if SOA formation is modest at room temperature, it might be interesting to carry out studies with conditions closer to those of biomass fires. Finally, an in-depth study of the optical, hygroscopic and toxicological properties would reveal whether these "modest" yields could have a significant effect on climate and health. The list of prospects could go on for several pages, but the best prospect for this study would be that it serves as an impetus for future researchers, as the first stone of a huge edifice.



# **Appendices**

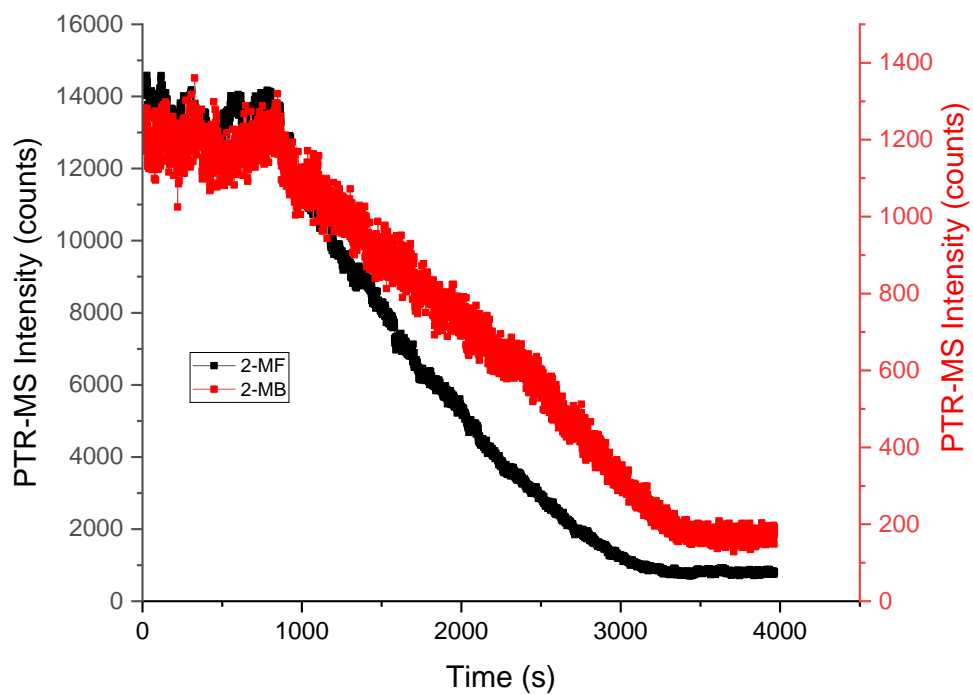


Figure S1: Time profiles of 2-MF and 2-MB followed by the PTR-ToF-MS.

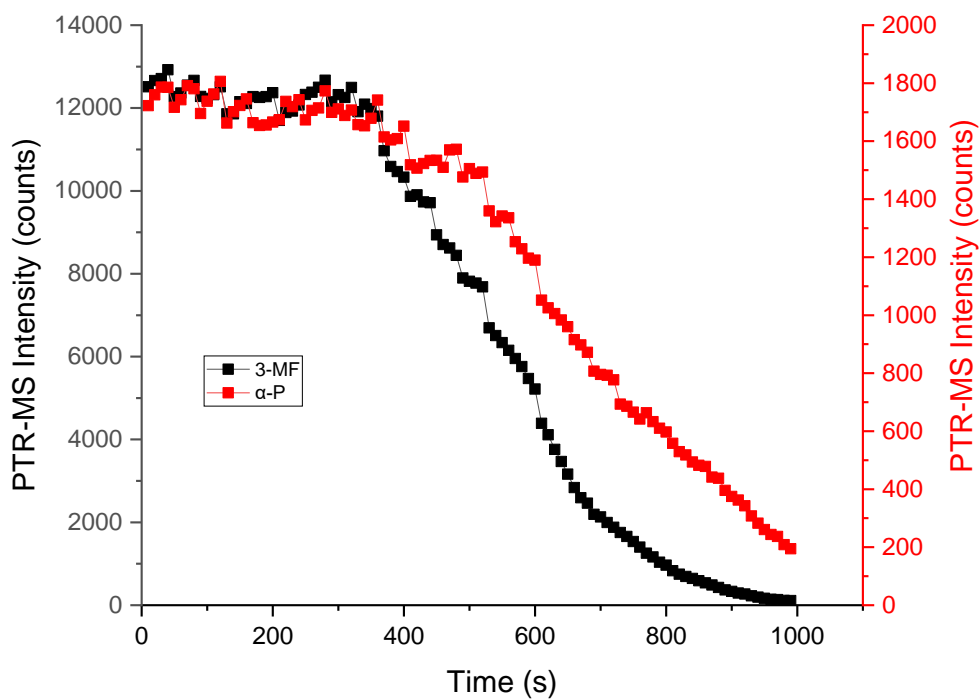


Figure S2: Time profiles of 3-MF and  $\alpha$ -P followed by the PTR-ToF-MS.

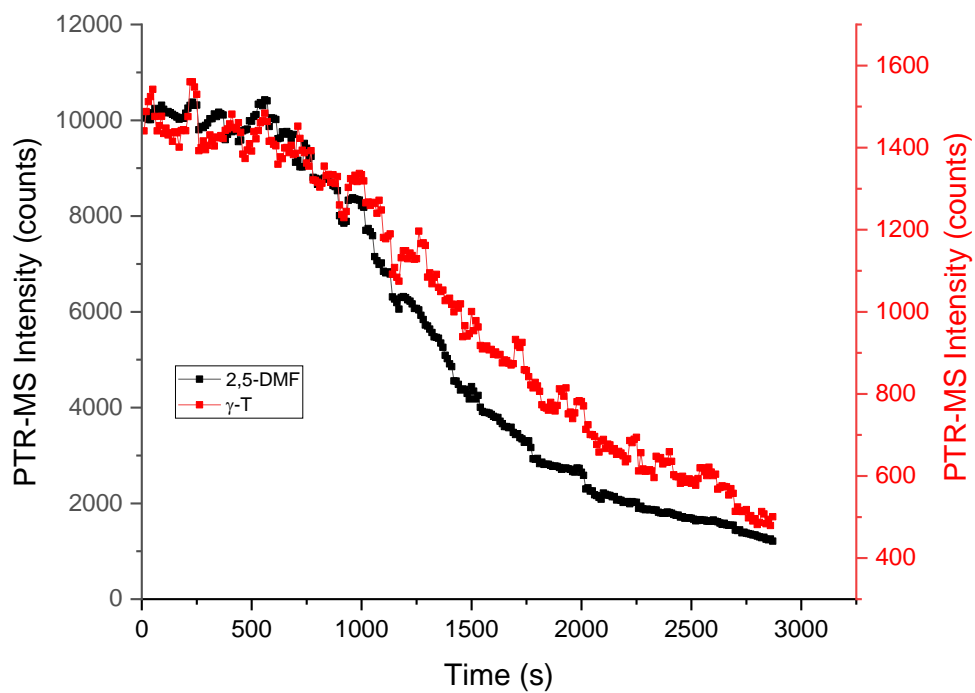


Figure S3: Time profiles of 3-MF and  $\gamma$ -T followed by the PTR-ToF-MS.

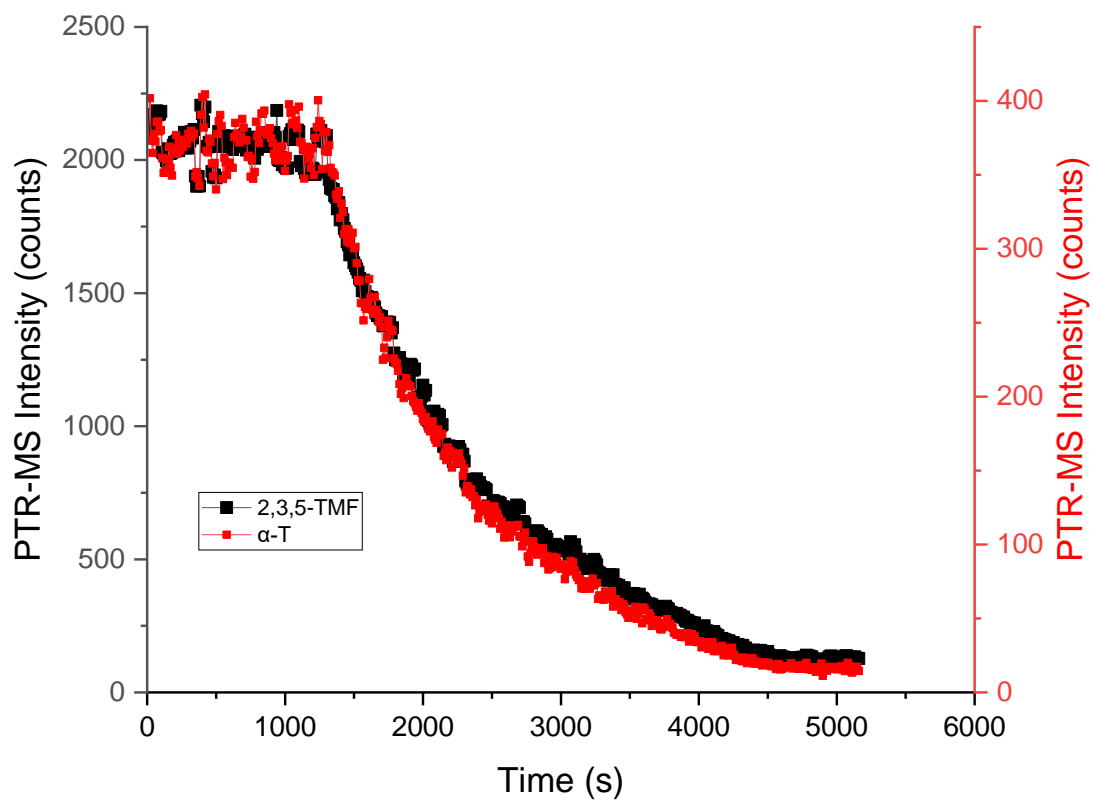


Figure S4: Time profiles of 2,3,5-TMF and  $\alpha$ -T followed by the PTR-ToF-MS.

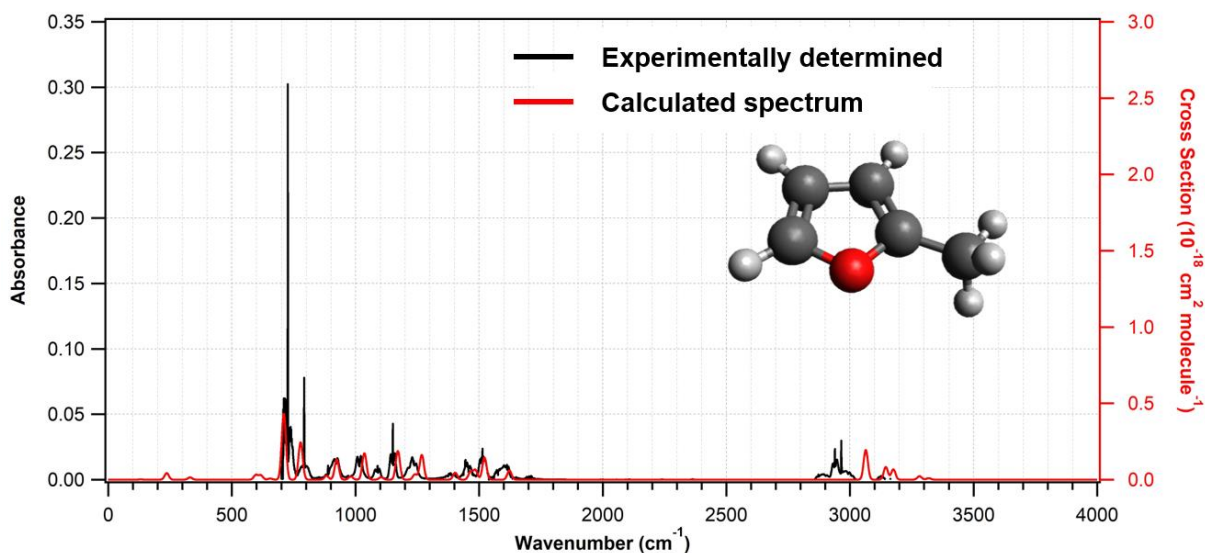


Figure S5: Experimentally determined IR spectrum of 2-MF (black) and theoretical calculated IR cross section spectrum (red) calculated. Calculated and experimental IR spectra are in reasonable agreement bands position-wise except from the C-H stretching features that appear around 3000  $\text{cm}^{-1}$ . The theoretical cross section spectrum has been broadened using gaussian type function and FWHM = 20  $\text{cm}^{-1}$ .

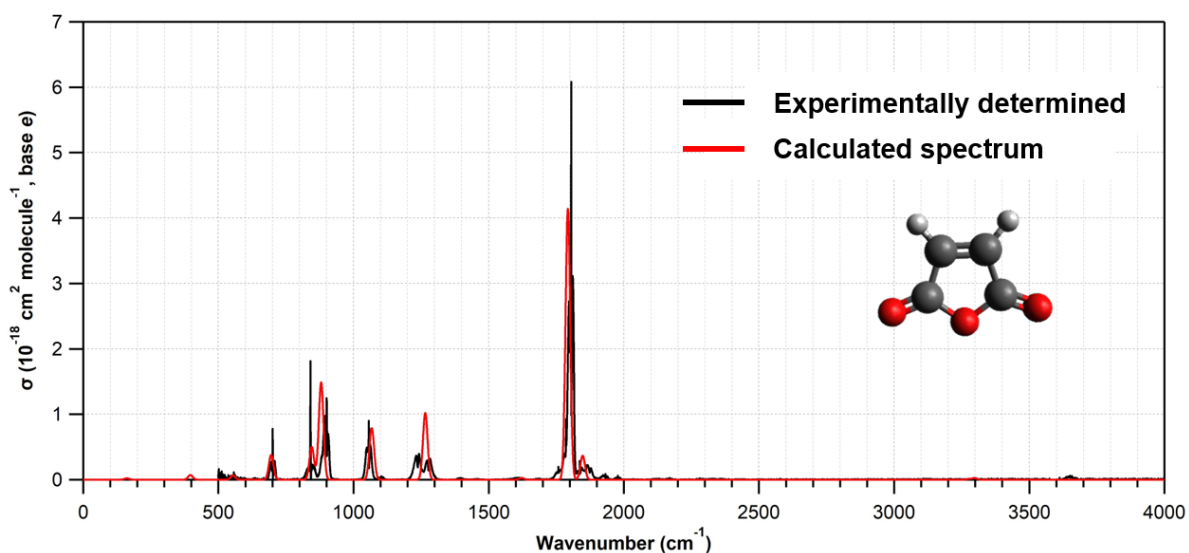


Figure S6: Comparison of the experimentally determined (in black) and calculated (in red) IR cross section spectra of maleic anhydride. Calculated and experimental IR spectra are in reasonable agreement bands position and cross section-wise, while small shifting could be attributed to limitations of the theory. The theoretical cross section spectrum has been broadened using gaussian type function and FWHM = 20  $\text{cm}^{-1}$ .

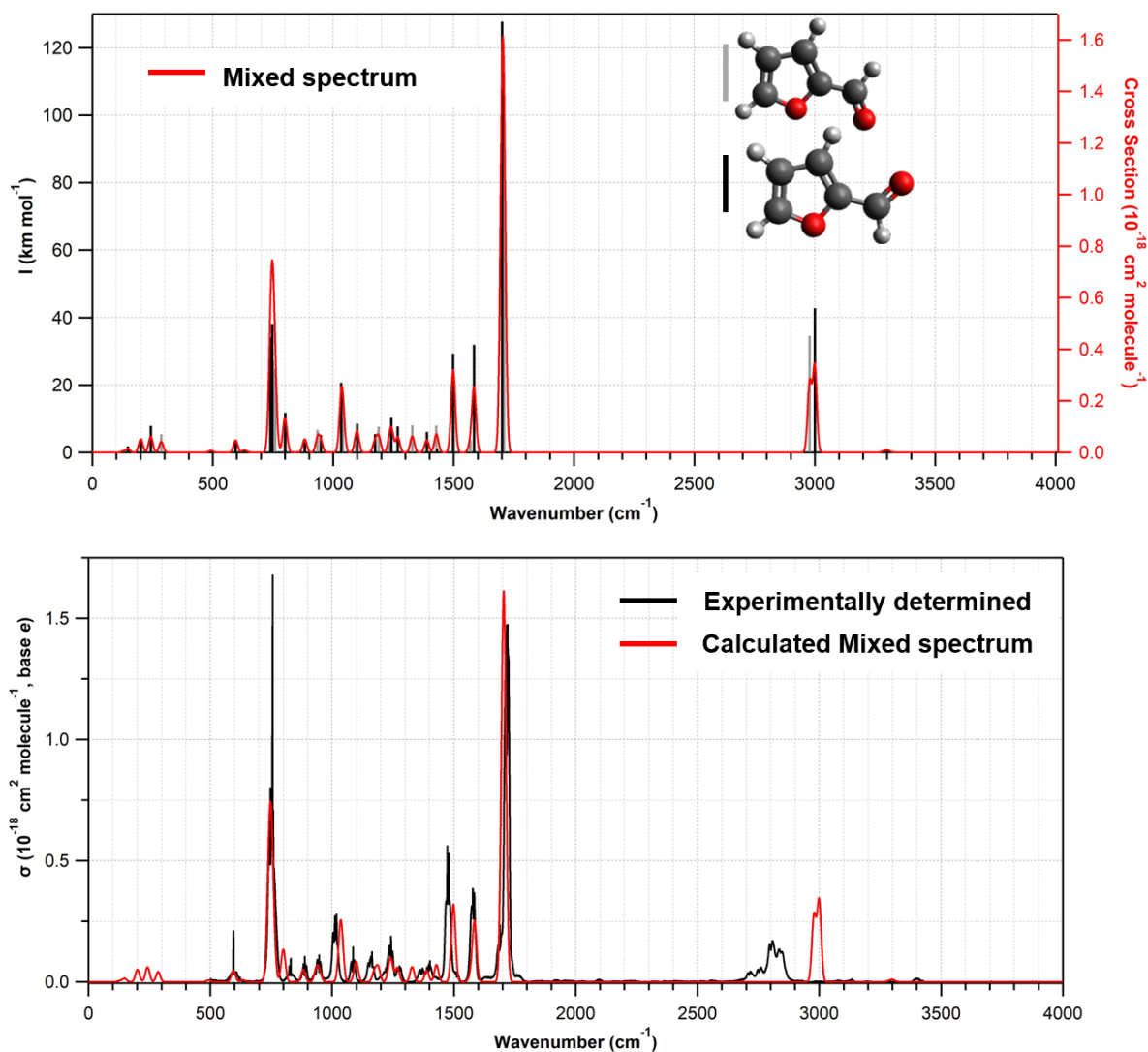


Figure S7: Upper panel: Furfural conformers stick and gaussian-broadened ( $\text{FWHM} = 20 \text{ cm}^{-1}$ ) composite IR spectra calculated at MP2/AUG-ccc-pVDZ level of theory. Two different conformers were found and their relative abundance for the two conformers was determined to be 41% (grey sticks), and 59 %, (black sticks) based on the energetics and the Boltzmann equilibrium distribution. Lower panel: Experimental (black) and theoretical (red) IR absorption cross-section spectra comparison for furfural. As shown there is a reasonable agreement between theory and experiment in both terms of positioning and integrated band intensities. Calculated and experimental IR spectra are in reasonable agreement bands position and cross section-wise, except from the C-H stretching features that appear around  $3000 \text{ cm}^{-1}$ . The theoretical cross section spectrum has been broadened using gaussian type function and  $\text{FWHM} = 20 \text{ cm}^{-1}$ .

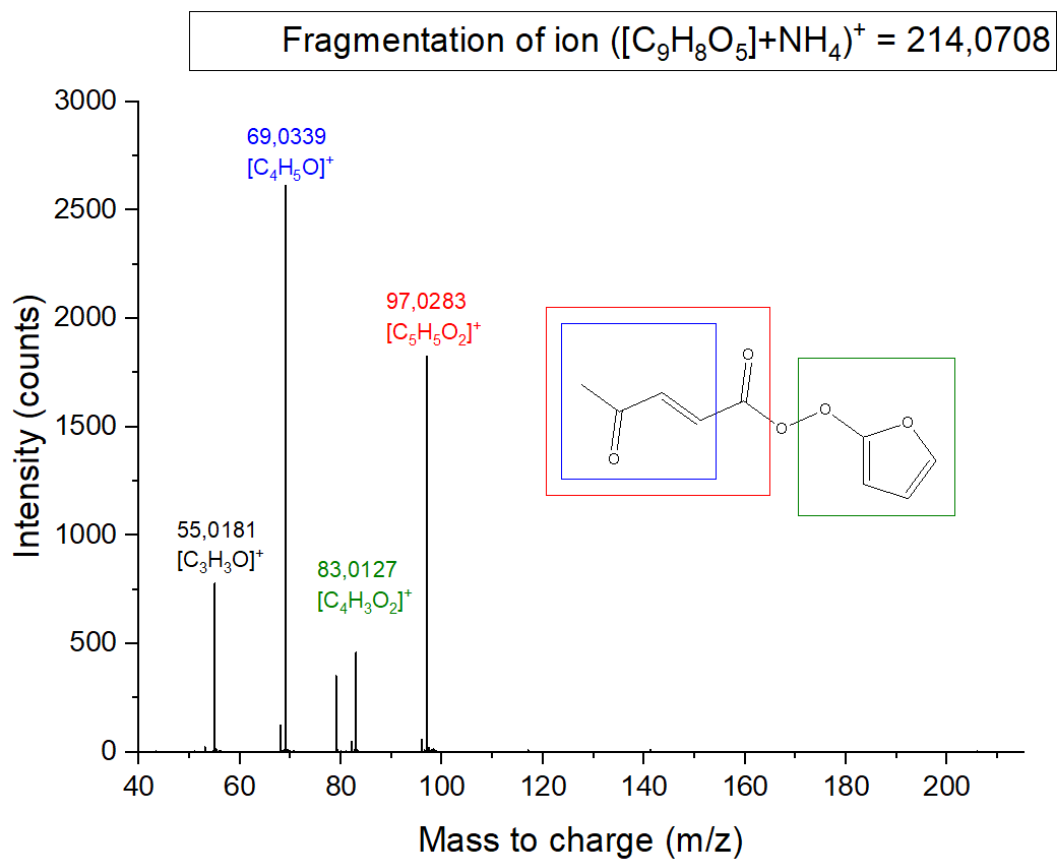


Figure S8: Fragmentation spectrum of ion  $([C_9H_8O_5]+NH_4)^+$  with mass = 214,0708 within the LCMSMS.

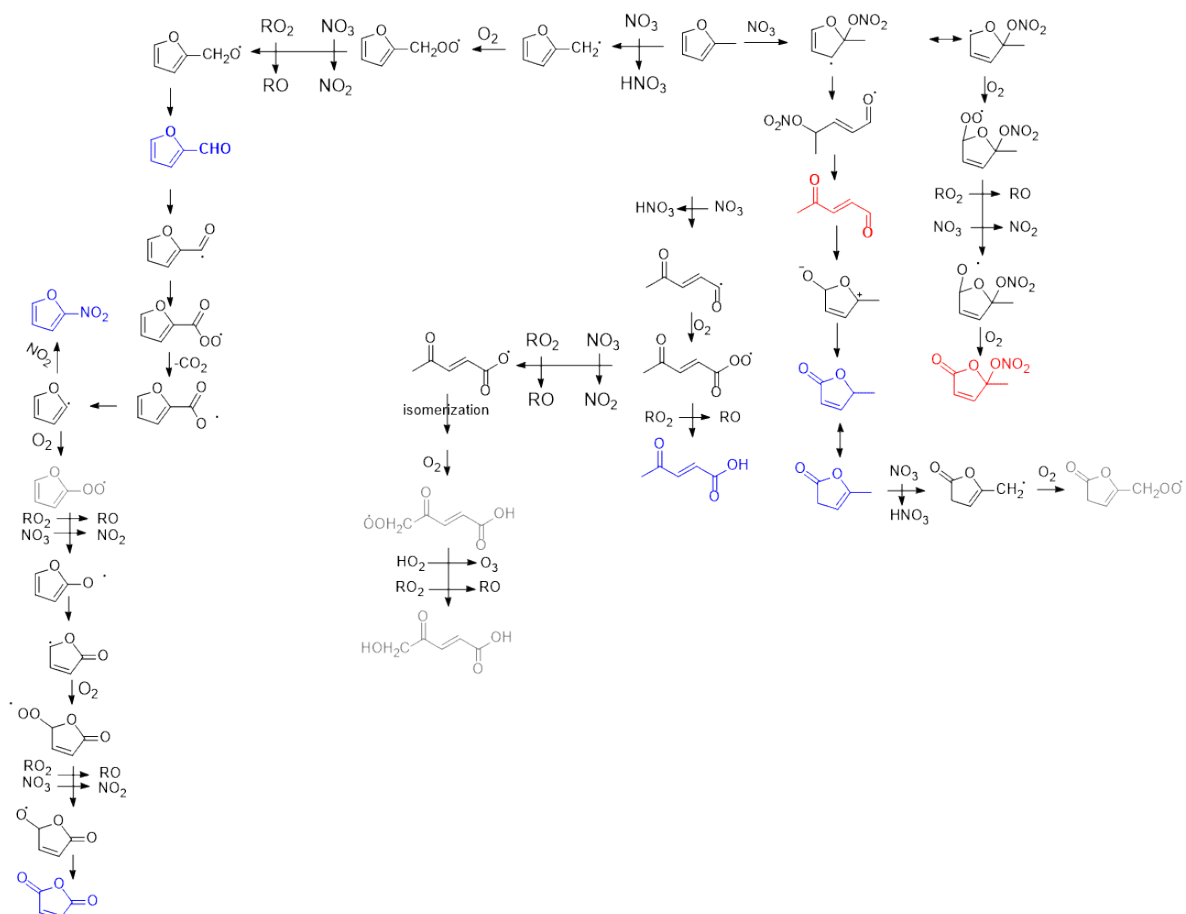
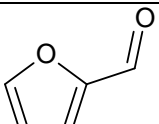

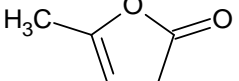
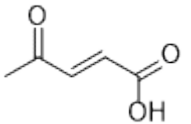
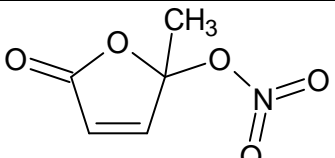
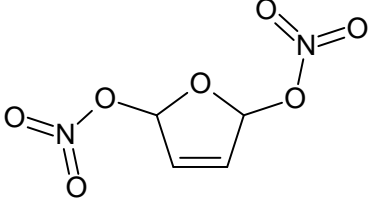
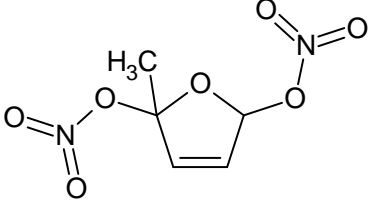
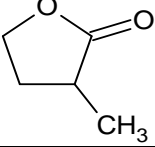
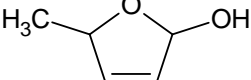
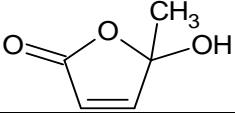
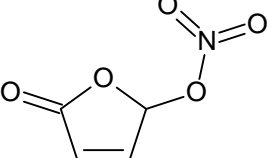
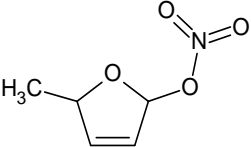
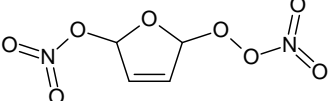


Figure S9: Mechanism of the reaction of 2-MF with  $\text{NO}_3$  radicals with intermediates/products labelled in grey leading to the formation of products in particulate phase.

Table S1: Structures of all species calculated with gaussian aiming to identify their presence in the residual IR spectrum.

Compound	PTR-ToF-MS	GC-EI-MS	FTIR
	✓	✓	
	✓	✓	
	✓	✓	
	✓	✓	✓
	✓	✓	

			v
			Possible
			
			
			
			
			
			



## Résumé en Français

### 1. Introduction

La combustion de la biomasse est la combustion de végétaux vivants ou morts, incluant les incendies naturels, le chauffage domestique et les incendies volontaires à des fins de déforestations ou d'adaptation de terrains... A cause de la croissance démographique et de la demande en denrées alimentaires, la déforestation pour l'exploitation agricole (Durigan et al., 2017; Brando et al., 2020) a grandement augmenté durant les dernières décennies (Paquet et al., 2019) et aucune tendance à la baisse n'est prévue dans un avenir proche (Stehfest et al., 2019) La combustion de la biomasse joue un rôle clé dans la capacité oxydante de l'atmosphère. Durant la journée, dans les panaches de fumée, les concentrations en radicaux OH sont 5 à 10 fois plus élevées que celles mesurées dans l'air ambiant (Crouse et al., 2009), ce qui contribue à une augmentation de plus de 120% de la réactivité totale des radicaux OH pendant les événements de CB (Kumar et al., 2018). Durant la nuit, il a été récemment établi que le mélange d'ozone avec des NO<sub>x</sub> dans un panache amené à une formation de radicaux NO<sub>3</sub> (l'oxydant atmosphérique nocturne majeur) avec une vitesse de formation de l'ordre d'1 ppb.h<sup>-1</sup> (Decker et al., 2021). Par conséquent, des transformations chimiques nocturnes significatives se produisent potentiellement dans les fumées, ce qui pourrait avoir un fort impact sur la qualité de l'air et la capacité oxydante de l'atmosphère. Toutefois, ces transformations sont encore très peu étudiées dans la littérature scientifique.

L'impact des émissions lors de la combustion de la biomasse sur la qualité de l'air et le climat est lié aux mélanges complexes de gaz et de particules émis dans l'atmosphère. Très récemment, les furanes ont été identifiés comme une famille de composés organiques volatiles (COV) majeurs des émissions gazeuses provenant de la pyrolyse de la cellulose lors d'incendies de forêt (Gilman et al., 2015; Hatch et al., 2017; Koss et al., 2018; Andreae, 2019). Les furanes représentent environ 30% du nombre totale de COV identifiés dans les fumées avec des niveaux de concentrations significatifs compris entre 68 et 118 ppbv pour 1 ppm de CO formé. La concentration en COV émise à partir de la combustion de la biomasse dépend du type de végétation et des conditions de la combustion. Toutefois, la caractérisation de Stockwell et al., (2015) des émissions de feux résidentiels, de la tourbe, de résidus agricoles et d'autres combustibles a montré que pour ces différents combustibles issus de la biomasse les facteurs d'émissions des furanes ( $\cong 0.1\text{--}2.3 \text{ g Kg}^{-1}$ ) sont supérieurs à ceux des composés de la famille des phénols ( $\cong 0.05\text{--}0.8 \text{ g Kg}^{-1}$ ), mais inférieurs à la famille des composés aromatiques ( $\cong 0.2\text{--}5 \text{ g Kg}^{-1}$ ) (Stockwell et al., 2015) Il a été démontré que les furanes contribuent significativement ( $\cong 20\%$ ) à la réactivité globale des radicaux NO<sub>3</sub> (Decker et al., 2021) et OH (Coggon et al., 2019) lors des émissions dû à la combustion de feux sauvages et de combustibles domestiques. Par comparaison, Decker et al., (2021) ont montré que la contribution des furanes dans la réactivité de OH (25%) est supérieure à celle des phénols (16.4 %), mais inférieur à celle des alcènes (33 %). Cependant, la réactivité avec NO<sub>3</sub> est principalement dominée par les phénols (64.4%), une contribution bien plus grande que les furanes (19%) et les alcènes (5%) (Decker et al., 2021). D'autres sources de furanes ont pour origines l'incinération de déchets, la combustion de carburants et biocarburants, les procédés industriels à haute température (Krause et al., 2014). Le 2-méthylfurane et le 2,5-diméthylfurane étant très prometteurs comme biocarburants, une augmentation de leurs émissions est attendu dans les prochaines années (Qian et al., 2015; Thewes et al., 2011). Les

furanes sont des molécules très réactives qui sont rapidement consommées dans l'atmosphère lors de leur oxydation en phase gazeuse. De façon notable, une étude expérimentale et de modélisation récente a montré que durant la journée, la dégradation des furanes est au cœur de la chimie à l'intérieur des fumées formées à partir de la combustion de la biomasse (Coggon et al., 2019), produisant des polluants secondaires qui contribuent probablement à la formation d'ozone troposphérique et d'aérosols organiques secondaires (AOS). Le rôle de la dégradation des furanes durant la nuit sur la chimie troposphérique est encore très peu étudiée.

## 2. But de la thèse

L'objectif de ce travail de thèse est d'améliorer notre compréhension de l'oxydation nocturne de différents furanes (furane F, 2-méthylfurane 2-MF, 3-méthylfurane 3-MF, 2,5-diméthylfurane 2,5-DMF, et 2,3,5-triméthylfurane 2,3,5-TMF) par les radicaux  $\text{NO}_3$ . L'objectif est triple, avec dans un premier temps l'évaluation de la cinétique des réactions, dans un second temps la caractérisation des produits de réaction ainsi que les mécanismes menant à ceux-ci et finalement évaluer la formation d'AOS et les caractériser chimiquement. Le choix de furanes méthylés et leur réaction avec  $\text{NO}_3$  est justifiée par plusieurs raisons. Premièrement, le peu d'études sur l'oxydation avec  $\text{NO}_3$  de cette famille de composés démontre une cinétique extrêmement rapide et donc un rôle important est attendu quant à la chimie atmosphérique nocturne, encore plus importante que la chimie de jour (Atkinson et al., 1983b; Kind et al., 1996b; Newland et al., 2022). Deuxièmement, ces composés sont une part importante de la famille des furanes émis lors de la combustion de la biomasse (Liang et al., 2022). Troisièmement, contrairement à la réactivité atmosphérique de jour, qui a déjà été largement étudiée, la réactivité de nuit avec  $\text{NO}_3$  est encore très peu comprise. Enfin, ces composés sont considérés comme étant les principaux furanes émis directement par le processus de combustion parmi tous les furanes identifiés dans la combustion de la biomasse, et de ce fait sont à l'origine de toute la chimie des furanes dans les panaches de fumée (durant le jour et la nuit).

Cette thèse est composée de quatre chapitres. Dans le premier chapitre, un résumé sur les connaissances générales de la réactivité atmosphérique des furanes est décrit avec pour conclusion les objectifs de la thèse. Dans le second chapitre, les deux chambres de simulation atmosphérique utilisées dans ces travaux ainsi que les techniques analytiques mises en œuvre afin d'étudier les espèces gazeuses et particulaires sont illustrées, accompagnées des méthodologies employées afin d'atteindre nos objectifs. Ce chapitre décrit les techniques analytiques et d'échantillonnage précédemment utilisées dans d'autres travaux (Meng et al., 2020; Fayad et al., 2021) et des méthodes utilisées spécialement pour la première fois pour cette étude. Le troisième chapitre concerne la détermination des constantes de vitesse de 5 furanes à température ambiante et en fonction de la température pour le F, 2-MF et 2,5-DMF. La mesure de ces constantes a permis d'une part de calculer les temps de vie atmosphérique de ces espèces et d'autre part de déduire l'effet de la température sur ceux-ci, nous offrant une première compréhension sur les mécanismes de ces réactions. Cette étude cinétique a montré comment la position et le nombre de groupements méthyl ( $\text{CH}_3$ ) influent sur les constantes de réaction des furanes avec  $\text{NO}_3$ . Dans le quatrième chapitre, la caractérisation qualitative et quantitative des produits d'oxydations atmosphériques dans les phases gazeuse et particulaire a été réalisée et a permis d'établir les mécanismes réactionnels détaillés qui

pourront être utilisés dans les modèles de chimie atmosphérique afin de simuler l'évolution des fumées émis lors de la combustion de la biomasse. Ces travaux vont également permettre de mettre en évidence des traceurs communs à la famille des furanes ou unique pour chaque furane étudié. Plus encore, ils montrent la répartition des différents COV entre les phases gazeuse et particulaire et quels sont les mécanismes qui mènent aux composés organiques semi-volatiles dans les AOS. L'objectif final de ce dernier chapitre est de déterminer les rendements en AOS de ces réactions afin de déterminer l'impact sur la qualité de l'air et du climat. Il est crucial de savoir si les composés de cette famille sont des contributeurs importants d'AOS dans l'atmosphère.

Cette étude a été conduite dans deux laboratoires : Le Laboratoire de Physico-Chimie de l'Atmosphère (LPCA) de l'Université du Littoral - Côte d'Opale (ULCO) à Dunkerque et le département Sciences de l'Atmosphère et Génie de l'Environnement (SAGE) de l'IMT Nord Europe à Douai. Deux chambres de simulation atmosphérique ont été utilisées : the CHamber for Atmospheric Reactivity and Metrology of Environment (CHARME) au LPCA et the Thermally Regulated Atmospheric Simulation Chamber (THALAMOS) au SAGE. Les deux chambres sont décrites dans le chapitre II soulignant l'aspect complémentaire de ces deux installations. Cette complémentarité est cruciale pour la validation croisée des résultats et la conduite d'études en fonction de la température. Ces objectifs visent à combler un vide significatif de connaissances dans la compréhension de l'oxydation atmosphérique des COVs émis par la combustion de biomasse.

### 3. Matériels et méthodes

CHARME a été utilisée pour mesurer les coefficients de réactions pour les réactions de F, 2-MF, 3-MF, 2,5-DMF et 2,3,5-TMF avec les radicaux  $\text{NO}_3$  à température ambiante. La caractérisation des produits gazeux et particulaires a également été effectuée ainsi que la mesure des rendements de formation en AOS. Un diagramme détaillé (figure 1) reprend les différentes techniques analytiques utilisées dans cette chambre.

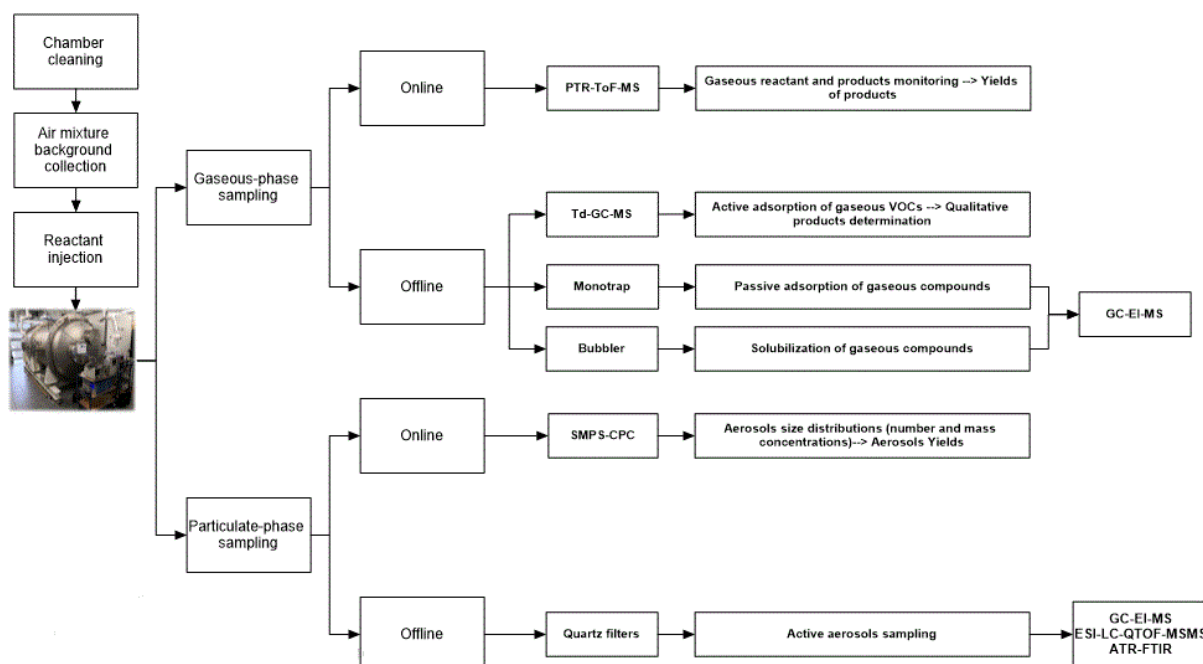
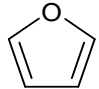
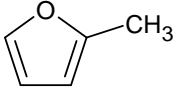
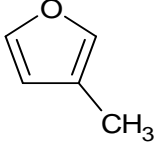
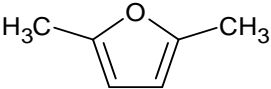
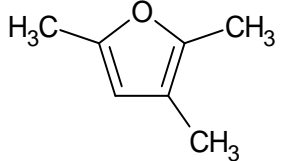






Tableau 1 : Constantes de vitesse pour la réaction d'oxydation des furanes par le radical NO<sub>3</sub>.

Composé	Référence	[FC] <sub>0</sub> (ppbv)	[Ref] <sub>0</sub> (ppbv)	[N <sub>2</sub> O <sub>5</sub> ] <sub>0</sub> (ppbv)	k <sub>FC</sub> /k <sub>ref</sub> <sup>a</sup>	k <sub>FC</sub> <sup>b</sup>	k <sub>FC</sub> <sup>b,c</sup> (moyenne)
<b>F</b> 	α-P	590	600	1850	$(24.5 \pm 0.2) \times 10^{-2}$	$(1.52 \pm 0.36) \times 10^{-12}$	$(1.51 \pm 0.38) \times 10^{-12}$
		790	800	1760	$(24.6 \pm 0.1) \times 10^{-2}$	$(1.52 \pm 0.35) \times 10^{-12}$	
		1000	1000	3660	$(25.2 \pm 0.1) \times 10^{-2}$	$(1.56 \pm 0.36) \times 10^{-12}$	
		1300	1300	8770	$(25.3 \pm 0.3) \times 10^{-2}$	$(1.57 \pm 0.37) \times 10^{-12}$	
	β-P	500	500	1740	$(56.5 \pm 0.2) \times 10^{-2}$	$(1.41 \pm 0.39) \times 10^{-12}$	
		990	1000	2000	$(62.1 \pm 0.3) \times 10^{-2}$	$(1.55 \pm 0.43) \times 10^{-12}$	
1300		1300	4170	$(59.5 \pm 0.2) \times 10^{-2}$	$(1.48 \pm 0.41) \times 10^{-12}$		
<b>2-MF</b> 	2-MB	630	640	9400	$2.06 \pm 0.01$	$(1.93 \pm 0.10) \times 10^{-11}$	$(1.91 \pm 0.32) \times 10^{-11}$
		830	860	6520	$2.17 \pm 0.01$	$(2.03 \pm 0.11) \times 10^{-11}$	
		1100	870	5120	$2.21 \pm 0.02$	$(2.07 \pm 0.12) \times 10^{-11}$	
	γ-T	410	500	2500	$(61.0 \pm 0.4) \times 10^{-2}$	$(1.79 \pm 0.50) \times 10^{-11}$	
		550	500	2700	$(62.8 \pm 0.3) \times 10^{-2}$	$(1.84 \pm 0.51) \times 10^{-11}$	
		1100	830	2870	$(63.6 \pm 0.3) \times 10^{-2}$	$(1.87 \pm 0.52) \times 10^{-11}$	
	DMB	550	1340	8400	$(41.8 \pm 0.7) \times 10^{-2}$	$(1.88 \pm 0.19) \times 10^{-11}$	
		280	540	3400	$(43.4 \pm 0.7) \times 10^{-2}$	$(1.95 \pm 0.20) \times 10^{-11}$	
800		800	2140	$(41.2 \pm 0.4) \times 10^{-2}$	$(1.85 \pm 0.18) \times 10^{-11}$		
<b>3-MF</b> 	α-P	830	830	3400	$2.38 \pm 0.01$	$(1.48 \pm 0.34) \times 10^{-11}$	$(1.49 \pm 0.33) \times 10^{-11}$
		630	630	1400	$2.37 \pm 0.04$	$(1.47 \pm 0.36) \times 10^{-11}$	
		1100	1100	3100	$2.23 \pm 0.01$	$(1.38 \pm 0.32) \times 10^{-11}$	
	γ-T	280	250	1140	$(53.7 \pm 0.5) \times 10^{-2}$	$(1.57 \pm 0.45) \times 10^{-11}$	
		600	830	2700	$(53.6 \pm 0.3) \times 10^{-2}$	$(1.57 \pm 0.44) \times 10^{-11}$	
		700	600	3580	$(56.8 \pm 0.4) \times 10^{-2}$	$(1.67 \pm 0.47) \times 10^{-11}$	
	2-MB	550	740	1370	$(14.9 \pm 0.2) \times 10^{-1}$	$(1.41 \pm 0.09) \times 10^{-11}$	
		830	1060	5219	$(13.99 \pm 0.08) \times 10^{-1}$	$(1.31 \pm 0.07) \times 10^{-11}$	
		280	420	1420	$(17.0 \pm 0.2) \times 10^{-1}$	$(1.59 \pm 0.10) \times 10^{-11}$	
<b>2,5-DMF</b> 	γ-T	800	800	1430	$1.91 \pm 0.02$	$(5.61 \pm 1.60) \times 10^{-11}$	$(5.82 \pm 1.21) \times 10^{-11}$
		1400	1300	2800	$1.98 \pm 0.01$	$(5.82 \pm 1.63) \times 10^{-11}$	
		600	600	1790	$1.89 \pm 0.02$	$(5.55 \pm 1.58) \times 10^{-11}$	
	DMB	600	620	1890	$(13.5 \pm 0.2) \times 10^{-1}$	$(6.07 \pm 0.62) \times 10^{-11}$	
		800	800	1500	$(13.2 \pm 0.2) \times 10^{-1}$	$(5.98 \pm 0.60) \times 10^{-11}$	
		1011.3	1020.82	7580	$(13.21 \pm 0.27) \times 10^{-1}$	$(5.94 \pm 0.64) \times 10^{-11}$	

<p style="text-align: center;"><b>2,3,5-TMF</b></p> 	DMB	615	940	1650	$3.62 \pm 0.02$	$(1.62 \pm 0.15) \times 10^{-10}$	$(1.66 \pm 0.69) \times 10^{-10}$
		410	671	1560	$3.74 \pm 0.06$	$(1.68 \pm 0.17) \times 10^{-10}$	
		821	1208	2190	$3.66 \pm 0.01$	$(1.64 \pm 0.15) \times 10^{-10}$	
	$\alpha$ -T	600	600	5700	$(92.96 \pm 0.48) \times 10^{-2}$	$(1.69 \pm 0.97) \times 10^{-10}$	
		840	850	1990	$(91.23 \pm 0.38) \times 10^{-2}$	$(1.66 \pm 0.95) \times 10^{-10}$	
		410	450	1080	$(93.09 \pm 0.46) \times 10^{-2}$	$(1.69 \pm 0.97) \times 10^{-10}$	

*a* L'erreur indiquée correspond à deux fois la déviation standard à partir de l'analyse de la régression linéaire *b* Exprimé en  $\text{cm}^3\text{molecule}^{-1}\text{s}^{-1}$  *c* moyenne des coefficients obtenus par toutes références utilisées.

## 5. Constantes de vitesse en fonction de la température pour la réaction des furanes avec les radicaux $\text{NO}_3$

Selon la littérature, seule des études à température ambiante ont été effectuées pour les réactions entre les radicaux  $\text{NO}_3$  et les composés de la famille des furanes, excepté pour le furane (Cabanas et al., 2004).

Durant cette thèse, les constantes de vitesse pour la réaction du F, 2-MF et le 2,5-DMF avec  $\text{NO}_3$  ont été étudiées en fonction de la température dans la chambre THALAMOS pour des températures comprises entre 263 à 373 K, à pression atmosphérique et en utilisant la méthode relative. Une équation d'Arrhenius a été proposée pour chaque composé.

L'utilisation de la méthode relative pour des études en fonction de la température de la réaction entre un COV et les radicaux  $\text{NO}_3$  nécessite l'utilisation de références pour lesquelles les constantes de vitesse ont été parfaitement établies. De plus, comme il est mentionné dans le chapitre 2, les constantes de vitesse des références doivent être de même ordre de grandeur que celles des composés étudiés pour avoir résultats précis. Toutefois, dans le cas des radicaux  $\text{NO}_3$ , il n'existe qu'un nombre limité d'études en fonction de la température et certaines sont parfois en désaccord pour un même composé (Manion et al., 2015; Burkholder et al., 2020). La grande majorité des études réalisées avec  $\text{NO}_3$  en fonction de la température au cours des 30 dernières années ont été effectuées par 2 groupes de recherche (Dlugokencky et Howard, 1989; Martinez et al., 1998), mais les résultats sont parfois en désaccord. Ces deux groupes ont utilisé la méthode absolue pour leurs études cinétiques dans des réacteurs à écoulement à basse pression. Le groupe de Martinez et al., (1998) a réalisé des mesures de constantes de vitesse qui sont particulièrement discutables et ne sont pas intégrés aux articles de review. Pour ces raisons, certaines références utilisées pour les études à température ambiante n'ont pu être choisies pour celles réalisées en fonction de la température.

Afin de pallier ces dépasser ces lacunes, plusieurs mesures cinétiques ont donc été réalisées afin de valider les constantes de vitesse des références utilisées pour déterminer les constantes des différents furanes considérés en fonction de la température. Le cheminement de cette approche est représenté par la figure 3.

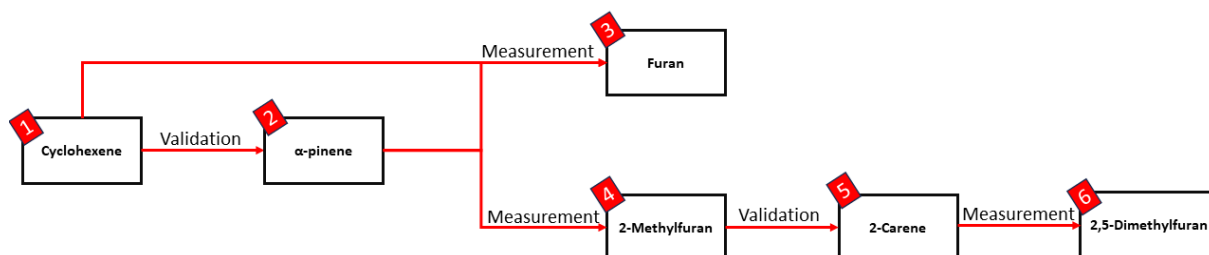


Figure 3 : Cheminement pour la mesure des coefficients en fonction de la température.

Sur cette base, une série de mesures a été réalisée avec le cyclohexène pour valider la cinétique de la réaction  $\alpha$ -pinène +  $\text{NO}_3$ . Ces deux composés ont été d'abord utilisés comme références dans cette étude pour la détermination des constantes de vitesse du furane. L' $\alpha$ -



pinène et le furane ont été utilisés pour l'étude cinétique du 2-MF. Ensuite le 2-MF a été utilisé pour l'étude du 2-carène avec  $\text{NO}_3$  et enfin ce même 2-carène a été utilisé pour le 2,5-DMF.

## 6. Tendances de la réactivité et premiers éléments à propos des mécanismes réactionnels

Il est crucial de comparer les constantes de vitesse à température ambiante des différents furanes pour comprendre l'effet de la structure des furanes sur la cinétique avec NO<sub>3</sub>. La comparaison entre le furane et les 2-MF et 3-MF montre que l'ajout d'un groupement méthyle sur le cycle du furane augmente la constante de vitesse d'environ un ordre de grandeur. Cette augmentation peut être due à l'effet inductif donneur du groupement méthyle qui augmente la densité électronique sur l'atome de carbone sur lequel il est lié et favorise l'addition de NO<sub>3</sub>. Cette addition est l'un des chemins réactionnels majeurs avec ces deux méthylfuranes. Toutefois, la position du groupe méthyle n'a pas d'influence significative sur la constante de vitesse. Le passage d'un groupe méthyle (2-MF et 3-MF) à deux groupes méthyles (2,5-DMF) triple la constante de la réaction, une augmentation également attribuée à l'effet inductif donneur des groupements méthyle. Une tendance similaire a été observée pour la réaction du radical NO<sub>3</sub> avec le 2,5-DMF et le 2,3,5-TMF (Kind et al., 1996b).

Les expressions d'Arrhenius pour les réactions du F, 2-MF, 2,5-DMF avec NO<sub>3</sub> obtenues sont présentées dans le tableau 2. Ces équations d'Arrhenius montrent une réduction de la constante de vitesse en fonction de la température et cette tendance est accentuée par l'ajout de groupes méthyle sur le cycle. Ces réactions s'effectuent sans barrière d'énergie potentielle, ce qui est typique pour des réactions d'associations avec une dépendance plutôt faible de la température. Les furanes forment avec NO<sub>3</sub> un adduit excité qui peut être soit de nouveau décomposé en réactifs, soit stabilisé par collision. L'étape déterminante de ces réactions est généralement la formation d'adduit (consistant avec la relation structure-réactivité avec NO<sub>3</sub> observé). Lorsque la température augmente, l'énergie interne dans l'adduit augmente et la décomposition en réactif est favorisée.

Tableau 2 : Expressions d'Arrhenius pour la réaction du F, 2-MF et 2,5-DMF avec NO<sub>3</sub>, gamme de température de chaque expression et énergie d'activation correspondante.

Composé	Equation d'Arrhenius	Gamme de Température (K)	Énergie d'activation (kJ/mol)
F	$(7.55 \pm 0.12) \times 10^{-13} \times e^{\frac{254 \pm 138}{T}}$	263 - 353	-(2.1 ± 1.1)
2-MF	$(7.76 \pm 0.14) \times 10^{-13} \times e^{\frac{922 \pm 151}{T}}$	263 - 373	-(7.7 ± 1.3)
2,5-DMF	$(5.04 \pm 0.19) \times 10^{-13} \times e^{\frac{1467 \pm 338}{T}}$	298 - 353	-(12.2 ± 2.8)

Après analyse des résultats expérimentaux, un effort a été réalisé pour tirer des conclusions par rapport aux mécanismes de ces réactions. Pour avoir un regard plus global, la réactivité d'autres composés organiques avec les radicaux NO<sub>3</sub> a été prise en compte et décrite dans des études précédentes (Atkinson, 1991a; Atkinson et al., 1997). Il a été observé que des constantes de vitesse dans la gamme de 10<sup>-17</sup> à 10<sup>-14</sup> cm<sup>3</sup> molecule<sup>-1</sup> s<sup>-1</sup> correspondent

typiquement à des mécanismes par abstraction d'hydrogène et affichent des énergies d'activation positive. A contrario, les réactions ayant des coefficients entre  $10^{-14}$  et  $10^{-11}$   $\text{cm}^3 \text{molecule}^{-1} \text{s}^{-1}$  sont souvent attribuées à des mécanismes d'addition sur des liaisons doubles et affichent des énergies d'activation négative. Les constantes de vitesse mesurées dans le cadre de nos études sont de l'ordre  $10^{-12}$ - $10^{-11}$   $\text{cm}^3 \text{molecule}^{-1} \text{s}^{-1}$  avec une énergie d'activation négative, ce qui démontre une première étape réactionnelle par addition de  $\text{NO}_3$  sur la double liaison C=C du cycle (ou par une étape d'addition-élimination) qui s'achève par l'abstraction d'un atome d'hydrogène du groupe méthyl lié au cycle. A haute température, la formation intermédiaire d'adduits devient moins favorable à cause de la réaction inverse (retour au réactif) qui est favorisée du fait de la haute énergie interne de l'adduit (plus difficile à stabiliser à travers une collision), ce qui au final réduit la vitesse de la réactivité totale.

Par ailleurs, du fait des similitudes entre les cinétiques et des propriétés réactives des furanes avec OH et  $\text{NO}_3$ , des déductions supplémentaires peuvent être établies en comparant nos résultats expérimentaux avec ceux obtenus avec OH (Eble et al., 2015; Romanias et al., soumis). Les réactions entre OH et F, 2-MF et 2,5-DMF ont également des énergies d'activations négatives, ce qui indique un mécanisme d'addition de OH sur les doubles liaisons C=C dans la gamme de température étudiée dans nos expériences.

### 7. Implications atmosphériques

Les temps de vies atmosphériques du furane et de ses dérivés méthylés avec  $\text{NO}_3$  ont été déterminés à partir des constantes de vitesse mesurée dans cette étude à température ambiante (298 K). Les résultats sont présentés dans le tableau 3 avec les temps de vies d'autres furanes et d'autres oxydants atmosphériques. Comme indiqué dans le tableau 3, pour le furane, la réactivité atmosphérique avec OH est supérieure à celle avec  $\text{NO}_3$  avec un temps de vie d'environ 3.3 heures. En revanche, pour les quatre dérivés méthylés étudiés, la réaction avec  $\text{NO}_3$  est majoritaire, avec des durées de vie de quelques minutes. Il est intéressant de noter que même de jour, la réactivité avec  $\text{NO}_3$  avec ces furanes est du même ordre de grandeur avec celle des radicaux OH.

De plus, on peut noter que les durées de vie du F et du 3-MF avec l'ozone sont élevées, mais qu'elles sont du même ordre de grandeur pour la réaction du 2,5-DMF avec OH et  $\text{NO}_3$  ce qui suggère une réactivité élevée avec l'ozone des dérivés diméthylés et triméthylés des furanes (Matsumoto, 2011). La réaction avec les atomes de chlore est moins importante comparée à celle avec les autres oxydants atmosphériques. Celle-ci pourrait cependant avoir une plus grande contribution dans les zones côtières où les concentrations en atomes de chlore sont plus élevées (Matsumoto, 2011).

Un intérêt supplémentaire concernant les fumées de combustion est que la concentration en radicaux nitrates augmente significativement durant le jour et la nuit. Cela augmente donc la réactivité de ces composés dans les fumées avec des temps de vie de l'ordre de la minute à quelques heures durant la nuit et le jour. Ces découvertes ont donc de grandes implications dans la compréhension de la chimie dans les fumées lors de combustions de la biomasse.

Tableau 3 : Temps de vie atmosphérique des furanes (réactions avec NO<sub>3</sub>, OH, O<sub>3</sub> et Cl).

Composé	$\tau(\text{NO}_3)$ (min) <sup>a, b</sup> (Nocturne)	$\tau(\text{NO}_3)$ (min) <sup>c</sup> (Diurne)	$\tau(\text{OH})$ (min) <sup>d</sup>	$\tau(\text{O}_3)$ (min) <sup>e</sup>	$\tau(\text{Cl})$ (min) <sup>f</sup> (Matsumoto, 2011)
F	52	1035	199 (Olariu et al., 2004)	8550 (~6 jours) (Cabañas et al., 2005)	8160 (~5 jours)
2-MF	4	85	114 (Aschmann et al., 2011)	–	4380 (~3 jours)
3-MF	6	112	95 (Aschmann et al., 2011)	1080 (~1 jour) (Cabañas et al., 2004)	4200 (~3 jours)
2,5-DMF	1	26	66 (Aschmann et al., 2011)	54 (Hein et al., 1997)	3480 (~2 jours)
2,3,5-TMF	0.5	10	-	-	-

<sup>a</sup> Cette étude

<sup>b</sup>  $[\text{NO}_3] = 2 \times 10^8$  molécules  $\text{cm}^{-3}$  (concentration nocturne moyenne) (Brown & Stutz, 2012)

<sup>c</sup>  $[\text{NO}_3] = 1 \times 10^7$  molécules  $\text{cm}^{-3}$  (concentration diurne moyenne) (Brown & Stutz, 2012)

<sup>d</sup>  $[\text{OH}] = 2 \times 10^6$  12-h moyenne diurne (Hein et al., 1997)

<sup>e</sup>  $[\text{O}_3] = 7.5 \times 10^{11}$  molécules  $\text{cm}^{-3}$  (Matsumoto, 2011)

<sup>f</sup>  $[\text{Cl}] = 1 \times 10^4$  molécules  $\text{cm}^{-3}$  (Wingenter et al., 1996)

### 8. Les produits de réaction des furanes méthylés avec NO<sub>3</sub>

Il existe un nombre limité d'études concernant les mécanismes réactionnels entre NO<sub>3</sub> et les furanes (Tapia et al., 2011; Berndt et al., 1997; Colmenar et al., 2020; Joo et al., 2019). Dans ces travaux, les produits d'oxydation du furane et des furanes méthylés ont été étudiés qualitativement et quantitativement à température ambiante. L'analyse des produits formés a permis de proposer des mécanismes réactionnels principaux afin de déterminer l'origine de la formation des composés de premières générations ainsi que les mécanismes auxiliaires menant aux composés de seconde génération. L'un des produits majoritaires formés qui est commun à toutes les réactions étudiés est le dicarbonyl insaturé produit à partir de l'addition de NO<sub>3</sub> sur les carbones C-2 ou C-5 du cycle. Ce produit est formé avec un haut rendement dans toutes les réactions étudiées.

En plus de l'analyse des produits à température ambiante, la variation du rendement des produits majoritaires des réactions entre NO<sub>3</sub> et le 2-MF et 2,5-DMF pour des températures entre 298 et 353 K a été réalisée. L'étude des rendements en fonction de la température aide à la compréhension de l'évolution des mécanismes et permet de comprendre les processus chimiques atmosphériques se produisant à des températures élevées. Comme cela a déjà été évoqué, les furanes sont principalement émis lors des épisodes de combustion de biomasse où la température est souvent plus élevée que la température ambiante. Ainsi, la compréhension des rendements en fonction de la température nous aide à comprendre la chimie nocturne dans les fumées issues de la combustion de biomasse.

Les rendements en aérosol organique secondaire (AOS) pour la réaction de trois méthylfuranes (2-MF, 2,5-DMF, 2,3,5-TMF) avec NO<sub>3</sub> ont été étudiés. Les résultats indiquent que les furanes méthylés ont des rendements maximaux en AOS de 2 à 12% et qu'ils ont un faible potentiel de formation en AOS lorsqu'ils réagissent avec NO<sub>3</sub>.

## 9. Mécanisme général pour la réaction du furane et des furanes méthylés avec les radicaux NO<sub>3</sub>

En comparant les produits et les mécanismes des réactions pour les 5 furanes étudiés avec NO<sub>3</sub>, un mécanisme global a été proposé, incluant les chemins réactionnels menant à la formation des composés primaires majoritaires et minoritaires. La figure 4 montre ce mécanisme général avec les rendements pour chaque produit étudié dans ces travaux ou la littérature. Pour les 5 composés, le mécanisme principal est l'addition du NO<sub>3</sub> sur les atomes de carbone C-2 ou C-5 du cycle qui conduit à la formation du premier composé majoritaire, un dicarbonyl insaturé. Un autre composé formé à partir de l'addition de NO<sub>3</sub> est un carbonyle cyclique nitraté, mais celui-ci n'est majoritaire que dans le cas des furanes comportant un seul groupement méthyl (2-MF et 3-MF). Pour les furanes pluri-méthylés (2,5-DMF et 2,3,5-TMF), l'addition de NO<sub>3</sub> peut être suivie de l'abstraction d'un hydrogène d'un groupement méthyl lié au cycle ce qui conduit à la formation d'un furaldéhyde méthylé(s) comme deuxième produit majoritaire.

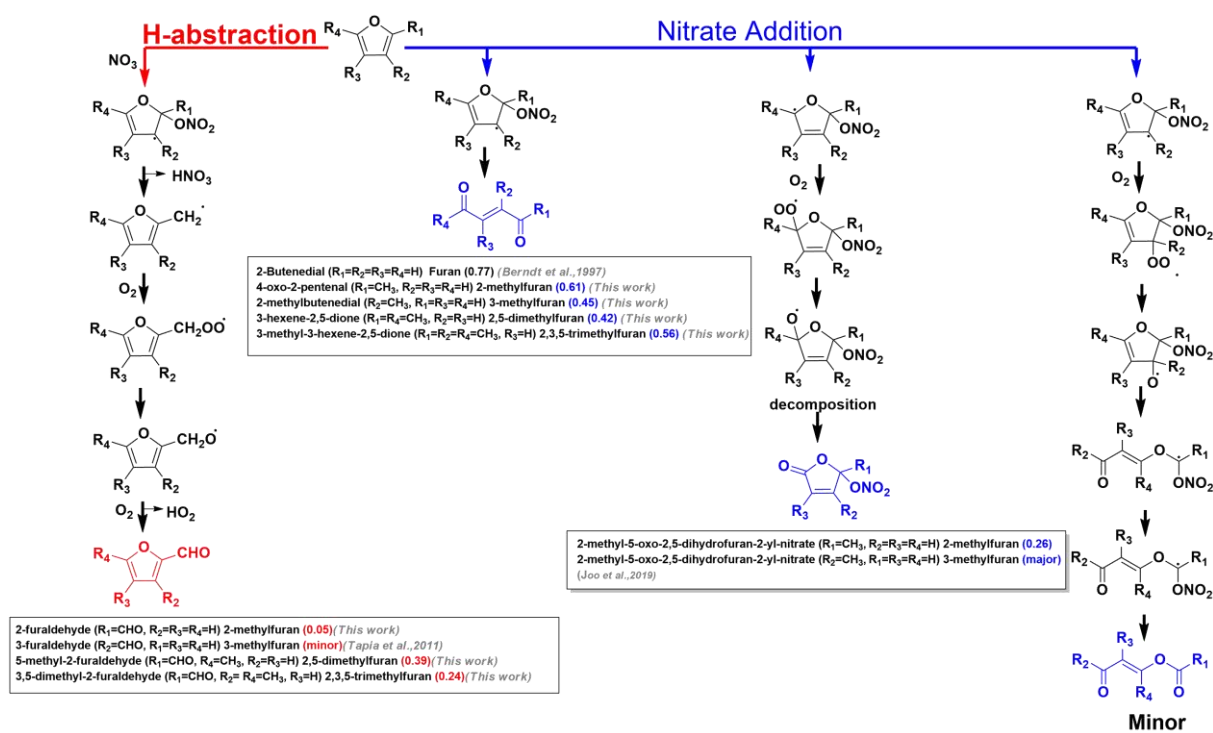


Figure 4 : Mécanismes de la réaction entre le furane et les furanes méthylés avec NO<sub>3</sub> menant à la formation des produits primaires. Les produits en bleu sont formés à partir de l'addition de NO<sub>3</sub> et ceux en rouge sont formés à partir de l'abstraction d'hydrogène. Les rendements sont également indiqués.

## 10. Conclusion et Perspectives

Ce travail de recherche sur l'étude des réactions entre le radical NO<sub>3</sub> et les furanes méthylés émis par la combustion de la biomasse a été réalisé dans les chambres de simulation atmosphériques CHARME et THALAMOS. Ces travaux ont permis de déterminer les durées de vie de ces composés et d'identifier et quantifier les produits d'oxydation formés dans les phases gazeuse et particulaires (AOS). Les mécanismes réactionnels ont été établis pour chaque composé, ce qui a permis de proposer un mécanisme global de formation des produits de première génération pour les furanes méthylés. Les analyses ont été réalisées en utilisant

différentes techniques : PTR-ToF-MS, GC-EI-MS et ESI-LC-QToF-MS/MS pour les mesures réalisées dans CHARME et SIFT-MS, GC-EI-MS pour celles effectuées dans THALAMOS. De plus, des analyses en spectroscopie infrarouge ont permis de valider l'identification de produits observés ou d'apporter des éléments supplémentaires à l'étude des AOS.

Comme cela a déjà été mentionné, la réactivité des furanes avec  $\text{NO}_3$  est encore peu étudiée, spécialement dans les conditions de combustion de la biomasse où on les retrouve principalement. Cette thèse a donc essayé d'ouvrir la voie à ce nouveau champ de recherche. De nombreux objectifs ont été atteints durant ces années de recherches, mais d'autres restent encore à être entrepris car même si nous avons répondu à un certain nombre de questions, d'autres restent en suspens voir de nouvelles questions ont été soulevés par nos travaux. Ainsi, les perspectives sont nombreuses et multidisciplinaires.

Du point de vue de la chimie atmosphérique, ces travaux ont permis d'identifier des produits primaires et secondaires qui ont eux aussi une réactivité significative avec  $\text{NO}_3$ . Il y a donc un intérêt réel à l'étude leur réactivité afin de déterminer leurs implications atmosphériques. La différence de chimie entre les furanes simplement méthylés et pluri-méthylés est aussi toujours en attente de réponse. Pourquoi les uns favorisent la formation de composés nitrates et ne sont pas affectés par l'ozone quand les autres favorisent la formation de furaldéhyde et sont largement affectés par l'ozone ? Concernant la phase particulaire, même si la formation d'AOS est modeste à température ambiante, il pourrait être intéressant de mener une des études de rendement avec des conditions plus proche de celles des fumées de la combustion de biomasse. Enfin, l'étude approfondie des propriétés optiques, hygroscopiques et toxicologiques permettrait de savoir si ces rendements « modestes » peuvent avoir un effet significatif sur le climat et la santé. Nous pourrions encore continuer la liste des perspectives sur plusieurs pages mais la meilleure perspective à cette étude serait qu'elle serve d'impulsion pour les futurs chercheurs comme première pierre d'un immense édifice.

## Références

- Akagi, S. K., Burling, I. R., Mendoza, A., Johnson, T. J., Cameron, M., Griffith, D. W. T., Paton-Walsh, C., Weise, D. R., Reardon, J., & Yokelson, R. J. (2014). Field measurements of trace gases emitted by prescribed fires in southeastern US pine forests using an open-path FTIR system. *Atmospheric Chemistry and Physics*, *14*(1), 199–215. <https://doi.org/10.5194/acp-14-199-2014>
- Akagi, S. K., Yokelson, R. J., Burling, I. R., Meinardi, S., Simpson, I., Blake, D. R., McMeeking, G. R., Sullivan, A., Lee, T., Kreidenweis, S., Urbanski, S., Reardon, J., Griffith, D. W. T., Johnson, T. J., & Weise, D. R. (2013). Measurements of reactive trace gases and variable O<sub>3</sub> formation rates in some South Carolina biomass burning plumes. In *Atmospheric Chemistry and Physics* (Vol. 13, Issue 3). <https://doi.org/10.5194/acp-13-1141-2013>
- Akagi, S. K., Yokelson, R. J., Wiedinmyer, C., Alvarado, M. J., Reid, J. S., Karl, T., Crouse, J. D., & Wennberg, P. O. (2011). Emission factors for open and domestic biomass burning for use in atmospheric models. *Atmospheric Chemistry and Physics*, *11*(9), 4039–4072. <https://doi.org/10.5194/acp-11-4039-2011>
- Akele, E. S., & Tarekegn, M. M. (2017). Assessment of dioxin and furan emission levels and management practices in Addis Ababa, Ethiopia. *Journal of Health and Pollution*, *7*(15), 85–94. <https://doi.org/10.5696/2156-9614-7.15.85>
- Al Ali, F., Coeur, C., Houzel, N., Bouya, H., Tomas, A., & Romanias, M. N. (2022). Rate Coefficients for the Gas-Phase Reactions of Nitrate Radicals with a Series of Furan Compounds. *Journal of Physical Chemistry A*, *126*(46), 8674–8681. <https://doi.org/10.1021/acs.jpca.2c03828>
- Alan Buis. (2019). *Earth's Atmosphere: A Multi-layered Cake*. <https://climate.nasa.gov/news/2919/earths-atmosphere-a-multi-layered-cake/>
- Alcock, R. E., & Jones, K. C. (1996). Dioxins in the environment: A review of trend data. *Environmental Science and Technology*, *30*(11), 3133–3143. <https://doi.org/10.1021/es960306z>
- Alicke, B., & Platt, U. (2002). *Impact of nitrous acid photolysis on the total hydroxyl radical budget during the Limitation of Oxidant Production / Pianura Padana Produzione di Ozono study in Milan*. 107. <https://doi.org/10.1029/2000JD000075>
- Alvarado, A., Atkinson, R., & Arey, J. (1996). Kinetics of the gas-phase reactions of NO<sub>3</sub> radicals and O<sub>3</sub> with 3-methylfuran and the OH radical yield from the O<sub>3</sub> reaction. *International Journal of Chemical Kinetics*, *28*(12), 905–909. [https://doi.org/10.1002/\(SICI\)1097-4601\(1996\)28:12<905::AID-KIN7>3.0.CO;2-R](https://doi.org/10.1002/(SICI)1097-4601(1996)28:12<905::AID-KIN7>3.0.CO;2-R)
- Alwe, H. D., Walavalkar, M. P., Sharma, A., Dhanya, S., & Naik, P. D. (2014). Tropospheric oxidation of cyclic unsaturated ethers in the day-time: Comparison of the reactions with Cl, OH and O<sub>3</sub> based on the determination of their rate coefficients at 298K. *Atmospheric Environment*, *82*, 113–120. <https://doi.org/10.1016/j.atmosenv.2013.10.009>
- Andersen, C., Nielsen, O. J., Østerstrøm, F. F., Ausmeel, S., Nilsson, E. J. K., & Sulbaek Andersen, M. P. (2016). Atmospheric Chemistry of Tetrahydrofuran, 2-Methyltetrahydrofuran, and 2,5-Dimethyltetrahydrofuran: Kinetics of Reactions with Chlorine Atoms, OD Radicals, and Ozone. *Journal of Physical Chemistry A*, *120*(37), 7320–7326. <https://doi.org/10.1021/acs.jpca.6b06618>
- Andreae, M. (2019). Emission of trace gases and aerosols from biomass burning. Global Biogeochemical. *Atmospheric Chemistry and Physics*, *15* (4)(April), 955–966. <https://www.atmos-chem-phys-discuss.net/acp-2019-303/acp-2019-303.pdf>
- Andreae, M. O. (2001). [ *Ca Because of the carbon to permits*. *15*(4), 955–966.

- Aschmann, S. M., Nishino, N., Arey, J., & Atkinson, R. (2011). Kinetics of the Reactions of OH Radicals with 2- and 3-Methylfuran, 2,3- and 2,5-Dimethylfuran, and E- and Z-3-Hexene-2,5-dione, and Products of OH p 2,5-Dimethylfuran. *Environmental Science and Technology*, 45(7), 1859–1865. <https://doi.org/10.1002/kin.550140706>
- Aschmann, S. M., Nishino, N., Arey, J., & Atkinson, R. (2014a). Products of the OH Radical-Initiated Reactions of Furan, 2- and 3-Methylfuran, and 2,3- and 2,5-Dimethylfuran in the Presence of NO. *The Journal of Physical Chemistry*, 118, 457–466. <https://doi.org/10.1021/jp410345k>
- Aschmann, S. M., Nishino, N., Arey, J., & Atkinson, R. (2014b). Sara M. Aschmann, Noriko Nishino, † Janet Arey, \*, ‡ and Roger Atkinson \*, ‡.
- Atkinson, R. (1991a). Kinetics and Mechanisms of the Gas-Phase Reactions of the NO<sub>3</sub> Radical with Organic Compounds. *Journal of Physical and Chemical Reference Data*, 20(3), 459–507. <https://doi.org/10.1063/1.555887>
- Atkinson, R. (1991b). Kinetics and Mechanisms of the Gas-Phase Reactions of the NO<sub>3</sub> Radical with Organic Compounds. *Journal of Physical and Chemical Reference Data*, 20(3), 459–507. <https://doi.org/10.1063/1.555887>
- Atkinson, R. (2000). Atmospheric chemistry of VOCs and NO(x). *Atmospheric Environment*, 34(12–14), 2063–2101. [https://doi.org/10.1016/S1352-2310\(99\)00460-4](https://doi.org/10.1016/S1352-2310(99)00460-4)
- Atkinson, R., & Arey, J. (2003). ARTICLE IN PRESS Gas-phase tropospheric chemistry of biogenic volatile organic compounds : a review. 2(2). [https://doi.org/10.1016/S1352-2310\(03\)00391-1](https://doi.org/10.1016/S1352-2310(03)00391-1)
- Atkinson, R., Arey, J., Tuazon, E. C., & Aschmann, S. M. (1992). Gas-phase reactions of 1,4-benzodioxan, 2,3-dihydrobenzofuran, and 2,3-benzofuran with OH radicals and O<sub>3</sub>. *International Journal of Chemical Kinetics*, 24(4), 345–358. <https://doi.org/10.1002/kin.550240404>
- Atkinson, R., Aschmann, S. M., & Carter, P. L. (1983a). *Radicals with Furan and Thiophene at. 15*, 51–61.
- Atkinson, R., Aschmann, S. M., & Carter, W. P. L. (1983b). Kinetics of the reactions of O<sub>3</sub> and OH radicals with furan and thiophene at 298 ± 2 K. *International Journal of Chemical Kinetics*, 15(1), 51–61. <https://doi.org/10.1002/kin.550150106>
- Atkinson, R., Aschmann, S. M., & Carter, W. P. L. (1984). Kinetics of the reactions of O<sub>3</sub> and OH radicals with a series of dialkenes and trialkenes at 294 ± 2 K. *International Journal of Chemical Kinetics*, 16(8), 967–976. <https://doi.org/10.1002/kin.550160804>
- Atkinson, R., Aschmann, S. M., & Pitts, J. N. (1988). Rate constants for the gas-phase reactions of the NO<sub>3</sub> radical with a series of organic compounds at 296 ± 2 K. *Journal of Physical Chemistry*, 92(12), 3454–3457. <https://doi.org/10.1021/j100323a028>
- Atkinson, R., Aschmann, S. M., Tuazon, E. C., Arey, J., & Zielinska, B. (1989). Formation of 3-Methylfuran from the gas-phase reaction of OH radicals with isoprene and the rate constant for its reaction with the OH radical. *International Journal of Chemical Kinetics*, 21(7), 593–604. <https://doi.org/10.1002/kin.550210709>
- Atkinson, R., Aschmann, S. M., Winer, A. M., & Carter, W. P. L. (1985a). *for Reactions with Pyrrole ± 1 Atmospheric. I*, 87–90.
- Atkinson, R., Aschmann, S. M., Winer, A. M., & Carter, W. P. L. (1985b). Rate Constants for the Gas-Phase Reactions of NO<sub>3</sub> Radicals with Furan, Thiophene, and Pyrrole at 295 ± 1 K and Atmospheric Pressure. *Environmental Science and Technology*, 19(1), 87–90. <https://doi.org/10.1021/es00131a010>



- Atkinson, R., Aschmann, S. M., Winer, A. M., & Pitts, J. N. (1985). Kinetics and Atmospheric Implications of the Gas-Phase Reactions of NO<sub>3</sub> Radicals with a Series of Monoterpenes and Related Organics at 294 ± 2 K. *Environmental Science and Technology*, 19(2), 159–163. <https://doi.org/10.1021/es00132a009>
- Atkinson, R., Baulch, D. L., Cox, R. A., Hampson, R. F., Kerr, J. A., Rossi, M. J., & Troe, J. (1997). Evaluated Kinetic, Photochemical and Heterogeneous Data for Atmospheric Chemistry: Supplement V: IUPAC Subcommittee on Gas Kinetic Data Evaluation for Atmospheric Chemistry. *Journal of Physical and Chemical Reference Data*, 26(3), 521–784. <https://doi.org/10.1063/1.556011>
- Bahreini, R., Keywood, M. D., Ng, N. L., Varutbangkul, V., Gao, S., Flagan, R. C., Seinfeld, J. H., Worsnop, D. R., & Jimenez, J. L. (2005). Measurements of secondary organic aerosol from oxidation of cycloalkenes, terpenes, and m-xylene using an aerodyne aerosol mass spectrometer. *Environmental Science and Technology*, 39(15), 5674–5688. <https://doi.org/10.1021/es048061a>
- Berndt, T., Böge, O., & Rolle, W. (1997). Products of the gas-phase reactions of NO<sub>3</sub> radicals with furan and tetramethylfuran. *Environmental Science and Technology*, 31(4), 1157–1162. <https://doi.org/10.1021/es960669z>
- Bierbach, A., Barnes, I., & Becker, K. H. (1992). Rate coefficients for the gas-phase reactions of hydroxyl radicals with furan, 2-methylfuran, 2-ethylfuran and 2,5-dimethylfuran at 300 ± 2 K. *Atmospheric Environment Part A, General Topics*, 26(5), 813–817. [https://doi.org/10.1016/0960-1686\(92\)90241-C](https://doi.org/10.1016/0960-1686(92)90241-C)
- Bierbach, A., Barnes, I., & Becker, K. H. (1995). Product and kinetic study of the oh-initiated gas-phase oxidation of Furan, 2-methylfuran and furanaldehydes at ≈ 300 K. *Atmospheric Environment*, 29(19), 2651–2660. [https://doi.org/10.1016/1352-2310\(95\)00096-H](https://doi.org/10.1016/1352-2310(95)00096-H)
- Bierbach, A., Barnes, I., Becker, K. H., & Wiesen, E. (1994). Atmospheric Chemistry of Unsaturated Carbonyls: Butenedial, 4-Oxo-2-pentenal, 3-Hexene-2,5-dione, Maleic Anhydride, 3H-Furan-2-one, and 5-Methyl-3H-furan-2-one. *Environmental Science and Technology*, 28(4), 715–729. <https://doi.org/10.1021/es00053a028>
- Blake, R., Monks, P., & Ellis, A. (2009). Proton Transfer Reaction Mass Spectrometry (PTR-MS). *Chem.Rev.*, 109(0), 861–896. <https://doi.org/10.1002/9781118180730.ch28>
- Brando, P., Macedo, M., Silvério, D., Rattis, L., Paolucci, L., Alencar, A., Coe, M., & Amorim, C. (2020). Amazon wildfires: Scenes from a foreseeable disaster. *Flora: Morphology, Distribution, Functional Ecology of Plants*, 268. <https://doi.org/10.1016/j.flora.2020.151609>
- Brown, S. S., & Stutz, J. (2012). Nighttime radical observations and chemistry. *Chemical Society Reviews*, 41(19), 6405–6447. <https://doi.org/10.1039/c2cs35181a>
- Burkholder, J. B., Abbatt, J. P. D., Barnes, I., Roberts, J. M., Melamed, M. L., Ammann, M., Bertram, A. K., Cappa, C. D., Carlton, A. G., Carpenter, L. J., Crowley, J. N., Dubowski, Y., George, C., Heard, D. E., Herrmann, H., Keutsch, F. N., Kroll, J. H., McNeill, V. F., Ng, N. L., ... Ziemann, P. J. (2017). The Essential Role for Laboratory Studies in Atmospheric Chemistry. *Environmental Science and Technology*, 51(5), 2519–2528. <https://doi.org/10.1021/acs.est.6b04947>
- Burkholder, J. B., Sander, S. P., Abbatt, J. P. D., Barker, J. R., Huie, R. E., Kolb, C. E., Kurylo, M. J., Orkin, V. L., Wilmouth, D. M., & Wine, P. H. (2020). Chemical Kinetics and Photochemical Data for Use in Atmospheric Studies, Evaluation No. 19. *JPL Publications 19-5*, 19, 1–153. <http://jpldataeval.jpl.nasa.gov/>
- Burling, I. R., Yokelson, R. J., Griffith, D. W. T., Johnson, T. J., Veres, P., Roberts, J. M., Warneke, C., Urbanski, S. P., Reardon, J., Weise, D. R., Hao, W. M., & De Gouw, J. (2010). Laboratory

- measurements of trace gas emissions from biomass burning of fuel types from the southeastern and southwestern United States. *Atmospheric Chemistry and Physics*, 10(22), 11115–11130. <https://doi.org/10.5194/acp-10-11115-2010>
- Cabañas, B., Baeza, M. T., Salgado, S., Martín, P., Taccone, R., & Martínez, E. (2004). Oxidation of heterocycles in the atmosphere: Kinetic study of their reactions with NO<sub>3</sub> radical. *Journal of Physical Chemistry A*, 108(49), 10818–10823. <https://doi.org/10.1021/jp046524t>
- Cabañas, B., Villanueva, F., Martín, P., Baeza, M. T., Salgado, S., & Jiménez, E. (2005). Study of reaction processes of furan and some furan derivatives initiated by Cl atoms. *Atmospheric Environment*, 39(10), 1935–1944. <https://doi.org/10.1016/j.atmosenv.2004.12.013>
- Cabrera-perez, D., Taraborrelli, D., Sander, R., & Pozzer, A. (2016). *Global atmospheric budget of simple monocyclic aromatic compounds*. 6931–6947. <https://doi.org/10.5194/acp-16-6931-2016>
- Calogirou, A., Jensen, N. R., Nielsen, C. J., Kotzias, D., & Hjorth, J. (1999). Gas-phase reactions of nopinone, 3-isopropenyl-6-oxo-heptanal, and 5-methyl-5-vinyltetrahydrofuran-2-ol with OH, NO<sub>3</sub>, and ozone. *Environmental Science and Technology*, 33(3), 453–460. <https://doi.org/10.1021/es980530j>
- Carbajo, P. G., Smith, S. C., Holloway, A. L., Smith, C. A., Pope, F. D., Shallcross, D. E., & Orr-Ewing, A. J. (2008). Ultraviolet photolysis of HCHO: Absolute HCO quantum yields by direct detection of the HCO radical photoproduct. *Journal of Physical Chemistry A*, 112(48), 12437–12448. <https://doi.org/10.1021/jp8070508>
- Chattopadhyay, A., Papadimitriou, V. C., Marshall, P., & Burkholder, J. B. (2020). Temperature-dependent rate coefficients for the gas-phase OH + furan-2,5-dione (C<sub>4</sub>H<sub>2</sub>O<sub>3</sub>, maleic anhydride) reaction. *International Journal of Chemical Kinetics*, 52(10), 623–631. <https://doi.org/10.1002/kin.21387>
- Chipperfield, M. P., Bekki, S., Dhomse, S., Harris, N. R. P., Hassler, B., Hossaini, R., Steinbrecht, W., Thiéblemont, R., & Weber, M. (2017). Detecting recovery of the stratospheric ozone layer. *Nature*, 549(7671), 211–218. <https://doi.org/10.1038/nature23681>
- Christian, T. J., Kleiss, B., Yokelson, R. J., Holzinger, R., Crutzen, P. J., Hao, W. M., Saharjo, B. H., & Ward, D. E. (2003). Comprehensive laboratory measurements of biomass-burning emissions: 1. Emissions from Indonesian, African, and other fuels. *Journal of Geophysical Research: Atmospheres*, 108(23). <https://doi.org/10.1029/2003jd003704>
- Ciccioli, P., Brancaleoni, E., Frattoni, M., Cecinato, A., & Pinciarelli, L. (2001). Determination of volatile organic compounds (VOC) emitted from biomass burning of Mediterranean vegetation species by GC-MS. *Analytical Letters*, 34(6), 937–955. <https://doi.org/10.1081/AL-100103604>
- Coeur-tourneur, C., Tomas, A., & Menu, D. (2008). *Secondary organic aerosol formation from the gas phase reaction of hydroxyl radicals with m-, o- and p-cresol*. 42, 3035–3045. <https://doi.org/10.1016/j.atmosenv.2007.12.043>
- Coggon, M. M., Lim, C. Y., Koss, A. R., Sekimoto, K., Yuan, B., Gilman, J. B., Hagan, D. H., Selimovic, V., Zarzana, K. J., Brown, S. S., M Roberts, J., Müller, M., Yokelson, R., Wisthaler, A., Krechmer, J. E., Jimenez, J. L., Cappa, C., Kroll, J. H., De Gouw, J., & Warneke, C. (2019). OH chemistry of non-methane organic gases (NMOGs) emitted from laboratory and ambient biomass burning smoke: Evaluating the influence of furans and oxygenated aromatics on ozone and secondary NMOG formation. *Atmospheric Chemistry and Physics*, 19(23), 14875–14899. <https://doi.org/10.5194/acp-19-14875-2019>
- Collard, F. X., & Blin, J. (2014). A review on pyrolysis of biomass constituents: Mechanisms and

- composition of the products obtained from the conversion of cellulose, hemicelluloses and lignin. *Renewable and Sustainable Energy Reviews*, 38, 594–608. <https://doi.org/10.1016/j.rser.2014.06.013>
- Colmenar, I., Cabañas, B., Martínez, E., Salgado, M. S., & Martín, P. (2012). Atmospheric fate of a series of furanaldehydes by their NO<sub>3</sub> reactions. *Atmospheric Environment*, 54(3), 177–184. <https://doi.org/10.1016/j.atmosenv.2012.02.087>
- Colmenar, I., Martín, P., Cabañas, B., Salgado, S., Villanueva, F., & Ballesteros, B. (2020). Evaluation of the SOA formation in the reaction of furfural with atmospheric oxidants. *Atmosphere*, 11(9). <https://doi.org/10.3390/atmos11090927>
- Corchnoy, S., & Atkinson, R. (1990). Kinetics of the Gas-Phase Reactions of OH and NO<sub>3</sub> Radicals with 2-Carene, 1,8-Cineole, p-Cymene, and Terpinolene. *Environ. Sci. Technol.* 1990, 24(10), 1497–1502.
- Crouse, J. D., DeCarlo, P. F., Blake, D. R., Emmons, L. K., Campos, T. L., Apel, E. C., Clarke, A. D., Weinheimer, A. J., McCabe, D. C., Yokelson, R. J., Jimenez, J. L., & Wennberg, P. O. (2009). Biomass burning and urban air pollution over the Central Mexican Plateau. *Atmospheric Chemistry and Physics*, 9(14), 4929–4944. <https://doi.org/10.5194/acp-9-4929-2009>
- Cuisset, A., Coeur, C., Mouret, G., Ahmad, W., Tomas, A., & Pirali, O. (2016). Infrared spectroscopy of methoxyphenols involved as atmospheric secondary organic aerosol precursors: Gas-phase vibrational cross-sections. *Journal of Quantitative Spectroscopy and Radiative Transfer*, 179, 51–58. <https://doi.org/10.1016/j.jqsrt.2016.03.020>
- Davis, A. C., & Sarathy, S. M. (2013). Computational study of the combustion and atmospheric decomposition of 2-methylfuran. *Journal of Physical Chemistry A*, 117(33), 7670–7685. <https://doi.org/10.1021/jp403085u>
- De gouw, J., & Warneke, C. (2007). MEASUREMENTS OF VOLATILE ORGANIC COMPOUNDS IN THE EARTH'S ATMOSPHERE USING PROTON-TRANSFER-REACTION MASS SPECTROMETRY. *Wiley InterScience*, i, 221–235. <https://doi.org/10.1002/mas>
- Decker, Z. C. J., Zarzana, K. J., Coggon, M., Min, K. E., Pollack, I., Ryerson, T. B., Peischl, J., Edwards, P., Dubé, W. P., Markovic, M. Z., Roberts, J. M., Veres, P. R., Graus, M., Warneke, C., De Gouw, J., Hatch, L. E., Barsanti, K. C., & Brown, S. S. (2019). Nighttime Chemical Transformation in Biomass Burning Plumes: A Box Model Analysis Initialized with Aircraft Observations. *Environmental Science and Technology*, 53(5), 2529–2538. <https://doi.org/10.1021/acs.est.8b05359>
- Decker, Z., Robinson, M., Barsanti, K., Bourgeois, I., Coggon, M., DiGangi, J., Diskin, G., Flocke, F., Franchin, A., Fredrickson, C., Hall, S., Halliday, H., Holmes, C., Huey, L. G., Lee, Y. R., Lindaas, J., Middlebrook, A., Montzka, D., Moore, R., ... Brown, S. (2021). Nighttime and Daytime Dark Oxidation Chemistry in Wildfire Plumes: An Observation and Model Analysis of FIREX-AQ Aircraft Data. *Atmospheric Chemistry and Physics Discussions*, November, 1–45. <https://doi.org/10.5194/acp-2021-267>
- Dlugokencky, E. J., & Howard, C. J. (1989a). + (1.28. 17, 1091–1096.
- Dlugokencky, E. J., & Howard, C. J. (1989b). Studies of NO<sub>3</sub> radical reactions with some atmospheric organic compounds at low pressures. *Journal of Physical Chemistry*, 93(3), 1091–1096. <https://doi.org/10.1021/j100340a015>
- Dodge, M. C. (2000). Chemical oxidant mechanisms for air quality modeling: Critical review. *Atmospheric Environment*, 34(12–14), 2103–2130. [https://doi.org/10.1016/S1352-2310\(99\)00461-6](https://doi.org/10.1016/S1352-2310(99)00461-6)

- Durigan, M. R., Cherubin, M. R., de Camargo, P. B., Ferreira, J. N., Berenguer, E., Gardner, T. A., Barlow, J., Dias, C. T. dos S., Signor, D., de Oliveira, R. C., & Cerri, C. E. P. (2017). Soil organic matter responses to anthropogenic forest disturbance and land use change in the eastern Brazilian Amazon. *Sustainability (Switzerland)*, *9*(3). <https://doi.org/10.3390/su9030379>
- Dusanter, S., Vimal, D., Stevens, P. S., Volkamer, R., Molina, L. T., Baker, A., Meinardi, S., Blake, D., Sheehy, P., Merten, A., Zhang, R., Zheng, J., Fortner, E. C., Junkermann, W., Dubey, M., Rann, T., Eichinger, B., Lewandowski, P., Prueger, J., & Holder, H. (2009). Measurements of OH and HO<sub>2</sub> concentrations during the MCMA-2006 field campaign - Part 2: Model comparison and radical budget. *Atmospheric Chemistry and Physics*, *9*(18), 6655–6675. <https://doi.org/10.5194/acp-9-6655-2009>
- Eble, J., Bänisch, C., & Olzmann, M. (2015). *Kinetic Investigation of the Reactions of 2, 5-Dimethylfuran and 2-Methylfuran with Hydroxyl Radicals*. 2–5.
- Elshorbany, Y., Barnes, I., Becker, K. H., Kleffmann, J., & Wiesen, P. (2010). Sources and cycling of tropospheric hydroxyl radicals - An overview. *Zeitschrift Fur Physikalische Chemie*, *224*(7–8), 967–987. <https://doi.org/10.1524/zpch.2010.6136>
- Elshorbany, Y. F., Kurtenbach, R., Wiesen, P., Lissi, E., Rubio, M., Villena, G., Gramsch, E., Rickard, A. R., Pilling, M. J., & Kleffmann, J. (2009). Oxidation capacity of the city air of Santiago, Chile. *Atmospheric Chemistry and Physics*, *9*(6), 2257–2273. <https://doi.org/10.5194/acp-9-2257-2009>
- Elwardany, A., Es-Sebbar, E., Khaled, F., & Farooq, A. (2016). A chemical kinetic study of the reaction of hydroxyl with furans. *Fuel*, *166*, 245–252. <https://doi.org/10.1016/j.fuel.2015.10.098>
- Evtugina, M., Alves, C., Calvo, A., Nunes, T., Tarelho, L., Duarte, M., Prozil, S. O., Evtuguin, D. V., & Pio, C. (2014). VOC emissions from residential combustion of Southern and mid-European woods. *Atmospheric Environment*, *83*, 90–98. <https://doi.org/10.1016/j.atmosenv.2013.10.050>
- Evtugina, M., Calvo, A. I., Nunes, T., Alves, C., Fernandes, A. P., Tarelho, L., Vicente, A., & Pio, C. (2013). VOC emissions of smouldering combustion from Mediterranean wildfires in central Portugal. *Atmospheric Environment*, *64*, 339–348. <https://doi.org/10.1016/j.atmosenv.2012.10.001>
- Fayad, L. (2019). *Caractérisation de la nouvelle chambre de simulation atmosphérique CHARME et étude de la réaction d'ozonolyse d'un COV biogénique, le  $\gamma$ -terpinène* Loyal FAYAD Acknowledgments (Vol. 104).
- Fayad, L., Coeur, C., Fagniez, T., Secordel, X., Houzel, N., & Mouret, G. (2021). Kinetic and mechanistic study of the gas-phase reaction of ozone with  $\gamma$ -terpinene. *Atmospheric Environment*, *246*(August 2020). <https://doi.org/10.1016/j.atmosenv.2020.118073>
- Ferdous, D., Dalai, A. K., Bej, S. K., & Thring, R. W. (2002). Pyrolysis of lignins: Experimental and kinetics studies. *Energy and Fuels*, *16*(6), 1405–1412. <https://doi.org/10.1021/ef0200323>
- Finlayson-Pitts, B. J. (2010). Atmospheric chemistry. *Proceedings of the National Academy of Sciences of the United States of America*, *107*(15), 6566–6567. <https://doi.org/10.1073/pnas.1003038107>
- Finlayson-Pitts, B. J., & Pitts, J. N. (1993). Atmospheric chemistry of tropospheric ozone formation: Scientific and regulatory implications. *Air and Waste*, *43*(8), 1091–1100. <https://doi.org/10.1080/1073161X.1993.10467187>
- Finlayson-Pitts, Barbara J., & James N. Pitts Jr. (1999). *Chemistry of the upper and lower atmosphere: theory, experiments, and applications*. El Sevier.
- Fuchs, J. D. H., Seakins, A. K. P., & Editors, J. W. (n.d.). *A Practical Guide to Atmospheric*.
- George, C., Ammann, M., D'Anna, B., Donaldson, D. J., & Nizkorodov, S. A. (2015). Heterogeneous

Photochemistry in the Atmosphere. *Chemical Reviews*, 115(10), 4218–4258. <https://doi.org/10.1021/cr500648z>

- Gilman, J. B., Lerner, B. M., Kuster, W. C., Goldan, P. D., Warneke, C., Veres, P. R., Roberts, J. M., De Gouw, J. A., Burling, I. R., & Yokelson, R. J. (2015). Biomass burning emissions and potential air quality impacts of volatile organic compounds and other trace gases from fuels common in the US. *Atmospheric Chemistry and Physics*, 15(24), 13915–13938. <https://doi.org/10.5194/acp-15-13915-2015>
- Giri, B. R., Khaled, F., Szori, M., Viskolcz, B., & Farooq, A. (2017). An experimental and theoretical kinetic study of the reaction of OH radicals with tetrahydrofuran. *Proceedings of the Combustion Institute*, 36(1), 143–150. <https://doi.org/10.1016/j.proci.2016.06.016>
- Gómez Alvarez, E., Borrás, E., Viidanoja, J., & Hjorth, J. (2009). Unsaturated dicarbonyl products from the OH-initiated photo-oxidation of furan, 2-methylfuran and 3-methylfuran. *Atmospheric Environment*, 43(9), 1603–1612. <https://doi.org/10.1016/j.atmosenv.2008.12.019>
- Graedel, T. E., & Keene, W. C. (1996). The budget and cycle of Earth's natural chlorine. *Pure and Applied Chemistry*, 68(9), 1689–1697. <https://doi.org/10.1351/pac199668091689>
- Graham, B., Mayol-Bracero, O. L., Guyon, P., Roberts, G. C., Decesari, S., Facchini, M. C., Artaxo, P., Maenhaut, W., Köll, P., & Andreae, M. O. (2002). Water-soluble organic compounds in biomass burning aerosols over Amazonia 1. Characterization by NMR and GC-MS. *Journal of Geophysical Research Atmospheres*, 107(20), LBA 14-1-LBA 14-16. <https://doi.org/10.1029/2001JD000336>
- Greenberg, J. P., Zimmerman, P. R., Heidt, L., & Pollock, W. (1984). Hydrocarbon and carbon monoxide emissions from biomass burning in Brazil. *Journal of Geophysical Research*, 89(D1), 1350–1354. <https://doi.org/10.1029/JD089iD01p01350>
- Griira, A., Amarandei, C., Romanias, M. N., El Dib, G., Canosa, A., Arsene, C., Bejan, I. G., Olariu, R. I., Coddeville, P., & Tomas, A. (2020). Kinetic measurements of Cl atom reactions with C5-C8 unsaturated alcohols. *Atmosphere*, 11(3), 1–15. <https://doi.org/10.3390/ATMOS11030256>
- Guenther, A., Nicholas, C., Fall, R., Klinger, L., Mckay, W. A., & Scholes, B. (1995). A global model of natural volatile organic compound emissions s Raja the balance Triangle changes in the atmospheric accumulation rates of greenhouse Triangle Several inventories of natural and Exposure Assessment global scales have been two classes Fores. *J. Geophys. Res.*, 100(94), 8873–8892.
- Hartikainen, A., Yli-Pirilä, P., Tiitta, P., Leskinen, A., Kortelainen, M., Orasche, J., Schnelle-Kreis, J., Lehtinen, K. E. J., Zimmermann, R., Jokiniemi, J., & Sippula, O. (2018). Volatile Organic Compounds from Logwood Combustion: Emissions and Transformation under Dark and Photochemical Aging Conditions in a Smog Chamber. *Environmental Science and Technology*, 52(8), 4979–4988. <https://doi.org/10.1021/acs.est.7b06269>
- Hatch, L. E., Luo, W., Pankow, J. F., Yokelson, R. J., Stockwell, C. E., & Barsanti, K. C. (2015). Identification and quantification of gaseous organic compounds emitted from biomass burning using two-dimensional gas chromatography-time-of-flight mass spectrometry. *Atmospheric Chemistry and Physics*, 15(4), 1865–1899. <https://doi.org/10.5194/acp-15-1865-2015>
- Hatch, L. E., Yokelson, R. J., Stockwell, C. E., Veres, P. R., Simpson, I. J., Blake, D. R., Orlando, J. J., & Barsanti, K. C. (2017). Multi-instrument comparison and compilation of non-methane organic gas emissions from biomass burning and implications for smoke-derived secondary organic aerosol precursors. *Atmospheric Chemistry and Physics*, 17(2), 1471–1489. <https://doi.org/10.5194/acp-17-1471-2017>

- Hein, R., Crutzen, P. J., & Heimann, M. (1997). An inverse modeling approach to investigate the global atmospheric methane cycle. *Global Biogeochemical Cycles*, 11(1), 43–76. <https://doi.org/10.1029/96GB03043>
- Holly Zell. (2013). *Earth's Atmospheric Layers*. [https://www.nasa.gov/mission\\_pages/sunearth/science/atmosphere-layers2.html](https://www.nasa.gov/mission_pages/sunearth/science/atmosphere-layers2.html)
- Huang, Z., Zhao, N., Ma, X., Xu, F., Zhang, Q., Zhuang, T., & Wang, W. (2019). Theoretical study on the atmospheric oxidation reaction of 2-furaldehyde initiated by NO<sub>3</sub> radicals. *Chemical Physics Letters*, 722(3), 50–57. <https://doi.org/10.1016/j.cplett.2019.03.009>
- Hynes, R. G., Angove, D. E., Saunders, S. M., Haverd, V., & Azzi, M. (2005). Evaluation of two MCM v3.1 alkene mechanisms using indoor environmental chamber data. *Atmospheric Environment*, 39(38), 7251–7262. <https://doi.org/10.1016/j.atmosenv.2005.09.005>
- Identification, I., Flux, V., & Atkinson, R. (1990). *Radicals with*. 24(10), 1497–1502.
- Illés, Á., Rózsa, Z. B., Thangaraj, R., Décsiné Gombos, E., Dóbbé, S., Giri, B. R., & Szóri, M. (2021). An experimental and theoretical kinetic study of the reactions of hydroxyl radicals with tetrahydrofuran and two deuterated tetrahydrofurans. *Chemical Physics Letters*, 776. <https://doi.org/10.1016/j.cplett.2021.138698>
- IUPAC. (2016). *IUPAC Task Group on Atmospheric Chemical Kinetic Data Evaluation – Data Sheet NO<sub>3</sub>\_VOC*. [iupac.pole-ether.fr](http://iupac.pole-ether.fr)
- Jenkin, M. E., & Hayman, G. D. (1999). Photochemical ozone creation potentials for oxygenated volatile organic compounds: Sensitivity to variations in kinetic and mechanistic parameters. *Atmospheric Environment*, 33(8), 1275–1293. [https://doi.org/10.1016/S1352-2310\(98\)00261-1](https://doi.org/10.1016/S1352-2310(98)00261-1)
- Jiang, G., Nowakowski, D. J., & Bridgwater, A. V. (2010). Effect of the temperature on the composition of lignin pyrolysis products. *Energy and Fuels*, 24(8), 4470–4475. <https://doi.org/10.1021/ef100363c>
- Jiang, J., Carter, W. P. L., Cocker, D. R., & Barsanti, K. C. (2020). Development and Evaluation of a Detailed Mechanism for Gas-Phase Atmospheric Reactions of Furans. *ACS Earth and Space Chemistry*, 4(8), 1254–1268. <https://doi.org/10.1021/acsearthspacechem.0c00058>
- Joo, T., Rivera-Rios, J. C., Takeuchi, M., Alvarado, M. J., & Ng, N. L. (2019a). Secondary Organic Aerosol Formation from Reaction of 3-Methylfuran with Nitrate Radicals. *ACS Earth and Space Chemistry*, 3(6), 922–934. <https://doi.org/10.1021/acsearthspacechem.9b00068>
- Joo, T., Rivera-Rios, J. C., Takeuchi, M., Alvarado, M. J., & Ng, N. L. (2019b). Secondary Organic Aerosol Formation from Reaction of 3-Methylfuran with Nitrate Radicals [Research-article]. *ACS Earth and Space Chemistry*, 3(6), 922–934. <https://doi.org/10.1021/acsearthspacechem.9b00068>
- Kawamoto, H. (2017). Lignin pyrolysis reactions. *Journal of Wood Science*, 63(2), 117–132. <https://doi.org/10.1007/s10086-016-1606-z>
- Keene, W. C., Maring, H., Maben, J. R., Kieber, D. J., Pszenny, A. A. P., Dahl, E. E., Izaguirre, M. A., Davis, A. J., Long, M. S., Zhou, X., Smoydzin, L., & Sander, R. (2007). Chemical and physical characteristics of nascent aerosols produced by bursting bubbles at a model air-sea interface. *Journal of Geophysical Research Atmospheres*, 112(21), 1–16. <https://doi.org/10.1029/2007JD008464>
- Kind, I., Berndt, T., Bisge, O., & Rolle, W. (1996a). *Gas-phase rate constants for the reaction of*. 2614(3), 2–6.
- Kind, I., Berndt, T., Bisge, O., & Rolle, W. (1996b). *Gas-phase rate constants for the reaction of NO<sub>3</sub> radicals with furan and methyl-substituted furans*. 2614(3), 2–6.

- Kind, I., Berndt, T., Böge, O., & Rolle, W. (1996). Gas-phase rate constants for the reaction of NO<sub>3</sub> radicals with selected oxiranes. *Chemical Physics Letters*, 249(1–2), 35–39. [https://doi.org/10.1016/0009-2614\(95\)01327-X](https://doi.org/10.1016/0009-2614(95)01327-X)
- Koolen, C. D., & Rothenberg, G. (2019). Air Pollution in Europe. *ChemSusChem*, 12(1), 164–172. <https://doi.org/10.1002/cssc.201802292>
- Koppmann, R. (2007). Volatile Organic Compounds in the Atmosphere. In *Volatile Organic Compounds in the Atmosphere*. <https://doi.org/10.1002/9780470988657>
- Koppmann, R., Khedim, A., Rudolph, J., Poppe, D., Andreae, M. O., Helas, G., Welling, M., & Zenker, T. (1997). Emissions of organic trace gases from savanna fires in southern Africa during the 1992 Southern African Fire Atmosphere Research Initiative and their impact on the formation of tropospheric ozone. *Journal of Geophysical Research Atmospheres*, 102(15), 18879–18888. <https://doi.org/10.1029/97jd00845>
- Koss, A. R., Sekimoto, K., Gilman, J. B., Selimovic, V., Coggon, M. M., Zarzana, K. J., Yuan, B., Lerner, B. M., Brown, S. S., Jimenez, J. L., Krechmer, J., Roberts, J. M., Warneke, C., Yokelson, R. J., & De Gouw, J. (2018). Non-methane organic gas emissions from biomass burning: Identification, quantification, and emission factors from PTR-ToF during the FIREX 2016 laboratory experiment. *Atmospheric Chemistry and Physics*, 18(5), 3299–3319. <https://doi.org/10.5194/acp-18-3299-2018>
- Krause, T., Tubbesing, C., Benzing, K., & Schöler, H. F. (2014). Model reactions and natural occurrence of furans from hypersaline environments. *Biogeosciences*, 11(10), 2871–2882. <https://doi.org/10.5194/bg-11-2871-2014>
- Kumar, V., Chandra, B. P., & Sinha, V. (2018). Large unexplained suite of chemically reactive compounds present in ambient air due to biomass fires. *Scientific Reports*, 8(1), 1–15. <https://doi.org/10.1038/s41598-017-19139-3>
- Lalchandani, V., Srivastava, D., Dave, J., Mishra, S., Tripathi, N., Shukla, A. K., Sahu, R., Thamban, N. M., Gaddamidi, S., Dixit, K., Ganguly, D., Tiwari, S., Srivastava, A. K., Sahu, L., Rastogi, N., Gargava, P., & Tripathi, S. N. (2021). Effect of biomass burning on PM 2.5 composition and secondary aerosol formation during post-monsoon and winter haze episodes in Delhi. *Journal of Geophysical Research: Atmospheres*, 1–21. <https://doi.org/10.1029/2021jd035232>
- Lambe, A. T., Chhabra, P. S., Onasch, T. B., Brune, W. H., Hunter, J. F., Kroll, J. H., Cummings, M. J., Brogan, J. F., Parmar, Y., Worsnop, D. R., Kolb, C. E., & Davidovits, P. (2015). Effect of oxidant concentration, exposure time, and seed particles on secondary organic aerosol chemical composition and yield. *Atmospheric Chemistry and Physics*, 15(6), 3063–3075. <https://doi.org/10.5194/acp-15-3063-2015>
- Lancar, I., Daele, V., Le Bras, G., & Poulet, G. (1991). Étude de la réactivité des radicaux NO<sub>3</sub> avec le diméthyl-2,3 butène-2, le butadiène-1,3 et le diméthyl-2,3 butadiène-1,3. *J. Chim. Phys*, 88, 1777–1792. <https://doi.org/10.1051/jcp/1991881777>
- Lançar, I., Daele, V., Le Bras, G., & Poulet, G. (1991). Étude de la réactivité des radicaux NO<sub>3</sub> avec le diméthyl-2,3 butène-2, le butadiène-1,3 et le diméthyl-2,3 butadiène-1,3. *Journal de Chimie Physique*, 88, 1777–1792. <https://doi.org/10.1051/jcp/1991881777>
- Lange, J. P., Price, R., Ayoub, P. M., Louis, J., Petrus, L., Clarke, L., & Gosselink, H. (2010). Valeric biofuels: A platform of cellulosic transportation fuels. *Angewandte Chemie - International Edition*, 49(26), 4479–4483. <https://doi.org/10.1002/anie.201000655>
- Lauraguais, A., Coeur-tourneur, C., Cassez, A., & Seydi, A. (2012). Rate constant and secondary organic

- aerosol yields for the gas-phase reaction of hydroxyl radicals with syringol ( 2,6-dimethoxyphenol ). *Atmospheric Environment*, 55, 43–48. <https://doi.org/10.1016/j.atmosenv.2012.02.027>
- Lê Thành, K., Commandré, J. M., Valette, J., Volle, G., & Meyer, M. (2015). Detailed identification and quantification of the condensable species released during torrefaction of lignocellulosic biomasses. *Fuel Processing Technology*, 139, 226–235. <https://doi.org/10.1016/j.fuproc.2015.07.001>
- Lee, J. H., & Tang, I. N. (1982). Absolute rate constants for the hydroxyl radical reactions with ethane, furan, and thiophene at room temperature. *The Journal of Chemical Physics*, 77(9), 4459–4463. <https://doi.org/10.1063/1.444367>
- Liang, Y., Weber, R. J., Misztal, P. K., Jen, C. N., & Goldstein, A. H. (2022). Aging of Volatile Organic Compounds in October 2017 Northern California Wildfire Plumes. *Environmental Science and Technology*, 56(3), 1557–1567. <https://doi.org/10.1021/acs.est.1c05684>
- Liley, P. E., Buck, E., & Ch, M. S. E. (1999). 493-Physical and Chemical Data 物性数据. *Perry's Chemical Engineers Handbook*, 2–86.
- Liljegren, J. A., & Stevens, P. S. (2013). Measurements of the kinetics of the reaction of OH radicals with 3-methylfuran at low pressure. *International Journal of Chemical Kinetics*, 45(12), 787–794. <https://doi.org/10.1002/kin.20814>
- Lin, Y., Cho, J., Tompsett, G. A., Westmoreland, P. R., & Huber, G. W. (2009). Kinetics Mechanism Cellulose Pyrolysis. *Phys. Chem. C*, 113, 20097–20107.
- Lindinger, W., Hansel, A., & Jordan, A. (1998). On-line monitoring of volatile organic compounds at pptv levels by means of Proton-Transfer-Reaction Mass Spectrometry (PTR-MS) Medical applications, food control and environmental research. *International Journal of Mass Spectrometry and Ion Processes*, 173(3), 191–241. [https://doi.org/10.1016/s0168-1176\(97\)00281-4](https://doi.org/10.1016/s0168-1176(97)00281-4)
- Ljungström, E., Wängberg, I., & Langer, S. (1993). Absolute rate coefficients for the reaction between nitrate radicals and some cyclic alkenes. *Journal of the Chemical Society, Faraday Transactions*, 89(16), 2977–2982. <https://doi.org/10.1039/FT9938902977>
- Manion, J., Huie, R. E., Burgess, D. R., Orkin, V. L., Tsang, W., McGivern, W. ., Hudgens, J. W., Knyazev, V. D., Atkinson, D. B., Chai, E., Tereza, A. M., Lin, C. Y., Allison, T. C., Mallard, W. G., Westley, F., Herron, J. T., Hampson, R. F., & Frizzell, D. H. (2015). *NIST Chemical Kinetics Database, NIST Standard Reference Database 17, Version 7.0 (Web Version), Release 1.6.8, Data version 2015.09*.
- Martín, P., Cabañas, B., Colmenar, I., Salgado, M. S., Villanueva, F., & Tapia, A. (2013). Reactivity of E-butenedial with the major atmospheric oxidants. *Atmospheric Environment*, 70, 351–360. <https://doi.org/10.1016/j.atmosenv.2013.01.041>
- Martinez, E., Cabanas, B., Aranda, A., & Martín, P. (1998). Kinetics of the reactions of NO<sub>3</sub> radical with selected monoterpenes: A temperature dependence study. *Environmental Science and Technology*, 32(23), 3730–3734. <https://doi.org/10.1021/es970899t>
- Martínez, E., Cabañas, B., Aranda, A., Martín, P., Notario, A., & Salgado, S. (1999). Study on the NO<sub>3</sub> Radical Reactivity: Reactions with Cyclic Alkenes. *Journal of Physical Chemistry A*, 103(27), 5321–5327. <https://doi.org/10.1021/jp9847181>
- Martinez, E., Cabañas, B., Aranda, A., Martín, P., & Salgado, S. (1999). Absolute Rate Coefficients for the Gas-Phase Reactions of NO<sub>3</sub> Radical with a Series of Monoterpenes at T = 298 to 433 K. *Journal of Atmospheric Chemistry*, 33(3), 265–282. <https://doi.org/10.1023/A:1006178530211>



- Mathematics, A. (2016). 濟無No Title No Title No Title. *19*(1), 1–23.
- Matsumoto, J. (2011). Kinetics of the reactions of ozone with 2,5-dimethylfuran and its atmospheric implications. *Chemistry Letters*, *40*(6), 582–583. <https://doi.org/10.1246/cl.2011.582>
- Mcdonald, J. D., Zielinska, B., Fujita, E. M., Sagebiel, J. C., Chow, J. C., & Watson, J. G. (2000). Fine particle and gaseous emission rates from residential wood combustion. *Environmental Science and Technology*, *34*(11), 2080–2091. <https://doi.org/10.1021/es9909632>
- Mellouki, A., & Chen, J. (2015). *Atmospheric Chemistry of Oxygenated Volatile Organic Compounds : Impacts on Air Quality and Climate*. <https://doi.org/10.1021/cr500549n>
- Meng, L., Coeur, C., Fayad, L., Houzel, N., Genevray, P., Bouzidi, H., Tomas, A., & Chen, W. (2020). Secondary organic aerosol formation from the gas-phase reaction of guaiacol (2-methoxyphenol) with NO<sub>3</sub> radicals. *Atmospheric Environment*, *240*(July). <https://doi.org/10.1016/j.atmosenv.2020.117740>
- Mettler, M. S., Mushrif, S. H., Paulsen, A. D., Javadekar, A. D., Vlachos, D. G., & Dauenhauer, P. J. (2012). Revealing pyrolysis chemistry for biofuels production: Conversion of cellulose to furans and small oxygenates. *Energy and Environmental Science*, *5*(1), 5414–5424. <https://doi.org/10.1039/c1ee02743c>
- Molina, M. J., & Molina, L. T. (2004). Megacities and atmospheric pollution. *Journal of the Air and Waste Management Association*, *54*(6), 644–680. <https://doi.org/10.1080/10473289.2004.10470936>
- Moriarty, J., Sidebottom, H., Wenger, J., Mellouki, A., & Le Bras, G. (2003). Kinetic studies on the reactions of hydroxyl radicals with cyclic ethers and aliphatic diethers. *Journal of Physical Chemistry A*, *107*(10), 1499–1505. <https://doi.org/10.1021/jp021267i>
- Mudhoo, A., Thayalan, G., Muthoora, N. J., Muthoora, M. N., Oozer, B. Z., Rago, Y. P., Ramphul, M. P., Valaydon, A. K., & Kumar, S. (2013). *Dioxins and Furans: Sources, Impacts and Remediation*. [https://doi.org/10.1007/978-3-319-02387-8\\_10](https://doi.org/10.1007/978-3-319-02387-8_10)
- Müller, M., Anderson, B. E., Beyersdorf, A. J., Crawford, J. H., Diskin, G. S., Eichler, P., Fried, A., Keutsch, F. N., Mikoviny, T., Thornhill, K. L., Walega, J. G., Weinheimer, A. J., Yang, M., Yokelson, R. J., & Wisthaler, A. (2016). In situ measurements and modeling of reactive trace gases in a small biomass burning plume. *Atmospheric Chemistry and Physics*, *16*(6), 3813–3824. <https://doi.org/10.5194/acp-16-3813-2016>
- Müller, M., Graus, M., Wisthaler, A., Hansel, A., Metzger, A., Dommen, J., & Baltensperger, U. (2012). Analysis of high mass resolution PTR-TOF mass spectra from 1,3,5-trimethylbenzene (TMB) environmental chamber experiments. *Atmospheric Chemistry and Physics*, *12*(2), 829–843. <https://doi.org/10.5194/acp-12-829-2012>
- Munger, J. W., Jacob, D. J., Waldman, J. M., & Hoffmann, M. R. (1983). Fogwater chemistry in an urban atmosphere. *Journal of Geophysical Research*, *88*(C9), 5109–5121. <https://doi.org/10.1029/JC088iC09p05109>
- Newland, M. J., Ren, Y., Mcgillen, M. R., Michelat, L., Daële, V., & Mellouki, A. (2022). NO<sub>3</sub>chemistry of wildfire emissions: A kinetic study of the gas-phase reactions of furans with the NO<sub>3</sub> radical. *Atmospheric Chemistry and Physics*, *22*(3), 1761–1772. <https://doi.org/10.5194/acp-22-1761-2022>
- Nguyen, T. B., Coggon, M. M., Bates, K. H., Zhang, X., Schwantes, R. H., Schilling, K. A., Loza, C. L., Flagan, R. C., Wennberg, P. O., & Seinfeld, J. H. (2014). Organic aerosol formation from the reactive uptake of isoprene epoxydiols (IEPOX) onto non-acidified inorganic seeds. *Atmospheric Chemistry*

- and Physics*, 14(7), 3497–3510. <https://doi.org/10.5194/acp-14-3497-2014>
- Odum, J. R., Hoffmann, T., Bowman, F., Collins, D., Flagan, R. C., & Seinfeld, J. H. (1996). Gas/particle partitioning and secondary organic aerosol yields. *Environmental Science and Technology*, 30(8), 2580–2585. <https://doi.org/10.1021/es950943+>
- Oh, H. J., Ma, Y., & Kim, J. (2020). Human inhalation exposure to aerosol and health effect: Aerosol monitoring and modelling regional deposited doses. *International Journal of Environmental Research and Public Health*, 17(6), 1–2. <https://doi.org/10.3390/ijerph17061923>
- Olariu, R. I., Bejan, I., Barnes, I., Klotz, B., Becker, K. H., & Wirtz, K. (2004). Rate coefficients for the gas-phase reaction of NO<sub>3</sub> radicals with selected dihydroxybenzenes. *International Journal of Chemical Kinetics*, 36(11), 577–583. <https://doi.org/10.1002/kin.20029>
- Olariu, R. I., Cuza, A. I., Chemistry, A., Tomas, A., Douai, M. De, Chimie, D., Barnes, I., Bejan, I., Becker, K. H., Wuppertal, B. U., Wirtz, K., Centro, F., & Ambientales, D. E. (1998). *Atmospheric Ozone Degradation Reaction of 1, 2-dihydroxybenzene : Aerosol Formation Study*. 1–12.
- Osseiran, N., Romanias, M. N., Gaudion, V., Angelaki, M. E., Papadimitriou, V. C., Tomas, A., Coddeville, P., & Thevenet, F. (2020). Development and validation of a thermally regulated atmospheric simulation chamber (THALAMOS): A versatile tool to simulate atmospheric processes. *Journal of Environmental Sciences (China)*, 95(xxxx), 141–154. <https://doi.org/10.1016/j.jes.2020.03.036>
- Pankow, J. F. (1994). An absorption model of the gas/aerosol partitioning involved in the formation of secondary organic aerosol. *Atmospheric Environment*, 28(SUPPL.), 189–193. <https://doi.org/10.1016/j.atmosenv.2007.10.060>
- Papadimitriou, V. C., Lazarou, Y. G., Talukdar, R. K., & Burkholder, J. B. (2011). *Atmospheric Chemistry of CF<sub>3</sub>CF<sub>2</sub>*. 2(3), 167–181.
- Paquet, M., Arlt, D., Knape, J., Low, M., Forslund, P., & Pärt, T. (2019). Quantifying the links between land use and population growth rate in a declining farmland bird. *Ecology and Evolution*, 9(2), 868–879. <https://doi.org/10.1002/ece3.4766>
- Qian, Y., Zhu, L., Wang, Y., & Lu, X. (2015). Recent progress in the development of biofuel 2,5-dimethylfuran. *Renewable and Sustainable Energy Reviews*, 41, 633–646. <https://doi.org/10.1016/j.rser.2014.08.085>
- Ravishankara, A. R., & Davis, D. D. (1978). Kinetic rate constants for the reaction of OH with methanol, ethanol, and tetrahydrofuran at 298 K [2]. *Journal of Physical Chemistry*, 82(26), 2852–2853. <https://doi.org/10.1021/j100515a022>
- Reddington, C. L., Spracklen, D. V., Artaxo, P., Ridley, D. A., Rizzo, L. V., & Arana, A. (2016). Analysis of particulate emissions from tropical biomass burning using a global aerosol model and long-term surface observations. *Atmospheric Chemistry and Physics*, 16(17), 11083–11106. <https://doi.org/10.5194/acp-16-11083-2016>
- Ren, X., Brune, W. H., Olliger, A., Metcalf, A. R., Simpas, J. B., Shirley, T., Schwab, J. J., Bai, C., Roychowdhury, U., Li, Y., Cai, C., Demerjian, K. L., He, Y., Zhou, X., Gao, H., & Hou, J. (2006). *OH, HO<sub>2</sub>, and OH reactivity during the PMTACS – NY Whiteface Mountain 2002 campaign : Observations and model comparison*. 111, 1–12. <https://doi.org/10.1029/2005JD006126>
- Ren, X., Gao, H., Zhou, X., Crouse, J. D., Wennberg, P. O., Browne, E. C., LaFranchi, B. W., Cohen, R. C., McKay, M., Goldstein, A. H., & Mao, J. (2010). Measurement of atmospheric nitrous acid at Bodgett forest during BEARPEX2007. *Atmospheric Chemistry and Physics*, 10(13), 6283–6294. <https://doi.org/10.5194/acp-10-6283-2010>

- Ren, X., Harder, H., Martinez, M., Leshner, R. L., Oligier, A., Simpas, J. B., Brune, W. H., Schwab, J. J., Demerjian, K. L., He, Y., Zhou, X., & Gao, H. (2003). OH and HO<sub>2</sub> chemistry in the urban atmosphere of New York City. *Atmospheric Environment*, 37(26), 3639–3651. [https://doi.org/10.1016/S1352-2310\(03\)00459-X](https://doi.org/10.1016/S1352-2310(03)00459-X)
- Rissanen, M. (2021). Anthropogenic Volatile Organic Compound (AVOC) Autoxidation as a Source of Highly Oxygenated Organic Molecules (HOM). *Journal of Physical Chemistry A*, 125(41), 9027–9039. <https://doi.org/10.1021/acs.jpca.1c06465>
- Roberts, J. M., Stockwell, C. E., Yokelson, R. J., De Gouw, J., Liu, Y., Selimovic, V., Koss, A. R., Sekimoto, K., Coggon, M. M., Yuan, B., Zarzana, K. J., Brown, S. S., Santin, C., Doerr, S. H., & Warneke, C. (2020). The nitrogen budget of laboratory-simulated western US wildfires during the FIREX 2016 Fire Lab study. *Atmospheric Chemistry and Physics*, 20(14), 8807–8826. <https://doi.org/10.5194/acp-20-8807-2020>
- Román-Leshkov, Y., Barrett, C. J., Liu, Z. Y., & Dumesic, J. A. (2007). Production of dimethylfuran for liquid fuels from biomass-derived carbohydrates. *Nature*, 447(7147), 982–985. <https://doi.org/10.1038/nature05923>
- Romanias, M. N., Coggon, M., Al Ali, F., Burkholder, J. B., Dagaut, P., Warneke, C., Stockwell, C. E., Decker, Z., Tomas, A., Houzel, N., Coeur, C., & Brown, S. (n.d.-a). Atmospheric chemistry of furanoids: insights into the sources and atmospheric fate. *Atmospheric Environment*.
- Romanias, M. N., Coggon, M. M., Al Ali, F., Burkholder, J. B., Dagaut, P., Warneke, C., Stockwell, C. E., Decker, Z. C. J., Tomas, A., Houzel, N., Coeur, C., & Brown, S. S. (n.d.-b). Atmospheric chemistry of furanoids: insights into the sources and atmospheric fate. *ASC ACS Earth and Space Chemistry*.
- Schellenberg, C. (2009). Conducta irascible y recalcitrante tras una infección de gripe: Efectos de una acupuntura dispersante en el H 3 en lactantes y niños pequeños. *Revista Internacional de Acupuntura*, 3(2), 78–79. [https://doi.org/10.1016/S1887-8369\(09\)71579-0](https://doi.org/10.1016/S1887-8369(09)71579-0)
- Schumann, U. (2012). Atmospheric Physics. In *Physics Today* (Vol. 15, Issue 5). <https://doi.org/10.1063/1.3058219>
- Seinfeld, J. H., Pandis, S. N., & Noone, K. (1998). Atmospheric Chemistry and Physics: From Air Pollution to Climate Change. In *Physics Today* (Vol. 51, Issue 10). <https://doi.org/10.1063/1.882420>
- Sekimoto, K., Koss, A. R., Gilman, J. B., Selimovic, V., Coggon, M. M., Zarzana, K. J., Yuan, B., Lerner, B. M., Brown, S. S., Warneke, C., Yokelson, R. J., Roberts, J. M., & De Gouw, J. (2018). High- and low-temperature pyrolysis profiles describe volatile organic compound emissions from western US wildfire fuels. *Atmospheric Chemistry and Physics*, 18(13), 9263–9281. <https://doi.org/10.5194/acp-18-9263-2018>
- Selimovic, V., Yokelson, R. J., Warneke, C., Roberts, J. M., De Gouw, J., Reardon, J., & Griffith, D. W. T. (2018). Aerosol optical properties and trace gas emissions by PAX and OP-FTIR for laboratory-simulated western US wildfires during FIREX. *Atmospheric Chemistry and Physics*, 18(4), 2929–2948. <https://doi.org/10.5194/acp-18-2929-2018>
- Si, Z., Wang, C. G., Bi, K., Zhang, X. H., Yu, C. L., Dong, R. J., Ma, L. L., & Changle, P. (2017). Py-GC/MS study of lignin pyrolysis and effect of catalysts on product distribution. *International Journal of Agricultural and Biological Engineering*, 10(5), 214–225. <https://doi.org/10.25165/j.ijabe.20171005.2852>
- Simoneit, B. R. T. (2002). Biomass burning - A review of organic tracers for smoke from incomplete combustion. In *Applied Geochemistry* (Vol. 17, Issue 3). <https://doi.org/10.1016/S0883->

- Smith, D., & Španěl, P. (2005). Selected ion flow tube mass spectrometry (SIFT-MS) for on-line trace gas analysis. *Mass Spectrometry Reviews*, *24*(5), 661–700. <https://doi.org/10.1002/mas.20033>
- Song, C., NA, K., & Cocker, D. R. (2005). Impact of the Hydrocarbon to NO. *Environmental Science & Technology*, *39*(9), 3143–3149.
- Španěl, P., Dryahina, K., & Smith, D. (2013). A quantitative study of the influence of inhaled compounds on their concentrations in exhaled breath. *Journal of Breath Research*, *7*(1). <https://doi.org/10.1088/1752-7155/7/1/017106>
- Stehfest, E., van Zeist, W. J., Valin, H., Havlik, P., Popp, A., Kyle, P., Tabeau, A., Mason-D’Croz, D., Hasegawa, T., Bodirsky, B. L., Calvin, K., Doelman, J. C., Fujimori, S., Humpenöder, F., Lotze-Campen, H., van Meijl, H., & Wiebe, K. (2019). Key determinants of global land-use projections. *Nature Communications*, *10*(1), 1–10. <https://doi.org/10.1038/s41467-019-09945-w>
- Stockman, R. A. (2007). Heterocyclic chemistry. In *Annual Reports on the Progress of Chemistry - Section B* (Vol. 103). <https://doi.org/10.1039/b614418g>
- Stockwell, C. E., Christian, T. J., Goetz, J. D., Jayarathne, T., Bhave, P. V., Praveen, P. S., Adhikari, S., Maharjan, R., DeCarlo, P. F., Stone, E. A., Saikawa, E., Blake, D. R., Simpson, I. J., Yokelson, R. J., & Panday, A. K. (2016). Nepal Ambient Monitoring and Source Testing Experiment (NAMaSTE): Emissions of trace gases and light-absorbing carbon from wood and dung cooking fires, garbage and crop residue burning, brick kilns, and other sources. *Atmospheric Chemistry and Physics*, *16*(17), 11043–11081. <https://doi.org/10.5194/acp-16-11043-2016>
- Stockwell, C. E., Veres, P. R., Williams, J., & Yokelson, R. J. (2015). Characterization of biomass burning emissions from cooking fires, peat, crop residue, and other fuels with high-resolution proton-transfer-reaction time-of-flight mass spectrometry. *Atmospheric Chemistry and Physics*, *15*(2), 845–865. <https://doi.org/10.5194/acp-15-845-2015>
- Strollo, C. M., & Ziemann, P. J. (2013). Products and mechanism of secondary organic aerosol formation from the reaction of 3-methylfuran with OH radicals in the presence of NO<sub>x</sub>. *Atmospheric Environment*, *77*, 534–543. <https://doi.org/10.1016/j.atmosenv.2013.05.033>
- Tajuelo, M., Rodríguez, A., Baeza-Romero, M. T., Aranda, A., Díaz-de-Mera, Y., & Rodríguez, D. (2019). Secondary organic aerosol formation from  $\alpha$ -methylstyrene atmospheric degradation: Role of NO<sub>x</sub> level, relative humidity and inorganic seed aerosol. *Atmospheric Research*, *230*(July), 104631. <https://doi.org/10.1016/j.atmosres.2019.104631>
- Tajuelo, M., Rodríguez, D., Baeza-Romero, M. T., Díaz-de-Mera, Y., Aranda, A., & Rodríguez, A. (2019). Secondary organic aerosol formation from styrene photolysis and photooxidation with hydroxyl radicals. *Chemosphere*, *231*, 276–286. <https://doi.org/10.1016/j.chemosphere.2019.05.136>
- Tajuelo, M., Rodríguez, D., Rodríguez, A., Escalona, A., Viteri, G., Aranda, A., & Diaz-de-Mera, Y. (2021). Secondary organic aerosol formation from the ozonolysis and oh-photooxidation of 2,5-dimethylfuran. *Atmospheric Environment*, *245*, 118041. <https://doi.org/10.1016/j.atmosenv.2020.118041>
- Takekawa, H., Minoura, H., & Yamazaki, S. (2003). *Temperature dependence of secondary organic aerosol formation by photo-oxidation of hydrocarbons*. *37*, 3413–3424. [https://doi.org/10.1016/S1352-2310\(03\)00359-5](https://doi.org/10.1016/S1352-2310(03)00359-5)
- Tapia, A., Villanueva, F., Salgado, M. S., Cabañas, B., Martínez, E., & Martín, P. (2011). Atmospheric degradation of 3-methylfuran: Kinetic and products study. *Atmospheric Chemistry and Physics*, *11*(7), 3227–3241. <https://doi.org/10.5194/acp-11-3227-2011>

- Thewes, M., Muether, M., Pischinger, S., Budde, M., Brunn, A., Sehr, A., Adomeit, P., & Klankermayer, J. (2011). Analysis of the impact of 2-methylfuran on mixture formation and combustion in a direct-injection spark-ignition engine. *Energy and Fuels*, 25(12), 5549–5561. <https://doi.org/10.1021/ef201021a>
- Tomas, A., Henry, F., & Visez, N. (2009). Aerosol formation yields from the reaction of catechol with ozone. 43, 2360–2365. <https://doi.org/10.1016/j.atmosenv.2008.12.054>
- Tuan Hoang, A., & Viet Pham, V. (2021). 2-Methylfuran (MF) as a potential biofuel: A thorough review on the production pathway from biomass, combustion progress, and application in engines. *Renewable and Sustainable Energy Reviews*, 148(June), 111265. <https://doi.org/10.1016/j.rser.2021.111265>
- Tuazon, E. C., Aschmann, S. M., & Atkinson, R. (2000). Atmospheric degradation of volatile methylsilicon compounds. *Environmental Science and Technology*, 34(10), 1970–1976. <https://doi.org/10.1021/es9910053>
- Vallero, D. (2008). *Fundamentals of Air Pollution* (Fourth). El Sevier.
- Villanueva, F., Barnes, I., Monedero, E., Salgado, S., Gómez, M. V., & Martin, P. (2007). Primary product distribution from the Cl-atom initiated atmospheric degradation of furan: Environmental implications. *Atmospheric Environment*, 41(38), 8796–8810. <https://doi.org/10.1016/j.atmosenv.2007.07.053>
- Villanueva, F., Cabañas, B., Monedero, E., Salgado, S., Bejan, I., & Martin, P. (2009). Atmospheric degradation of alkylfurans with chlorine atoms: Product and mechanistic study. *Atmospheric Environment*, 43(17), 2804–2813. <https://doi.org/10.1016/j.atmosenv.2009.02.030>
- Wallington, T. J., Dagaut, P., Liu, R., & Kurylo, M. J. (1988). The gas phase reactions of hydroxyl radicals with a series of esters over the temperature range 240–440 K. *International Journal of Chemical Kinetics*, 20(2), 177–186. <https://doi.org/10.1002/kin.550200210>
- Wang, J., Doussin, J. F., Perrier, S., Perraudin, E., Katrib, Y., Pangui, E., & Picquet-Varrault, B. (2011). Design of a new multi-phase experimental simulation chamber for atmospheric photochemistry, aerosol and cloud chemistry research. *Atmospheric Measurement Techniques*, 4(11), 2465–2494. <https://doi.org/10.5194/amt-4-2465-2011>
- Wang, L., Slowik, J. G., Tripathi, N., Bhattu, D., Rai, P., Kumar, V., Vats, P., Satish, R., Baltensperger, U., Ganguly, D., Rastogi, N., Sahu, L. K., Tripathi, S. N., & Prévôt, A. S. H. (2020). Source characterization of volatile organic compounds measured by proton-transfer-reaction time-of-flight mass spectrometers in Delhi, India. *Atmospheric Chemistry and Physics*, 20(16), 9753–9770. <https://doi.org/10.5194/acp-20-9753-2020>
- Wang, Q., Song, H., Pan, S., Dong, N., Wang, X., & Sun, S. (2020). Initial pyrolysis mechanism and product formation of cellulose: An Experimental and Density functional theory(DFT) study. *Scientific Reports*, 10(1), 1–18. <https://doi.org/10.1038/s41598-020-60095-2>
- Wang, S., Wei, W., Du, L., Li, G., & Hao, J. (2009). Characteristics of gaseous pollutants from biofuel-stoves in rural China. *Atmospheric Environment*, 43(27), 4148–4154. <https://doi.org/10.1016/j.atmosenv.2009.05.040>
- Whelan, C. A., Eble, J., Mir, Z. S., Blitz, M. A., Seakins, P. W., Olzmann, M., & Stone, D. (2020). Kinetics of the Reactions of Hydroxyl Radicals with Furan and Its Alkylated Derivatives 2-Methyl Furan and 2,5-Dimethyl Furan. *Journal of Physical Chemistry A*, 124(37), 7416–7426. <https://doi.org/10.1021/acs.jpca.0c06321>
- Wine, P. H., & Thompson, R. J. (1984). Kinetics of OH reactions with furan, thiophene, and

- tetrahydrothiophene. *International Journal of Chemical Kinetics*, 16(7), 867–878. <https://doi.org/10.1002/kin.550160707>
- Winer, M., Darnall, K. R., & Lloyd, A. C. (1977). *REACTION set-BUTYL*. 5(2), 221–226.
- Wingenter, O. W., Blake, D. R., Blake, N. J., Sive, B. C., Rowland, F. S., Atlas, E., & Flocke, F. (1999). Tropospheric hydroxyl and atomic chlorine concentrations, and mixing timescales determined from hydrocarbon and halocarbon measurements made over the Southern Ocean. *Journal of Geophysical Research Atmospheres*, 104(D17), 21819–21828. <https://doi.org/10.1029/1999JD900203>
- Wingenter, O. W., Kubo, M. K., Blake, N. J., Smith, T. W., Blake, D. R., & Rowland, F. S. (1996). Hydrocarbon and halocarbon measurements as photochemical and dynamical indicators of atmospheric hydroxyl, atomic chlorine, and vertical mixing obtained during Lagrangian flights. *Journal of Geophysical Research Atmospheres*, 101(D2), 4331–4340. <https://doi.org/10.1029/95JD02457>
- World Health Organization. (2016). WORLD HEALTH STATISTICS - MONITORING HEALTH FOR THE SDGs. *World Health Organization*, 1.121. <https://doi.org/10.1017/CBO9781107415324.004>
- Xu, L., Guo, H., Weber, R. J., & Ng, N. L. (2017). Chemical Characterization of Water-Soluble Organic Aerosol in Contrasting Rural and Urban Environments in the Southeastern United States. *Environmental Science and Technology*, 51(1), 78–88. <https://doi.org/10.1021/acs.est.6b05002>
- Yang, H., Li, S., Liu, B., Chen, Y., Xiao, J., Dong, Z., Gong, M., & Chen, H. (2020). Hemicellulose pyrolysis mechanism based on functional group evolutions by two-dimensional perturbation correlation infrared spectroscopy. *Fuel*, 267(July 2019), 117302. <https://doi.org/10.1016/j.fuel.2020.117302>
- Yang, X., Zhao, Y., Li, W., Li, R., & Wu, Y. (2019). Unveiling the Pyrolysis Mechanisms of Hemicellulose: Experimental and Theoretical Studies. *Energy and Fuels*, 33(5), 4352–4360. <https://doi.org/10.1021/acs.energyfuels.9b00482>
- Yokelson, R. J., Burling, I. R., Gilman, J. B., Warneke, C., Stockwell, C. E., De Gouw, J., Akagi, S. K., Urbanski, S. P., Veres, P., Roberts, J. M., Kuster, W. C., Reardon, J., Griffith, D. W. T., Johnson, T. J., Hosseini, S., Miller, J. W., Cocker, D. R., Jung, H., & Weise, D. R. (2013). Coupling field and laboratory measurements to estimate the emission factors of identified and unidentified trace gases for prescribed fires. *Atmospheric Chemistry and Physics*, 13(1), 89–116. <https://doi.org/10.5194/acp-13-89-2013>
- Yokelson, R. J., Burling, I. R., Urbanski, S. P., Atlas, E. L., Adachi, K., Buseck, P. R., Wiedinmyer, C., Akagi, S. K., Toohey, D. W., & Wold, C. E. (2011). Trace gas and particle emissions from open biomass burning in Mexico. *Atmospheric Chemistry and Physics*, 11(14), 6787–6808. <https://doi.org/10.5194/acp-11-6787-2011>
- Yokelson, R. J., Saharjo, B. H., Stockwell, C. E., Putra, E. I., Jayarathne, T., Akbar, A., Albar, I., Blake, D. R., Graham, L. L. B., Kurniawan, A., Meinardi, S., Ningrum, D., Nurhayati, A. D., Saad, A., Sakuntaladewi, N., Setianto, E., Simpson, I. J., Stone, E. A., Sutikno, S., ... Cochrane, M. A. (2022). Tropical peat fire emissions: 2019 field measurements in Sumatra and Borneo and synthesis with previous studies. *Atmospheric Chemistry and Physics*, 22(15), 10173–10194. <https://doi.org/10.5194/acp-22-10173-2022>
- Yokelson, R. J., Susott, R., Ward, D. E., Reardon, J., & Griffith, D. W. T. (1997). Emissions from smoldering combustion of biomass measured by open-path Fourier transform infrared spectroscopy. *Journal of Geophysical Research Atmospheres*, 102(15), 18865–18877. <https://doi.org/10.1029/97jd00852>

- Young, C. J., Washenfelder, R. A., Edwards, P. M., Parrish, D. D., Gilman, J. B., Kuster, W. C., Mielke, L. H., Osthoff, H. D., Tsai, C., Pikelnaya, O., Stutz, J., Veres, P. R., Roberts, J. M., Griffith, S., Dusanter, S., Stevens, P. S., Flynn, J., Grossberg, N., Lefer, B., ... Brown, S. S. (2014). Chlorine as a primary radical: Evaluation of methods to understand its role in initiation of oxidative cycles. *Atmospheric Chemistry and Physics*, *14*(7), 3427–3440. <https://doi.org/10.5194/acp-14-3427-2014>
- Yuan, Y., Zhao, X., Wang, S., & Wang, L. (2017). Atmospheric Oxidation of Furan and Methyl-Substituted Furans Initiated by Hydroxyl Radicals. *Journal of Physical Chemistry A*, *121*(48), 9306–9319. <https://doi.org/10.1021/acs.jpca.7b09741>
- Zhao, D., Schmitt, S. H., Wang, M., Acir, I. H., Tillmann, R., Tan, Z., Novelli, A., Fuchs, H., Pullinen, I., Wegener, R., Rohrer, F., Wildt, J., Kiendler-Scharr, A., Wahner, A., & Mentel, T. F. (2018). Effects of NO<sub>x</sub> and SO<sub>2</sub> on the secondary organic aerosol formation from photooxidation of  $\alpha$ -pinene and limonene. *Atmospheric Chemistry and Physics*, *18*(3), 1611–1628. <https://doi.org/10.5194/acp-18-1611-2018>
- Zhao, X., & Wang, L. (2017). Atmospheric Oxidation Mechanism of Furfural Initiated by Hydroxyl Radicals. *Journal of Physical Chemistry A*, *121*(17), 3247–3253. <https://doi.org/10.1021/acs.jpca.7b00506>
- Zhou, X., Beine, H. J., Honrath, R. E., Fuentes, J. D., Simpson, W., & Bottenheim, J. W. (2001). Snowpack Photochemical Production of HONO: a Major Source of OH in the Arctic Boundary Layer in Springtime. *Geophysical Research Letters*, *28*, 4087–4090. <https://doi.org/10.1029/2001GL013531>
- Zhou, X., Li, W., Mabon, R., & Broadbelt, L. J. (2018). A mechanistic model of fast pyrolysis of hemicellulose. *Energy and Environmental Science*, *11*(5), 1240–1260. <https://doi.org/10.1039/c7ee03208k>
- Ziemann, P. J., & Atkinson, R. (2012). Kinetics, products, and mechanisms of secondary organic aerosol formation. *Chemical Society Reviews*, *41*(19), 6582–6605. <https://doi.org/10.1039/c2cs35122f>
- Zogka, A. G., Romanias, M. N., & Thevenet, F. (2022). Formaldehyde and glyoxal measurement deploying a selected ion flow tube mass spectrometer (SIFT-MS). *Atmospheric Measurement Techniques*, *15*(7), 2001–2019. <https://doi.org/10.5194/amt-15-2001-2022>
- Zysman, B., & Skelly, P. D. (1992). *T*: 1992.

**Abstracts**  
**(English & French Version)**



## **Title: Investigation of Nocturnal Atmospheric Reactivity of Furan Compounds with NO<sub>3</sub> Radicals in Simulation Chambers: Kinetics, Products, Mechanisms, and Secondary Organic Aerosol (SOA) Formation**

Keywords: Atmospheric Simulation Chamber, Characterization, Furan, 2-Methylfuran, 3-Methylfuran, 2,5-Dimethylfuran, 2,3,5-Trimethylfuran, NO<sub>3</sub>, Rate coefficient, Mechanistic study, Secondary Organic Aerosols

The study of atmospheric processes is among the central topics of current environmental research. The most direct and significant way to investigate the transformation of pollutants and the formation of aerosols in the atmosphere, is to simulate these processes under controlled and simplified conditions. In this regard, the atmospheric reaction of a series of furan compounds highly emitted from biomass burning (furan (F), 2-methylfuran (2-MF), 3-methylfuran (3-MF), 2,5-dimethylfuran (2,5-DMF), and 2,3,5-trimethylfuran (2,3,5-TMF)) with nitrate radical (NO<sub>3</sub>) has been in the Chamber for the Atmospheric Reactivity and the Metrology of the Environment (CHARME) simulation chamber at the laboratoire de Physico-Chimie de l'Atmosphere (LPCA) laboratory (Dunkerque, France) and in the Thermally Regulated Atmospheric Simulation Chamber (THALAMOS) at SAGE laboratory- IMT Nord Europe.

The first part of this research focused on the determination of the room temperature rate coefficients of the latter reactions with NO<sub>3</sub>, together with the temperature dependence data of F, 2-MF, 2,5-DMF and two monoterpenes ( $\alpha$ -pinene, 2-carene). For the room temperature kinetics, experiments were performed in the dark, under dry conditions (RH <2%), atmospheric pressure and room temperature (294  $\pm$  2 K) using the relative rate method in both simulation chambers (CHARME & THALAMOS). The measurement of the rate coefficients allowed to calculate the atmospheric lifetimes of these furan compounds. The following rate coefficients (in units cm<sup>3</sup> molecule<sup>-1</sup> s<sup>-1</sup>) are determined:  $k(\text{F}) = (1.61 \pm 0.28) \times 10^{-12}$ ,  $k(2\text{-MF}) = (1.96 \pm 0.25) \times 10^{-11}$ ,  $k(3\text{-MF}) = (1.49 \pm 0.33) \times 10^{-11}$ ,  $k(2,5\text{-DMF}) = (6.49 \pm 0.95) \times 10^{-11}$  and  $k(2,3,5\text{-TMF}) = (1.66 \pm 0.69) \times 10^{-10}$ . This work shows that the reaction between furan and methylated furan compounds with nitrate radical (NO<sub>3</sub>) is the dominant removal pathway during the night with lifetimes between 0.5 and 55 min for the studied molecules. The temperature-dependent kinetic studies were studied in THALAMOS in the dark, under dry conditions (RH <2%), atmospheric pressure using relative rate method too. The negative temperature dependence evidenced in the reaction rates of furanoids with NO<sub>3</sub> shows that the major reaction pathway is governed by NO<sub>3</sub> addition or addition-elimination to the ring.

The second part of this research focused on the qualitative and quantitative products determination formed in the gas- and particulate- phase formed from these reactions and the mechanism leading to these oxidation products was proposed. For the five studied furan compounds, the major pathway occurs by NO<sub>3</sub> addition to C-2/C-5 of the ring leading to the formation of unsaturated dicarbonyls. For single methylated furan compounds (2-MF and 3-MF), cyclic nitrooxy carbonyls are also formed as major primary product from the NO<sub>3</sub> addition to C-2. For multi-methylated furanoids (2,5-DMF and 2,3,5-TMF), another major pathway occurs by NO<sub>3</sub> addition followed by H atom-abstraction from one of the methyl groups

attached to the furan ring leading to the formation of methylated-furfurals as second major products.

Comparing the SOA yield obtained from the reaction of 2-MF, 2,5-DMF AND 2,3,5-TMF with NO<sub>3</sub>, the maximum aerosol yield obtained from the reaction of 2-MF was  $\approx$  2% which is 5-6 times lower than those obtained from the reaction of 2,5-DMF ( $\approx$  12 %) and 2,3,5-TMF ( $\approx$  10 %). This shows that increasing the methylation on the furan ring increases the SOA yield of formation from the reaction. This is due to the the presence of methyl groups on the ring reducing the volatility or the vapor pressure of a compound.

Regarding the composition of the SOA formed from title reaction, it can be concluded that some products identified in the gas-phase where also identified in the particulate phase including the major ones, this shows that these products partition between the gas- and particulate- phase. In addition to these products, other dimers and trimers which are formed from the RO<sub>2</sub> radicals formed during the course of the reaction.

## **Titre: Etude de la réactivité atmosphérique nocturne des furanes avec les radicaux NO<sub>3</sub> en chambres de simulation: Cinétiques, Produits, Mécanismes et formation d'Aérosol Organique Secondaire (AOS)**

Mots clés: Chambre de Simulation Atmosphérique, Caractérisation, Furane, 2-Méthylfurane, 3-Méthylfurane, 2,5-Diméthylfurane, 2,3,5-Triméthylfuran, NO<sub>3</sub>, Coefficient de réaction, étude mécanistique, Aérosol Organique Secondaire

L'étude des procédés atmosphériques est parmi les sujets centraux concernant la recherche environnementale. La méthode la plus directe et la significative d'étudier la transformation des polluants et la formation d'aérosols dans l'atmosphère est de simuler ces procédés dans conditions contrôlée et simplifiée. Dans cette optique, les réactions atmosphériques d'une série de furanes fortement émis par la combustion de biomasse (furane (F), 2-méthylfuran (2-MF), 3-méthylfuran (3-MF), 2,5-diméthylfuran (2,5-DMF), 2,3,5-triméthylfuran (2,3,5-TMF)) avec les radicaux nitrates (NO<sub>3</sub>) ont été étudiées dans la chambre de simulation CHARME (CHamber for the Atmospheric Reactivity and the Metrology of the Environnement) au Laboratoire de Physico-Chimie de l'atmosphère (LPCA) à Dunkerque (France) et dans la chambre THALAMOS (Thermally Regulated Atmospheric Simulation Chamber) au laboratoire SAGE de l'IMT Nord Europe à Douai (France).

La première partie de ces recherches se focalise sur la détermination des coefficients à température ambiante des réactions déjà citées et en fonction de la température pour les F, 2-MF, 2,5-DMF et deux monoterpènes ( $\alpha$ -pinène et 2-carène). Pour la cinétique à température ambiante, les études ont été réalisées dans le noir, en condition sèche (RH<2%), à pression atmosphérique et à une température de  $294 \pm 2$  K) en utilisant la méthode relative dans les deux chambres (CHARME et THALAMOS). La mesure des coefficients ont permis de calculer le temps de vie atmosphérique pour ces furanes. Les coefficients suivants (En  $\text{cm}^3 \text{molecule}^{-1} \text{s}^{-1}$ ) ont été déterminés:  $k(\text{F}) = (1.61 \pm 0.28) \times 10^{-12}$ ,  $k(2\text{-MF}) = (1.96 \pm 0.25) \times 10^{-11}$ ,  $k(3\text{-MF}) = (1.49 \pm 0.33) \times 10^{-11}$ ,  $k(2,5\text{-DMF}) = (6.49 \pm 0.95) \times 10^{-11}$  and  $k(2,3,5\text{-TMF}) = (1.66 \pm 0.69) \times 10^{-10}$ . Ces résultats montrent que les réactions des furanes méthylés avec les radicaux nitrates est la voie principale de réactivité avec des temps de vie entre 0.5 et 55 min pour ces molécules. La cinétique en fonction de la température a été étudiée dans le noir, en condition sèche (RH<2%), à pression atmosphérique et en utilisant aussi la méthode relative. La dépendance négative à la température mise en évidence des coefficients des réactions pour ces furanes avec NO<sub>3</sub> montre que la voie majeure de la réaction est réalisée par l'addition de NO<sub>3</sub> et l'addition-élimination sur l'anneau.

La deuxième partie de ces recherches se focalise sur l'identification et la quantification des produits formés dans la phase gazeuse et particulaire de ces réactions et les mécanismes menant à ces produits d'oxydation. Pour les 5 furanes étudiés, la voie principale de réaction est réalisée l'addition de NO<sub>3</sub> sur le C-2/C-5 de l'anneau menant à la formation de dicarbonyles insaturés. Pour un furane simplement méthylé (2-MF et 3-MF), un carbonyle cyclique nitraté est aussi formé comme produit primaire majeur par addition de NO<sub>3</sub> sur le C-2. Pour les furanes multi-méthylés (2,5-DMF et 2,3,5-TMF), une autre voie majeure apparaît via une

addition de  $\text{NO}_3$  suivi d'une abstraction d'hydrogène sur le groupe méthyle attaché à l'anneau du furane menant à la formation de furaldéhydes méthylés comme autres produits majeurs.

Comparant les rendements en AOS obtenus lors des réactions du 2-MF, 2,5-DMF et 2,3,5-TMF avec  $\text{NO}_3$ , le rendement maximal d'aérosol du 2-MF était d'environ 2% ce qui est 5 à 6 fois inférieur au 2,5-DMF (environ 12%) et au 2,3,5-TMF (environ 10%). Cela montre que le nombre de méthyle sur l'anneau réduit la volatilité ou la pression de vapeur saturante du composé.

La composition des AOS de ces réactions permet de conclure que certains des produits identifiés dans la phase gazeuse ont aussi été identifiés dans la phase particulaire (produits majoritaires inclus) montrant que ces produits se partagent entre les phases gazeuse et particulaire. En plus de ces produits, des dimères et des trimères formés à partir de radicaux  $\text{RO}_2$  sont produits lors de ces réactions.

